PROGRESS IN THEORETICAL CHEMISTRY AND PHYSICS

Theoretical Chemistry and Physics of Heavy and Superheavy Elements

U. Kaldor
S. Wilson (Eds.)

Springer-Science+Business Media, B.V.

THEORETICAL CHEMISTRY AND PHYSICS OF HEAVY AND SUPERHEAVY ELEMENTS

Progress in Theoretical Chemistry and Physics

VOLUME 11

Honorary Editor:

W.N. Lipscomb *(Harvard University, Cambridge, MA, U.S.A.)*

Editors-in-Chief:

J. Maruani *(Laboratoire de Chimie Physique, Paris, France)*
S. Wilson *(Rutherford Appleton Laboratory, Oxfordshire, U.K.)*

Editorial Board:

H. Ågren *(Royal Institute of Technology, Stockholm, Sweden)*
D. Avnir *(Hebrew University of Jerusalem, Israel)*
J. Cioslowski *(Florida State University, Tallahassee, FL, U.S.A.)*
R. Daudel *(European Academy of Sciences, Arts and Humanities, Paris, France)*
G. Delgado-Barrio *(Instituto de Matematicas y Fisica Fundamental, Madrid, Spain)*
E.K.U. Gross *(Freie Universität, Berlin, Germany)*
W.F. van Gunsteren *(ETH-Zentrum, Zürich, Switzerland)*
K. Hirao *(University of Tokyo, Japan)*
I. Hubač *(Komensky University, Bratislava, Slovakia)*
M.P. Levy *(Tulane University, New Orleans, LA, U.S.A.)*
R. McWeeny *(Università di Pisa, Italy)*
P.G. Mezey *(University of Saskatchewan, Saskatoon, SK, Canada)*
M.A.C. Nascimento *(Instituto de Quimica, Rio de Janeiro, Brazil)*
N. Rahman *(Dipartimento di Scienze Chimiche, Trieste, Italy)*
S.D. Schwartz *(Yeshiva University, Bronx, NY, U.S.A.)*
S. Suhai *(Cancer Research Center, Heidelberg, Germany)*
O. Tapia *(University of Uppsala, Sweden)*
P.R. Taylor *(University of Warwick, Coventry, U.K.)*
R.G. Woolley *(Nottingham Trent University, Nottingham, U.K.)*

Former Editors and Editorial Board Members:

I. Prigogine (deceased)
J. Rychlewski (deceased)
Y.G. Smeyers (deceased)
G.L. Malli (resigned)

The titles published in this series are listed at the end of this volume.

Theoretical Chemistry and Physics of Heavy and Superheavy Elements

Edited by

U. Kaldor

School of Chemistry,
Tel Aviv University, Tel Aviv, Israel

and

S. Wilson

Rutherford Appleton Laboratory,
Chilton, Oxfordshire, England

Springer-Science+Business Media, B.V.

A C.I.P. Catalogue record for this book is available from the Library of Congress.

ISBN 978-90-481-6313-7 ISBN 978-94-017-0105-1 (eBook)
DOI 10.1007/978-94-017-0105-1

Printed on acid-free paper

All Rights Reserved
© 2003 Springer Science+Business Media Dordrecht
Originally published by Kluwer Academic Publishers in 2003.
Softcover reprint of the hardcover 1st edition 2003
No part of this work may be reproduced, stored in a retrieval system, or transmitted
in any form or by any means, electronic, mechanical, photocopying, microfilming, recording
or otherwise, without written permission from the Publisher, with the exception
of any material supplied specifically for the purpose of being entered
and executed on a computer system, for exclusive use by the purchaser of the work.

Progress in Theoretical Chemistry and Physics

A series reporting advances in theoretical molecular and material sciences, including theoretical, mathematical and computational chemistry, physical chemistry and chemical physics

Aim and Scope

Science progresses by a symbiotic interaction between theory and experiment: theory is used to interpret experimental results and may suggest new experiments; experiment helps to test theoretical predictions and may lead to improved theories. Theoretical Chemistry (including Physical Chemistry and Chemical Physics) provides the conceptual and technical background and apparatus for the rationalisation of phenomena in the chemical sciences. It is, therefore, a wide ranging subject, reflecting the diversity of molecular and related species and processes arising in chemical systems. The book series *Progress in Theoretical Chemistry and Physics* aims to report advances in methods and applications in this extended domain. It will comprise monographs as well as collections of papers on particular themes, which may arise from proceedings of symposia or invited papers on specific topics as well as initiatives from authors or translations.

The basic theories of physics – classical mechanics and electromagnetism, relativity theory, quantum mechanics, statistical mechanics, quantum electrodynamics – support the theoretical apparatus which is used in molecular sciences. Quantum mechanics plays a particular role in theoretical chemistry, providing the basis for the valence theories which allow to interpret the structure of molecules and for the spectroscopic models employed in the determination of structural information from spectral patterns. Indeed, Quantum Chemistry often appears synonymous with Theoretical Chemistry: it will, therefore, constitute a major part of this book series. However, the scope of the series will also include other areas of theoretical chemistry, such as mathematical chemistry (which involves the use of algebra and topology in the analysis of molecular structures and reactions); molecular mechanics, molecular dynamics and chemical thermodynamics, which play an important role in rationalizing the geometric and electronic structures of molecular assemblies and polymers, clusters and crystals; surface, interface, solvent and solid-state effects; excited-state dynamics, reactive collisions, and chemical reactions.

Recent decades have seen the emergence of a novel approach to scientific research, based on the exploitation of fast electronic digital computers. Computation provides a method of investigation which transcends the traditional division between theory and experiment. Computer-assisted simulation and design may afford a solution to complex problems which would otherwise be intractable to theoretical analysis, and may also provide a viable alternative to difficult or costly laboratory experiments. Though stemming from Theoretical Chemistry, Computational Chemistry is a field of research

in its own right, which can help to test theoretical predictions and may also suggest improved theories.

The field of theoretical molecular sciences ranges from fundamental physical questions relevant to the molecular concept, through the statics and dynamics of isolated molecules, aggregates and materials, molecular properties and interactions, and the role of molecules in the biological sciences. Therefore, it involves the physical basis for geometric and electronic structure, states of aggregation, physical and chemical transformations, thermodynamic and kinetic properties, as well as unusual properties such as extreme flexibility or strong relativistic or quantum-field effects, extreme conditions such as intense radiation fields or interaction with the continuum, and the specificity of biochemical reactions.

Theoretical chemistry has an applied branch – a part of molecular engineering, which involves the investigation of structure–property relationships aiming at the design, synthesis and application of molecules and materials endowed with specific functions, now in demand in such areas as molecular electronics, drug design or genetic engineering. Relevant properties include conductivity (normal, semi- and supra-), magnetism (ferro- or ferri-), optoelectronic effects (involving nonlinear response), photochromism and photoreactivity, radiation and thermal resistance, molecular recognition and information processing, and biological and pharmaceutical activities, as well as properties favouring self-assembling mechanisms and combination properties needed in multifunctional systems.

Progress in Theoretical Chemistry and Physics is made at different rates in these various research fields. The aim of this book series is to provide timely and in-depth coverage of selected topics and broad-ranging yet detailed analysis of contemporary theories and their applications. The series will be of primary interest to those whose research is directly concerned with the development and application of theoretical approaches in the chemical sciences. It will provide up-to-date reports on theoretical methods for the chemist, thermodynamician or spectroscopist, the atomic, molecular or cluster physicist, and the biochemist or molecular biologist who wish to employ techniques developed in theoretical, mathematical or computational chemistry in their research programmes. It is also intended to provide the graduate student with a readily accessible documentation on various branches of theoretical chemistry, physical chemistry and chemical physics.

Contents

Preface xiii

Contributing Authors xvii

1
Theoretical Chemistry and Physics of Heavy and Superheavy Elements 1
S. Wilson and U. Kaldor
1. New Alchemies: from Rutherford to Rutherfordium 2
2. Theoretical Chemistry and Physics of Heavy and Superheavy Elements 10

2
Basic elements of relativistic quantum mechanics 15
S. Wilson and U. Kaldor
1. Introduction 16
2. The Fundamentals of Relativistic Electronic Structure Theory 18
   2.1 The Dirac Equation 20
   2.2 The Dirac Matrices 22
   2.3 The Dirac Spectrum 27
   2.4 Many-Body Systems and Operators 29
   2.5 The Electron-Electron Interaction 30
   2.6 The Furry Bound-State Interaction Picture of Quantum Electrodynamics 32
3. The algebraic approximation 34
   3.1 Non-relativistic Finite Basis Set Approximations 34
   3.2 The Dirac Equation in the Algebraic Approximation 35
   3.3 The Matrix Dirac-Hartree-Fock Approximation 39
   3.4 A Digression: Finite Nuclear Models 42
   3.5 Electron correlation, many-body perturbation theory, and the no virtual pair approximation 42
   3.6 Beyond the no virtual pair approximation 44
4. Summary and Conclusions 48

3
The Chemistry of the Heaviest Elements 55
V. Pershina and D.C. Hoffman
1. Introduction 56
1.1 Production and identification of the heaviest elements. A historical overview 56
1.2 Role of chemical studies 60
2. Relativistic effects in the chemistry of the heaviest elements 62
2.1 Relativistic effects on atomic electronic shells 62
2.2 Relativistic quantum chemical calculations 66
3. Predictions of chemical properties 69
3.1 Atomic properties 69
3.2 Properties of gas-phase compounds of elements 104 through 108 73
3.3 Solution chemistry of elements 104, 105 and 106 79
4. One-atom-at-a-time chemistry 86
4.1 Experimental techniques 86
4.2 Results of gas-phase chemistry experiments 89
4.3 Results of solution chemistry experiments 96
5. Prospects for chemical studies of elements heavier than 108 101
5.1 Production of longer-lived isotopes 101
5.2 Theoretical predictions of chemical properties 102
5.3 Experimental investigations and plans 106
6. Summary 107

4
Core and valence electron distributions in heavy elements by x-ray and electron spectroscopy 115
C. Bonnelle
1. Basic principles of electron and x-ray spectroscopy 118
1.1 General 118
1.2 Interactions with the probe particles 120
1.3 Photoemission 122
1.4 Discrete x-ray emission 123
1.5 Auger emission 125
1.6 Complementarity between the different core spectroscopies 126
2. Binding energies 127
2.1 Atomic effects 127
2.2 Effects due to the surrounding 131
3. Transitions between localized states 133
3.1 X-ray normal emissions and their satellites 133
3.1.1 Mn K emission spectrum 136
3.1.2 Rare earth x-ray emissions 139
3.1.3 Uranium x-ray emissions 139
3.2 Core photoemission 141
4. X-ray excited states 147
4.1 f states 147
4.1.1 Creation of the x-ray excited states 148
4.1.2 Decay of the x-ray excited states 150
4.1.3 Lanthanum $3d$ and $4d$ emissions 151
4.1.4 Erbium $3d$ emission 154

4.1.5 Uranium $3d$, $4d$ and $5d$ emissions 154
4.1.6 Plutonium $3d$ emission 155
4.1.7 Interaction with a state continuum 156
4.2 d states 157
4.3 Discussion 158
5. Valence states in solids 159
5.1 Elements with s and p valence electrons 161
5.2 Transition elements 163
5.3 Lanthanides and Actinides 165

5
Four-component electronic structure methods for atoms 171
Uzi Kaldor, Ephraim Eliav, and Arie Landau
1. Basic Equations 173
1.1 The relativistic Hamiltonian 173
1.2 The one-electron equation 175
1.3 SCF calculations 177
2. Incorporation of Electron Correlation 177
2.1 The Fock-space coupled-cluster method 178
2.2 The intermediate Hamiltonian coupled cluster method 180
3. Applications 182
3.1 Ionization potentials of alkali atoms 183
3.2 Gold and eka-gold (E111): Local maximum of relativistic effects 184
3.3 The f^2 levels of Pr^{3+}: Importance of dynamic correlation 187
3.4 Ground state of rutherfordium — interplay of relativity and correlation 189
3.5 Eka-lead (element 114) — an island of stability? 191
3.6 Element 118 — can a rare gas have positive electron affinity? 195
3.7 Eka-actinium (E121) — when is the Breit term important? 196
3.8 Electron affinities of alkali atoms — selection of P space 196
3.9 Electron affinities in group 13 — what about Ga? 200
3.10 Heavy atom electron affinities — multiple stable anionic states 201
3.11 Properties other than energy 202
4. Summary and Conclusion 203

6
Four-component electronic structure methods for molecules 211
T. Saue and L. Visscher
1. The Hamiltonian 213
1.1 The one-electron part 214
1.1.1 The Dirac equation in an electromagnetic field 214
1.1.2 Time reversal symmetry 218
1.1.3 Charge conjugation symmetry 222
1.1.4 Towards the non-relativistic limit 223
1.2 The two-electron part 225
1.3 Second quantization 227
2. Variational procedures 228

2.1 The standard approach 229
2.2 Towards QED 234
2.3 Discussion 240
2.4 The correlated level 245
3. Implementation and Computational Scaling 248
3.1 The algebraic approximation 248
3.2 Electron correlation methods 256
4. Conclusion 261

7
Relativistic electron correlation theory 269
Yasuyuki Ishikawa and Marius J. Vilkas
1. Relativistic electron correlation theory 271
1.1 The relativistic no-pair Dirac-Coulomb- Breit Hamiltonian 271
1.2 Single-configuration matrix Dirac-Fock SCF for closed- and open-shell systems 274
1.3 Relativistic electron correlation: Definition of the Dirac-Coulomb and Dirac-Coulomb- Breit correlation energies 283
1.4 Relativistic Moller-Plesset perturbation theory for systems with closed shells or one valence electron outside a closed core 284
1.5 Dirac-Coulomb and Dirac-Coulomb-Breit correlation corrections in noble gas atoms, group-IIB atoms and neon-like ions 288
1.6 Dirac-Coulomb and Dirac-Coulomb-Breit correlation in systems with one valence electron outside a closed core: the effects on the ionization energy 295
2. Nondynamical and dynamical correlation energies 303
2.1 The matrix multiconfiguration Dirac-Fock SCF method for multiple open-shell systems 303
2.2 Relativistic multireference many-body perturbation theory for quasidegenerate systems 306
2.3 Nondynamic and dynamic correlation energies in Zn 311
2.4 Contribution of relativistic correlation energies and Lamb shift to term energy separations in Pb 315
3. Summary 319

8
Matrix Approximations to the Dirac Hamiltonian for Molecular Calculations 325
Kenneth G. Dyall
1. The Modified Dirac Equation 327
2. Elimination of the Small Component and the Foldy-Wouthuysen Transformation 332
3. Matrix Elimination of the Small Component 335
4. The Atomic 4-spinor Approximation 339
5. The Nonrelativistic Atom Approximation 342
6. Properties in the Matrix Approximations 344

9
Two–component methods 349
M. Barysz
1. Unitary transformations of the Dirac Hamiltonian 356
2. The two–component Douglas–Kroll Hamiltonian and its extensions 360
3. Momentum space integrals: the Douglas–Kroll–Hess method 365
4. The infinite–order (exact) two–component method 367
5. The infinite–order two–component method: Numerical results 369
6. The change of picture problem 374
7. The two–electron Hamiltonian in the two–component approximation 378
8. Step by step solutions for the operator R 380
9. Summary 391

10
Relativistic Pseudopotentials 399
P. Schwerdtfeger
1. Introduction 399
2. The Pseudopotential approximation 404
   2.1 Selecting the core 404
   2.2 Introducing the pseudopotential approximation at the Hartree-Fock level 406
   2.3 The model core approximation 408
   2.4 The pseudopotential approximation 409
   2.5 Relativistic pseudopotentials 412
   2.6 Valence basis sets 414
   2.7 Beyond the frozen core approximation 415
3. The accuracy of the pseudopotential approximation 419
   3.1 Test case: the indium atom 419
   3.2 Test case: the mercury atom 420
   3.3 Test case: Au_2 and AuH 422
   3.4 Test case: TlH and (113)H 426
   3.5 Do pseudopotentials overestimate electron correlation effects ? 428
4. Summary 429

11
Relativistic Density Functional Theory 439
E. Engel
1. Introduction 440
2. RDFT Formalism 444
3. Exact Exchange Functional: Relativistic Optimized Potential Method 453
4. RDFT Results for Atoms 455
   4.1 Exchange-only limit: Role of transverse interaction 455
   4.2 Correlation 463
5. Construction of Relativistic Normconserving Pseudopotentials 465
   5.1 Relativistic Troullier-Martins scheme 465
   5.2 Exact exchange 471

6. Illustrative Results for Molecules 475
7. Open Questions 479

12
QED effects in atoms 487
Leonti Labzowsky and Igor Goidenko
1. The Furry picture for bound-state QED 489
   1.1 Dirac equation for the electron in an external field 489
   1.2 Interaction of the electromagnetic and electron-positron fields 493
   1.3 Feynman graph techniques for the bound electrons 496
   1.4 Regularization and renormalization 500
2. Interelectron interaction in atoms 507
   2.1 Adiabatic S-matrix formalism 507
   2.2 First order interelectron interaction 510
   2.3 Second order interelectron interaction 512
   2.4 Dirac-Hartree-Fock approximation 515
   2.5 Dirac-Coulomb-Breit Hamiltonian and beyond 517
3. QED theory of light atoms 519
   3.1 Lowest order radiative corrections 519
   3.2 Higher orders radiative corrections 523
   3.3 QED theory of many-electron atoms 525
4. QED theory of heavy atoms 527
   4.1 Electron self-energy: potential expansion 527
   4.2 Electron self-energy: partial wave renormalization 531
   4.3 Vacuum polarization 533
   4.4 Radiative corrections for the ns valence electrons in heavy atoms 536
   4.5 Radiative corrections to g-factors of the ns valence electron in heavy atoms 537

Index 557

Preface

Quantum mechanics provides the fundamental theoretical apparatus for describing the structure and properties of atoms and molecules in terms of the behaviour of their fundamental components, electrons and nuclei. For heavy atoms and molecules containing them, the electrons can move at speeds which represent a substantial fraction of the speed of light, and thus relativity must be taken into account. Relativistic quantum mechanics therefore provides the basic formalism for calculating the properties of heavy-atom systems.

The purpose of this book is to provide a detailed description of the application of relativistic quantum mechanics to the many-body problem in the theoretical chemistry and physics of heavy and superheavy elements. Recent years have witnessed a continued and growing interest in relativistic quantum chemical methods and the associated computational algorithms which facilitate their application. This interest is fuelled by the need to develop robust, yet efficient theoretical approaches, together with efficient algorithms, which can be applied to atoms in the lower part of the Periodic Table and, more particularly, molecules and molecular entities containing such atoms. Such relativistic theories and computational algorithms are an essential ingredient for the description of heavy element chemistry, becoming even more important in the case of superheavy elements. They are destined to become an indispensable tool in the quantum chemist's armoury. Indeed, since relativity influences the structure of every atom in the Periodic Table, relativistic molecular structure methods may replace in many applications the non-relativistic techniques widely used in contemporary research.

We are most grateful to the contributors to this volume for the time and effort they invested in creating the individual chapters included herein, which together afford a concise review of the theoretical appara-

tus upon which contemporary research on the chemistry and physics of heavy and superheavy elements is based.

U. KALDOR, S. WILSON

"Transmutation was, of course, an age-old dream. But to men like me, with a theoretical bent of mind, what was most exciting about the 1930s was that there began to open up the evolution of nature. ...

The first step in the evolution of the elements takes place in young stars, such as the sun. It is the step from hydrogen to helium, and it needs the great heat of the interior ...

In time the sun will become mostly helium. And then it will become a hotter star in which helium nuclei collide to make heavier atoms in turn. Carbon, for instance, is formed in a star whenever three helium nuclei collide at one spot within less than a millionth of a millionth of a second. Every carbon atom in every living creature has been formed by such a wildly improbable collision. Beyond carbon, oxygen is formed, silicon, sulphur and heavier elements. The most stable elements are in the middle of Mendeleev's table, roughly between iron and silver, But the process of building elements overshoots well beyond them.

If the elements are built up one by one, why does nature stop ? Why do we find only ninety-two elements, of which the last is uranium ? To answer that question we have, evidently, to build elements beyond it ..."

J. Bronowski,
The Ascent of Man,
British Broadcasting Corporation,
London (1973)

Contributing Authors

M. Barysz, Department of Quantum Chemistry, Institute of Chemistry, Nicholas Copernicus University, Gagarina 7, PL-87100 Toruń, Poland
teomjb@chem.uni.torun.pl

C. Bonnelle, Laboratoire de Chimie Physique - Matiére et Rayonnement, Université Pierre et Marie Curie, UMR-CNRS 7614, 11, rue Pierre et Marie Curie, F-75231 Paris, France
cbon@ccr.jussieu.fr

K.G. Dyall, Eloret Corporation, 690 W. Fremont Ave., Suite 8, Sunnyvale, California, CA 94087, U.S.A.
kgdyall@earthlink.net

E. Eliav, School of Chemistry, Tel Aviv University, 69978 Tel Aviv, Israel
ephraim@jade.tau.ac.il

E. Engel, Institut für Theoretische Physik, J.W. Goethe Universität Frankfurt, Robert Mayer Strasse 8-10, D-60054 Frankfurt/Main, Germany
engel@math.uni-frankfurt.de

I. Goidenko, Institute of Physics, St. Petersburg State University, 198904 Uljanovskaya 1, Petrodvorets, St Petersburg, Russia
igor@landau.phys.spbu.ru

D.C. Hoffman, Lawrence Berkeley National Laboratory, 1 Cyclotron Road, Berkeley, California, CA 94720, U.S.A.
University of California, Berkeley, California, CA 94720, U.S.A.
DCHoffman@lbl.gov

Y. Ishikawa, Department of Chemistry and The Chemical Physics Program, University of Puerto Rico, San Juan, Puerto Rico, PR 00931-3346, U.S.A.
ishikawa@rrpac.upr.clu.edu

U. Kaldor, School of Chemistry, Tel Aviv University, 69978 Tel Aviv, Israel
kaldor@jade.tau.ac.il

L.N. Labzowsky, Institute of Physics, St. Petersburg State University, 198904 Uljanovskaya 1, Petrodvorets, St Petersburg, Russia
leonti@landau.phys.spbu.ru

A. Landau, School of Chemistry, Tel Aviv University, 69978 Tel Aviv, Israel
arik@topaz.tau.ac.il

V. Pershina, Gesellschaft für Schwerionenforschung, Planckstr.1, D-64291 Darmstadt, Germany
V.Pershina@gsi.de

T. Saue, CNRS, UMR 7551, Laboratoire de Chimie Quantique, 4 Rue Blaise Pascal, F-67000 Strasbourg, France
saue@quantix.u-strasbg.fr

P. Schwerdtfeger, Department of Chemistry, The University of Auckland, Private Bag 92019, Auckland, New Zealand
p.schwerdtfeger@auckland.ac.nz

M.J. Vilkas, Department of Chemistry and The Chemical Physics Program, University of Puerto Rico, San Juan, Puerto Rico, PR 00931-3346, U.S.A.
marius@hpcf.upr.edu

L. Visscher, Department of Theoretical Chemistry, Faculty of Sciences, Vrije Universiteit Amsterdam, De Boelaan 1083, 1081 HV Amsterdam, The Netherlands
visscher@chem.vu.nl

S. Wilson, Rutherford Appleton Laboratory, Chilton, Oxfordshire, OX11 0QX, England
S.Wilson@rl.ac.uk

Chapter 1

THEORETICAL CHEMISTRY AND PHYSICS OF HEAVY AND SUPERHEAVY ELEMENTS - AN INTRODUCTION

S. Wilson
Rutherford Appleton Laboratory,
Oxfordshire OX11 0QX, England
S.Wilson@rl.ac.uk

U. Kaldor
School of Chemistry, Tel Aviv University,
69978 Tel Aviv, Israel
kaldor@jade.tau.ac.il

"**Transmutation** *late ME* The (supposed or alleged) conversion of one element or substance into another, esp. of a baser metal into gold or silver."

Oxford English Dictionary,
Clarendon Press, Oxford

"In 1919, during his last year at Manchester, he discovered that the nuclei of certain light elements, such as nitrogen, could be 'disintegrated' by the impact of energetic alpha particles coming from some radioactive source, and that during this process fast protons were emitted. Blackett later proved, with the cloud chamber, that the nitrogen in this process was actually transformed into an oxygen isotope, so that Rutherford was the first to deliberately transmute one element into another."

Nobel Lectures: Chemistry 1901-1921,
Elsevier Publishing Company,
Amsterdam (1970)

U. Kaldor and S. Wilson (eds.),
Theoretical Chemistry and Physics of Heavy and Superheavy Elements, 1- 14.
© 2003 *Kluwer Academic Publishers.*

1. New Alchemies: from Rutherford to Rutherfordium

In the Middle Ages, the Alchemists failed completely in their attempts to transmute lead or other base metals into gold[1]. Today, we can not only transmute one element to another but create new elements unknown to Nature. We can achieve this transmutation not only in our experiments but also in our theories. We have thus created New Alchemies!

This volume is concerned with the theoretical apparatus and associated computational algorithms for the description of the chemistry and physics of the heavy and superheavy elements. We are concerned with the structure and properties not only of isolated atoms of these elements but also of molecular species containing them.

Whilst it may appear pedantic, let us begin by defining the terms "heavy" and "superheavy" as used in our title with respect to the elements. We start with what is perhaps the more difficult of the two – "heavy". A dictionary definition of "heavy" reads "*of concentrated weight for the size*" [2]. This is, of course, a relative term. "Heavy water" refers to water composed of isotopes of hydrogen with mass greater than 1 or of oxygen with mass greater than 16 or both. It is applied especially to D_2O. The term "heavy element" is most often taken to refer to elements lying in the lower part of the Periodic Table, including the lanthanides and actinides. But the description "heavy atom" might, in different context, be applied to the single carbon atom in a methane molecule, which is twelve times heavier than other atoms in this system.

The theoretical basis for the description of atoms and molecules is provided by quantum mechanics. This was established in the first three decades of the twentieth century. Quantum mechanics has provided a theoretical foundation for studies in molecular physics and quantum chemistry for over seventy years [3]. The development of many "black box" computer programs over the past four decades has rendered molecular electronic structure calculations almost routine. One of the most widely used of these programs is the GAUSSIAN package [4], which, in common with many others, is based almost entirely on non-relativistic quantum theory. One of the most respected early computer programs was called ALCHEMY. Initially developed during the 1960s by A.D. McLean and his coworkers [5], this program used basis sets of exponential-type functions to carry out high quality calculations on diatomic and linear

[1] Read [1] describes this view of alchemy as "perfunctory" and sets it beside that of the German chemist Liebig (1803-1873) for whom alchemy "was essentially the chemistry of the Middle Ages".

polyatomic molecules. It was called ALCHEMY because atoms could be "transmuted" merely by changing the input data – in particular the nuclear charge. In common with other molecular codes developed in the 1960s – and, indeed, most molecular codes in use today – the ALCHEMY program was based on non-relativistic quantum mechanics. However, when electrons move in the regions of space close to a nucleus, they can achieve speeds which are a significant fraction of the speed of light. Moreover, the heavier the nucleus, the larger this fraction. The equations of quantum mechanics are obtained by applying the Schrödinger correspondence principle to the classical equations of motion. These equations – both classical and quantal – satisfy the Galilean principle of relativity which is known to be inadequate for particles moving at a substantial fraction of the speed of light. For such systems, quantum mechanical equations corresponding to the Special Theory of Relativity must be employed – that is, relativistic quantum mechanics. For high-accuracy treatment of many-electron systems we are ultimately led to the theory of quantum electrodynamics.

In modern work, the term "heavy element" is frequently taken to indicate an element for which the effects of relativity are important. But this must also be seen as a relative definition, since the importance of the "relativistic effects" will depend crucially on the property studied. For example, for some arbitrary system, relativistic effects may be unimportant in the study of valence shell excitations but crucial for core excitation processes. For properties such as nuclear magnetic resonance (NMR) coupling constants, which are sensitive to the wave function in regions close to the nucleus, relativistic effects can be found to be very important even though their influence on the structure and bonding may be very small.

An example of the increased importance of relativistic treatment with atomic number is provided by comparing the experimental ionization potentials of some of the alkali atoms with values calculated using large basis sets and high-order correlation in a non-relativistic and relativistic framework (Table 1.1) [55]. While the errors of the ionization potentials calculated in the relativistic formulation stay small, a systematic increase of the error with atomic number is observed in the non-relativistic scheme. Where exactly these errors justify calling the element "heavy" is, obviously, a matter of choice.

The theoretical study of molecules containing "heavy elements" demands the use of a relativistic formalism. The practical application of this theory requires a new ALCHEMY, a program capable of performing

Table 1.1 **Experimental and calculated ionization potentials of alkali atoms (cm^{-1}). Errors of calculated values with respect to experiment are given.**

Atom	Z	expt.	calc. error	
			rel.	nonrel.
Li	3	43487	−3	−6
K	19	35010	18	−26
Rb	37	33691	30	535
Cs	55	31407	36	1163
Fr	87	32849	−10	2780

high quality calculations for molecules within a fully relativistic framework. Some approaches to this problem are described in the present volume.

Much contemporary literature is concerned with the importance of "relativistic effects", by which is meant the difference between the value of some property calculated within the framework of non-relativistic quantum mechanics and the value obtained once relativity is taken into account. These "relativistic effects" are to large extent an accident of history, for had fully relativistic quantum mechanics been seen as the theoretical basis for molecular electronic structure theory from the beginning, we would surely have only spoken of the "non-relativistic error" introduced when a less appropriate theory – non-relativistic quantum mechanics – is introduced. As it was, non-relativistic quantum mechanics was seen as the foundation for molecular electronic structure theory for about half a century, and much work undertaken in the last two decades of the twentieth century was therefore devoted to the analysis and categorization of "relativistic effects". This statement should be qualified by two observations: (i) Non-relativistic theory leads to a much simpler mathematical machinery required to solve the equations at a given level of sophistication, and it was therefore naturally used in preference to relativistic theory; (ii) Trends in the chemical behaviour of elements show significant changes at the bottom of the Periodic Table. One example is seen in Table 1.1: while the ionization potentials go down from Li to Cs, the trend is reversed for Fr. Calculations indicate that ekafrancium (element 119) will have an even larger IP. Even if we had never heard of non-relativistic quantum mechanics or of "relativistic effects", this "heavy-element effect" would have still required consideration.

Atomic weights do not play a direct role in molecular electronic structure theory provided a point nucleus model is assumed – then the elec-

tronic structure depends on the positions of the clamped nuclei and the associated charges. But nuclei have a finite extent which is, of course, related to the number of component protons and neutrons and thus to the atomic weight. For heavy elements, the finite-nuclear size correction may be large, particularly for s and $p_{1/2}$ single particle state functions which have a non-vanishing amplitude at the nuclear position. The use of realistic nuclear models is essential in the evaluation of hyperfine and PNC (parity nonconserving) effects since some of the operators involved act only over the nuclear volume.

Atomic weights, or more correctly atomic masses, play a direct role in the nuclear motion problem and thus in the vibrational and rotational spectroscopy of heavy elements. By definition, the most abundant carbon isotope, ^{12}C, has a relative atomic mass of 12.0000000(0) amu. The relative atomic mass for each of the noble gases are given in Table 1.2 together with the isotopic abundances and standard atomic weights to provide the reader with a feeling for the range of values which arise.

The term "superheavy" is less ambiguous than "heavy". It is used to describe the heaviest elements, but there is no universal agreement as to when an element is heavy enough to merit the notation "superheavy". While some believe that only elements with atomic number above 100 are superheavy, others confer this title upon all synthetic elements beyond the heaviest naturally occurring element, uranium, which has an atomic number of 92.

By 1939, it was already established [8–11] that the creation of elements heavier than uranium, the heaviest element to occur naturally in significant amounts, is limited by this disintegration of the massive nucleus by nuclear fission. The liquid drop model [13, 23] assumes that nuclei have approximately constant density, an assumption supported by scattering experiments. For the nuclei of elements heavier than uranium, the repulsive Coulomb forces between the Z protons are not balanced by the strong but short-range attractive nuclear forces and the liquid drop model predicts fission.

The discovery of a shell structure in nuclei in which each nucleon moves in an effective potential created by the other nucleons led to the realization that shell effects, similar to those which arise in the electronic structure of atoms, can stabilize heavy nuclei. A key difference between the atom and the nuclear structure problems is that, whilst the Hamiltonian can be immediately written down for an atom, there exist no first principles derivation of the Hamiltonian for a nucleus. Over the years, a great deal of effort has been expended on the construction of potential

Table 1.2 Atomic Weights and Isotopic Compositions for the Noble Gases†

Z	Symbol	A	Atomic mass[a]	Isotopic composition[b]	Atomic weight[c]
2	He	3	3.0160293097(9)	0.000137(3)	4.002602(2)
		4	4.0026032497(10)	99.999863(3)	
10	Ne	20	19.9924401759(20)	90.48(3)	20.1797(6)
		21	20.99384674(4)	0.27(1)	
		22	21.99138551(23)	9.25(3)	
18	Ar	36	35.96754628(27)	0.3365(30)	39.948(1)
		38	37.9627322(5)	0.0632(5)	
		40	39.962383123(3)	99.6003(30)	
36	Kr	78	77.920386(7)	0.35(1)	83.80(1)
		80	79.916378(4)	2.28(6)	
		82	81.9134846(28)	11.58(14)	
		83	82.914136(3)	11.49(6)	
		84	83.911507(3)	57.00(4)	
		86	85.9106103(12)	17.30(22)	
54	Xe	124	123.9058958(21)	0.09(1)	131.29(2)
		126	125.904269(7)	0.09(1)	
		128	127.9035304(15)	1.92(3)	
		129	128.9047795(9)	26.44(24)	
		130	129.9035079(10)	4.08(2)	
		131	130.9050819(10)	21.18(3)	
		132	131.9041545(12)	26.89(6)	
		134	133.9053945(9)	10.44(10)	
		136	135.907220(8)	8.87(16)	
86	Rn	211	210.990585(8)		[222][d]
		220	220.0113841(29)		
		222	222.0175705(27)		

† Taken from the work of Coursey and Dragoset [7].

[a] Relative Atomic Mass of the given isotope. These values are scaled such that the relative atomic mass of ^{12}C is 12, where ^{12}C is a neutral atom in its nuclear and electronic ground state.

[b] Representative Isotopic Composition. These values represent the isotopic composition of the chemicals and/or materials most commonly encountered in the laboratory. The uncertainities are listed in parenthesis.

[c] Standard Atomic Weight (common usage) [more appropriately called relative atomic mass of the element]. The relative atomic mass of an element is derived by averaging the relative atomic masses of the isotopes of that element. The uncertainties are listed in parenthesis.

[d] Mass number of the most stable isotope.

functions for the modeling of the observed nuclear energy levels. Solving the resulting equations yields a series of energy levels. These energy levels increase with orbital angular momentum quantum number ℓ. The s, p, d, f ... symbols are used for ℓ=0, 1, 2, 3 ... just as in the atomic case. However, there is no analog to the principal quantum number n, which takes the values $n = 1, \ldots$. The quantum number for orbital angular momentum, ℓ, is not limited by n as in the case of atomic electronic structure.

Nuclear energy levels depend on the details of the potential function and the quantum numbers arising in the nuclear shell model; they also exhibit splitting caused by spin-orbit interaction. This splitting increases with orbital quantum number, leading sometimes to overlapping of adjacent levels. The multiplicity of a given state is $2j + 1$, where j is the total angular momentum.

The first eleven transuranium elements, with their atomic numbers and year discovered (or, rather, first produced), are:

- neptunium (93, 1940)
- plutonium (94, 1940)
- americium (95, 1944)
- curium (96, 1944)
- berkelium (97, 1949)
- californium (98, 1950)
- einsteinium (99, 1952)
- fermium (100, 1952)
- mendelevium (101, 1955)
- nobelium (102, 1958)
- lawrencium (103, 1961).

In this series of elements, electrons are successively added to the inner $5f$ shell. These elements are, therefore, members of a fourteen-member heavy rare earth series, called the actinide elements. This series is chemically analogous to the fourteen-member lanthanide series of naturally occurring elements consisting of cerium (atomic number 58) through lutetium (atomic number 71), in which the $4f$ shell is sequentially filled. Hence the superheavy element curium (96) is chemically homologous with the lanthanide element gadolinium (atomic number 64), whilst the

superheavy element lawrencium (103) is similarly related with the lanthanide lutetium (71).

The synthetic transuranium elements beyond atomic number 103 (lawrencium) are termed the transactinide elements. These elements, which have been called rutherfordium (atomic number 104), hahnium (atomic number 105), seaborgium (atomic number 106), etc., are expected to have chemical properties analogous to those of the elements beyond atomic number 71 – hafnium (atomic number 72), tantalum (atomic number 73), tungsten (atomic number 74), etc., since for both series a *d* shell is being filled.

At the time of writing, the known transactinide elements are

- rutherfordium (104, 1964)
- dubnium (105, 1967)
- seaborgium (106, 1974)
- bohrium (107, 1981)
- hassium (108, 1984)
- meitnerium (109, 1982)
- ununnilium (110, 1994)
- unununium (111, 1994)
- ununbium (112, 1996)
- ununquadium (114, 1998).

Observations of the elements Ununhexium (Uuh) and Ununoctium (Uuo) with atomic numbers 116 and 118, respectively, were claimed in 1999 but were later retracted.

The first of the transactinide elements, rutherfordium, is named after Ernest Rutherford, the proponent of the nuclear atom. It was created in 1969 by Ghiorso and coworkers by bombarding californium-249 with beams of carbon-12 and carbon-13. This produced isotopes with half lives of 4+ and 3 seconds. With an atomic number of 104, one isotope has since been produced with a half-life greater than a minute: this is ^{261}Rf, with a half life of 82.7 seconds. Four isotopes have half lives in excess of a second but less than a minute: ^{255}Rf, ^{257}Rf, ^{259}Rf and ^{262}Rf have half lives of 1.4, 26.1, 3.1 and 1.2 seconds, respectively. The less stable isotopes ^{256}Rf, ^{258}Rf, and ^{260}Rf have half lives of 7.4, 13 and 21 *milli*seconds, respectively. The least stable isotopes ^{253}Rf and ^{254}Rf

Table 1.3 The known isotopes of rutherfordium, Rf†

Z	Symbol	A	Atomic mass[a]
104	Rf	253	253.10068(49)
		254	254.10017(31)
		255	255.10149(22)
		256	256.101180(29)
		257	257.10307(29)
		258	258.10357(22)
		259	259.105630(80)
		260	260.10643(22)
		261	261.10875(11)
		262	262.10992(30)
		263	263.11254(20)
		264	264.11398(48)

† Taken from the work of Coursey and Dragoset [7].
[a] Relative Atomic Mass (of the isotope): Ar(X), where X is an isotope. These values are scaled to Ar(^{12}C) = 12, where ^{12}C is a neutral atom in its nuclear and electronic ground state. Thus, the relative atomic mass of entity X is given by: Ar(X) = m(X) / [m(^{12}C) / 12]
.

have half lives of 48 and 22 μseconds, respectively. The known isotopes of rutherfordium are shown in Table 1.3.

The superheavy elements are produced in the laboratory by fusion of heavy ions. Experimental research into this area is centred around heavy-ion accelerators capable of delivering intense heavy ion beams at energies which can overcome the Coulomb barrier between the ions. These accelerators are located at

- Gesellschaft für Schwerionenforschung mbH (GSI),
  Darmstadt, Germany
  http://www.gsi.de/,

- Joint Institute for Nuclear Research (JINR),
  Dubna, Russia
  http://www.jinr.dubna.su/,

- Lawrence Berkeley National Laboratory (LBNL),
  Berkeley, USA
  http://www.lbl.gov/,

- Grand Accelerateur National d'Ions Lourds (GANIL), France
  http://www.ganil.fr/ ,

- The Institute of Physical and Chemical Research (RIKEN), Wako, Saitama, Japan
  http://www.riken.go.jp/.

These facilities have established a new alchemy. The transmutation of matter that has created the superheavy elements has resulted in an extended Periodic table and a new chemistry.

The chemical properties of the elements neptunium (93) through einsteinium (99) were studied at first by tracer techniques. Macroscopic quantities became available later. Experiments with very small quantities (single atoms for the heavier elements) have now been extended all the way to hassium (108). Experimental observations indicate that, in general, these elements exhibit chemical properties expected from their place in the Periodic Table.

2. Theoretical Chemistry and Physics of Heavy and Superheavy Elements

The first decades of the twentieth century saw the introduction of the nuclear model for the atom and the laying down of the foundations for a theoretical description of atomic and molecular structure which would ultimately provide a detailed understanding of the nature of the chemical bond and the rationalization of the ideas and concepts of molecular structure which had their infancy in the work of Dalton at the beginning of the nineteenth century.

The thirty years following Planck's seminal insight in 1900 saw the birth of quantum mechanics[2]. Bohr explained the spectrum of the hydrogen atom by considering Rutherford's nuclear model of the atom and established the 'old' quantum theory. In the 1920s, Schrödinger, Heisenberg, Dirac and others developed wave mechanics, matrix mechanics and the general theory of quantum mechanics. But physicists faced a contradiction between quantum mechanics, which was formulated in the Galilean (or non-relativistic) approximation, and the special theory of relativity introduced by Einstein in a famous paper[3] published in 1905.

[2]The historical development of quantum mechanics is described in the work of Mehra and Rechenberg [14–19].

[3]For an English translation of both Einstein papers on relativity and those of Lorentz, Minkkowski and Weyl see the volume entitled *The Principle of Relativity* published by Dover [20].

Dirac developed a relativistic wave equation for the electron, which was an important advance. The Dirac equation gave rise to a spectrum which admitted not only positive energy solutions, which are in corresponded with the solutions of the (non-relativistic) Schrödinger equation, but also negative energy solutions, which have no counterpart in non-relativistic quantum mechanics. Dirac writes [21]

> "... the wave equation for the electron admits of twice as many solutions as it ought to, half of them referring to states with negative values for the kinetic energy ... This difficulty ... is inherent in any relativistic theory. It occurs also in classical relativistic theory, but is not then serious since, owing to the continuity in the variation of all classical dynamical variables, if the kinetic energy is initially positive ..., it cannot subsequently be negative. In the quantum theory ... discontinuous transitions may take place, so that if the electron is initially in a state of positive kinetic energy it may make a transition to a state of negative kinetic energy. It is therefore no longer permissible simply to ignore the negative-energy states, as one can do in the classical theory."

Dirac postulated that the negative energy branch of the spectrum is filled with electrons, according to the Pauli principle, which prevent the decay of positive energy states. The electrons occupying the negative energy states are not directly observable, but excitations from this negative energy sea gives rise to holes or positrons which could be observed. Dirac described the situation as follows [22]:

> "We assume that *nearly all the negative-energy states are occupied*, with one electron in each state in accordance with the exclusion principle of Pauli. An unoccupied negative energy state will now appear as something with a positive energy, since to make it disappear, i.e. to fill it up, we should have to add to it an electron with negative energy. We assume that *these unoccupied negative-energy states are the positrons*".

A consequence of Dirac's work is that even the simplest of systems, the hydrogenic atom, is seen to be an infinitely many-bodied problem. The basic feature that had to be introduced to successfully unite quantum mechanics and special relativity is the possibility of the creation and annihilation of quanta (or 'particles'). The fundamental contradiction of special relativity and the non-relativistic quantum theory is that the latter does not have this feature. The theoretical framework in which quantum mechanics and special relativity are successfully reconciled is called quantum electrodynamics. This was developed by Tomonaga, Schwinger, Feynman and others in the late 1940s[4]. The general principles on which quantum electrodynamics or the quantum theory of fields are constructed

[4]For a collection of original papers in which quantum electrodynamics is developed see the volume edited by Schwinger [23]

allow for many different consistent theories. Of these theories one has been experimentally singled out. It is called the "standard model". The standard model is highly successful in accounting for a wide range of experiments to very high precision[5].

The twentieth century closed with the development of the theoretical and the associated computational machinery required for the description of the chemistry and physics of the heavy and superheavy elements. This volume describes the most important of these developments.

After the present Introduction, the volume contains a chapter presenting briefly the basic elements of relativistic atomic and molecular quantum mechanics.

The next two chapters describe some of the most important experimental studies of the chemistry and physics of heavy and superheavy elements. Hoffman and Pershina give an up-to-date account of the chemistry of the heaviest elements together with theoretical approaches intimately related to the experimental work, and Bonnelle describes the determination of core and valence electron distribution in heavy elements by X-ray and electron spectroscopy.

Four-component methods and calculations are reviewed in the following three chapter: Kaldor, Eliav and Landau discuss atomic systems, Saue and Visscher describe molecular methods and applications, and Ishikawa and Vilkas concentrate on correlation methods within relativistic quantum chemistry. Four-component methods are the most accurate but also the most demanding in terms of computational resources.

Less expensive two-component methods are described in the next two chapters. Dyall gives matrix approximations to the Dirac Hamiltonian for molecular calculations, and Barysz reviews a series of two-component methods, from Douglas-Kroll to the exact infinite order method.

The treatment of large systems requires methods which are more approximate and computationally feasible; two chapters describe such schemes. The pseudopotential approach, reviewed by Schwerdtfeger, has the distinction of being the oldest and most computationally tractable ansatz for incorporating relativity in molecular electronic structure calculations. A more recent method, also widely used, is the relativistic density functional theory, described by Engel.

The volume concludes with a review of quantum electrodynamic effects, which are necessary in high-accuracy descriptions of many-electron systems, by Labzowsky and Goidenko.

[5] A comprehensive account of the quantum theory of fields can be found in the 3 volume trattise by Weinberg [24–26]

Acknowledgments

SW acknowledges the support of the Engineering and Physical Sciences Research Council. UK acknowledges support of the Israel Science Foundation and the U.S.-Israel Binational Science Foundation.

References

[1] Read J., (1961) *From Alchemy to Chemistry*, Bell, London; (1995) Dover, New York.

[2] *Oxford English Dictionary*, Clarendon Press, Oxford

[3] Wilson S., Bernath P.F., and McWeeny, R. (editors), (2003) *Handbook of Molecular Physics and Quantum Chemistry*, Wiley, Chichester.

[4] Frisch Æleen and Frisch M.J., (1999), *Gaussian 98 User's Reference*, 2nd edition, Gaussian Inc., Carnegie Office Park, Pittsburgh, PA 15106, U.S.A.

[5] McLean A.D., (1971) in *Proceedings of the Conference on Potential Energy Surfaces in Chemistry*, August 10-13, 1970, University of California, Santa Cruz, edited by W.A. Lester, Jr., p. 87, IBM Research Laboratory, San Jose, California, U.S.A.

[6] Eliav E., Kaldor U., and Ishikawa Y., (1994) *Phys. Rev. A* **50**, 1121.

[7] Coursey J.S. and Dragoset R.A., (2001) *Atomic Weights and Isotopic Compositions (version 2.2.1)*, [Online]. Available: http://physics.nist.gov/Comp [2002, February 7]. National Institute of Standards and Technology, Gaithersburg, MD.

[8] Hahn O. and Strassmann F., (1939) *Naturwissenschaften* **27**, 11.

[9] Meitner L. and Frisch O., (1939) *Nature* **143**, 239.

[10] Frisch O.R., (1939) *Nature* **143**, 276.

[11] Bohr N., (1939) *Nature* **143**, 330.

[12] Bethe H.A. and Bacher F., (1936) *Rev. Mod. Phys.* **8**, 82.

[13] von Weizsäcker C.F., (1936) *Z. Phys.* **96**, 431.

[14] Mehra J. and Rechenberg H., (1982) *The historical development of quantum theory.* Volume 1 *The quantum theory of Planck, Einstein, Bohr and Sommerfeld*, Springer-Verlag, Berlin.

[15] Mehra J. and Rechenberg H., (1982) *The historical development of quantum theory.* Volume 2 *the discovery of quantum mechanics 1925* Springer-Verlag, Berlin.

[16] Mehra J. and Rechenberg H., (1982) *The historical development of quantum theory.* Volume 3: *The formulation of matrix mechanics and its modifications 1925-1926* Springer-Verlag, Berlin.

[17] Mehra J. and Rechenberg H., (1982) *The historical development of quantum theory.* Volume 4. Part 1: *The fundamental equations of quantum mechanics 1925-1926.* Part 2: *The reception of the new quantum mechanics 1925-1926* Springer-Verlag, Berlin.

[18] Mehra J. and Rechenberg H., (1982) *The historical development of quantum theory.* Volume 5: *Erwin Schrodinger and the rise of wave mechanics.* Part 1: *Schrodinger in Vienna and Zurich 1887-1925* Springer-Verlag, Berlin.

[19] Mehra J. and Rechenberg H., (2000) *The historical development of quantum theory.* Volume 6: Part 1: *The completion of quantum mechanics 1926-1941.* Part 2: *The conceptual completion and the extensions of quantum mechanics 1942-1999* Springer-Verlag, Berlin.

[20] Einstein A., Lorentz H.A., Weyl H., and Minkowski H., (1952) *The principles of relativity*, Dover, New York.

[21] Dirac P.A.M., (1958) *The principles of quantum mechanics*, 4th edition, p. 273, Clarendon Press, Oxford.

[22] Dirac P.A.M., (1958) *The principles of quantum mechanics*, 4th edition, pp. 274-5, Clarendon Press, Oxford.

[23] Schwinger J., (1958) *Selected Papers in Quantum Electrodynamics*, Dover, New York.

[24] Weinberg S., (1995) *The quantum theory of fields: foundations*, Cambridge University Press, Cambridge.

[25] Weinberg S., (1996) *The quantum theory of fields: modern applications*, Cambridge University Press, Cambridge.

[26] Weinberg S., (2000) *The quantum theory of fields: supersymmetry*, Cambridge University Press, Cambridge.

Chapter 2

BASIC ELEMENTS OF RELATIVISTIC ATOMIC AND MOLECULAR QUANTUM MECHANICS

S. Wilson
Rutherford Appleton Laboratory,
Oxfordshire OX11 0QX, England
S.Wilson@rl.ac.uk

U. Kaldor
School of Chemistry, Tel Aviv University,
69978 Tel Aviv, Israel
kaldor@jade.tau.ac.il

Abstract The basic elements of relativistic quantum mechanics are presented in a form suitable for application to the atomic and molecular structure problem.

Keywords: relativistic quantum mechanics, atomic structure, molecular electronic structure, Dirac equation, Dirac-Hartree-Fock-Coulomb method, Dirac-Hartree-Fock-Breit method, Breit interaction, no-virtual-pair approximation, Furry picture of quantum electrodynamics

---

"Einstein's great achievement, the principle of relativity, imposes conditions which all physical laws have to satisfy. It profoundly influences the whole of physical science, from cosmology, which deals with the very large, to the study of the atom, which deals with the very small."

P.A.M. DIRAC,
Rev. Mod. Phys. **21**, 392 (1949)

U. Kaldor and S. Wilson (eds.),
Theoretical Chemistry and Physics of Heavy and Superheavy Elements, 15–53.
© 2003 *Kluwer Academic Publishers.*

1. Introduction

Non-relativistic quantum mechanics is inadequate as a theoretical basis for the description of the structure and properties of molecular systems which contain "heavy" or "superheavy" elements. The mean speed of electrons in the region close to the nucleus is a substantial fraction of the speed of light, and a fully relativistic electronic structure theory is, therefore, required, both at the independent particle level and beyond. Indeed, at the "heavy" and "superheavy" end of the Periodic Table we may expect a complex interplay between the effects of relativity, many-body effects and quantum electrodynamics. Electric and magnetic properties of atoms and molecules can display pronounced relativistic effects, particularly when the energy of the interaction is high and the use of a non-relativistic treatment of the radiation field is invalid.

The development of methods for relativistic atomic structure calculations began with the the work of Swirles [1] in the 1930s. This occurred in spite of Dirac's 1929 statement [2] that relativity was of

> *"no importance in the consideration of atomic and molecular structure, and ordinary chemical reactions, in which it is, indeed, usually sufficiently accurate if one neglects relativistic variation of mass with velocity and assumes only Coulomb forces between the various electrons and atomic nuclei."*

The ground state energy of a non-relativistic hydrogenic atom with nuclear charge Z is

$$E_{\text{non-relativistic}} = -\frac{1}{2}Z^2, \tag{2.1}$$

whereas for the relativistic hydrogenic atom

$$E_{\text{relativistic}} = -c^2\left[1 - \left(1 - \frac{Z^2}{c^2}\right)^{\frac{1}{2}}\right], \tag{2.2}$$

where c is the speed of light. Thus, for example, for Sn^{49+} ($Z = 50$), the non-relativistic ground state energy is -1250 hartree, whilst the relativistic ground state energy is -1294.626156 hartree. The difference between these two energies is then 44.626156 hartree. For a "superheavy" nucleus, for example Fm^{99+} ($Z = 100$), the non-relativistic energy of the ground state is -5000 hartree and the relativistic ground state energy is -5939.195384 hartree, so that "relativistic effects" account for 939.195384 hartree, or more than 15% of the total energy of this simple one-electron system.

It was not until the late 1970s that Pyykkö [3] pointed out to molecular electronic structure theorists that for a hydrogenic atom with a nuclear

charge of 80 the average radial velocity is some 58% of the speed of light and leads to an electron mass increase of about 23%. Prior to this time, the importance of relativity in studies of atomic structure was widely appreciated [4, 5]. However, atomic structure theory fell largely within 'physics' and was primarily concerned with the interpretation of atomic spectra. On the other hand, molecular electronic structure theory was driven by the needs of 'chemistry' and studied the shape, structure and properties of molecular systems. Several reasons can be advanced for the failure of the theoretical chemistry community to incorporate the effects of relativity in molecular electronic structure calculations until the final quarter of the twentieth century:

1. Willingness to accept Dirac's dictum. In particular, the belief that, since relativistic effects are primarily associated with the atomic cores, they are of no chemical significance.

2. Lack of familiarity with relativistic quantum mechanics.

3. Concentration on the theoretical chemistry of molecules containing light atoms. Electronic structure studies of organic species frequently involve conformation studies of molecules containing C together with N, O and H.

4. The computational demands raised by studies of molecular systems containing heavy atoms.

5. Technical difficulties associated with the implementation of the algebraic approximation in relativistic electronic structure theory.

The growing interest in the influence of relativity on molecular structure is well documented in three bibliographies entitled *Relativistic theory of atoms and molecules* and compiled by Pyykkö [6–8]. Much early work published prior to 1990 is represented in the volumes entitled *Relativistic Effects in Atoms and Molecules* [9] and *The Effects of Relativity in Atoms, Molecules and the Solid State* [10].

The purpose of this chapter is to provide a brief introduction to the basic elements of relativistic atomic and molecular quantum mechanics suitable for the reader who is familiar with the corresponding non-relativistic theory. It is not possible in the space available to provide a detailed exposition of the apparatus of relativistic atomic and molecular structure theory. Such detail can be found elsewhere[1]. Here we aim to demonstrate that the relativistic electronic structure problem contains formal

[1] In addition to the volumes cited above [6–10] and the following chapters in this volume, the interested reader should consult the recent volume edited by Hess [11] and the contribution by Quiney [12].

subtleties and technical difficulties not found in the non-relativistic formalism.

The second section of the present chapter deals with the fundamentals of relativistic electronic structure theory beginning with the Dirac equation, the Dirac matrices, and the Dirac spectrum, and then turning to relativistic many-body systems and operators, the electron-electron interaction, and, finally, the Furry bound-state interaction picture of quantum electrodynamics. The third section addresses the algebraic approximation, which remains fundamental to the vast majority of practical applications of molecular electronic structure theory in both non-relativistic and relativistic formulations. A robust implementation of the algebraic approximation is an essential ingredient of relativistic quantum chemistry. After briefly reviewing non-relativistic finite basis set approximations, attention is focussed on the central problem of the Dirac equation in the algebraic approximation, before turning to the matrix formulation of Dirac-Hartree-Fock theory and relativistic many-body perturbation theory. Section 3 closes by considering a simple model problem which unequivocally demonstrates the contribution of the negative energy states to solutions of a relativistic electronic structure problem.

2. The Fundamentals of Relativistic Electronic Structure Theory

The principle of relativity states that the velocity of propagation of interactions is the same in all inertial frames of reference. This velocity, or strictly speaking maximum velocity, of propagation is the velocity of light in vacuum, which is usually designated c and takes the value $c \approx 2.997925 \times 10^8$ m sec^{-1}. c is a universal constant. The relativistic mechanics, originally introduced by Einstein [13], combines the principle of special relativity with the finite velocity of propagation of interactions. A theory which may be applied to high speed particles must conform to the principle of special relativity.

Quiney et al. [14] have underlined "the dangers associated with a complacent attitude towards relativistic many-body theory." They remark

> "An instinctive approach to the non-relativistic problem is fine, since classical instincts are usually valid, even when set in the context of quantum mechanics, when the energies involved are small. Rather less defensible is the heuristic approach to relativistic quantum mechanics which "fixes up" non-relativistic quantum mechanics through a series of mathematically ill-defined corrections. In particular, the instinctive route to relativistic quantum mechanics, which quantizes the classical relativistic energy functional, leads *not* to the Dirac equation, but to the Klein-Gordon equation, which is applicable only for relativistic spin-free particles. Attempts to deal with relativistic effects by seeking operator

> expansions in powers of $1/c$ ... [indicated] that the connection between relativistic and non-relativistic quantum mechanics is far from transparent."

According to relativistic mechanics [15, 16], the energy of a particle with momentum p is given by

$$E^2 = c^2p^2 + m^2c^4. \tag{2.3}$$

Immediately, we note that (2.3) can be written as

$$E = \pm\sqrt{c^2p^2 + m^2c^4}, \tag{2.4}$$

where the "+" sign corresponds to real classical solutions and the "−" sign respresents solutions of negative energy without physical significance.

Following the methods developed for obtaining the non-relativistic quantum mechanical equations of motion from the classical equations of motion, an attempt may be made to transform (2.3) to quantum mechanics by means of Schrödinger's correspondence rule (see, for example, the treatise by Messiah [17]), that is

$$E \to i\hbar\frac{\partial}{\partial t} \tag{2.5}$$

and

$$\begin{aligned} p_x &\to \frac{\hbar}{i}\frac{\partial}{\partial x}, \\ p_y &\to \frac{\hbar}{i}\frac{\partial}{\partial y}, \\ p_z &\to \frac{\hbar}{i}\frac{\partial}{\partial z}. \end{aligned} \tag{2.6}$$

This leads to a wave equation of the form

$$-\hbar^2\frac{\partial^2\psi}{\partial t^2} = -c^2\hbar^2\nabla^2\psi + m^2c^4\psi, \tag{2.7}$$

which is known as the Klein-Gordon equation (see, for example, Messiah [17] pp. 884-888). It is a second order wave equation and can be written as

$$-\hbar^2\frac{\partial^2\psi}{\partial t^2} = H_{KG}\psi, \tag{2.8}$$

where H_{KG} is the Klein-Gordon Hamiltonian

$$H_{KG} = -c^2\hbar^2\nabla^2 + m^2c^4. \tag{2.9}$$

The Klein-Gordon equation is relativistically invariant, and may be written in a form which brings this out explicitly. Defining the Dalembertian by

$$\Box = \frac{1}{c^2}\frac{\partial^2}{\partial t^2} - \nabla^2 = \frac{1}{c^2}\frac{\partial^2}{\partial t^2} - \frac{\partial^2}{\partial x^2} - \frac{\partial^2}{\partial y^2} - \frac{\partial^2}{\partial z^2}, \tag{2.10}$$

one obtains from (2.7)

$$(\hbar^2\Box + m^2c^2)\psi = 0. \tag{2.11}$$

The Klein-Gordon equation can be shown to go over to the Schrödinger equation in the non-relativistic limit; this is done by multiplying the speed of light by a scaling parameter λ and then putting $\lambda c \to \infty$. The eigenfunctions of the equation depend on the coordinates x, y, z and t. It contains no spin variables. The Klein-Gordon equation describes particles of zero spin.

2.1 The Dirac Equation

The principle of superposition requires that the relativistic wave equation be linear. Therefore, the relativistic generalization of the Schrödinger equation should contain only the first derivatives with respect to time, just as the Schrödinger equation itself does. Moreover, since all relativistically invariant expressions must involve spatial coordinates and time in an equivalent fashion, the relativistic generalization of the Schrödinger equation must also contain first derivatives with respect to the coordinates.

Following Dirac [18], one may attempt to obtain an equation with the required properties by replacing the left-hand side of the Klein-Gordon equation (2.7) by the linear form

$$i\hbar\frac{\partial}{\partial t}, \tag{2.12}$$

but the corresponding right-hand side is more problematical. How is one to interpret the operator

$$\sqrt{H_{KG}} = \sqrt{-c^2\hbar^2\nabla^2 + m^2c^4}? \tag{2.13}$$

Dirac assumed a linear form for the relativistic wave equation. Specifically, he introduced a new dynamical variable p_0 equal to the energy, E, divided by the speed of light, c,

$$p_0 = \frac{E}{c}. \tag{2.14}$$

Since $x_0 = ct$, the transformation

$$E \to i\hbar \frac{\partial}{\partial t}, \tag{2.15}$$

which leads to the Schrödinger formulation of quantum mechanics, may then be replaced by

$$p_0 \to \frac{1}{c} i\hbar \frac{\partial}{\partial t} = i\hbar \frac{\partial}{\partial x_0}. \tag{2.16}$$

The introduction of this new dynamical variable p_0 leads to four p's which, like the four x's, can be treated on the same footing.

Since $i\hbar\partial/\partial t = cp_0$, the Klein-Gordon equation (2.7) may be written

$$c^2 p_0^2 \psi = H_{KG}\psi, \tag{2.17}$$

where the Klein-Gordon Hamiltonian is

$$H_{KG} = c^2(p_x^2 + p_y^2 + p_z^2) + m^2c^4. \tag{2.18}$$

Again following Dirac, we can write the relativistic wave equation for a free particle by replacing the left-hand-side of equation (2.17) by the linear term cp_0 and the Hamiltonian operator on the right-hand-side by the Dirac Hamiltonian

$$cp_0\psi = H_D\psi. \tag{2.19}$$

The Dirac Hamiltonian, H_D, is unknown at this point. However, it is known that the square of the Dirac Hamiltonian must be equal to the Klein-Gordon Hamiltonian, H_{KG}, that is

$$(H_D)^2 = H_{KG}. \tag{2.20}$$

The left-hand-side of equation (2.19) is linear in p_0. A Hamiltonian is required, therefore, which is linear in p_x, p_y and p_z. The most general form of such a linear Hamiltonian will give

$$cp_0\psi = c\left(\alpha_x p_x + \alpha_y p_y + \alpha_z p_z + \beta\right)\psi, \tag{2.21}$$

and the Dirac Hamiltonian is therefore of the form

$$H_D = c\left(\alpha_x p_x + \alpha_y p_y + \alpha_z p_z + \beta\right). \tag{2.22}$$

The α's and β are independent of the momenta p and position coordinates x but are not defined at this stage.

By writing out the Klein-Gordon Hamiltonian explicitly, it can be seen that

$$H_D^2 \equiv c^2\left(p_x^2 + p_y^2 + p_z^2\right)^2 + m^2c^4. \tag{2.23}$$

It will be shown below that this identity implies that:

i) α_x, α_y, α_z and β are 4×4 matrices which anticommute and have a square of unity.

ii) the eigenfunction ψ is a four-component vector.

Explicit consideration of this identity will be shown to lead to the Dirac matrices and then to the Dirac equation.

2.2 The Dirac Matrices

Squaring the the Dirac Hamiltonian, H_D, given in (2.22), we have

$$\begin{aligned}(H_D)^2 &= c^2[\alpha_x^2 p_x^2 + \alpha_y^2 p_y^2 + \alpha_z^2 p_z^2 + \beta^2 \\ &\quad (\alpha_x\alpha_y + \alpha_y\alpha_x)\, p_x p_y + \\ &\quad (\alpha_y\alpha_z + \alpha_z\alpha_y)\, p_z p_y + \\ &\quad (\alpha_x\alpha_z + \alpha_z\alpha_x)\, p_x p_z + \\ &\quad (\alpha_x\beta + \beta\alpha_x)\, p_x + \left(\alpha_y\beta + \beta\alpha_y\right) p_y + (\beta\alpha_z + \alpha_z\beta)\, p_z].\end{aligned} \tag{2.24}$$

The squared operator $(H_D)^2$ will be equivalent to the Klein-Gordon Hamiltonian, H_{KG}, if in the first line of the above expression

$$\alpha_x^2 = \alpha_y^2 = \alpha_z^2 = 1 \tag{2.25}$$

and

$$\beta^2 = m^2c^2, \tag{2.26}$$

whilst in the remaining lines the equivalence requires that

$$\alpha_\mu\alpha_\lambda + \alpha_\lambda\alpha_\mu = 0, \quad \lambda \neq \mu, \quad \lambda, \mu = x, y, z \tag{2.27}$$

and

$$\alpha_\mu\beta + \beta\alpha_\mu = 0. \tag{2.28}$$

Putting

$$\alpha_m = \frac{1}{mc}\beta \tag{2.29}$$

enables equations (2.25)–(2.28) to be written as

$$\alpha_a\alpha_b + \alpha_b\alpha_a = 2\delta_{ab} \quad (a, b = x, y, z, m) \tag{2.30}$$

or

$$[\alpha_a, \alpha_b]_+ = 2\delta_{ab} \quad (a, b = x, y, z, m)\,, \tag{2.31}$$

where $[x, y]_+ = xy + yx$ is an anticommutator. Any set of matrices for which [18] "the four α's all anticommute with one another and the square

of each is unity" are called Dirac matrices. Equation (2.19) with the α and β in the Hamiltonian H_D (equation (2.22)) chosen so as to satisfy (2.30) is called the Dirac equation. An explicit form for the α_μ, $\mu = x, y, z, m$ is required to make further progress.

Again following Dirac, we seek the explicit form of the operators α_μ, $\mu = x, y, z, m$. We begin by noting that these operators cannot simply be constant numbers, since then it would not be possible to satisfy the anticommutation relations (2.31). Therefore, we seek a set of matrices of dimension n which satisfy the anticommutation relations, i.e.

$$\alpha_a \alpha_b = -\alpha_b \alpha_a = (-\mathbf{I})\, \alpha_b \alpha_a, \; a \neq b \tag{2.32}$$

where $\mathbf{I}$ is a unit matrix of dimension n.

Since in general $\det \mathbf{AB} = \det \mathbf{A} \det \mathbf{B}$, equation (2.32) implies that

$$\det \alpha_a \det \alpha_b = \det(-\mathbf{I}) \det \alpha_b \det \alpha_a, \; a \neq b$$

and, therefore, $\det(-\mathbf{I}) = 1$ or $(-1)^n = 1$, which constrains n to be even.

We consider the simplest case, that is $n = 2$. The well-known Pauli spin matrices

$$\sigma_x^P = \begin{pmatrix} 0 & 1 \\ 1 & 0 \end{pmatrix} \tag{2.33}$$

$$\sigma_y^P = \begin{pmatrix} 0 & -i \\ i & 0 \end{pmatrix} \tag{2.34}$$

$$\sigma_z^P = \begin{pmatrix} 1 & 0 \\ 0 & -1 \end{pmatrix} \tag{2.35}$$

satisfy the relations

$$\sigma_x^P \sigma_y^P = -\sigma_y^P \sigma_x^P = i\sigma_z^P \tag{2.36}$$

$$\sigma_y^P \sigma_z^P = -\sigma_z^P \sigma_y^P = i\sigma_x^P \tag{2.37}$$

$$\sigma_z^P \sigma_x^P = -\sigma_x^P \sigma_z^P = i\sigma_y^P \tag{2.38}$$

and

$$\left(\sigma_\mu^P\right)^2 = \begin{pmatrix} 1 & 0 \\ 0 & 1 \end{pmatrix} = \mathbf{I}, \quad \mu = x, y, z. \tag{2.39}$$

Equations (2.36)–(2.38) lead to the anticommutation relations

$$\left[\sigma_x^P, \sigma_y^P\right]_+ = 0 \tag{2.40}$$

$$\left[\sigma_y^P, \sigma_z^P\right]_+ = 0 \tag{2.41}$$

$$\left[\sigma_z^P, \sigma_x^P\right]_+ = 0. \tag{2.42}$$

The three Pauli matrices together with the unit matrix

$$\mathbf{I} = \begin{pmatrix} 1 & 0 \\ 0 & 1 \end{pmatrix} \tag{2.43}$$

provide four linearly independent 2×2 numerical matrices. However, the unit matrix commutes with each of the Pauli matrices $\sigma_\mu^P, \mu = x, y, z$

$$[\sigma_\mu^P, \mathbf{I}] = 0 \tag{2.44}$$

and, therefore, this set of four matrices does not satisfy the anticommutation conditions (2.31). We must conclude, therefore, that the Dirac matrices cannot be of dimension 2.

Let us consider the case $n = 4$. Again we follow Dirac and express the α's in terms of the σ_μ^P and a second similar set of three anticommuting variables whose squares are unity, ρ_1, ρ_2, ρ_3 say. We write

$$\sigma_1 = \begin{pmatrix} \sigma_x^P & 0 \\ 0 & \sigma_x^P \end{pmatrix} \tag{2.45}$$

$$\sigma_2 = \begin{pmatrix} \sigma_y^P & 0 \\ 0 & \sigma_y^P \end{pmatrix} \tag{2.46}$$

$$\sigma_3 = \begin{pmatrix} \sigma_z^P & 0 \\ 0 & \sigma_z^P \end{pmatrix}, \tag{2.47}$$

or more explicitly

$$\sigma_1 = \begin{pmatrix} 0 & 1 & 0 & 0 \\ 1 & 0 & 0 & 0 \\ 0 & 0 & 0 & 1 \\ 0 & 0 & 1 & 0 \end{pmatrix} \tag{2.48}$$

$$\sigma_2 = \begin{pmatrix} 0 & -i & 0 & 0 \\ i & 0 & 0 & 0 \\ 0 & 0 & 0 & -i \\ 0 & 0 & i & 0 \end{pmatrix} \tag{2.49}$$

$$\sigma_3 = \begin{pmatrix} 1 & 0 & 0 & 0 \\ 0 & -1 & 0 & 0 \\ 0 & 0 & 1 & 0 \\ 0 & 0 & 0 & -1 \end{pmatrix}. \tag{2.50}$$

The σ_μ's are Hermitian. We can now write down a second set of three anticommuting matrices whose squares are unity. Let us designate them as

$$\rho_\mu, \quad \mu = 1, 2, 3. \tag{2.51}$$

These 4×4 matrices have the following properties

$$[\rho_\mu, \rho_\lambda]_+ = 0, \ \mu \neq \lambda, \ \mu, \lambda = 1, 2, 3 \tag{2.52}$$

and

$$(\rho_\mu)^2 = \mathbf{1}. \tag{2.53}$$

The matrices ρ_μ are independent of the σ's and commute with them

$$[\rho_\mu, \sigma_\lambda] = 0, \ \forall \mu, \lambda. \tag{2.54}$$

In terms of 2×2 submatrices, the ρ_μ's may be written

$$\rho_1 = \begin{pmatrix} \mathbf{0} & \mathbf{I} \\ \mathbf{I} & \mathbf{0} \end{pmatrix} \tag{2.55}$$

$$\rho_2 = \begin{pmatrix} \mathbf{0} & -\imath\mathbf{I} \\ \imath\mathbf{I} & \mathbf{0} \end{pmatrix} \tag{2.56}$$

and

$$\rho_3 = \begin{pmatrix} \mathbf{I} & \mathbf{0} \\ \mathbf{0} & -\mathbf{I} \end{pmatrix} \tag{2.57}$$

Explicitly, these matrices have the form

$$\rho_1 = \begin{pmatrix} 0 & 0 & 1 & 0 \\ 0 & 0 & 0 & 1 \\ 1 & 0 & 0 & 0 \\ 0 & 1 & 0 & 0 \end{pmatrix} \tag{2.58}$$

$$\rho_2 = \begin{pmatrix} 0 & 0 & -\imath & 0 \\ 0 & 0 & 0 & -\imath \\ \imath & 0 & 0 & 0 \\ 0 & \imath & 0 & 0 \end{pmatrix} \tag{2.59}$$

$$\rho_3 = \begin{pmatrix} 1 & 0 & 0 & 0 \\ 0 & 1 & 0 & 0 \\ 0 & 0 & -1 & 0 \\ 0 & 0 & 0 & -1 \end{pmatrix} \tag{2.60}$$

The ρ_μ's are also Hermitian.

Following Dirac, we may choose, amongst other possibilities, the matrices α_μ to be defined as

$$\alpha_1 = \rho_1 \sigma_1 \tag{2.61}$$

$$\alpha_2 = \rho_1 \sigma_2 \tag{2.62}$$

$$\alpha_3 = \rho_1 \sigma_3 \tag{2.63}$$

and

$$\alpha_m = \rho_3. \tag{2.64}$$

It can be shown by using the definitions (2.61)–(2.64) that the $\alpha_\mu{}'s$ will satisfy the anticommutation relations (2.31). By way of example, we note that we can use (2.61) and (2.62) to write

$$[\alpha_1, \alpha_2]_+ = \rho_1\sigma_1\rho_1\sigma_2 + \rho_1\sigma_2\rho_1\sigma_1, \tag{2.65}$$

which, since $[\sigma_1, \rho_1] = [\sigma_2, \rho_1] = 0$, yields

$$[\alpha_1, \alpha_2]_+ = \rho_1\rho_1\sigma_1\sigma_2 + \rho_1\rho_1\sigma_2\sigma_1 \tag{2.66}$$

or

$$[\alpha_1, \alpha_2]_+ = \rho_1^2 [\sigma_1, \sigma_2]_+ = 0, \tag{2.67}$$

so that the required anitcommutation relation is satisfied. The matrices defined in (2.61)–(2.64) therefore form a set of Dirac matrices. They may be written as

$$\begin{aligned} \alpha_\mu &= \rho_1\sigma_\mu \\ &= \begin{pmatrix} \mathbf{0} & \mathbf{I} \\ \mathbf{I} & \mathbf{0} \end{pmatrix} \begin{pmatrix} \sigma_\mu^P & 0 \\ 0 & \sigma_\mu^P \end{pmatrix} \\ &= \begin{pmatrix} 0 & \sigma_\mu^P \\ \sigma_\mu^P & 0 \end{pmatrix}, \quad \mu = x, y, z \end{aligned} \tag{2.68}$$

and

$$\alpha_m = \begin{pmatrix} \mathbf{I} & \mathbf{0} \\ \mathbf{0} & -\mathbf{I} \end{pmatrix}. \tag{2.69}$$

The set of Dirac matrices given in our discussion above is not unique. Pauli [19] and Good [20] have made a detailed study of the Dirac matrices. These matrices form a set of hypercomplex numbers of the type first studied by Clifford [21], and were studied from this perspective by van der Waerden [22]. A fundamental property of the Dirac matrices is that any set of 4 by 4 matrices which satisfy the anticommutation relations (2.31) are connected by a similarity transformation. Thus if γ_μ, $\mu = 1, 2, 3, 4$ and γ'_μ, $\mu = 1, 2, 3, 4$ are two sets of 4×4 matrices such that

$$\gamma_\mu\gamma_\nu + \gamma_\nu\gamma_\mu = 2\delta_{\mu\nu} \tag{2.70}$$

and

$$\gamma'_\mu\gamma'_\nu + \gamma'_\nu\gamma'_\mu = 2\delta_{\mu\nu}, \tag{2.71}$$

then there exists a nonsingular 4 by 4 matrix $\mathbf{S}$ such that

$$\gamma'_\mu = \mathbf{S}\gamma_\mu\mathbf{S}^{-1}. \tag{2.72}$$

The matrix **S** which connects two sets of Dirac matrices is uniquely determined by the two sets to within an arbitrary numerical factor. The introduction of a different set of (Hermitian) Dirac matrices corresponds to a unitary transformation among the four components of the wave function. Different sets of Dirac matrices are more convenient in different situations; for example, in approaching the Schrödinger-Pauli limit.

It should be noted that using matrices of rank greater than 4 does not violate the formal theory. However, when 4×4 matrices are used, the Dirac equation describes the properties of spin-$\frac{1}{2}$ particles.

2.3 The Dirac Spectrum

A schematic representation of the Dirac spectrum for a hydrogenic atom is compared with the more familiar Schrödinger spectrum in Figure 2.1. For an infinitely-massive point nucleus, bound-state solutions of s-symmetry exist in the range $0 < Z < c$, where c is the speed of light, which in atomic units takes the value 137.0359895 a.u. We choose the zero of energy to be that of an electron at rest. The Dirac spectrum divides into two branches: the negative energy continuum in the interval $(-\infty, -mc^2)$, and the positive energy solutions which are bounded in the interval $(+mc^2, +\infty)$. The positive-energy solutions for an attractive potential may be further classified as having either bound or continuum character.

The non-relativistic limit of the Dirac equation is obtained by scaling the speed of light, c, by a parameter λ and then taking the limit $\lambda c \to \infty$. In this limit, the negative-energy states vanish, and the positive-energy solutions become the familiar Schrödinger spectrum. Whilst in the non-relativistic case the solutions of the Schrödinger operator form a complete set, it is important to recognize that in the relativistic case neither the eigenfunction set belonging to the positive-energy branch of the Dirac spectrum nor the negative-energy branch form, on their own, a complete set. Both positive-energy and negative-energy solutions are required for a complete set.

In the Dirac *hole theory* of the positron, or in one of the more modern versions of relativistic quantum field theory, the negative energy states are taken to be filled with electron according to the Pauli Exclusion Principle in the description for the vacuum state. This negative energy "sea" prevents the radiative decay of an electron in a positive-energy state into a negative-energy continuum state. The negative energy "sea" is, however, unobservable, because only differences between state vectors can be observed, so that, to a good approximation, the contribution from the infinite density of vacuum electrons vanishes by cancellation.

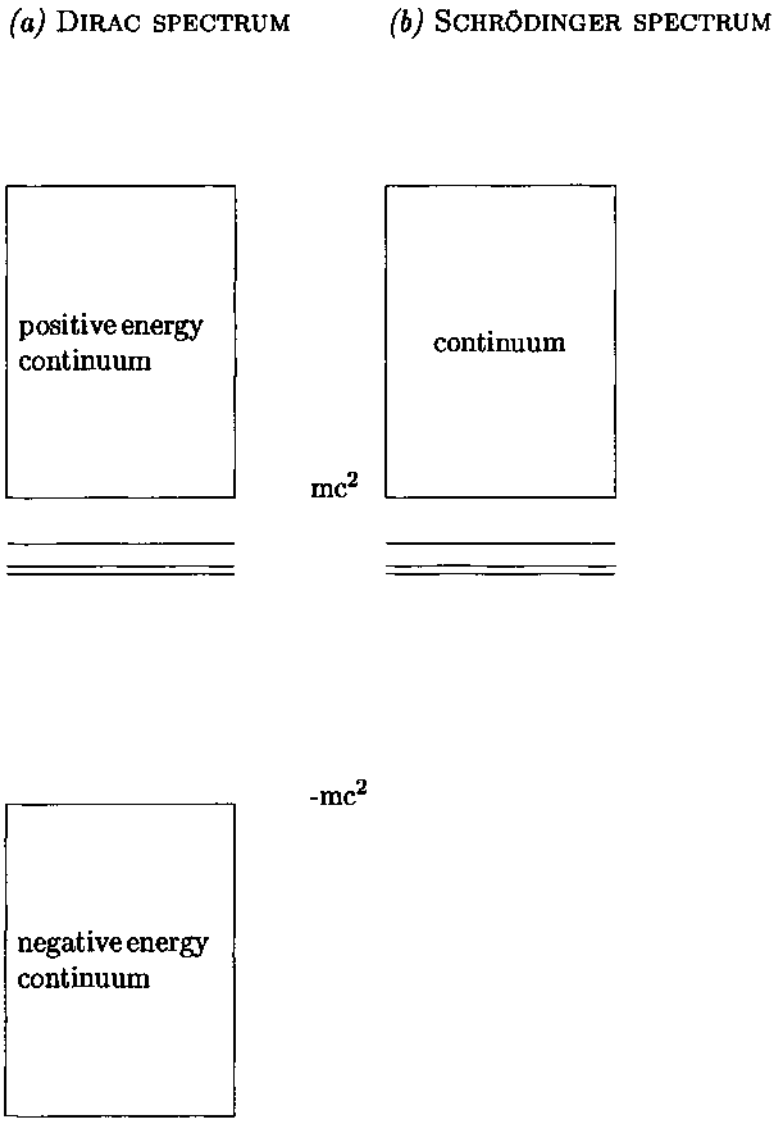

Figure 2.1 Comparison of schematic representations of *(a)* the Dirac spectrum and *(b)* the Schrödinger spectrum for a hydrogenic atom

The Dirac hole theory has a remarkable consequence – even the simplest atomic and molecular systems are infinitely-many-bodied. For example, the many-body character of the hydrogen atom is encountered when the interactions of its single electron with the radiation field and with the filled vacuum are considered. This is the first step on the road to quantum electrodynamics. Within hole theory, a vacancy in the density of negative-energy electrons is interpreted as a positron. (More sophisticated theories exist which put the electron and the positron on an equal footing, but the essential physical content of the theory remains unchanged.) The vacuum is best considered within a second-quantized framework in which the observable effects arise through the polarization of the "sea", or *vacuum polarization*, and through zero-point quantum fluctuations which result in the electron *self-energy*.

2.4 Many-Body Systems and Operators

The standard derivation of equations for relativistic many-body calculations follows the methods of non-relativistic quantum mechanics. The single-particle Dirac operator is given in atomic units as (with m made explicit to bring out the dimensionality)

$$h_{\mathrm{D}}(i) = c\alpha_i \cdot \mathbf{p}_i + (\beta_i - 1)\, mc^2 - \frac{Z}{r_i}, \tag{2.73}$$

whilst the N-electron Dirac-Coulomb operator is

$$H_{\mathrm{DC}} = \sum_i h_{\mathrm{D}}(i) + \sum_{i>j} \frac{1}{r_{ij}}, \tag{2.74}$$

and the Dirac-Coulomb-Breit operator is

$$H_{\mathrm{DCB}} = \sum_i h_{\mathrm{D}}(i) + \sum_{i>j} \frac{1}{r_{ij}} + \sum_{i>j} B_{ij}, \tag{2.75}$$

with the Breit operator B discussed below. In equations (2.73), (2.74) and (2.75) the indices i and j label the N electrons in the system. The Born-Oppenheimer approximation has been assumed which, although it gives serious problems of principle in a relativistic formulation, appears to have negligible practical consequences.

We have seen in the preceding section that the Dirac hole theory has the remarkable consequence that even the simplest atomic and molecular systems are infinitely-many-bodied. For the one-electron problem one can, by working with an unquantized field, ignore many-body effects to a good approximation. However, if for the helium atom we specify

a Hartree two-electron configuration as a model and then switch on the instantaneous Coulomb interaction, there exist an infinite number of two-electron configurations with which the initial configuration is degenerate in energy, but which include contributions from both the positive- and negative-energy branches of the spectrum. This problem has been termed "continuum dissolution". We have to impose the requirement that the negative-energy states are considered filled and therefore unavailable for the "continuum dissolution" process. This is most elegantly achieved by working within a second-quantized formalism, since then interactions with the negative-energy states can be included and, in particular, the creation of electron-positron pairs described. If we wish to explore the origin of quantum electrodynamic effects in many-electron systems, then we must be prepared to expand Dirac wavefunctions in a complete basis set including both positive- and negative-energy contributions, so that the use of a second-quantization approach is mandatory.

2.5 The Electron-Electron Interaction

The vast majority of atomic and molecular electronic structure calculations assume that the electrons interact solely through an instantaneous Coulomb mechanism. Additional interactions are then added, based largely on classical arguments and the assumption that they may be considered to be small corrections to the Coulomb interaction. The orbital motion of the electrons gives rise to currents which result in a system of interacting magnetic moments. An additional "spin" magnetic moment is appended to the electron, which further interacts with the orbital magnetic moments, giving the familiar spin-orbit interactions.

Classical models of the electron-electron interaction may not be trivially extended to include relativistic dynamics without introducing ambiguities. A well-known example of this is the familiar form of the spin-orbit interaction, which includes a non-classical factor of $\frac{1}{2}$ due to the Thomas precession. This additional factor is required to maintain relativistic invariance under relativistic frame transformations between laboratory-fixed axes of the model nucleus and a coordinate system fixed on the orbiting electron. Relativistic many-body theory should contain none of these uncertainties and *ad hoc* corrections, especially if we wish to remain in contact with the theory of quantum electrodynamics and to recover the familiar non-relativistic limit.

Let us briefly sketch the derivation of the Breit operator. Following the account of Bethe and Salpeter [23], we use perturbation theory. Two electrons may interact not only by their mutual Coulomb repulsion, but also through the exchange of virtual photons in the quantized

electromagnetic field. Let the electromagnetic field, A, be expanded in the complete set of relativistic plane-waves characterized by wavevector $\boldsymbol{k}$. The exchange matrix elements of this subsidiary interaction is then given, to second order, by

$$\langle ab|B_{\rm tr}|ba\rangle = -\frac{c}{4\pi^2}\sum_{\pi}\int\frac{d^3k}{k}\sum_{n}\frac{\langle ab|\alpha_{1\pi}\epsilon^{i\mathbf{k}.\mathbf{r}_1}|n\rangle\langle n|\alpha_{2\pi}\epsilon^{i\mathbf{k}.\mathbf{r}_2}|ab\rangle}{kc+E_n-\epsilon_a-\epsilon_b},$$

together with a term in which the labels 1 and 2 are interchanged. The initial two-electron state is the product function $|a(1)b(2)\rangle$, α is a Dirac matrix, π labels transverse polarization directions, and the complete set of intermediate states $\{|n\rangle\}$ are the product functions $\{|c(1)d(2)\rangle\}$. Each matrix element is separable into a product of factors depending only on the coordinates of a single electron.

Using orthogonality and sum-rules we obtain a definition of the operator

$$B_{\rm tr} = -\frac{1}{2\pi^2}\int_0^\infty\frac{d^3k}{(k^2-\omega^2)}e^{i\mathbf{k}\cdot\mathbf{R}}\left[\boldsymbol{\alpha}_1\cdot\boldsymbol{\alpha}_2-\frac{(\boldsymbol{\alpha}_1\cdot\mathbf{k})(\boldsymbol{\alpha}_2\cdot\mathbf{k})}{k^2}\right]$$

where $R = r_1 - r_2$ and $\omega = (\epsilon_a - \epsilon_b)/c$.

If we assume that $\omega \ll k$, which is valid for energy differences smaller than the binding energy, then further use of commutativity of the Dirac matrices $\boldsymbol{\alpha}_1$ and $\boldsymbol{\alpha}_2$ with $\mathbf{k}$ and $\mathbf{R}$ gives the commonly quoted form of the Breit operator

$$B = -\frac{1}{2\pi}\left[\boldsymbol{\alpha}_1\cdot\boldsymbol{\alpha}_2-\frac{(\boldsymbol{\alpha}_1\cdot\mathbf{R})(\boldsymbol{\alpha}_2\cdot\mathbf{R})}{R^2}\right]. \tag{2.76}$$

Bethe and Salpeter emphasize that the neglect of ω-dependence in the definition of B limits the use of the Breit operator to the calculation of expectation values of bound states of weak external fields in the first order of perturbation theory. Breit pointed out that the second-order relativistic many-body operator given by equation (2.76) gives an unphysically large correction to the helium ground state. The unphysical terms can be traced to the contributions from the negative-energy branch of the Dirac spectrum. A pragmatic solution was devised in which unphysical terms were identified and then rejected. However, if we wish to consider interactions which involve virtual photons of high energy then we may not ignore the ω-dependence in the transverse interaction. A configuration-space representation of the complete electron-electron interaction was presented by Brown [24]. The Brown interaction is similar in form to the sum of the Coulomb and Breit interactions but is suitable for use in systems involving large energy differences, because the

ω-dependence in $B_{\rm tr}$ is made explicit. The Brown interaction or, as it is more commonly known, the frequency-dependent Breit interaction, appears in a different context in Feynman's original work on the relativistic theory of quantum electrodynamics in Møller scattering [25, 26]. Feynman makes no use of perturbation theory and obtains the relativistic electron-electron interaction operator in configuration space as

$$V_{\rm F} = \frac{1}{R}\left(1 - \boldsymbol{\alpha}_1 \cdot \boldsymbol{\alpha}_2\right) e^{i\mathbf{kR}},$$

which is derived from the photon propagator in Lorentz (Feynman) gauge. In the Coulomb gauge the same quantity is given by

$$V_{\rm C} = \frac{1}{R} - \frac{1}{R}\boldsymbol{\alpha}_1 \cdot \boldsymbol{\alpha}_2 e^{i\mathbf{kR}} + \left(\boldsymbol{\alpha}_1 \cdot \nabla_R\right)\left(\boldsymbol{\alpha}_2 \cdot \nabla_R\right)\frac{e^{i\mathbf{kR}} - 1}{k^2 R},$$

where $R = |\mathbf{r}_1 - \mathbf{r}_2|$ and $k = \left(\epsilon_a - \epsilon_c\right)/c = \left(\epsilon_b - \epsilon_d\right)/c$, which is the momentum transferred by the exchanged photon. The real part gives rise to the level shift, while the imaginary part corresponds to the width. There has been some discussion about the relative merits of using of the interactions $V_{\rm F}$ and $V_{\rm C}$ in atomic and molecular electronic structure calculations. Gauge invariance is maintained only if the complete interaction is employed in either case. This implies that both parts of $V_{\rm C}$ should be treated on the same footing rather than as separate perturbations. The introduction of the algebraic approximation has made possible the use of the interaction $V_{\rm C}$ in relativistic atomic and molecular electronic structure studies.

2.6 The Furry Bound-State Interaction Picture of Quantum Electrodynamics

For relativistic bound-state problems, the Furry interaction picture of quantum electrodynamics [27] relies on the expansion of the many-particle state vector in a complete basis of single-particle Dirac spinors (for a more recent discussion see the work of Quiney et al [28, 29]). The Furry picture depends on the existence of a complete set of relativistic solutions to the Dirac equation for some time-independent potential. This complete set comprises both positive-energy and negative-energy branches of the Dirac spectrum.

The Dirac-Hartree-Fock approximation is defined by analogy with the familiar non-relativistic Hartree-Fock theory. The Dirac-Hartree-Fock equations are derived by assuming some mean, time-independent potential governing the motion of the electrons. This is a basic requirement of the Furry picture. The mean, time-independent potential is determined by a self-consistent field procedure.

If the electrons are taken to interact solely through an instantaneous Coulomb mechanism, then the resulting self-consistent field equations define the Dirac-Hartree-Fock-Coulomb approximation. The Fock operator takes the form

$$\mathbf{F}_{\mathrm{DHFC}} = \mathbf{h}_{\mathrm{D}} + \mathbf{g}_{\mathrm{C}},$$

where $\mathbf{h}_{\mathrm{D}}$ is the bare-nucleus Dirac matrix which has the form

$$\mathbf{h}_{\mathrm{D}} = \begin{bmatrix} V^{\mathrm{LL}} & c\Pi^{\mathrm{LS}} \\ c\Pi^{\mathrm{SL}} & V^{\mathrm{SS}} - 2c^2 \end{bmatrix} \tag{2.77}$$

and $\mathbf{g}_{\mathrm{C}}$ is the matrix of the instantaneous Coulomb interaction,

$$\mathbf{g}_{\mathrm{C}} = \begin{bmatrix} J^{\mathrm{LL}} - K^{\mathrm{LL}} & -K^{\mathrm{LS}} \\ -K^{\mathrm{SL}} & J^{\mathrm{SS}} - K^{\mathrm{SS}} \end{bmatrix}. \tag{2.78}$$

In equation (2.77), V^{XX} describes the electron-nucleus attraction and $c\Pi^{\mathrm{XY}}$ is associated with the electronic kinetic energy. The superscripts X and Y label either large (L) or small (S) components of the relativistic wavefunction. In equation (2.78), J^{XX} and K^{XY} are Coulomb and exchange operators. If the low-frequency Breit interaction is included in the description of the electron-electron interaction, the Dirac-Hartree-Fock-Breit approximation is obtained. The Fock operator then takes the form

$$\mathbf{F}_{\mathrm{DHFB}} = \mathbf{h}_{\mathrm{D}} + \mathbf{g}_{\mathrm{B}},$$

where

$$\mathbf{g}_{\mathrm{B}} = \mathbf{g}_{\mathrm{C}} + \mathbf{b}$$

and

$$\mathbf{b} = \begin{bmatrix} B^{\mathrm{LL}} & B^{\mathrm{LS}} \\ B^{\mathrm{SL}} & B^{\mathrm{SS}} \end{bmatrix}.$$

The self-consistent field procedure in the Dirac-Hartree-Fock approximation generates a series of Furry pictures, each characterized by a complete set of single-particle states. The self-consistent field iterations mixes positive-energy and negative-energy branches of the Dirac spectrum. When the iterative procedure is completed, diagrams involving single excitations cancel corresponding diagrams involving the self-consistent field potential through infinite order in the many-body perturbative analysis. The self-consistent field potential involves contributions from the negative-energy states of the unscreened spectrum, so that the Dirac-Hartree-Fock method defines a stationary point in the space of possible configurations, rather than a variational minimum as in the non-relativistic case.

3. The algebraic approximation

In practical molecular electronic structure studies the algebraic approximation is almost ubiquitous. Finite difference and finite element methods have been applied to the atomic Hartree-Fock problem and, in more recent times, to diatomic molecular systems. For arbitrary polyatomic molecules and for studies which go beyond the Hartree-Fock model the use of finite basis set expansions has significant advantages. The integro-differential Hartree-Fock equations become a set of algebraic equations for the expansion coefficients. The solution of the matrix Hartree-Fock equations yields a representation of the Schrödinger spectrum, in terms of which a description of electron correlation effects can be developed.

During the 1960s, Roothaan's group in Chicago [30–32] attempted to formulate the Dirac-Hartree-Fock equations within the algebraic approximation so as to facilitate applications to arbitrary polyatomic molecules. These early calculations (most notable those of Kim [31, 32]) identified a spurious behaviour which was dubbed the "finite basis set disease". A solution to this problem was not realized until the early 1980s [14,33–39] (see also [40–43]). In recent years, the growing interest in the treatment of relativistic and quantum electrodynamic effects in atoms and molecules has necessitated the reintroduction of physics that has been known for over forty years. A key to this development for molecular systems is a rigorous and robust implementation of the algebraic approximation for Dirac and Dirac-like equations. The algebraic approximation provides a representation of both the positive-energy and negative-energy branches of the Dirac spectrum. Relativistic many-body perturbation theory, relativistic coupled pair approximations and relativistic coupled cluster theories can be formulated within the "no-virtual-pair" approximation. Such formulations are restricted to the positive energy branch of the spectrum. However, the negative-energy states make an essential contribution to the description of atomic and molecular electronic structure. The investigation of this contribution is facilitated by proper implementation of the algebraic approximation using formulations which are amenable to systematic refinement.

3.1 Non-relativistic Finite Basis Set Approximations

There are many reviews describing the choice of finite basis sets for non-relativistic molecular electronic structure calculations. Most approaches begin by designing basis sets suitable for the component atoms. For the vast majority of molecular calculations the basis set of Gaussian-

type functions is employed because of the ease with which the two-electron integrals can be evaluated. The atom-centred basis sets are then supplemented by polarization functions to obtain a basis set suitable for a molecular system. Although the choice of basis set is a most important element of any molecular structure calculation, we shall not dwell upon this aspect here, since it is discussed thoroughly in many review articles.

Two aspects of basis set development for non-relativistic studies deserve further mention. First, the development of a systematic sequence of basis sets capable of approaching a complete set as the number of functions is increased. The most transparent of these are the even-tempered sets, for which the orbital exponents are given by

$$\zeta_k = \alpha\beta^k, \qquad \alpha > 0, \qquad \beta > 1, \qquad k = 1, 2, ..., N.$$

As the number of basis functions, N, is increased, the parameters α and β are varied according to empirical formulae such that

$$\begin{aligned} \alpha &\rightarrow 0 \\ \beta &\rightarrow 1 \\ \beta^N &\rightarrow \infty \end{aligned}$$

For both atomic and molecular systems this method can be used to systematically approach both the Hartree-Fock limit [44–48] and some correlated limits [49–52].

The second aspect of basis set development for non-relativistic studies that should be mentioned here is that solution of the matrix Hartree-Fock equation provides a representation of the whole spectrum. In addition to an approximation to the occupied orbitals, a set of unoccupied functions is obtained which can be employed in studies of correlation effects.

3.2 The Dirac Equation in the Algebraic Approximation

The implementation of the algebraic approximation for the Dirac and Dirac-like equations to obtain a matrix formulation requires some care if a clean separation of the positive and negative energy branches of the single particle spectrum is to be obtained. The Dirac spectrum can be divided into three regions:

1. the region with energies E satisfying

$$E < -mc^2, \tag{2.79}$$

which is the negative energy branch or "negative-energy sea";

2. the region with energies satisfying

$$E > mc^2, \tag{2.80}$$

3. the region with bound state energies,

$$-mc^2 < E < mc^2. \tag{2.81}$$

The last two regions form the positive energy branch. Failure to develop a robust implementation of the algebraic approximation leads to "intruder"states in the region $[-mc^2, mc^2]$ which effectively undermine the Furry picture and result in the "finite basis set" disease mentioned above.

The solution of the Dirac equation in the algebraic approximation introduces difficulties which are not present in the corresponding non-relativistic problem.

For an electron in an electrostatic field $V(r)$ the Dirac equation may be written

$$h_D\psi(\mathbf{r}) = \left[c\boldsymbol{\alpha}\cdot\mathbf{p} + \beta mc^2 + V(r)\right]\psi(\mathbf{r}) = E\psi(\mathbf{r}), \tag{2.82}$$

where $\psi(\mathbf{r})$ is a four-dimensional vector. In equation (2.82) $\boldsymbol{\alpha}$ is a vector

$$\boldsymbol{\alpha} = (\alpha_x, \alpha_y, \alpha_z) \tag{2.83}$$

whose elements are the 4×4 matrices

$$\alpha_\mu = \begin{bmatrix} \mathbf{0_2} & \sigma_\mu \\ \sigma_\mu & \mathbf{0_2} \end{bmatrix}, \quad \mu = x, y, z \tag{2.84}$$

in which $\mathbf{0_2}$ is a 2×2 null matrix and the σ_μ are the Pauli spin matrices

$$\sigma_x = \begin{bmatrix} 0 & 1 \\ 1 & 0 \end{bmatrix}, \quad \sigma_y = \begin{bmatrix} 0 & -i \\ i & 0 \end{bmatrix}, \quad \sigma_z = \begin{bmatrix} 1 & 0 \\ 0 & -1 \end{bmatrix} \tag{2.85}$$

so that

$$\alpha_x = \begin{bmatrix} 0 & 0 & 0 & 1 \\ 0 & 0 & 1 & 0 \\ 0 & 1 & 0 & 0 \\ 1 & 0 & 0 & 0 \end{bmatrix},$$

$$\alpha_y = \begin{bmatrix} 0 & 0 & 0 & -i \\ 0 & 0 & i & 0 \\ 0 & -i & 0 & 0 \\ i & 0 & 0 & 0 \end{bmatrix},$$

$$\alpha_z = \begin{bmatrix} 0 & 0 & 1 & 0 \\ 0 & 0 & 0 & -1 \\ 1 & 0 & 0 & 0 \\ 0 & -1 & 0 & 0 \end{bmatrix}. \tag{2.86}$$

$\mathbf{p}$ is the momentum vector

$$\mathbf{p} = \begin{pmatrix} p_x \\ p_y \\ p_z \end{pmatrix} \tag{2.87}$$

with elements

$$p_\mu = \frac{\hbar}{i}\frac{\partial}{\partial \mu}, \quad \mu = x, y, z. \tag{2.88}$$

The matrix β has the form

$$\beta = \begin{bmatrix} \mathbf{I_2} & \mathbf{0} \\ \mathbf{0} & -\mathbf{I_2} \end{bmatrix}, \tag{2.89}$$

where $\mathbf{I_2}$ is the 2×2 unit matrix. The Dirac Hamiltonian operator can therefore be written

$$h_D = \begin{bmatrix} mc^2 + V(r) & c\boldsymbol{\sigma}\cdot\mathbf{p} \\ c\boldsymbol{\sigma}\cdot\mathbf{p} & -mc^2 + V(r) \end{bmatrix}. \tag{2.90}$$

Shifting the zero of energy from $E = mc^2$ to $E = 0$ makes comparison with the corresponding non-relativistic formalism more transparent. The Dirac Hamiltonian then becomes

$$h_D - mc^2 = \begin{bmatrix} V(r) & c\boldsymbol{\sigma}\cdot\mathbf{p} \\ c\boldsymbol{\sigma}\cdot\mathbf{p} & -2mc^2 + V(r) \end{bmatrix}. \tag{2.91}$$

The four-component eigenspinors in equation (2.82) take the form

$$\psi(\mathbf{r}) = \begin{pmatrix} \psi^L(\mathbf{r}) \\ \psi^S(\mathbf{r}) \end{pmatrix}, \tag{2.92}$$

where $\psi^L(\mathbf{r})$ is the large component and $\psi^S(\mathbf{r})$ is the small component. $\psi^L(\mathbf{r})$ and $\psi^S(\mathbf{r})$ are two-component spinors or Pauli spinors. For a four-component spinor corresponding to a positive energy eigenvalue, the large component, $\psi^L(\mathbf{r})$, approaches the non-relativistic Pauli two-spinor and the small component, $\psi^S(\mathbf{r})$, vanishes in the limit $\lambda c \to \infty$, where c is the speed of light and λ is a scaling parameter.

The so-called "finite basis set disease"arose from attempts to implement the algebraic approximation by expanding the components of $\psi^L(\mathbf{r})$ and $\psi^S(\mathbf{r})$ in arbitarily chosen sets of basis functions. The basis functions used in a relativistic electronic structure calculation must reflect the four-component structure of a relativistic spinor. In particular, if the large component is approximated by the expansion

$$\psi^L(\mathbf{r}) = \sum_{p=1}^{N} \chi_p^L(\mathbf{r})\, c_p^L \tag{2.93}$$

and the small component by the expansion

$$\psi^S(\mathbf{r}) = i\sum_{p=1}^{N} \chi_p^S(\mathbf{r})\, c_p^S, \tag{2.94}$$

where $\chi_p^L(\mathbf{r})$ and $\chi_p^S(\mathbf{r})$ are the two-component spinors

$$\chi_p^L(\mathbf{r}) = N_p^L \frac{1}{r_p} R_p^L(r_p)\Omega_{\kappa_p,m_p}(\theta_p,\varphi_p) \tag{2.95}$$

and

$$\chi_p^S(\mathbf{r}) = N_p^S \frac{1}{r_p} R_p^S(r_p)\Omega_{-\kappa_p,m_p}(\theta_p,\varphi_p), \tag{2.96}$$

respectively, and the spin-angular spinors take the form

$$\Omega_{\kappa_p,m_p}(\theta_p,\varphi_p) = \begin{bmatrix} \left(\frac{j+m}{2j}\right)^{\frac{1}{2}} Y_{j-1/2}^{m-1/2}(\theta\varphi) \\ \left(\frac{j-m}{2j}\right)^{\frac{1}{2}} Y_{j-1/2}^{m+1/2}(\theta\varphi) \end{bmatrix}, \quad \kappa < 0 \tag{2.97}$$

and

$$\Omega_{-\kappa_p,m_p}(\theta_p,\varphi_p) = \begin{bmatrix} -\left(\frac{j+1-m}{2j+2}\right)^{\frac{1}{2}} Y_{j+1/2}^{m-1/2}(\theta\varphi) \\ \left(\frac{j+1+m}{2j+2}\right)^{\frac{1}{2}} Y_{j+1/2}^{m+1/2}(\theta\varphi) \end{bmatrix}, \quad \kappa > 0, \tag{2.98}$$

then the two-spinors $\chi_p^L(\mathbf{r})$ and $\chi_p^S(\mathbf{r})$ must satisfy the relation

$$\chi_p^S(\mathbf{r}) = \boldsymbol{\sigma}\cdot\mathbf{p}\chi_p^L(\mathbf{r}) \tag{2.99}$$

which is termed the *(restricted) kinetic balance* condition. In (2.95) and (2.96) N_p^L and N_p^S are normalization constants and $R_p^L(r_p)$ and $R_p^S(r_p)$ are radial functions. For molecular applications the radial functions $R_p^L(r_p)$ and $R_p^S(r_p)$ will be chosen to be Gaussian-type functions $G_p^L(r_p)$ and $G_p^S(r_p)$ because of the economy and accuracy with which the associated molecular integrals may be evaluated. Specifically, the functions $G_p^L(r_p)$ may be chosen to have the form

$$G_p^L(r_p) = r_p^{\ell_p+1}\, e^{-\zeta_p r_p^2} \tag{2.100}$$

and the exponents ζ_p generated according to some systematic scheme, such as that outlined in section 3.1, whereby the basis set approaches completeness as the size of the set is increased. The (restricted) kinetic balance condition then dictates that

$$G_p^S(r_p) = r_p^{\ell_p}\left[(\kappa_p + \ell_p + 1) - 2\zeta_p r_p^2\right] e^{-\zeta_p r_p^2}\,. \tag{2.101}$$

3.3 The Matrix Dirac-Hartree-Fock Approximation

For closed-shell systems, the matrix Dirac-Hartree-Fock equations take the form of block-diagonal generalized matrix eigenvalue equations

$$\mathbf{F}_\kappa \mathbf{C}_\kappa = \mathbf{E}_\kappa \mathbf{S}_\kappa \mathbf{C}_\kappa,$$

in which $\mathbf{F}_\kappa$ is the matrix representation of the appropriate Fock operator – usually corresponding to the Dirac-Hartree-Fock-Coulomb approximation, $\mathbf{F}_{\mathrm{DHFC}}$, or the Dirac-Hartree-Fock-Breit approximation, $\mathbf{F}_{\mathrm{DHFB}}$, $\mathbf{C}_\kappa$ is the matrix of expansion coefficients, $\mathbf{E}_\kappa$ is a diagonal matrix of eigenvalues and $\mathbf{S}_\kappa$ is a block-diagonal overlap matrix for relativistic symmetry-type κ. The angular quantum number κ can take the values

$$\begin{aligned} \kappa &= \ell \\ \kappa &= -(\ell+1) \end{aligned}$$

where ℓ is the orbital quantum number. The total angular momentum, j, is thus given by

$$j = |\kappa| - \tfrac{1}{2}$$

Following Goldstone [53], the Fock potential, V, may be chosen so as *to make it allow for the first-order interactions with passive unexcited particles.* Thus V is defined by

$$\langle r\,|V|\,s\rangle = \sum_p \{\langle rp\,|v|\,sp\rangle - \langle rp\,|v|\,ps\rangle\} \tag{2.102}$$

where $v = v_C$ and the sum is over all unexcited states, which are determined by

$$(T+V)\,\psi_p = E_p\psi_p \tag{2.103}$$

These two equations constitute the Dirac-Hartree-Fock-Coulomb self-consistent field equations.

In Table 2.1 we illustrate the accuracy with which the matrix Dirac-Hartree-Fock-Coulomb equations (*i.e.* the Dirac-Hartree-Fock-Coulomb equations within the algebraic approximation) can be solved by employing a systematically constructed sequence of even-tempered basis sets. These results, which are taken from the work of Quiney, Grant and Wilson [14], confirm that a sequence of even-tempered basis sets, constructed according to formulae which ensure that the basis set becomes formally complete in the limit of an infinitely large set, will support a total energy which agrees with the corresponding finite difference result given in the final row of Table 2.1.

Table 2.1 Matrix Dirac-Hartree-Fock-Coulomb calculations for the argon atom ground state spanned by a systematic sequence of even-tempered basis sets of exponential-type functions.

N	α	β	$-E$ (hartree)
9	0.500	1.550	528.643 948 19
10	0.484	1.516	528.683 364 15
11	0.470	1.486	528.684 311 73
12	0.458	1.462	528.684 289 73
13	0.447	1.440	528.684 430 68
14	0.437	1.421	528.684 432 46
15	0.429	1.404	528.684 448 56
16	0.421	1.389	528.684 449 90
17	0.413	1.376	528.684 450 50
∞			528.684 450 77

Table 2.2 Iterative sequence in a relativistic self-consistent field calculation for the argon atom ground state.

i	$-E$(hartree)
1	598.077 562 767
2	543.663 518 292
3	524.411 745 366
4	528.429 807 069
5	528.645 698 663
6	528.676 614 683
7	528.682 728 387
8	528.684 045 061
9	528.684 349 369
10	528.684 423 276
∞	528.684 448 557

In Table 2.2, the iterative sequence involved in the solution of the self-consistent field equations for the case $N = 15$ in Table 2.1 serves to demonstrate that convergence can be from below. This should be contrasted with the iterative sequence associated with non-relativistic self-consistent field calculations, which, because of the variation theorem,

always converge from above. Again, these results are taken from the work of Quiney, Grant and Wilson [14].

In Table 2.3 we illustrate the accuracy that may be achieved in molecular matrix Dirac-Hartree-Fock-Coulomb calculations. Matrix Hartree-Fock, matrix Dirac-Hartree-Fock-Coulomb and matrix Dirac-Hartree-Fock-Breit carried out with a distributed Gaussian basis set are compared with finite difference and finite element calculations which essential define the basis set limit. Further details and similar comparisons for other molecules are given in the work of Quiney, Glushkov and Wilson [54,55].

Table 2.3 A comparison of Hartree-Fock (HF), Dirac-Hartree-Fock-Coulomb (DHFC) and Dirac-Hartree-Fock-Breit (DHFB) energies for the ground state of the LiH molecule. R=3.015 bohr.†

Quantity	Symbol	Energy/Hartree
Matrix HF energy [a]	E_{mHF}	−7.987 351 392 9
Finite difference HF energy [b]	E_{fdHF}	−7.987 352 236 7
Δ_{HF}		+0.000 000 843 8
Matrix DHFC energy	E_{mDHFC}	−7.988 163 041 1
Finite element DHFC energy [c]	E_{feDHFC}	−7.988 163 911 2
Δ_{DHFC}		+0.000 000 870 1
Basis set first order Breit energy	$E^{(1)}_{\mathrm{Breit}}$	+0.000 270 225 9
Matrix DHFC energy plus first order Breit energy	$E_{\mathrm{mDHFC}} + E^{(1)}_{\mathrm{Breit}}$	−7.987 892 815 2
Matrix DHFB energy	E_{mDHFB}	−7.987 892 826 0
$\delta_{\text{first order Breit}}$		+0.000 000 010 8
$\Delta^{\mathrm{Coulomb}}_{\mathrm{Relativity}}$		+0.000 811 648 2
$\Delta^{\mathrm{Breit}}_{\mathrm{Relativity}}$		+0.000 541 433 1
Δ_{Breit}		+0.000 270 225 9

† taken from the work of HM Quiney, VN Glushkov and S Wilson *Intern. J. Quantum Chem* **89** 227 (2002)

[a] 50s distributed finite Gaussian basis set

[b] from J Kobus, D Moncrieff & S Wilson *J Phys B: At Mol Opt Phys* **34** 5127 (2001)

[c] from O Kullie, C Düsterhöft and D Kolbe *Chem Phys Lett* **314** 307 (1999)

3.4 A Digression: Finite Nuclear Models

The vast majority of non-relativistic atomic and molecular electronic structure studies employ a point nucleus model. This model involves a cusp singularity at each nucleus. The successful description of this singularity in calculations carried out within the algebraic approximation may require a suitable choice of basis set. For example, in calculations employing the widely-used Gaussian-type basis functions it is necessary to include functions with relatively high exponent for each of the component atoms. In practice, nuclei have a finite extent and the nuclear cusp is seen to be an artefact of the point nucleus model.

In the case of "heavy" and "superheavy" elements, corrections to energies and other expectation values arising from finite nuclear size may be large. This is particularly true if the single-particle wave function has a non-vanishing amplitude at $r = 0$ as, for example, in the case of s and $p_{1/2}$ states. If the nucleus is modelled as a homogeneously charged sphere then the wave function is approximately Gaussian over the nuclear dimension, but exhibits near singular behaviour in regions just outside the classical nuclear volume [56]. For many-electron systems, the use of finite-nuclear models induces "sympathetic" effects throughout the valence orbitals because of substantial modification of the electron density in the "core" region. Even orbitals which have negligible amplitude over the nucleus can therefore be affected by the use of a finite-nuclear model.

3.5 Electron correlation, many-body perturbation theory, and the no virtual pair approximation

In nonrelativistic molecular electronic structure theory, diagrammatic many-body perturbation theory provides a natural vehicle for the evaluation of corrections to single-particle models; that is, the study of electron correlation effects [57–65]. Within the algebraic approximation, the solution of the matrix Hartree-Fock equations provides a set of occupied and unoccupied states in terms of which the many-body perturbation expansion can be developed. Other methods for describing the non-relativistic electron correlation problem in molecules, in particular configuration interaction expansions [66] and coupled cluster ansatz [67], can be readily analysed in terms of the many-body perturbation theory.

In his original development of the many-body perturbation theory, Goldstone [53] adapted the diagrammatic methods developed by Feynman for the formulation of quantum field theory. It might be expected

that the connection between the relativistic and nonrelativistic correlation problem would be at its most transparent in diagrammatic many-body perturbation theory[2]. There are, however, crucial differences between the nonrelativistic and relativistic formulations. In the nonrelativistic formulation the particle number is always conserved, whereas in the relativistic theory this is not the case and we must be able to describe the creation and annihilation of real and virtual electron-positron pairs. The essential ingredients of the relativistic model are:

(a) the accurate specification of a complete set of Dirac spinors for some mean field potential;

(b) the second quantized description of the fields;

(c) the relativistic treatment of the electromagnetic interaction.

A relativistic many-body perturbation theory which is a straightforward generalization of the nonrelativistic theory can be obtained if we neglect interactions with the filled negative energy sea. We then have what is termed the "no-virtual-pair" approximation. Virtual electron-positron pair creation processes are excluded. Relativistic many-body perturbation theory can be implemented in the "no-virtual-pair" approximation as a natural extension of the methods used in non-relativistic theory. Solution of the matrix Dirac-Hartree-Fock equations provides a discretized representation of the whole Dirac spectrum. From this the negative energy states are discarded and sum-over-states formulae entirely analogous to the nonrelativistic formulae can be written down and evaluated. The negative energy states only enter the calculation in the solution of the matrix Dirac-Hartree-Fock problem.

Other methods for handling the correlation problem in non-relativistic theory, such as configuration interaction and coupled cluster expansions, can also be implemented within the no-virtual-pair approximation in a similar fashion. Over the past decade, a number of relativistic many-body perturbation theory and coupled cluster calculations have been reported, most notably by Kaldor and his collaborators [69–84]. It is important to recognize that the separation of the Dirac spectrum into positive-energy and negative-energy branches depends on the choice of model employed to generate the single particle state functions. A change of this model will result in an admixture of positive-energy and negative-energy states.

[2]See, for example, the discussion of the relation between many-body perturbation theory and quantum electrodynamics by Sapirstein [68].

3.6 Beyond the no virtual pair approximation

The exact description of a relativistic many-body problem must explicitly take account of the negative energy solutions of the Dirac equation. Such exact descriptions must go beyond the "no virtual pair" approximation. We have remarked above that in relativistic quantum mechanics even the ground state of the hydrogen atom is an infinitely many-bodied problem. In this section, we consider a simple model problem which affords unequivocal evidence of the need to include the negative energy states in order to approach the exact solution of a relativistic many-body problem.

Let us consider a simple model problem consisting of a ground state hydrogenic atom with nuclear charge Z subjected to a perturbation which increases the nuclear charge to $Z + z$ [85–89]. Analytic solutions can be written down for this model in both the non-relativistic and the relativistic formulation. These analytic results can be compared with the sum-over-states perturbation coefficients. In the relativistic case, the negative-energy contributions are essential in order to reproduce the known analytic perturbation expansion at each order. The unquantized nature of the interaction results in an unrestricted summation over both positive- and negative-energy branches of the spectrum. Failure to include the negative-energy contributions results in inaccuracy in the perturbation coefficients.

The non-relativistic zero-order energy is

$$E_0^{nr} = -\frac{1}{2}Z^2, \tag{2.104}$$

whilst the first order energy is

$$E_1^{nr} = -Zz \tag{2.105}$$

and the second order energy is

$$E_2^{nr} = -\frac{1}{2}z^2. \tag{2.106}$$

The sum-over-states formula for the second order energy is

$$E_2^{nr} = \sum_{q\neq 0} \frac{\langle 0 \left| -\frac{z}{r} \right| q \rangle \langle q \left| -\frac{z}{r} \right| 0 \rangle}{E_0^{nr} - E_q^{nr}}. \tag{2.107}$$

For the non-relativistic problem the exact energy of the perturbed system is recovered in second order. The total energy coefficients in third and higher orders is zero. Although individual diagrammatic components in a given order beyond second may be non-zero, their sum vanishes.

The zero order relativistic energy is

$$E_0^r = \left(\sqrt{1 - \frac{Z^2}{c^2}} - 1\right) c^2, \tag{2.108}$$

the first order energy is

$$E_1^r = -\frac{Z}{\sqrt{1 - \frac{Z^2}{c^2}}} z, \tag{2.109}$$

and the second order energy is

$$E_2^r = -\frac{1}{2\left(\sqrt{1 - \frac{Z^2}{c^2}}\right)^3} z^2. \tag{2.110}$$

The exact energy of the perturbed problem is not recovered for the relativistic formulation when taken through second order.

The second order energy can be written in the form

$$E_2^r = E_2^{r+} + E_2^{r-}, \tag{2.111}$$

where E_2^{r+} arises from the summation over the positive energy branch of the spectrum and E_2^{r-} from that over the negative energy branch. The sum-over-states expression for E_2^{r+} is

$$E_2^{r+} = \sum_{p \in P, p \neq 0} \frac{\langle 0 | -\frac{z}{r} | p \rangle \langle p | -\frac{z}{r} | 0 \rangle}{E_0^r - E_p^r}, \tag{2.112}$$

whilst that for E_2^{r-} is

$$E_2^{r-} = \sum_{n \in N} \frac{\langle 0 | -\frac{z}{r} | n \rangle \langle n | -\frac{z}{r} | 0 \rangle}{E_0^r - E_n^r}. \tag{2.113}$$

The third order non-relativistic energy coefficient can be written in the form

$$E_3^{nr} = E_3^{nr}(p) + E_3^{nr}(h), \tag{2.114}$$

where

$$E_3^{nr}(p) = \sum_{q,r \neq 0} \frac{\langle 0 | -\frac{z}{r} | q \rangle \langle q | -\frac{z}{r} | r \rangle \langle r | -\frac{z}{r} | 0 \rangle}{\left(E_0^{nr} - E_q^{nr}\right)\left(E_0^{nr} - E_r^{nr}\right)} \tag{2.115}$$

and

$$E_3^{nr}(h) = \sum_{q \neq 0} \frac{\langle 0 | -\frac{z}{r} | q \rangle \langle 0 | -\frac{z}{r} | 0 \rangle \langle q | -\frac{z}{r} | 0 \rangle}{\left(E_0^{nr} - E_q^{nr}\right)^2}. \tag{2.116}$$

The diagrammatic representation of both $E_3^{nr}(p)$ and $E_3^{nr}(h)$ involves a single Fermion loop and three interaction lines. They differ in that for $E_3^{nr}(p)$ the middle interaction involves particle lines whereas for $E_3^{nr}(h)$ it involves a hole line. It can be shown analytically for the non-relativistic model problem that

$$E_3^{nr}(p) = -\frac{3}{4}\frac{z^3}{Z} \tag{2.117}$$

and that

$$E_3^{nr}(h) = \frac{3}{4}\frac{z^3}{Z}, \tag{2.118}$$

so that their sum E_3^{nr} vanishes.

For the relativistic hydrogenic model problem the total third order energy coefficient may be written

$$E_3^r = E_3^r(p) + E_3^r(h), \tag{2.119}$$

where

$$E_3^r(p) = E_3^{r++}(p) + E_3^{r+-}(p) + E_3^{r-+}(p) + E_3^{r--}(p). \tag{2.120}$$

The first term is the only term to be considered in the "no-virtual-pair" approximation and corresponds to the sum-over-state expression

$$E_3^{r++}(p) = \sum_{p,q\in P, p,q\neq 0} \frac{\langle 0|-\frac{z}{r}|p\rangle\langle p|-\frac{z}{r}|q\rangle\langle q|-\frac{z}{r}|0\rangle}{\left(E_0^r - E_p^r\right)\left(E_0^r - E_q^r\right)}, \tag{2.121}$$

in which the summation is restricted to the postive energy branch, P, of the Dirac spectrum. In contrast with the nonrelativistic case, E_3^r does not vanish.

The energy coefficients for the hydrogenic model problem in the non-relativistic and the relativistic formalism are shown in Table 2.4 for two values of Z, namely $Z = 50, 100$, and z=1. These results, which are taken from the work of Wilson [89] and of Grant and Quiney [95], correspond to estimates of the values in the limit of a complete basis set. The column headed $E_{\lambda c\to\infty}$ shows the non-relativistic energy components whilst the column headed $E_{\lambda c=c}$ gives the relativistic components. The third column, headed δ, presents the differences between the relativistic and non-relativistic energies. $\%p$ denotes $\left(E_2^+/E_2\right)\times 100$ and $\%q$ denotes $\left(E_2^-/E_2\right)\times 100$. This simple model problem demonstrates both that the negative energy states must be included in the perturbation summation if the exact energy is to be recovered and that the magnitude of the negative energy component, E_2^-, increases with Z.

Table 2.4 Energy coefficients for the hydrogenic model problem in the non-relativistic and the relativistic formalism. See text for details. Energies are given in hartree.

		$Z = 50, z = 1$	
	$E_{\lambda c \to \infty}$	$E_{\lambda c = c}$	δ
E_0	−1250.000000	−1294.626156	−44.626156
E_1	−50.000000	−53.702267	−3.702267
E_2	−0.500000	−0.619495	−0.119495
E_2^+	−0.500000	−0.625648	−0.125648
$\%p$	100.00%	100.99%	105.15%
E_2^-	0	0.006153	0.006153
$\%q$	0.00%	0.99%	5.15%
		$Z = 100, z = 1$	
	$E_{\lambda c \to \infty}$	$E_{\lambda c = c}$	δ
E_0	−5000.000000	−5939.195384	−939.195384
E_1	−100.0	−146.256615	−46.256615
E_2	−0.500000	−1.564287	−1.064287
E_2^+	−0.500000	−1.611339	−1.111339
$\%p$	100.00%	103.01%	104.42%
E_2^-	0	0.047052	0.047052
$\%q$	0.00%	3.01%	4.42%

In general, beyond the no-pair approximation, vacuum-induced corrections to the many-body perturbation theory appear at second order. The correct relativistic energy expressions can be obtained from a time-independent approach using standard rules, provided we remember that the observable is the difference between two infinitely many-bodied states. Particular care must be taken in the evaluation of expectation values over creation and annihilation operators for electrons and positrons, which contribute additional sign changes to the values of many-body diagrams. We may, alternatively, adopt Feynman's original prescription and interpret positrons as electrons propagating backwards in time.

The effects of the polarization of the negative-energy sea (vacuum polarization), the modifications to the magnetic moment of the electron (the anomalous electron magnetic moment) and the interaction with the zero-point fluctuations in the radiation field of the electron (the electron self-energy) are observable phenomena. The finite basis set represen-

tation of the Dirac spectrum furnished by the algebraic approximation facilitates the evaluation of Furry QED corrections. These quantum electrodynamic effects have been evaluated for few-electron atomic systems (see, for example, [90–95]). Recently calculations for neutral or nearly neutral atoms and molecules with a large number of electrons have been carried out [96–100]. QED corrections are discussed in more detail in the last chapter of this volume.

4. Summary and Conclusions

A firm foundation for the fully relativistic theory of atomic and molecular electronic structure has been laid down allowing the *ab initio* study of systems containing any atom of the Periodic Table including 'heavy' and 'superheavy' elements. The theory is a precisely defined model which is consistent with the Furry bound-state interaction picture of quantum electrodynamics. The application of this machinery to molecular systems represents a considerable computational challenge. Applications of high quality can be achieved for atoms and small molecular systems. There is, however, no limit on the size of a molecular unit (or unit cell for a periodic system) and the development of theoretical methods for larger molecular systems containing "heavy" and "superheavy" elements requires the development of more approximate techniques. It is the development of these techniques which forms the core of the present volume.

Acknowledgments

SW acknowledges the support of the Engineering and Physical Sciences Research Council. UK acknowledges support by the Israel Science Foundation and by the U.S.-Israel Binational Science Foundation.

References

[1] Swirles B., (1935) *Proc. Roy. Soc. (London) A* **152**, 625; *ibid.* **157** (1935) 680

[2] Dirac P.A.M., (1929) *Proc. Roy. Soc. A (London)* **123**, 714

[3] Pyykkö P., (1978) *Adv. Quantum Chem.* **11**, 353

[4] Grant I.P., (1961) *Proc. Roy. Soc. A* **262**, 555

[5] Grant I.P., (1970) *Adv. Phys.* **19**, 747.

[6] Pyykkö P., *Relativistic theory of atoms and molecules. I.*, Lecture Notes in Chemistry **41** Springer, Berlin.

[7] Pyykkö P., (1993) *Relativistic theory of atoms and molecules. II.*, Lecture Notes in Chemistry **60** Springer, Berlin.

[8] Pyykkö P., (2000) *Relativistic theory of atoms and molecules. III.*, Lecture Notes in Chemistry **76** Springer, Berlin.

[9] Wilson S., (1988) in *Relativistic effects in atoms and molecules*, ed Wilson S. *Meth. Comput. Chem.* **2**, 73

[10] Wilson S., Grant I.P., and Gyorffy B.L. (eds), (1991) *The Effects of Relativity in Atoms, Molecules and the Solid State*, Plenum Press, New York.

[11] Hess, B.A. *(ed.)*, (2002) *Relativistic Effects in Heavy Element Chemistry and Physics*, John Wiley & Sons, Chichester.

[12] Quiney H.M., (2003) in *Handbook of Molecular Physics and Quantum Chemistry*, Vol. 2, edited by S. Wilson, P.F. Bernath and R. McWeeny, John Wiley & Sons, Chichester.

[13] Einstein A., (1905) *Ann. d. Physik* **17**, 37.

[14] Quiney H.M., Grant I.P. and Wilson S., (1989) in *Many-Body Methods in Quantum Chemistry*, ed Kaldor U., Lecture Notes in Chemistry **52**, 331

[15] Levich B.G., (1970) *Theoretical Physics 1*, Wiley Interscience, New York.

[16] Rindler W., (1991) *Introduction to the Special Theory of Relativity*, Clarendon Press, Oxford.

[17] Messiah A., (1961) *Quantum Mechanics*, North-Holland Publishing Company, Amsterdam.

[18] Dirac P.A.M., (1958) *The Principles of Quantum Mechanics*, 4th edition, p. 256, Clarendon Press, Oxford.

[19] Pauli W., (1936) *Ann. inst. Henri Poincaré* **6**, 109

[20] Good Jr. R.H., (1955) *Rev. Mod. Phys.* **27**, 187.

[21] Clifford W.K., (1878) *Am. J. Math.* **1**, 350.

[22] van der Waerden B.L., (1932) *Die Gruppentheoretische Methode in der Quantenmechanik*, Springer, Berlin.

[23] Bethe H. and Salpeter E.E., *The Quantum Mechanics of One- and Two-Electron Systems*, Springer-Verlag, Berlin

[24] Brown G.E., (1952) *Phil. Mag.* **43**, 467.

[25] Feynman R.P., (1949) *Phys. Rev.* **76**, 749

[26] Feynman R.P., (1949) *Phys. Rev.* **76**, 769

[27] Furry W.H., (1951) *Phys. Rev.* **81**, 115.

[28] Quiney H.M., Grant I.P. and Wilson S., (1989) *J. Phys. B: At. Mol. Phys.* **22**, L15

[29] Grant I.P. and Quiney H.M., (1988) *Adv. At. Mol. Phys.* **23**, 37.

[30] Synek M., (1964) *Phys. Rev.* **136**, 1556

[31] Kim Y.-K., (1967) *Phys. Rev.* **154**, 17

[32] Kim Y.-K., (1968) *Phys. Rev.* **159**, 190

[33] Lee Y.S. and McLean A.D., (1982) *J. Chem. Phys.* **76**, 735

[34] Dyall K.G., Grant I.P. and Wilson S., (1984) *J. Phys. B.: At. Mol. Phys.* **17**, 493

[35] Dyall K.G., Grant I.P. and Wilson S., (1984) *J. Phys. B.: At. Mol. Phys.* **17**, L45

[36] Dyall, K.G., Grant I.P. and Wilson S., (1984) *J. Phys. B.: At. Mol. Phys.* **17**, 1201

[37] Stanton R.E. and Havriliak S., (1984) *J. Chem. Phys.* **81**, 1910

[38] Quiney H.M., Grant I.P. and Wilson S., (1987) *J. Phys. B: At. Mol. Phys.* **20**, 1413

[39] Quiney H.M., Grant I.P. and Wilson S., (1987) *Physica Scripta* **36**, 460

[40] Drake, G.W.F. and Goldman S.P., (1981) *Phys. Rev.* **A 24**, 183

[41] Goldman S.P., (1985) *Phys. Rev.* **A31**, 3541

[42] Goldman S.P. and Dalgarno A., (1986) *Phys. Rev. Lett.* **57**, 408

[43] Goldman S.P., (1988) *Phys. Rev.* **A37**, 16

[44] Wells B.H. and Wilson S., (1989) *J. Phys. B: At. Mol. Opt. Phys.* **22**, 1285.

[45] Schmidt M.W. and Ruedenberg K., (1979) *J. Chem. Phys.* **71**, 3951.

[46] Moncrieff D. and Wilson S., (1993) *Chem. Phys. Lett.* **209**, 423.

[47] Moncrieff D. and Wilson S., (1993) *J. Phys. B: At. Mol. Opt. Phys.* **26**, 1605.

[48] Kobus J., Moncrieff D., and Wilson S., (2000) *Phys. Rev. A* **62**, 062503.

[49] Moncrieff D. and Wilson S., (1996) *J. Phys. B: At. Mol. Opt. Phys.* **29**, 2425

[50] Moncrieff D. and Wilson S., (1996) *J. Phys. B: At. Mol. Opt. Phys.* **29**, 6009

[51] Moncrieff D. and Wilson S., (1998) *J. Phys. B: At. Mol. Opt. Phys.*

[52] Moncrieff D. and Wilson S., (1999) *J. Phys. B: At. Mol. Opt. Phys.* **32**, 5379

[53] Goldstone J., (1957) *Proc. Roy. Soc. (London) A* **239**, 267

[54] Quiney H.M., V.N. Glushkov and Wilson S., (2001) *Adv. Quantum Chem.* **39**, 242.

[55] Quiney H.M., Glushkov V.N., and Wilson S., (2002) *Intern. J. Quantum Chem.* **89**, 227.

[56] Bohr A. and Weisskopf V., (1950) *Phys. Rev.* **77**, 94

[57] March N.H., Young W.H., and Sampanthar S., (1967) *The many body problem in quantum mechanics*, Cambridge University Press, Cambridge.

[58] Wilson S., (1981) in *Specialist Periodical Reports: Theoretical Chemistry* **4**, 1

[59] Wilson S., (1984) *Electron correlation in molecules*, Clarendon Press, Oxford.

[60] Urban M., Černušák I., Kellö V., and Noga J., (1987) in *Electron correlation in atoms and molecules*, Meth. Comput. Chem. **1**, 117

[61] McWeeny R., (1989) *Methods of Molecular Quantum Mechanics*, Academic Press, London.

[62] Harris F.E., Monkhorst H.J., and Freeman D.L., (1992) *Algebraic and diagrammatic methods in many-fermion theory*, Oxford University Press, New York.

[63] Wilson S., (1997) in *Problem Solving in Computational Molecular Science*, eds. Wilson S. and G.H.F. Diercksen, Kluwer Academic Publishers, Dordrecht.

[64] Wilson S., (2000) in *Chemical Modelling: Applications and Theory.*, Senior Reporter: A. Hinchliffe, Specialist Periodical Reports (Royal Society of Chemistry, London) **1**, 364; (2002) *ibid.* **2**, 329

[65] Wilson S., (2003) in *Handbook of Molecular Physics and Quantum Chemistry*, Vol. 2, edited by S. Wilson, P.F. Bernath and R. McWeeny, John Wiley & Sons, Chichester.

[66] Karwowski J. and Shavitt I., (2003) in *Handbook of Molecular Physics and Quantum Chemistry*, Vol. 2, edited by S. Wilson, P.F. Bernath and R. McWeeny, John Wiley & Sons, Chichester.

[67] Paldus J., (2003) in *Handbook of Molecular Physics and Quantum Chemistry*, Vol. 2, edited by S. Wilson, P.F. Bernath and R. McWeeny, John Wiley & Sons, Chichester.

[68] Sapirstein J., (1993) *Physica Scripta* **T46**, 52

[69] Ilyabaev E. and Kaldor U., (1992) *Chem. Phys. Lett.* **194**, 95.

[70] Ilyabaev E. and Kaldor U., (1994) *J. Chem. Phys.* **97**, 8455.

[71] Ilyabaev E. and Kaldor U., (1993) *Phys. Rev. A* **47**, 137.

[72] Eliav E., Kaldor U., and Ishikawa Y., (1994) *Chem. Phys. Lett.* **222**, 82.

[73] Eliav E., Kaldor U., and Ishikawa Y., (1994) *Phys. Rev. A* **50**, 1121.

[74] Eliav E., Kaldor U., and Ishikawa Y., (1994) *Intern. J. Quantum Chem. Symp.* **28**, 205.

[75] Eliav E., Kaldor U., and Ishikawa Y., (1996) *Phys. Rev. Lett.* **74**, 1079.

[76] Eliav E., Kaldor U., and Ishikawa Y., (1995) *Phys. Rev. A* **51**, 225.

[77] Eliav E., Kaldor U., and Ishikawa Y., (1995) *Phys. Rev. A* **52**, 291.

[78] Eliav E., Kaldor U., and Ishikawa Y., (1995) *Phys. Rev. A* **52**, 2765.

[79] Eliav E., Kaldor U., and Ishikawa Y., (1996) *Phys. Rev. A* **53**, 3050.

[80] Eliav E., Kaldor U., and Ishikawa Y., (1998) *Molec. Phys.* **94**, 181.

[81] Eliav E., Kaldor U., Y. Ishikawa, M. Seth and P. Pyykkö, (1996) *Phys. Rev. A* **53**, 3926.

[82] Eliav E., Kaldor U., P. Schwerdtfeger, B.A. Hess and Y. Ishikawa, (1994) *Phys. Rev. Lett.* **73**, 3203.

[83] Eliav E., Kaldor U., Y. Ishikawa and P. Pyykkö, (1996) *Phys. Rev. Lett.* **77**, 5350.

[84] Kaldor U. and E. Eliav, (2000) in *Quantum Systems in Chemistry and Physics: Basic problems and model systems*, eds. A. Hernández-Laguna, J. Maruani, R. McWeeny and Wilson S., Progr. Theoret. Chem. & Phys. **2**, 161.

[85] Wilson S., (1984) in *Proc. Sixth Seminar on Computational Methods in Quantum Chemistry*, Schloss Ringberg, West Germany, eds. W.P. Kraemer and W.C. Nieuwpoort, Max-Planck-Institut fur Physik und Astrophysik, Garching.

[86] Quiney H.M., Grant I.P. and Wilson S., (1985) *J. Phys. B: At. Mol. Phys.* **18**, 2805.

[87] Quiney H.M., Grant I.P. and Wilson S., (1985) *J. Phys. B: At. Mol. Phys.* **18**, 3027.

[88] Grant I.P. and Quiney H.M., (2000) *Phys. Rev. A* **62**, 022508.

[89] Wilson S., (2001) *J. Molec. Struct.* THEOCHEM **547**, 279.

[90] Persson H., Salomenson S., Sunnergren P., and Lindgren I., (1996) *Phys. Rev. Lett.* **76**, 204.

[91] Lindgren I., (1996) *Intern. J. Quantum Chem.* **57**, 683.

[92] Mohr P.J., Plunien G., and Soff G., (1998) *Phys. Rept.* **293**, 228.

[93] Lindgren I., (1998) *Molec. Phys.* **94**, 19.

[94] Lindgren I., (2000) *Molec. Phys.* **98**, 1159.

[95] Grant I.P. and Quiney H.M., (2000) *Intern. J. Quantum Chem.* **80**, 283.

[96] Pyykkö P., Tokman M., and Labzowsky L., (1998) *Phys. Rev.* A **57**, R689.

[97] Labzowsky L., Goidenko I., Tokman M., and Pyykkö P., (1999) *Phys. Rev.* A **59**, 2701.

[98] Pyykkö P., Dyall K. G., Csaszar A. G., Tarczay G., Polyancky O. L., and Tennyson J., (2001) *Phys. Rev.* A **63**, 024502.

[99] Dyall K. G., Bauschlicher C. W. Jr., Schwenke D. W., and Pyykkö P., (2001) *Chem. Phys. Lett.* **348**, 497.

[100] Goidenko I., Labzowsky L., Eliav E., Kaldor U., and Pyykkö P, to be published.

Chapter 3

THE CHEMISTRY OF THE HEAVIEST ELEMENTS

Theory and Experiment

V. Pershina* and D. C. Hoffman**

**Gesellschaft für Schwerionenforschung, D-64291 Darmstadt, Germany; **Lawrence Berkeley National Laboratory and University of California, Berkeley, CA94720, USA*

Abstract: Theoretical and experimental investigations of the chemical properties of the heaviest elements are among the most fundamental and important in all of chemistry. They seek to probe the uppermost reaches of the periodic table of the elements where the influence of relativistic effects on chemical properties should be the strongest and where deviations from simple extrapolation of known trends within chemical groups have been observed. The improvement in experimental techniques for "atom-at-a-time" studies of elements with both short half-lives and small production rates has made the last decade especially fruitful in furnishing new results for elements through 108 and preliminary reports of element 112 chemistry. The new wave of theoretical investigations based on molecular relativistic calculations aimed at helping experimentalists design these sophisticated and resource intensive experiments to answer important theoretical questions have resulted in landmark accomplishments. These synergistic interactions between theory and experiment have led to a better understanding of the chemistry of the heaviest elements and the role and magnitude of relativistic effects. Theoretical predictions and experimental results to date are reviewed and compared, and predictions of chemical properties for elements as heavy as 118 are summarized.

Key words: chemistry of elements 101-118, relativistic calculations, "one-atom-at-a-time" experimental techniques

U. Kaldor and S. Wilson (eds.),
Theoretical Chemistry and Physics of Heavy and Superheavy Elements, 55–114.
© 2003 *Kluwer Academic Publishers.*

1. INTRODUCTION

1.1 Production and identification of the heaviest elements. A historical overview

Uranium was discovered in 1789 by Klaproth [1] in pitchblende from Saxony, Germany, and it remained the heaviest element known for more than 150 years. In the mid-1930s, spurred by the discovery of the neutron in 1932 and artificial radioactivity in 1934, both chemists and physicists began experiments to synthesize new "artificial" elements not found in nature. First reports of the synthesis of transuranium elements in 1934 and up to 1938 could not be confirmed and further studies involving meticulous radiochemical separations showed that the new radioactivities were actually fission products. These experiments culminated in early 1939 in the discovery of nuclear fission and the development of the framework for the theory of this new type of nuclear reaction, dubbed "nuclear fission", including the huge amount of energy released and the recoil energy of the fission fragments. Ironically, a study of the recoil energies, begun later in 1939 by E. M. McMillan at the University of California, Berkeley, ultimately led to the discovery of the first "real" transuranium element, with proton number 93. It was produced and identified chemically by McMillan and Abelson [2] in 1940. Shortly thereafter, the next transuranium element with 94 protons was identified as the beta-decay of product of element 93 which had been produced in deuteron bombardments of uranium and its chemical separation from uranium and neptunium was accomplished in early February 1941. The periodic table of that time placed elements 93 and 94 as heavy members of groups 7 and 8 of the periodic table and properties similar to rhenium and osmium were expected which actually delayed chemical identification of element 93. These discoveries thus fulfilled the earlier nuclear scientists' dreams of artificially producing elements beyond uranium. The elements 93 and 94 were subsequently named neptunium and plutonium, respectively, after Neptune and Pluto which are the next planets beyond Uranus for which uranium was originally named.

Later attempts to identify elements 95 and 96 (americium and curium) based on chemical similarities to groups 9 and 10 or even to neptunium and plutonium, all failed. Then in 1944, G. T. Seaborg began to formulate an "actinide" hypothesis in which he placed an actinide series beginning with actinium (Z=89) below the lanthanide (Z=57) series in the periodic table [3]. Using chemistry designed to separate elements 95 and 96 as trivalent homologs of the lanthanides europium and gadolinium, his group was able to successfully separate them from irradiation products. Element 96 was

identified in 1944 and element 95 in early 1945. His actinide hypothesis also laid the framework for predicting the chemical properties of the remaining members of the actinide series that should end with filling of the 5*f* electron shell at element 103, lawrencium.

Another consequence of the actinide concept is the so-called "actinide" contraction, analogous to the lanthanide contraction, in which the radii of the 3+ ions decrease as the positive charge on the nucleus increases with increasing atomic number. Thus the actinides and lanthanides can be separated from each other according to their radii by elution from cation exchange resin columns with a wide variety of complexing agents.

The remaining members of the actinide series were discovered rather quickly as shown in the time line of the discovery of the transuranium elements given in Figure 1.1, and by 1961 the elements through 103 were all known.

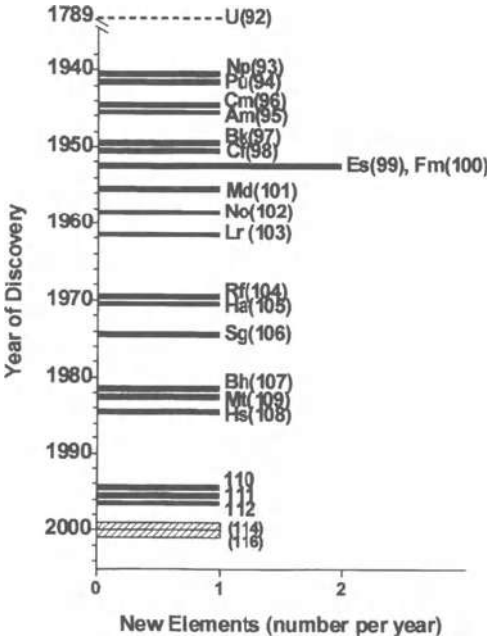

Figure 1.1. Time-line for discovery of the heaviest elements.

By 1970, the actinide concept was further validated by studies of the chemical properties of nobelium, lawrencium, and rutherfordium, showing that nobelium had a stable 2+ state in aqueous solution (similar to Yb which can be reduced to the 2+ state), while the 3+ state is again the most stable in Lr, the last of the actinides. It was also shown that Rf is most stable in the 4+

state, indicating that as predicted it is the first of the transactinides and should be placed as the heaviest member of group 4 of the periodic table, thus beginning the new 6*d* transition series.

The elements beyond 101 have been identified first by "physical" techniques because of their very small production rates and short half-lives. In order to positively identify a new element and place it in its proper position in the periodic table, its proton number, that is, its atomic number, Z, must be determined or deduced in some way, and it became necessary to develop new methods for positive identification of atomic number. One widely used technique is that of α–α correlation of the element's α–decay to a known daughter and/or granddaughter that also decays by α–emission. Positive identification becomes even more difficult for species that decay predominantly by spontaneous fission (SF). Although detection of SF is a very sensitive technique, it is very difficult to determine what the Z of the fissioning species might have been since only the fission fragments are detected. The Z of *both primary fragments* would have to be identified in coincidence in order to add them together to get the Z of the new element. This led to many controversies concerning the discoveries of elements 102 through 105. A correspondingly rather long "gap" can be seen in the time line (Figure 1.1) between the discovery of element 103 in 1961 and of elements 104, 105, and 106 beginning in 1969 while new techniques were perfected, new projectile-target combinations were explored, and new accelerators were built.

Table 1.1. Names of transfermium elements, IUPAC August 1997

Element	Name	Symbol
101	Mendelevium	Md
102	Nobelium	No
103	Lawrencium	Lr
104	Rutherfordium	Rf
105	Dubnium (Hahnium)*	Db (Ha)*
106	Seaborgium	Sg
107	Bohrium	Bh
108	Hassium	Hs
109	Meitnerium	Mt

*Many publications of chemical studies prior to 1997 use hahnium (Ha) for element 105.

The long time interval between discovery of seaborgium (106) in 1974 and bohrium (107) in 1981 can be attributed to the necessity to devise a new type of nuclear reaction ("cold" rather than "hot" fusion) to increase the

production rates and the development of the new separation and detection system SHIP (Separator for Heavy Ion reaction Products) at the Gesellschaft für Schwerionenforschung (GSI) at Darmstadt, Germany that could separate and identify very short-lived species. It was used to discover elements 107 through 109 [4] between 1981 and 1984. The names and symbols for elements 101 through 109 approved [5] by the International Union of Pure and Applied Chemistry in August 1997 are listed in Table 1.1.

Improvements were made in the efficiency of separation and detection of the SHIP and elements 110 through 112 were identified [6-8] between 1994 and 1996, but they have not yet been named. A periodic table as of 2002 is shown in Figure 1.2.

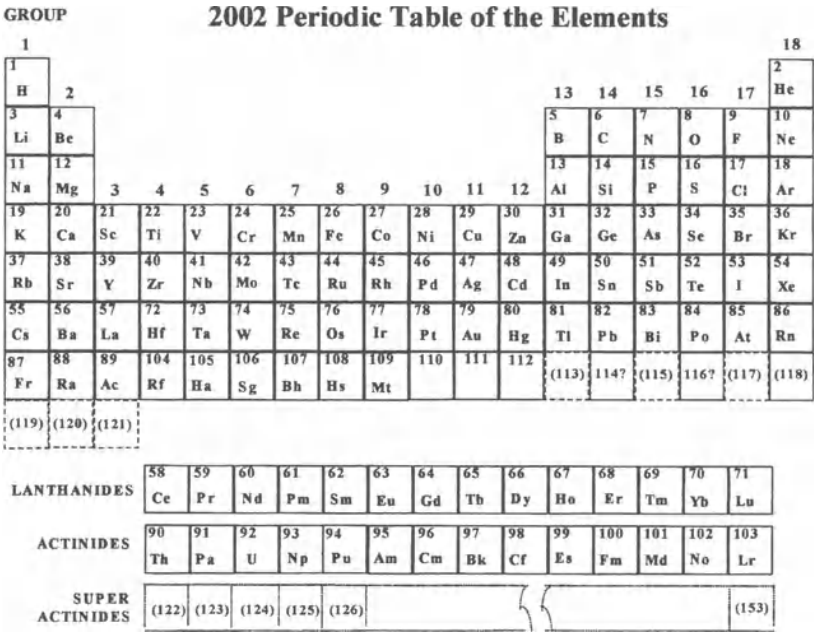

Figure 1.2. Modern periodic table of the elements.

Production of the SuperHeavy elements (SHEs) elements 114 and 116 using "hot" fusion reactions between ^{48}Ca ions and ^{244}Pu and ^{248}Cm targets has recently been reported [9,10] by a Dubna/Livermore collaboration working at the Joint Institutes for Nuclear Research (JINR) in Dubna, Russia. These results have not yet been confirmed but are of considerable interest for chemical studies because the reported half-lives are much longer than those produced at GSI using "cold" fusion reactions which lead to more neutron-deficient species. A number of review papers have been published

which give details on the production and decay properties of the elements from 104 through 112 [11-14]. A chart of the isotopes reported for elements 106 through 116 is given in Figure 1.3.

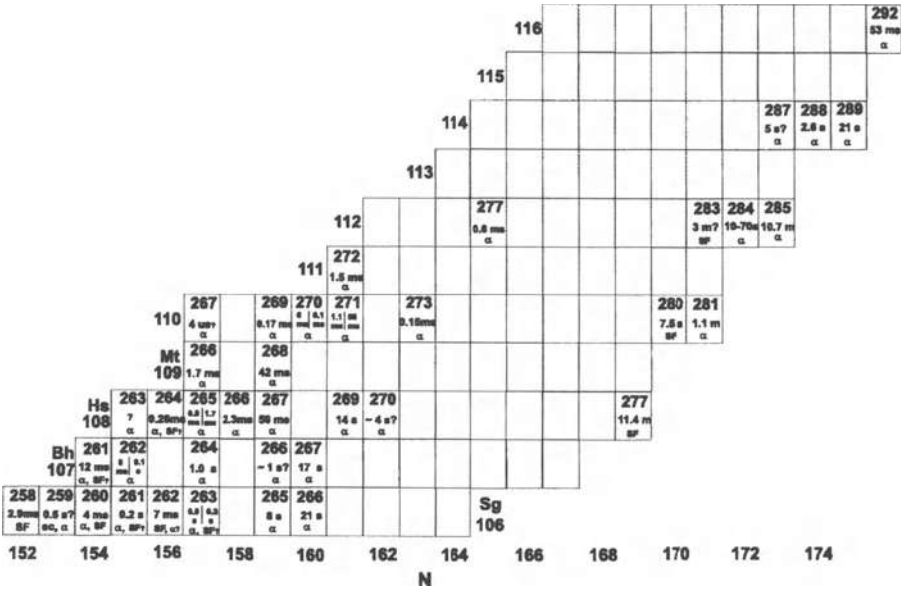

Figure 1.3. The upper part of the chart of nuclides.

1.2 Role of chemical studies

Placement of a new element in the periodic table requires knowledge of its atomic number or electronic configuration. The elements heavier than 101 were first discovered by physical techniques and positive proof of the Z of the new element had to be furnished before discovery of elements 102 through 109 was officially recognized by the International Unions of Pure and Applied Chemistry (IUPAC) and Pure and Applied Physics (IUPAP). However, as discussed earlier, this has led to considerable controversy about what constitutes proof of Z and the validity of various methods. Even though the atomic number is positively assigned, no knowledge is obtained about the electronic configurations or chemical properties of a new element from these physical methods. The elements are just placed in the periodic table by atomic number in various groups or series based on simple extrapolation of known periodic table trends or from theoretical calculations and predictions of the electronic structures. It remains to the experimental chemist to attempt to validate or contradict these predictions.

Beyond element 101, classical chemical separation techniques that depend on the presence of large numbers of atoms can no longer be used. Special chemical separations must be chosen that come to equilibrium rapidly compared to the half-lives of the species involved and give the same results for "one atom-at-a-time" chemistry as would be obtained in a macroscopic experiment [15,16]. (See discussion in Section 4).

The chemistry of elements 104 through 106 has been successfully studied on an "atom-at-a-time" basis (see [17-21]) and Kratz [19] has given a comprehensive review of the results as of 1999. Recently, the chemistry of bohrium (element 107) has been investigated for the first time by using an isothermal gas-phase system [22] and the first chemical studies of element 108 (hassium), the heaviest element whose chemical properties have been investigated so far, have been reported [23]. Experiments with still heavier elements such as 112 [24] are underway and others are planned.

Unfortunately, volatility and complex formation are practically the only properties that can presently be studied experimentally. Some other important properties like ionic radii (IR) or stabilities of oxidation states can only be judged indirectly, e.g., by comparison of elution properties within a series. Even the chemical composition of compounds is not known and can only be assumed on the basis of analogy in the experimental behaviour. Ionisation potentials (IP), electron affinities (EA), dissociation energies or geometrical structures can presently only be determined via quantum-chemical calculations. Thus, the theory starts to be extremely important for the heaviest elements and is often the only source of useful chemical information.

Even before the discovery of the actinides, predictions were made based on the periodic table of the time. Although these were usually helpful, attempts to separate neptunium (93) based on its chemical similarity to rhenium as predicted by the periodic table of the 1930s actually impeded efforts to chemically identify it. Simple extrapolations of existing periodic properties must be made cautiously, a caveat that still remains valid today. That is especially true for the heaviest elements where relativistic effects on their electron shells are extremely strong [25-27]. Some properties of their compounds are expected to deviate from trends found within the lighter homologs in the chemical groups. From the theoretical point of view, the use of relativistic quantum theory and corresponding molecular and atomic programs is mandatory. It has been shown [28-29] that using non-relativistic codes for the elements of the 7th row of the periodic table even gives erroneous predictions of trends.

Numerous relativistic calculations based on Dirac-Slater (DS) and Dirac-Fock (DF) models were performed by chemical theoreticians using the "high-speed" computers of about 30 year ago to predict electronic ground-

state configurations and energy levels for elements through Z=172 [25,30,31]. These calculations guided experimentalists in designing the chemistry to be used for identifying new elements. Later on, some more sophisticated methods like multiconfiguration DF (MCDF) or couple cluster (CC) methods (see the Chapter of U. Kaldor in this book) taking into account correlation effects provided more detailed electronic structures of those elements. Nowadays, the emphasis is on molecular relativistic calculations for the heaviest systems [28,29,32].

In order to predict properties studied experimentally such as adsorption enthalpies in the gas-phase experiments or distribution coefficients in the liquid chromatography experiments, some additional techniques have to be developed that go beyond the usual scope of quantum-chemical calculations. All this makes both theoretical and experimental investigations of the chemistry of the heaviest elements challenging.

The goal of the present chapter is to describe some of the experimental research on the chemistry of the heaviest elements and theoretical attempts to help suggest relevant experiments and predict their outcome.

2. RELATIVISTIC EFFECTS IN THE CHEMISTRY OF THE HEAVIEST ELEMENTS

2.1 Relativistic effects on atomic electronic shells

The relativistic mass increase is known as

$$m = \frac{m_0}{\sqrt{1-(v/c)^2}} \tag{1}$$

where m_0 is the rest mass and v is the velocity of the electron. The effective Bohr radius

$$a_B = \frac{\hbar^2}{mc^2} = a_B{}^0 \sqrt{1-(v/c)^2} \tag{2}$$

decreases, as a consequence, for an inner electron. Thus, the direct relativistic effect is the contraction and, hence, stabilization of the hydrogen-like s and $p_{1/2}$ electrons and it was shown to originate from the inner K and L shell region [33]. This effects was originally thought to be large only for the "fast" electrons in inner core shells of heavy atoms. It was, however, shown that the direct relativistic stabilization is still large for the outer s and $p_{1/2}$ valence orbitals. Thus, e.g., 7s orbital for element 105, Db, is $\Delta_R \langle r \rangle_{7s} = 25\%$ relativistically contracted, where $\Delta_R \langle r \rangle_{ns} = \langle r \rangle_{nr} - \langle r \rangle_{rel} / \langle r \rangle_{nr}$ (Figure 2.1).

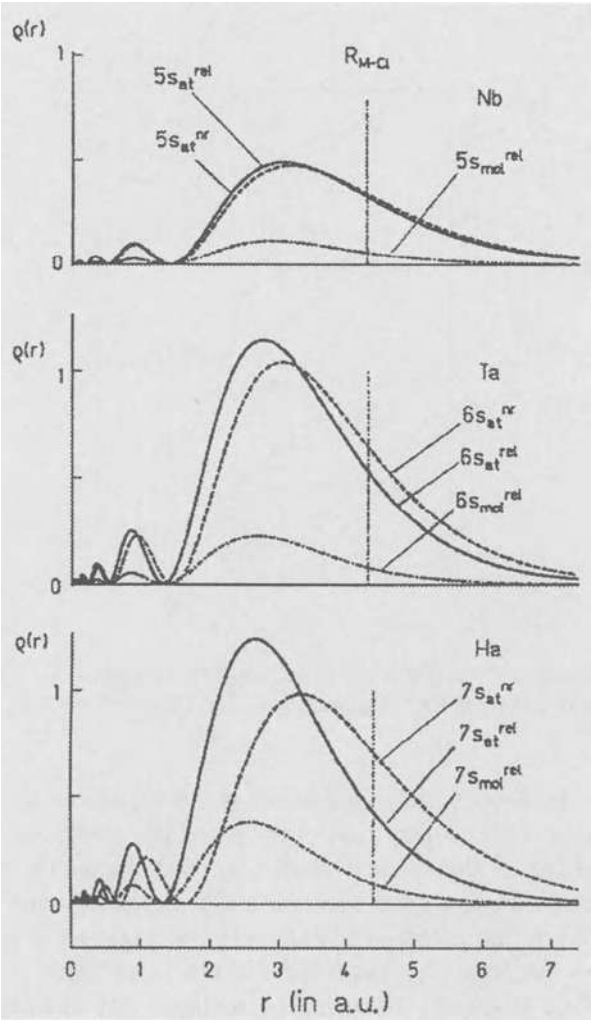

Figure 2.1. Relativistic (solid line) and non-relativistic (dashed line) radial distribution of the ns valence electrons in Nb, Ta, and element 105, Db (Ha on the picture). (From [28]).

The effect of the ns orbital contraction reaches its maximum in the 6th row on Au (17.3%) and in the 7th row on element 112 (31%), the phenomenon being called the relativistic effects gold maximum and group-12 maximum, respectively [32]. The contraction of the outer s and $p_{1/2}$ orbitals was recently explained as due to the admixing of higher bound and (partially) continuum orbitals due to relativistic perturbations [33].

In Figure 2.2, the relativistic stabilization of the 7s and $7p_{1/2}$ orbitals is shown for the group of the noble gas elements (the DF calculations [34]). The relativistic stabilization of the 7s orbital is of 14.2 eV.

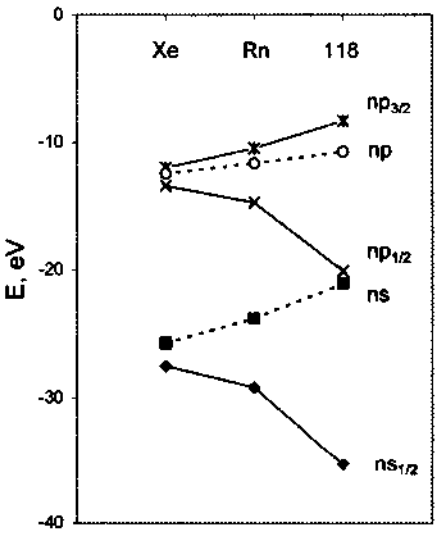

Figure 2.2. Relativistic stabilization of the ns and $np_{1/2}$ orbitals and the SO splitting of the np-orbitals for the noble gases Xe, Rn and element 118. (The DF values are from [34] and the HF values are from [32]).

The second (indirect) relativistic effect is the expansion of outer d and f orbitals. The relativistic contraction of the s and $p_{1/2}$ shells results in a more efficient screening of the nuclear charge, so that the outer orbitals which never come close to the core become more expanded and energetically destabilized. While the direct relativistic effects originate in the immediate vicinity of the nucleus, the outer core shells contribute to the indirect relativistic effect. It should, however, be realized that though contracted s and $p_{1/2}$ core (innermost) orbitals cause indirect destabilization of the outer orbitals, relativistically expanded d and f orbitals cause their indirect stabilization. That partially explains the very large relativistic stabilization of the 6s and 7s orbitals in Au (Z=79) and element 112, respectively: Since d

shells (it is also valid for the f shells) become populated at the end of the nd series, there will occur a maximum of indirect stabilization of the valence s and p orbitals [33].

Figure 2.3 demonstrates the relativistic destabilization of the (n-1)d orbitals, as well as the stabilization of the ns orbitals, for group-6 elements, as an example. One can see that the trends in the relativistic and non-relativistic energies of the valence electrons are opposite from the 5d to the 6d elements. Thus, the non-relativistic description would still give the right trend in properties from the 4d to the 5d elements, while it would result in the opposite and wrong trend in going over to the 6d elements.

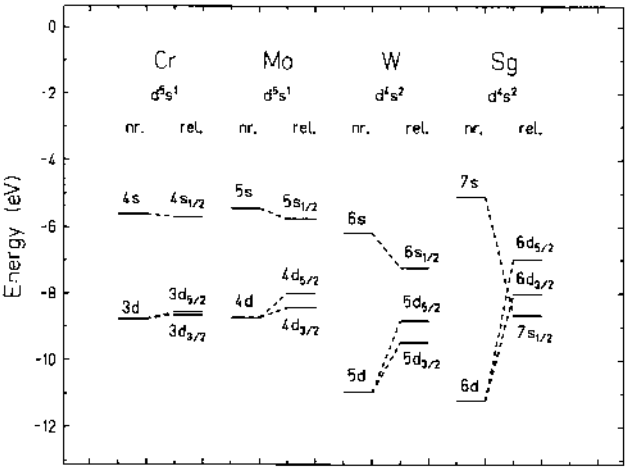

Figure 2.3. Relativistic (DF) and non-relativistic (HF) energy levels of the valence ns and (n-1)d electrons. (The data are from [34]).

The third relativistic effect is the well-known spin-orbit (SO) splitting of levels with $l > 0$ (p, d, f, etc. electrons) into $j = l \pm ½$. It also originates in the vicinity of nucleus. The SO splitting of the valence 7p levels in the 7p elements is very large, e.g., of 11.8 eV for element 118 (Figure 2.2). All the three effects are of the same order of magnitude and grow roughly as Z^2.

Breit effects (accounting for magnetostatic interactions) on energies of the valence orbitals and on IP are usually small (e.g., 0.02 eV for element 121 [35]). They can, however, reach few % for the fine structure level splitting.

The influence of the QED effects (vacuum polarization and self-energy) on the energies of the valence orbitals was tested by Pyykkö *et al.* [36] for the coinage metals. The effects were shown to be not negligible and to be of the order of 1-2 % of the kinetic relativistic effects. That means that existing studies of relativistic effects are up to 99% correct.

2.2 Relativistic quantum-chemical calculations

Methods for calculating the electronic structures of very heavy element compounds are the same relativistic methods which can be applied to any other relativistic system. They have been overviewed in other publications in application to transition elements [26], actinides [37], and transactinides [28,29,32] and are extensively represented in this book.

Most atomic calculations for the heaviest elements were performed by using the Dirac-Fock (DF) [34], Dirac-Slater (DS) (see [25] and references therein, as well as [38,39]), multiconfiguration Dirac-Fock (MCDF) [40-49] and Dirac-Coulomb-Breit Coupled Cluster Single Double excitations (DCB CCSD) [50-60] methods, with the latter being presently the most accurate. Calculations using the CCSD method have shown, e.g., some fundamentally different results for the ground state electronic configuration of Rf (s^2d^2) [53] in contrast to the MCDF results (d^2sp) [42,43], since the former method includes dynamic correlations omitted in the MCDF method. Due to the limitation of the CCSD method in treating electronic configurations with more than two electrons (holes) beyond the closed shell, the predictions for the middle of the 6d-series (elements 105 through 108) were made using the MCDF method [44-46,49].

Most molecular calculations for the transactinide elements were performed using the fully relativistic (four-component) Dirac-Slater discrete variational (DS-DV) method (see [28,29] and references therein) and later, based on it the density functional theory (DFT) method with the RGGA approximation for the exchange-correlation potential [61-64].

In the DFT method, the total energy is expressed as a functional of the charge density $\rho(r)$ [65,66]

$$E = \sum_i n_i \langle \phi_i | t | \phi_i \rangle + \int \rho V^n d^3 r + \frac{1}{2} \int \rho V^c d^3 r + E^{xc}(\rho) + \sum_{p>q} \frac{Z_p Z_q}{|R_p - R_q|} \tag{3}$$

where t is the Dirac kinetic energy operator, a (4 x 4) matrix in spinor space, V^n represents the potential energy of the interaction of the electrons with the nuclei, and V^c is the direct Coulomb-interaction potential among the electrons. The last two terms represent the exchange-correlation energy and the nucleus-nucleus Coulomb interaction energy, respectively. The total energy functional $E(\rho)$, eq. (3), has a minimum with the ground state density ρ of the system. Application of the variational principle with the constraint

of conservation of the number of electrons leads to the single particle Kohn-Sham equations

$$\left[t+V^{n}+V^{c}+V^{xc}\right]\left|\phi_i\right\rangle=\varepsilon_i\left|\phi_i\right\rangle, \quad i = 1 \ldots N \tag{4}$$

The exchange-correlation potential V^{xc} is a functional derivative of the exchange-correlation energy E^{xc} with respect to the density, that is,

$$\rho(\mathbf{r})=\sum_i n_i\phi_i^{+}(\mathbf{r})\phi_i(\mathbf{r}) \tag{5}$$

where n_i are the occupation numbers. The parametrized exchange-correlation potential of Vosko, Wilk, Nusair [67] is used for the local density approximation (LDA). The generalised gradient approximation (GGA) of Becke [68] is included perturbatively in order to consider non-local contributions.

$$E_{xc}^{GGA} = \int f(\rho(r),|\nabla\rho(r)|)dr \tag{6}$$

In both the LDA and GGA calculations, the relativistic form of the exchange-correlation potentials developed by Engel *et al.* [69] has been used (see the Chapter of E. Engel in this book).

In order to solve the Kohn-Sham equations (eq. 4), the molecular orbital-linear combination of atomic orbitals (MO-LCAO) approach was used. The molecular wave functions ϕ_i are expanded via the symmetry adapted χ_j which are also expanded in terms of the atomic orbitals $\xi_{n_\nu}(r)$. These atomic orbitals are four-component Dirac spinors. The symmetrization coefficients are obtained by the use of group theoretical projection operators [70]

$$\phi_i(r) = \sum_j \chi_j c_{ji} = \sum_j \xi_{n_\nu}(r) d_{n_\nu j} c_{ji} \tag{7}$$

where $n_\nu = (\nu, n, k, m)$. Here ν indicates atomic site and m and k are magnetic and Dirac quantum numbers. The variational coefficients are determined by using standard procedure for solving the secular equation

$$\mathbf{HC}=\varepsilon\mathbf{SC} \tag{8}$$

where **H** and **S** are the Hamiltonian and overlap matrices, respectively. The matrix elements are evaluated numerically by using the modified version for relativistic numerical wave functions [71] with the integration scheme of Boerrigter, Velde and Baerends [72]. The direct Coulomb potential V^c has been calculated via an additional variational procedure, which reduces the numerical errors and yields a variationally consistent total energy [65,66].

As is known [73,74], the DFT methods are well suited for description of properties of chemically interesting systems, including complexes in solutions or adsorption processes. Systems with large number of atoms can be treated with sufficient accuracy very economically. Using these methods, electronic structures of various gas phase chemical compounds of elements 104 through 108, as well as aqueous complexes of element 104 through 106 have been theoretically studied. Predictions of the experimental behaviour have been made on their basis [28,29,61-64]. The Beijing Density Functional method (BDF) was also applied to the calculations of some dimers of element 111 [75-77].

Another group of methods successfully used for calculations of the electronic structure of the heaviest elements was the energy-adjusted pseudo potentials (PP) (see [32,78] and references therein, as well as the Chapter of P. Schwerdtfeger in this book). Properties of open-shell compounds of elements at the end of the 6d series (111 and 112), as well as at the beginning of the 7p series (113 and 114) were studied using this method. Another group of the PP methods, the relativistic effective core potentials, RECP, were also applied to the calculations of the electronic structures of the heaviest element systems [79-84].

Molecular relativistic *ab initio* DF codes with electron correlation are still at the stage of development (see the corresponding chapters in this book). They are too sophisticated and still not sufficiently economic to be applied to the heaviest element systems studied experimentally. They were applied only to very small molecules of the heaviest elements. The main aim was to study relativistic or correlation effects on some model systems like 111H, 117H, $(113)_2$ or $114H_4$ [85-91]. Results of the molecular calculations mainly in the application to experimental needs will be discussed in the following chapters.

3. PREDICTIONS OF CHEMICAL PROPERTIES

3.1 Atomic properties

Electronic configurations, ionisation potentials (IP), atomic/ionic radii (AR/IR), polarizability (α) and stability of oxidation states are important atomic properties. From knowledge of trends in these properties one can assess the similarity of the heaviest elements to their lighter homologs in the chemical groups. Differences in the chemical behaviour of the transactinides and their lighter homologs can result from larger ionic radii, different energies and a radial extension of the valence orbitals. Earlier predictions of chemical properties on the basis of atomic DS and DF calculations are summarized in the review of Fricke [25].

3.1.1 Electronic configurations

Relativistic changes in the energies of the 7s, 7p and 6d electrons of the transactinide elements result in the stability of the $7s^2$ electronic pair in the ground states over the entire 7th row of the periodic table which is different from some elements of the 6th row like Pt($5d^9 6s$) and Au($5d^{10}6s$).

Both the MCDF and CCSD calculations [41,59] have agreed on the $7s^2 7p$ ground state for element 103, Lr, different than its lanthanide homolog Lu ($7s^2 6d$), due to the strong relativistic stabilization of the 7p electrons. For Rf, MCDF calculations [42,43] have shown a different electronic configuration, $7s^2 6d7p$, than the $6s^2 5d^2$ state of its homolog, Hf. The $7s^2 6d7p$ ground state of Rf was, however, not confirmed by the more accurate CCSD calculations [53]. Inclusion of correlation effects of higher order (f electrons) in the CCSD calculations resulted in the inversion of the $7s^2 6d7p$ and $7s^2 6d^2$ configurations, with the latter being more stable. For elements 105 through 108, the MCDF calculations have confirmed the $7s^2 6d^q$ ground states [44-46]. The CCSD calculations have also confirmed the $7s^2 6d^q$ electronic configurations of elements 111 and 112 [54,55], as well as $7s^2 7p^q$ ground states for elements 113, 114 and 115 [56-58] obtained by earlier DF and DS and later MCDF calculations for elements 113 through 118 [49]. For element 121, the CCSD calculations have also shown the $8s^2 8p$ configuration [35], as was predicted by the DF calculations [34].

The relativistic stabilization of the $7s^2$ and $7p_{1/2}$ electrons was a reason to think earlier about an enhanced stability of lower oxidation states of Lr^+ and some lighter transactinides, Db^{3+} or Sg^{4+}, as well as to design gas-phase experiments to detect a p-character of Lr and Rf, since the volatilities of d- and p-element compounds are essentially different (see Section 4.2.1). The

MCDF calculations of multiple IPs for elements 104 through 108 [43-46] and estimates of redox potentials (see Section 3.1.3) did not confirm the stability of lower oxidation states, as is shown in Section 3.1.3. Neither was the p character of Rf confirmed by molecular calculations [28,29].

3.1.2 Ionization potentials and stabilities of oxidation states

The DF and DS calculated IPs for elements with Z up to 166 are summarized in [25]. The MCDF results for elements 104 through 108 are given in [43-46] and for elements 113-118 in [49]. The recent CCSD IPs for elements 104, 111-115 are published in [53-58].

The calculations have shown that the relativistic stabilization of the 7s and the destabilization of the 6d electrons of the 6d elements cause the excitation energies between the valence orbitals to decrease in comparison with those of the 5d elements, so that the highest oxidation states are easier to reach. Recent MCDF calculations of IP for elements 104 through 108 [43-46] have indeed shown a decrease in the IP($0 \rightarrow Z^{+}_{max}$), as illustrated in Figure 3.1.

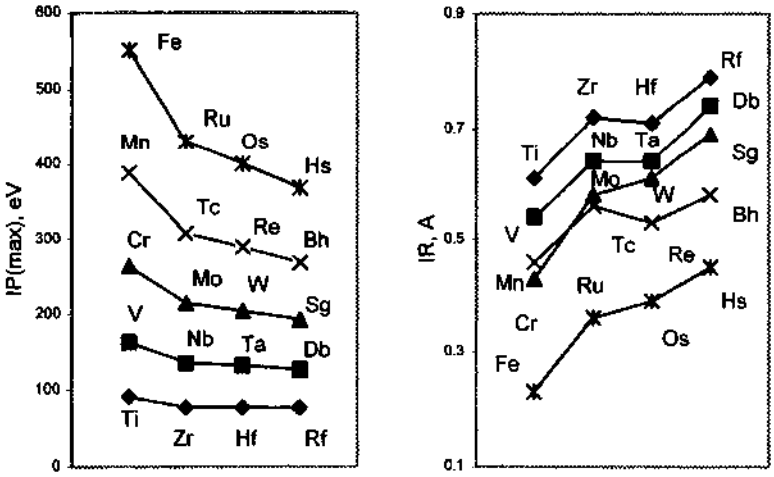

Figure 3.1. Multiple ionization potentials (IP_{max}) and ionic radii (IR) for elements 104 through 108 in their maximum oxidation states obtained from the MCDF calculations [43-46].

This is also the reason why lower oxidation states are not stable at the beginning of the 6d series: the 7s and 6d levels are so close spatially that the step-wise ionization process, for example, for Db or Sg results in the $6d^2$ and not in the $7s^2$ configuration for Db^{3+} or Sg^{4+} (see Figure 10 in [92]). Since

the 6d orbitals of the 6d elements are more destabilized than the (n-1)d orbitals of the 4d and 5d elements, the 3+ and 4+ ionized states of Db and Sg, respectively, will even be less stable than those of Ta and W.

The destabilization of the 6d orbitals at the end of the transactinide series is a reason for the 6d electrons to be chemically active. As a consequence, an enhanced stability of higher oxidation states can be expected like, e.g., of the 3+ and 5+ states of element 111, or 4+ state of element 112 [25,78].

For element 112, the CCSD calculations [55] have confirmed the largest IP=11.97 eV in the group. Thus, element 112 is expected to be more inert than Hg, but still not as inert as Xe.

The large relativistic stabilization of the $7s^2$ electrons (a large 7s-6p gap hindering the hybridisation) is the reason for an enhanced stability of lower oxidation states at the beginning of the 7p series. However, the destabilization of the 6d levels would also contribute to a more transition-element character of these elements [32,78].

The IP of element 118 of 8.7 eV [25] is about the same as the IP for element 114 of 8.54 eV [57] and smaller than IP(Rn) = 10.74 eV and IP(112) = 11.97 eV [55]. Thus, element 118 is expected to be the least inert and most electropositive of all the noble gases. The oxidation states 2+ and 4+ will be more important than 6+ because of the strong binding of the $7p_{1/2}$ electrons. The outer 8s orbital of element 118 is relativistically stabilized to give the atom a positive electron affinity of 0.056 eV [60]. The inclusion of both relativistic and correlation effects was required to obtain this result. Similar calculations did not give a ^2S bound state for Rn^-.

3.1.3 Redox potentials

The knowledge of the relative stability of oxidation states, redox potentials, is very important for a chemical application. A way to calculate redox potentials is to calculate the free energy $\Delta G°$ of an oxidation-reduction reaction

$$M^{z+n} + ne \leftrightarrow M^{z+}. \tag{9}$$

The redox potential $E°$ is then defined as

$$E° = -\Delta G°/nF, \tag{10}$$

where F is the Faraday number. The practice, however, shows that the predictions of $E°$ via total energy calculations of reaction components do not reach the sufficient accuracy (see, for example, [93]). Another way to do it

was suggested [92,94] using a linear correlation between calculated IPs and experimental redox potential, since

$$\Delta G^{o} = -(\mathrm{IP} + \Delta G^{\circ}_{\mathrm{hydr}}), \tag{11}$$

where $\Delta G^{\circ}_{\mathrm{hydr}}$ is a free energy of hydration. The latter was shown to be a smooth function of atomic number and can be evaluated. Thus, using calculated MCDF IP [43-46] and experimental E° [95], redox potentials of Rf, Db and Sg and, where unknown, of their lighter homologs were determined [92,94,96]. One of those correlations for group-6 species is shown in Figure 3.2 as an example.

The results of those investigations have, indeed, shown that the stability of the maximum oxidation state increases in groups 4 through 6, while that of lower oxidation states decreases. In going along the 6d series, the stability of the maximum oxidation state decreases: $E^{\circ}(Lr^{3+}/Lr^{2+}) = -2.6$; $E^{\circ}(Rf^{4+}/Rf^{3+}) = -1.5$; $E^{\circ}(Db^{5+}/Db^{4+}) = -0.93$; and $E^{\circ}(Sg^{6+}/Sg^{5+}) = -0.05$ V [28]. Comparison of the relativistic with non-relativistic calculated energies has shown that the increasing stability of the maximum oxidation state is a relativistic effect due to the destabilization of the 6d orbitals.

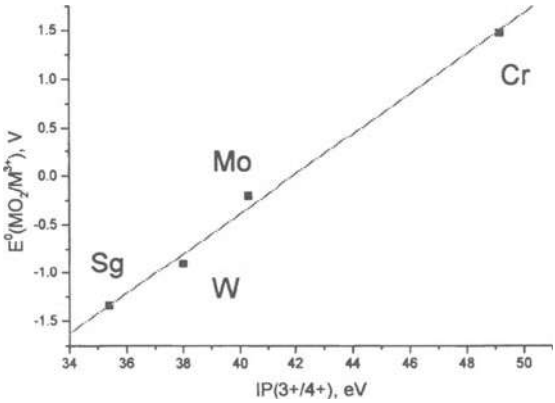

Figure 3.2. Correlation between MCDF IP(3+/4+) and standard potentials $E^{\circ}(MO_2/M^{3+})$ [95], where M = Cr, Mo, W, and Sg. (From [92]).

The estimates of redox potentials have also demonstrated that the 3+ and 4+ states for Db and Sg, respectively, will not be stable. (See Figure 3.2). Based on these predictions, experiments to attempt to reduce Sg with a strongly reducing metal such as Al ($E^{\circ} = -1.662$ V) are planned.

3.1.4 Ionic radii

Ionic radii (IR) are usually defined by the maximum of the radial charge density, R_{max}, or an expectation value, $\langle r_{nj} \rangle$, of an outer valence orbital. The DF expectation values of various electrons for elements up to Z = 120 have been tabulated by Desclaux [34]. The MCDF R_{max} for elements 104 through 108 are given in refs. [43-46]. They were used to estimate the IR of the transactinide elements in various oxidation states using a linear correlation between R_{max} and IR [97]. An example of one of these correlations is shown in Figure 3.3.

The predictions of IR for elements 104 through 108 in their maximum oxidation states are summarized in Figure 3.1. The Figure shows that the IR of the 4d and 5d elements are almost equal due to the lanthanide contraction (which is 86% a non-relativistic effect), while the IR of the transactinides are about 0.05 Å larger than the IR of the 5d elements due to an orbital expansion of the $6p_{3/2}$ orbitals. Nevertheless, they are still smaller than the IR of the actinides due to the actinide contraction (of 0.030 Å) which is mostly a relativistic effect [26,98].

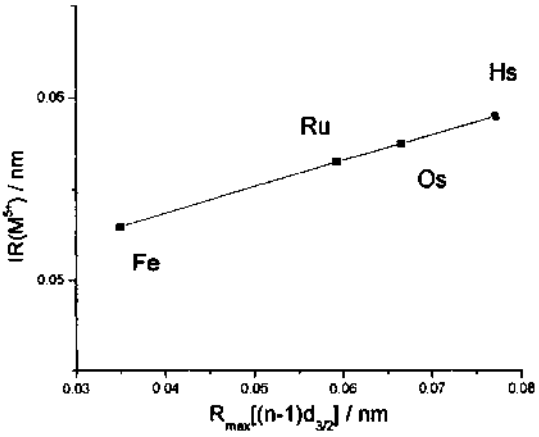

Figure 3.3. Correlation between the $R_{max}[(n-1)d_{3/2}]$ and IR(M^{5+}) for group-8 elements Fe, Ru, Os and Hs. The IR(Hs^{5+}) = 0.059 nm. (From [46]).

3.2 Properties of gas-phase compounds of elements 104 through 108

Transactinides are now known to form volatile halides and oxyhalides as do the lighter homologs in their respective chemical groups. These were the first gas-phase compounds to be studied experimentally. Therefore, there

was widespread interest in their electronic structures and fundamental properties such as ionicity or covalence, bonding and thermochemical stability, as well as the trends within the groups. The question of the magnitude of the influence of relativistic effects on those properties was also of great interest.

3.2.1 Electronic structures and role of relativity

A large series of calculations has been performed for halides and oxyhalides of elements 104 through 106 using density-functional methods, mostly the DS-DV: MCl_4 (M = Zr, Hf, and Rf), MCl_5 and MBr_5, $MOCl_3$ and $MOBr_3$ (M = V, Nb, Ta and Db), MF_6 and MCl_6, $MOCl_4$, MO_2Cl_2, MO_4^{2-}, $M(CO)_6$ (M = Mo, W and Sg). (See [28,29] and references therein). Various electronic structure properties (IP, EA, electron transition energies, charge density distribution and bonding) and their trends have been predicted for the transactinides and their lighter homologs. Calculations of binding energies, D_e, and optimization of geometry (equilibrium bond lengths, R_e) have been performed for MCl_4 (M = Ti, Zr, Hf and Rf) [61], MCl_6 (M = Mo, W and Sg) [62], MO_3Cl (M = Tc, Re and Bh) [63], and MO_4 (M = Ru, Os and Hs) [64] using the RGGA DFT method. Recently, CCSD(T) RECP calculations have also been performed for halides and oxyhalides of elements 104 through 106, such as $RfCl_4$, MCl_6, $MOCl_4$, MO_2Cl_2, MO_3 (M = W and Sg), MCl_5 and MBr_5 (M = Ta and Db) [79]. The influence of relativistic effects on the electronic structure and properties of the transactinide compounds has been analysed in detail in [99] for the example of MCl_5 (M = V, Nb, Ta, and Db).

The Mulliken analysis of the valence orbital population has shown the bonding in the 6d elements to be dominated by a large participation of both the $6d_{3/2}$ and $6d_{5/2}$ orbitals (e.g., 70% in $DbCl_5$) and is typical of d-element compounds [99]. The 7s, as well as both $6p_{1/2}$ and $6p_{3/2}$ orbitals, each contribute about 15 % to the bonding. Thus, the most important conclusion for the design of experimental investigations was that the 6d elements are close homologs of the 5d elements and should exhibit similar chemical properties.

The most common feature for all the compounds found in both the DFT [61-64] and RECP [79] calculations was an increase in covalence (a decrease in effective charges, Q_M, and an increase in the overlap population, OP) in going down the transition element groups, as it is shown in Figures 3.4 and 3.5. Comparison of the relativistic with non-relativistic calculations (Figure 3.4) has shown this increase to be a purely relativistic effect due to the increasing contribution of the relativistically stabilized and contracted 7s and $7p_{1/2}$ AO, as well as of expanded 6d AO in bonding [99].

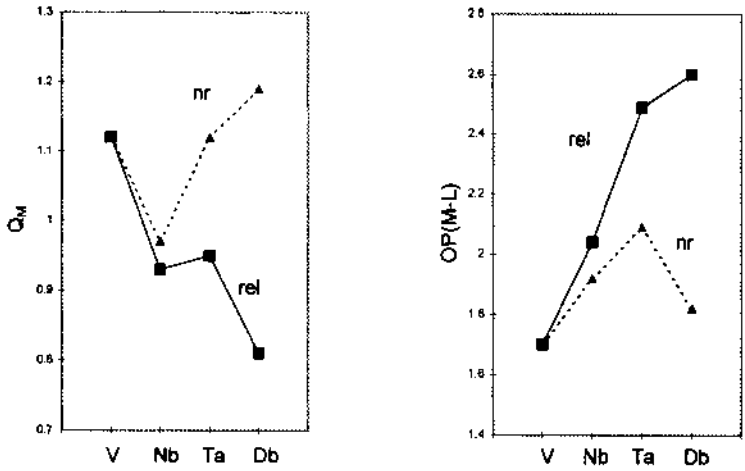

Figure 3.4. Relativistic (rel) and non-relativistic (nr) values of effective charges (Q_M) and overlap populations (OP) in MCl_5, where M = V, Nb, Ta and Db. (Results are from [99]).

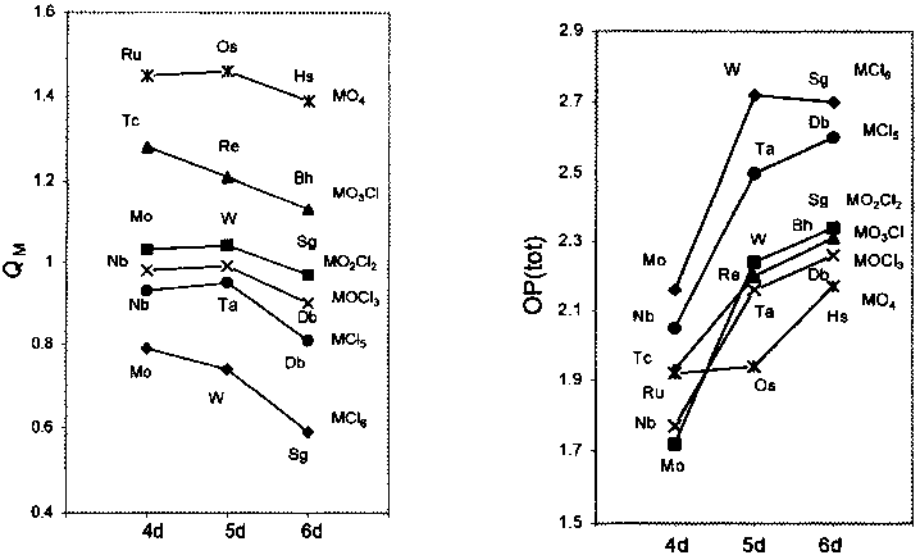

Figure 3.5. Effective charges (Q_M) and total overlap populations (OP) for group-4-8 halides and oxyhalides obtained as a result of the Mulliken analysis in the DS-DV and DFT calculations [28,63,64].

The molecular calculations [99,29] have also shown that an increase in IP, a decrease in EA, and an increase in the stability of the maximum oxidation states is a relativistic effect. It is important to note that non-relativistically, trends in all these properties would be just the opposite from the 5d to the 6d compounds (like, e.g., Q_M and OP in Figure 3.4).

The trends in D_e and R_e for various types of compounds are summarised in Figure 3.6. There is a decrease in D_e from 5d to the 6d elements for almost all the compounds except for the group-8 MO_4 and the group-6 MCl_6. In all the groups, relativistic effects steadily enhance the bonding in going down the groups, though increasing SO splitting of the d orbitals partially diminishes it by about 1.5 eV, as was shown by the RECP calculations [79]. This is one of the reasons for most of the transactinide compounds having atomization energies lower than those of the previous 5d elements. The other reason is a decrease in the ionic contribution to bonding which is also a relativistic effect. The calculated R_e (Figure 3.6) reflect the experimentally known similarity of bond lengths for the 4d and the 5d elements due to the lanthanide contraction and an increase in R_e of about 0.05 Å in the transactinide compounds in comparison with the 5d elements.

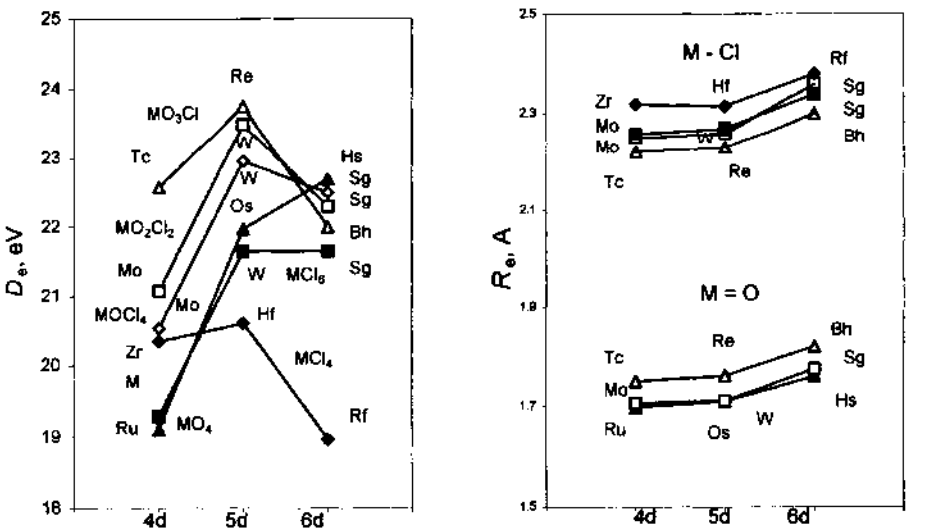

Figure 3.6. Atomization energies (D_e) and optimized bond length (R_e) for various halides, oxides and oxyhalides of group-4 - 8 elements [63,64,79,100,101].

Among other important trends, one should mention a decrease in the strength of a single metal-ligand bond from the group-4 to group-6 halides, as well as a decrease in the relative stability of the maximum oxidation state.

Thus, the volatile species like $SgCl_6$ and $SgOCl_4$ will decompose at high temperatures by analogy with $MoCl_6$ and $MoOCl_4$ (a weak Sg-Cl bond), transforming into Mo (V). The SgO_2Cl_2 was shown to be the most stable and was recommended for the gas-phase experiments [101]. This theoretical result has influenced the decision of the chemists to use oxygen containing chlorination agents in the experiments with Sg and SgO_2Cl_2 was obviously formed in those experiments in good agreement with the prediction (see Section 4.2.1).

An increase in dipole moments, μ, of the low symmetry molecules within the transition element groups was predicted for all the group-4 through 8 compounds. However, the μ and α, as well as the molecular size, are decreased by relativistic effects. The IP and covalence, in turn, are relativistically increased. Since all these quantities contribute to the molecule-surface interactions (see Section 3.2.3), volatility is, therefore, increased as a result of relativistic effects.

3.2.2 Predictions of trends in volatility

Theoretical treatment of volatility is a very complicated subject since this quantity does not correlate with a single electronic structure parameter. Nevertheless, a larger series of the DS-DV calculations [28,29,63,64] enabled one to establish some relationships between molecular properties such as covalence (OP) or dipole moment and volatility. Thus, the following relationships have been established for the highest halides and oxyhalides of groups 4 through 8:

- higher OPs in the 5d halides compared to the 4d halides correspond to their higher volatility;
- higher OPs in the group-5 halides compared to the group-4 halides are consistent with their higher volatility;
- smaller OPs for oxyhalides compared to corresponding pure halides are related to their lower volatility;
- much lower OPs for halides of the actinides compared to those of halides of the d elements are in line with the lower volatility of the actinides;
- increasing dipole moments in the low symmetry compounds of the group-5 $MOCl_3$, group-6 $MOCl_4$, MO_2Cl_2, or group-7 MO_3Cl are the reason for the observed decrease in volatility within those groups.

These observations led to conclusions that the higher covalence (larger OP) of high symmetry halides or oxides of the transactinides should result in higher volatility compared to those of their 4d and 5d homologs. The largest μ of lower symmetry transactinide compounds should result in their lowest volatility as compared to those of the lighter homologs within the groups. Experimentalists were also advised to use the equilibrium vapour pressure,

known in macrochemistry as a measure of volatility, as a benchmark for "one-atom-at-a-time" measurements of the adsorption temperatures or $T_{50\%}$ of the chemical yield, and some hypothetical P_{mm} was predicted for transactinide compounds [102]. As a result of these theoretical considerations, it was predicted that volatility should change as $RfCl_4$ > $HfCl_4$, $DbCl_5$ > $DbOCl_3$, MoO_2Cl_2 > WO_2Cl_2 > SgO_2Cl_2 or TcO_3Cl > ReO_3Cl > BhO_3Cl [29,101,103,63]. This was, indeed, confirmed experimentally by the observation of higher volatility for $RfCl_4$ than that for $HfCl_4$ and lower volatility of $DbOCl_3$, SgO_2Cl_2, or BhO_3Cl in comparison with similar compounds of their lighter homologs (see Section 4.2).

3.2.3 Predictions of adsorption enthalpies

A further step was undertaken by Pershina *et al.* [63,64] to predict the quantity studied experiementally: ΔH_{ads} of 107 and 108 compounds on the surface of the chromatography column were determined using some models of physisorption. (Direct calculations of adsorption enthalpies are still not feasible both due to the limitations of the methods, e.g. of the DFT one in treating weak interactions, and the fact that there is no detailed information about the surface: it can be quartz covered with some reactive material). The used models were based on the principle of molecule-slab interactions subdivided into usual types for the long-range forces: the dipole-dipole, dipole-polarizability and dispersion interactions [104]. Thus, for the case of the interaction of MO_3Cl (M = Tc, Re and Bh) with a surface charge Q (located on Cl, since HCl was adsorbed on the surface), the interaction energy is expressed as

$$E(x) = -\frac{2Qe\mu_{mol}^{2}}{x^2} - \frac{Q^2e^2\alpha_{mol}}{2x^4} - \frac{3}{2}\frac{\alpha_{mol}\alpha_{slab}}{\left(\frac{1}{h\nu_{mol}} + \frac{1}{h\nu_{slab}}\right)} \qquad (12)$$

where μ, $h\nu_{mol}$ (roughly IP) and α_{mol} belong to the molecule and those with index "slab" to the surface. The calculated contributions to $E(x)$ are given in Table 3.1.

Table 3.1. Contributions to the interaction energy *E(x)* between MO_3Cl (M = Tc, Re and Bh) and Cl^{ϱ} of the surface [63].

Molecule	μ-*Qe*	α-*Qe*	α-α(Cl)
	$E10^{28}\,x^2$ (erg cm^2)	$E10^{44}\,x^4$ (erg cm^3)	$E10^{60}\,x^6$ (erg cm^6)
TcO_3Cl	3.58	9.12	607.32
ReO_3Cl	4.96	10.91	738.05
BhO_3Cl	7.49	13.84	947.17

The only value which can not be calculated directly according to this model is the molecule-surface interaction distance x. It can, however, be deduced from experiment if ΔH_{ads} for at least one molecule in a homologous series is known. Thus, the x for ReO_3Cl was obtained by setting the calculated interaction energy (from Table 3.1) to the experimental $\Delta H_{ads}(ReO_3Cl)$ = -61 kJ/mol. Assuming then the proportionality between x and molecular size, $\Delta H_{ads}(TcO_3Cl)$ = -48.2 and ΔH_{ads} (BhO_3Cl) = -78.5 kJ/mol were defined using the calculated *E(x)* of Table 3.1. The obtained adsorption enthalpies indicate that volatility changes as $TcO_3Cl > ReO_3Cl > BhO_3Cl$. The predicted sequence and the ΔH_{ads} were in excellent agreement with experiment [22], as will be shown in Section 4.2.2.

Analogously, ΔH_{ads} for HsO_4 was predicted [64] using a molecule-slab interaction model according to which the energy of the van der Waals interaction of the molecule with the quartz surface is expressed as

$$E(x) = -\frac{3}{16}\left(\frac{\varepsilon-1}{\varepsilon+2}\right)\frac{\alpha_{mol}}{\left(\frac{1}{h\nu_{slab}}+\frac{1}{h\nu_{mol}}\right)x^3} \tag{13}$$

where $h\nu$ denotes roughly IP of the molecule and slab (quartz), and ε is the dielectric constant of the latter. The calculated contributions to *E(x)* between MO_4 (M = Ru, Os, and Hs) and various types of surfaces are shown in Table 3.2. Using the same technique to define x as that used in the case of the group-7 oxychlorides, i.e. by setting the interaction energies from Table 3.2 equal to the experimentally known ΔH_{ads} (OsO_4) = -38 ± 1.5 kJ/mol, $\Delta H_{ads}(RuO_4)$ = -40.4 ± 1.5 kJ/mol and $\Delta H_{ads}(HsO_4)$ = -36.7 ± 1.5 kJ/mol were obtained. Consequently, the volatility of group-8 tetroxides in the particular experiments was expected to change as $RuO_4 < OsO_4 \leq HsO_4$ [64]. This sequence would be in accord with the idea of increasing volatility with increasing covalence of the compounds. Results of the experimental investigations in comparison with these predictions are discussed in Section 4.2.3.

Table 3.2. The DFT calculated polarizabilities (α) and ionisation potentials (IP), as well as contributions to the interaction energy $E(x)$ between MO_4 (M = Ru, Os and Hs) and a) pure quartz surface; b) surface covered with O_2; c) surface with an effective charge Qe. (From [64]).[a]

Molecule	$10^{24}\alpha$ (cm^3)	IP (eV)	α-$\alpha(SiO_2)$ $E10^{24}x^3$ (eV cm^3)	α-$\alpha(O_2)$ $E10^{24}x^3$ (eV cm^3)	α-Qe $E10^{32}x^4$ (eV cm^4)
RuO_4	6.48	12.15	4.73	5.31	10.01
OsO_4	5.96	12.35	4.48	4.75	9.41
HsO_4	6.26	12.28	4.63	4.90	9.73

[a] The calculated values are in very good agreement with experimental values: $\alpha(OsO_4)$ = 6.3 cm^3, $IP(RuO_4)$ = 12.19 eV and $IP(OsO_4)$ = 12.35 eV (see references in [64]).

3.3 Solution chemistry of elements 104, 105 and 106

Complex formation is a property which can be studied experimentally by liquid-liquid extractions, or anion exchange separations. For a simple complex ML_n, the stability, or the cumulative complex formation constant, can be expressed as follows

$$\beta_n = [ML_n][M]^{-1}[L]^{-n} \tag{14}$$

(For cosequitive steps, constants K_i are used). Complex formation is known to increase in the transition element groups. The aim of the investigations has, therefore, been to establish whether this trend is continued with the heaviest elements.

If one molecular complex, ML_i, among many others is extracted into an organic phase, the distribution coefficient, K_d, is a good measure of its stability (β_i) and a sequence in the K_d values for a studied series reflects the sequence in stability of the complexes [105]. Thus, by predicting β_i, one can predict sequences in the extraction of complexes into an organic phase or their sorption by cation or anion exchange resins.

The complex formation of group-4 through 6 elements is usually accompanied by strong hydrolysis of cations and/or of complexes themselves [106]. The hydrolysis of cations is described as a process of a successive loss of protons

$$M(H_2O)_n^{z+} \Leftrightarrow MOH(H_2O)_{n-1}^{(z-1)+} + H^+ \tag{15}$$

In acidic solutions, hydrolysis involves the cation, anion, or both, and is competing with complex formation described by the following equilibrium

$$xM(H_2O)_{w^o}^{z+} + yOH^- + iL^- \Leftrightarrow M_xO_u(OH)_{z-2u}(H_2O)_wL_a^{(xz-y-i)+}$$

$$+ (xw^{\circ} + u - w)H_2O \tag{16}$$

3.3.1 Theoretical model for prediction of complex formation

For a reaction, like eq. (15),

$$\log K_i = -\Delta G^{r}/2.3RT \tag{17}$$

where ΔG^{r} is the free energy change of the reaction. To define it in a straightforward way, binding (or total) energies, of species in the left and right parts of equation (15) should be calculated. Since it is almost impossible to do it with sufficient accuracy for very large, highly coordinated aqueous species (see [93] as an example), the following model was suggested by Pershina [107-112].

In a fashion analogous to that of Kassiakoff and Harker [106,113], the following expression for the free energy of formation of the $M_xO_u(OH)_v(H_2O)_w^{(z-2u-v)+}$ species from the elements was adopted

$$\begin{aligned} &-\Delta G^{f}(u,v,w)/2.3RT = \\ &\sum a_i + \sum a_{ij} + \log P - \log(u!v!w!2^{w}) + (2u+v+1)\log 55.5 \end{aligned} \tag{18}$$

The first term on the right hand side of eq. (18), $\sum a_i$, is the non-electrostatic contribution from M, O, OH, and H_2O, which is related to the overlap population, OP. For a reaction,

$$\Delta \sum a_i = \Delta E^{OP} = k\,\Delta OP, \tag{19}$$

where k is an empirical coefficient. The next term, $\sum a_{ij}$, is a sum of each pairwise electrostatic (Coulomb) interaction

$$E^{C} = \sum a_{ij} = -B\sum_{ij} Q_i Q_j / d_{ij} \tag{20}$$

where d_{ij} is the distance between moieties i and j; Q_i and Q_j are their effective charges and $B = 2.3RTe^2/\varepsilon$, where ε is a dielectric constant. For a reaction, ΔE^{C} is the difference in E^{C} for the species in the left and right parts of a reaction. P in eq. (18) is the partition function representing the contribution of structural isomers if there are any. The last two terms are statistical: one is a correction for the indistinguishable configurations of the species, and the other is a conversion to the molar scale of concentration for

the entropy. $\sum a_{ij}$ and $\sum a_i$ for each compound are then calculated directly via Mulliken numbers implemented in the DS-DV or DFT methods (see Section 2.2). To predict $\log K_i$ or $\log \beta_i$ for transactinide complexes, coefficients k and B should be defined by fitting $\log K_i$ to experimental values for the lighter homologs, as it is shown in [110].

The advantage of this method is that there is no need to perform geometry optimisation in order to define trends in the complex formation or even approximate values of complex formation constants for homologous species. For the lighter elements, geometries and experimental bond lengths can be used where known, or their IR, provided the bond lengths are not known. For the transactinides, bond lengths can be calculated for some simpler molecules. Then by varying them in a reasonable interval for a particular complex in solution an error bar for predicted values can be obtained. This saves a lot of computing time and makes the work highly efficient. Using this model, hydrolysis and complex formation constants were predicted for a large number of aqueous compounds of group-4 through 6 elements [107-113] in excellent agreement with experiment (see Section 4.3). Results of these calculations and comparison with experiment have also shown the predominant contribution in ΔG^r to be a change in the electrostatic metal-ligand interaction energy, ΔE^C. Thus, just by calculating this term all the trends in the complex formation can correctly be predicted.

3.3.2 Element 104

Element 104 has been extensively studied experimentally. The accumulated experimental results have revealed quite a number of surprises and disagreements. Thus, it was not clear whether Rf is more or less hydrolysed than Hf, and there were often disagreements in the sequences for the K_d values of Zr, Hf and Rf in HF and HCl solutions obtained by ion exchange separations (see [19]).

Hydrolysis of group-4 elements and their complex formation were studied theoretically [111] using the model described in the previous section. The following reactions were considered: the first hydrolysis step

$$M(H_2O)_8^{4+} \Leftrightarrow MOH(H_2O)_7^{3+}, \tag{21}$$

the step-wise fluorination process

$$M(H_2O)_8^{4+} \Leftrightarrow MF(H_2O)_7^{3+} \ldots \Leftrightarrow \ldots MF_3(H_2O)_5^{+} \ldots \Leftrightarrow \tag{22a}$$

$$MF_4(H_2O)_4 \Leftrightarrow \ldots MF_5(H_2O)^{-} \Leftrightarrow MF_6^{2-}, \tag{22b}$$

and the chlorination processes

$$M(H_2O)_8^{4+} + 6HCl \Leftrightarrow MCl_6^{2-} \quad (23)$$

The DFT calculated E^C for the complexes indicated in eqs. (21-23) are given in Table 3.3. The following trend in hydrolysis for the group-4 elements (reaction 22) was obtained based on the ΔE^C values:

$$Zr > Hf > Rf \quad (24)$$

The first hydrolysis constant $\log K_{11}(Rf) \approx -4$ was then defined using the data of Table 3.3 (first two lines) by fitting eq. (18) with unknown k and B (eqs. 19 and 20) to experimental values of log K_{11} for Zr and Hf (see ref. [111]).

Table 3.3. Calculated Coulomb contribution to the binding energy, E^C (in eV), for various complexes of Zr, Hf and Rf. (From [111]).

Complex	Zr	Hf	Rf
$M(H_2O)_8^{4+}$	-53.36	-52.09	-50.93
$MOH(H_2O)_7^{3+}$	-58.05	-56.70	-55.04
$MF(H_2O)_7^{3+}$	-53.36	-52.07	-50.53
$MF_2(H_2O)_6^{2+\,a}$	-50.40	-49.14	-47.38
$MF_2(H_2O)_6^{2+\,b}$	-49.77	-48.56	-46.79
$MF_3(H_2O)_5^{+}$	-45.44	-44.20	-42.32
$MF_4(H_2O)_4$	-37.50	-36.25	-34.41
MF_4 (T_d)	-12.79	-12.36	-11.61
MF_6^{2-}	-2.59	-1.18	0.23
MCl_4 (T_d)	-5.37	-4.26	-3.28
MCl_6^{2-}	-1.21	0.41	2.13

[a] *cis*-position, [b] *trans*-position of F atoms.

For various fluorination and chlorination reactions (22-23) taking place at different acid molarities, the calculated ΔE^C show the following. For the cation exchange separations (CIX) performed at $< 10^{-2}$ M HF, i.e., for the extraction of the positively charged complexes, the K_d values will have the following trend in group 4

$$Zr \leq Hf < Rf \quad (25a)$$

This is caused by the decreasing trend in the formation of the positively charged complexes according to eq. (22a)

$$Zr \geq Hf > Rf \quad (25b)$$

(For the formation of positively charged complexes from complexes with a higher charge, eq. 22a, the sequence in the K_d values is opposite to the sequence in the complex formation, since complexes with a lower charge are worse sorbed on the CIX resin than those with a higher charge).

For the formation of anionic complexes separated by the anion exchage (AIX) resins, the trend becomes more complicated depending on pH, i.e., depending on whether the fluorination process starts from hydrated or hydrolyzed species. Thus, for experiments conducted in 10^{-3}-10^{-1} M HF (where some hydrolyzed or partially fluorinated species are present), the trend for the formation of the anionic MF_6^{2-} (eq. 23b) is reversed within the group-4 elements:

$$Rf \geq Zr > Hf \tag{26}$$

This trend should then be experimentally observed in the K_d values. For the AIX separations at 4-8 M HCl (chlorination process according to eq. 23, no hydrolysis), the trend in the complex formation and K_d values will definitely be continued with Rf

$$Zr > Hf > Rf \tag{27}$$

The predicted sequences are in agreement with experiments on the CIX and AIX separations of Zr, Hf and Rf, as will be discussed in Section 4.3.

3.3.3 Element 105

A motivation for the theoretical study of the complex formation of element 105 was its unexpected behaviour in extractions into triisoctyamine (TIOA) from mixed HCl/HF solutions [114]: Db was extracted similarly to Pa and not to Ta. Therefore, a theoretical study of the complex formation in pure HF, HCl and HBr solutions was undertaken in an attempt to understand this behaviour [108,109].

In HCl solutions, a large variety of complexes, such as $M(OH)_2Cl_4^-$, $MOCl_4^-$, $MOCl_5^{2-}$ and MCl_6^- (M = Nb, Ta, Db and Pa) can be formed with different degrees of hydrolysis. Their formation is described in a general form by the following equilibrium

$$M(OH)_6^- + iL^- \Leftrightarrow MO_u(OH)_{z-2u}L_i^{(6-i)-} \tag{28}$$

To predict stability of those complexes of Nb, Ta, Db and Pa, calculations of the electronic structures were performed using the DFT method [108,109]. As a result, the ΔE^C for reaction (28) are given in Table 3.4.

Table 3.4. ΔE^C (in eV) for the formation of complexes of Nb, Ta, Db and Pa. (From [108]).

Metal	$M(OH)_2Cl_4^-$	$MOCl_4^-$	MCl_6^-
Nb	13.56	18.40	19.57
Ta	14.32	19.80	20.78
Db	14.29	19.67	20.46
Pa	11.68	16.29	17.67

The data of Table 3.4 show the following trend in the complex formation of group-5 elements: Pa >> Nb > Db > Ta. Taking into account the work of transfer of the complexes between the phases, the following trend has been predicted for the extraction of group-5 anions by an anion exchanger

$$Pa >> Nb \geq Db > Ta \tag{29}$$

The calculations predicted the following sequence in the formation of various types of complexes as a function of the acid concentration (Table 3.4)

$$M(OH)_2Cl_4^- > MOCl_4^- > MCl_6^- \tag{30}$$

in full agreement with experimental results for Nb, Ta and Pa. The calculations have also reproduced the sequence in the formation of ML_6^- (L = F, Cl, and Br) as a function of the ligand, as the data of Table 3.5 show.

Table 3.5. ΔE^C (in eV) for reaction $M(OH)_6^- \Leftrightarrow ML_6^-$, where M = Nb, Ta, Db and Pa, and L = F, Cl and Br [108,109].

Complex	F	Cl	Br
NbL_6^-	12.20	19.57	21.40
TaL_6^-	12.69	20.78	22.63
DbL_6^-	12.38	20.46	22.11
PaL_6^-	12.19	17.67	19.91

The theoretical investigations [108,109] have shown that the trend in the complex formation (eq. 29) and extraction known for Nb, Ta and Pa turned out to be *reversed* in going to Db. This could not be predicted by any extrapolation of properties within the group, but came as a result of considering real chemical equilibria and calculating relativistically the electronic structure of the complexes. According to these results, a recommendation was made to conduct the AIX separations in pure HCl or HF solutions, and the sequences given in eqs. (29-30) were predicted. These were, indeed, fully confirmed by experiments, as will be shown in Section 4.3.2.

3.3.4 Element 106

Experiments on the CIX separations of element 106 from 0.1 M HNO_3 solutions have shown that Sg was not eluted from the CIX column, in contrast to Mo and W [115]. This non-tungsten-like behaviour of Sg was tentatively attributed to its lower tendency to hydrolyse (deprotonate) compared to that of W. To interpret the behaviour of Sg in these experiments and to predict its hydrolysis at various pH values, free energies of the following protonation reactions for Mo, W and Sg

$$MO_4^{2-} \Leftrightarrow MO_3(OH)^- \Leftrightarrow MO_2(OH)_2(H_2O)_2 \Leftrightarrow$$

$$MO(OH)_3(H_2O)_2^+ \Leftrightarrow M(OH)_4(H_2O)_2^{2+} \Leftrightarrow \ldots \Leftrightarrow M(H_2O)_6^{6+} \qquad (31)$$

were considered theoretically. Using the model described above, ΔE^C for the consecutive protonation steps were calculated using the DFT method [110] and are shown in Table 3.6.

Table 3.6. ΔE^C (in eV) for the step-wise protonation of MO_4^{2-} (M = Mo, W and Sg) [110].

Reaction	ΔE^C		
	Mo	W	Sg
$MO_4^{2-} + H^+ \Leftrightarrow MO_3(OH)^-$	-12.28	-13.13	-12.96
$MO_3(OH)^- + H^+ + 2H_2O \Leftrightarrow MO_2(OH)_2(H_2O)_2$	-21.43	-22.08	-21.61
$MO_2(OH)_2(H_2O)_2 + H^+ \Leftrightarrow MO(OH)_3(H_2O)_2^+$	-5.84	-6.35	-6.65
$MO(OH)_3(H_2O)_2^+ + H^+ \Leftrightarrow M(OH)_4(H_2O)_2^{2+}$	-0.43	-0.76	-1.23
$M(OH)_4(H_2O)_2^{2+} + 4H^+ \Leftrightarrow \ldots M(H_2O)_6^{6+}$	41.97	38.71	37.11

The data of Table 3.6 show that for the first two protonation steps, the trend in group 6 is reversed:

$$Mo < Sg < W \qquad (32)$$

For the further protonation process, the trend is continued with Sg, so that

$$Mo < W < Sg \qquad (33)$$

Thus, the same reversal in trend is predicted for the protonation of oxyanions of the group-6 elements as that for the complex formation of the group-4 and -5 elements. The predicted trends in log$K$ are in agreement with experiments on Mo and W at various pHs [106]. For the protonation/hydrolysis of positively charged complexes, the trend (33) is in line with the experimental observations for Sg [115] (see Section 4.3.3). By fitting log$K$ of eq. (18) for

the reactions shown in Table 3.6 to the known experimental values for Mo and W, coefficients k and B and then log$K$ were defined for Sg [110].

Even though the aqueous chemistry of elements heavier than 106 is very promising, theoretical studies have not yet been performed.

4. "ONE-ATOM-AT-A-TIME" CHEMISTRY

4.1 Experimental techniques

Because normal chemical analysis techniques are not usually applicable, special techniques have been developed to detect a single atom at a time, normally by measuring its radioactive decay. Typically, the longest-lived known isotope of the element is used which is not necessarily the isotope first discovered. A knowledge of the nuclear decay properties and a measurement technique which positively identifies that the detected decay arises from the element in question are required. Alpha-alpha correlation to a known daughter activity can provide such positive identification while detection of spontaneous fission usually does not.

The chemical procedures must be fast compared to the half-lives of the isotopes used in the studies and give the same results for a few atoms as for macro amounts. Chemical methods in which a single atom rapidly participates in many identical chemical interactions in two-phase systems which reach equilibrium quickly have proven to be valid. Then the results obtained from many identical experiments, each performed with only a single atom, can be added together to obtain statistically significant information about chemical behaviour [16,116]. Some methods which meet these requirements include ion-exchange and liquid-liquid extractions, and gas-chromatographic separations. The chemistry of Md and No was initially investigated using "atom-at-a-time" chemistry in which elutions from cation-exchange resins were performed to separate the individual actinides. These elements have since been produced in much larger quantities and it has been possible to verify that such "atom-at-a-time" results using ion-exchange techniques were valid. The comparison of the chemical properties of a new element of known Z with those of its homologs in the appropriate group in the periodic table as predicted by theoretical calculations or empirical trends is usually used to decide placement of the element in the corresponding chemical group.

Techniques have been devised for transporting atoms recoiling from the target in an accelerator beam to a collection site outside the radiation field where chemistry can be carried out within a few seconds, either manually or with computer-controlled automated systems. A variety of computer-

controlled automated systems for both aqueous and gas-phase chemistry has been developed to carry out the many repetitive experiments that are required to get statistically significant information. Several detailed reviews [19-21,117] are available.

4.1.1 Gas-phase chemistry

Both thermochromatographic and isothermal methods have been used to study gas-phase properties of the heaviest elements. These methods are particularly useful for short-lived isotopes because the lengthy process of evaporating liquid samples as required in most of the aqueous chemistry experiments is avoided. Gas-phase chromatographic methods permit determination of the adsorption enthalpy, ΔH_{ads}, by using correlations between measured properties such as temperature of adsorption and ΔH_{ads}. The latter was shown [118] to be linearly related to the sublimation enthalpy, ΔH_{sub}, which is used to compare the volatility with lighter homologs. Pioneering studies of the volatilities of the halides of elements 104 and 105 were carried out in the late 1960s and 1970s by Zvara *et al.* [17,119,120] using thermochromatographic separations. In this method, a longitudinal, negative temperature gradient is established along the chromatographic column through which a gas stream is conducted. It contains the volatile species of interest which deposit on the surface of the column according to their volatilities. Later, the deposition zones are determined from fission tracks registered in detectors positioned along the column. These fissions are then associated with specific deposition temperatures, which are then correlated with ΔH_{ads}. The advantage of this method is that production and separation of the detected species takes place very rapidly. It also has some disadvantages. Positions of the deposition zones are determined only after the experiments are finished. This makes the interpretation of the results very difficult because it is necessary to correct for the half-lives of the various species involved before their volatilities can be compared. Furthermore, real-time observation of the nuclear decay and the determination of the half-lives of the detected species is not possible. Another difficulty is that if only SF activity is measured in the experiments, it is difficult to prove what the atomic number of the detected species actually was since only the fission fragments are detected (see earlier discussion in Section 1.1). Relatively recently, investigations of Sg chemistry have also been performed using this technique [121].

More recent studies of gas-phase chemistry have used isothermal chromatographic systems such as the On-Line Gas Analyzer (OLGA) developed by Gäggeler *et al.* [122] and the Heavy Element Volatility Instrument (HEVI) [123] to compare the behaviour of the halides and

oxyhalides of elements 104 through 108 with those of their lighter homologs in groups 4 through 8 of the periodic table. In such systems the entire chromatographic column (usually quartz) is kept at a constant temperature. Volatile species pass through the column and undergo numerous sorption/desorption steps. Retention time is indicative of volatility at the given isothermal temperature. A series of temperatures is run and the chemical yield of the volatile species is studied as a function of temperature. At the temperature at which 50% of the plateau yield is observed, $T_{50\%}$, the retention time is equal to one half life, and can be used as a relative measure of volatility. A Monte Carlo program taking account of all the experimental conditions is used to deduce the ΔH_{ads} for the measured species. Examples of those curves are shown in Figures 4.1-4.4 and discussed in Section 4.2.

4.1.2 Solution chemistry

The Automated Rapid Chemistry Apparatus (ARCA) and the microcentrifuge system SISAK are two automated systems that have been used recently in studies of aqueous systems. The ARCA can perform rapid, repeated, high-pressure liquid chromatography column experiments on the seconds time scale, but the same experiment must often be repeated several hundred or several thousand times in order to obtain statistically significant results for the heaviest elements whose production rates are very small. The separations usually involve AIX/CIX exchange column separations. The absorbed fractions are eluted from the chromatography columns, and elution curves are obtained (e.g., Figure 7 in ref. [19]). The collected liquid samples must then be dried prior to measurement of α–emission and SF decay with high resolution solid-state detectors, thus limiting detection to nuclides with half-lives longer than ~30 seconds although longer-lived daughter products can be used to infer properties of the parent element. The distribution coefficient, K_d, is then determined from the retention time (related to the peak of the elution curve) as

$$K_d = (t_r - t_0)\frac{V}{M} \tag{34}$$

where t_r is retention time, t_0 - column hold-up time due to the free column volume, V - flow rate of the mobile phase, and M - mass of the ion exchanger. The ARCA system was used for successful separations of elements 104 through 106 (see reviews [18-20]). There is a further development of this technique, the so called three-column technique [124]. It has the advantage of measuring longer lived daughter products of the

transactinides without preparing numerous samples for the short-lived mother.

The SISAK system performs liquid-liquid extractions on a few second time scale and has been coupled to a continuously flowing liquid scintillation system to provide continuous separation and measurement of α–α correlations and SF for nuclides as short as a few seconds [125]. This permits chemical studies of shorter-lived nuclides, but the detection energy resolution is not as good. However, some physical method of rapid pre-separation by an instrument such as the Berkeley Gas-filled Separator (BGS) has been shown to be highly beneficial in studies of elements 104 and 105 [126] and should permit much more rapid and detailed studies of the chemical properties of these elements as well as still heavier elements.

4.2 Results of gas-phase chemistry experiments

4.2.1 Elements 103-106

As is indicated in Section 3.1.1, the $7s^27p_{1/2}$ ground state electronic configuration of atomic Lr might exhibit p-character because of a relativistically stabilized $7p_{1/2}$ electron. Therefore, experiments were conducted [127] to "detect" the p-character of atomic Lr. The idea was that if the configuration of Lr with a $7p_{1/2}$ electron exists as the ground state, this would influence the chemical properties and it might exhibit high volatility in the elemental state as do the p elements In and Tl. Accordingly, estimates were made for ΔH_{sub} of Lr(d) (Lr in the $7s^26d$ configuration) of -350 to -410 kJ/mol and Lr(p) of -135 kJ/mol [128]. Based on these predicted differences in ΔH_{sub} a procedure for separation of Lr from other actinides using high-temperature (1000 °C) gas-phase chromatography in quartz columns was devised [127]. These experiments indicated that Lr was not more volatile than the other actinides (which were strongly adsorbed on the column) and a lower limit for ΔH_{sub} for Lr of -290 kJ/mol, significantly lower (more negative) than the expected values for Lr(p). However, the result did not exclude the existence of the $7s^27p$ ground state because when the atom interacted with the surface of the column, it might possibly have reached its next, $7s^26d$, excited state, which is separated by only 0.24 eV from the ground state and thus lose its "p" character.

The first experiments with Rf were initially designed to chemically identify a 0.3 s Rf isotope by observing its SF decay, but it could not be found and the SFs detected were attributed to the longer-lived 3 s ^{259}Rf although its SF branch is now known to be < 5%. It was investigated using thermochromatography [17,118-120] and Rf was reported to form the tetrachloride, $RfCl_4$, by analogy with Hf and its deposition zone on the

chromatography column coincided with that of Hf [129]. Both elements were found to be more volatile than chlorides of actinides (which deposited in the zone at the beginning of the column). However, it has not been established that these fissions were due to Rf.

Since that time, quite a number of experiments has been conducted for various halides and oxyhalides of Rf. We refer the reader to the reviews of Türler, Gäggeler and Kratz [130,21,19]. The latest gas-phase experiments on Rf were conducted at the Lawrence Berkeley National Laboratory (LBNL), using the isothermal chromatography system HEVI [123,131]. ^{261}Rf was produced via the ^{248}Cm(^{18}O,5n) reaction with a half-life of 75 ± 7 s and behaviour of its chlorides and bromides was compared with those of short-lived Hf and Zr isotopes measured in the same system. The activity recoiling from the target was attached to aerosols of either KCl, MoO_3, or KBr in a flowing helium transport system and the aerosols containing the activity were deposited at the beginning of HEVI on a quartz wool plug at 900 °C and chlorinated or brominated with the appropriate halide gas mixture. The volatile species exiting the isothermal column enter a recluster chamber where the gas stream was cooled via adiabatic expansion and the activity was reattached to new aerosols and transported to an appropriate detector for measurement. The ^{261}Rf could be positively identified by its characteristic α-α decay chain and the Zr and Hf isotopes were identified via γ-spectroscopy.

Under those conditions, Rf obviously produced a volatile $RfCl_4$ which had 50% of the relative yield at about the same temperature as $ZrCl_4$ indicating their similar volatilities. $HfCl_4$ was unexpectedly less volatile which could be associated with the formation of $HfOCl_2$. The relative yield curves for the Zr, Hf and Rf-chlorides are shown in Figure 4.1.

The analysis of the data using the Monte Carlo model [123] gives the following ΔH_{ads} for group-4 chlorides on SiO_2: -74 ± 5 kJ/mol for Zr, -96 ± 5 kJ/mol for Hf, and -77 ± 6 kJ/mol for Rf (Figure 4.2). $RfCl_4$ shows the about the same volatility as $ZrCl_4$ within the error bars as expected from relativistic calculations [96]. "Non-relativistic" extrapolations give lower volatility for $RfCl_4$ (see [130]). Experiments with the bromides [131] show that they are generally less volatile than the chlorides and that $RfBr_4$ is more volatile than $HfBr_4$ (Figure 4.2), in agreement with theoretical predictions [29].

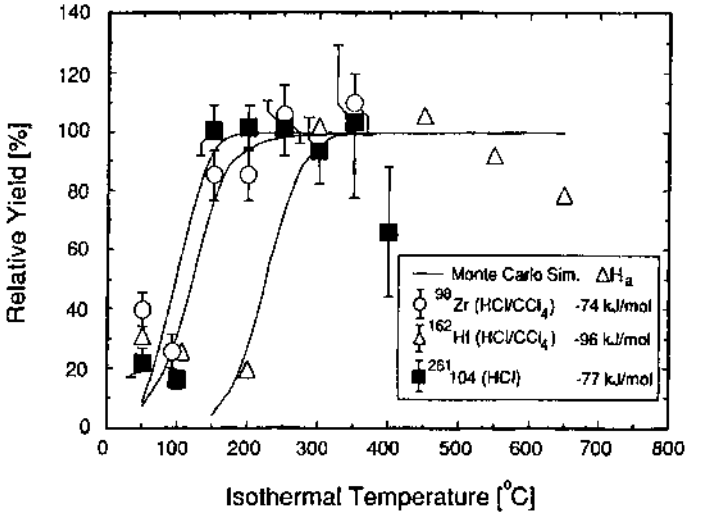

Figure 4.1. The relative yield curves are shown for Zr, Hf and Rf-chloride molecules. (The solid lines drawn through the data points are from the Monte Carle simulations). (From [130]).

First experiments on the volatility of element 105 chlorides and bromides were performed with 1.8 s ^{261}Db by Zvara *et al.* using the same set up as for Rf [119,120]. Later the OLGA isothermal gas-chromatography system, was used at PSI to study volatility of the bromides of Nb, Ta and Db [122,132, 133]. According to theoretical predictions based on the DS-DV relativistic calculations [102], $DbBr_5$ was expected to be more volatile than $TaBr_5$. However, a lower volatility of Db was observed in those experiments and was attributed to the formation of $DbOBr_3$. Relativistic calculations [103] have shown a stronger tendency for Db to form oxyhalide compounds than Nb and Ta. In later experiments with the chlorides of group-5 elements two steps have indeed been observed in the yield curve for Db. These are probably associated with the formation of $DbCl_5$ and $DbOCl_3$ [132]. It was also found that $DbOCl_3$ is less volatile than $DbCl_5$ and that the dubnium chlorides are more volatile than the bromides [130,134]. This is also in agreement with the theoretical predictions [102,103] as discussed in Section 3.2.2.

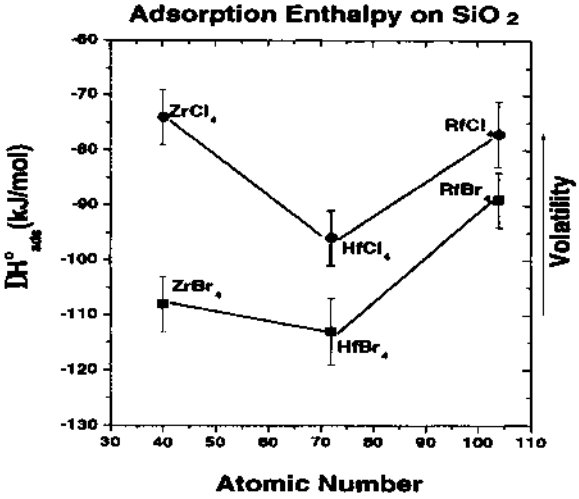

Figure 4.2. Measured adsorption enthalpies for Zr, Hf and Rf-chlorides and bromides on the SiO_2 surface. (From [131]).

First attempts to chemically characterize element 106 using 0.9 s ^{263}Sg produced via the $^{249}Cf(^{18}O,4n)$ reaction, were reported by researchers at Dubna between 1992 and 1996 [121,135] using the fast on-line thermochromatography system in which the surface of the quartz column served as track detector for spontaneous fissions. Flowing argon gas carried the thermalized recoils to the entry to the quartz column where they were treated with air saturated with $SOCl_2$ to produce the oxychlorides and then transported through the 120-cm long column with a temperature gradient between abou 400 °C and room temperature. Fission tracks attributed to Sg were observed at a lower deposition temperature (~160 °C) than its lighter homolog W (~250 °C) which was identified by γ-spectroscopy. This difference was attributed to the presence of two different chemical species, SgO_2Cl_2 and $WOCl_4$, with the latter resulting from conversion of the originally formed WO_2Cl_2 into $WOCl_4$ due to the longer half-life of the W isotope. Later, a critical analysis of the experimental conditions and the assignment of the observed SFs by Kratz [19] concluded that the interpretation of the SF events as being due only to Sg "falls short of demonstrating that other sources of SF tracks were rigorously excluded".

Around the same time, an international collaboration centered around nuclear chemistry groups at the GSI, Darmstadt, the University of Mainz, and the PSI, Villigen, began working on detection of Sg using a

thermochromatography system with an external detection system. This was different than the Dubna internal detection technique and needed longer-lived isotopes. Fortunately, in 1994 a Dubna/Livermore group reported discovery of $^{266,265}Sg$ with half-lives estimated to be (10-30 s) and (2-30 s), respectively, formed in $^{248}Cm(^{22}Ne,4n,5n)$ reactions [136,137]. The first chemical experiments on Sg were gas-phase experiments with OLGAIII conducted in 1995 and 1996 using these reactions with ^{152}Gd in the target to produce also W, so it could be measured at the same time as Sg [138,139]. The oxychlorides of the recoiling products were formed by treatment with Cl_2, $SOCl_2$ and O_2. Two decay chains attributed to ^{265}Sg and one to ^{266}Sg were observed and the half-lives were measured to be 21 s and 7 s for ^{266}Sg and ^{265}Sg, respectively [140]. It was possible to show [138,139] that Sg formed a volatile oxychloride, presumably SgO_2Cl_2, of lower or equal volatility to the WO_2Cl_2, consistent with DS-DV calculations [101]. The relative yield curves obtained for the Sg oxychloride along with its homologs Mo and W are shown in Figure 4.3.

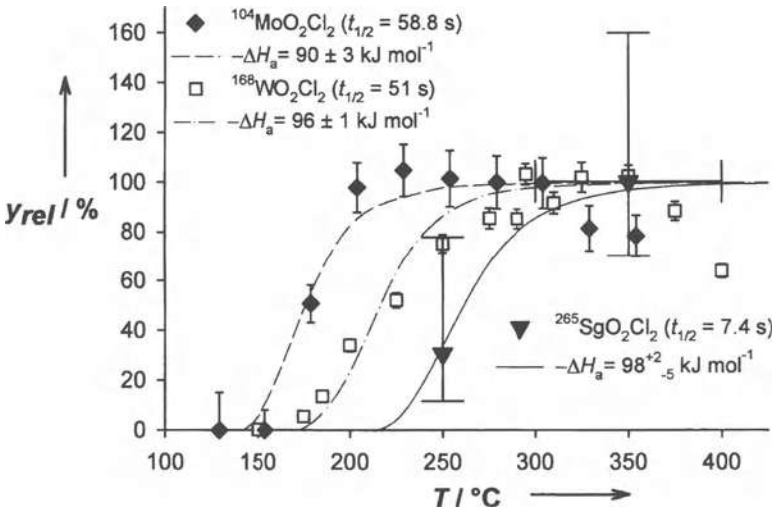

Figure 4.3. Relative yields vs. isothermal temperature for UCl_6 (full lozenges), MoO_2Cl_2 (open hexagons), WO_2Cl_2 (full squares) and SgO_2Cl_2 (open triangle). (From [139]).

The position of the SgO_2Cl_2 curve was in agreement with the ΔH_{ads} estimated from the experimental data for the adsorption of MoO_2Cl_2 and WO_2Cl_2. The resulting volatility sequence was $MoO_2Cl_2 > WO_2Cl_2 > SgO_2Cl_2$, with ΔH_{ads}

values deduced from Monte Carlo simulations as -90 kJ/mol, -96 kJ/mol and -100 kJ/mol, respectively. Thus, it was shown that Sg forms oxyhalides analogous to those of Mo and W, while U forms a different type of a molecule, UCl_6, under these experimental conditions and has a higher volatility (ΔH_{ads} of -91 kJ/mol). The experimentally observed formation of SgO_2Cl_2 and the decreasing trend in volatility Mo > W > Sg was in agreement with theoretical predictions and recommendations [101] as discussed in Section 3.2.2.

Recently, it was shown that Sg forms volatile oxide hydroxide by analogy with the group-6 elements Mo and W, as well as with U [141]. Using high temperature on-line isothermal gas chromatography, Sg and W were studied in the O_2-$H_2O(g)/SiO_2(s)$ system. The 21 s ^{266}Sg nuclide was produced in the same reaction as described above (^{248}Cm + ^{22}Ne) and reaction products were transported by a $He(MoO_3)$-jet into the chromatography apparatus. Group-6 element oxide hydroxides volatile at temperatires above 1000 K were formed at 1325 K by adding oxygen as reactive gas. ^{266}Sg was unambiguously detected after gas chromatographic separation by measuring ^{266}Sg-^{262}Rf mother-daughter α-SF correlations.

4.2.2 Element 107 (bohrium)

The recently discovered isotope, 17 s ^{267}Bh [142], produced in the ^{249}Bk (^{22}Ne,4n) reaction was used to compare the volatility of the oxychlorides of Bh with those of its group-7 homologs Re and Tc in on-line isothermal gas chromatographic experiments using the OLGA III [22]. The recoiling reaction products were sorbed on carbon particles suspended in He gas and continuously transported a distance of a few meters to the OLGA where they were treated with HCl and oxygen to produce the volatile oxychlorides and conducted into the quartz chromatographic column. The molecules passing through the column were reattached to new aerosols and then deposited stepwise on foils on the circumference of a rotating wheel where their decay by α-emission and SF was measured to identify them positively as ^{267}Bh by their decay sequences to known daughter activities. Six such decay chains were observed over nearly a month of irradiation time. The relative yields vs. isothermal temperature curves are shown in Figure 4.4.

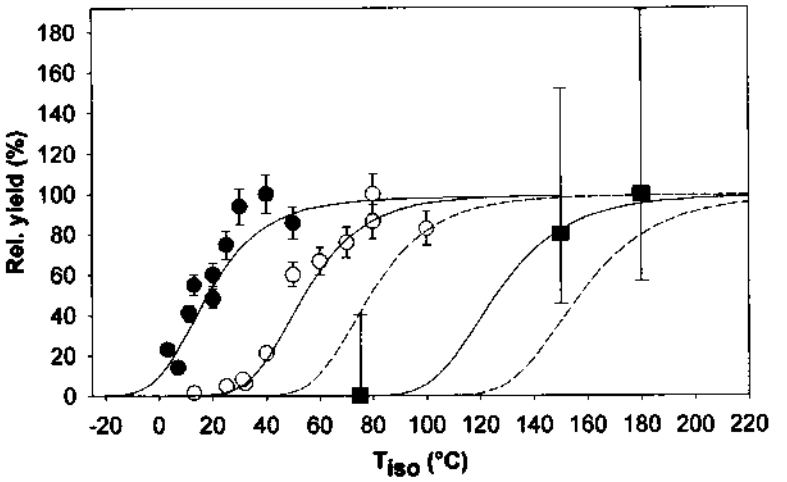

Figure 4.4. The relative yields of TcO_3Cl (black circles), ReO_3Cl (open cicrles) and $^{267}BhO_3Cl$ (black squares) as a function of the isothermal temperatures (T_{iso}) (From [22]).

A Monte Carlo program was used to deduce ΔH_{ads} of -75 kJ/mol with a 68% confidence interval of –66 kJ/mol to –81 kJ/mol for BhO_3Cl, the most probable oxychloride under these conditions. The values for the Tc and Re oxychlorides studied under the same conditions are -51 kJ/mol and -61 kJ/mol, respectively. Thus, BhO_3Cl shows a stronger adsorption interaction with the chlorinated quartz surface then either the TcO_3Cl or ReO_3Cl and is more similar to Re than to Tc. This is in very good agreement with the calculations [63] where ΔH_{ads} of –48.2 kJ/mol for Tc and –78.5 kJ/mol for Bh were predicted giving a volatility sequence of TcO_3Cl > ReO_3Cl > BhO_3Cl (see section 3.2.3).

4.2.3 Element 108 (hassium)

An international team of scientists recently performed the first studies of the chemistry of hassium, the heaviest element to date whose chemistry has been successfully investigated [23]. The $^{248}Cm(^{26}Mg,5n)$ reaction whose estimated production cross section is only ~6pb was used to produce ~10 second ^{269}Hs using three ^{248}Cm targets positioned on a rotating wheel to increase the production rate. A cryo-thermochromatography system was developed for separating and detecting Hs as a volatile oxide similar to that of its expected group-8 homolog, osmium. The recoiling Hs atoms were treated with oxygen at high temperature to produce the tetroxide which was then carried in helium through a narrow channel formed by opposing rows of semiconductor diodes with a negative temperature gradient from room temperature to -176 °C. Based on detection of three decay chains attributable

to ^{269}Hs and two to a new nuclide ^{270}Hs [143], it was found that HsO_4 condenses at a higher temperature than OsO_4 under similar conditions, indicating that the Hs oxide is less volatile. According to the prediction [64], the ΔH_{ads} for the Hs and Os oxides should be nearly the same. This was also expected from the extrapolation of this property within the group. Because so few events were detected it is premature to say whether or not the experimental data are in disagreement with the predictions.

4.2.4 Summary of the gas phase chemistry study

Observed trends in volatility of groups 4 through 8 compounds compared to the theoretical predictions are summarized in Table 4.1.

Table 4.1. Trends in volatility of the heaviest element compounds and their lighter homologs in chemical groups.

Group	Compounds	Theoretically predicted	Ref.	Experimentally observed	Ref.
4	MCl_4, MBr_4	Hf < Rf	29	Hf < Rf	123,131
5	ML_5 (L = Cl, Br)	Nb < Ta < Db	102,103	($DbOBr_3$)	132
		$DbCl_5$ > $DbOCl_3$	102,103	$DbCl_5$ > $DbOCl_3$	132,120
6	MO_2Cl_2	Mo > W > Sg	101	Mo > W > Sg	138,139
7	MO_3Cl	Tc > Re > Bh	63	Tc > Re > Bh	22
8	MO_4	Ru < Os ≤ Hs	64	Os > Hs	23

4.3 Results of solution chemistry experiments

Chemical properties of aqueous solution species of elements 104 through 106 have been studied using aqueous chemistry separation techniques as described in Section 4.1.2 and the results have been summarized in a number of previous publications [18,19,20,117].

4.3.1 Element 104

The paper of Kratz [19] gives an excellent overview of experimental details and recent results. Therefore, we will discuss mostly those cases where theoretical predictions were especially important.

The first experimental results of the CIX separations [144] have already shown that Rf is a homolog of Zr and Hf: The elution of those elements by 6 M HCl demonstrated that the chloride complexation of Rf is similar to that of Hf and much stronger than that of the actinides. This is in agreement with the relativistic calculations [28,111] showing that the electronic structure, as well as formation enthalpies of the Rf complexes, are very similar to those of Hf and Zr (see Table 3.3.).

As was mentioned in Section 3.3.2, results of later experiments on the extraction of Zr, Hf and Rf from HF and HCl solutions disagreed concerning trends in the extraction sequences (see [19]). CIX separations of Zr, Hf and Rf from HF solutions have given the following trend in K_d values: Zr ≤ Hf < Rf << Th (Figure 4.5). That means that the complex formation in group-4 elements according to reaction (22a) changes as Zr ≥ Hf > Rf >> Th (see comments on page 29). In AIX separations, although Rf and Hf behaved similarly, they were much less absorbed on the AIX column than Zr [145]. In contrast to the work of Strub *et al.* [145], results of the AIX separations of the group-4 elements from mixed 0.02 M HF and 0.3-0.4 M HCl solutions have shown the K_d of Rf to be slightly larger than those of Zr and Hf [146]. Recent AIX separation experiments [147] of group-4 elements from aqueous 4-8 M HCl solutions have shown an inverse sequence in K_d values (and in the complex formation): Rf > Zr > Hf. However, the TBP extraction of group-4 elements from 8 M HCl, showed K_d of Rf to be in between those of Zr and Hf: Zr > Rf > Hf [148].

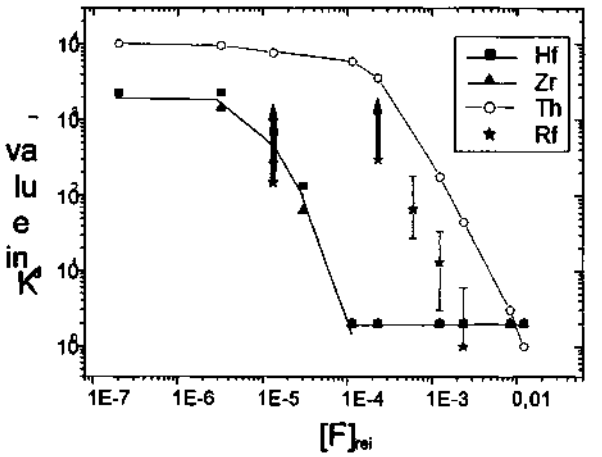

Figure 4.5. Sorption of Zr, Hf, Th and Rf on the CIX resin (Aminex A6) in 0.1 M HNO_3 at various HF concentrations. (From [145,149]).

The sequence in the K_d values Zr ≤ Hf < Rf obtained in the CIX separations from HF solutions (Figure 4.5) [145,149] is in agreement with the theoretically predicted trend shown by eq. (25a) (Section 3.3.2). For the AIX separation from HF solutions, the theoretically predicted trend in the complex formation and K_d (eq. 26) is in agreement with experiments [146] showing that it becomes reversed at these specific experimental conditions. This could not be predicted by any extrapolation of the properties within the group, but came as a result of relativistic calculations of the complex

formation equilibria. Taking into account those theoretical predictions, the weaker sorption of Rf from HF solutions of > 10^{-3} M on the AIX column [145] is explained (and also shown by additional experiments) by a strong competition between NO_3^- and Rf complexes for adsorption on the active resin sites. A reversal of the trend in the extraction of group-4 elements from HCl solutions by TBP [148] is also consistent with the theoretical trend for the formation of the MCl_4 species (see [111]), though some further calculations for the $MCl_4(TBP)_2$ complexes have to be performed.

Another open question in the chemistry of group-4 elements was that of hydrolysis of Rf. A conclusion about stronger hydrolysis of Rf in comparison with that of Zr was drawn in the study of sorption of group-4 elements and Th on cobalt ferrocyanite surfaces [150], while results of the AIX separations [151] came to a different conclusion and showed the following trend in hydrolysis: Zr > Hf > Rf. The theoretical results [111] agreed with the conclusion [151] that the hydrolysis of Rf was weaker. In addition, the theoretically estimated first hydrolysis constant $\log K_1 = -4$ for Rf is close to the value of -2.6 ± 0.7 obtained from the linear correlation between experimentally measured complex formation constants for the $M(TTA)_x$ (TTA is thenoyltrifluoroacetone) and hydrolysis constants of group-4 elements [151].

4.3.2 Element 105

The first aqueous chemistry of element 105 using 34 s ^{262}Db was performed manually in a series of some 800 identical liquid-liquid extractions requiring ~50 seconds for the entire procedure [152]. These experiments showed that element 105 behaved more like the lighter homolog Nb than like Ta, but no evidence was found for the 3+ oxidation state that had sometimes been predicted based on strong stabilization of the $7s^2$ electrons due to relativistic effects. The instability of lower oxidation states was, indeed, shown by later relativistic calculations and predicted redox potentials [94] (see Chapter 3.1.3).

Later, a larger series of ARCA II separations were conducted to investigate the extraction behaviour of group-5 elements including Db (Ha at that time) and Pa by TiOA from HF/HCl [114]. Element 105 showed a striking non-Ta-behaviour, while it was close in behaviour to Nb and Pa. This result has given impetus to the theoretical investigations described in Section 3.3.3. Based on results of those investigations, it was recommended that the experiments should be repeated separately containing with HF and HCl, as well as HBr solutions. The trends were predicted as shown in eqs. (30-31) [108,109]. Accordingly, the amine separations of the group-5 elements were systematically redone by Paulus *et al.* [153]. The result of those separations from HCl solutions is shown in Figure 4.6.

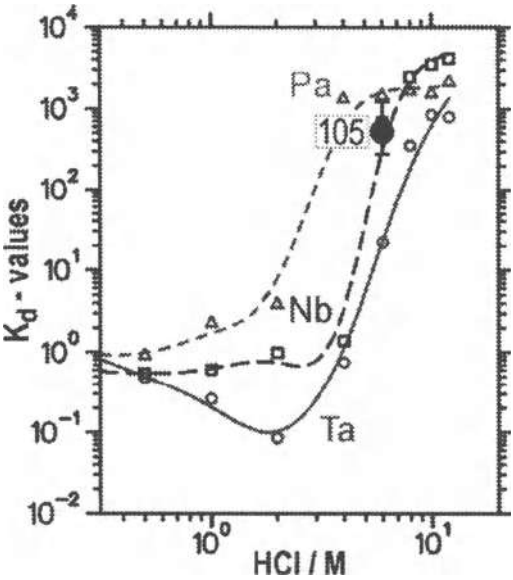

Figure 4.6. Distribution coefficients of Pa, Nb and Ta in the system Aliquat 336/HCl. The position of K_d for Db in 6 M HCl is indicated with the bar. (From [153]).

Thus, the reversed extraction sequence Pa >> Nb ≥ Db > Ta has been established exactly as theoretically predicted by eq. (29). That was the first time that predictions of extraction behaviour of the heaviest elements based on quantum-chemical calculations were made, and also confirmed by specially designed experiments. Only by considering all possible equilibria in the aqueous phase including hydrolysis could this unexpected behaviour be predicted. Simple extrapolations of properties within the group would have shown the straightforward and, consequently, the wrong trend.

4.3.3 Element 106

The first aqueous chemistry experiments on Sg were conducted in 1997 [138,154] using ^{266,265}Sg produced by bombardment of a ^{248}Cm target with ^{22}Ne projectiles. The activity was transported to ARCA II where it was sorbed on chromatographic columns filled with the cation exchange resin Aminex A6. Then, the activity was eluted with 0.1 M HNO_3/5·10^{-4} M HF solution. In the eluted fraction, three α-α correlations were observed that were assigned to the decay of ^{261}Rf, as the decay product of ^{265}Sg. From this observation, it was concluded that for the first time, a chemical separation of Sg was performed in aqueous solutions and that Sg behaved as a typical hexavalent group-6 element (the behaviour of W under similar conditions was studied before) forming $SgO_2F_3^-$ or SgO_2F_2 by analogy with its Mo and

W homologs and different from the pseudo-homolog U which remained as UO_2^{2+} on the CIX column.

In order to check whether Sg could form SgO_4^{2-} which could not be detected in the first experiments, due to the presence of F ions, a new series of experiments were conducted in which Sg and W were eluted by 0.1 M HNO_3 without HF [115]. The results have shown that in the absence of HF, Sg was retained on the CIX column (no events were observed in the eluted fraction), while W was eluted from the CIX column. This non-W behaviour of Sg was tentatively attributed to its weaker tendency to hydrolyze.

This assumption was tested theoretically by considering hydrolysis of group-6 elements, as described in Section 3.3.4. The theoretical calculations [110] have indeed shown that hydrolysis of group-6 cations (the process opposite to the protonation) under these experimental conditions should follow the trend opposite to that of eq. (33). Thus, it was confirmed theoretically that between pH = 0 and 1 Sg is in the form of mono- or di-positively charged complexes and is retained on the CIX column, while W forms neutral complexes which were eluted. The theoretical predictions (Table 3.6) cover practically all the range of the pH values, so that further experiments can be planned. An interesting case would be to check for a reversed trend, eq. (32), which can occur at higher pH values. Experimental studies of aqueous chemistry of elements 107 and heavier have not yet been conducted.

4.3.4 Summary of the solution chemistry study

Trends in hydrolysis, complex formation and extraction of complexes at various experimental conditions observed experimentally in comparison with theoretical predictions are summarized in Table 4.2.

Table 4.2 Trends in hydrolysis and complex formation of the heaviest element compounds and their lighter homologs in chemical groups.

Group	Complexes	Experimental conditions	Theoretically predicted[a]	Experimentally observed	Ref.
4	Hydrolysis of M^{4+}	pH ≤ 2	Zr > Hf > Rf	Zr > Hf > Rf	151
	$MF_x(H_2O)^{z-x}_{8-x}$ (x ≤ 4)	[HF] < 10^{-1} M	Zr > Hf > Rf	Zr > Hf > Rf	145 149
	MF_6^-	[HF] > 10^{-3} M	Rf ≥ Zr > Hf	Rf ≥ Zr > Hf	146
	MCl_6^-	4-8 M [HCl]	Zr > Hf > Rf	Rf > Zr > Hf	147
5	Hydrolysis of M^{5+}	all pH	Nb > Ta > Db	Nb > Ta	106
	$M(OH)_2Cl_4^-$, $MOCl_4^-$, MCl_6^-	all [HCl]	Pa >> Nb ≥ Db > Ta	Pa >> Nb ≥ Db >Ta	153
6	Hydrolysis of M^{6+}	pH = 0 ÷ 1	Mo > W > Sg	Mo > W > Sg	115
	Hydrolysis of $MO_2(OH)_2$	pH > 1	Mo > Sg > W	Mo > W	106

[a] Refs. [111,108,110].

5. PROSPECTS FOR CHEMICAL STUDIES OF ELEMENTS HEAVIER THAN 108

5.1 Production of longer-lived isotopes

Unfortunately, production rates as well as half-lives tend to decrease rapidly in going to ever higher atomic numbers and range from about an atom per minute for element 104 to an atom per week or less for element 109 using current techniques. Considerable research to explore new types of production reactions and methods for using multiple targets and higher beam currents are required if we are to extend chemical studies as far as 118. If relatively long-lived species are discovered, then methods for "stockpiling" them or producing them as by-products must be considered.

The production of isotopes of elements 110, 112, 114 and 116 with half-lives in the range of seconds to minutes has now been reported using "warm/hot" fusion reactions. For example, half-lives of 3 min (SF) for ^{283}112 from the ^{238}U (^{48}Ca,3n) reaction and ~5 s and ~2 s for ^{287,288}114 from ^{242,244}Pu (^{48}Ca,3n,4n) reactions were given [9,10]. If these results can be confirmed and the production rates can be increased, experimental investigations of their chemical properties should be feasible. The isotope ^{280}110 with a half-life of ~7 s has also been reported as a decay product of ^{288}114, and it may also be possible to produce ^{277}110 directly in the ^{232}Th(^{48}Ca,3n) reaction. Longer-lived isotopes of element 109 (Mt) are expected around the deformed shell at 162 neutrons and might be produced using the ^{238}U(^{37}Cl,4n) or the ^{249}Bk(^{26}Mg,4n) reaction to make ^{271}Mt with a half-life predicted to be ~10 seconds. ^{237}Np targets with ^{40}Ar or ^{48}Ca projectiles might be used to make elements 111 and 113 and ^{249}Bk targets with ^{48}Ca projectiles might be used to make more neutron rich 117 isotopes. Other highly radioactive targets such as ^{243}Am, ^{249}Cf, or even ^{254}Es with appropriate projectiles might be used to make more neutron-rich isotopes of elements as heavy as 118, but considerable development work will be required. The Dubna/Livermore group plans to use ^{249}Cf (48Ca,3,4n)^{294,293}118 "warm/hot" fusion reactions to try to make neutron-rich isotopes of element 118 with longer half-lives.

5.2 Theoretical predictions of chemical properties

5.2.1 Elements 109 through 111

Molecular DS-DV calculations have been performed for fluorides of elements 109 and 110 [155] showing a similarity in their electronic structures with those of the Ir and Pt compounds. Element 111, a homolog of

Au, has received much attention due to the maximum of relativistic effects in group 11. The electronic structure of 111H, a sort of a test molecule, like AuH, was calculated via a variety of methods, HF, DF, DK, PP, PP CCSD(T), etc. [76,78,85]. Comparison of relativistic (DF or ARPP) with non-relativistic (HF or NRPP) calculations [85] have shown the bonding to be considerably increased by relativistic effects doubling the dissociation energy, though the SO splitting diminishes it by 0.7 eV (the ARPP CCSD – SOPP CCSD difference). The BDF calculations have also been performed for 111H and other dimers AuX and 111X (X = F, Cl, Br, O, Au, 111) [76]. Stabilities of higher oxidation state for element 111 were considered on the basis of PP molecular calculations for the reactions $MF_6^- \rightarrow MF_4^- + F_2$ and $MF_4^- \rightarrow MF_2^- + F_2$ [78,156]. The PP MP2 and CCSD results confirmed that relativistic effects stabilize higher oxidation states due to a larger involvement of the 6d orbitals in bonding.

5.2.2 Element 112

Element 112 is the most interesting for chemical studies since the maximum of relativistic effects on the 7s electron shell is expected to dramatically influence its properties. In addition, chemical identification will be the only way to confirm its production [9,10], since it decays by SF in previously unknown nuclei.

Element 112 is expected to be rather inert due to the relativistic contraction and stabilization of the 7s shell, making the $7s^2$ electron pair inactive. The relativistic effects maximum for element 112 was confirmed by molecular PP calculations [78,157]. They have, indeed, shown $R_e(112H^+)$ to be the shortest among CdH^+, HgH^+ and $112H^+$, and to be similar to $R_e(ZnH^+)$. The investigations [157] have also come to the conclusion that element 112 would exhibit a typical transition element character in higher oxidation states, since 6d orbitals are relativistically destabilized and, therefore, should be more involved in the coordination bonding. Thus, its 4+ oxidation state may be accessible and the 2+ state may not.

Since the most exciting property of element 112 is expected to be its high volatility [25,158-160], experiments are planned to detect it in the elemental state by gas-phase chromatography. Element 112 and its nearest homolog Hg should be sorbed on Au and Pd metal surfaces (see Section 5.2). The adsorption position of element 112 would indicate its volatility in relation to the two extreme cases: Hg and Rn. Element 112 is expected to have adsorption enthalpies on Au and Pd surfaces between those of Hg and Rn, as semi-empirical estimates of ΔH_{ads} show [158].

To predict the outcome of those experiments on the quantum-mechanical level, calculations of adsorption of Hg and element 112 on metal

surfaces of interest are highly desirable. As a first step, the ability of element 112 to form intermetallic compounds was tested by the DFT calculations for 112M, where M = Cu, Pd, Pt, Ag and Au [161]. The calculated D_e are shown in Figure 5.1 together with "experimental" (deduced from adsorption temperatures) ΔH_{ads} of Hg on the corresponding metal surfaces [162]. The calculations revealed an increase in R_e of about 0.06 Å and a decrease in D_e of about 15–20 kJ/mol from HgX to 112X. The Mulliken population analysis has shown that this decrease is due to a drastic relativistic stabilization and, therefore, inertness of the $7s^2$ shell leading to a large decrease in the 7s(112)-6s(Au) overlap compared to the 6s(Hg)-6s(Au) one. The contribution of the other orbitals is almost unchanged.

One can see good agreement (Figure 5.1) for the trends between the two types of data, the "experimental" ΔH_{ads} for Hg and the calculated D_e for HgM and 112M, with the interaction of Hg and element 112 with Pd being the strongest. Thus, the DFT calculations obviously describe bonding in these systems correctly, so that the difference in D_e between HgX and 112X can be related to the difference in ΔH_{ads} of Hg and element 112 on the metal surfaces. Thus, element 112 is expected to be more weakly adsorbed than Hg, though not as weakly sorbed as expected earlier [158]. Calculations of adsorption of Hg and element 112 on the metal surfaces are in progress using the embedded cluster model [163].

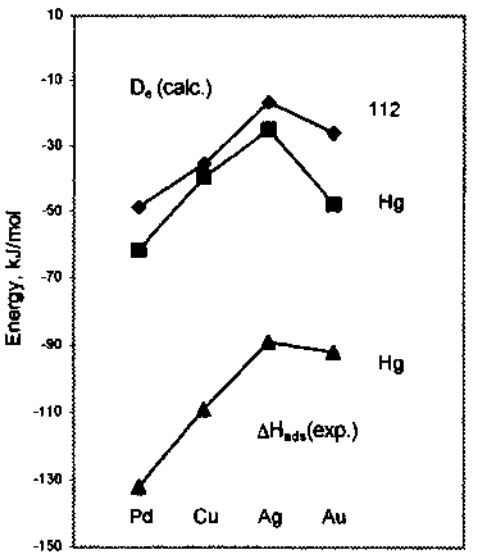

Figure 5.1. Calculated binding energies for HgX and 112X (X = Pd, Cu, Ag and Au) and "experimental" ΔH_{ads} on the corresponding metal surfaces [159]. (From [161]).

5.2.3 Elements with Z > 112

Predictions of chemical properties of elements heavier than 112 on the basis of relativistic atomic calculations were summarized by Fricke [25]. There are now a few relativistic calculations for compounds of these elements, mostly for simple hydrides and fluorides.

The most interesting element after 112 from both the theoretical and experimental point of view is 114, a homolog of Pb. The large relativistic stabilization of the 7s and $7p_{1/2}$ electrons and its closed-shell configuration due to the very large SO splitting of the 7p orbitals was the reason to predict its inertness. That was, indeed, confirmed by calculations of stability of some 114 compounds. Thus, weakening of the metal-ligand bond in comparison with the Pb-X bond was found for 114X (X = F, Cl, Br, I, O, O_2) by the RECP, ZORA and BDF calculations [80,90,77]. Energies of the decomposition reactions $MX_4 \rightarrow MX_2 + X_2$ and $MX_2 \rightarrow M + X_2$ (X = H, F and Cl) were calculated at the PP CCSD(T) and DHF levels [90,87]. The results show a decreasing trend in the stability of the 4+ oxidation state in the group in agreement with the conclusion of [164] where atomic calculations and simple bonding models were used. The instability was shown to be a relativistic effect. The neutral state was found to be more stable for element 114 than for Pb. The possibility of the existence of $114F_6^{2-}$ was considered although this compound will undergo strong hydrolysis in aqueous solutions. Thus, for aqueous chemistry of element 114, complexes like $114Br_3^-$ or $114I_3^-$ should be more stable.

The next chemically interesting element (though still to be produced) is 118, a homolog of the rare gases. A relatively high reactivity of element 118 was foreseen by earlier considerations [164,25]. Element 118 was predicted to be the most electropositive in the group and able to form a 118-Cl bond. The RECP calculations for the reactions $M + F_2 \rightarrow MF_2$ and $MF_2 + F_2 \rightarrow MF_4$, where M = Xe, Rn and element 118 [82], confirmed an increase in the stabilities of the 2+ and 4+ oxidation states due to the very large SO interaction of the 7p electrons and inert $7s^2$ electrons. The SO effects were shown to stabilize $118F_4$ by a significant amount of about 2 eV, though they elongate R_e by 0.05 Å.

The influence of the SO interaction on the geometry of MF_4 was investigated by the RECP-SOCI [84] and RECP-CCSD calculations [82]. In both papers it was found that a D_{4h} geometrical configuration for XeF_4 and RnF_4 becomes slightly unstable for $118F_4$. A T_d configuration was shown to be more stable than D_{4h} by 0.25 eV [84] and 0.17 eV [82] in agreement with each other. The reason for that was the availability of the only stereochemically active $7p_{3/2}$ electrons for bonding. An important observation has been made that the fluorides of element 118 will most probably be ionic rather than covalent, as in the case of Xe: they are,

therefore, predicted to be non-volatile. Those conclusions might be important for future gas-phase chromatography experiments.

The electronic structures of compounds of elements heavier that 118 have not yet been calculated. They will be much more influenced by relativistic effects, so that any comparison with lighter congeners may become impossible. Obviously, investigation of those systems will belong to the far future.

5.3 Experimental investigations and plans

5.3.1 Gas-phase chemistry

The first chemical experiments on element 112 have been reported by Yakushev *et al.* [24,165] using the spontaneously fissioning nuclide $^{283}112$ (~3 min) reported by Oganessian *et al.* [166] to be formed in the ^{238}U (^{48}Ca,3n) reaction with a cross section of 5 pb. The experiment was designed to determine whether element 112 behaved similarly to its periodic table homolog Hg which had been shown to deposit on Au- or Pd-coated silicon surface barrier detectors [24] or whether it behaved as a noble gas like Rn and remained in the gas phase. However, no SF or α-decay events associated with the production of element 112 were detected in the initial experiment [24], so an unambiguous answer about the physical or chemical properties of elements 112 was not provided. Therefore, the system was improved by introducing a special ionisation chamber after the silicon detectors to measure α-decays and SF events of nuclei remaining in the gas. More than 95% of the simultaneously produced Hg isotopes were deposited on the first Au-coated detector. Again, no events attributable to element 112 were detected on either the Au- or Pd-coated silicon detectors, but 8 SF events were registered in the ionization chamber [165]. These SF events were attributed to element 112 which would indicate that it is more chemically inert than Hg and remained in the gas phase. The ΔH_{ads} of element 112 was estimated as below (in absolute value) -55 kJ/mol. Further experiments with a temperature gradient in the chromatography column are now planned to better define ΔH_{ads}. It is also important to confirm that the observed SF events belong to element 112. If it were possible to use the α-decaying $^{284}112$ (~10 s), reported [9,10] previously as the daughter of $^{288}114$ (3 s), it would help confirm that element 112 was actually being observed.

Similar chemical experiments to those conducted in Dubna on element 112 are being planned by researchers at PSI [167] using a chromatographic column with a negative temperature gradient from. Silicon detectors coated with Au and Pd will be placed along the chromatographic column to detect element 112 and its deposition temperature will be determined relative to

those of Hg at 155 °C and Rn at about -170 °C [168] in order to deduce the ΔH_{ads} of element 112.

Researchers at LBNL plan to use BGS [169] to investigate the production of 112 isotopes in $^{238}U(^{48}Ca,xn)$ reactions down to a cross section sensitivity of 0.5 pb. If suitable isotopes are found, collaborative experiments will be undertaken to measure the properties of element 112. These experiments will also help to assess the usefulness of "warm" fusion reactions for production of a broad range of heavy element reactions for chemical studies.

5.3.2 Solution chemistry

There are some prospects for aqueous chemistry studies of elements heavier than 106 as well as more detailed studies of elements 104, 105, and 106 using shorter-lived isotopes which may have higher production rates. A recoil transfer chamber has been designed [23] to replace the focal plane detection system in the BGS so that separated isotopes can be slowed in an inert gas and attached to aerosols for transport to a rapid chemical separation system such as the SISAK described earlier [126] for few-second liquid-liquid extractions or some other rapid chemical separation system. Such systems might permit detailed studies of complex formation of elements 107 and 109 which would be of special interest in acid solutions. Experiments to study the chemistry of element 109 as a homolog of the group-9 elements Ir and Rh are being planned at Berkeley, but await production and identification using the BGS of the predicted longer-lived isotope ^{271}Mt mentioned earlier.

Plans to separate elements with $Z > 108$ as noble metals by electrochemical deposition from aqueous solutions have also been described [19]. The choice of an appropriate electrode material is very important and estimates of suitable electrodes have already been made for lighter homologs of the heaviest elements [170]. Pd or Pt were found to be suitable electrode metals for the deposition of Hg, Tl, Pb, Bi and Po, the homologs of elements 112-116. The chemical behaviour of the group-14 elements Sn and Pb in aqueous solutions is being studied at the Lawrence Livermore National Laboratory in preparation for experiments for the separation of element 114.

6. SUMMARY

Examples of both experimental and theoretical investigations of the chemical properties of the heaviest elements have been described. Recent interactions between theory and experiment have been mutually beneficial and have resulted in a much deeper understanding of the physics and chemistry of these exotic elements. Relativistic atomic and molecular calculations in combination with various models were useful in designing

the sophisticated and expensive chemical experiments required in order to study single atoms at a time. The synergism between theoretical and experimental research has allowed establishment of trends in properties of the heaviest elements and their lighter homologs within chemical groups in the periodic table.

To predict properties with greater accuracy, quantum-chemical methods as well as computational facilities still need to be further developed for application to the heaviest elements. Thus, *ab initio* molecular quantum-chemical methods are at the stage of improving the treatment of correlation effects and will need further development of computing facilities to use them in a routine manner. For calculations of adsorption processes of single atoms and molecules on various surfaces, embedded cluster models based on the DFT philosophy still must be further developed to take proper account of effects of the cluster environment, as well as of weak interactions.

From the experimental point of view, some results are ambiguous and need to be repeated to obtain more statistically significant information for comparison with the various theoretical predictions. In addition, evaluation of the experimental results is especially difficult when only spontaneous fission decay is detected. Thus, it will be important to try to produce new isotopes of the heaviest elements which decay by α-emission with half-lives and production rates suitable for experimental measurements of chemical properties. Continued close interactions between theorists and experimentalists should give rise to exciting progress in the next decade.

REFERENCES

1. Klaproth, M. H. Crell's Ann. **12**, (1789) 387.
2. McMillan, E. M., Abelson, P. H. Phys. Rev. **57**, (1940) 1185.
3. Seaborg, G. T. Chem. Eng. News **23**, (1945) 2190.
4. Münzenberg, G. Rep. Prog. Phys. **51**, (1988) 57.
5. Commission on Nomenclature of Inorganic Chemistry, Pure & Appl. Chem. **69**, (1997) 2471.
6. Hofmann, S., Ninov, V., Hessberger, F.P., Armbruster, P., Folger, H., Münzenberg, G., Schött, H.J., Popeko, A.G., Yeremin, A.V., Andreev, A.N., Saro, S., Janik, R., Leino, M. Z. Phys. A **350**, (1995) 277.
7. Hofmann, S., Ninov, V., Hessberger, F.P., Armbruster, P., Folger, H., Münzenberg, G., Schött, H.J., Popeko, A.G., Yeremin, A.V., Andreev, A.N., Saro, S., Janik, R., Leino, M. Z. Phys. A **350**, (1995) 281.
8. Hofmann, S., Ninov, V., Hessberger, F.P., Armbruster, P., Folger, H., Münzenberg, G., Schött, H.J., Popeko, A.G., Yeremin, A.V., Saro, S., Janik, R., Leino, M. Z. Phys. A **354**, (1996) 229.
9. Oganessian, Yu. Ts., Utyonkov, V.K., Lobanov, Yu. V., Abdulin, F. Sh., Polyakov, A.N., Shirokovsky, I.V., Tsyganov, Yu. S., Gulbekian, G.G., Bogomolov, S.L., Gikal, B.N., Mezentsev, A.N., Iliev, S., Subbotin, V.G., Sukhov, A.M., Ivanov, O.V., Buklanov, G.V., Subotic, K., Itkis, M.G., Moody, K.J., Wild, J.F., Stoyer, N.J., Stoyer,

M.A., Lougheed, R.W., Laue, C.A., Karelin, Ye. A., Tatarinov, A.N. Phys. Rev. C **63**, (2000) 011301 (R).
10. Oganessian, Yu. Ts. Nucl. Phys. A **685** (2001) 17c.
11. Seaborg, G. T. and Loveland, W. D. The elements beyond uranium, John Wiley and Sons, Inc., New York, 1990.
12. Flerov, G. N. and Ter-Akopian, G. M. Rep. Prog. Phys. **46**, (1983) 817.
13. Münzenberg, G. and Hofmann, S. "Discovery of the Heaviest Elements". In.: *Heavy Elements and Related New Phenomena,* Eds. Greiner, W., Gupta, R.K., World Scientific, Singapore, (1999, pp. 9-42.
14. Hofmann, S. and Münzenberg, G. Rev. Mod. Phys. **72**, (2000) 733.
15. Keller, Jr., O.L., Seaborg, G. T. Ann. Rev. Nucl. Sci. **77**, (1977) 139.
16. Guillaumont, J.-P., Adloff, A., Peneloux, A. Radiochim. Acta **46**, (1989) 169.
17. Zvara, I., Eichler, B., Belov, V. Z., Zvarova, T.S., Korotkin, Yu. S., Shalaevsky, M. R., Shegolev, V. A., Hussonnois, M. Sov. Radiochem. **16**, (1974) 709.
18. Schädel, M. Radiochim. Acta **70/71**, (1995), 207.
19. Kratz, J.V. "Fast Chemical Separation Procedures for Transactinides". In: *Heavy Elements and Related New Phenomena,* Eds. Greiner, W., Gupta, R.K., World Scientific, Singapore, (1999), pp. 43-63.
20. Hoffman, D.C. Chem. Eng. News, May 24 (1994).
21. Gäggeler, H.W. "Chemistry of the Transactinide Elements". In: Proceedings of "The Robert A. Welch Foundation Conference on Chemical Research XXXIV. Fifty Years with Transuranium Elements", Houston, Texas, 22-23 October 1990, pp. 255-276.
22. Eichler, R., Brüchle, W., Dressler, C.E., Düllman, C.E., Eichler, B., Gäggeler, H.W., Gregorich, K.E., Hoffman, D.C., Hübener, S., Jost, D.T., Kirbach, U.W., Laue, C.A., Lavanchy, V.M., Nitsche, H., Patin, J.B., Piguet, D., Schädel, M., Shaughnessy, D.A., Strellis, D.A., Taut, S., Tobler, L., Tsyganov, Y. S., Türler, A., Vahle, A., Wilk, P.A., Yakushev, A.B. Nature **407**, (2000) 63.
23. Düllman, Ch., Brüchle, W., Dressler, R., Eberhardt, K., Eichler, B., Eichler, R., Gäggeler, H. W., Ginter, T. N., Glaus, F., Gregorich, K. E., Hoffman, D. C., Jäger, E., Jost, D. T., Kirbach, U. W., Lee, D. E., Nitsche, H., Patin, J. B., Pershina, V., Piguet, D., Qin, Z., Schädel, M., Schausten, B., Schimpt, E., Schött, H.-J., Soverna, S., Sudowe, R., Thörler, P., Timohkin, S. N., Trautmann, N., Türler, A., Vahle, A., Wirth, G., Yakushev, A. B., Zielinski, P. M. Nature (Letters), **418,** (2002) 859, ; Kirbach, U.W., Folden III, C. M., Ginter, T. N., Gregorich, K. E., Omtvedt, J. P., Ninov, V., Lee, D. M., Patin, J. B., Seward, N. K., Strellis, D. A., Sudowe, R., Türler, A., Wilk, P. A., Zielinski, P. M., Hoffman, D. C., Nitsche, H., Nucl. Instr. & Methods in Phys. Res. A **484,** (2002) 587.
24. Yakushev, A.B. , Buklanov, G.V., Chelnokov, M.L., Chepigin, V.I., Dmitriev, S.N., Gorshkov, V.A., Hübener, S., Lebedev, V.Ya, Malyshev, O.N., Oganessian, Yu.Ts., Popeko, A.G., Sokol, E.A., Timokhin, S.N., Türler, A., Vasko, V.M., Yeremin, A.V., Zvara, I. Radiochim. Acta **89**, (2001) 743.
25. Fricke, B. Struct. Bond. **21**, (1975) 89.
26. Pyykkö, P. Chem. Rev. **88**, (1988) 563.
27. Grant I.P. In: *The Effects of Relativity in Atoms, Molecules and the Solid State*, Eds. Wilson, S., Grant, I.P. and Gyorffy, B.L., Plenum, New York, (1991), pp. 17-43.
28. Pershina, V. Chem. Rev. **96**, (1996) 1977.
29. Pershina, V. and Fricke, B. "Electronic Structure and Chemistry of the Heaviest Elements". In: *Heavy Elements and Related New Phenomena,* Eds. Greiner, W., Gupta, R.K., World Scientific, Singapore, (1999), pp. 194-162.
30. Seaborg, G. T. "From Mendeleev to Mendelevium". In: Proceedings of "The Robert A. Welch Conference on Chemical Research XIII. The Transuranium Elements-The Mendeleev Centennial", Houston, Texas, 17-19 November 1969, pp. 5-40.
31. Waber, J. T. "The Quantum Chemistry of the Super-Actinide Elements", ibid, pp. 353-443.

32. Schwerdtfeger, P. and Seth, M. "Relativistic Effects on the Superheavy Elements". In: *Encyclopedia of Computational Chemistry*, Wiley, New York, (1998), Vol. 4, pp. 2480-2499.
33. Schwarz, W.H.E., van Wezenbeek, E.M., Baerends, E.J., Snijders, J.G. J. Phys. B: At. Mol. Opt. Phys. **22**, (1989) 1515; Baerends, E.J., Schwarz, W.H.E., Schwerdtfeger, P., Snijders, J.G. J. Phys. B: At. Mol. Opt. Phys. **23**, (1990) 3225.
34. Desclaux, J.P. At. Data Nucl. Data Tables **12**, (1973) 311.
35. Eliav, E., Shmulyian, S., Kaldor, U., Ishikawa, Y. J. Chem. Phys. **109**, (1998) 3954.
36. Pyykkö, P., Tokman, M., Labzowsky, L.N., Phys. Rev. A **57**, (1998) R689.
37. Pepper, M. and Bursten, B.E. Chem. Rev. **91**, (1991) 719.
38. Mann, J.B. J. Chem. Phys. **51**, (1969) 841; Mann, J.B. and Waber, J.T. J. Chem. Phys. **53**, (1970) 2397.
39. Fricke, B., Greiner, W., Waber, J.T. Theoret. Chim. Acta **21**, (1971) 235.
40. Desclaux, J.P. Comp. Phys. Comm. **9**, (1975) 31.
41. Desclaux, J.P. and Fricke, B. J. Phys. **41**, (1980) 943.
42. Glebov, V.A., Kasztura, L., Nefedov, V.S., Zhuikov, B.L. Radiochim. Acta **46**, (1989) 117.
43. Johnson, E., Fricke, B., Keller, Jr., O.L., Nestor, Jr., C.W., Ticker, T.C. J. Chem. Phys. **93**, (1990) 8041.
44. Fricke, B., Johnson, E., Rivera, G.M. Radiochim. Acta **62**, (1993) 17.
45. Johnson, E., Pershina, V., Fricke, B. J. Phys. Chem. **103**, (1999) 8458.
46. Johnson, E., Fricke, B., Jacob, T., Dong, C.Z., Fritzsche, S., Pershina, V. J. Phys. Chem. **116**, (2002) 1862.
47. Grant, I.P. J. Phys. B **19**, (1986) 3187.
48. Parpia, F.A., Froese-Fisher, S., Grant, I.P. CPC **94**, (1996) 249.
49. Pyper, N.C. and Grant, I.P. Proc. R. Soc. Lond. A **376**, (1981) 483.
50. Kaldor, U. and Eliav, E. Adv. Quantum. Chem. **31**, (1998) 313.
51. Kaldor, U. and Eliav, E. "Energies and Other Properties of Heavy Atoms and Molecules". In: *Quantum Systems in Chemistry and Physics*, Ed. Hernandes-Laguna, v. II, (2000) 185.
52. Ishikawa, I. and Kaldor, U. In: *Computational Chemistry, Reviews of Current Trends*, Ed. Leszynski, J., World Scientific, Singapore, (1996) Vol. 1.
53. Eliav, E., Kaldor, U., Ishikawa, Y. Phys. Rev. Lett. **74**, (1995) 1079.
54. Eliav, E., Kaldor, U., Schwerdtfeger, P., Hess, B.A., Ishikawa, Y. Phys. Rev. Lett. **73**, (1994) 3203.
55. Eliav, E., Kaldor, U., Ishikawa, Y. Phys. Rev. A **52**, (1995) 2765.
56. Eliav, E., Kaldor, U., Ishikawa, Y., Seth, M., Pyykkö, P. Phys. Rev. A **53**, (1996) 3926.
57. Landau, A., Eliav, E., Ishikawa, Y., Kaldor, U. J. Chem. Phys. **114**, (2001) 2977.
58. Eliav, E., Kaldor, U., Ishikawa, Y. Mol. Phys. **94**, (1998) 181.
59. Eliav, E., Kaldor, U., Ishikawa, Y. Phys. Rev. A **52**, (1995) 291.
60. Eliav, E., Kaldor, U., Ishikawa, Y., M., Pyykkö, P. Phys. Rev. Lett. **77**, (1996) 5350.
61. Varga, S., Fricke, B., Hirata, M., Bastug, T., Pershina, V., Fritzsche, S. J. Phys. Chem. A **104**, (2000) 6495.
62. Pershina, V., Bastug, T., Fricke, B. J. Alloy Comp. **271-273**, (1998) 283.
63. Pershina, V. and Bastug, T. J. Chem. Phys. **113**, (2000) 1441.
64. Pershina, V., Bastug, T., Fricke, B., Varga, S. J. Chem. Phys. **115**, (2001) 1.
65. Bastug, T., Heinemann, D., Sepp, W.-D., Kolb, D., Fricke, B. Chem. Phys. Lett. **211** (1993) 119.
66. Varga, S., Engel, E., Sepp, W.-D., Fricke, B. Phys. Rev. A **59**, (1999) 4288.
67. Vosko, S. H., Wilk, L., Nusair, M. Can. J. Phys. **58**, (1980) 1200.
68. Becke, A. D. Phys. Rev. A **38**, (1988) 3098.
69. Engel, E., Keller, S., Dreizler, R.M., Phys. Rev. A **53**, (1996) 1367.

70. Rosen, A., Ellis, D.E. J. Chem. Phys. **62**, (1975) 3039; Rosen, A. Int. J. Quant. Chem. **13**, (1978) 509.
71. Bastug, T., Sepp, W.-D., Kolb, D., Fricke, B., te Velde, G., Baerends, E. J. J. Phys. B. **28**, (1995) 2325.
72. Boerrigter, P. M., te Velde, G., Baerends, E. J. Int. J. Quant. Chem. **33**, (1988) 87; te Velde, G., Baerends, E. J. J. Comput. Phys. **99**, (1992) 84.
73. Kohn, W., Becke, A.D., Parr, R.G. J. Phys. Chem. **100**, (1996) 12974.
74. Rosen, A. Adv. Quant. Chem. **29**, (1997) 1.
75. Liu, W., Hong, G., Dai, D., Li, L., Dolg, M. Theor. Chem. Acc. **96**, (1997) 75.
76. Liu, W. and van Wüllen, Ch. J. Chem. Phys. **110**, (1999) 3730.
77. Liu, W., van Wüllen, Ch., Han, Y. K., Choi, Y. J., Lee, Y.S. Adv. Quant. Chem. **39**, (2001) 325.
78. Seth, M. "The Chemistry of Superheavy Element", Thesis, University of Auckland, 1998.
79. Han, Y.-K., Son, S.-K., Choi, Y.J., Lee, Y.S. J. Phys. Chem. **103**, (1999) 9109.
80. Han, Y.-K., Bae, C., Son, S.-K., Lee, Y.S. J. Chem. Phys. **112**, (2000) 2684.
81. Choi, Y. J., Han, Y.K., Lee, Y.S. J. Chem. Phys. **115**, (2001) 3448.
82. Han, Y.K. and Lee, Y.S. J. Phys. Chem. A **103**, (1999) 1104.
83. Nash, C. S., Bursten, B. E. J. Phys. Chem. A **103**, (1999) 402.
84. Nash, C.S. and Bursten, B.E. J. Phys. Chem. A **103**, (1999) 632.
85. Seth, M., Schwerdtfeger, P., Dolg, M., Faegri, K., Hess, B.A., Kaldor, U. Chem. Phys. Lett. **250**, (1996) 461.
86. Faegri, K. and Saue, T. J. Chem. Phys. **115**, (2001) 2456.
87. Faegri, K. and Saue, T., to be piblished.
88. Saue, T., Faegri, K., Gropen, O. Chem. Phys. Lett. **263**, (1996) 360.
89. Seth, M., Schwerdtfeger, P., Faegri, K. J. Chem. Phys. **111**, (1999) 6422.
90. Seth, M., Faegri, K., Schwerdtfeger, P. Angew. Chem. Int. Ed. Engl. **37**, (1998) 2493.
91. Wood, X. and Pyper, N.C. Chem. Phys. Lett. **84**, (1981) 614.
92. Pershina, V., Johnson, E., Fricke, B. J. Phys. Chem. A **103**, (1999) 8463.
93. Martin, R. L., Hay, P. J., Pratt, L. R. J. Phys. Chem. A **102**, (1998) 3565.
94. Ionova, G. V., Pershina, V., Johnson, E., Fricke, B., Schädel, M. J. Phys. Chem. **96**, (1992) 11096.
95. Bratsch, S. G. Phys. Chem. Ref. Data **18**, (1989) 1.
96. Pershina, V., Fricke, B. J. Phys. Chem. **98**, (1994) 6468.
97. Shannon, R.D. Acta Crystallogr., Sect. A **32**, (1976) 751.
98. Seth, M., Dolg, M., Fulde, P., Schwerdtfeger, P. J. Am. Chem. Soc. **117**, (1995) 6597.
99. Pershina, V. and Fricke, B. J. Chem. Phys. **99**, (1993) 9720.
100. Pershina, V. and Fricke, B. J. Phys. Chem. **99**, (1995) 144.
101. Pershina, V. and Fricke, B. J. Phys. Chem. **100**, (1996) 8748.
102. Pershina, V., Sepp, W.-D., Fricke, B., Kolb, D., Schädel, M., Ionova, G. V. J. Chem. Phys. **97**, (1992) 1116.
103. Pershina, V., Sepp. W.-D., Bastug, T., Fricke, B., Ionova, G. V. J. Chem. Phys. **97**, (1992) 1123.
104. Adamson, A.W. Physical Chemistry of Surfaces, Wiley, New York, 1976.
105. Ahrland, S., Liljenzin, J. O., Rydberg, J. In: *Comprehensive Inorganic Chemistry*, ed. Bailar, J., Pergamon Press, Oxford, 1973, Vol. 5, pp. 519-542.
106. Baes, Jr., C.F. and Mesmer, R.E. The Hydrolysis of Cations, John Wiley, New York, 1976.
107. Pershina, V. Radiochim. Acta **80**, (1998) 65.
108. Pershina, V. Radiochim. Acta **80**, (1998) 75.
109. Pershina, V. and Bastug, T. Radiochim. Acta **84**, (1999) 79.
110. Pershina, V. and Kratz, J.V. Inorg. Chem. **40**, (2001) 776.
111. Pershina, V., Trubert, D., Le Naour, C., Kratz, J. V. Radiochim. Acta **90**, (2002) 869.

112. Kratz, V. and Pershina, V. "Experimental and Theoretical Study of the Chemistry of the Heaviest Elements". In: *Relativistic Effects in Heavy-Element Chemistry and Physics*, Ed. Hess, B.A., John Wiley and Sons, Ltd. (2003), pp. 219-244.
113. Kassiakoff, A. and Harker, D. J. Am. Chem. Soc. **60**, (1938) 2047.
114. Kratz, J.V., Zimmermann, H.P., Scherer, U.W., Schädel, M., Brüchle, W., Gregorich, K.E., Gannett, C.M., Hall, H.L., Henderson, R.A., Lee, D.M., Leyba, J.D., Nurmia, M., Hoffman, D.C., Gäggeler, H.W., Jost, D., Baltensprenger, U., Ya Nai-Qi, Türler, A., Lienert, Ch. Radiochim. Acta **48**, (1989) 121.
115. Schädel, M., Brüchle, W., Jäger, E., Schausten, B., Wirth, G., Paulus, W., Günther, R., Eberhardt, K., Kratz, J.V., Seibert, A., Strub, E., Thörle, P., Trautmann, N., Waldek, W., Zauner, S., Schumann, D., Kirbach, U., Kubica, B., Misiak, R., Nagame, Y., Gregorich, K.E. Radiochim. Acta **83**, (1998) 163.
116. Guillaumont, R., Adloff, J. P., Peneloux, A., Delamoye, P. Radiochim. Acta **54** (1991) 1.
117. Hoffman, D. C. J. Chem. Ed. **76**, (1999) 331.
118. Zvara, I., Chuburkov, Yu. Ts., Belov, V. Z., Buklanov, G. V., Zakhvataev, B. B., Zvarova, T. S., Maslov, O. D., Caletka, R., Shalaevsky, M. R. J. Inorg. Nucl. Chem. **32**, (1970) 1885.
119. Zvara, I., Eichler, B., Belov, V. Z., Zvarova, T. S., Korotkin, Yu. S., Shalaevsky, M. R., Shegolev, V. A., Hussonois, M. Sov. Radiochem. **16**, (1974) 709.
120. Zvara, I., Belov, V. Z., Domanov, V. P., Shalaevski, M. R. Sov. Radiochem. **18**, (1976) 328.
121. Timokhin, S. N., Yakushev, A. B., Honggui, Xu., Perelygin, V. P., Zvara, I. J. Radioanal. Nucl. Chem. Lett. **212**, (1996) 31.
122. Gäggeler, H. W. J. Radioanal. Nucl. Chem. Articles **183**, (1994) 261.
123. Kadkhodayan, B., Türler, A., Gregorich, K. E., Baisden, P. A., Czerwinski, K. R., Eichler, B., Gäggeler, H. W., Hamilton, T. M., Jost, T. M., Kacher, C. D., Kovacs, A., Kreek, S. A., Lane, M. R., Mohar, M. F., Neu, M. P., Stoyer, N. J., Sylwester, E. R., Lee, D. M., Nurmia, M. J., Seaborg, G. T. , Hoffman, D. C. Radiochim. Acta **72**, (1996) 169.
124. Pfrepper, G., Pfrepper, R., Yakushev, A. B., Timokhin, S. N., Zvara, I. Radiochim. Acta **77**, (1997) 201; ibid. **80**, (1998) 7.
125. Omtvedt, J.-P., Alstad, J., Eberhardt, K., Fure, K., Malmbeck, R., Mendel, M., Nähler, A., Skarnemark, G., Trautmann, N., Wiehl, N., Wierczinski, B. J. Alloys and Comp. **271**, (1998) 303.
126. Omtvedt, J.-P., Alstadt, J., Breivik, H., Dyve, J. E., Eberhardt, K., Folden III, C. M., Ginter, T., Gregorich, K. E., Hult, E. A., Johansson, M., Kirbach, U. W., Lee, D. M., Mendel, M., Nähler, A., Ninov, V., Omtvedt, L. A., Patin, J. B., Skarnemark, G., Stavsetra, L., Sudowe, R., Wiehl, N., Wierczinski, B., Wilk, P. A., Zielinski, P. M., Kratz, J. V., Trautmann, N., Nitsche, H., Hoffman, D. C. J. Nucl. & Radiochem. Sci., Japan **3**, (2002) 121.
127. Jost, D. T., Gäggeler, H. W., Vogel, Ch., Schädel, M., Jäger, E., Eichler, B., Gregorich, K. E., Hoffman, D. C. Inorg. Chem. Acta **146**, (1988) 255.
128. Eichler, B., Hübner, S., Gäggeler, H. W., Jost, D. T. Inorg. Chim. Acta **146**, (1988) 261.
129. Zvara, I., Belov, V. Z., Domanov, V. P., Korotkin, Yu. S., Chelnokov, L. P., Shalaevsky, M. R., Shchegolev, V. A., Hussonois, M. Sov. Radiochem. **14**, (1971) 115.
130. Türler, A. Radiochim. Acta **72**, (1996) 7.
131. Sylwester, E. R., Gregorich, K. E., Lee, D. M., Kadkhodayan, B., Türler, A., Adams, J. L., Kacher, C. D., Lane, M. R., Laue, C. A., McGrath, C. A., Shaughnessy, D. A., Strellis, D. A., Wilk, P. A., Hoffman, D. C. Radiochim. Acta **88**, (2000) 837.
132. Türler, A., Eichler, B., Jost, D. T., Piguet, D., Gäggeler, H. W., Gregorich, K. E., Kadkhodayan, B., Kreek, S. A., Lee, D. M., Mohar, M., Sylwester, E., Hoffman, D. C., Hübener, S. Radiochim. Acta **73**, (1996) 55.
133. Gäggeler, H. W., Jost, D. T., Kovacs, J., Scherer, U. W., Weber, A., Vermeulen, D., Türler, A., Gregorich, K. E., Henderson, R. A., Czerwinski, K. R., Kadkhodayan, B.,

Lee, D. M., Nurmia, M. J., Hoffman, D. C., Kratz, J. V., Gober, M. K., Zimmermann, H. P., Schädel, M., Brüchle, W., Schimpf, E., Zvara, I. Radiochim. Acta **57**, (1992) 93.
134. Kadkhodayan, B. "On-Line Gas Chromatographic Studies of Rutherfordium (Element 104), Hahnium (Element 105), and Homologs", Doctoral Thesis, LBL, Berkeley, 1993; Türler, A., Buklanov, G. V., Euchler, B., Gäggeler, H. W., Grantz, M., Hübener, S., Jost, D. T., Labedev, V. Ya., Piguet, D., Timokhin, S. N., Yakishev, A. B., Zvara, I. J. Alloys and Comp. **271**, (1998) 287.
135. Yakushev, A. B., Timokhin, S. N., Vedeneev, M. V., Honggui Xu, Zvara, I., J. Radioanal. Nucl. Chem., Articles **205**, (1996) 63.
136. Lazarev, Yu. A., Lobanov, Yu.V., Oganessian, Yu.Ts., Utyonkov, V.K., Abdullin, F. Sh., Buklanov, G. V., Gikal, B.N., Iliev, S., Mezentsev, A.N., Polyakov, A.N., Sedykh, I.M., Shirokovsky, I.V., Subbotin, V.G., Sukhov, A.M., Tsyganov, Yu.S., Zhuchko, V.E., Lougheed, R.W., Moody, K.J., Wild, J.F., Hulet, E.K., McQuaid, J.H. Phys. Rev. Lett. **73**, (1994) 624.
137. Lougheed, R.W., Moody, K.J., Wild, J.F., Hulet, E.K., McQuaid, J.H., Lazarev, Yu. A., Lobanov, Yu.V., Oganessian, Yu. Ts., Utyonkov, V.K., Abdullin, F. Sh., Buklanov, G. V., Gikal, B. N., Iliev, S., Mezentsev, A. N., Polyakov, A.N., Sedykh, I.M., Shirokovsky, I.V., Subbotin, V.G., Sukhov, A.M., Tsyganov, Yu.S., Zhuchko, V.E. J. Alloys and Compounds **213/214**, (1994) 61.
138. Schädel, M., Brüchle, W., Dressler, R., Eichler, B., Gäggeler, H. W., Günther, R., Gregorich, K. E., Hoffman, D. C., Hübener, S., Jost, D. T., Kratz, J. V., Paulus, W., Schumann, D., Timokhin, S., Trautmann, N., Türler, A., Wirth, G., Yakushev, A. Nature (Letters) **388**, (1997) 55.
139. Türler, A., Brüchle, W., Dressler, R., Eichler, B., Eichler, R., Gäggeler, H. W., Gärtner, M., Glatz, J.-P., Gregorich, K. E., Hübener, S., Jost, D. T., Lebedev, V. Ya., Pershina, V., Schädel, M., Taut, S., Timokhin, N., Trautmann, N., Vahle, A., Yakushev, A. B. Angew. Chem. Int. Ed. **38**, (1999) 2212.
140. Türler, A., Dressler, R., Eichler, B., Gäggeler, H. W., Jost, D. T., Schädel, M., Brüchle, W., Gregorich, K. E., Trautmann, N., Taut, S. Phys. Rev. C **57**, (1998) 1648.
141. Hübener, S., Taut, S., Vahle, A., Dressler, R., Eichler, B., Gäggeler, H. W., Jost, D. T., Piguet, D. T., Türler, A., Brüchle, W., Jäger, E., Schädel, M., Schimpf, E., Kirbach, U., Trautmann, N., Yakushev, A. B. Radiochim. Acta **89**, (2001) 737.
142. Wilk, P., Gregorich, K. E., Türler, A., Laue, C. A., Eichler, R., Ninov, V., Adams, J. L., Kirbach; U. W., Lane, M. R., Lee, D. M., Patin, J. B., Shaughnessy, D. A., Strellis, D. A., Nitsche, H., Hoffman, D. C. Phys. Rev. Lett. **85**, (2001) 2697.
143. Türler, A., Düllman, Ch. E., Gäggeler, H. W., Kirbach, U. W., Yakushev, A. B., Schädel, M., Brüchle, W., Dressler, R., Eberhardt, K., Eichler, B., Eichler, R., Ginter, T. N., Glaus, F., Gregorich, K. E., Hoffman, D. C., Jäger, E., Jost, D. T., Lee, D. M., Nitsche, H., Patin, J. B., Pershina, V., Piguet, D., Qin, Z., Schausten, B., Schimpf, E., Schött, H.-J., Soverna, S., Sudowe, R., Thörle, P., Timokhin, S. N., Trautmann, N., Vahle, A., Wirth, G., Zielinski, P. Eur. Phys. J, submitted.
144. Silva, R. J., Harris, J., Nurmia, M., Eskola, K., Ghiorso, A. Inorg. Nucl. Chem. Lett. **6**, (1970) 871.
145. Strub, E., Kratz, J.V., Kronenberg, A., Nähler, A., Thörle, P., Zauner, S., Brüchle, W., Jäger, E., Schädel, M., Schausten, B., Schimpf, E., Zongwei, Li, Kirbach, U., Schumann, D., Jost, D., Türler, A., Asai, M., Nagame, Y., Sakara, M., Tsukada, K., Gäggeler, H.W., Glanz, J.P. Radiochim. Acta **88**, (2000) 265.
146. Trubert, D., Le Naour, C., Hussonois, M., Brillard, L., Montroy Gutman, F., Le Du, J. F., Constantinescu, O., Barci, V., Weiss, B., Gasparro, J., Ardisson, G. In: Abstracts of the 1st Intern. Conf. on Chemistry and Physics of Transactinides, Seeheim, Sept 26-30, 1999.
147. Haba, H., Tsukada, K., Asai, M., Goto, S., Toyoshima, A., Nishinaka, I., Akiyama, K., Hirata, M., Ichikawa, S., Nagame, Y., Shoji, Y., Shigekawa, M., Koike, T., Iwasaki, M., Shinohara, A., Kaneko, T., Maruyama, T., Ono, S., Kudo, H., Oura, Y., Sueki, K.,

Nakahara, H., Sakama, M., Yokoyama, A., Kratz, J.V., Schädel, M., Brüchle, W. J. Nucl. & Radiochem. Sci., Japan **3**, (2002) 143.
148. Günther, R., Paulus, W., Kratz, J. V., Seibert, A., Thörle, P., Zauner, S., Brüchle, W., Jäger, E., Pershina, V., Schädel, M., Schausten, B., Schumann, D., Eichler, B., Gäggeler, H. W., Jost, D. T., Türler, A. Radiochim. Acta **80**, (1998) 121.
149. Kronenberg, A. "Entwicklung einer online-Chromatographie für Element 106 (Seaborgium)", Doctoral Thesis, University of Mainz, 2001.
150. Bilewicz, A., Siekerski, S., Kacher, C. D., Gregorich, K. E., Lee, D. M., Stoyer, N. J., Kadkhodayan, B., Kreek, S. A., Lane, M. R., Sylwester, E. R., Neu, M. P., Mohar, M. F., Hoffman, D. C, Radiochim. Acta **75**, (1996) 121.
151. Czerwinski, K. R. "Studies of Fundamental Properties of Rutherfordium (Element 104) Using Organic Complexing Agents", Doctoral Thesis, LBL Berkeley, 1992.
152. Gregorich, K. E., Henderson, R. A., Lee, D. M., Nurmia, M. J., Chasteler, R. M., Hall, H. L., Bennett, C. M., Chadwick, R. B., Leyba, J. D., Hoffman, D. C., Herrmann, G. Radiochim. Acta **43**, (1988) 223.
153. Paulus, W., Kratz, J.V., Strub, E., Zauner, S., Brüchle, W., Pershina, V., Schädel, M., Schausten, B., Adams, J.L., Gregorich, K.E., Hoffman, D.C., Lane, M.R., Laue, C., Lee, D.M., McGrath, C.A., Shaughnessy, D.K., Strellis, D.A., Sylwester, E.R. Radiochim. Acta **84**, (1999) 69.
154. Schädel, M., Brüchle, W., Schausten, B., Schimpf, E., Jäger, E., Wirth, G., Günther, R., Kratz, J. V., Paulus, W., Seibert, A., Thörle, P., Trautmann, N., Zauner, S., Schumann, D., Andrassy, M., Misiak, R., Gregorich, K. E., Hoffman, D. C., Lee, D. M., Sylwester, E. R., Nagame, Y., Oura, Y. Radiochim. Acta **77**, (1997) 149.
155. Rosen, A., Fricke, B., Morovic, T., Ellis, D.E. J. Phys. C-4, Suppl. **4**, **40**, (1979) C-4/218.
156. Seth, M., Cooke, F., Schwerdtfeger, P., Heully, J.-L., Pelissier, M. J. Chem. Phys. **109**, (1998) 3935.
157. Seth, M., Schwerdtfeger, P., Dolg, M. J. Chem. Phys. **106**, (1997) 3623.
158. Eichler, B., Rossbach, H. and Eichler, B. Radiochim. Acta **33**, (1983) 121.
159. Pitzer, K.S. J. Chem. Phys. **63**, (1975) 1032.
160. Ionova, G. V., Pershina, V., Zuraeva, I. T., Suraeva, N. I. Sov. Radiochem. **37**, (1995) 282.
161. Pershina, V., Bastug, T., Jacob, T., Fricke, B., Varga, S. Chem. Phys. Lett. **365**, (2002) 176.
162. Rossbach, H. and Eichler, B. ZfK-527 Report, Akademie der Wissenschaft der DDR, Juni 1984.
163. Jacob, T., Geschke, D., Fritzsche, S., Sepp, W.-D., Fricke, B., Anton, J., Varga, S. Surf. Sci. **486**, (2001) 194.
164. Pitzer, K.S. J. Chem. Soc., Chem. Commun. (1975) 760.
165. Yakushev, A. Workshop on Recoil Separator for Superheavy Element Chemistry, March 20-21, 2002, Darmstadt.
166. Oganessian, Yu., Yeremin, A. Y., Gulbekian, G.G., Bogomolov, S. L., Chepigin, V. I., Gikal, B. N., Gorshkov, V. A., Itkis, M. G., Kabachenko, A. P., Kutner, V. B., Lavrentev, A. Yu., Malyshev, O. N., Popeko, A. G., Rohac, J., Sagaidak, R. N., Hofmann, S., Münzenberg, G., Veselsky, M., Saro, S., Iwasa, N. Morita, K. Eur. Phys. J. A **5**, (1999) 63.
167. Soverna, S., Aebersold, H. U., Düllman, Ch. E., Eichler B., Gäeggeler, H. W., Tobler, L., Türler, A., Thi, Q., The GDCh Conference, Würzburg, Germany, September 2001.
168. Eichler, R., Haenssler, F., Gäggeler, H. W., Qin, Z., Soverna, S., Dressler, R., Eichler, B., Piguet, D. PSI Auual Report 2002, p. 4; Niklaus, J.-P., Eichler, R., Soverna, S., Gäggeler, H. W., Tobler, L. ibid., p. 8.
169. Gregorich, K. *et al.*, Workshop on Recoil Separator for Superheavy Element Chemistry, March 20-21, 2002, Darmstadt, Germany.
170. Eichler, B., Kratz, J. V. Radiochim. Acta **88**, (2000) 475.

Chapter 4

CORE AND VALENCE ELECTRON DISTRIBUTIONS IN HEAVY ELEMENTS BY X-RAY AND ELECTRON SPECTROSCOPY

C. Bonnelle

Laboratoire de Chimie Physique - Matire et Rayonnement, Universit Pierre et Marie Curie, UMR-CNRS 7614, 11 rue Pierre et Marie Curie, F-75231 Paris Cedex 05, France

cbon@ccr.jussieu.fr

Abstract X-ray emission spectroscopy, Auger spectroscopy and x-ray photoemission provide a means of determining the electron distributions in any material. We give a short description of the principles of these methods. We then consider perturbations of spectra that are due to the emission process itself. Several examples are given. The behaviour of the valence electrons of different symmetry in the condensed matter is discussed. In particular we dwell on the characteristics of the f states in rare earths and actinides as well as on the creation of excited states with a core hole in the presence of an f incomplete sub-shell.

Keywords: X-ray emission, photoemission, Auger effect, Lanthanides, Actinides.

Introduction

Photon and electron spectroscopy provides the most reliable information about the electronic structure of free atoms as well as atoms bound in any material. These techniques have been powerful in elucidating the variation of the electronic structure of an element as a function of its chemical and structural surrounding in the system under analysis. Molecular gases, liquids as well as metallic, semiconductor or insulator solids may all be studied alike. It is the purpose of this article to introduce several of these techniques, show their applications to specific electronic structures in atoms and solids and discuss their relative merits.

U. Kaldor and S. Wilson (eds.),
Theoretical Chemistry and Physics of Heavy and Superheavy Elements, 115–170.
© 2003 *Kluwer Academic Publishers.*

While diffraction methods give a spatial description of the electron distributions, the spectroscopic methods give information on the energy distributions of the electronic states and on energy level diagrams. Among these methods, core-level spectroscopy such as x-ray emission spectroscopy (XES) [1, 2], Auger emission (AES) [3] and x-ray photoemission spectroscopy (XPS) [4] give an almost direct view of the core and valence electronic orbitals. X-ray absorption spectroscopy (XAS) [1], electron energy loss spectroscopy (EELS) [5] and bremsstrahlung isochromat spectroscopy (BIS) [6] provide a similar view of the unoccupied levels. Except valence electron XPS and ELS as well as BIS, the concerned electronic transitions involve a core sub-shell.

The most difficult feature of the core-level methods is that the presence of the core hole induces a perturbation of all the filled and empty orbitals. The response of the system to this perturbation differs according its electronic properties. The importance and the characteristics of the perturbations have thus to be considered for each type of material. Interpretation difficulties exist but they offer possibilities of interesting studies. For example, the importance of electron-electron correlations can be deduced by comparing the experimental results with the theoretical data obtained in an one-electron model. Conversely, the validity of the electron-electron interaction energies obtained from *ab initio* calculations can successfully be determined by comparing the theoretical andexperimental distributions. Establishing reliable data from only one type of experiment is often difficult and the simultaneous use of several spectroscopic methods is required for a careful interpretation.

Spectroscopy is a time-dependent methodology. In XAS and EELS as also in XPS, interaction takes place between incident ionizing particles and the material in a very short time, equivalent to the "information time", before the perturbed states are created. *Static* information on these states are obtained from these methods. The study of the decay processes of the perturbed states to more stable states is a source of information about their dynamics. XES and AES can be used for this purpose; both are thus *dynamic* methods

Under charged particle bombardment, excited and ionized states can be created simultaneously. By comparing their decay rates, information on their relative stability can be deduced. Radiative and non radiative decays of an excited state with a core hole are observable only if the state is localized, i.e. if it is a discrete bound state of lifetime shorter or equal to that of the core hole. This condition is satisfied in the free atoms. In solids, it is generally not satisfied because the excited electrons are well described by extended wave functions. However, exceptions exist: they concern the excitonic-like states, the states associated with any

defect present in the material, involving impurity, vacancy or interstitial, surface or interface, and also electrons excited in f orbitals normally unoccupied in the absence of the core hole.

Included in the general aim of this article is a comparison of the behaviour of the s, p, d and f valence electrons. A specific objective concerns the f electrons of the lanthanides and the actinides. Emphasis will be put on experiments capable of determining the localized or itinerant character of the $5f$ electrons. Previously, it had been widely accepted, from energy-band calculations and indirect experimental methods that used cohesive energy values or magnetic properties, that in plutonium and lighter actinides the $5f$ electrons are not localized. Only in the heavier part of the series, the actinides start to resemble the rare earth metals and their $5f$ electrons become localized. Experimental x-ray spectra which can only be understood in a localized picture of the $5f$ states will be discussed. Great importance will be given to the study of excited states with an nd core hole because the observation of emissions from these states is a prove of the localized-like character of the excited f electrons in the solid. Experiment-theory comparison will be used as a test of the validity of the interpretations. This will be made by simulating the spectra with the help of an atomic model based on the *ab initio* calculations of the energies and probabilities of the lines. This model will also be used to simulate transitions between inner levels.

In solids, valence electron distributions can generally be predicted using a noninteracting electron gas model. Precision in the band calculations has considerably increased in the last decade for a large category of materials having valence s and p electrons, whatever their physicochemical states. The predictions are obtained by taking into account the crystalline arrangement and by supposing that the material is infinite, perfect and at the absolute zero temperature. Problems remain how describe the influence of the temperature, of the surface, of the defects or of any deformation.

The d electron distributions pose a critical problem because in some cases they cannot be treated with the same non interacting model as the s and p electrons. As an example, for the heavier $3d$ transition elements, the one-electron energy band calculations and molecular orbital calculations can only predict certain ground-state properties. Physical properties associated with excited or ionized states have to be treated beyond the one-electron picture.

XES and XPS supply many possibilities as methods for chemical analysis. Identification of the elements is possible by XES with a large sensitivity. Changes of the electron distributions are observed between the free atom, the molecule, the condensed material; for a solid, changes ex-

ist between the bulk, its surface, an interface, an aggregate, crystalline or amorphous phases, and so on. These changes involve all the core and valence electrons. Indeed the electron distributions are characteristic of the surrounding of the emitting atom, that is to say of its nearest neighbours and of the crystalline structure. They depend on its charge state, i.e. of its oxidation state and the electronegativity of neighbouring atoms. Electron distributions can be used to characterize the chemical bond and the physical-chemistry properties of the material under consideration. A few examples will be presented.

This brief review is not intended to be exhaustive. In all the models considered here, the coupling between the electronic terms and the thermal vibrations is not taken into account. Possibilities to observe the spin distributions or the angular dependence of the electronic distributions are not considered. Another restriction is the selection of examples that concern especially solids. All these, however, do not reduce the general approach of this article whose scope is to introduce the fundamental aspects of the subject and to present the contribution of the spectroscopic methods to improving our knowledge of the electron distributions.

1. Basic principles of electron and x-ray spectroscopy

1.1 General

In the absence of external perturbation, an atomic system is stable and does not emit radiation. When it is irradiated by ionising radiation, inelastic collisions take place between the incident, or *probe* particles, and those of the medium, or *target* particles. The atoms are perturbed, the system is unstable and photons, electrons, and eventually ions, are emitted. Information on the electronic structure is obtained from spectroscopic methods which analyse the perturbations of the system subsequent to the ionising collisions [7]. In these methods, the target particles are atomic electrons while the probe particles and the emitted particles are, indiscriminately, photons or charged particles.

In an inelastic collision between an ionizing particle and an electron of an atom Z, the atomic electron, initially present in the nlj sub-shell, makes a transition to an empty level, either discrete (excitation) or belonging to the continuum of the positive energies (ionization). The atom is left with a nlj vacancy; it is *singly excited* or *singly ionized*. During this transition, the system moves from the initial ground state i to the perturbed state e, which is the final state of the excitation or ionization process.

The perturbed atom reorganizes by emitting photons or electrons [8]. In emission spectroscopy, each transition corresponds to one of the reorganisation processes of the perturbed atom in the state e. In the case of first order processes, the $i \to e \to f$ transformation is considered as two independent processes. Thus, the $e \to f$ transition can be treated independently of the initial perturbation as a transition between an initial state $i = e$ and a final state f.

A quantum state is characterized by its energy distribution. The shape of this distribution depends on the evolution of the system with time. An excited or ionized atomic state with a vacancy nlj decays exponentionally as a function of time. The life-time τ_{nlj} is defined as the time it takes the state to decay in the e (2.732) ratio. Consequently, an nlj quantum state of life-time τ_{nlj} has a Lorentzian energy distribution whose full width at half maximum (FWHM) Γ_{nlj} satisfies the relation $\Gamma_{nlj} = \hbar\tau_{nlj}$. The energy of the state is equal to the energy of the distribution maximum. The ground state has an infinite life-time; its width is nil and its energy perfectly defined.

The inverse of the life-time is equal to the sum of probabilities of all the decay processes. The transition probabilities are defined by reciprocal time units. They are proportional to the square of a matrix element which depends on the electron wave functions of the initial and final states and the interaction operator between the atomic electron and the emitted particle. For a first order electron-photon interaction, it is the electric dipolar operator; for an electron-electron interaction, it is the Coulomb operator. In both cases, the magnitude of the matrix element depends on the overlap of the initial and final wave functions.

An $i \to f$ transition is associated, in the experimental spectrum, with a *spectral density* characterized by four parameters, energy, intensity, shape and width. The energy is the difference of the initial and final state energies. The intensity is proportional to the transition probability. The shape is the convolution product of the energy distributions of the initial and final states. For lorentzian distributions, the spectral density is lorentzian and its width is the sum of the widths of the initial and final distributions. If one of the states is known, it is possible to determine the characteristics of the another state.

In reality, the spectra are more complicated than those predicted by a simple model of transitions between monoionized degenerate states. The charge redistribution which accompagnies the creation of the inner holes induces additional perturbations. Perturbed states are present; they generate secondary peaks, labelled *satellites*, which are observed in the vicinity of the main transitions. The satellites represent the response of the system to the perturbation created by the presence of the core hole.

This response differs according the electronic characteristics, thus the type of the material considered. Consequently, different types of satellites exist and will be discussed. Among the perturbations accompanying the creation of an inner hole, the most probable are the ***shake-up*** and ***shake-off*** processes, which correspond to the excitation or the ionization of a second electron [9]. In an atom, their probabilities, nevertheless, remain small with respect to those of monoexcitation or monoionization.

On the other hand, when the atoms have partially filled sub-shells retaining an atomic character in the studied material, each singly ionized state shows multiplet splitting and the number of J-levels associated with both the initial and final states depends on the sub-shells. The spectral density shows a more or less marked multiplet splitting and this fine structure can make the shape of the spectrum rather complex.

It should be remarked that the broadening of the spectral line due to the measurement process is always present and hinders the determination of its shape and width. Indeed, the spectrometers have a finite resolving power, represented by an instrumental function. This function, often Gaussian, is the response of the instrument to a purely monochromatic radiation. Consequently, an observed line is the convolution product of the intrinsic line by the instrumental function.

1.2 Interactions with the probe particles

In order to choose the most convenient method for resolving a given problem and to deduce quantitative information from observed spectra, the interactions between the probe particles and the medium [10,11] and the characteristics of the irradiation must be known.

In the soft x-rays and X-UV ranges (few tens eV to few keV), individual excitations and ionisations, already mentioned above, are the most probable interaction processes of the electrons and the photons with the matter. All the atomic electrons which have a binding energy lower or equal to the energy of the incident photons ($h\nu$) or electrons (E) can be ionized. However, other processes have to be taken into account. Due to their charge, the electrons produce collective excitations of the electrons of the medium with the creation of plasmons. Elastic collisions of the probe particle must be considered. In the case of the electrons, they produce deviations of the trajectories with the possibility of backscattering and consequently a decrease of the number of electrons in the incident direction. For an incident photon beam, diffusion in various spatial directions is also present but its probability in the considered energy range is small.

The interaction strength between two particles is defined by the cross section σ, which is equal to the probability per unit range that the probe particle interacts with a target particle. This is the probability per time unit, w, referred to the flux of the probe particles ($\sigma = w/vn_s$, where v and n_s are the velocity and the number of the probe particles incident per volume unity). The cross sections depend on the energy of the particles in interaction. Since the target particles are considered at the rest, the cross sections depend on the energy of the probe particles.

Because the characteristics of the photons and the electrons, e.g. mass, charge, spin, are different, fundamental differences exist between their interaction modes with the matter. In an inelastic collision, the photon is annihilated and the totality of its energy is transferred to the system. Consequently, when a photon beam interacts by photoabsorption with the material, the number of photons decreases but their individual energy remains the same. In contrast, the electrons are deccelerated, they loose all or part of their energy but their number remains the same. After having crossed a sufficient thickness, the electrons are thermalized and free to move in the empty states of the material. The decrease dn of the number n of the probe particles (photons $h\nu$ or electrons having energy E), in the thickness dx, is given by

$$dn = -\sum_i \sigma_i n N dx$$

where σ_i is the cross section of the process i and N is the number of the target atoms per unity volume.

One defines the attenuation depth Λ as the mean path travelled by the probe particle between two interactions; it is

$$\Lambda = \frac{1}{\sum_i \sigma_i N}$$

For the photons, $\Lambda_{h\nu}$ is the inverse of the total absorption coefficient. For the electrons, Λ_e is the mean free path. Another important datum is the range of the electrons, $R(E_0 - E)$, i.e. the path in the target along which the mean energy of the electrons decreases from the incident energy E_0 down to E. After each collision, the electrons are deviated and move in any direction. If E is the threshold energy of a collisional process, the thickness contributing to this process, or *effective thickness*, can be deduced from $R(E_0 - E)$ by taking into account the deviations. Semiempirical formulas exist to calculate electron ranges and effective thicknesses [12, 13].

As already underlined, while $h\nu$ is constant, E varies from the incident energy E_0 up to a few eV, making the interaction of the electrons in

the target selective with the depth. The operators involved in the cross sections, $\sigma(h\nu)$ and $\sigma(E)$, are different, making their behaviour different. Thus, the cross section for photoabsorption is largest for the electrons nearest to the nucleus, i.e. the electrons most strongly bound. In contrast, the most probable electron-electron collisions are those with the smallest energy loss.

1.3 Photoemission

In photoemission, the sample is irradiated by photons of known energy and one measures the kinetic energy of the ionized electrons, or photoelectrons. The energy required to eject one electron from its initial nlj sub-shell to the vacuum level is labelled *binding energy*. When the incident photon energy is larger than the ionization thresholds of the atomic electrons, all electrons can be ionized. Peaks appear in the spectrum, each being characteristic of one or several non degenerate orbitals. In a solid, peaks characteristic of the core electrons and the valence densities of states (valence DOS) are present simultaneously. Photoemission is a direct method to determine the energies of the occupied orbitals [14].

Comparison between the experimental and theoretical binding energies requires that the energies be referred to the same reference level. For free atoms, the reference level is always the vacuum level. For solids, the experiments are referred to the Fermi level, but in the case of non conductor materials, the Fermi energy may be difficult to define. Moreover, secondary effects, such as charge effect and polarization effect of the surface, shift the experimental energies and corrections must be applied to take into account these different effects.

The peak intensity is proportional to the photoionization cross section of the incident photons. It depends also on the probability of the photoelectron to be emitted from the sample without being slowed down. An electron having suffered an inelastic collision, loses a part, or the totality, of its energy and does not contribute to the photoelectron peak. The solid thickness contributing to the spectrum is labelled *escape depth*; it is smaller than $3\Lambda_e$. For the electrons of 1 keV, it is of the order of 5 nm. Consequently, photoemission analyses only a superficial zone of the sample.

In photoemission, the initial state is the ground state. Therefore, each photoelectron peak describes the energy distribution of the corresponding final state. When the photoemission concerns an nlj atomic sub-shell, one expects the peak to be a lorentzian curve whose width is the inverse of the life-time of the nlj vacancy. Indeed, several effects make the spectra more complicated. Secondary peaks can be present and asymmetry can

obscure the true shape of the peaks. The predominant effects are the following:

- multiplet splitting due to the presence of unpaired electrons at the ground state.
- double excitation or ionization processes producing shake-up or shake-off satellites located towards the higher binding energy with respect to the single ionization peak.
- discrete and collective characteristic energy losses due to the inelastic collisions suffered by the photoelectron in its path up to the surface of the material. In conductors, this effect produces a continuum which broadens the original photoelectron peak towards the lower kinetic energy, i.e. towards higher binding energy. This introduces an asymmetry of the peaks, very large when the energy of the photoelectron is small and the density of states at the Fermi energy is large.
- presence of Auger peaks (cf. § 1.5).
- instrumental broadening that can deform the lines asymmetrically.

For the valence states, the photoemission peak describes the valence distribution weighted by the photoabsorption cross sections. Since valence states of different symmetries are generally present, the role of the cross sections can be important. As an example, the photoionization cross section of the s electrons is larger than that of the p or d electrons because the s electrons are closer to the nucleus. For an element, valence states of different symmetries can be mixed. Mixing is also present between the valence states belonging to different atoms in a compound. Consequently, in photoemission, the spectral density is the sum of all the valence states, each being weighted by its photoionization probability.

1.4 Discrete x-ray emission

The ionized or excited atomic states with an inner nlj hole decay by radiative processes to final states with a hole in a more external sub-shell. The energy of the emitted photons is equal to the difference between the energies of the two states; they are characteristic of the emitter atom. The probability of the radiative transitions depends on the characteristics of the wave functions associated with the two states. Only the electric dipolar transitions are intense. They fulfill the dipolar selection rules, $l' = l \pm 1, j' = j$ or $j \pm 1$, except $j = 0 \rightarrow j' = 0$. Significant departures from the dipole approximation are commonly thought to occur at

wavelenghts comparable to or smaller than the spatial dimensions of the electronic orbitals. Consequently, electric quadripolar emissions are observed only for the heavy elements. Indeed, their probability increases as Z^6 while the intensity of the dipolar emissions increases approximately as Z^4.

Radiative transitions between two states monoionized in an inner shell correspond to atomic lines, usually designated as $n'l'j' - nlj$ emissions; we label them *normal lines*. The x-ray normal lines can be defined as emissions at one vacancy (figure 4.1). This simple description is valid only for atoms or ions with closed sub-shells. In atoms with an open sub-shell, multiplet splitting is present. On the other hand, radiative transitions in excited atoms with an inner vacancy have been observed. These transitions will be discussed largely in section 4.. As in photoemission, satellite emissions are also present. The more intense ones correspond to transitions in doubly ionized or ionized-excited systems and are located towards the higher photon energy. Weak satellites corresponding to the simultaneous emission of one photon and one electron have been detected towards the lower photon energy; they are labelled *radiative Auger effect* [15].

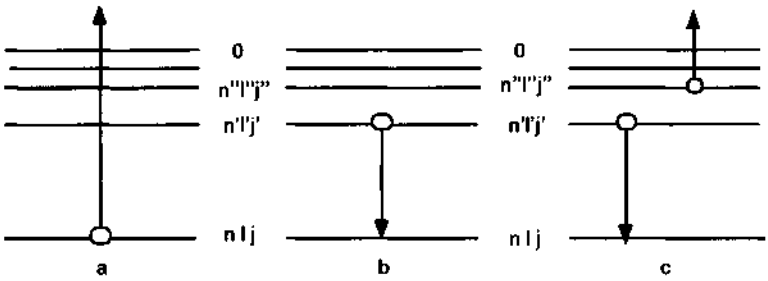

Figure 4.1 Radiative and non radiative transitions: initial state (a); final state of a normal line (b) and of Auger emission (c).

The transitions between a state missing an electron in the nlj inner shell and a final state with a hole in the valence band are labelled *emission bands*. The non vanishing transition probability matrix elements are those whose valence state wave functions overlap the atomic core ones and only they contribute to this emission. The transitions involved then satisfy the corresponding selection rules. Consequently the final hole is present in the states of the valence band which are characteristic of the ionized element and have the $l \pm 1$ symmetry. The corresponding spectral density is the convolution product of this local and partial valence DOS

by the lorentzian distribution of the inner hole. The energy distribution of the inner hole is known and the transition probability can be considered as constant along the width of the emission. Then, XES is the method from which direct information on the partial and local valence DOS can be obtained.

In order to deduce information on the electronic structure from the x-ray emission spectra, the shape of the emission bands has to be determined and their components identified. Fine structure, shape and intensity are better obtained from high-resolution experiments. The spectral resolution is higher for lower photon energy, making the soft x-ray region favorable for this type of analysis.

The intensity of an emission line depends on three factors: the number of atoms or ions created in the intermediate state, the transition probability and the self-absorption that this radiation undergoes. The effective depth depends on the creation of the ionized or excited state and on the reabsorption of the emitted radiation. It can vary from a few nm to a few μm. Because the intensity is proportional to the number of the emitting atoms, XES is largely used as a quantitative, non-destructive method of analysis of thin films as well as solids. Its sensitivity can reach several ppm [16]. When electrons are used as probe particles, the in-depth distributions of the ionizations and of the characteristic x-ray production can be determined from convenient simulation models, making possible the analysis of the depth profiles.

1.5 Auger emission

An ionized or excited atomic state with an nlj hole can decay by non radiative, or Auger, processes. An $n'l'j'$ electron jumps to the nlj hole and the energy difference is used to ionize another $n"l"j"$ electron. The two holes, $n'l'j'$ and $n"l"j"$, are present in the final state (figure 4.1). An Auger transition is designated by the $nlj - n'l'j'n"l"j"$ (or $K - LL$, $K - LM$, ...) notation. When the nlj and $n'l'j'$ sub-shells belong to the same shell ($n = n'$), the Auger transition is labelled *Coster-Kronig transition*. If the three electrons belong to the same shell, it is a super-Coster-Kronig transition.

The energy of the Auger peaks is characteristic of the atom and independent of the energy of the probe particles. Like in XES, the intensity of the Auger peaks depends on the overlap of the wave functions associated with the sub-shells involved and the number of initial states created by the interaction with the probe particles. Moreover, like in photoemission, the intensity depends on the probability of the Auger electron

to be emitted from the sample without being slowed down. AES is an analysis method of the surface.

Auger transitions create doubly and multiply ionized states. Indeed, cascades of Auger transitions can take place in an ionized state. When Coster-Kronig transitions are energetically possible, they can be very intense. As an example, in heavy elements, an L_I vacancy has more than 50% probability to decay by the $L_I - L_{III}X$ Coster-Kronig transitions and about 20% by $L_I - L_{II}X$ transitions [17]. Consequently, the probability to create doubly ionized states by Auger effect is generally larger than by shake-off effect.

1.6 Complementarity between the different core spectroscopies

XES, AES, XPS and XAS are complementary methods and interpretations obtained from one of these methods must be verified from the others.

First, let us consider XES and AES. From an ionized state, radiative and Auger transitions take place simultaneously. One, or several, Auger peaks correspond to each x-ray line. Indeed, in the x-ray range, the energy of the emissions is higher than the threshold energy of the most external atomic shells, making the Auger processes energetically possible. The same considerations are valuable for the excited states. Consequently, whether excited states with a core hole are deduced from AES in a material, transitions characteristic of these states must be observed by XES in this same material and vice versa.

Let us consider a state i with a vacancy in the nlj sub-shell. The sum of the probabilities of all the radiative (P_{ri}) and Auger (P_{nri}) transitions from this state is equal to the unity. The fluorescence yield ω_{nlj} of the state i is

$$\omega_{nlj} = \Sigma P_{ri}/\Sigma(P_{ri} + P_{nri}).$$

The Auger yield ω_{Anlj} is complementary of the fluorescence yield

$$\omega_{Anlj} = 1 - \omega_{nlj}.$$

The Auger yields are roughly Z independent while fluorescence yields vary roughly as Z^4. For the light elements, ω_{Anlj} is much larger than ω_{nlj} while for the inner shells of the heavy elements, the two yields become comparative.

Secondly, let us consider XPS and XES. The x-ray normal emissions take place between two inner sub-shells, nlj and $n'l'j'$, in the singly ionized element. Consequently, their energies are equal to the difference between the binding energies of the two nlj and $n'l'j'$ sub-shells, or nlj

and $n'l'j'$ energy levels. This property has been used to determine the energy levels of elements. Conversely, the energies of normal x-ray emissions can be determined from the energy levels as deduced by photoemission. Relation between XPS and XES can, thus, be used to identify the photoemission main peak when several peaks of comparable intensity are simultaneously present in the spectrum. Finally, energy differences between excited and ionized states can be deduced by comparing XAS and XPS.

In BIS, the continuous radiation, or bremsstrahlung, emitted by the sample irradiated by an electon beam is analysed at pre-fixed photon energy as a function of the energy E of the incident electrons. When E crosses an nlj threshold, the spectrum describes the energy electron distribution of the empty states. No core hole is present in contrast to XAS. The total DOS corresponding to the distribution of a hole in the valence band or an electron in the conduction band can be deduced from valence photoemission and BIS.

2. Binding energies

2.1 Atomic effects

In a multielectron system with N electrons, the binding energy E_b of the nlj electrons is determined from photoemission. Indeed, the ejection of a nlj electron is described by the relation of energy conservation

$$E_{tot}(N) + h\nu = E_{tot}(N-1) + E_k$$

where $E_{tot}(N)$ and $E_{tot}(N-1)$ are the total energies of the system with N or $N-1$ electrons, $h\nu$ is the energy of the incident photon and E_k is the kinetic energy of the photoelectron. The binding energy of the nlj electron is the difference between the energies of the initial ($E_i = E_{tot}(N)$) and final ($E_f = E_{tot}(N-1)$) states of the ionization transition.

For a free atom of atomic number Z, the E_i and E_f energies are the eigenvalues of the hamiltonians with Z or $Z-1$ electrons. In the final state, all the $Z-1$ electrons are perturbed by the change of potential which follows the ionization process. In the single particle picture, i.e. in the approximation of the frozen orbitals or Koopman's theorem, the binding energy of the nlj sub-shell should be equal to its one electron orbital energy $-\epsilon_i$. The difference between $-\epsilon_i$ and $(E_i - E_f)$, labelled *relaxation energy* E_{rel}, is positive [18].

$$E_b = E_i(Z) - E_f(Z-1) = -\epsilon_i + E_{rel}$$

This relaxation energy is labelled the *intra-atomic relaxation* term; it introduces a decrease of the binding energies with respect to the one-

electron energies. Indeed, the atom orbitals adjust to screen the positive charge created by the ionization and this supplementary screening explains the decrease of the binding energies. Tables exist giving the calculated binding energies of the sub-shells of all the elements [19].

Comparison between the experimental [20,21]. and computed energies is presented in Table 4.1 for Xe. The calculations are made with a MCDF program [22]. The total energies, $E_i(Z)$ and $E_f(Z-1)$, are determined with respect to the vacuum level. The differences $E_i(Z) - E_f(Z-1)$ and the intra-atomic relaxations E_{rel} are calculated for all the sub-shells (cf. columns 2 and 3). The relative value of the relaxation energy increases with the quantum number n from 0.6% for $n = 1$ to about 7% for the more external sub-shells. The energy differences E_{if} obtained by computing simultaneously the initial and final state energies from the average level extension of the MCDF method coupled with the Slater transition state [23] are also plotted (column 4). The energies E_i, E_f and E_{if} are determined by taking into account the contributions due to the Breit operator, to the self energy, the vacuum polarisation and the nucleus volume. All these corrections increase the energy of the Xe ground state by about 0.1%.

The differences between the experimental (column 5) and computed energies, $E_i - E_f$ or E_{if}, are of the order of the experimental error. The relative error is higher in the lower energy range; it is the highest for the ns sub-shells because the lifetimes of the ns holes are the shortest, resulting in a broadening of the spectra and contributing to reduce the precision of the measurement. A particular case exists for $4p$ sub-shells. In the elements around Xe, the energies of the $4p$ sub-shells are close to the energy of the $4d^{-2}4f$ double ionization-excitation process where the excitation involves the final $4d^{-1}4f^1\ {}^1P_1$ excited level. Thus quasi resonance exists between the $4p^{-1}$ and $4d^{-2}4f$ configurations, inducing the $4p^{-1}$ ionized state to decay by a particularly intense $4p^{-1} - 4d^{-2}4f$ super Coster-Kronig process. Consequently, the $4p$ sub-shell peaks are disturbed [25]. This is a typical example of strong many-electron effect in core hole spectrum.

The change of the potential due to the creation of the inner hole can induce a change of the electronic configuration. Such changes take place in the atoms having d or f open sub-shells, that is to say for the transition elements, the lanthanides and the actinides, but also for the elements situated just before them in the periodic table. They correspond to an increase of the number of the d or f electrons in the presence of an inner hole.

Calculations are performed as indicated above. In a first step, the ground configuration of the neutral atom and of the ions having lost one,

Table 4.1 Energies (eV) in Xe.

	$\lvert E_i - E_f \rvert$	E_{rel}	$\lvert E_{if} \rvert$	exp
$1s$	34563.3	192.2	34556.8	$34561.6^{(a)}$
$2s$	5459.4	49.8	5456.4	$5452.8^{(b)}$
$2p_{1/2}$	5107.8	53.7	5104.7	$5103.7^{(b)}$
$2p_{3/2}$	4787.2	48.3	4783.4	$4782.2^{(b)}$
$3s$	1151.6	18.8	1150.5	$1148.7^{(c)}$
$3p_{1/2}$	1005.5	19.3	1004.5	$1002.1^{(c)}$
$3p_{3/2}$	943.4	18.0	942.0	$940.6^{(c)}$
$3d_{3/2}$	689.2	18.8	688.0	$689.0^{(c)}$
$3d_{5/2}$	676.5	18.5	675.2	$676.4^{(c)}$
$4s$	222.7	6.7	222.4	$213.2^{(c)}$
$4p_{1/2}$	169.2	6.3	168.9	$146.7^{(b)}$
$4p_{3/2}$	156.8	5.9	156.4	$145.5^{(c)}$
$4d_{3/2}$	68.5	5.2	68.2	$69.5^{(c)}$
$4d_{5/2}$	66.5	5.1	66.2	$67.5^{(c)}$
$5s$	26.5	1.0	26.4	$23.3^{(c)}$
$5p_{1/2}$	12.5	0.8	12.6	$13.4^{(c)}$
$5p_{3/2}$	11.2	0.8	11.2	$12.1^{(c)}$

[a] Ref. [24]. [b] Ref. [21]. [c] Ref. [14].

two or three valence electrons is verified by taking into account all the configurations which can contribute to the optical spectrum, as indicated in Moore's tables [26]. Then, the ground configuration of the free atom in the presence of a core hole is determined. All the J-levels of each configuration are taken into account. For the transition elements with $nd^m(n+1)s^2$ as ground configuration and with $nd^{m+1}(n+1)s^1$ as the lower excited one, the presence of a core hole in any X sub-shell intro-

duces a remarkable reverse of order and the ground configuration of the ion becomes $X^{-1}nd^{m+1}(n+1)s^1$. In contrast, if the lower excited configuration is of the nd^{m+1} type, this reverse of order does not take place and the ground configuration of the valence electrons remains unchanged in the presence of the core hole.

This result is in agreement with the empirical model according to which the ionization of a core electron can be considered as equivalent to the increase of the proton number by one unit. In this concept, labelled *equivalent-core model*, the spectral characteristics of a Z atom with a core hole are considered as equivalent to those of a $(Z+1)$ atom monoionized in its external shell. For the transition elements, the corresponding configuration is well of the $nd^{m+1}(n+1)s^1$ type, except for Cr and Mo. In both elements, the ground configuration is d^5s^1 while that of the $Z+1$ element is d^5s^2. Consequently, the configuration remains of the d^5s^1 type in the presence of a core hole.

For the lanthanides, the $5d$ and $4f$ open sub-shells are in competition, making the situation to be complex. The ground configuration of the neutral atoms is either $4f^m5d6s^2$ or $4f^{m+1}6s^2$. Their lower excited configuration is $4f^m5d^26s$ or $4f^{m+1}5d6s$. The ground configurations of the singly charged ions are $4f^m5d6s$ or $4f^{m+1}6s$ and of the doubly ones are $4f^m5d$ or $4f^{m+1}$. Only for the three time charged ions, the ground configuration is $4f^m$ for all the lanthanides. When a core hole is created in any core sub-shell of the $4f^m(5d+6s)^{m'}$ ion (with $m' = 3, 2, 1, 0$), MCDF calculations show that the ground configuration is of the $X^{-1}4f^{m+1}(5d+6s)^{m'-1}$ type. In contrast, for atoms and ions of $4f^{m+1}(5d+6s)^{m'}$ $(m' = 2, 1, 0)$ ground configuration, no change of the f electron number is predicted in the presence of core hole.

For the actinides, the $6d$ and $5f$ open sub-shells follow the behaviour of the lanthanides. The ground configurations of neutral and several times charged uranium are given in Table 4.2, simultaneously with MCDF calculations of the uranium $3s$ sub-shell for various valence configurations. Neutral uranium has the $5f^36d7s^2$ ground configuration. In the presence of a core hole, its ground configuration is $X^{-1}5f^46d7s$. However, the probability to observe this configuration is weak and the spectra are well described from the $X^{-1}5f^36d7s^2$ configuration.

An interesting example concerns neutral barium whose ground configuration is $6s^2$. In the presence of one $4d$ or $5p$ vacancy, the ground configuration becomes $5d^2$. In the case of the $4d^94f^1$ and $5p^54f^1$ excited configurations, the ground configuration is again $6s^2$, i.e. the same as for the neutral atom [27]. The $4f$ excited electron screens sufficiently the core hole for that configuration change does not occur.

Table 4.2 Configurations and energies (eV) in the U atom.

	ground configuration	$3s^1$ binding energy
U	$5f^36d^17s^2$	$3s^15f^36d^17s^2 = 5558.9$ eV
U^+	$5f^36d^17s^1$	$3s^15f^47s^2 = 5555.5$ eV
U^{2+}	$5f^36d^1$	
U^{3+}	$5f^3$	$3s^15f^36d^1 = 5573.0$ eV
U^{4+}	$5f^2$	$3s^15f^4 = 5568.4$ eV

In summary, when an atom with a d or f open sub-shell is ionized in its valence shell, the s and p electrons, characterized by the most extended wave function, are preferentially ejected. In the presence of a core hole, the d and f electrons are partially stabilized and electron redistribution between the valence orbitals can take place. This redistribution is one of the possible responses of the atom to the perturbation accompanying the creation of the core hole; it leads towards an increase of the screening. Only a small number of the core-ionized atoms are concerned by this electron distribution, most of them preserving the configuration of the non perturbed atom. In photoemission, it corresponds to the perturbed configuration a peak located towards the lower energies of the main peak. Such a peak of weak intensity has been observed for a few cases; it has been labelled *shake-down* peak (cf. § 3.2).

2.2 Effects due to the surrounding

During the conversion from a free atom to an atom in the solid state, all the electron shells are affected and the binding energies of the inner levels decrease. The difference, ΔE_b, is the sum of several factors. One of these factors is due to the change of the valence electron distribution. In the free atom, the valence electrons are bound while in the solid they are partially delocalized because the interatomic interactions with the nearest neighbour atoms can dominate the intra-atomic interactions. This introduces an increase of the repulsive term in the potential energy of the inner electrons and consequently a decrease of their binding energy.

A second factor is due to the change of the relaxation energy with the change of the valence electron distribution. This term is labelled the *extra-atomic relaxation energy*. It, too, contributes to the decrease of the binding energies. Its magnitude changes according to whether the valence electrons are bound or delocalized in the solid. It increases

with the delocalization of the valence electrons, thus with theirmobility. Consequently, it varies with the characteristics of the binding and is larger for conductors than for insulators. Indeed, the relaxation of the valence-band electron towards the hole is quasi complete when the valence electrons are quasi free, i.e. in the simple metals (*sp* metals). The calculation of both factors is difficult.

To these factors one must add the possibility of changes in the electronic configuration in the presence of an inner hole. The variation in the binding energies associated with a configuration change is clearly larger than that due to the other terms. When the configuration is modifies in the free atom, one can expect a modification of the same type in the solid. These changes involve an increase of the number of the *d* or *f* electrons. In metallic solids, a *d* or *f* orbital close to the Fermi energy could be pulled down by the core hole, making this orbital occupied in the ionized state. It should correspond to it a shake-down peak.

In non conductor compounds, if a metal ion has empty orbitals which can be localized in the presence of the core hole, electron transfer can take place from the ligand to these orbitals. The probabilities of this process increases with the covalence by following the same order as that of the nephelauxetique series [28, 29]. The satellites obtained are often designated as *charge transfer peaks*. They correspond to a doubly excitation-ionization process from the ground state. They are thus shake-up-like satellites. All these considerations must be taken into account in the interpretation of the photoemission spectra. They will consider in details in section 3.2.

A change of the charge density around an atom introduces a change of the potential in which the atomic electrons move and, consequently, a change of their binding energy. This is the origin of the inner level shift with a modification in the environment of the atom, labelled *chemical shift* [30]. The binding energies depend on the fractional charge of the element, thus on the polarisability of the medium and the electroaffinity of the neighbouring atoms [31, 32]. Their variation with respect to the pure element increases with the ionicity of the binding. They depend also on the crystal field; they are different for the bulk, the surface or an interface. From the precise measurement of the binding energies, it is possible to characterise the binding state of an element present in a material, solid, liquid or gazeous and its variation as a function of the chemical surrounding. Tables giving the binding energies of the elements in their various compounds are available.

3. Transitions between localized states

When transitions take place between localized states, the spectra can be simulated with the help of an atomic treatment. This is the case for the transitions between core levels, such as the normal emissions and their satellites in XES (§ 3.1), and for the core peaks in XPS (§ 3.2). From the observation of the x-ray normal emissions, informations on the dynamic of the ionized states in an inner shell and numerous atomic parameters can be deduced. Precise values of the differences between the core level energies are obtained from the position of the lines. The energies of the electrostatic and spin-orbit interactions are determined from the fine structure. The relative probabilities of the radiative decay processes are deduced from the measurement of the intensities. These data are necessary to obtain the atomic parameters on which depend the excitation and ionization processes and the radioactive processes, electron capture and internal conversion. From the relative intensity of the high and low energy satellites, the relative importance of the secondary effects which give rise to them is determined. All these parameters depend on the external electronic configuration of the emitting atom and on its chemical environment in the studied material. Lastly, comparisonbetween the spectroscopic parameters and the calculated data can be used to test the validity of the theoretical simulations.

Excited states with a core hole can also be created in solids. When excited states have a localized character, their decay introduces interesting peculiarities in the spectra that can be treated in the atomic model. Creation and decay of these states will be discussed in section 4..

3.1 X-ray normal emissions and their satellites

X-ray normal emissions are calculated for atoms or ions of different external configurations with the help of the above-mentioned MCDF program. Wave functions, energies and transition probabilities are computed. The initial and final configurations of the emissions are obtained simultaneously from the Average Level Extension of the MCDF method coupled with the Slater transition state (method I). In this model, each vacancy is shared between both sub-shells and the correlation effects are minimized. Another weighting model can also be used, in which the weight assigned to each initial or final configuration is equal to its statistic weight (method II). The length and velocity forms of the transition matrix elements are used. The simulated emission is obtained by folding the theoretical probability with a Lorentzian broadening function whose width is equal to the intrinsic width of the transition, as defined from the lifetimes of the initial and final configurations. The width of the state i,

Γ_i, is proportional to the sum of all the radiative, P_{ri}, and non radiative, P_{nri}, decay probabilities from this state (cf. § 1.6). If the fluorescence yields ω_i and ω_f are known [33, 34], the width Γ of a line between the monoionized states i and f can be determined first by calculating ΣP_{ri} and ΣP_{rf} and then by using the relation

$$\Gamma = \Gamma_i + \Gamma_f = \hbar \Sigma P_{ri}/\omega_i + \hbar \Sigma P_{rf}/\omega_f$$

Finite experimental resolution is taken into account with a Lorentzian or Gaussian broadening function.

The shorter the life-time the broader the line width; for a given level, the width increases with increasing E_{nlj}, i.e. as Z increases. For the $1s$ level, the life-time varies from some 10^{-14} s for Li to about 10^{-17} s for U. This intrinsic broadening limits the spectral resolution and the lines profiles should be studied in the soft x-ray region. However, low energy levels can be broader than those of a more inner sub-shell if Coster-Kronig non radiative transitions are possible from these levels. As an example, the width of Ni L_{III} (855 eV) is only 0.6 eV whereas that of M_{III} (68 eV) is 3.8 eV because of the presence of the intense $M_{III} - M_{IV,V}M_{IV,V}$ super-Coster-Kronig transitions [35].

For atoms having one, or several, open sub-shells, the ionized configurations split into J-levels. All the J-levels of an ionized configuration are populated statistically and the interaction between them is strong. The radiative emission is the sum of all the allowed lines that connect the various J-levels of the initial and final configurations. The simulated emission is obtained by summing over all the electric dipole lines, each being weighted by the statistical weight of its initial J level. The energy of the emission is the average energy, or barycenter, obtained by making the weighted average of energies of all the lines. The probability is the average value obtained by making the weighted sum of probabilities.

Let us consider the $np - 1s$ emissions of the transition elements. When the np spin-orbit interaction is large with respect to the electrostatic interaction between the np hole and the open d sub-shell, the peaks associated with the $np_{3/2} - 1s$ and $np_{1/2} - 1s$ transitions are well separated; their intensities are in a ratio close of 2/1 and their shape is almost symmetrical. This is verified for $n = 2$. In contrast, for $n = 3$ and the $3d$ transition elements, the interaction between the $3p$ hole present at the final state of the transition and the open $3d$ sub-shell is largely predominating. It creates a large splitting of the $3p - 1s$ emission which spreads on 10 eV and more. In this case, the width of the emission is governed by the energy distribution of the initial and final states and not by their life-times. The same considerations are valid for the $nd - 2p$ transitions. When the spin-orbit interaction is large enough, one ex-

pects three distinct symmetric lines, $nd_{5/2} - 2p_{3/2}$, $nd_{3/2} - 2p_{3/2}$ and $nd_{3/2} - 2p_{1/2}$, allowed by the electric dipolar selection rules. The three lines are observed for the $3d - 2p$ transitions of the elements of $Z > 36$. In contrast, the $4d - 2p$ transitions of the rare earths are strongly split by the interaction between the $4d$ sub-shell and the open $4f$ sub-shell.

High-energy satellites are due to transitions in doubly, or multiply, ionized atoms. An additional inner hole shifts the transitions towards the higher energies and the shift is the greater the deeper the shell containing the additional hole. Simulation of satellites can be performed and comparison between energies of normal and satellite emissions can be made. It is found that their transition probabilities are similar. However, the experimental intensities of the two types of transitions are very different. As seen § 1.4, the intensity of the emissions depends both on the transition probability and the number of atoms in the initial state. In the case of the satellites, this number is the number of atoms in doubly ionized states. Consequently, the relative intensities of the satellite and the normal emission contains information on the probability to create the doubly ionized states.

For K emissions, only double ionization by shake-off process is to be taken into account. These processes satisfy the monopole selection rule. They are described in the sudden approximation and their probabilities increase with the ejection velocity of the first electron, i.e. with the energy of the probe particles, approximatively up to twice the ionization threshold. The second hole is most likely to be in the outer sub-shell, i.e. in the valence states. As an example, following a $1s$ vacancy in argon, the probability of shake-off from the $3p$ shell is 17.3% whereas from $1s$, it is only 0.001% [36]. Shake-up and shake-off processes accompany the hole creation, whatever the nlj sub-shell, and are present in the free atoms as well as in the solids. However, since the core hole induces a change in the potentiel in the core region, these processes are all the more probable if almost localized valence states are present in the material. Consequently, they have an important role in the spectra of the rare earths and the actinides.

For L, M, ... emissions, double ionization by Auger and Coster-Kronig processes are the more probable. It is possible to identify the double ionization satellites by decreasing the energy of the probe particles. As an example, non resolved features are present towards the higher energy of the Cu $L\alpha$ ($3d \rightarrow 2p_{3/2}$) emission. For probe particles of energy lower than the $2s$ and especially $2p_{1/2}$ thresholds, there is a considerable decrease of the intensity of these features [37]. This result shows that the $L_I - L_{III}X$ and $L_{II} - L_{III}X$ Coster-Kronig transitions have an important role in the creation of doubly ionized states with a $2p_{3/2}$ hole

and the appearance of secondary emissions. Consequently, if Coster-Kronig satellites are present, they must be taken into account in the determination of the shape of the principal lines.

Among the low-energy satellites, transitions due to radiative Auger effect (RAE) have been studied extensively in the $3d$ transition element range. According to theoretical predictions based on the shake model [38], the $K - MM$ RAE components should be the most probable. Their relative probability with respect to that of the $3p - 1s$ normal emission should be about 4%. Experimentally, the intensity of $K - MM$ satellites is clearly weaker than the predicted value [39]. This result shows that the RAE probability is not well described in the shake approximation. A new model is necessary to describe this process.

It has been suggested in numerous works published on the $3d$ transition elements that most of their atomic parameters are linear functions of the number of $3d$ electrons. As a new example, a recent study of the Mn K spectrum varying the number of $3d$ electrons is presented below. The L and M emission spectra of the rare earths have been widely studied. The influence of the n-$4f$ strong interaction, with $n = 4$, on the shape of the emissions is shown here. Concerning the actinides, the fine structure of the uranium N normal lines has been studied. An example is presented; it shown the important role of the nl-$5f$ interactions (with $n = 5$) on the spectrum.

3.1.1 Mn K emission spectrum [40]. The previously described *ab initio* calculation was used in the simulation of the $K\alpha_{1,2}$ ($2p \rightarrow 1s$) and $K\beta_{1,3}$ ($3p \rightarrow 1s$) normal emissions and their satellites for the Mn (Ar) $3d^n$, $3d^n4s^1$ or $3d^{n-1}4s^2$ configurations with n varying between 6 and 4. The energies and the intensities are deduced for each valence configuration. Each emission results from several thousands of closely bunched lines. However, the $K\alpha_1$ and $K\alpha_2$ peaks are well resolved; their width is only 4 eV and their shape is almost symmetrical. In contrast, the non resolved $K\beta_{1,3}$ emission spreads on about 20 eV and its energy broadening is governed by the energy distribution of the final state.

In figure 4.2, the experimental and the simulated $K\alpha_{1,2}$ doublets are plotted. The theoretical curve has been ajusted to the maximum of the $K\alpha_1$ emission (5898.7 eV) by shifting it by 3.5 eV towards the lower energies, i.e. by 0.06% of the absolute value of the energy. Good agreement exists between both curves. Indeed, the $K\alpha_1 - K\alpha_2$ splitting, the relative intensities and the shapes of $K\alpha_1$ and $K\alpha_2$ emissions are similar. When the experimental spectrum is plotted on a logarithmic scale to enhance the weak intensity emissions, a structure is observed towards the higher energies of $K\alpha_{1,2}$, at the position calculated for the $KL - LL$

double ionization satellites. In contrast, no structure is seen towards the lower energies of the $K\alpha_{1,2}$ doublet and the shape of the spectrum is characteristic of a pure x-ray emission in this energy range.

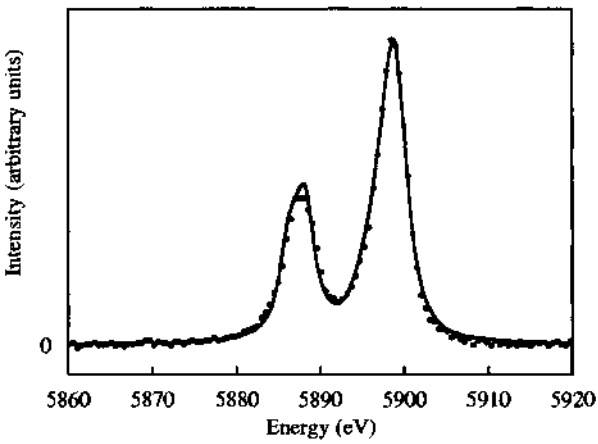

Figure 4.2 Experimental (dots) and simulated (line) $K\alpha_{1,2}$ emission of metal Mn.

Experimental and simulated $K\beta_{1,3}$ emissions are plotted in figure 4.3. They are ajusted at their top. The $K\beta_{1,3}$ emission is asymmetrical towards the lower energies and this asymmetry varies with n. No satellite is seen in this range. The simulated curve reproduces well the low-energy tail of the experimental curve which spreads out about 20 eV. The asymmetry of the $K\beta_{1,3}$ emission is due to the interaction between the open $3d$ sub-shell and the $3p$ hole. Our calculations, carried out for free atoms, support this interpretation. Indeed, the $3p$-$3d$ exchange energy, about 10 eV, is the dominant interaction. It is much larger than splitting due to the $3p$ spin-orbit and to the ligand field (âabout 1 eV for the Mn d orbitals in a cubic field). This explains why the atomic calculations fit well the experimental data for the solid. The shape of the $K\beta_{1,3}$ emission is governed by the large splitting of the final configuration, i.e. by its energy distribution. It depends on the number of the unpaired $3d$ electrons and is very sensitive to the oxidation degree of Mn, i.e. to the chemical environment of the emitting atom.

Towards higher energies, the experimental spectrum is higher than the simulated one. The difference can be explained by the presence of the satellites arising from the KM double initial ionization. They have been calculated and are plotted in figure 4.3. Double ionization $KM - MM$ satellites are not resolved from the normal line because of the complexity

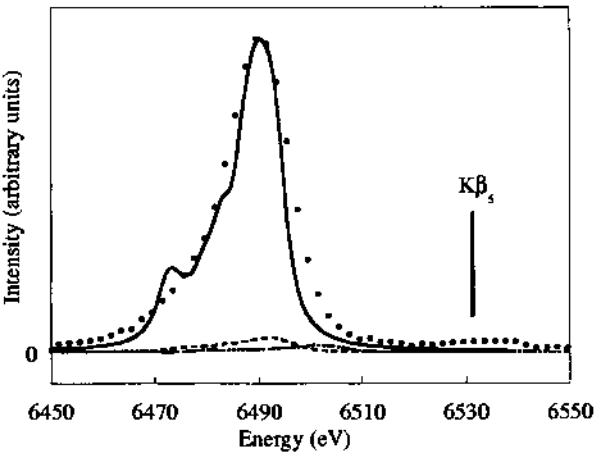

Figure 4.3 Experimental (dots) and simulated (line) $K\beta_{1,3}$ emission of metal Mn; $KM - MM$ satellites (dashed lines).

of the configurations with a supplementary hole. They appear only as a tail on the high-energy side of the emission. The satellites due to KL doubly ionized atoms, are clearly separated from the normal emission; their intensity can be neglected because the shake-off creation of the KL states is much less probable than that of the KM states.

Weak emission is observed in the metal spectrum at 6531 eV, the expected energy for the $K\beta_5$ ($3d \rightarrow 1s$) transition. From the theoretical calculation in the free ion, its relative intensity should be very weak, less than 0.1% of $K\beta_{1,3}$. However, because the $3d$ and $4sp$ valence electrons are energetically mixed in the solid, one expects to observe a $4p - 1s$ emission at the position of $K\beta_5$ with an intensity clearly higher than that calculated for the quadrupolar transition. This result shows that the mixing between the valence states of different symmetries of the same element can be derived from x-ray emissions. In the same way, mixing between the states owing to two different elements present in a same compound can be deduced from XES. Examples will be given in section 5..

The energies of the $K\alpha_{1,2}$ and $K\beta_{1,3}$ normal emissions of Mn (Ar) $3d^n$ vary with n in an opposite manner. When the oxidation degree of Mn increases, i.e. n decreases, $K\alpha_{1,2}$ shifts towards the lower energies while $K\beta_{1,3}$ shifts in the opposite direction. These predictions are in agreement with the experimental data. The average probability of the $K\alpha_{1,2}$

emission decreases by less 0.1% with n decreasing while the probability of the $K\beta_{1,3}$ emission increases by about 10% with n decreasing.

This study establishes, for the transition elements, the dependence of the atomic parameters on the electronic configuration, more specifically on the number of its d electrons. Conversely, these parameters, in particular the energy of the x-ray emissions, can be used to determine the oxidation degree of the transition elements in their different compounds.

3.1.2 Rare earth x-ray emissions. The normal lines of rare earths were known as showing a large splitting. This is the strongest for the lines involving the $n = 4$ sub-shell. The present example concerns the Er $4d - 2p$ emissions. The $2p$ spin-orbit coupling is large and the $4d - 2p_{3/2}$ and $4d - 2p_{1/2}$ emissions are separated by about 900 eV. They are simulated by using the method described above. The neutral Er ground configuration is $4f^{12}5s^2$. In the trivalent ion, it is $4f^{11}$. The simulated spectra of Er^{3+} ion are plotted in figure 4.4 and compared to the experimental spectra observed for the trivalent oxide. The arrays of 21708 allowed lines of $4d - 2p_{3/2}$ and the 11442 allowed lines of $4d - 2p_{1/2}$ are taken into account simultaneously in the calculations. Each spectrum spreads over several tens of eV and shows fine structure characteristic of the large number of multiplets of the initial and final states. General agreement exists between the experimental and calculated emissions.

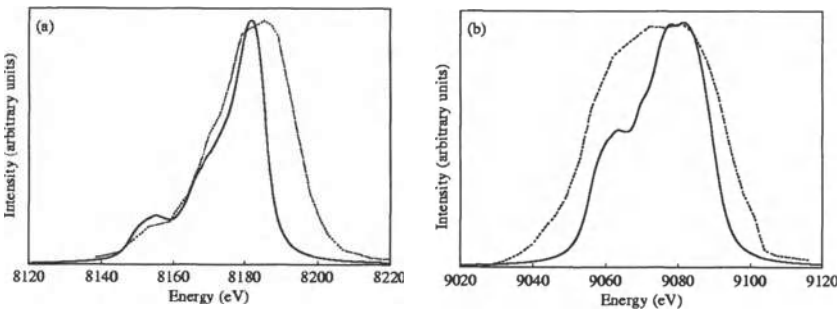

Figure 4.4 Experimental (dashed line) and simulated (solid line) emission of Er in oxide: $4d - 2p_{3/2}$ (a); $4d - 2p_{1/2}$ (b).

3.1.3 Uranium x-ray emissions [41]. In order to determine the importance of the interaction between a core hole and the open $5f$ sub-shell in the actinides, the shape of U $5p_{3/2} - 4d_{5/2}$ emission in UO_2 has been studied. Four electrons are present in the valence band and are

partially delocalized in the solid. Thus, uranium can be approximated as a U^{4+} ion with ground configuration $5f^2$. The observed spectrum is plotted figure 4.5. It spreads over about 7 eV and shows an extensive fine structure with a maximum situated at 546 eV and a shoulder at 543 eV. The simulated spectrum of the U^{4+} $5f^2$ free ion, obtained using the same method is plotted by shifting it by 12 eV towards the higher energy to make easier the comparison between the shapes of both curves. In the absence of the open $5f$ sub-shell, one expects one Lorentzian line centred at about 543 eV. For U^{4+}, the initial and final states, $4d_{5/2}^{-1}5f^2$ and $5p_{3/2}^{-1}5f^2$, have 62 and 45 J-levels respectively, all included in the calculation. The structures of the calculated spectrum reproduce rather well those of the experimental one; it spreads about 8 eV. This large spreading is not a lifetime effect; it results from the large splitting associated with the presence of the open $5f$ sub-shell.

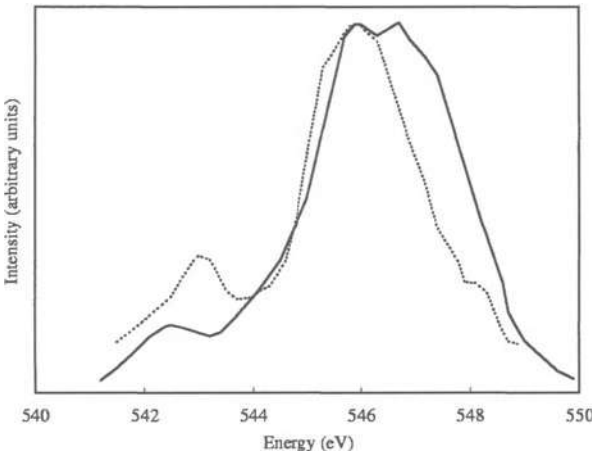

Figure 4.5 **Experimental (dashed line) and simulated (solid line) $5p \rightarrow 4d$ emission of U in UO_2.**

In summary, the experiments presented here were made for solids where the intra-atomic interactions are expected to be smaller than for the free ion. The agreement between the shape of the experimental and simulated spectra shows that, in the presence of a core hole, the effect of splitting due to the open d or f sub-shells is noticeable in solids. The main characteristics of the normal x-ray emissions originating from transitions between core levels observed in a solid can thus be obtained by using our atomic model. Energy shifts between the experimental and simulated spectra are directly related to the difference between the real

charge seen by the atom in the solid and the atomic charge assumed in the calculation. Since this shift is noticeable for uranium, it means that the charge for solid U is smaller than 4. For Er metal and compounds, no shift is observed proving that the charge 3 used is the correct one.

3.2 Core photoemission

As already underlined, various secondary processes can be associated with the creation of the core hole: shake-off or shake-up which results in satellites located towards the higher binding energies of the main peak; characteristic energy losses of the photoelectron, resulting in asymmetry and structures towards the higher binding energy; shake-down giving peaks towards the lower binding energies.

For the systems with s and p valence electrons, the secondary processes are essentially the characteristic energy losses. Photoemission spectra of the core sub-shells for an element of well defined physicochemical state are characterized by non structured intense peaks and their interpretation is easy. On the other hand, when an element is present in various crystalline structures or various compounds, several peaks are associated with each sub-shell because the binding energies vary with the structural and chemical environment. The observation of the various photoemission peaks and the measurement of their relative intensities make possible the determination of the physicochemical characteristics of an element in a complex material.

For transition elements, lanthanides and actinides, the presence of a d or f open sub-shell increases the secondary effects and the spectra become more complex. The probability of shake-off and shake-up processes increases. At the same time shake-down processes become possible. The peaks can be strongly split and sometimes several components of comparable intensity are observed. Then, identification of the main peak can be difficult and results obtained for the same sample from other spectroscopic methods such as, for example, XES must be taken into account in the interpretation.

It had been predicted that d and f orbitals could be populated by relaxation from a core hole ionized state $nl^{-1}n'l'^{m}$ to $nl^{-1}n'l'^{m+1}V^{-1}$ configuration, where nl^{-1} and V^{-1} designate a hole in the nl core sub-shell and the valence band respectively and n'l' designates the d or f orbital. The $nl^{-1}n'l'^{m+1}V^{-1}$ relaxed configuration had been called *well-screened* [42]. In this model [43], labelled the *screening model*, the creation of the well-screened configuration depends on the coupling of the empty screening orbitals with the valence states. This coupling has been described in terms of the hybridization degree of the d or f electrons with

the valence electrons. If the coupling energy is higher than the distance between the top of the valence band and the empty orbital, the probability of transferring a valence electron to the n'l' orbital should be large. Then the importance of the transfer should reflect directly the hybridization of the $n'l'$ occupied orbital with the valence states. The screening model has been largely used to interpret the x-ray photoemission spectra and it has been suggested that well-screened and poorly-screened peaks corresponding to the final $nl^{-1}n'l'^{m+1}V^{-1}$ and $nl^{-1}n'l'^{m}$, configurations should be present in the photoemission spectra of rare earths and transition metals and compounds.

Let us consider the changes of the electron distributions following the creation of a core hole in systems with d or f valence electrons. The energies of all the core levels increase. An energy shift of filled or empty localized-like orbitals, $n'l'$, accompanies that of the core levels. In contrast, the valence and conduction free-like states are shifted only slightly. The energy shift that a core hole can cause to empty localized-like orbitals can be large enough to pull them down below the top of the valence band. Then an electron can be transfered from a valence state to the localized-like orbital leading to an $nl^{-1}n'l'^{m+1}$ configuration. Such a relaxation process is not selective: all the J-levels of the $nl^{-1}n'l'^{m+1}$ configuration are populated with probabilities proportional to their statistical weights and the energy of the configuration can be taken as equal to the energy of its barycentre. The corresponding photoemission peak is a shake-down satellite (figure 4.6). In this model, satellite of $nl^{-1}n'l'^{m+1}$ final configuration is present when the $n'l'$ orbital and the valence states overlap energetically and the transfer of one of the valence electrons to the $n'l'$ orbital requires no energy.

The weak low binding energy peak present in the $3d$ photoemission of light rare earth metals has successfully been considered to provide the shake-down process of the $3d^{-1}4f^{m+1}$ final configuration, due to the relaxation of the ionized state with a $3d$ hole [44]. This configuration is more stable than $3d^{-1}4f^{m}$ in the metal. Indeed, as shown by BIS and XAS, in the presence of a $3d$ core-hole, the $4f$ level undergoes a reduction of energy and mixes with the valence states of the metal. The large mobility of valence electrons favors the population of the $4f$ level. However, the intensity of the corresponding shake-down satellite is only a few percent of the main peak.

In lanthanide insulator compounds, in the presence of a core hole, the f^{m+1} localized-like orbital is generally located in the band gap. In this case the creation of a $3d^{-1}4f^{m+1}V^{-1}$ final state from the $3d^{-1}4f^{m}$ ion necessitates supplementary energy. According to the screeningmodel, a peak designated by its $3d^{-1}4f^{m+1}V^{-1}$ final configuration could be

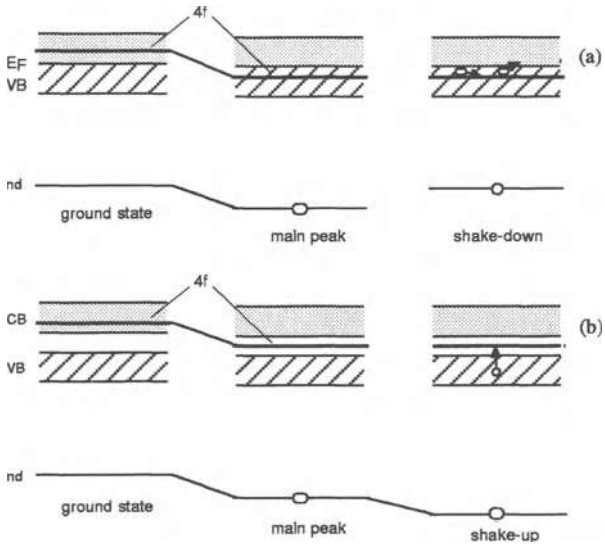

Figure 4.6 Photoemission: main peak, shake-down and shake-up satellites; conductor (a); insulator (b).

present towards the lower energies of the main peak if strong interaction exists between the f and the valence electrons [43].

As an example, let us consider La $3d_{5/2}$ photoemission. In La metal, the energy of the main peak, which corresponds to the binding energy of the $3d_{5/2}$ sub-shell, is 835.6 eV. A weak feature is observed at 832.4 eV [44]. This energy is close to that of the $3d_{5/2}^{-1}4f^1$ configuration (cf. § 4.1.3). In the presence of the core hole, an empty $4f$ orbital, situated above the Fermi level, becomes localized and mixes with the valence states, making possible the creation of the $3d_{5/2}^{-1}4f^1$ state. This state is more stable than the $3d_{5/2}^{-1}$ ionized state because presence of the $4f$ electron screens the positive charge due to the $3d$ hole. This shake-down peak accounts for the perturbation that the lanthanum undergoes during the creation of the core hole.

The energy of the $3d_{5/2}^{-1}4f^1$ configuration has the same value in La metal and its compounds (cf.§ 4.1.3). No peak is seen at the vicinity of 832.4 eV in $3d_{5/2}$ photoemission of La insulator compounds, making no process of $3d_{5/2}^{-1}4f^1$ final configuration observable, unlike the predictions of the screening model. The La $3d_{5/2}$ photoemission varies strongly from one compound to another. In La_2O_3 insulator oxide, two peaks are

observed at 837.7 and 841.6 eV [45]. In order to determine the peak corresponding to the singly ionized state, comparison of energies is made with the $3d_{5/2}$ binding energy deduced from the absorption and emission x-ray spectra. This energy is equal to 838 eV [20] and corresponds to that of the main peak located at 837.7 eV. Different possibilities exist to explain the peak at 841.6 eV. It could correspond to a shake-up process: the creation of $3d_{5/2}$ hole should be accompanied by an electron transfer between the valence band and the empty $4f$ orbitals, i.e. between the ligands and the metal ion (figure 4.6). On the other hand, both La $3d_{5/2}$ peaks could be explained by considering the crystalline structure of La_2O_3. Two different La-O distances, 2.42 and 2.69 Å, i.e. two different environments exist in this compound, making possible the presence of two $3d_{5/2}$ peaks. The large variety of energies and shapes observed for the photoemission peaks of the La compounds could be attributed to the difference of their structural arrangements.

Results for metal Ce are analogous to that obtained for metal La [44]. The main peak is observed at 883.8 eV; a weak feature is present at 878.5 eV; it corresponds to the $3d_{5/2}^{-1}4f^2$ configuration whose barycentre, calculated for the Ce^{3+} free ion, is at 879.8 eV. Results for the Ce compounds are more complex because cerium has two oxidation numbers and the hybridization between the f states and the valence states varies according to the oxidation number. Moreover, it appears difficult to obtain pure compounds, i.e. in which all the atoms have the same oxidation number. In Ce_2O_3, no structure is observed at the energy of the $3d_{5/2}^{-1}4f^2$ configuration. A peak is present at 887.5 eV; it is accompanied by a structure at 884 eV (cf. figure 4.7). The $3d_{5/2}$ binding energy, obtained as previously described for La, is 889 eV; it corresponds to the peak observed at 887.5 eV which is the main peak of this oxide. The structure could be explained by the presence of the two different crystalline surroundings since the crystalline structure of both La_2O_3 and Ce_2O_3 compounds is the same. It can also be due to the presence of Ce^{4+} ions as can be seen in the following paragraph.

In the tetravalent oxide, CeO_2, the energy of the shake-down satellite should be the energy of the barycentre of the $3d_{5/2}^{-1}4f^1$ configuration, whose value calculated for Ce^{4+} free ion is 883.4 eV. Experimentally, two peaks are observed at 883.8 and 899.7 eV and two structures at 886.2 and 889.8 eV [46] (cf. figure 4.7). No value of the CeO_2 $3d_{5/2}$binding energy deduced from x-ray spectra is available. However, the calculated energy separation between the $3d_{5/2}^{-1}$ and $3d_{5/2}^{-1}4f^1$ configurations indicates that the main peak is at 899.7 eV, the peak at 883.8 eV being the shake-down satellite, in agreement with the calculated value. The two weak

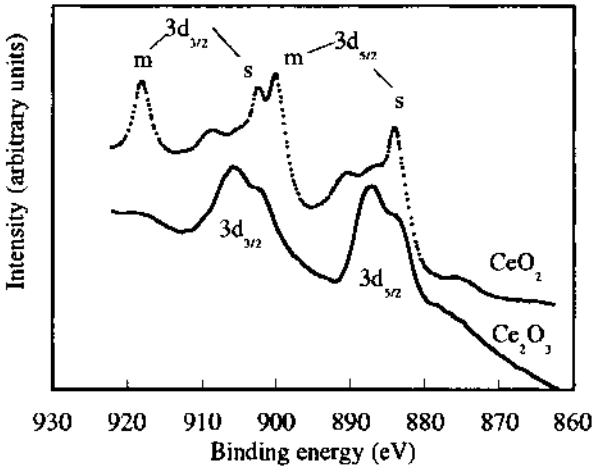

Figure 4.7 Ce 3d photoemission in Ce_2O_3 and CeO_2: main peak (m); shake-down (s).

structures should be due to the presence of some Ce^{3+} ions in various environments.

In summary, for La and light rare earth metals, because the $4f$ and valence orbitals overlap energetically in the presence of a core hole, the $3d^{-1}4f^{m+1}V^{-1}$ well-screened states are close in energy to that of the $3d^{-1}4f^{m+1}$ excited states as determined experimentally from EELS or theoretically from the atomic model. Consequently they produce the peaks (labelled here *shake-down satellites*) seen in the $3d$ photoemission. Their intensity is weak because the hybridization of $4f$ with valence states is very small.

For La insulator compounds, from energy considerations based on the x-ray spectra, one deduces that the $4f$ orbital lies in the band gap in the presence of the $3d$ core hole and does not interact with the valence states. This agrees with the x-ray and Auger emission results (cf. § 4.1.3) according to which the hybridization is weaker in the oxide than in the metal. Consequently, no shake-down satellite due to the relaxation of the core hole ion is observed in the $3d$ photoemission. The La $3d$ photoemission peak at lower binding energy corresponds to the $3d^{-1}$ ionized configuration and that at higher binding energy to a shake-up satellite; the latter is intense because the probability is large for a ligand electron to be excited to the localized empty $4f$ orbital located in the band gap. In tetravalent Ce compounds, in the presence of the $3d$ hole, an $4f$ orbital, energetically mixed with the valence states, relaxes [47, 48]. As

the hybridization of the f and valence electrons is known to be large in the Ce^{4+} compounds, the conditions required for the observation of the well-screened configuration appear to be fulfilled. The peak at 883.8 eV, located towards the lower energies of the main peak in CeO_2, can be attributed to the shake-down satellite of $3d^9 4f^1$ final configuration whereas the peak with the highest binding energy corresponds to the $3d^9 4f^0$ final configuration. Peaks observed at the same energy in the Ce_2O_3 and CeO_2 spectra reveal in each of these compounds the presence of a small contribution of the other ion. This interpretation was made possible only owing to the data obtained by XES and discussed in section 4.1.3.

For the transition elements, strong configuration interaction exists between the ground and excited configurations of the neutral atom as well as of the ion with one electron missing in a core sub-shell. Energy distributions of these configurations are broad and overlapping. Stabilisation of one d electron takes place in the presence of a core hole and provides the screening to the hole. By analogy, photoemission spectra of the solids have been discussed in terms of screening effects and the existence of "well screened" and "no screened" holes has been proposed to interpret the core spectra in the transition element compounds [42].

We discuss rhodium as an example for which atomic calculations have been performed using the previous method. The ground configuration of the neutral atom is $4d^8 4s^1$. In the singly ionized atom, strong interaction exists between the $3p^5 4d^8 4s^1$ and $3p^5 4d^9$ configurations whose energies partially overlap. The lower configuration is $3p^5 4d^9$ and the energy difference between the barycentres of both configurations is a few eV. This could suggest that in the solid annp photoemission peak of lower binding energy corresponding to the $np^5 d^{m+1} V^{-1}$ configuration could be present: such a peak is not observed. It needs to underline that the atomic model must be used judiciously for the transition elements. No localized excited state occurs for these elements in the solid (cf. § 4.). Therefore the d electrons cannot be treated in an atomic-like picture. In solid compounds of transition elements, the hybridization of the d and valence electrons is large and the d band spreads on several eV. The interaction due to the crystalline field is of the same order of magnitude as the d-d intra-atomic interactions and must be taken into account. Consequently, the previous atomic model may not be applicable for the d valence electrons in solids.

In the core photoemission spectrum of the transition metals, the main peak corresponds to the ground state of the ionized configuration where the mean number of the d electrons in the band remains unchanged with respect to that of the ground configuration. Satellite structures are observed towards the higher binding energies of the main peak in the spectra of the heavier $3d$ transition elements. For example, for the $2p_{1/2}$,

$2p_{3/2}$, $3s$ and $3p$ core spectra in Ni metal, satellite structure is found at â 6 eV from the main peak [49]. These satellite structures are generally interpreted as being due to the simultaneous creation of core and $3d$ holes by shake-up effect. A feature corresponding to these satellites is also present in the np emission spectra. There is a strong probability that the $3d$ additional hole be localized on the site of the core hole because the intra-atomic Coulomb interaction between the two holes is strong. Consequently, the final state of the satellite has one d electron less than the final state of the main peak, making the corresponding state more bound. This behaviour is characteristic of the heavy nd elements.

4. X-ray excited states

Excited states with an nd core hole and an additional excited electron in the $4f$ sub-shell have been observed in the rare earths from x-ray emission and Auger spectra [7, 50]; we have labelled them *excited x-ray states.* Their decay introduces specific atomic-like transitions in the nd spectra which reveal the localized- like behaviour of the f electrons in these elements. Concerning the actinides, their nd emission spectra show similar peculiarities due to the presence of localized states, as those already seen for the rare earths [51]. It is clear that the f states are localized at the time scale of the XES and AES. Indeed, the analysis of the radiative, as well as non radiative, decay processes enables us to probe the dynamics of the excited x-ray states, making a direct comparison to that of the ionized states having the same core hole. This probing takes place during a time scale defined by the lifetime of the core hole. Consequently, this localization of the f states could not be inferred from other properties and this shows the interest of these two spectroscopic techniques.

Generally, the d electrons of the transition elements present in a condensed system must be treated in a band model. However, in some cases, they have a behaviour similar to that of the free atom. This behaviour exists if the distance between the neighbouring transition elements is sufficiently great so that the intra-atomic d-d interactions are clearly larger than the interatomic interactions.

4.1 f states

The nature of the f electrons in lanthanides and actinides has been discussed at length. The f electrons are not considered as having a unique behaviour, that could account for all the physical properties of the lanthanides and actinides in all materials, in particular in the conductors. Hybridization between the f electrons and the valence electrons

has been invoked in the interpretation of some physical as well as spectral properties of elements such as cerium and light actinides. For the other rare earths, the f electrons are known to have a behaviour similar in the bulk solid and in the free atom.

It is clearly established that the localized character of the $4f$ and $5f$ electrons increases in the presence of a core hole. As already mentioned, nd x-ray excited states of the $nd^9n'f^{m+1}$ type are expected in all the lanthanides and the actinides. From these localized-like states, electronic transitions have been observed in the metals as well as in the insulator compounds. Various models have been considered to explain the creation of the x-ray excited states. They are discussed briefly, previously the description of x-ray and Auger emissions from these states. It is shown that the observation of x-ray and Auger transitions from excited states reveals the weak interaction of these states with continuum states of the solid.

4.1.1 Creation of the x-ray excited states. It has been suggested that the creation of the excited states should take place by relaxation from the corresponding ionized state. If the x-ray excited states were created from this process, there should be a relation between the intensity of x-ray emissions from the excited states and the intensity of the shake-down satellite in photoemission. However, the intensities observed for these transitions in the metallic light lanthanides are in disagreement with this interpretation. As an example, for La metal, the shake-down satellite, which corresponds to $3d^{-1}4f^1$ excited configuration, is very weak whereas the emissions in $3d^{-1}4f^1$ excited La are more intense than the emissions in $3d^{-1}$ ion.

The proportion of the relaxed states from the ion is smaller than initially predicted for the f elements. The theories developed to explain the relaxation process involve a strong hybridization of the f and valence electrons. Because the x-ray excited states decay before they interact with other states, one expects the intra-atomic d-f interactions to be strong whereas the interactions of the $nd^9n'f^{m+1}$ excited states with the ionized states, i.e. with the extended states of the solid, to be weak.

In the first experiments showing the decay of the x-ray excited states, excitation was created by electron-electron interaction. Let us consider electrons as probe particles. The energy distribution of the incident electrons spreads over some eV and becomes broaden upon crossing the material. Indeed, during their collisions with the atomic electrons, the probe electrons may loose any amount of their energy due to excitation or ionisation concurrently. Generally, the energy of the incident electron beam exceeds the excitation threshold by over 10 eV. From the energy

distributions of the incident electrons it is clear that no interference exists between the excitation and decay processes. The emission process is treated in the step model and the emissions of characteristic radiations and Auger electrons are treated as independent processes by using first-order time dependent perturbation theory.

The excitation and ionization collisional cross sections vary with the incident electron energy. The excitation by an incident electron with energy close to the threshold is not governed by selection rules. All the J-levels of the excited configuration are populated proportionally to their statistical weight, as in the relaxation process. On the other hand, when the Born approximation is valid, i.e. the incident electron energy is about twice the threshold one, the generalized oscillator strengths approach the optical values and the J-levels accessible by photoexcitation are populated preferentially, making the shape of the collisional excitation spectrum rather similar to the photoabsorption. However, electronic redistribution is fast so that all the J-levels of the excited configuration become statistically populated before the decay takes place. The direct excitation by electron-electron collisions is possible far above the threshold, i.e. in a broad energy range, but its probability decreases with increasing electron energy. In the energy range close to the threshold, the excitation cross section is larger than the ionisation cross section, making the creation of excited states predominant and the electron-electron interactions favourable for the study of the excited states.

Let us now consider photons as probe particles. Only the photons whose energy is equal to the excitation energy are efficient. Monochromatic radiation has been used to create the $4d^9 4f^1$ excited configuration of Ba^{2+} [52] and La^{3+} [53]. Among the 20 levels of the $4d^9 4f^1$ configuration, only three, $^3P_1$, $^3D_1$ and $^1P_1$, can be excited from the ground state, $^1S_0$. Photons of energy close to these three levels have been used. Two distinct cases appear: if the discret level, $^{2S+1}L_J$, is mixed with continuum states, the excitation is followed by a reorganisation of all the J-levels of the excited configuration which are statistically populated. Decay processes take place from all the J-levels and are analogous to those observed in the case of the collisional excitation. The photonic excitation can, therefore, be described as photoabsorption followed by reorganisation and the emission process must be treated as a two-step process. In this model, the emission spectrum does not depend on the excitation process.

When the discret level, $^{2S+1}L_J$, is not perturbed by other levels, it is the only one populated and radiative and non radiative emissions take place from this single level. Let us note that its life-time, which strongly depends on the Auger processes, is independent of the excitation mode.

In summary, in the case of the photoexcitation, the excitation characteristics depend on the interactions which bind the J-levels of the excited configuration.

4.1.2 Decay of the x-ray excited states. The strong intra-atomic interaction between the d hole and the localized f electron makes in turn the transfer of the excited f electron to the continuum states by tunnel effect improbable. Consequently radiative and non radiative decays of the excited configuration take place in the solid before it relaxes. This has been shown for the first time in the lanthanide $3d$ emission spectra. Such excited states have an exciton-like character. However, they differ from excitonic states because the decay transitions are analogous to those in the free atom and independent of the considered solid.

The decay of the x-ray excited states can proceed via several channels:

- radiative or non radiative decays to the ground state or to a monoionized state, labelled *resonant processes*; the resonant Auger effect is often designated as *resonant photoemission* [54].

- normal radiative or non radiative transitions in the presence of the excited spectator electron.

In the x-ray emission spectra, the resonant transitions are the most intense nd lines. In the Auger spectra, no general rule exists. The analysis of the de-excitation processes in the presence and in the absence of a spectator f electron can be used to probe the dynamics of the excited and ionized atoms having an nd core hole.

In the x-ray excited states of lanthanides and actinides, the supplementary f electron screens the nuclear charge, and the energies of all core levels decrease with respect to the energies of the ionized states. Generally, in the presence of a f electron, the energy of the nd sub-shell decreases more than the energies of the outer other sub-shells. Then the transitions from the excited nd states are located towards the lower photon energies with respect to that from the ionized nd states.

In the $3d$ range, the $3d$ spin-orbit interaction is stronger than the Coulomb interaction between the $3d$ hole and the f electrons, making the excited $3d^9 4f^{m+1}$ configuration separate into two sub-groups, $3d_{5/2}^{-1} n' f^{m+1}$ and $3d_{3/2}^{-1} n' f^{m+1}$. Each group of states is spread over a range of a few eV due to the splitting and its energy is lower than that of the corresponding $3d^9$ ionization threshold. In the lanthanide $4d$ range, the Coulomb interaction is the dominant one. The $4d_{5/2}^{-1} 4f^{m+1}$ and $4d_{3/2}^{-1} 4f^{m+1}$ levels of the excited configuration are mixed and spread over about 20 eV. Some levels can be located above the $4d_{3/2}$ ioniza-

tion threshold. The same behaviour is observed in the $5d$ spectra of the actinides. Owing to the large difference between the electrostatic and spin-orbit interactions in the various energy ranges, the spectral characteristics of nd emissions vary strongly with n. However, it is important to underline that the same theoretical model is capable of interpreting the various spectra. The examples presented here are for the cases where the excited and ionized states are produced by an electron beam.

4.1.3 Lanthanum $3d$ and $4d$ emissions. The main radiative decay channel of the La^{3+} $nd^{-1}4f^1$excited configuration gives rise to the $4f$-nd resonance lines; They correspond to the jump of the excited $4f$ electron to the nd hole, i.e. the return to the ground configuration of the trivalent (Xe) $^1S_0$ ion [55]. The identification of the resonance lines is easy because they result from the inverse process of the nd photoexcitation and they are in coincidence with the photoabsorption lines, to within the precision of the measurement, i.e. 0.1 eV. Three lines are expected from the $^3P_1$, $^3D_1$ and $^1P_1$ levels of the $3d^{-1}4f^1$configuration but the line from $^3P_1$ is less than 1% of the two others. The $^3D_1$ (834.6 eV) and $^1P_1$ (850.9 eV) levels lie above the barycentres of $3d_{5/2}^{-1}4f^1$ (831.8eV) and $3d_{3/2}^{-1}4f^1$ (848.5eV) configurations. Two intense symmetrical lines have been observed at 834.9 and 851.5 eV in La $3d$ spectra of the metal, the La_2O_3 oxide and the LaF_3 fluoride. They correspond to resonant lines from $^3D_1$ and $^1P_1$.

The $5p - 3d$ transitions are located in the same energy range as the resonance lines. The energies of normal emissions are deduced from the energies of $3d$ and $5p$ photoemission peaks. For La_2O_3, La $5p_{3/2}$ and $5p_{1/2}$ peaks are present at 18.8 and 21.3 eV. Two $3d_{5/2}$ peaks are observed at 837.7 and 841.6 eV. The $5p_{3/2} - 3d_{5/2}$ emission is consequently expected at either 818.9 or 822.8 eV. No emission is seen in this energy range. The emission observed at 812.4 eV cannot be identified as a transition due to the radiative decay of the $3d$ hole ion. It has been identified as the $3d_{5/2}^{-1}4f^1 - 5p_{3/2}^{-1}4f^1$ transition, i.e. $5p_{3/2} - 3d_{5/2}$ emission taking place in the singly excited element in the presence of a $4f$ spectator electron. Theoretical simulation confirms that the emission at 812.4 eV corresponds to the $3d_{5/2}^{-1}4f^1 - 5p_{3/2}^{-1}4f^1$ transition. The resonance lines and the emissions in the presence of the excited spectator electron have the same energy in La metal and compounds, in contrast with the normal emissions. This energy is in good agreement with the value predicted from atomic calculations.

It should be underlined that the emission from the $3d_{5/2}^{-1}4f^1$ initial state, located at 812.4 eV, cannot be anticipated from the La_2O_3 pho-

toemission spectra; it does not correspond to one of the La_2O_3 photoemission peaks, confirming that no shake-down satellite is observed in this compound (cf.§ 3.2). On the other hand, according to the theoretical simulations which take into account only the transition probabilities, the $3d_{5/2}^{-1} - 5p_{3/2}^{-1}$ emission in the ion should be more intense than the $3d_{5/2}^{-1}4f^1 - 5p_{3/2}^{-1}4f^1$ emission in the excited configuration. Experimentally the inverse is observed (cf. figure 4.8). This confirms that the number of the $3d^9 4f^1$ excited species created by direct transfer of an $3d$ electron to an empty $4f$ orbital is large.

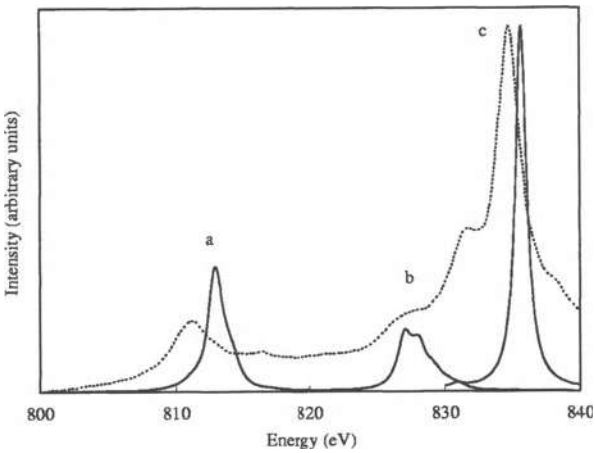

Figure 4.8 Experimental (dashed line) and simulated (solid line) emission of La in oxide: $3d_{5/2}^{-1}4f^1 \rightarrow 5p_{3/2}^{-1}4f^1$ (a); $3d_{3/2}^{-1}4f^1 \rightarrow 5p_{1/2}^{-1}4f^1$ (b); $3d_{5/2}^{-1}4f^1 \rightarrow 3d^{10}$ (c).

Spectra obtained in the $4d$ range have been interpreted by the same model [56]. In this range, strong interaction exists between the $4d^9 nf^1$ (with $n > 4$) excited configurations and one level of the $4d^9 4f^1$ excited configuration, $^1P_1$, lies above the $4d_{3/2}^{-1}$ threshold. The excitation to this level is represented by a very high peak in the photoabsorption spectrum. It had been suggested [57] that this peak is dominated by the transitions to $4d^9$ with an f electron in the continuum. The creation of a $4d$ inner hole has then been described as a competition between discrete and continuum excitations, $4d - (4f, \epsilon f)$ and the peak was labelled *giant resonance*. In such an approach, the x-ray emission spectrum should be dominated by the transitions from $4d^9$ and, in particular, the $4d^9 - 5p^5$ emissions should be the most intense. In reality, these emissions have a very weak intensity, as in the $3d$ range. In contrast, the $4d^9 - 5p^5$

emissions in the presence of the $4f$ spectator electron are intense and the lines from $^1P_1$ are clearly observed. This already indicates that the above approach should be considered very cautiously.

The same results are obtained from $4d$ Auger spectrum. In figure 4.9, the simulated spectra from $4d^94f^1$ and $4d^9$ are plotted next to the experimental spectrum. The number of possible transitions is larger than in x-ray emission and their energies overlap. However, the importance of the transitions from $4d^94f^1$ with respect to the ones from $4d^9$ is clearly demonstrated. Indeed, if transitions from the $4d^9$ configuration predominate, the most intense peak should be located between 45 and 55 eV.

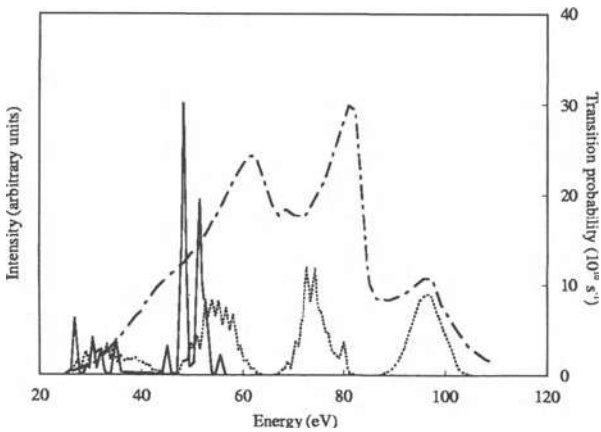

Figure 4.9 **Experimental (dashed-dotted line) and simulated from $4d^9$ (solid line) and $4d^94f^1$ (dashed line) Auger spectra of La.**

The comparison between the experimental and simulated spectra shows that the number of excited species is larger than the number of ionized species and that all the J-levels of the excited configuration, including $^1P_1$, contribute to the radiative and non radiative decay processes. The importance of recombinations from the $4d^94f^1$ $^1P_1$ state to discrete states has been derived from the observation of the x-ray resonance emission and the Auger resonance peak and it has been found that the decay probability of the $4d^94f^1$ $^1P_1$ state to discrete states is larger than that of other states of the $4d^94f^1$ configuration. Consequently, the screening model as well as the "giant resonance" approach cannot be used to explain the La experimental results. But this is not necessary since these are well described by considering the decay of localized-like excited states created directly under electron impact.

4.1.4 Erbium 3*d* emission. The heavy lanthanides are those beyond the half $4f$ shell, i.e. they contain more than seven $4f$ electrons. In order to determine the relative importance of the excited and ionized configurations created in these elements, the experimental spectrum is compared to the one simulated involving the $nd^{-1}4f^{m+1}$ excited configuration. Such a simulation takes into account the resonance emissions and the emissions in the presence of the $4f$ spectator electron. The theoretical transitions from Er^{3+} $3d_{5/2}^{-1}4f^{12}$ are plotted in figure 4.10 along with the experimental $3d$ emission and photoabsorption curves. Agreement exists between the experimental and simulated spectra in both$3d_{3/2}$ and $3d_{5/2}$ ranges. This shows that the $4f - 3d$ emission spectrum is dominated by the transitions from the excited states. The satisfactory simulation of the spectrum in both $3d$ ranges shows that no change of the model is required when the excited levels are situated above one of the $3d$ ionization threshold, as is the case for the $3d_{3/2}^{-1}4f^{12}$ levels with respect to the $3d_{5/2}$ ionization.

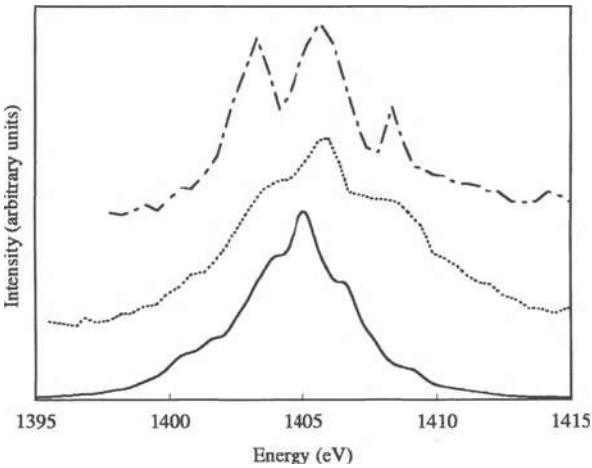

Figure 4.10 Experimental (dashed line) and simulated (solid line) $3d_{5/2}^{-1}4f^{12} \rightarrow 4f^{11}$ emission of Er; experimental $3d_{5/2}$ absorption (dashed-dotted line.

4.1.5 Uranium 3*d*, 4*d* and 5*d* emissions [41]. >From the experimental data obtained in the $3d$, $4d$ and $5d$ ranges of uranium in UO_2 and their corresponding simulated spectra for U^{4+}, the dynamics of U $nd^{-1}5f^{m+1}$ excited states have been derived. There is an analogy between the U $3d$ and $4d$ spectra, where the nd spin-orbit is the dominant

interaction. In contrast, the U $5d$ spectrum is dominated by the $5d$-$5f$ interaction. The shape of the spectrum is clearly different. These differences are due to the evolution from the jj dominated coupling scheme valid for the $3d$ and $4d$ sub-shells to the LS dominated scheme for the $5d$ sub-shell. This causes a redistribution of the probabilities towards the higher energy transitions.

The emissions due to the radiative decay of the excited states, i.e. resonance emission and emission in the presence of the spectator f electron, have been observed in the three nd ranges. The same theoretical model was able to account for all the experimental results. This shows that the U nd excited states have the same localized-like character in the $3d$, $4d$ and $5d$ ranges in spite of large difference in the shape of the spectra. However, 3d and 4d simulated spectra are shifted by about ten eV with respect to the experimental ones.

Experimental problems are different in the three spectral ranges and should be carefully taken into account. The radiative transition probabilities decrease from $3d$ to $4d$, then to $5d$. The fluorescence yield also decreases with the transition energy whereas the self-absorption increases strongly. In the $4d$ and especially, $5d$ range, the intensity of the emissions is weak. The effect due to self- absorption is very important for the resonance emissions. It increases from $3d$ to $4d$ and especially to $5d$ because the photoexcitation cross sections increase strongly. In the $5d$ range, a strong photoexcitation is known to be present; it is situated above the $5d_{3/2}$ threshold towards the higher energies and corresponds to that observed in the lanthanide $4d$ spectra. A strong excitation cross section can introduce experimental perturbations which change the relative intensities of the peaks and result in broadenings, thus modifying strongly the shape of the spectra. These perturbations are observed in photoexcitation as well as in x-ray emission and favorable experimental conditions must be used to eliminate them. These difficulties made the shape of the spectra not easy to obtain.

4.1.6 Plutonium $3d$ emission. Resonance emissions have been observed in the Pu $3d$ spectra of the metal and the oxide PuO_2. As in the lanthanides, no chemical shift of the transitions from $3d$ excited states is seen within the experimental error. Pu $3d_{3/2}$ experimental and simulated emission spectra are plotted in figure 4.11. The simulation is made for the Pu^{4+} ion; it includes all the 26794 lines corresponding to the resonance emission and the $5f - 3d_{3/2}$ emission in the presence of the $5f$ spectator electron simultaneously. Due to experimental difficulties, the emitted intensity was weak. In order to obtain satisfactory statistics, the incident electron energy had been choosen relatively high, equal to

1.9 times the threshold energy. Consequently, strong self-absorptionis present. This causes a change of the emission shape, corresponding to a cut off of the part of the emission situated towards the higher photon energies. On the other hand, the good agreement previously obtained between the experimental energies of the lanthanide in excited states and their calculated values is demonstrated now also for plutonium.

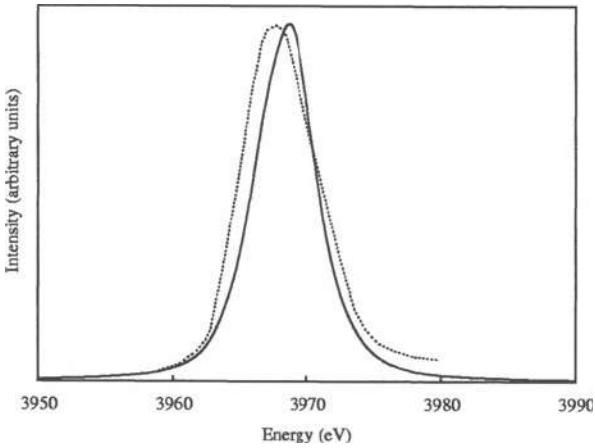

Figure 4.11 Experimental (dashed line) and simulated (solid line) $3d_{3/2}^{-1}5f^5 \rightarrow 5f^4$ emission of Pu

4.1.7 Interaction with a state continuum. The direct decay of an excited state is all the more probable as its atomic character is more pronounced, i.e. its interaction with the conduction or valence states is weaker. When the empty $4f$ orbitals are situated high in the continuum, their localization in the presence of a core hole is weak. This is the case of solid barium where the empty $4f$ orbitals are situated in the continuum of the conduction states and their interaction with these states by tunnel effect is possible, making them partially delocalized. Consequently the number of atoms in the $nd^{-1}4f^1$ excited states is small and the emissions from Ba $nd^{-1}4f^1$ are weak with respect to the emissions from Ba nd^{-1} ion. In contrast, in lanthanum insulator compounds, the emission lines from $nd^{-1}4f^1$ dominate the spectrum because the $4f$ states are not energetically mixed with continuum states; they are situated in the band gap and are "localized" on the atom.

When interaction between the excited state and the continuum states exists, changes of the resonance emission shape are expected. The

lorentzian shape of the no-interaction case becomes a Fano shape [58]. This change is small for Ba. For thorium, resonance lines of assymmetric shape have been observed. From the shape of the lines one deduces that the localization of the $5f$ states in the light actinides is smaller than in the lanthanides. The Th $3d$ resonance lines of ThO_2 are plotted in figure 4.12 along with the calculated lines for Th^{4+}(Rn).

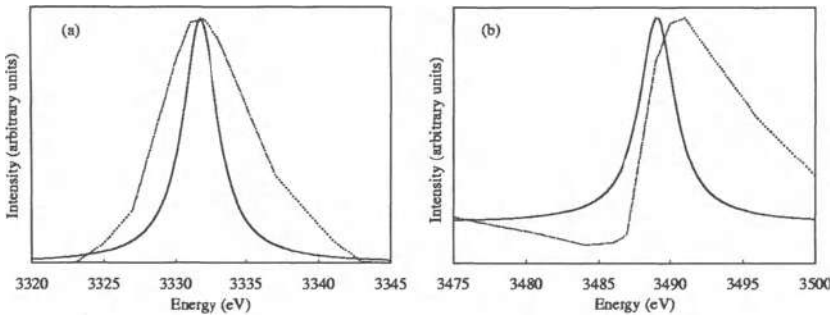

Figure 4.12 Experimental (dashed line) and simulated (solid line) emission of Th: $3d_{5/2}^{-1}5f^1 \rightarrow 3d^{10}$ (a); $3d_{3/2}^{-1}5f^1 \rightarrow 3d^{10}$ (b).

On the other hand, if the $4f$ and valence electrons are energetically mixed in the presence of the core hole, the localization of the f electrons decreases. The emissions from the excited states become weaker but nevertheless they remain the most intense of the nd spectra. This is the case for cerium in its tetravalent compounds and for the metals with respect to their insulator compounds. Then, resonance emissions observed in metal La as well as in metal light actinides such as U are weaker than resonance emissions in La_2O_3 or UO_2.

4.2 *d* states

Hybridization of the d and valence electrons and delocalization of the d electrons increases with the atomic volume. These both characteristics are larger in the heavy elements than in the first transition series and decrease along the transition series. Among the d elements, the nickel is the one for which the intra-atomic d-d correlation terms are predicted be the strongest. No x-ray excited states are created in the Ni bulk metal and compounds. Indeed, spectral characters seen in the lanthanide and actinide nd spectra are absent in the transition element np spectra. This shows that the d electrons are not localized in the bulk solids.

However, the Ni $3d$ electrons cannot be treated from the one-electron band model, valid for the s and p valence electrons. A narrowing of the Ni $3d$ spectral band with respect to the one-electron calculated d band is observed from $3d - 2p$ emission and $3d$ photoemission. This will be discussed in § 5..

On the other hand, changes of the Ni $3d$ distribution revealing its partial localization have been observed to be a function of the sample size. Narrowing of the Ni $3d$ spectral density is observed in very thin films and a resonant line has been identified in 1 nm diameter clusters [59]. In both examples, a majority of Ni atoms have a number of first neighbours smaller than in the bulk and, for these atoms, the intra-atomic interactions dominate the interatomic ones. Consequently, partial localization of the Ni $3d$ electrons exists when the atomic environment acts as a potential barrier confining them to the nickel atoms. Similar effects have been observed on other heavy transition elements.

4.3 Discussion

The presence of atomic-like x-ray excited states in solids is a specific property of the elements having f orbitals. This atomic behaviour of f electrons is in agreement with the small f-extended state hybridization. When this hybridization is weak, the $nd^{-1}n'f^{m+1}$ excited states are created by collisions with incident probe particles and they decay by radiative and nonradiative recombination processes before the relaxation takes place. Information on the dynamics of high-energy excited states is obtained from the analysis of their decay processes, in a time scale which is a function of the core hole lifetime, i.e. of the order of 10^{-14}-10^{-16} s. When interaction exists between the f and extended states, the decay transitions have the same characteristics as in the previous case but they are weaker. It is important to underline that the f excited states in the rare earths as well as in the actinides can be treated using same model for any material considered. In contrast, in the transition elements, even those with a narrow d band such as Ni, this model is not convenient, thus showing that the behaviour of the d and f electrons is clearly different in solids.

The good agreement between the experimental spectrum and its theoretical simulation based on an atomic model confirms the localized-like character of the excited configurations and reflects their purety. Thus, erbium in the trivalent oxide is well simulated by Er^{3+} ion. In the same way, thorium and plutonium are well simulated by Th^{4+} and Pu^{4+} ions whereas uranium in its tetravalent oxide is not pure U^{4+} ions. The U experimental binding energies are shifted with respect to the calculated

values. Consequently, from the excited states, information can also be deduced on the charge of the elements in solid compounds and on the character of the chemical binding.

5. Valence states in solids

An analysis of the x-ray emissions, due to the transition of the valence electrons to a discrete core level of known characteristics, usually provides the most straightforward means of determining the energy distribution of the valence orbitals, or the density of states (DOS) making up the valence band of solids. As mentioned in § 1.4, local and partial valence distributions are obtained by XES. The spectral densities of an element present in various materials reveal its valence orbital change as a function of its chemical surrounding, i.e. of the chemical binding. The analysis of the partial valence orbitals belonging to each type of atoms in a compound offers possibilities for determining energy diagrams of the orbitals, which can directly be compared with the theoretical results. Energy overlap of the occupied orbitals belonging to different atoms of a compound can be deduced directly from these observations. Similar observations can be made for the empty orbitals by XAS and EELS.

The spectral densities are widened by the broadening effect of the inner hole lorentzian distribution. To obtain a good intrinsic resolution, this broadening must be as small as possible. This is generally realized in the soft x-ray range (cf. § 3.1). Broadening due to the valence hole can be described as a lorentzian of FWHM at the energy ϵ equal to

$$\Gamma_v \left[(\epsilon - \epsilon_F)/(\epsilon_0 - \epsilon_F)\right]^2$$

The quadratic term takes into account the variation of the valence hole lifetime which decreases from the Fermi energy, ϵ_F, where it is infinite until it reaches the bottom of the valence band, ϵ_0, where it has its minimum value, i.e. $\hbar/\Gamma_v$.

The spectral density as a function of the photon energy, $D(h\nu)$, is

$$D(h\nu) \propto \nu^3 \left[\int_{l+1\to l} \overline{|M|^2} N_{l+1}(\epsilon) L(h\nu - \epsilon) d\epsilon + \int_{l-1\to l} \overline{|M|^2} N_{l-1}(\epsilon) L(h\nu - \epsilon) d\epsilon\right]$$

where M is the electric dipole matrix element, N_l is the distribution of the valence electrons of symmetry l and L is the broadening function. The energy ϵ is measured relative to an average electron potential in the solid. The matrix elements are usually found to depend only weakly on the energy. The probability of emission from the valence band to the nl

core hole of an element Z is a function of the valence electron number of symmetry $l \pm 1$ present in the vicinity of the Z nl hole. It depends on the charge of the Z element in the considered material.

Secondary effects must be taken into account for determining the true valence DOS from the observed spectral densities [60]. These effects are the response of the electrons to the perturbation accompanying the creation of the inner hole and the hole in the valence band. Two cases must be considered: - the adiabatic approximation, in which the core electron is slowly ejected to excitation states; the relaxation is complete. - the sudden approximation, in which the electron goes out very rapidly. The screening is incomplete because the response of the valence electrons is not rapid enough and perturbed states are created during the charge redistribution.

When the charge redistribution is associated with an almost uniform electron gas (simple metals), two specific effects are observed. First, a singularity at the Fermi level [61]. It is due to the creation of many electron-hole pairs of very low energy accompanying the creation of the core hole. This singularity has been observed in the soft x-ray region for Mg, Al K and L emission bands and the observations are in agreement with the theoretical calculations [62]. Secondly, a dynamic response to the electron gas leading to the creation of plasmon waves. The free-like electrons are very rapidly attracted by the field of holes. An excess of negative charge is brought in and removed quickly thus creating an oscillating motion of the negative charge cloud. Because of the strong cancellation that exists between the negative charge clouds associated with the holes present in the initial and final states of the emission process, there are no plasmon satellite of the atomic x-ray lines and only weak satellites are observed on the low energy side of the emission band [62]. They correspond to the simultaneous emission of one photon and one plasmon.

In semiconductors and insulators the screening of valence electrons is less efficient. No perturbation of the top of the valence bands is possible because of the presence of the band gap. The screening effects are described by an excitonic model: due to the correlations between the excited electrons and the core hole, an electron can be trapped by the core hole atom and an excitonic electron-hole pair can be created [63]. In such a pair the electron and the hole are bound together by Coulomb interaction. An excitonic electron-hole pair can de-excited with the return of the electron to the hole, the excess energy being either converted into radiation or transmitted to a secondary electron which is ejected. The corresponding emissions are observed towards the higher photon energies of the emission band, just under the photoabsorption threshold [64].

In the compounds, the sudden creation of a core hole in a metal ion can induce electron excitation from the ligand valence states to the empty orbitals of the metal ion. Satellites of the shake-up type are observed towards the higher photon energies of the emission band. They correespond to "charge transfer satellites" seen in photoemission (cf.§ 2.2).

5.1 Elements with *s* and *p* valence electrons

The partial spectral densities observed for elements such as Mg, Al, Si, Ge, As, Sb, etc, are described, to a good approximation, by an one-electron band model, whatever the solid considered. *Ab initio* methods such APW, KKR, pseudopotentials, based on the local density approximation (LDA), have been widely used to investigate these spectral densities. Good agreement is obtained between the experimental and theoretical spectral densities of the pure elements or those present in compounds. Shapes as well as widths of the filled and empty distributions are correctly predicted. Only the direct energy gap of the insulators is systematically underestimated by a few eV, a common problem of all the LDA-based methods.

The good agreement between the experiment and the one-electron theory is explained by the weakness of the secondary effects in these materials. Indeed, the wave functions describing the s and p valence electrons of a solid extend over several atomic sites. A hole created in the valence band is thus not localized on a particular atom but delocalized in the crystal. Since the screening of an inner hole is almost complete the valence configuration is the same for the initial and final states of the transition. Consequently, the perturbations due to the holes intervene essentially by a life-time broadening. The $N(\epsilon)$ curves are only lightly perturbed if the width of the broadening function is small compared to that of the electron distributions to be determined. This condition is generally satisfied in the soft x-ray range. Consequently, effects due to the inner hole can be neglected when comparing the spectra of an element in two various compounds.

Usually the chemical surrounding influences the electron distributions. This influence is the strongest for the p valence orbitals because they are very directional, contrary to the s orbitals. They are also more delocalized than the d orbitals, thus more sensitive to mean distance order. The x-ray emission band of an element in a compound is usually shifted towards the lower photon energies with respect to the corresponding emission of the pure element. The shift is proportional to the degree of oxidation, i.e. to the decreasing of the effective electron density on the element in the compound. Consequently, the degree of oxidation of

the element in any compound can be deduced from the analysis of its x-ray spectrum. On the other hand, mixing exists between the valence states of the various elements present in a compound. As an example, for the III-V materials, overlap between the states of different symmetries is present on all the spreading of the valence band [65,66] (cf. figure 4.13). Likewise, mixing exists in the oxides such as MgO, Al_2O_3, ..., between the O $2s$ and $2p$ states and the valence states of the cation. Numerous other examples exist. In the cation spectrum features due to this mixing are observed to have weak intensity because they correspond to emissions from spatially extended electronic distributions. In the spectrum of ligands, the main peak generally overlaps the DOS of the metallic element and, as a consequence, its shape changes considerably from one compound to another. The relative energies of the different orbitals can be deduced from the measurement of their x-ray emissions, after the relative energies of the different core levels have been established [8].

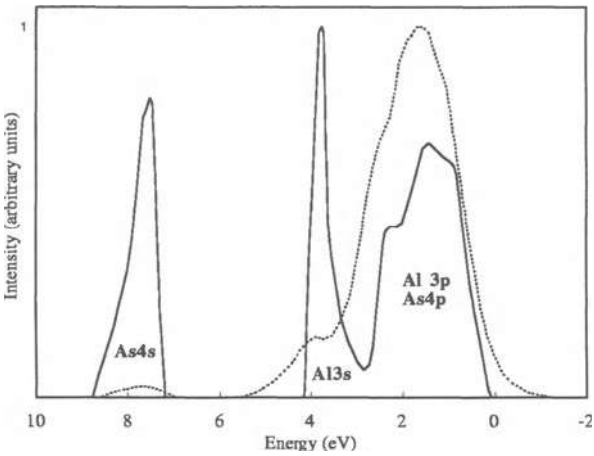

Figure 4.13 Spectral density of Al (dashed line) and theoretical partial DOS of Al and As (solid line) in AlAs.

Information on the electron redistribution around each element in a chemical compound can also be obtained from XES. The only case for which this has been made up to now is Mg in the metal and the oxide [67]. The $3p$ electron mean number present around Mg has been determined from the measurement of the intensity of Mg $3p \rightarrow 1s$ emission with respect to that of Mg $2p \rightarrow 1s$. Both emissions were observed under the same experimental conditions, indicating that the number of the initial states is the same. In the first approximation, the probability of the Mg

$2p \rightarrow 1s$ normal emission is independent of the material. Consequently, the intensity ratio $R = 3p \rightarrow 1s/2p \rightarrow 1s$ depends only on the number of $3p$ electrons present near the Mg $1s$ inner hole. The ratio R_{MgO}/R_{Mg}, which is then equivalent to the ratio $3p \rightarrow 1s_{MgO}/3p- \rightarrow 1s_{Mg}$, was measured to be 1.2 ± 0.1, in agreement with the theoretical value of 1.37. From this result, no p charge transfer exists in MgO. The theoretical Mg $3s$ charge distribution shows a weak s charge transfer from cation to anion. From experimental and theoretical data, the charge in the interstitial region is greater than one. Consequently, a large amount of the charge present around the O site is due to charge superposition, besides charge transfer. These results are in agreement with the relatively large energy of the O $1s$ photoemission in MgO which reveals also a weak polarizability of the oxide. Classification of the simple oxides based on the O $1s$ binding energy has recently been proposed [68]. It has been shown that their character varies from semicovalent oxides such as SiO_2, Al_2O_3, Ga_2O_3, MgO, to true ionic oxides as SrO, CdO, BaO, La_2O_3, ...

In summary, methods using the emission band energies and intensities give information on the mean number of electrons present around an element in a compound and are of fundamental importance in relation to the character of the chemical bonds. Changes of the spectral densities as a function of atomic arrangement, defects, reactivity of surface, etc, are also widely studied. Large shape variations of the ligand spectral densities with the type of cation are used to determine the interactions present at the contact between two solid materials, especially in the case of the metal-ceramic interfaces. Indeed, the presence of chemical compounds, or of a simple mixing of the DOS, gives information about the strenght of the interfacial interactions in relation with the adhesion properties. From a general point of view, properties depending on the valence DOS can be deduced from these spectroscopic methods.

5.2 Transition elements

In valence electron photoemission of the nd transition elements, the main peak corresponds to the ionization of a single d electron delocalized in the metal valence band [69]. Spectral contribution of the s states is also observed, enhanced by the photoabsorption cross section. In the "first" transition elements, i.e. the elements with the d sub-shell less half-filled, the d electrons can be treated in the itinerant electron model and their behaviour is fairly similar to that of the s and p electrons. In the heavier $3d$ transition metals such as Ni, Co, relaxation of the $3d$ electrons towards the final $3d$ hole causes an increase of the intra-atomic correlations. The perturbation takes place in the unit cell containing the

hole. The $4sp$ charge density adjusts to maintain charge neutrality in a volume of the size of this cell and a $3d$ hole can be described as a hole accompanied by its $4sp$ screening charge propagating together through the lattice. The spectrum is well represented by the strongly correlated band model. The large intra-atomic d-d correlations cause the narrowing of the $3d$ spectral distribution and the width of $3d$ distribution is smaller than the calculated one-electron valence DOS. The contribution of the s-d interaction is only by a hybridization of the bands.

In XES,the $nd \rightarrow n'p$ emission bands and the main peak of the nd photoemission result from the distribution of the same final state, making the resultats similar.

The transition element compounds can be separated into two large groups, those with delocalized-like d orbitals, well described in a band model, and those with a narrow d band. In the latter case, the behaviour of the d states is clearly different from that of nearly-free electronic states for which the screening is total [70]. the d orbitals are more localized than typical H-F orbitals used in conventional DOS calculations and the s-d hybridization decreases. The d states are correlated electron states. However, the d electrons or holes are no longer well localized, in agreement with the fact that strong d-d hopping is present. No atomic-like excited states are observed by XES and AES in bulk materials. The crystal-field interaction has to be taken into account. As an example, from angle-resolved photoemission, it has been shown that the Ni $3d$ distribution in NiO is split by the crystal field into two peaks, the width of each d peak being less than 2 eV [71]. The EXES results are in agreement with these data: from the Ni $3d - 2p$ emission band of NiO, a feature due to the crystal field splitting is clearly observed in the $3d$ valence DOS.

The spectra of transition metal oxides have been extensively analysed. While most theoretical calculations use a pure ionic model to describe the binding in these oxides, the importance of the covalent interactions between the metal d states and the anion p states cannot be neglected. As for the magnesium oxide, the electron number within each atomic sphere gives a picture of the charge transfer that is different from that suggested by the ionic model [72]. The repartition of the charges in the space is only slightly modified with respect to that of the pure elements. Redistribution of the electron symmetry character in each atomic sphere and energy mixing of the different symmetry electron states are responsible for the changes of the electron distribution. Thus, a strong p-d mixing due to the hybridization between the transition metal d orbitals and the oxygen p orbitals is present. The covalency effect between oxygen p and metal d states has as a consequence the reduction of the intra-atomic

Coulomb integral and it is the dominant source of the ligand-field splitting [73].

5.3 Lanthanides and Actinides

As discussed in section 4., emissions from $nd^{-1}n'f^{m+1}$ localized-like excited states are observed in these elements. As shown for Er (§ 4.1.4), the spectrum is well described by a simulation which supposes that the occupied as well as excited $4f$ states are localized. Indeed, the spectrum is dominated by the transitions from the excited configuration. No transition from the ionized configuration is observed and the Er $4f$ occupied states are seen only from their emission in the presence of the spectator electron. This confirms the atomic-like character of the $4f$ electrons. With the already mentioned exception of cerium, the same behaviour is expected throughout the series. However, it must be mentioned that actually no calculation has been made for the elements in the middle of the series because of the very large number of J-levels associated with each configuration.

Observation by XPS have confirmed these interpretations. Indeed, strong splitting of the f^{m-1} final configuration has been observed for all the lanthanides.

In the U $3d_{5/2}$ emission of metal U and UO_2, an additional transition is observed towards the higher binding energies (lower photon energies) of the simulated spectrum. It corresponds to the transition in the ion and involves the $5f^m$ occupied electron distribution. It is clearly separated from the emission from the excited configuration and shifted in the oxide with respect to the metal. Thus the separation between the occupied $5f^m$ and excited $5f^{m+1}$ distributions is about 3 eV in the metal and 6 eV in the oxyde. However these distances must be corrected by taking into account the role of the core hole. In the excited state, the $5f$ excited electron screens the core hole whereas in the ionized state, one expects the screening to be incomplete thus increasing the energies. Consequently, the distance of 6 eV is an overestimate. From XPS and BIS, discrete $5f^{m-1}$ and $5f^{m+1}$ final states have been identified [74] (figure 4.14). They are separated by 4.6 eV to 6 eV by XES, the difference being due to the role of the core hole. The 4.6 eV energy corresponds to the $5f$ intra-atomic Coulomb correlation energy and gives a direct estimate of this parameter.

The separation of the occupied and excited $5f$ electron distribution in the metallic uranium reveals their localized-like character. As expected, the localization increases in the oxide and it clearly appears that the U $5f$ electrons cannot be described in a band model. Indeed, the $5f$

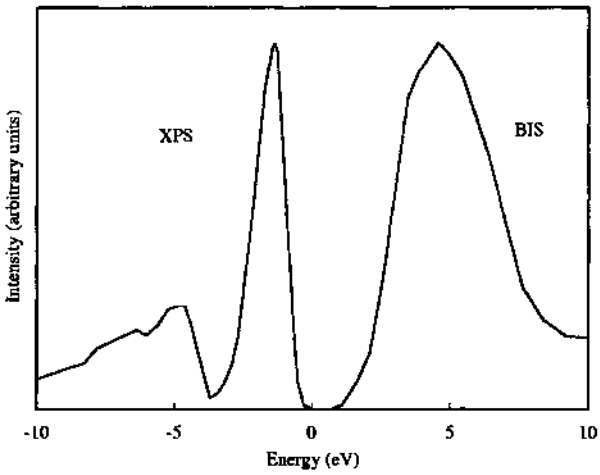

Figure 4.14 XPS and BIS in UO_2.

intra-atomic Coulomb correlation energy is larger than the width of the excitation levels. However, the observation of a $5f^m$ emission from the ionized configuration which suffers a noticeable chemical shift and the gap which is found between the experimental and simulated energies of the emissions show that the localization is not complete in uranium.

The s and d electrons which form the valence band are seen towards the lower binding energy with respect to the $5f^m$ distribution. As expected, they are present at the Fermi level in the metal and are energetically mixed with the O $2p$ states in the oxide.

For Pu, the experimental and simulated energies are separated by less than 1 eV, i.e. less than 2.10^{-4} (cf. figure 4.11). The simulation has been made for the Pu^{4+} $5f^4$ ion. Consequently four $5f$ electrons are localized in PuO_2. Only the emissions from the excited configuration are observed and no measurement of the intra-atomic correlation energy is possible. Still, it is possible to conclude that the localisation of the $5f$ electrons is very strong.

All the spectrocopic results tend to show that the behaviour of the $5f$ electrons in the actinides is closer to that of the $4f$ electrons in lanthanides than to the strongly correlated d electrons of the heavier $3d$ elements.

Acknowledgment

The author wishes to thank Dr. Nissan Spector of the Soreq Research Center for his enlightening remarks concerning the manuscript.

References

[1] Cauchois, Y., (1948) Les spectres de rayons X et la structure électronique de la matière, Gauthier-Villars, Paris.

[2] Parratt, L. G., (1959) Rev. Mod. Phys., 31, 616.

[3] Burhop, E.H.S. (1952) "The Auger Effect and Other Radiationless Transitions", London, Cambridge Univ. Press.

[4] Siegbahn, K., Nordling, C., Fahlman, A., Nordberg, R., Hamrin, K., Hedman, J., Johannson, G., Bergmark, T., Karlsson, S.E., Lindgren, I., Lindberg, B., (1967) "ESCA Atomic, Molecular and Solid State Structure Studied by Means of Electron Spectroscopy", Nova Acta Regiae Soc. Sci. Upsal.

[5] Marton, L., Leder L.B., Mendlowitz, H., (1955) Advances in Electronics and Electron Physics, 17.

[6] Claus, H., Ulmer, K., (1965) Z. Phys. 185, 139.

[7] "Advances in X-ray Spectrocopy" (1982), Oxford, Pergamon Press, Edited by C. Bonnelle and C. Mandé.

[8] Bonnelle, C., (1987) Annual Report C 1987, Royal Society of Chemistry, London, 201.

[9] Aberg, T., (1967) Phys. Rev. 156, 35.

[10] "Atomic Inner-Shell Processes" (1975) New York, Academic Press, edited by B. Crasemann.

[11] Fano, U., Rau, A.R.P., (1986) "Atomic Collisions and Spectra", Academic Press, 1986.

[12] Staub, P.-F., (1998) X-Ray Spectrom. 27, 43

[13] Staub, P.-F., Jonnard, P., Vergand, F., Bonnelle, C., (1998) X-Ray Spectrom. 27, 58.

[14] Cardona, M., Ley, L., (1978-1980) "Photoemission in Solids", Topics in Applied Physics 26, 27, Berlin, Springer-Verlag.

[15] Aberg, T., Utriainem, J., (1969) Phys. Rev. Lett. 22, 1346.

[16] "Modern Developments and Applications in Microbeam Analysis" (2002) Mikrochimica Acta, 138, No 3-4.

[17] Krause, M.O., (1979) J. Phys. Chem. Ref. Data 8, 307.

[18] Hedin, L., Johansson, A., (1969) J. Phys. B 2, 1336.

[19] Huang, K.-N., Aoyagi, M., Hsiung Chen, M., Crasemann, B., Mark, H., (1976) Atomic Data and Nuclear Data Tables 18, 243.

[20] Cauchois, Y., (1952) J. Phys. Radium 13, 113, (1955), J. Phys. Radium 16, 253.

[21] Bearden, J.A., Burr, A.F., (1967) Rev. Mod. Phys. 19, 125.

[22] Bruneau, J., (1983) J. Phys. B 16, 4135.

[23] Rose, S.J., Pyper, N.D.C., Grant, I.P., (1978) J. Phys. B 11, 755.

[24] Kraft, S., Stümpel, J., Becker, P., Kuetgens, U., (1996) Rev. Sci. Instr. 67, 681.

[25] Wendin, G., (1981) Structure and Bonding 45, 1.

[26] Moore, C.E., (1949) "Atomic Energy Levels", Nat. Bur. Stand. (U.S.) Cir. No 467, Washington, D.C.

[27] Bonnelle, C., Spector, N., Bruneau, J., (2002) Phys. Scr. 65, 476.

[28] Jorgensen, C.K., (1971) "Modern Aspects of Ligand-Field Theory, Amsterdam, North-Holland.

[29] Gerard, I., Krupa, J.C., Simoni, E., Martin, P., (1994) J. Alloys Compounds, 207/208, 120.

[30] Meisel, A., "Advances in X-ray Spectrocopy" (1982), Oxford, Pergamon Press, p. 302.

[31] Khoudir, A., Maruani, J., Tronc, M., (2000) Quantum Systems in Chemistry and Physics, Kluwer Academic Publishers, A. Hernandez-Laguna et al. eds, Vol. 2, 57.

[32] Maruani, J., Khoudir, A., Kuleff, A., Tronc, M., Giorgi, G., Bonnelle, C., (2001) Adv. Quant. Chem., 39, 307.

[33] Chen, M.H., Crasemann,B, Mark, H., (1979) Phys. Rev. A 19, 2253.

[34] Chen, M.H., Crasemann,B, Mark, H., (1980) Phys. Rev. A 21, 436.

[35] Krause, M.O., Oliver, J.H., (1979) J. Phys. Chem. Ref. Data, 8, 329.

[36] Carlson, T.A., Nestor, C.W., (1973) Phys. Rev. A, 8, 2887.

[37] Guennou, H., Sureau, A., Hague, C.F., Dufour, G., Mariot, J.-M., (1981) "Inner-Shell and X-ray Physics of Atoms and Solids", Plenum Press, edited by Fabian D.J., Kleinpoppen, H., and Watson, L.M., p. 797.

[38] Scofield, J.H., (1974) Phys. Rev. A 9, 1041.

[39] Keski-Rakhonen, O., Ahopelto, J., (1980) J. Phys. C 13, 71.

[40] Jonnard, P., Giorgi, G., Bonnelle, C., (2002) Phys. Rev. A 65, 32507.

[41] Bonnelle, C., Jonnard, P., Barré. C., Giorgi, G., Bruneau, J., (1997) Phys. Rev. A 55, 3422.

[42] Fuggle, J.C., Campagna, M., Zolnierek, Z., Lässer, R., Platau, A., (1980) Phys. Rev. Lett. 45, 1597.

[43] Gunnarsson, O. Schönhammer, K., (1983) Phys. Rev. B 28, 4315.

[44] Crecelius, G., Wertheim, G.K., Buchanan, D.N.E., (1978) Phys. Rev. B 18, 6519.

[45] Berthou, H., (1976) Thèse de Doctorat d'Etat, Université de Paris.

[46] Wuilloud, E., Delley, B., Schneider, W.-D., Bear, Y., (1984) Phys. Rev. Lett. 53, 202.

[47] Jo, T., Kotani, A., (1986) J. Phys. Soc. Jpn. 55, 2457.

[48] Kotani, A., Okada, K., Okada, M., (1987) Sol. State Commun. 64, 1479.

[49] Hufner, S., Wertheim, G.W., (1975) Phys. Lett 51A, 301.

[50] Bonnelle, C., (1984) X-ray and Inner-shell Processes in Atoms, Molecules and Solids, Leipzig, Karl-Marx-Universität, edited by A.Meisel and J.Finster, 263.

[51] Bonnelle, C., (1976) Struc. Bonding 31, 23.

[52] Rubensson, J.-E., Lüning, J., Eisebitt, S., Eberhardt, W., (1995) Phys. Rev. B 51, 13 856.

[53] Moewes, A., Postnikov, A.V., Kurmaev, E.Z., Grush, M.M. Ederer, D.L., (2000) Europhys. Lett. 49, 665.

[54] Lenth, W., Lutz, F., Barth, J., Kalkoffen, G., Kunz, C., (1978) Phys. Rev. Lett. 41, 1185.

[55] Motais, P., Belin, E., Bonnelle, C., (1984) Phys. Rev. B 30, 4399.

[56] Bonnelle, C., Giorgi, G., Bruneau, J., (1994) Phys. Rev. B 50, 16255.

[57] "Giant Resonances in Atoms, Molecules and Solids" (1987) New York, Plenum, edited by J.P.Connerade, J.M.Esteva, R.C.Karnatak.

[58] Fano, U., Cooper, J.W., (1968) Rev. Mod. Phys. 40, 441.

[59] Fargues, D., Vergand, F., Belin, E., Bonnelle, C., Olivier, D., Bonneviot, L., Che, M., (1981) Surf. Sci. 106, 239.

[60] Hedin, L. in "X-ray Spectroscopy" (1974) edited by Azaroff, L.V., New York, McGraw-Hill, p. 226.

[61] Nozières, P., de Dominicis, C.T., (1969) Phys. Rev. 178, 1097.

[62] Sénémaud, C., Costa-Lima, M.T., (1974) Phys. Lett. A 47, 395.

[63] Strinati, G., (1984) Phys. Rev. B 29, 5718.

[64] Carson, R.D., Schnatterly, S.E., (1987) Phys. Rev. Lett. 59, 319.

[65] Min, B.I., Massida, S., Freeman, A.J., (1988) Phys. Rev. B 38, 1970.

[66] Vergand, F., Jonnard, P., Bonnelle, C., (1989) Europhys. Lett. 10, 67.

[67] Jonnard, P., Vergand, F., Bonnelle, C., Orgaz, E., Gupta, M., (1998) Phys. Rev. B 57, 12111.

[68] Dimitrov, V., Komatsu, T., (2002) J. Solid State Chem. 163, 100.

[69] Eastman, D.E., Janak, J.F., Williams, A.R., Coleman, R.V., Wendin, G., (1979), J. Appl. Phys. 50, 7423.

[70] Zaanen, J., Westra, C., Sawatzky, G.A.,(1986) Phys. Rev. B 33, 8060.

[71] McKay, J.M., Henrich, V.E. (1984) Phys. Rev. Lett. 53, 2343.

[72] Xu, J.H., Jarlborg, T., Freeman, A.J., (1989) Phys. Rev. B 40, 7939.

[73] Grenet, G., Jugnet, Y., Tran Minh Duc, Kibler, M., (1981), J. Chem. Phys. 74, 2163.

[74] Baer, Y., Schoenes, J., (1980) Solid State Commun. 33, 885.

Chapter 5

FOUR-COMPONENT ELECTRONIC STRUCTURE METHODS FOR ATOMS

Uzi Kaldor, Ephraim Eliav, and Arie Landau
School of Chemistry, Tel Aviv University, Tel Aviv, Israel
kaldor@jade.tau.ac.il

Abstract Four-component methods for high-accuracy atomic calculations are reviewed. The projected (or no-virtual-pair) Dirac-Coulomb-Breit Hamiltonian serves as the starting point and defines the physical framework. One-electron four-component Dirac-Fock-Breit functions, similar in spirit to Hartree-Fock orbitals in the nonrelativistic formulation, are calculated first, followed by treatment of electron correlation. Correlation methods include multiconfiguration Dirac-Fock and many-body perturbation theory or its all-order limit, the coupled cluster approach. The Fock-space CC and its extension to the intermediate Hamiltonian approach are described. Applications address mostly transition energies in various atoms. Very large basis sets, going up to $l = 8$, are used. High l orbitals are particularly important for transitions involving f electrons. The Breit term is required for fine-structure splittings and for f transitions. Representative applications are described, including the gold atom, with relativistic effects of 3–4 eV on transition energies; eka-gold (E111), where relativity changes the ground state from $6d^{10}7s$ to $6d^{9}7s^{2}$; Pr^{3+}, where the many f^2 levels are reproduced with great precision; Rf (E104), where opposite effects of relativity and correlation lead finally to a $7s^26d^2$ ground state, ~0.3 eV below the $7s^26d7p$ predicted by MCDF; eka-lead (E114), a potential member of the "island of stability" forecast by nuclear physics, predicted to have ionization potentials higher than all other group-14 atoms except carbon; and eka-radon (E118), which has a unique property for a rare gas, positive electron affinity. Heavy anions are described, showing instances of multiple stable excited states. Finally, applications to properties other than energy are discussed.

Keywords: Four-component methods, atomic structure, heavy atoms, superheavy atoms, relativity, electron correlation, atomic transition energies.

U. Kaldor and S. Wilson (eds.),
Theoretical Chemistry and Physics of Heavy and Superheavy Elements, 171–210.
© 2003 *Kluwer Academic Publishers.*

Introduction

The structure, spectroscopy and chemistry of heavy atoms exhibit large relativistic effects. These effects play an important role in lighter elements too, showing up in phenomena such as fine or hyperfine structure of electronic states. Perturbative approaches, starting from a non-relativistic Hamiltonian, are often adequate for describing the influence of relativity on light atoms; for heavier elements, the Schrödinger equation must be supplanted by an appropriate relativistic wave equation.

No closed-form relativistic many-body equation is known, and one must resort to approximate schemes. Most commonly, the Dirac Hamiltonian is used for the one-body terms, with the Coulomb repulsion serving as the two-body interaction, yielding the Dirac-Coulomb equation. The frequency-independent Breit operator is often added to give the Dirac-Coulomb-Breit scheme. Approximate one-electron solutions to these equations may be obtained by the self-consistent-field procedure. The resulting Dirac-Fock or Dirac-Fock-Breit functions are conceptually similar to the familiar Hartree-Fock functions; the Hartree-Fock orbitals are replaced, however, by four-component spinors. Correlation is no less important in the relativistic regime than it is for lighter elements, and may be included in a similar manner. Four-component methods, complemented by high-level treatment of correlation, provide the most accurate approach to heavy-atom studies; they are also the most expensive in terms of computational resources. Less demanding methods are often used; they are described in other chapters of the present volume.

The basic relativistic equations are described in section 1, with section 2 discussing correlation methods. Representative applications are shown in section 3, to illustrate the level of accuracy one can expect and the predictions current methods afford regarding properties of hard to access superheavy atoms. It should be noted that a complete listing of applications is beyond the scope of this chapter; the interested reader is referred to Pyykkö's exhaustive database, comprising three volumes and a periodically updated web site [1].

The no-virtual-pair Dirac-Coulomb-Breit Hamiltonian, correct to second order in the fine-structure constant α, provides the framework for the four-component method described below. Many-body methods, and in particular the coupled cluster (CC) approach, give the most successful approach to the treatment of correlation. The method is described in the next section, followed by representative applications. The gold atom provided the first test of the relativistic coupled cluster method and demonstrated its accuracy. Eka-gold (element 111) is an example of a superheavy atom where relativity leads to properties (in this case

the ground state electronic configuration) different from those of lighter homologs. The f^2 levels of Pr^{3+} are studied in the following subsection, demonstrating the ability of the method to give accurate results for a manifold of f-shell levels by including dynamic correlation; the importance of the Breit term for getting correct fine structure splittings is also shown.

Next we study the nature of ground-state configuration of Rf, where contradictory predictions have been made in the past, since relativity favors p over d orbitals whereas correlation has the opposite effect. It is shown that dynamic correlation is the decisive factor, making the $7s^26d^2$ configuration lower than $7s^26d7p$, contrary to multiconfiguration Dirac-Fock results. The recently developed intermediate Hamiltonian Fock-space coupled cluster approach provides higher accuracy by allowing much larger P spaces; this is demonstrated by application to the electron affinities of the alkali atoms. The method is also applied to eka-lead (element 114), which nuclear physics predicts to be in an "island of stability" and have isotopes with much longer lifetime than other superheavy elements. Another interesting superheavy atom is the rare gas eka-radon (E118), which is predicted to have a positive electron affinity, an uncharacteristic property for a rare gas. Transitions involving f electrons in atoms such as La and E121 are shown to require the Breit term and at least i ($l = 6$) functions in the basis to attain the desired accuracy. Several studies of electron affinities, a tough property to calculate, are then listed. A brief discussion of properties other than energy concludes the roster of applications.

1. Basic Equations

A brief review of the basic equations providing the framework to relativistic atomic structure calculations is presented below, followed by reference to early calculations at the SCF level.

1.1 The relativistic Hamiltonian

The relativistic many-electron Hamiltonian cannot be written in closed form; it may be derived perturbatively from quantum electrodynamics [2]. The simplest form is the Dirac-Coulomb (DC) Hamiltonian, where the nonrelativistic one-electron terms in the Schrödinger equation are replaced by the one-electron Dirac operator h_D,

$$H_{\mathrm{DC}} = \sum_i h_D(i) + \sum_{i<j} 1/r_{ij}\,, \tag{5.1}$$

with

$$h_D = c\boldsymbol{\alpha} \cdot \boldsymbol{p} + \beta c^2 + V_{\text{nuc}}. \tag{5.2}$$

$\boldsymbol{\alpha}$ and β are the four-dimensional Dirac matrices, and V_{nuc} is the nuclear attraction operator, with the nucleus modeled as a point or finite-size charge. Only the one-electron terms in the DC Hamiltonian are relativistic, and the two-electron repulsion remains in the nonrelativistic form. The lowest-order correction to the two-electron term in Coulomb gauge is the Breit operator [3]

$$B_{12}^{\omega} = -\frac{\boldsymbol{\alpha}_1 \cdot \boldsymbol{\alpha}_2 \cos(\omega r_{12})}{r_{12}} + (\boldsymbol{\alpha}_1 \cdot \boldsymbol{\nabla}_1)(\boldsymbol{\alpha}_2 \cdot \boldsymbol{\nabla}_2)\frac{\cos(\omega r_{12}) - 1}{\omega^2 r_{12}}. \tag{5.3}$$

Usually, the frequency-independent Breit operator is taken,

$$B_{12} = -\frac{1}{2}[\boldsymbol{\alpha}_1 \cdot \boldsymbol{\alpha}_2 + (\boldsymbol{\alpha}_1 \cdot \boldsymbol{r}_{12}) \cdot (\boldsymbol{\alpha}_2 \cdot \boldsymbol{r}_{12})/r_{12}^2]/r_{12}\,, \tag{5.4}$$

yielding the Dirac-Coulomb-Breit (DCB) Hamiltonian

$$H_{\text{DCB}} = \sum_i h_D(i) + \sum_{i<j}(1/r_{ij} + B_{ij})\,. \tag{5.5}$$

All equations are in atomic units.

The DC or DCB Hamiltonians may lead to the admixture of negative-energy eigenstates of the Dirac Hamiltonian in an erroneous way [4,5]. The no-virtual-pair approximation [6,7] is often invoked to correct this problem: the negative-energy states are eliminated by the projection operator Λ^+, leading to the projected Hamiltonians

$$H_{\text{DC}}^{+} = \Lambda^+ H_{\text{DC}} \Lambda^+ \tag{5.6}$$

or

$$H_{\text{DCB}}^{+} = \Lambda^+ H_{\text{DCB}} \Lambda^+\,. \tag{5.7}$$

H_{DCB}^{+} is correct to second order in the fine-structure constant α, and is expected to be highly accurate for all neutral and weakly-ionized atoms [8]. Higher quantum electrodynamic (QED) terms are required for strongly-ionized species; these are outside the scope of this chapter. A comprehensive discussion of higher QED effects and other aspects of relativistic atomic physics may be found in the proceedings of the 1988 Santa Barbara program [9]. An up-to-date review of QED effects in atoms appears in the last chapter of the present book.

1.2 The one-electron equation

The no-pair DCB Hamiltonian (5.7) is used as a starting point for variational or many-body relativistic calculations [10]. The procedure is similar to the nonrelativistic case, with the Hartree-Fock orbitals replaced by the four-component Dirac-Fock-Breit (DFB) functions. The spherical symmetry of atoms leads to the separation of the one-electron equation into radial and spin-angular parts [11]. The radial four-spinor has the so-called large component $P_{n\kappa}$ in the upper two places and the small component $Q_{n\kappa}$ in the lower two. The quantum number κ (with $|\kappa| = j + 1/2$) comes from the spin-angular equation, and n is the principal quantum number, which counts the solutions of the radial equation with the same κ. Defining

$$\phi_{n\kappa} = \begin{pmatrix} P_{n\kappa}(r) \\ Q_{n\kappa}(r) \end{pmatrix}, \tag{5.8}$$

the DFB equation has the form

$$F_\kappa \phi_{n\kappa} = \varepsilon_{n\kappa} \phi_{n\kappa}, \tag{5.9}$$

where the one-electron DFB operator F_κ is [12–16]

$$F_\kappa = \begin{pmatrix} V_{\text{nuc}} + U^{LL} & c\Pi_\kappa + U^{LS} \\ c\Pi_\kappa^+ + U^{SL} & V_{\text{nuc}} + U^{SS} - 2c^2 \end{pmatrix}, \tag{5.10}$$

with

$$\Pi_\kappa = -d/dr + \kappa/r \tag{5.11}$$

and

$$\Pi_\kappa^+ = d/dr + \kappa/r. \tag{5.12}$$

V_{nuc} is the nuclear attraction potential. The point-charge model employed in light atom calculations gives significant errors for heavy elements, and the finite extent of the nucleus must be considered. Several models for the distribution of the nuclear charge are commonly used [17, 18]. In the uniform charge distribution model, the charge of a nucleus of atomic mass A is distributed uniformly over a sphere with radius $R = 2.2677 \times 10^{-5} A^{-1/3}$. The nuclear potential for a nucleus with charge Z is then

$$V_{\text{nuc}} = \begin{cases} -Z/r & \text{for } r > R \\ -(Z/2R)(3 - r^2/R^2) & \text{for } r \leq R. \end{cases} \tag{5.13}$$

Two other commonly used potentials employ Fermi or Gaussian charge distributions. Dirac-Fock calculations for all elements up to Mt (E109)

[18] found that significant differences exist between point-charge and finite nuclei, while the three finite nuclei models give very close values. Table 5.1 lists some results for atomic Fm. The effect of selecting a different finite nuclear model is two orders of magnitude smaller than going from a finite to a point-charge nucleus. These results are typical, indicating that a finite nucleus should be used, but the choice of the exact model is secondary.

Table 5.1 **Effect of nuclear model on DF calculated properties of Fm (E100). Values from ref. [18]. Absolute and percent differences are shown. Energies in hartree, distances in bohr units.**

	Differences between	
	point and finite nuclei	finite nuclear models
Total energy	42(0.12%)	0.53(0.0015%)
$1s$ orbital energy	16(0.3%)	0.20(0.0038%)
$7s$ orbital energy	6×10^{-4}(0.3%)	7×10^{-6}(0.0034%)
$\langle r\rangle$ of $1s$	1.2×10^{-4}(0.24%)	1.5×10^{-6}(0.0030%)
$\langle r\rangle$ of $7s$	0.010(0.24%)	1.2×10^{-4}(0.0029%)
$\langle r^{-1}\rangle$ of $1s$	1.6(1.1%)	0.024(0.016%)
$\langle r^{-1}\rangle$ of $7s$	9×10^{-4}(0.3%)	1.1×10^{-5}(0.004%)

The terms U^{LL} etc. in (5.10) represent the one-body mean-field potential, which approximates the two-electron interaction in the Hamiltonian, as is the practice in SCF schemes. In the DFB equations this interaction includes the Breit term (5.4) in addition to the electron repulsion $1/r_{ij}$. The radial functions $P_{n\kappa}(r)$ and $Q_{n\kappa}(r)$ may be obtained by numerical integration [19,20] or by expansion in a basis (for more details see recent reviews [21,22]). Since the Dirac Hamiltonian is not bound from below, failure to observe correct boundary conditions leads to "variational collapse" [23,24], where admixture of negative-energy solutions may yield energies much below experimental. To avoid this failure, the basis sets used for expanding the large and small components must maintain "kinetic balance" [25,26]. In the nonrelativistic limit ($c \to \infty$), the small component is related to the large component by [23]

$$Q_{n\kappa}(r) = (2c)^{-1}\Pi_\kappa^+ P_{n\kappa}(r)\,, \tag{5.14}$$

where Π_κ^+ is defined in (5.12). The simplest way to obtain kinetic balance is to derive the small-component basis functions from those used to span

the large component by

$$\chi^S_{\kappa j} = \Pi^+_\kappa \chi^L_{\kappa j} \,. \tag{5.15}$$

Ishikawa and coworkers [16,27] have shown that G-spinors, with functions spanned in Gaussian-type functions (GTF) chosen according to (5.15), satisfy kinetic balance for finite c values if the nucleus is modeled as a uniformly-charged sphere.

1.3 SCF calculations

The earliest Dirac-Fock calculations of atomic wavefunctions used numerical integration of the radial equations [28, 29]. Of particular note is the work of Desclaux [29], who tabulated the functions of all atoms to element 120. Other calculations in the 1970's used the Dirac-Slater method, with exchange parametrized as a function of electron density [30–32]. Mann and Waber [33] added the Breit term and semiempirical correlation to the DF Hamiltonian. A major goal of these calculations was to establish the ground state electron configuration of the heavy and superheavy elements, which are often different from those of the lighter atoms in the same group. Many features of the structure and spectra of heavy atoms could be understood, at least qualitatively, on the basis of these calculations; more accurate, quantitative treatment was made possible by the advent of powerful methods to incorporate electron correlation and the availability of computational resources allowing their implementation.

2. Incorporation of Electron Correlation

The first method used extensively to include correlation in relativistic calculations was the numerical multiconfiguration Dirac-Fock (MCDF) scheme [34–36]. This method gives, in general, good atomic term energies and transition probabilities. It is particularly successful in treating nondynamic correlation, where a few hundred configuration state functions are sufficient; the many thousands of CSFs required for accurate description of dynamic correlation are sometimes beyond its reach (see, e.g., the recent calculation of Rodrigues et al. [37] for atomic Cs, where the MCDF results could not be converged with respect to configuration space). Atomic MCDF has recently been implemented in a Gaussian basis by Vilkas et al [38].

A different class of methods goes under the heading "many-body methods", reviewed recently by Sapirstein [39]. For highly ionized atoms, second-order many-body perturbation theory (2nd-order MBPT, better known to chemists as Møller-Plesset or MP2 theory) is accurate enough to see QED effects from the differences between MBPT and experimen-

tal values. Neutral or weakly ionized atoms, on the other hand, require higher order treatment of correlation. One approach to the problem is relativistic multireference MBPT, implemented recently in a Gaussian basis by Ishikawa and coworkers [40]. An alternative scheme involves infinite-order summation of perturbation terms, accomplished by the coupled cluster method [41–43]. A numerical procedure for solving the relativistic many-body Dirac-Coulomb equation, based on the pair approximation of the CC approach, has been developed by Lindgren and coworkers [44]. A different approach to the many-body problem employs a discrete basis set of local or global functions. The CC or MBPT sums over an infinite set of bound states and integrals over positive-energy continuum states are replaced by finite summation over the pseudospectrum. The implementation of the projection operators is made easy by the clean separation of positive- and negative-energy states; it amounts to limiting summations to the positive-energy branch of the one-electron pseudospectrum. A relativistic CC technique based on local splines (piecewise polynomial fitting) has been developed and implemented to a number of atoms [46, 47]. Another kind of local basis set has been introduced to relativistic CC by Salomonson and Öster [48], who discretized the radial space. This technique is similar in spirit to the spline method and may be regarded as its limiting case (single-point representation rather than polynomial fitting).

A particular variant of the coupled cluster method, called Fock-space or valence-universal [49,50], gave remarkable agreement with experiment for many transition energies of heavy atoms [51]. This success makes the scheme a useful tool for reliable prediction of the structure and spectrum of superheavy elements, which are difficult to access experimentally. A brief description of the method is given in the next subsection; this is followed by an account of a recent improved approach called intermediate Hamiltonian Fock-space coupled cluster, where preliminary applications promise even higher accuracy and an extended domain of applicability.

2.1 The Fock-space coupled-cluster method

The Dirac-Coulomb-Breit Hamiltonian H^+_{DCB} may be rewritten in second-quantized form [6, 16] in terms of normal-ordered products of spinor creation and annihilation operators $\{r^+s\}$ and $\{r^+s^+ut\}$,

$$H = H^+_{\mathrm{DCB}} - \langle 0|H^+_{\mathrm{DCB}}|0\rangle = \sum_{rs} f_{rs}\{r^+s\} + \frac{1}{4}\sum_{rstu}\langle rs||tu\rangle\{r^+s^+ut\}, \tag{5.16}$$

where

$$\langle rs||tu\rangle = \langle rs|tu\rangle - \langle rs|ut\rangle \tag{5.17}$$

and

$$\langle rs|tu\rangle = \int d\mathbf{x}_1 d\mathbf{x}_2 \Psi_r^*(\mathbf{x}_1)\Psi_s^*(\mathbf{x}_2)(r_{12}^{-1} + B_{12})\Psi_t(\mathbf{x}_1)\Psi_u(\mathbf{x}_2). \quad (5.18)$$

Here f_{rs} and $\langle rs||tu\rangle$ are, respectively, elements of one-electron Dirac-Fock-Breit and antisymmetrized two-electron Coulomb-Breit interaction matrices over Dirac four-component spinors. The effect of the projection operators Λ^+ is now taken over by normal ordering, denoted by the curly braces in (5.16), which requires annihilation operators to be moved to the right of creation operators as if all anticommutation relations vanish. The Fermi level is set at the top of the highest occupied positive-energy state, and the negative-energy states are ignored.

By adopting the no-pair approximation, a natural and straightforward extension of the nonrelativistic open-shell CC theory emerges. The multireference valence-universal Fock-space coupled-cluster approach is employed [49, 50], which defines and calculates an effective Hamiltonian in a low-dimensional model (or P) space, with eigenvalues approximating some desirable eigenvalues of the physical Hamiltonian. The effective Hamiltonian has the form [44]

$$H_{\text{eff}} = PH\Omega P\,, \quad (5.19)$$

where Ω is the normal-ordered wave operator,

$$\Omega = \{\exp(S)\}. \quad (5.20)$$

The Fock-space approach starts from a reference state (closed-shell in our applications, but other single-determinant functions may also be used), correlates it, then adds and/or removes electrons one at a time, recorrelating the whole system at each stage. The sector (m, n) of the Fock space includes all states obtained from the reference determinant by removing m electrons from designated occupied orbitals, called valence holes, and adding n electrons in designated virtual orbitals, called valence particles. The practical limit is $m + n \leq 2$, although higher sectors have also been tried [45]. The excitation operator is partitioned into sector operators

$$S = \sum_{m\geq 0}\sum_{n\geq 0} S^{(m,n)}. \quad (5.21)$$

This partitioning allows for partial decoupling of the open-shell CC equations. The equations for the (m, n) sector involve only S elements from sectors (k, l) with $k \leq m$ and $l \leq n$, so that the very large system of coupled nonlinear equations is separated into smaller subsystems, which are solved consecutively: first, the equations for $S^{(0,0)}$ are iterated to

convergence; the $S^{(1,0)}$ (or $S^{(0,1)}$) equations are then solved using the known $S^{(0,0)}$, and so on. This separation, which does not involve any approximation, reduces the computational effort significantly. The effective Hamiltonian (5.19) is also partitioned by sectors. An important advantage of the method is the simultaneous calculation of a large number of states.

Each sector excitation operator is, in the usual way, a sum of virtual excitations of one, two, ..., electrons,

$$S^{(m,n)} = \sum_l S_l^{(m,n)}, \tag{5.22}$$

with l going, in principle, to the total number of electrons. In practice, l has to be truncated. The level of truncation reflects the quality of the approximation, i.e., the extent to which the complementary Q space is taken into account in the evaluation of the effective Hamiltonian. The series (5.22) is truncated at l=2 in the applications described below. The resulting CCSD (coupled cluster with single and double excitations) scheme involves the fully self-consistent, iterative calculation of all one- and two-body virtual excitation amplitudes, and sums all diagrams with these excitations to infinite order. As negative-energy states are excluded from the Q space, the diagrammatic summations in the CC equations are carried out only within the subspace of the positive-energy branch of the DF spectrum.

2.2 The intermediate Hamiltonian coupled cluster method

The accuracy and convergence of the Fock-space coupled cluster method discussed above depends on an appropriate partitioning of the function space into P and Q subspaces. Ideally, the P space should include all functions which are important to the states considered, since the effective Hamiltonian is diagonalized in P, whereas Q-space contributions are included approximately. On the other hand, convergence of the coupled cluster iterations is enhanced by maximal separation and minimal interaction between P and Q. These requirements are not always easy to reconcile. Relatively high P functions have often strong interaction with or are energetically close to Q states, making convergence slow or impossible. The offending functions are usually included in P because of their significant contribution to the lower P states, and we may not be particularly interested in the correlated states generated from them by the wave operator; however, the FSCC is an all-or-nothing method, and lack of convergence means that no states at all are obtained. The intermediate

Hamiltonian coupled cluster method developed recently [52] addresses this problem, making possible larger and more flexible P spaces, thereby extending the scope of the coupled cluster method and increasing its precision.

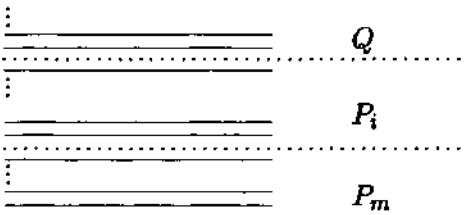

Figure 5.1 Model spaces in the intermediate Hamiltonian method

The intermediate Hamiltonian method has been proposed by Malrieu [53] in the framework of degenerate perturbation theory. The P space is partitioned into the main P_m and the intermediate P_i (see fig. 5.1), with the corresponding operators satisfying

$$P_m + P_i = P \ , \qquad P + Q = 1 \ . \tag{5.23}$$

Two sets of wave-like operators are defined and expanded in coupled-cluster normal-ordered exponential ansätze. $\Omega = 1 + \chi$ is a standard wave operator in P_m,

$$\Omega P_m|\Psi_m\rangle = \{\exp S\}P_m|\Psi_m\rangle = |\Psi_m\rangle \ , \tag{5.24}$$

where $|\Psi_m\rangle$ denotes an eigenstate of the Hamiltonian H with the largest components in P_m, and $R = 1 + \Delta$ is an operator in P, satisfying

$$RP|\Psi_m\rangle = \{\exp T\}P|\Psi_m\rangle = |\Psi_m\rangle. \tag{5.25}$$

It should be noted that the last equation, and therefore all equations derived from it, applies when operating on $|\Psi_m\rangle$ but not necessarily on $|\Psi_i\rangle$. This feature distinguishes R from a bona fide wave operator. The cluster equation for S in the (n) sector of the Fock space is [52]

$$Q[S^{(n)}, H_0]P_m = Q(\overline{VQ_i\Omega} - \overline{\chi P_m VQ_i\Omega})^{(n)}P_m, \tag{5.26}$$

where $Q_i = 1 - P_i = Q + P_m$. No P_iSP_m elements appear in the equation, so that P_i acts as a buffer between P_m and Q, facilitating convergence and avoiding intruder states. Eq. (5.26) is valid provided $QSP_m \simeq QTP_m$,

which can be achieved by choosing an appropriate P_i. Table 5.2 shows the dependence of $Q(S-T)P_m$ amplitudes on the size of P_i for the test case of Mg. These amplitudes are monitored in all applications, making sure they are of order 10^{-6} or less.

Table 5.2 Dependence of $Q(S-T)P_m$ on size of P_i. Test on Mg atom, with a $18s13p8d4f$ basis. Mg^{2+} is the reference state, $2s2p$ electrons are correlated, P_m includes all Mg determinants with $3s$, $4s$, $3p$, $4p$, and $3d$ electrons.

P_i orbitals	$Q(S-T)P_m$ amplitudes
5–6s, 5p, 4d	$< 10^{-3}$
5–7s, 5–6p, 4–5d, 4f	$< 10^{-4}$
5–8s, 5–7p, 4–6d, 4–5f	$< 7 \cdot 10^{-6}$

After (5.26) is solved for QSP_m, QTP is obtained from

$$(E-H_0)QT^{(n)}P = \qquad (5.27)$$
$$Q\left(S(E-H_0)P_m + (\overline{VR}) - (\overline{\chi P_m VR})\right)^{(n)} P.$$

E is an arbitrary constant, chosen to facilitate convergence. Tests have shown that E may be changed within broad bounds (hundreds of hartrees) with minute effect (a few wave numbers) on calculated transition energies. The final step is the construction of the intermediate Hamiltonian

$$H_I = PHRP\,, \qquad (5.28)$$

which gives upon diagonalization the correlated energies of $|\Psi_m\rangle$,

$$H_I P|\Psi_m\rangle = E_m P|\Psi_m\rangle\,. \qquad (5.29)$$

The dimension of the H_I matrix is that of P; however, only the eigenvalues corresponding to $|\Psi_m\rangle$ are required to satisfy (5.29). The other eigenvalues, which correspond to states $|\Psi_i\rangle$ with the largest components in P_i, may include larger errors.

3. Applications

As noted above, high-level inclusion of correlation is essential if a quantitative description of the atom is desired. It should be emphasized that correlation and relativistic effects (by the latter we mean the difference

between the results of relativistic and equivalent nonrelativistic formulations) are non-additive for heavy atoms. The cause is clear: since the relativistic spatial distribution of the orbitals differs significantly from that of nonrelativistic counterparts (s and p orbitals undergo contraction, whereas d and f orbitals expand), correlation energy changes. This affects in particular inner shells, but more diffuse orbitals are not exempt. Thus, the CCSD correlation energy of the $4s$ and higher electrons in Au^- came out as -1.3702 hartree in the nonrelativistic scheme, -1.4644 hartree in the Dirac-Coulomb Hamiltonian, and -1.4669 hartree in the DCB formulation [54].

Representative applications of the Fock-space coupled cluster method to atomic systems will now be presented. The applications were selected to illuminate features of the method or phenomena exhibited by the various atoms and ascribed to relativistic effects. The spherical symmetry of atoms, which leads to angular decomposition of the wave function and coupled-cluster equations, is used at both the Dirac-Fock-Breit [16] and CC [54, 55] stages of the calculation. The energy integrals and CC amplitudes, which appear in the Goldstone-type diagrams defining the CC equations, are decomposed in terms of vector-coupling coefficients, expressed by angular-momentum diagrams, and reduced Coulomb-Breit or S matrix elements, respectively. The reduced equations for single and double excitation amplitudes are derived using the Jucys-Levinson-Vanagas theorem [44] and solved iteratively. This technique makes possible the use of large basis sets with high l values, as a basis orbital gives rise to two functions at most, with $j = l \pm 1/2$, whereas in Cartesian coordinates the number of functions increases rapidly with l. Typically we go to h ($l = 5$) or i ($l = 6$) orbitals, but higher orbitals (up to $l = 8$) have been used. To account for core-polarization effects, which may be important for many systems, we correlate at least the two outer shells, usually 20–40 electrons. Finally, uncontracted Gaussians are used, since contraction leads to problems in satisfying kinetic balance and correctly representing the small components. On the other hand, it has been found that high-energy virtual orbitals have little effect on the transition energies we calculate, since these orbitals have nodes in the inner regions of the atom and correlate mostly the inner-shell electrons, which we do not correlate anyway. These virtual orbitals, with energies above 80 or 100 hartree, are therefore eliminated from the CC calculation.

3.1 Ionization potentials of alkali atoms

Alkali atoms are basically one-valence-electron systems, and correlation would therefore not be expected to play a major role in the de-

termination of properties such as ionization potentials. Nevertheless, a Hartree-Fock (or, for the heavier alkali atoms, a Dirac-Fock) calculation gives sizable errors for this property. In particular, if accuracy below the one percent level is desired, as would be needed, for example, in studies of parity nonconservation effects [56], high-level treatment of correlation is essential. Large basis set calculations were carried out by the Notre Dame group in second-order MBPT for Li to Cs [57] and in CCSD for Cs [58]; the Fock-space CC method was applied to all atoms by Eliav et al. [55]. Results for atomic cesium, collected in table 5.3, show that all-order summation is indeed necessary to obtain highly accurate ionization potentials. The Fock-space CC values are within 0.02%–0.11% of experiment. Fine structure splittings are also reproduced well: 548 cm^{-1} for the $6p$ level (experimental 554) and 96.5 cm^{-1} for $5d$ (experimental 97.6).

Table 5.3 Ionization potential of Cs (hartree). Percent error in parentheses.

	$6s_{1/2}$	$6p_{1/2}$	$6p_{3/2}$	$7s_{1/2}$
DF [57]	0.12737 (11%)	0.08562 (7.1%)	0.08378 (6.5%)	0.05519 (5.9%)
MBPT-2 [57]	0.14511 (1.4%)	0.09253 (0.4%)	0.08996 (0.4%)	0.05939 (1.3%)
CC [58]	0.14257 (0.4%)	0.09198 (0.2%)	0.08951 (0.15%)	0.05845 (0.3%)
FSCC [55]	0.14326 (0.11%)	0.09212 (0.05%)	0.08962 (0.02%)	0.05867 (0.03%)
Expt. [59]	0.14310	0.09217	0.08964	0.05865

3.2 Gold and eka-gold (E111): Local maximum of relativistic effects

The gold atom exhibits very large relativistic effects on its chemical and physical properties, due to the contraction and stabilization of the $6s$ orbital. The compactness of the atom relative to its neighbors leads to a local maximum in relativistic effects, called by Pyykkö the "gold maximum". Nonrelativistic calculations lead to large errors, including the reversal of the two lowest excited states [60,61]. Gold was therefore selected as the first heavy atom to be treated by the CC method [54]. Two closed-shell states can be used as starting points for the Fock-space treatment, defining the (0,0) sector, namely Au^+ or Au^-. Electrons are then added or removed according to the schemes

$$Au^+(0,0) \rightarrow Au(0,1) \rightarrow Au^-(0,2), \tag{5.30}$$

or

$$\mathrm{Au}^-(0,0) \rightarrow \mathrm{Au}(1,0) \rightarrow \mathrm{Au}^+(2,0). \tag{5.31}$$

The basis consisted of $21s17p11d7f$ Gaussian spinors [61], and correlated shells included $4spdf5spd6s$. Table 5.4 shows the nonrelativistic, Dirac-Coulomb, and Dirac-Coulomb-Breit total energies of the two ions. As expected, relativistic effects are very large, over 1100 hartree. The nonadditivity of relativistic and correlation corrections to the energy, apparent in table 5.4, has been noted above.

Table 5.4 Total energies of the closed-shell systems Au^+ and Au^- (hartree), with nonrelativistic, DC, and DCB Hamiltonians. Correlation includes $4s$ and higher shells.

	Au^+		Au^-	
	Uncorrelated	Correlation	Uncorrelated	Correlation
NR	−17863.46301	−1.29756	−17863.68392	−1.37018
DC	−19029.01322	−1.36150	−19029.32077	−1.46436
DCB	−19007.42385	−1.36430	−19007.73063	−1.46690

Table 5.5 CCSD transition energies in Au (eV). IP is the ionization potential, EA denotes electron affinity, and EE — excitation energy relative to the ground state. FS denotes fine-structure splittings.

			NR	DC	DCB	Expt. [59]
IP	$5d^{10}6s$	$^2S_{1/2}$	6.981	9.101	9.086	9.22
EE	$5d^9 6s^2$	$^2D_{3/2}$	5.301	2.661	2.669	2.658
	$5d^9 6s^2$	$^2D_{5/2}$	5.301	1.115	1.150	1.136
	$5d^{10}6p_{1/2}$	$^2P_{1/2}$	3.313	4.723	4.720	4.632
	$5d^{10}6p_{3/2}$	$^2P_{3/2}$	3.313	5.193	5.184	5.105
FS		^2D	0	1.546	1.519	1.522
		^2P	0	0.470	0.466	0.473
EA	$5d^{10}6s^2$	$^1S_0$	1.267	2.278	2.269	2.31

The various transition energies of the gold atom and its ions are shown and compared with experiment [59] in table 5.5. The nonrelativistic results have errors of several eV. The CC values, on the other hand, are highly accurate, with an average error of 0.06 eV. More recent (unpublished) values, obtained with a larger $31s26p21d17f14g11h8i$ basis, are

even closer to experiment, giving 9.17 eV for the IP and 2.29 eV for the EA. The inclusion of the Breit effect does not change the results by much, except for some improvement of the fine-structure splittings.

A major relativistic effect in the gold atom is the stabilization of the $6s$ orbital. This is manifested by the energy separation between the $5d^{10}6s\ ^2S$ ground state and the $5d^9 6s^2\ ^2D$ excited state. Looking at group 11 (coinage metal) atoms, the ^2D excitation energies of Cu are 1.389 ($J = 5/2$) and 1.642 ($J = 3/2$) eV, increasing to 3.749 and 4.304 eV for Ag [59]. Were it not for relativity, one would expect even higher energies for Au. Indeed, nonrelativistic CCSD (table 5.5) puts the ^2D energy at 5.301 eV above the ^2S ground state, in line with expectations. Relativistic effects reduce this value radically, giving 1.150 and 2.669 eV for the excited ^2D sublevels, within 0.015 eV of experiment [59]. Even larger stabilization may be expected for the next member of the group, element 111. The question arose whether this stabilization would be sufficient to push the ^2D level below the ^2S and make it the ground state of the atom.

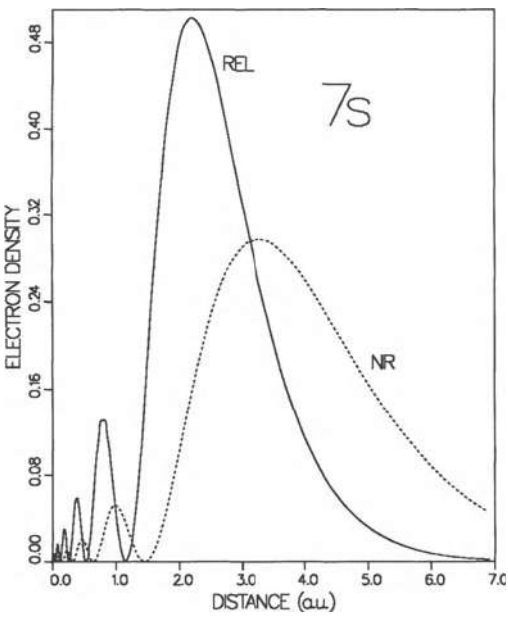

Figure 5.2 Relativistic and nonrelativistic densities of element 111 $7s$ orbital

Table 5.6 CCSD excitation energies, electron affinity and ionization potentials of element 111 (eV).

	Transition	DC	DCB	NR
EE	$6d^9 7s^2\ ^2D_{5/2} \rightarrow 6d^9 7s^2\ ^2D_{3/2}$	2.719	2.687	0
	$6d^9 7s^2\ ^2D_{5/2} \rightarrow 6d^{10} 7s\ ^2S_{1/2}$	3.006	2.953	−5.430
EA	$6d^9 7s^2\ ^2D_{5/2} \rightarrow 6d^{10} 7s^2\ ^1S_0$	1.542	1.565	6.484
IP	$6d^9 7s^2\ ^2D_{5/2} \rightarrow 6d^8 7s^2\ ^3D_4$	10.57	10.60	22.98
	$6d^9 7s^2\ ^2D_{5/2} \rightarrow 6d^9 7s\ ^3D_3$	12.36	12.33	0.92
	$6d^9 7s^2\ ^2D_{5/2} \rightarrow 6d^{10}\ ^1S_0$	15.30	15.23	−0.44

The calculations were carried out as for gold above, starting with the $E111^-$ anion as reference [62]. As expected, very large relativistic effects are observed, demonstrated by the large contraction of the $7s$ orbital of neutral E111 (Fig. 5.2). The $7s$ orbital energy of the anion goes down from −0.018 to −0.136 hartree, while the $6d$ goes up from −0.355 to −0.186 ($j = 3/2$) and −0.080 ($j = 5/2$) hartree. Atomic energies also show dramatic changes (see table 5.6). Of particular interest to us is the $6d^9 7s^2\ ^2D_{5/2}$ state, predicted by nonrelativistic CCSD to lie 5.43 eV above the $6d^{10} 7s\ ^2S$ state, but reduced relativistically to 3 eV *below* the ^2S, thus becoming the ground state. Ionization potentials of the atom show relativistic effects of 12–15 eV! Similar effects were observed in eka-mercury (E112) [63] and eka-thallium (E113) [64].

3.3 The f^2 levels of Pr^{3+}: Importance of dynamic correlation

Lanthanides and actinides possess open f shells, which give rise to large manifolds of closely spaced states. As an example of these systems we discuss the energy levels of the Pr^{3+} ion, which has an f^2 ground state configuration. The spectrum is well characterized experimentally [65] and provides a good test for high-accuracy methods incorporating relativity and correlation. The system has been studied by both MCDF and Fock-space CC, and comparison between these methods can therefore be made.

The MCDF calculations [66] involved between 354 and 1708 CSFs for the different J states. The number of CSFs was much larger in the CC calculations [67], since all excitations from the $4spdf5sp$ orbitals to virtual orbitals (except virtuals with energies above 100 hartree), as well

as excitations from $4spd5sp$ to the partially filled $4f$, were included. Thus, a much larger part of dynamic correlation was accounted for. The Pr^{5+} closed shell state served as reference, and two electrons were added in the $4f$ shell to obtain the levels of interest. Three basis sets were used, with l going up to 4, 5 and 6. The calculated excitation energies are compared with experiment [65] in table 5.7.

Table 5.7 Excitation energies of Pr^{3+} $4f^2$ levels (cm^{-1}). The ground state is $^3H_4$.

Level	Expt. [65]	MCDF [66]	CCSD [67]		
			$l \leq 4$	$l \leq 5$	$l \leq 6$
$^3H_5$	2152.09	2337	2273	2273	2270
$^3H_6$	4389.09	4733	4645	4641	4635
$^3F_2$	4996.61	4984	4749	4832	4843
$^3F_3$	6415.24	6517	6266	6345	6354
$^3F_4$	6854.75	6950	6808	6844	6843
$^1G_4$	9921.24	10207	10019	10014	10001
$^1D_2$	17334.39	18153	16803	16961	16998
$^3P_0$	21389.81	22776	20802	21109	21155
$^3P_1$	22007.46	23450	21443	21747	21791
$^1I_6$	22211.54	25854	22267	22061	22010
$^3P_2$	23160.61	24653	22719	23009	23051
$^1S_0$	50090.29	50517	48448	49072	49194
Avrg. error		853	394	245	222

The Fock-space CC excitation energies are in better agreement with experiment than MCDF values, and improve with the size of the basis. All 13 levels appear in the correct order (in MCDF the $^3P_2$ level appears 1200 cm^{-1} below the $^1I_6$ instead of 950 cm^{-1} above it). Convergence with respect to the l value in the virtual space seems good, and the best basis gives an average error of 222 cm^{-1} for the excitation energies. A full half of the total error is due to the high $^1S_0$ state; these states are notoriously difficult to calculate. While inclusion of the Breit term has a rather small effect on the excitation energies of Pr^{3+}, it improves the fine-structure splittings (table 5.8). This is a general phenomenon, and may be traced to the spin-other-spin interaction in the two-electron Breit term [68]. Fine-structure splittings are less sensitive to the amount of correlation retrieved.

Table 5.8 Fine structure in Pr^{3+} (cm^{-1}).

	Expt. [65]	MCDF	DC $l \leq 4$	DC $l \leq 5$	DCB $l \leq 5$	DC $l \leq 6$
$^3H_5 - ^3H_4$	2152	2337	2273	2273	2081	2270
$^3H_6 - ^3H_5$	2237	2396	2369	2368	2169	2365
$^3F_3 - ^3F_2$	1419	1533	1517	1513	1373	1511
$^3F_4 - ^3F_3$	440	433	542	499	465	489
$^3P_1 - ^3P_0$	618	674	631	638	585	636
$^3P_2 - ^3P_1$	1153	1203	1276	1262	1090	1260
Avrg. error		95	98	89	51	86

3.4 Ground state of rutherfordium — interplay of relativity and correlation

The nature of the rutherfordium ground state has been a subject of interest for a long time. Rutherfordium is the first atom after the actinide series, and in analogy with the lighter group-4 elements it should have the ground-state configuration $[Rn]5f^{14}6d^27s^2$. Keller [69] suggested that the relativistic stabilization of the $7p_{1/2}$ orbital would yield a $7s^27p_{1/2}^2$ ground state. MCDF calculations [70, 71] found that the $7p^2$ state was rather high; they indicated a $6d7s^27p$ ground state, with the lowest state of the $6d^27s^2$ configuration higher by 0.5 [70] or 0.24 eV [71]. The two calculations are similar, using numerical MCDF [34] in a space including all possible distributions of the four external electrons in the $6d$, $7s$ and $7p$ orbitals, and the difference may be due to the different programs used or to minor computational details. These MCDF calculations take into account nondynamic correlation only, which is due to near-degeneracy effects and can be included by using a small number of configurations. A similar approach by Desclaux and Fricke [72] gave errors of 0.4–0.5 eV for the energy differences between $(n-1)d$ and np configurations of Y, La and Lu, with the calculated np energy being too low. Desclaux and Fricke corrected the corresponding energy difference in Lr by a similar amount [72]. If a shift of similar magnitude is applied to the MCDF results for Rf, the order of the two lowest states may be reversed. It should also be noted that dynamic correlation, largely omitted from MCDF, has been shown to play a significant role in determining atomic excitation energies (see

above), reducing the average error in calculating Pr^{3+} excitation energies by a factor of four relative to MCDF results. The FSCC method was therefore applied to Rf [73]. Starting from Rf^{2+} with the closed-shell configuration $[Rn]5f^{14}7s^2$, two electrons were added, one at a time, in the $6d$ and $7p$ orbitals, to form the low-lying states of Rf^+ and Rf. A large basis set of $34s24p19d13f8g5h4i$ G-spinors was used, and the external 36 electrons were correlated, leaving only the $[Xe]4f^{14}$ core uncorrelated. A series of calculations, with increasing l values in the virtual space, was performed to assess the convergence of the results. Some of the calculated transition energies are shown in table 5.9. Others may be found in the original publication [73].

Table 5.9 Transition energies in Rf^+ and Rf (eV).

	Rf^+		Rf	
	$7s^26d_{3/2}$ $^2D_{3/2}$ IP	$7s^26d_{5/2}$ $^2D_{5/2}$ EE	$7s^26d^2$ $^3F_2$ IP	$7s^27p6d$ $^3D_2$ EE
MCDF [71]	13.47		5.30	−0.24
MCDF [70]				−0.50
CCSD				
$l \leq 2^a$	13.37	0.79	5.15	−0.60
$l \leq 3^a$	13.95	0.82	5.65	−0.11
$l \leq 3$	14.05	0.87	5.76	0.03
$l \leq 4$	14.20	0.90	5.90	0.17
$l \leq 5$	14.34	0.92	5.99	0.25
$l \leq 6$	14.37	0.92	6.01	0.27
$l \leq 5^b$	14.34	0.87	5.99	0.27

[a] $5f$ electrons not correlated
[b] With Breit interaction.

The salient feature of the calculated transition energies is their monotonic behavior with the amount of correlation accounted for. The correlation of the $5f$ electrons and the gradual inclusion of higher l spaces all increase the four transition energies in table 5.9, as well as those not shown here. The MCDF results fall invariably between the d and f limits. This makes sense, since the MCDF function optimizes the orbitals and CI coefficients in a space including configuration state functions which correspond to all possible distributions of the four external electrons in the $6d$, $7s$ and $7p$ orbitals. Nondynamic correlation, resulting from in-

teractions of configurations relatively close in energy, is thus described very well; the dynamic correlation, which is more difficult to include and requires many thousands of configurations, is not described as well, leading to an error in the identification of the Rf ground state. The latter is determined by the sign of the excitation energy in the last column of table 5.9. A negative energy means that the $7s^2 7p6d$ configuration is lower than $7s^2 6d^2$, and is therefore the ground state. From the calculations reported, we estimate the CCSD converged value for this energy at 0.30–0.35 eV, making the $7s^2 6d^2$ state the ground state of atomic Rf. Recent state-of-the-art experiments with Rf confirmed [74] that the chemistry of the atom is similar to that of Hf, which has a $6s^2 5d^2$ ground state.

This example shows the intricate interplay of relativity and correlation. It is well known that relativity stabilizes p vs. d orbitals, and correlation has the opposite effect. When both effects are important and the result not obvious *a priori*, one must apply methods, such as relativistic CC, which treat relativity and correlation simultaneously to high order.

3.5 Eka-lead (element 114) — an island of stability?

Great progress has been made in recent years in creating new superheavy elements. After the synthesis of elements 110–112 in 1994–96 [75–78], elements 114 [79], 116 and 118 [80] were reported in 1999. While claims for elements 116 and 118 have been retracted, and too few atoms of the E114 have been identified so far to confirm unambiguously its creation, these atoms are the subject of great interest, as they fall within the "island of stability" predicted by nuclear physics. The exact location of this island is not certain. There seems to be general agreement that the next neutron magic number is 184, but the proton magic number (which determines the atomic number of the element) is variously predicted at 114 [81], 120 [82], or 126 [83]. Current technology produces isotopes with too few neutrons to get maximum stability; nevertheless, longer lifetimes than for other superheavy elements have been reported (e.g., 30 seconds [79] for element 114 with atomic weight 289 vs. only 240μs for $^{277}_{112}$Uub). One reason for studying these elements, apart from the nuclear physics involved, is the hope that the strong relativistic effects for the heavier elements would lend them exotic chemical properties, unknown for their lighter homologs. The discussion of eka-gold above provides an example where the ground-state configuration of a superheavy element differs from that of the lighter atoms in the group; another case of unusual behavior of a superheavy element is given in the next subsection. Here we

compare the properties of eka-lead with those of lead and lighter group-4 elements. The IHFSCC method is used to obtain high accuracy.

Two series of calculations were carried out [84]. The first started from the closed-shell M^{4+} ion, adding two electrons in the Fock-space scheme

$$M^{4+}(\text{sector } 0) \rightarrow M^{3+}(\text{sector } 1) \rightarrow M^{2+}(\text{sector } 2). \tag{5.32}$$

Thirty two electrons $[(n-1)s^2(n-1)p^6(n-1)d^{10}(n-2)f^{14}$, with $n = 6$ for Pb and 7 for E114] are correlated in the reference state. We were interested in the few lowest states only for these sectors, so a relatively small P_m was taken, including only states with ns and np electrons added to the reference. The P space was considerably larger, including in addition the next four s, four p, four d, three f and two g orbitals. In this case, the traditional FSCC converges with a model space constructed from the ns and np orbitals, and the advantage of IHFSCC lies in enhancing accuracy by allowing a larger P space.

The closed-shell M^{2+} ns^2 state is taken as reference in the second Fock-space sequence,

$$M^{2+}(\text{sector } 0) \rightarrow M^{+}(\text{sector } 1) \rightarrow M(\text{sector } 2). \tag{5.33}$$

Here 34 electrons are correlated in the reference state. Basis sets going to $l = 8$ were used, with $35s26p21d16f11g9h9i7k7l$ Gaussian orbitals. The FSCC iterations converge only when the np orbitals serve as the sole valence particles, i.e., only ns^2np^2 states could be obtained. The IHFSCC method allows many more valence orbitals and, consequently, many more states. The P_m for lead included all states constructed from the $7s$, $8s$, $6p$, $7p$, and $6d$ orbitals; P included, in addition, states with occupied $9s - 12s$, $8p - 11p$, $7d - 9d$, $5f - 7f$, and $5g$ orbitals. For E114 we were interested in fewer states, so that P_m was smaller, with $8s$, $7p$, and $8p$ orbitals; $9s - 13s$, $9p - 12p$, $7d - 10d$, $6f - 8f$, and $5g$ orbitals complete the P space.

The ionization potentials and low excitation energies of the lead and eka-lead cations are reported, together with Pb experimental values [59], in table 5.10. For easy comparison, terms are listed in the LS coupling as in Moore's Tables [59], although the validity of this coupling scheme for Pb, and even more so for E114, is questionable; the only good quantum number in the reported levels (and the calculation procedures) is J. The average deviation of the Pb results from experiment is 334 cm^{-1}, and the largest error is 861 cm^{-1}. This close agreement indicates that the eka-lead values provide good predictions for the electronic spectrum of this superheavy element. Table 5.11 gives the transition energies of the neutral atoms. It is noteworthy that many Pb states can be obtained

Table 5.10 Ionization potentials (IP) and excitation energies (EE) of lead and eka-lead cations (cm^{-1}). $n = 6$ for Pb, 7 for E114.

	Transition		Pb		E114
			Expt. [59]	Calc.	Calc.
	M^{3+}. Ground state $(n-1)d^{10}ns\ ^2S_{1/2}$				
IP	$\rightarrow(n-1)d^{10}$	$^1S_0$	341350	341748	373208
EE	$\rightarrow(n-1)d^{10}np_{1/2}$	$^2P_{1/2}$	76158	76839	86676
	$\rightarrow(n-1)d^{10}np_{3/2}$	$^2P_{3/2}$	97219	97803	138047
	M^{2+}. Ground state $(n-1)d^{10}ns^2\ ^1S_0$				
IP	$\rightarrow(n-1)d^{10}ns$	$^2S_{1/2}$	257592	257617	288256
EE	$\rightarrow(n-1)d^{10}nsnp_{1/2}$	$^3P_0$	60397	60396	73135
	$\rightarrow$	$^3P_1$	64391	64451	79832
	$\rightarrow(n-1)d^{10}nsnp_{3/2}$	$^3P_2$	78985	78964	119597
	$\rightarrow$	$^1P_1$	95340	95716	135170
	$\rightarrow(n-1)d^{10}np^2_{1/2}$	$^3P_0$	142551	143412	166645
	M^{+}. Ground state $(n-1)d^{10}ns^2np_{1/2}\ ^2P_{1/2}$				
IP	$\rightarrow(n-1)d^{10}ns^2$	$^1S_0$	121243	121077	136074
EE	$\rightarrow(n-1)d^{10}ns^2np_{3/2}$	$^2P_{3/2}$	14081	13885	39355
	$\rightarrow(n-1)d^{10}ns^2(n+1)s$	$^2S_0$	59448	59253	71993

accurately by the IHFSCC method (the average error for the 22 P_m excitations is 602 cm^{-1} or 1.6%), while only the $6s^26p^2$ states are accessible by traditional FSCC. There are many P_i states above 51000 cm^{-1}; these come out less well, as expected from theory. In contrast, the higher P_m states are roughly as accurate as the lower levels. The predicted transition energies of E114 given in the same table show ionization potentials higher by 0.2–0.3 eV than those reported by Seth et al. [85]. Our values are probably more accurate, due to the inclusion of the Breit term and the use of a larger basis and a much extended model space, which more than compensates for the perturbative inclusion of triples. The transition energies reported here should be roughly as accurate as those of Pb, with errors of a few hundredths of an eV, and provide therefore good predictions for future experimental values.

The most prominent feature of the energies collected in tables 5.10 and 5.11 is that ionization potentials and excitation energies of E114 are much higher than analogous Pb values. Table 5.12 collects the first four ionization potentials of all group-14 elements (experimental values [86]

Table 5.11 Ionization potential (IP) and excitation energies (EE) of neutral lead and eka-lead (cm^{-1}). States belong to P_m, unless noted otherwise. Ground state is $(n-1)d^{10}ns^2np_{1/2}^2\ {}^3P_0$, with $n = 6$ for Pb, 7 for E114. P spaces for E114 are smaller than for Pb (see text), and some of the E114 states are therefore missing.

	Transition		Pb		E114
			Expt. [59]	Calc.	Calc.
IP	$\rightarrow ns^2np_{1/2}$	${}^2P_{1/2}$	59821	59276	68868
EE	$\rightarrow ns^2np^2$	${}^3P_1$	7819	7531	26342
	$\rightarrow$	${}^3P_2$	10650	10307	28983
	$\rightarrow$	${}^1D_2$	21458	20853	60956
	$\rightarrow$	${}^1S_0$	29467	29259	67817
	$\rightarrow ns^2np_{1/2}(n+1)s$	${}^3P_0$	34960	34405	43111
	$\rightarrow$	${}^3P_1$	35287	34711	43441
	$\rightarrow ns^2np_{1/2}(n+1)p$	${}^3P_0$	42919	42255	52487
	$\rightarrow$	${}^3P_1$	44401	43655	54647
	$\rightarrow$	${}^3D_1$	44675	43969	51302
	$\rightarrow$	${}^3D_2$	44809	44089	54814
	$\rightarrow ns^2np_{1/2}nd$	${}^3F_2$	45443	44525	56026[a]
	$\rightarrow$	${}^3F_3$	46328	45627	56494[a]
	$\rightarrow$	${}^3D_2$	46060	45173	56418[a]
	$\rightarrow$	${}^3D_1$	46068	45165	56456[a]
	$\rightarrow ns^2np_{3/2}(n+1)s$	${}^3P_2$	48188	47414	79473
	$\rightarrow$	${}^1P_1$	49439	48682	80455
	$\rightarrow ns^2np_{1/2}(n+2)s$	${}^3P_1$	48687	47988	
	$\rightarrow$	${}^3P_0$	48726	48031	
	$\rightarrow ns^2np_{3/2}(n+1)p$	${}^3D_3$	57372	57336	92205
	$\rightarrow ns^2np_{3/2}nd$	${}^3D_3$	58518	58080	95851[a]
	$\rightarrow$	${}^3P_1$	59427	59291	
	$\rightarrow ns^2np_{3/2}(n+2)s$	${}^3P_2$	62621	61728	

[a] P_i state.

for C–Pb, calculated for Pb and E114), and Fig. 5.3 shows the first IP for these elements. The usual trend of IPs decreasing for heavier atoms holds from C to Sn; reversal of this trend begins in Pb and increases greatly for E114, with IPs surpassing those of Si. This reversal is due to relativistic stabilization of the valence s and $p_{1/2}$ orbitals, which becomes stronger in the superheavy elements. The higher IPs of eka-lead indicate it will be more inert and less metallic than lead.

Table 5.12 Ionization potentials of group 14 elements (eV). Experimental data from the Handbook [86], calculated data: present work.

	Experimental					Calculated	
	C	Si	Ge	Sn	Pb	Pb	E114
IP1	11.260	8.152	7.900	7.344	7.417	7.484	8.539
IP2	24.383	16.346	15.935	14.632	15.032	15.012	16.871
IP3	47.888	33.493	34.224	30.503	31.937	31.941	35.739
IP4	64.494	45.142	45.713	40.735	42.322	42.372	46.272

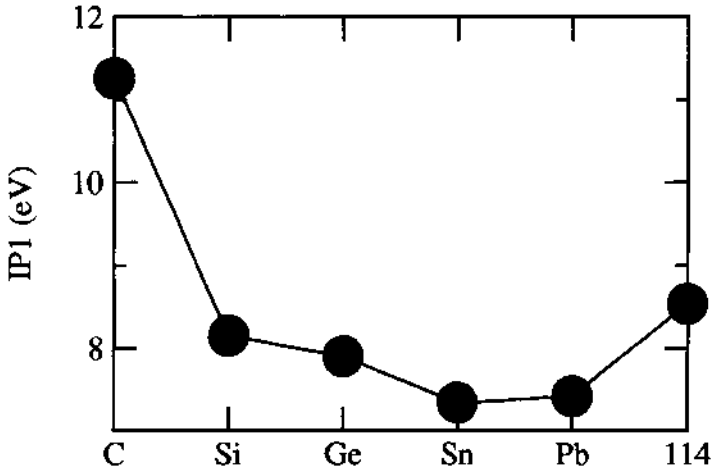

Figure 5.3 First ionization potentials of group 14 elements

3.6 Element 118 — can a rare gas have positive electron affinity?

One of the most dramatic effects of relativity is the contraction and concomitant stabilization of s orbitals. An intriguing question is whether the $8s$ orbital of element 118, the next rare gas, would be stabilized sufficiently to give the atom a positive electron affinity. Using the neutral atom Dirac-Fock orbitals as a starting point raises a problem, since the $8s$ orbital has positive energy and tends to "escape" to the most diffuse basis functions. This may be avoided by calculating the unoccupied orbitals in an artificial field, obtained by assigning partial charges to some of the occupied shells. The nonphysical fields are compensated by including an appropriate correction in the perturbation operator. A series

of calculations with a variety of fields gave electron affinities differing by a few wave numbers [87]. Thus, assigning a charge of 0.8e to the $7p_{3/2}$ electrons gave an EA of 454 cm^{-1}; a charge of 0.75e on the $7s$ electrons yielded 449 cm^{-1}; and putting 0.9e on all $7s$ and $7p$ electrons yielded an electron affinity of 437 cm^{-1}. Several other tests of the stability and reliability of the calculations were carried out. The basis set convergence was checked by calculating several l limits (with a charge of $0.8e$ on the $7p_{3/2}$ electrons). The f, g, and h limits came out as 427, 447, and 452 cm^{-1}, respectively. The correlated relativistic electron affinity is put at 0.056 eV, with an estimated error of 0.01 eV [87]. It should be emphasized that correlated nonrelativistic or relativistic uncorrelated calculations yield no electron affinity. The Rn atom does not show a bound state of the anion even at the relativistic CC level.

3.7 Eka-actinium (E121) — when is the Breit term important?

Examples given above show small effects of the frequency-independent Breit term on transition energies, except for fine-structure splittings. A calculation on La, Ac and E121 [88] revealed another case with significant Breit effect. Table 5.13 shows the DC and DCB transition energies of E121, calculated in a $35s26p21d16f10g6h5i$ basis, with 43 electrons correlated in the neutral species.

Relativistic effects occur as expected. The ground state of E121 is $8s8p_{1/2}$, in contrast with the $ns^2(n-1)d$ exhibited by all other group 3 elements, namely Sc, Y, La and Ac. The $(n-1)d \rightarrow np$ transition energies are 1.31 eV in Y [59], 1.89 eV in La [65], and 0.98 eV in Ac [88]. The point to note involves the differences between DC and DCB transition energies (table 5.13). These differences are small (below 0.02 eV) in most cases, but go up to nearly 0.1 eV for transitions involving f electrons. The same phenomenon appears already for the much lighter La [88]. Another feature of f transitions is their dependence on high l functions. While omitting i ($l = 6$) functions from the basis changes most transitions by 0.01–0.02 eV, transitions affecting f shell occupancies show shifts of up to 0.1 eV.

3.8 Electron affinities of alkali atoms — selection of P space

Alkali atoms are conceptually simple one-valence-electron systems, and have consequently attracted many experimental and theoretical studies. The electron affinities of the atoms up to Cs are known with great precision [89]; only a semiempirical value of 492 meV (with an un-

Table 5.13 Ionization potentials and excitation energies of element 121 and its cations by the Dirac-Coulomb and Dirac-Coulomb-Breit CCSD method (in eV).

	Final state		DC	DCB
	E121^{2+}, ground state [E118]$8s$ $^2S_{1/2}$			
IP	[E118]	$^1S_0$	18.67	18.65
EE	$7d$	$^2D_{3/2}$	2.883	2.859
		$^2D_{5/2}$	3.507	3.478
	$8p$	$^2P_{1/2}$	4.186	4.196
		$^2P_{3/2}$	6.831	6.819
	$6f$	$^2F_{5/2}$	4.557	4.471
		$^2F_{7/2}$	5.050	4.960
	E121^{+}, ground state $8s^2$ $^1S_0$			
IP			12.67	12.66
EE	$7d8s$	$^3D_1$	2.764	2.744
		$^3D_2$	2.850	2.829
		$^3D_3$	3.209	3.185
		$^1D_0$	3.800	3.775
	$8s8p$	$^3P_0$	3.001	3.010
		$^3P_1$	3.331	3.338
		$^3P_2$	5.293	5.284
	$5f8s$	$^3F_2$	5.149	5.082
		$^3F_3$	5.314	5.238
		$^3F_4$	5.635	5.558
	E121, ground state $8s^28p_{1/2}$ $^2P_{1/2}$			
IP	$8s^2$	$^1S_0$	4.458	4.447
EE	$8s^27d_{3/2}$	$^2D_{3/2}$	0.412	0.389
	$8s^27d_{5/2}$	$^2D_{5/2}$	0.738	0.714
	$8s^28p_{3/2}$	$^2P_{3/2}$	1.436	1.424
		E121^{-}		
EA	$8s^28p_{1/2}^2$	$^1S_0$	0.580	0.569
	$8s^28p_{1/2}7d_{3/2}$	$J=2$	0.270	0.272

certainty of 2.2%) is available for Fr [90]. An interesting aspect of these systems is the suggestion made some years ago [91–93] that Cs^- might have bound excited states, an idea refuted by more recent experimental [94] and theoretical [90] work. One of the first applications of the relativistic Fock-space coupled cluster (FSCC) method described above has been to transition energies of alkali atoms [55]. Excellent agreement with experiment was obtained for ionization potentials (an average error of 0.09%) and excitation energies (0.2% error), but electron affinities, particularly those of the heavier elements in the group, were less satisfactory, with errors of 4–9% for K, Rb, and Cs. The newly developed intermediate Hamiltonian method made possible more extensive calculations with much larger P spaces, and the problem was therefore revisited recently [95].

Table 5.14 Electron affinity of Cs with different model spaces (meV). The experimental value is 472 meV (Ref. [89]).

Model space	P_m orbitals	P_i orbitals	EA
A	$6s$	–[a]	516
B	$6s,6p,5d$	$7\text{-}11s,7\text{-}10p,6\text{-}9d,4\text{-}6f$	511
C	$6\text{-}7s,6\text{-}7p,5\text{-}6d$	$8\text{-}11s,8\text{-}10p,7\text{-}9d,4\text{-}6f$	490
D	$6\text{-}9s,6\text{-}8p,5\text{-}7d,4f$	$10\text{-}12s,9\text{-}11p,8\text{-}9d,5\text{-}6f$	481
E	$6\text{-}10s,6\text{-}9p,5\text{-}7d,4\text{-}5f$	$11\text{-}12s,10\text{-}11p,8\text{-}9d,6f$	480
F	$6\text{-}9s,6\text{-}8p,5\text{-}7d,4f$	$10\text{-}13s,9\text{-}12p,8\text{-}9d,5\text{-}6f$	475
G	$6\text{-}9s,6\text{-}8p,5\text{-}7d,4f$	$10\text{-}12s,9\text{-}11p,8\text{-}10d,5\text{-}7f$	480

[a]FSCC, no P_i space

The dependence of the electron affinity on the structure of the P_m and P_i spaces was investigated for Cs. Orbitals defining P_m and P_i are selected largely in order of increasing orbital energies. Results are shown in table 5.14. P_m reached optimal size and convergence with set D, and further increase (set E) has little effect. Augmenting P_i by s and p orbitals (set F) led to further improvement, whereas adding d and f functions (set G) had little effect, as did other attempts to augment set F. Model spaces of the latter set, suitably adapted to the shell structure of the different atoms, were therefore used for all atoms; they are listed in table 5.15. The number of correlated electrons in the cation reference

states varied from 8 in Na^+ to 50 in $E119^+$ (see table 5.15); corresponding anions have two additional correlated electrons.

Table 5.15 Correlated electrons in the reference cations and structure of model spaces.

Atom	Correlated electrons		P_m orbitals	P_i orbitals
	number	orbitals		
Na	8	$2s2p$	3-6s,3-5p,3-5d,4f	7-10s,6-9p,6-7d,5-7f
K	16	$2s2p3s3p$	4-7s,4-6p,3-5d,4f	8-11s,7-10p,6-7d,5-6f
Rb	26	$3s3p3d4s4p$	5-8s,5-7p,4-6d,4f	9-12s,8-11p,7-8d,5-6f
Cs	26	$4s4p4d5s5p$	6-9s,6-8p,5-7d,4f	10-13s,9-12p,8-9d,5-6f
Fr	40	$4f5s5p5d6s6p$	7-10s,7-9p,6-8d,5f	11-14s,10-13p,9-10d,6-7f
E119	50	$4f5d6s6p6d7s7p$	8-11s,8-10p,7-9d,5-6f	12-15s,11-13p,10-11d,7-8f

Calculated electron affinities are collected and compared with experiment in table 5.16. The power of the intermediate Hamiltonian method is demonstrated by the excellent agreement with experiment. The Fock space values start well for Na, but errors increase to 5%, 7% and 9% for the heavier K, Rb and Cs, respectively. IHFSCC values, on the other hand, are all within 5 meV or 1% of experiment. It should be noted that the FSCC function of the anions includes only one determinant in the P space, whereas the IHFSCC P space includes several thousand. The importance of these additional determinants (and of excitations from them to Q) increases with the size of the alkali anion.

The excellent agreement with known experimental values allows us to propose with confidence a reference value for the yet unmeasured electron affinity of Fr, 491±5 meV. This is in agreement with the recent semiempirical value [90] of 492±10 meV. It is interesting to observe the increase of the electron affinity for the heaviest alkalis, due to relativistic stabilization of the s orbitals. While the EAs go down from Na to Cs, Fr exhibits a modest increase, and the superheavy element 119 is predicted to have a much larger affinity, larger in fact than any other alkali atom. This dramatic stabilization effect on the 8s orbital has been observed for element 118, which is predicted to be the first rare gas with positive electron affinity (see above). Finally, we also note that no stable excited states of Cs^- or other alkali anions were obtained, in agreement with recent observations [90, 94] and refuting earlier predictions [91–93].

Table 5.16 Electron affinities of the alkali atoms (meV). Fock-space (FS) and intermediate Hamiltonian (IH) compared with experimental [89] (semiempirical [90] for Fr) values.

Atom	Expt.	FS	IH	% error	
				FS	IH
Na	547.9	549.1	549.9	0.3	0.4
K	501.5	525.4	506.8	4.8	1.1
Rb	485.9	519.3	490.8	6.9	1.0
Cs	471.6	516.0	474.6	9.4	0.6
Fr	492±2.2%	542.2	491.3		
E119		717.1	662.5		

3.9 Electron affinities in group 13 — what about Ga?

The Hotop and Lineberger tables [89] show reliable electron affinities for the two lightest elements, B and Al; other values have error limits of 50–100%. High-precision measurements for all five elements were reported since 1998 [96–100]. Few calculations have appeared for the latter atoms before 1997. These include the multireference configuration interaction (MRCI) of Arnau et al. using pseudopotentials [101], the Fock-space coupled cluster work on Tl [64], and the multiconfiguration Dirac-Fock computation of Wijesundera [102].

MRCI values for Al (0.45 eV) and MCDF results for B (0.26 eV) and Al (0.43 eV) are in good agreement with experimental values. MRCI and MCDF EAs for the other atoms agree with each other (0.29 and 0.30 eV for Ga, 0.38 and 0.39 eV for In, 0.27 and 0.29 eV for Tl). The CC EA of Tl is much higher at 0.40(5) eV. A major difference between the CC and the other two methods lies in the number of electrons correlated. While [101] and [102] correlate valence electrons only, three for the neutral atom and four for the anion, Eliav et al. [64] correlated 35 electrons in Tl and 36 in Tl^-. A FSCC study of all five elements was undertaken [103], with the aim of determining their EAs and, in particular, the effect of inner-shell correlation and virtual space used on the calculated values.

Large basis sets of Gaussian-type orbitals (up to $35s27p21d9g6h4i$) were used, taken from the universal basis set of Malli *et al.* [104]. Many electrons were correlated (5 in B, 11 in Al, 27 in Ga, 21 in In, and 35 in Tl), to account for core polarization. Triple excitations proved impor-

tant for B but not for the heavier elements (see [103] for details). The calculated EAs are shown in Table 5.17 and compared with experiment [96–100]. Agreement with experimental values for B, Al and In is very good, but a significant deviation is observed for Ga. A detailed analysis of the calculation [105] did not come up with an acceptable explanation for this disagreement. The recently measured EA of Tl [100] is in good agreement with the FSCC value, but not with the significantly lower MRCI and MCDF results. The advantage of the FSCC calculation lies in correlating both valence and inner shells, so that core polarization and correlation are included properly, while only valence electrons are correlated in the other applications. Results show that inner-shell correlation contributes about one quarter or 0.1 eV of the total affinity. The rather large error limit quoted in the FSCC result appears because two Fock-space schemes, starting from Tl^+ and Tl^- respectively, give significant differences. This problem, together with the outstanding disagreement between FSCC and measured values for Ga, remains to be clarified.

Table 5.17 Group 13 electron affinities (eV).

Atom	Expt.		CCSD [103]
B	0.279 723(25)	[96]	0.279
Al	0.432 83(5)	[97]	0.427
Ga	0.43(3)	[98]	0.301
In	0.404(9)	[99]	0.419
Tl	0.377(13)	[100]	0.40(5)

3.10 Heavy atom electron affinities — multiple stable anionic states

Calculated electron affinities for other heavy and superheavy atoms are collected in Table 5.18. Unfortunately, experimental values are not available for most of these atoms. FSCC values are in good agreement with measured EAs of Bi (0.95 eV [89]) and Lu (0.343 eV [106]), but La (0.47 eV [107]) shows a larger difference between experiment and calculation. An interesting prediction is that many of these elements may have bound excited states of the anion. Such excited states have been observed for La [107] and Lu [106]; measured electron affinities (0.17 and 0.16 eV, respectively) are in agreement with FSCC predictions.

Table 5.18 **Electron affinities of some heavy and superheavy elements (eV).**

Atom	configuration		EA
	atom	anion	
La [88]	$6s^2 5d_{3/2}\ ^2D_{3/2}$	$6s^2 6p5d\ ^1D_2$	0.33
		$6s^2 5d^2\ ^3F_2$	0.19
		$6s^2 5d^2\ ^3F_3$	0.11
Ac [88]	$7s^2 6d_{3/2}\ ^2D_{3/2}$	$7s^2 7p6d\ ^1D_2$	0.35
E121 [88]	$8s^2 8p_{3/2}\ ^2P_{1/2}$	$8s^2 8p^2_{1/2}\ ^1S_0$	0.57
		$8s^2 8p_{1/2} 7d_{3/2}$, J=2	0.27
Lu [116]	$6s^2 5d\ ^2D_{3/2}$	$6s^2 6p5d\ ^1D_2$	0.26
		$6s^2 6p^2\ ^3P_0$	0.09
Lr [116]	$7s^2 7p_{1/2}\ ^2P_{1/2}$	$7s^2 7p^2\ ^3P_0$	0.31
		$7s^2 7p6d\ ^3P_0$	0.16
Bi [117]	$6p^2_{1/2} 6p_{3/2}\ ^4S_{3/2}$	$6p^2_{1/2} 6p^2_{3/2}\ ^3P_2$	1.03
		$6p^2_{1/2} 6p^2_{3/2}\ ^3P_0$	0.18
E115 [117]	$7p^2_{1/2} 7p_{3/2}\ ^4S_{3/2}$	$7p^2_{1/2} 7p^2_{3/2}\ ^3P_2$	0.38

3.11 Properties other than energy

Most of the applications to heavy atoms were aimed at obtaining energy levels and transition energies (excitations, ionization, electron affinities). Other properties were also calculated. Foremost among them are transition probabilities and lifetimes. In particular, few-electron atoms and ions were subject to extensive studies. Johnson et al. [108] studied two-electron atoms with atomic number to 100, while Safronova et al. [109] treated four- and ten-electron systems. The latter group also calculated transition moments, hyperfine interactions and dipole polarizabilities for the alkali atoms up to Fr [110]. The hyperfine structure of many atomic states was studied by Bieroń and coworkers [111]. Inner-shell transitions present a different kind of challenge, where correlation is not as difficult to incorporate as for valence shells, but QED effects must be accounted for. Extensive studies of inner shells were carried out by Indelicato et al. [112].

Parity non-conservation effects are of fundamental interest in physics. It turns out that atomic measurements may provide one of the more sensitive sources for detecting such effects, and accurate computations of certain atomic enhancement factors, related to gradients of the poten-

tial, are necessary to extract such information as upper bounds on the dipole moment of the electron [56]. Relevant calculations were carried out by Hartley et al. [113]. A similar situation occurs for the extraction of nuclear quadrupole moments from spectroscopic data [114]. The quadrupole moment Q (in mb) is obtained from the quadrupole coupling constant B (in MHz) and the calculated electric field gradient at the nucleus q (in atomic units) by

$$Q = 4.255\ 957\ 9\frac{B}{q}\ . \tag{5.34}$$

The accuracy of Q is usually limited by the accuracy in which q can be calculated. A painstaking study of the Br and I atoms have been reported recently by Bieroń et al. [115].

4. Summary and Conclusion

Four-component methods provide the framework for the most accurate treatment of heavy atoms. When combined with high-level quantum chemical methods for inclusion of correlation, such as multiconfiguration Dirac-Fock or the coupled cluster scheme, remarkably high-quality results are obtained. Transition energies of heavy atoms, including ionization potentials, excitation energies and electron affinities, as well as fine-structure splittings, usually agree with experiment within a few hundredths of an eV. The frequency independent Breit term must be included in the Hamiltonian for this level of accuracy; it is particularly important for hyperfine splittings [54,67] and for transitions affecting the occupancy of f shells [88]. The latter transitions also require high l basis functions, with i ($l = 6$) orbitals contributing up to 0.1 eV in the case of La. The ability of these methods to reproduce available spectroscopic data lends credence to predictions made regarding the structure and spectroscopy of superheavy elements, which are slowly becoming accessible to experimental study. Useful contributions are also made by accurate calculations of such properties as transition moments, hyperfine splittings, electric field gradients and electron dipole enhancement factors.

While correlated four-component methods provide excellent results where applicable, they are too expensive to use for large systems, particularly larger molecules. Less computationally demanding methods are available and have proven to be of great value to the study of atomic and molecular systems, as shown in other chapters of this book. Nevertheless, four-component benchmark calculations for carefully selected systems will be necessary to test and calibrate the less expensive and more widely applicable schemes.

Acknowledgments

Many of the results reported here were obtained in collaboration with Professor Yasuyuki Ishikawa of the University of Puerto Rico. Research at Tel Aviv University was supported by the U.S.-Israel Binational Science Foundation and by the Israel Science Foundation.

References

[1] Pyykkö P. *Relativistic Theory of Atoms and Molecules*, Vol. I, 1916–1985 (Springer-Verlag, Berlin, 1986); Vol. II 1986–1992 (Springer-Verlag, Berlin, 1993) Vol. III, 1993–1999 (Springer-Verlag, Berlin, 2000; http://www.csc.fi/lul/rtam.

[2] See, e.g., Sucher J. in *Relativistic, Quantum Electrodynamic, and Weak Interaction Effects in Atoms*, ed. Johnson W., Mohr P., and Sucher J. (American Institute of Physics, New York, 1989), p. 28.

[3] Breit G. (1929) *Phys. Rev.* **B34**, 553; (1930) *Phys. Rev.* **36**, 383; (1932) *Phys. Rev.* **39**, 616.

[4] Brown G.E. and Ravenhall D.G. (1951) *Proc. Roy. Soc. A* **208**, 552.

[5] Bethe H.A. and Salpeter E.E. *Quantum Mechanics of One- and Two-Electron Atoms* (Springer-verlag, Berlin, 1957).

[6] Sucher J. (1980) *Phys. Rev. A* **22**, 348; (1987) *Phys. Scr.* **36**, 271.

[7] Buchmüller W. and Dietz K. (1980) *Z. Phys. C* **5**, 45.

[8] Lindgren I. in *Many-Body Methods in Quantum Chemistry*, ed. Kaldor U., Lecture Notes in Chemistry Vol. 52 (Springer-Verlag, Heidelberg, 1989) p. 293; (1988) *Nucl. Instrum. Methods* **B31**, 102.

[9] *Relativistic, Quantum Electrodynamic, and Weak Interaction Effects in Atoms*, ed. Johnson W., Mohr P., and Sucher J. (American Institute of Physics, New York, 1989).

[10] Mittleman M. (1971) *Phys. Rev. A* **4**, 893; (1972) *Phys. Rev. A* **5**, 2395; (1981) *Phys. Rev. A* **24**, 1167.

[11] Davydov A.S., *Quantum Mechanics* (NEO Press, Peaks Island, Maine, 1966) chap. VIII.

[12] Kim Y.-K. (1967) *Phys. Rev.* **154**, 17.

[13] Kagawa T. (1975) *Phys. Rev. A* **12**, 2245; (1980) *Phys. Rev. A* **22**, 2340.

[14] Johnson W.R. and Sapirstein J. (1986) *Phys. Rev. Lett.* **57**, 1126; Johnson W.R., Idrees M., and Sapirstein J., (1987) *Phys. Rev. A* **35**, 3218; Blundell S.A., Johnson W.R., Liu Z.W., and Sapirstein

J. (1989) *Phys. Rev. A* **39**, 3768; Johnson W.R., Blundell S.A., and Sapirstein J. (1988) *Phys. Rev. A* **37**, 307; (1988) *Phys. Rev. A* **37**, 2764; (1990) *Phys. Rev. A* **41**, 1689.

[15] Quiney H.M., Grant I.P., and Wilson S. (1987) *J. Phys. B* **20**, 1413; (1987) *Phys. Scr.* **36**, 460; in *Many-Body Methods in Quantum Chemistry*, ed. Kaldor U., Lecture Notes in Chemistry Vol. 52 (Springer-Verlag, Heidelberg, 1989); (1990) *J. Phys. B* **23**, L271; Grant I.P. and Quiney H.M., *Adv. Atom. Molec. Phys.* **23**, 37 (1988).

[16] Ishikawa Y., Binning R.C., and Sekino H. (1989) *Chem. Phys. Lett.* **160**, 206; Ishikawa Y. (1990) *Phys. Rev. A* **42**, 1142; (1990) *Chem. Phys. Lett.* **166**, 321; Ishikawa Y. and Quiney H.M. (1993) *Phys. Rev. A* **47**, 1732; Ishikawa Y. and Koc K. (1994) *Phys. Rev. A* **50**, 4733.

[17] Johnson W. R. and Soff G. (1985) *At. Data Nucl. Data Tables* **33**, 405.

[18] Visscher L. and Dyall K. G. (1997) *At. Data Nucl. Data Tables* **67**, 207.

[19] Desclaux J.-P. (1975) *Comput. Phys. Commun.* **9**, 31.

[20] Grant I.P., McKenzie B.J., Norrington P.H., Mayers D.F., and Pyper N.C. (1980) *Comput. Phys. Commun.* **21**, 207.

[21] Ishikawa Y. and Kaldor U., in *Computational Chemistry: Review of Current Trends*, ed. Leszczynski J. (World Scientific, Singapore, 1996), vol. I, p. 1.

[22] Kaldor U. and Eliav E. (1998) *Adv. Quantum Chem.* **31**, 313.

[23] Lee Y.-S. and McLean A.D. (1982) *J. Chem. Phys.* **76**, 735.

[24] Aerts P.J.C. and Nieuwpoort W.C. (1985) *Chem. Phys. Lett.* **113**, 165; *ibid.* **125**, 83 (1986).

[25] Stanton R. E. and Havriliak S. (1984) *J. Chem. Phys.* **81**, 1910.

[26] Ishikawa Y., Baretty R., and Binning R.C. (1985) *Intern. J. Quantum Chem. Symp.* **19**, 285; Ishikawa Y. and Sekino H. (1990) *Chem. Phys. Lett.* **165**, 243.

[27] Ishikawa Y., Binning R.C., and Sando K.M. (1983) *Chem. Phys. Lett.* **101**, 111; (1984) *Chem. Phys. Lett.* **105**, 189; (1985) *Chem. Phys. Lett.* **117**, 444; Ishikawa Y., Baretty R., and Binning R.C. (1985) *Chem. Phys. Lett.* **121**, 130; Ishikawa Y. and Quiney H.M. (1987) *Intern. J. Quantum Chem. Symp.* **21**, 523.

[28] Smith F. C. and Johnson W. R. (1967) *Phys. Rev.* **160**, 136.

[29] Desclaux J. P. (1973) *At. Data Nucl. Data Tables* **12**, 311.

[30] Fricke B., Greiner W., and Waber J. T. (1977) *Theor. Chim. Acta* **21**, 235.

[31] Fricke B. and Soff G. (1977) *At. Data Nucl. Data Tables* **19**, 83.

[32] Lu C. C., Carlson T. A., Malik F. B., Tucker T. C., and Nestor C. W. (1971) *At. Data* **3**, 1.

[33] Mann J. B. and Waber J. T. (1970) *J. Chem. Phys.* **53**, 2397.

[34] Grant I. P. (1970) *Adv. Phys.* **19**, 747; Grant I.P. and Quiney H.M. (1988) *Adv. At. Mol. Phys.* **23**, 37.

[35] Dyall K. G., Grant I. P., Johnson C. T., Parpia F. A., and Plummer E. P. (1989) *Comput. Phys. Commun.* **55**, 425.

[36] Parpia F. A., Froese-Fischer C., and Grant I. P. (1996) *Comput. Phys. Commun.* **94**, 249.

[37] Rodrigues G. C., Ourdane M. A., Bieroń J., Indelicato P., and Lindroth E. (2000) *Phys. Rev. A* **63**, 012510.

[38] Vilkas M. J., Koc K., and Ishikawa Y. (1997) *Chem. Phys. Lett.* **280**, 167; Vilkas M. J., Ishikawa Y., and Koc K. (1998) *Phys. Rev. E* **58**, 5096; Vilkas M. J., Ishikawa Y., and Koc K. (1998) *Intern. J. Quantum Chem.* **70**, 813.

[39] Sapirstein J. (1998) *Rev. Mod. Phys.* **70**, 55.

[40] Vilkas M. J., Ishikawa Y., and Koc K. (1999) *Phys. Rev. A* **60**, 2808; Ishikawa Y., Vilkas M. J., and Koc M. (2000) *Intern. J. Quantum Chem.* **77**, 433.

[41] Coester F. (1958) *Nucl. Phys.* **7**, 421; Coester F. and Kümmel H. (1960) *Nucl. Phys.* **17**, 477.

[42] Čížek J. (1969) *Adv. Chem. Phys.* **14**, 35.

[43] Bartlett R. J. (1991) *Theor. Chim. Acta* **80**, 71.

[44] Salomonson S., Lindgren I., and Mårtensson A.-M (1980) *Phys. Scr.* **21**, 351; Lindgren I. and Morrison J., *Atomic Many-Body Theory*, 2nd ed. (Springer Verlag, Berlin, 1986).

[45] Hughes S.R. and Kaldor U. (1992) *Chem. Phys. Lett.* **194**, 99; *ibid.* **204**, 339 (1993); (1993) *Phys. Rev. A* **47**, 4705; (1993) *J. Chem. Phys.* **99**, 6773; (1995) *Intern. J. Quantum Chem.* **55**, 127.

[46] Blundell S. A., Johnson W. R., Liu Z. W., and Sapirstein J. (1989) *Phys. Rev. A* **39**, 3768; (1989) *Phys. Rev. A* **40**, 2233; Blundell S. A., Johnson W. R., and Sapirstein J. (1990) *Phys. Rev. Lett.* **65**, 1411; (1991) *Phys. Rev. A* **43**, 3407.

[47] Liu Z. W. and Kelly H. P. (1991) *Phys. Rev. A* **43**, 3305.

[48] Salomonson S. and Öster P. (1989) *Phys. Rev. A* **40**, 5548.

[49] Pal S. and Mukherjee D. (1989) *Adv. Quantum Chem.* **20**, 292.

[50] Kaldor U. (1991) *Theor. Chim. Acta* **80**, 427.

[51] Kaldor U. and Eliav E. (1998) *Adv. Quantum Chem.* **31**, 313.

[52] Landau A., Eliav E., and Kaldor U. (1999) *Chem. Phys. Lett.* **313**, 399; Landau A., Eliav E., Ishikawa Y., and Kaldor U. (2000) *J. Chem. Phys.* **113**, 9905; Landau A., Eliav E., and Kaldor U. (2001) *Adv. Quantum Chem.* **39**, 172.

[53] Malrieu J.-P., Durand Ph., and Daudey J.-P. (1985) *J. Phys. A* **18**, 809.

[54] Eliav E., Kaldor U., and Ishikawa Y. (1994) *Phys. Rev. A* **49**, 1724.

[55] Eliav E., Kaldor U., and Ishikawa Y. (1994) *Phys. Rev. A* **50**, 1121.

[56] Mårtensson-Pendrill A.-M. in *Methods in Computational Chemistry*, Vol. 5, ed. Wilson S. (Plenum Press, New York, 1992) p. 99.

[57] Johnson W. R., Liu Z. W., and Sapirstein J. (1996) *At. Data Nucl. Data Tables* **64**, 279.

[58] Blundell S. A., Johnson W. R., and Sapirstein J. (1992) *Phys. Rev. D* **45**, 1602.

[59] Moore C.E., *Atomic Energy Levels*, Natl. Bur. of Stand. (U.S.) Circ. No. 467 (U.S. GPO, Washington, DC, 1948).

[60] Hay P.J., Wadt W.R., Kahn L.R., and Bobrowicz F.W. (1978) *J. Chem. Phys.* **69**, 984.

[61] Pizlo A., Jansen G., and Hess B.A. (1993) *J. Chem. Phys.* **98**, 3945.

[62] Eliav E., Kaldor U., Schwerdtfeger P., Hess B.A., and Ishikawa Y. (1994) *Phys. Rev. Lett.* **73**, 3203.

[63] E. Eliav, U. Kaldor, and Y. Ishikawa, (1995) *Phys. Rev. A* **52**, 2765.

[64] Eliav E., Kaldor U., Ishikawa Y., Seth M., and Pyykkö P. (1996) *Phys. Rev. A* **53**, 3926.

[65] Martin W.C., Zalubas R., and Hagan L. *Atomic Energy Levels — The Rare-Earth Elements*, Natl. Bur. Stand. Ref. Data Series, NBS Circ. No. 60 (U.S. GPO, Washington, DC, 1978).

[66] Cai Z., Meiser Umar V., and Froese Fischer C. (1992) *Phys. Rev. Lett.* **68**, 297.

[67] Eliav E., Kaldor U., and Ishikawa Y. (1995) *Phys. Rev. A* **51**, 225.

[68] Hess B.A., Marian C.M., and Peyerimhoff S.D. in *Modern Electronic Structure Theory*, ed. Yarkony D.R. (World Scientific, Singapore, 1995) p. 152.

[69] Keller O.L. (1984) *Radiochim. Acta* **37**, 169. See also Mann J. B., quoted by Fricke B. and Waber J. T. (1971) *Actinides Rev.* **1**, 433.

[70] Glebov V.A., Kasztura L., Nefedov V.S., and Zhuikov B.L. (1989) *Radiochim. Acta* **46**, 117.

[71] Johnson E., Fricke B., Keller O.L., Nestor C.W. Jr., and Tucker T. C. (1990) *J. Chem. Phys.* **93**, 8041.

[72] Desclaux J.-P. and Fricke B. (1980) *J. Phys.* **41**, 943.

[73] Eliav E., Kaldor U., and Ishikawa Y. (1995) *Phys. Rev. Lett.* **74**, 1079.

[74] Schädel M. (1995) *Radiochim. Acta* **70/71**, 207.

[75] Hofmann S. et al. (1995) *Z. Phys. A* **350**, 277.

[76] Hofmann S. et al. (1995) *Z. Phys. A* **350**, 281.

[77] Hofmann S. et al. (1996) *Z. Phys. A* **354**, 229.

[78] For a recent review see Hofmann S. (1998) *Rep. Progr. Phys.* **61**, 639.

[79] Oganessian Yu. Ts. et al. (1999) *Phys. Rev. Lett.* **83**, 3154.

[80] Ninov V. et al. (1999) *Phys. Rev. Lett.* **83**, 1104.

[81] Sobiczewski A. (1994) *Phys. Part. Nuclei* **25**, 295; Möller P. and Nix J. R. (1994) *J. Phys. G* **20**, 1681; Smolanczuk R., Skalski J., and Sobiczewski A. (1995) *Phys. Rev. C* **52**, 1871.

[82] Rutz K., Bender M., Bürvenich T., Schilling T., Reinhard P. G., Maruhn J. A., and Greiner W. (1997) *Phys. Rev. C* **56**, 238.

[83] Ćwiok S., Dobaczewski J., Heenen P. H., Magierski P., and Nazarewicz W.(1996) *Nucl. Phys. A* **611**, 211.

[84] Landau A., Eliav E., Ishikawa Y., and Kaldor U., (2001) *J. Chem. Phys.* **114**, 2977.

[85] Seth M., Fægri K., and Schwerdtfeger P. (1998) *Angew. Chem. Int. Ed.* **37**, 2493.

[86] Lide D. R. (Ed.), *Handbook of Chemistry and Physics*, 74th Ed., (CRC Press, Boca Raton FL, 1993).

[87] Eliav E., Kaldor U., Ishikawa Y., and Pyykkö P., (1996) *Phys. Rev. Lett.* **77**, 5350.

[88] Eliav E., Shmuliyan S., Kaldor U., and Ishikawa Y. (1998) *J. Chem. Phys.* **109**, 3954.

[89] Hotop H. and Lineberger W. C. (1975) JPCRD **4**, 539; (1985) *J. Phys. Chem. Ref. Data* **14**, 731.

[90] Bahrim C. and Thumm U. (2000) *Phys. Rev. A* **61**, 022722.

[91] Fabrikant I.I. (1982) *Opt. Spektrosk.* **53**, 223 [*Opt. Spectrosc. (USSR)* **53**, 131].

[92] Froese Fischer C. and Chen D. (1989) *J. Mol. Struct.* **199**, 61.

[93] Greene C. H., (1990) *Phys. Rev. A* **42**, 1405.

[94] Scheer M., Thogersen J., Bilodeau R. C., Brodie C. A., Haugen H. K., Andersen H. H., Kristensen P., and Andersen T. (1998) *Phys. Rev. Lett.* **80**, 684.

[95] Landau A., Eliav E., Ishikawa Y., and Kaldor U., (2001) *J. Chem. Phys.* **115**, 2389.

[96] Scheer M., Bilodeau R.C., and Haugen H.K. (1998) *Phys. Rev. Lett.* **80**, 2562.

[97] Scheer M., Bilodeau R.C., Thøgersen J., and Haugen H.K. (1998) *Phys. Rev. A* **57**, R1493.

[98] Williams W.W., Carpenter D.L., Covington A.M., Koepnick M.C., Calabrese D., and Thompson J.S. (1998) *J. Phys. B* **31**, L341.

[99] Williams W.W., Carpenter D.L., Covington A.M., Thompson J.S., Kvale T.J., and Seely D.G. (1998) *Phys. Rev. A* **58**, 3582.

[100] Carpenter D.L., Covington A.M., and Thompson J.S. (2000) *Phys. Rev. A* **61**, 042501.

[101] Arnau F., Mota F., and Novoa J.J. (1992) *Chem. Phys.* **166**, 77.

[102] Wijesundera W.P. (1997) *Phys. Rev. A* **55**, 1785.

[103] Eliav E., Ishikawa Y., Pyykkö P., and Kaldor U. (1997) *Phys. Rev. A* **56**, 4532.

[104] Malli G.L., Da Silva A.B.F., and Ishikawa Y. (1993) *Phys. Rev. A* **47**, 143.

[105] Sundholm D., Tokman M., Pyykkö P., Eliav E., and Kaldor U. (1999) *J. Phys. B* **32**, 5853.

[106] Davis V.T. and Thompson J.S. (2001) *J. Phys. B* **34**, L433.

[107] Covington A.M., Calabrese D., Thosmpson J.S., and Kvale T.J. (1998) *J. Phys. B* **31**, L855.

[108] Johnson W. R., Plante D. R., and Sapirstein J. (1995) *Adv. Atom. Molec. Phys.* **35**, 255.

[109] Safronova M. S., Johnsom W. R., and Safronova U. I. (1996) *Phys. Rev. A* **53**, 4036; (1997) *J. Phys. B* **30**, 2375; Safronova U. I., Derevianko A., Safronova M. S., and Johnson W. R. (1999) *J. Phys. B* **32**, 3527.

[110] Safronova M. S., Johnson W. R., and Derevianko A. (1999) *Phys. Rev. A* **60**, 4476.

[111] Bieroń J., Parpia F. A., Froese Fischer C., and Jönsson P. (1995) PRA **51**, 4603; Bieroń J., Jönsson P., and Froese Fischer C. (1996) *Phys. Rev. A* **53**, 2181; Bieroń J., and Grant I. P. (1998) *Phys. Rev. A* **58**, 4401; Bieroń J. (1999) *Phys. Rev. A* **59**, 4295.

[112] Indelicato S., Boucard P., and Lindroth E. (1998) *Eur. J. Phys. D* **3**, 29.

[113] Hartley C. A., Lindroth E., and Mårtensson-Pendrill A.-M. (1990) *J. Phys. B* **23**, 1990; Hartley C. A. and Mårtensson-Pendrill A.-M. (1990) *Z. Phys. D* **15**, 309; (1991) *J. Phys. B* **24**, 1193.

[114] Pyykkö P. (2001) *Molec. Phys.* **99**, 1617.

[115] Bieroń J., Pyykkö P., Sundholm D., Kellö V., and Sadlej A. J. (2001) *Phys. Rev. A* **64**, 052507.

[116] Eliav E., Kaldor U., and Ishikawa Y. (1995) *Phys. Rev. A* **52**, 291.

[117] Eliav E., Kaldor U., and Ishikawa Y. (1998) *Molec. Phys.* **94**, 181.

Chapter 6

FOUR-COMPONENT ELECTRONIC STRUCTURE METHODS FOR MOLECULES

T. Saue
CNRS, UMR 7551, Laboratoire de Chimie Quantique, 4 Rue Blaise Pascal, F-67000 Strasbourg, France
saue@quantix.u-strasbg.fr

L. Visscher
Department of Theoretical Chemistry, Faculty of Sciences, Vrije Universiteit Amsterdam, De Boelaan 1083, 1081 HV Amsterdam, The Netherlands
visscher@chem.vu.nl

Abstract In this chapter we consider the extension of 4-component relativistic methods from atomic to molecular systems, in particular the challenges arising from the introduction of the algebraic approximation. In order to analyze the variational stability of the relativistic many-electron Hamiltonian we derive a variational theory of QED in the semiclassical limit using the second quantization formalism and exponential parametrization. In QED the negative-energy orbitals are filled leading to a true minimization principle for the electronic ground state, whereas in the standard 4-component approach these orbitals are empty and treated as an orthogonal complement, thus leading to a minimax principle. We emphasize the non-uniqueness of the resulting no-pair Hamiltonian of the standard approach. 4-component methods allow the continuous update of the Hamiltonian and thereby complete relaxation of the electronic wave function. We also discuss more practical aspects of the implementation of 4-component relativistic methods. We carefully analyze their computational cost and conclude that the difference with respect to non-relativistic methods constitute a prefactor and not a difference in order. We furthermore discuss how computational cost may be reduced while staying at the 4-component level, e.g. by exploiting the atomic nature of the small component density.

U. Kaldor and S. Wilson (eds.),
Theoretical Chemistry and Physics of Heavy and Superheavy Elements, 211–267.
© 2003 *Kluwer Academic Publishers.*

Keywords: Relativistic Quantum Chemistry, Electronic Structure Theory, Computational Chemistry, 4-component methods, variational collapse, quantum electrodynamics, basis sets calculations, algebraic approximation, Dirac equation, molecules

Introduction

4-component electronic structure methods for atoms were introduced in chapter six. In the present chapter we consider the extension of these methods to molecular systems (see [1] and references therein for recent reviews). It is therefore natural in this chapter to focus on the additional complexities added when going from single atoms to polyatomic systems. An obvious difference is the lack of spherical symmetry. In the atomic case the high symmetry allows the separation of radial and angular degrees of freedom. The angular part can be solved completely by symmetry, particularly facilitated by the introduction of Racah algebra [2], whereas radial equations can be solved by finite difference methods. In molecular calculations one generally has to resort to the *algebraic approximation*, that is the use of finite basis set expansions. The first basis set calculations led to rather disastrous results (see [3] for references). Schwarz and Wechsel-Trakowski [4] identified two problems connected with 4-component relativistic calculations in the algebraic approach:

1. The coupling of the large and small components of the Dirac equation requires separate basis set expansions for each component.

2. The relativistic many-electron Hamiltonian is not bounded from below and, according to an argument given Brown and Ravenhall [5], gives only continuum solutions. This has been referred to as the "Brown-Ravenhall disease".

In the atomic case the first problem is avoided by the use of finite difference methods, and the second problem is solved by imposing the boundary conditions at $r = 0$ and $r \to \infty$ for bound solutions [6]. In practice the above two problems have also been solved in the algebraic approximations, and 4-component relativistic molecular calculations are thereby routinely carried out today. On the theoretical side things have apparently not been completely straightened out, as witnessed by a number of misunderstandings in the literature. After an initial overview of the relativistic many-electron Hamiltonian in section 1., we therefore give a variational formulation of QED in the semiclassical limit, that is with continuous electromagnetic fields, in section 2.. At this level of theory a true minimization principle is assumed to exist [7], and this puts the

discussion of the variational stability of the relativistic many-electron Hamiltonian on firm grounds.

The separate basis set expansion of the large and small components needed to solve the second problem above leads to increased computational cost. 4-component calculations are therefore considered limited to benchmark calculations, and more cost-efficient methods are sought by reducing the 4-component Hamiltonian to 1- or 2-component approximate forms. There is, however, another approach which consists of staying within the 4-component form and instead seek reduction of computational cost by reduction or elimination of intermediate quantities (e.g. two-electron integrals) appearing in the actual calculations. The current status and perspectives of this approach are discussed in section 3..

Notation and units: Unless otherwise stated, all formulas appearing in this chapter are in atomic units. In these units the electron mass m and the elementary charge e are both unity. We have, however, chosen to retain their symbols so that the reader can see how the fundamental characteristics of the electrons enter the equations. This is particular important for the electron charge since it provides the coupling to external fields as will be discussed in section 1.1.1. In this manner one can distinguish equations describing electrons from those describing its antiparticle, the positron. Operators generally come with operator hats, and vectors are written in bold characters. We shall also make extensive use of the Einstein summation convention or implicit summation, which means that a repeated index signals free summation over this index. A dot product is accordingly written $\mathbf{u} \cdot \mathbf{v} = u_i v_i$. This convention allows formulas to be written in a more compact manner, which is particularly useful in the section on QED.

1. The Hamiltonian

The general form of the many-electron Hamiltonian is

$$\hat{H} = \sum_i \hat{h}(i) + \frac{1}{2}\sum_{i \neq j} \hat{g}(i,j) + \hat{V}_{nn}; \quad \hat{V}_{nn} = \frac{1}{2}\sum_{A \neq B} \frac{Z_A Z_B e^2}{|\mathbf{R}_A - \mathbf{R}_B|} \tag{6.1}$$

where $\hat{h}(i)$ are one-electron operators, $\hat{g}(i,j)$ represents the two-electron interaction and $\hat{V}_{nn}$ is the classical repulsion of fixed nuclei. This form is valid in both the relativistic and the non-relativistic domain to the extent that three-particle and higher interactions can be ignored. For the development of the various methods of quantum chemistry it is rarely necessary to be more specific regarding the form of the many-electron Hamiltonian. This holds particularly true if the operator is recast in sec-

ond quantized form, as will be discussed in section 1.3. This observation signals that one should carefully distinguish Hamiltonians from methods. At the 4-component relativistic molecular level of theory one now finds an almost complete set of methods analogous to the arsenal developed in the non-relativistic domain, such as Hartree-Fock (HF) (see e.g. [8–16] and references therein), second-order Møller-Plesset perturbation theory (MP2) [17, 18], Multi-Configuration Self Consistent Field (MCSCF) [19,20], Restricted Active Space Configuration Interaction (RASCI) [21], Coupled Cluster (CC) [22, 23] and Density Functional Theory (DFT) (see e.g. [24–27]). We therefore find it unnecessary to elaborate on the general principles of these methods since this information is available in a number of textbooks [28–31]. We shall rather try to point out the specific adaptions and considerations needed to carry these methods over into the 4-component relativistic realm. We would also like to point out that in view of the distinction between Hamiltonians and methods emphasized above, we advise against the use of method names such as Dirac-Hartree-Fock and the shorter version Dirac-Fock (which is not very fair to Douglas Hartree who first suggested to Bertha Swirles the extension of the SCF method to the Dirac equation [32]) and instead recommend "the Hartree-Fock method at the 4-component relativistic level" or, more specifically, DC-HF (the Hartree-Fock method based on the Dirac-Coulomb Hamiltonian).

1.1 The one-electron part

1.1.1 The Dirac equation in an electromagnetic field. The starting point for 4-component molecular calculations is Dirac's celebrated relativistic wave equation [33, 34]. In covariant form (that is the form in which the equation "looks the same" in all Lorentz frames [35]) it is given by

$$(i\gamma_\mu\partial_\mu - mc)\,\psi = 0; \quad \begin{cases} \partial_\mu &= \left(\boldsymbol{\nabla}, -\dfrac{i}{c}\dfrac{\partial}{\partial t}\right) \\ \gamma_\mu &= \beta\,(\boldsymbol{\alpha}, iI_4) \end{cases} \tag{6.2}$$

in which appears the 4-gradient ∂_μ. Note that we do not distinguish between covariant and contravariant 4-vectors, as this is not necessary at the level of special relativity [35, p.6]. The quantity γ_μ is given in terms of the 4×4 identity matrix I_4 and the Dirac matrices

$$\boldsymbol{\alpha} = \begin{bmatrix} 0_2 & \boldsymbol{\sigma} \\ \boldsymbol{\sigma} & 0_2 \end{bmatrix} \quad \text{and} \quad \beta = \begin{bmatrix} I_2 & 0_2 \\ 0_2 & -I_2 \end{bmatrix} \tag{6.3}$$

and generates the C_4 Clifford algebra [36], the algebra of gamma matrices. The Pauli spin matrices

$$\sigma_x = \begin{bmatrix} 0 & 1 \\ 1 & 0 \end{bmatrix}; \quad \sigma_y = \begin{bmatrix} 0 & -i \\ i & 0 \end{bmatrix}; \quad \sigma_z = \begin{bmatrix} 1 & 0 \\ 0 & -1 \end{bmatrix} \tag{6.4}$$

are themselves generators of the C_3 Clifford algebra, that is the algebra of complex quaternions, a property that we shall make use of in section 1.1.2. Note also that the Dirac $\boldsymbol{\alpha}$ matrices can be expressed in terms of the 4×4 spin matrices

$$\boldsymbol{\alpha} = \zeta \boldsymbol{\Sigma}; \quad \boldsymbol{\Sigma} = \begin{bmatrix} \boldsymbol{\sigma} & 0_2 \\ 0_2 & \boldsymbol{\sigma} \end{bmatrix}; \quad \zeta = \begin{bmatrix} 0_2 & I_2 \\ I_2 & 0_2 \end{bmatrix} \tag{6.5}$$

upon the introduction of the auxiliary matrix ζ [37]. In order to align the relativistic and non-relativistic energy scales one usually performs the substitution

$$\beta \quad \rightarrow \quad \beta' = \beta - I_4 \tag{6.6}$$

but we will for the moment retain the original form of the Dirac equation.

The free-particle Dirac equation in its more familiar form is obtained by multiplication by βc from the left

$$\left[\hat{h}_{D;0} - i\frac{\partial}{\partial t}\right]\psi = 0; \quad \hat{h}_{D;0} = \beta mc^2 + c\,(\boldsymbol{\alpha} \cdot \mathbf{p}) \tag{6.7}$$

External fields are introduced through *the principle of minimal electromagnetic interaction* [38]

$$p_\mu \rightarrow \pi_\mu = p_\mu - qA_\mu \tag{6.8}$$

in which appears 4-momentum $p_\mu = -i\partial_\mu$ and the 4-potential $A_\mu = (\mathbf{A}, \frac{i}{c}\phi)$. We are interested in electrons and therefore *choose* the charge $q = -e$. The Dirac equation then attains the form

$$\hat{D}\psi = \left[\hat{h}_{D;A_\mu} - i\frac{\partial}{\partial t}\right]\psi = 0; \quad \hat{h}_{D;A\mu} = \beta mc^2 + c\,(\boldsymbol{\alpha} \cdot \boldsymbol{\pi}) - e\phi \tag{6.9}$$

It is important to note that the minimal substitution (6.8) follows from the term

$$\mathcal{L}_{\text{int}} = j_\mu A_\mu \tag{6.10}$$

in the Lagrangian describing the interaction between the particle and the electromagnetic field as the product of the 4-current $j_\mu = (\mathbf{j}, ic\rho)$ and the 4-potential. This term was first proposed by Schwarzschild [39] to satisfy Lorentz covariance. It is employed in *ad hoc* basis in the non-relativistic

domain, even though it does not represent the proper non-relativistic limit, which is electrostatics (see [40] and references therein). Comparing (6.9) and (6.10) we can identify the 4-current as

$$j_\mu = -ec\psi^\dagger\beta\gamma_\mu\psi; \quad \rho = -e\psi^\dagger I_4\psi; \quad \mathbf{j} = -ec\psi^\dagger\boldsymbol{\alpha}\psi \tag{6.11}$$

Classically the current density is given as charge multiplied by velocity and indeed one finds from Heisenbergs equation of motion that the velocity operator in the relativistic domain is $c\boldsymbol{\alpha}$. This may appear somewhat surprising, but may be interpreted as the electron oscillating at the speed of light c about its mean position ("Zitterbewegung" [37,41]). Note that just as we may identify $-ec\boldsymbol{\alpha}$ as the operator of current density, we may identify $-eI_4$ as the operator of charge density. This identification will prove useful in section 1.2.

External electric $\mathbf{E}$ and magnetic $\mathbf{B}$ fields appear in the Hamiltonian only indirectly through the scalar ϕ and vector $\mathbf{A}$ potentials

$$\mathbf{E} = -\boldsymbol{\nabla}\phi - \frac{\partial\mathbf{A}}{\partial t}; \quad \mathbf{B} = \boldsymbol{\nabla}\times\mathbf{A} \tag{6.12}$$

This can be considered an advantage as the freedom of gauge [42] leaves room to choose the most convenient form of the potentials. For instance, a uniform electric field may be represented by $A_\mu = \left(0, -\frac{i}{c}\mathbf{E}\cdot\mathbf{r}\right)$ as well as $A_\mu = (-\mathbf{E}t, 0)$, but the former choice is usually preferred since it can be handled by time-independent theory [43]. Quantum chemistry, be it relativistic or not, is usually expressed in Coulomb gauge, that is through the transversality condition $\boldsymbol{\nabla}\cdot\mathbf{A} = 0$. From Maxwell's equations and the definitions (6.12) the field equations in the presence of a density ρ and a current $\mathbf{j}$ can then be expressed as [44]

$$\nabla^2\phi = -4\pi\rho \tag{6.13}$$

$$\left(\nabla^2\mathbf{A} - \alpha^2\frac{\partial^2\mathbf{A}}{\partial t^2}\right) - \boldsymbol{\nabla}\alpha^2\frac{\partial\phi}{\partial t} = -4\pi\alpha^2\mathbf{j} \tag{6.14}$$

where α is the fine-structure constant. The equation for the scalar potential is simply the Poisson equation with solution

$$\phi(\mathbf{r},t) = \int\frac{\rho(\mathbf{r}',t)}{|\mathbf{r}-\mathbf{r}'|}d\tau' \tag{6.15}$$

At first sight, this result appears to be in contradiction with the theory of special relativity since the scalar potential is given by the *instantaneous* charge density. However, one must bear in mind that the scalar potential itself is not an observable. The effects of retardation, as well as magnetic interactions, enter through the vector potential. The Coulomb gauge

bears its name because it singles out the *instantaneous* Coulomb interaction which is the proper non-relativistic limit of classical electrodynamics and which is the dominant interaction of chemistry. All retardation and magnetic interactions enter as higher-order terms in a perturbation expansion of the total interaction in terms of the fine-structure constant α [45]. For instance, to first order the interaction between two point charges q_1 and q_2 is in Coulomb gauge given by [42,46,47]

$$L_{\text{int}} = \frac{q_1 q_2}{r_{12}} \left[-1 + \frac{1}{2c^2} \left\{ (\mathbf{v}_1 \cdot \mathbf{v}_2) + \frac{1}{r_{12}^2} (\mathbf{r}_{12} \cdot \mathbf{v}_1)(\mathbf{r}_{12} \cdot \mathbf{v}_2) \right\} \right] \quad (6.16)$$

where $\mathbf{v}_1$ and $\mathbf{v}_2$ are their velocities. The first term can be identified as a charge-charge interaction, whereas the second term is a current-current interaction.

In molecular theory we shall employ $\hat{h}_{D;V}$, the Dirac operator in the *molecular field.* It corresponds to the introduction of the 4-potential

$$\phi(\mathbf{r}_i) = \sum_A \frac{Z_A e}{|\mathbf{r}_i - \mathbf{R}_A|}; \quad \mathbf{A}(\mathbf{r}_i) = 0. \quad (6.17)$$

where $Z_A e$ and $\mathbf{R}_A$ is charge and position, respectively, of nucleus A. The nuclei are accordingly treated as sources of external scalar potentials and nuclear spins are ignored. This "clamped nucleus" approximation is essentially the same as the one introduced by Born and Oppenheimer [48] in non-relativistic theory in which the main assumption is that electrons follow the slower movements of nuclei adiabatically. However, in the relativistic domain two consequences of this approximation should be kept in mind. The first is that the restriction to a particular frame in which the nuclei are at rest invalidates Lorentz covariance. In reality, though, nuclei will always move relative to each other so that no frame can be found in which all nuclei are stationary. Second, from (6.16) it is clear that all charge-charge interactions involving nuclei will be neglected in the "clamped nucleus" approximation.

The operators appearing in the Dirac equation (6.9) are 4×4 matrix operators and the corresponding wave function is therefore a 4-component vector function

$$\psi = \begin{bmatrix} \psi^L \\ \psi^S \end{bmatrix}; \quad \psi^X = \begin{bmatrix} \psi^{X\alpha} \\ \psi^{X\beta} \end{bmatrix}, \quad X = L, S. \quad (6.18)$$

The four degrees of freedom come from the fact that the Dirac equation describes both electrons and positrons and explicitly includes spin. For a given potential the positive-energy solutions correspond to electronic solutions, and in the non-relativistic limit (to be discussed in section

1.1.4) the lower two components of these solutions go to zero, whereas the upper two components reduce to a spin orbital in which the spatial part becomes a solution of the corresponding non-relativistic Schrödinger equation. The upper and lower two components are therefore generally referred to as the large and small components, respectively. For the same potential the negative-energy branch of the spectrum gives the positronic solutions indirectly, that is by charge conjugation (see section 1.1.3) and in the non-relativistic limit it is now the large components that go to zero. For this reason it has been suggested [49] that one should rather speak of upper and lower components than large and small ones. However, since focus in chemistry is on electronic solutions we will retain the common terminology. On the other hand one should not forget that the large components of positive-energy solutions of the Dirac equation are large by a factor c^{-1} only in an averaged sense; there may be regions in space where the small components dominate.

It is important to realize that the four degrees of freedom in the Dirac spinor (6.18), as compared to the scalar eigenfunctions of the Schrödinger equation, are not to be associated with specific components. It is a common mistake to associate the small components with the positronic degrees of freedom. For instance, one cannot simply delete the small components of a given electronic solution. One can also see from (6.18) that spin (α or β) is associated with two components and not one.

1.1.2 Time reversal symmetry. In this and the following section we shall analyze two features of the Dirac equation (6.9) that are related to the four degrees of freedom in the relativistic wave equation. The first feature is charge conjugation symmetry, which reflects that the Dirac equation describes both electrons and positrons, but generally, as we shall see, not of the same system. The second feature is time reversal symmetry which to some extent can recover the lack of spin symmetry in the relativistic domain. It is interesting to note that both features involve a pairing of eigenfunctions of the Dirac equation. As we shall see, in the case of time reversal symmetry this pairing is broken by the introduction of an external vector potential. In the case of charge conjugation symmetry the pairing is broken by the introduction of *any* 4-potential.

Both features are represented by antiunitary operators $\widehat{\mathcal{K}}$ defined by

$$\widehat{\mathcal{K}}\langle\psi_1 \mid \psi_2\rangle = \left\langle \widehat{\mathcal{K}}\psi_1 \mid \widehat{\mathcal{K}}\psi_2 \right\rangle = \langle\psi_2 \mid \psi_1\rangle = \langle\psi_1 \mid \psi_2\rangle^* \tag{6.19}$$

An example of an antiunitary operator is provided by the complex conjugation operator $\widehat{\mathcal{K}}_0$. In the non-relativistic domain this operator commutes with the Hamiltonian in the absence of external magnetic fields. It's effect on the non-relativistic Schrödinger equation in the molecular

field (6.17)is thereby

$$\begin{aligned}\widehat{\mathcal{K}}_0\left[\hat{h}_{NR}-i\frac{\partial}{\partial t}\right]\widehat{\mathcal{K}}_0^{-1}\widehat{\mathcal{K}}_0\psi_{NR}(\mathbf{r},t) &= \left[\hat{h}_{NR}+i\frac{\partial}{\partial t}\right]\overline{\psi}_{NR}(\mathbf{r},t) \quad (6.20)\\ &= \left[\hat{h}_{NR}-i\frac{\partial}{\partial t}\right]\overline{\psi}_{NR}(\mathbf{r},-t)=0\end{aligned}$$

where $\overline{\psi}_{NR}=\widehat{\mathcal{K}}_0\psi_{NR}$. Through the substitution $t\to -t$ one recovers the form of the original equation. The complex conjugation operator is therefore identified as the time-reversal operator in non-relativistic systems [50]. Consider now the effect of $\widehat{\mathcal{K}}_0$ on the Dirac equation (6.9). Proceeding as in (6.20) we obtain

$$\left[\beta mc^2+c\zeta\mathbf{\Sigma}^*\cdot(-\mathbf{p}+e\mathbf{A})-e\phi+i\frac{\partial}{\partial t}\right]\widehat{\mathcal{K}}_0\psi(\mathbf{r},t)=0 \qquad (6.21)$$

In this case the substitution $t\to -t$ is not enough to recover the original equation and so the complex conjugation operator can not be identified as the time-reversal operator in the relativistic domain. To find the proper form we may note that the product of a unitary and an antiunitary operator is an antiunitary operator. We may therefore take as our starting point the generic form

$$\widehat{\mathcal{K}}=U\widehat{\mathcal{K}}_0 \qquad (6.22)$$

where U is a 4×4 unitary matrix. Next, we note that the problem with (6.21) is that Σ_y changes sign under complex conjugation, whereas the other 4×4 spin matrices (6.5) do not. If one wants an antiunitary transformation under which the individual terms of the Dirac equation are either symmetric or antisymmetric the unitary operator U (6.22) must therefore contain Σ_y. We then finally arrive at the choice $U_T=-i\Sigma_y$ which gives the time reversal operator $\widehat{\mathcal{K}}$ for relativistic systems. Its application gives

$$\left[\underbrace{\left\{\beta mc^2+c(\boldsymbol{\alpha}\cdot\mathbf{p})-e\phi\right\}}_{(+)}-\underbrace{\left\{ec(\boldsymbol{\alpha}\cdot\mathbf{A})-i\frac{\partial}{\partial t}\right\}}_{(-)}\right]\overline{\psi}(\mathbf{r},t)=0 \qquad (6.23)$$

where $\overline{\psi}=\widehat{\mathcal{K}}\psi$ and one can see that in the absence of external vector potentials, one recovers the correct form of the Dirac equation through the substitution $t\to -t$.

Equation (6.23) shows that under time reversal the Dirac equation splits into a symmetric (+) and an antisymmetric (−) part. Further insight is obtained by reordering the Dirac equation

$$\begin{bmatrix} \psi^L \\ \psi^S \end{bmatrix} = \begin{bmatrix} \psi^{L\alpha} \\ \psi^{L\beta} \\ \psi^{S\alpha} \\ \psi^{S\beta} \end{bmatrix} \rightarrow \begin{bmatrix} \psi^{L\alpha} \\ \psi^{S\alpha} \\ \psi^{L\beta} \\ \psi^{S\beta} \end{bmatrix} = \begin{bmatrix} \psi^{\alpha} \\ \psi^{\beta} \end{bmatrix} \tag{6.24}$$

The time-symmetric part of the Dirac equation can then be written as

$$\mathcal{D}_+ = \begin{bmatrix} mc^2 - e\phi & -icd_z & 0 & -icd_- \\ -icd_z & -mc^2 - e\phi & -icd_- & 0 \\ 0 & -icd_+ & mc^2 - e\phi & icd_z \\ -icd_+ & 0 & -icd_z & -mc^2 - e\phi \end{bmatrix} \tag{6.25}$$

where we have introduced the notation

$$d_z = \frac{\partial}{\partial z}; \quad d_\pm = \frac{\partial}{\partial x} \pm i\frac{\partial}{\partial y}. \tag{6.26}$$

In the same manner we find that the time-antisymmetric part can be written as

$$\mathcal{D}_- = \begin{bmatrix} -i\frac{\partial}{\partial t} & ecA_z & 0 & ecA_- \\ ecA_z & -i\frac{\partial}{\partial t} & ecA_- & 0 \\ 0 & ecA_+ & -i\frac{\partial}{\partial t} & -ecA_z \\ ecA_+ & 0 & -ecA_z & -i\frac{\partial}{\partial t} \end{bmatrix} \tag{6.27}$$

where $A_\pm = A_x \pm iA_y$. The above two forms can be summarized by the matrix structure

$$\mathcal{D}_t = \begin{bmatrix} A & B \\ -tB^* & tA^* \end{bmatrix}; \quad t = \pm 1. \tag{6.28}$$

It is then a simple exercise to show that if

$$\begin{bmatrix} A & B \\ -tB^* & tA^* \end{bmatrix} \begin{bmatrix} \psi^\alpha \\ \psi^\beta \end{bmatrix} = \epsilon \begin{bmatrix} \psi^\alpha \\ \psi^\beta \end{bmatrix} = \epsilon\psi \tag{6.29}$$

then

$$\begin{bmatrix} A & B \\ -tB^* & tA^* \end{bmatrix} \begin{bmatrix} -\psi^{\beta *} \\ \psi^{\alpha *} \end{bmatrix} = t\epsilon \begin{bmatrix} -\psi^{\beta *} \\ \psi^{\alpha *} \end{bmatrix} = t\epsilon\overline{\psi}. \tag{6.30}$$

This shows that the time symmetric part of the Dirac equation has doubly degenerate eigensolutions. In the reordered equation (6.24) the time reversal operator has the form

$$\mathcal{K} = \begin{bmatrix} 0_2 & -I_2 \\ I_2 & 0_2 \end{bmatrix} \mathcal{K}_0 \tag{6.31}$$

and one therefore easily sees that the eigenvectors ψ and $\overline{\psi}$ are related by time reversal symmetry. They will therefore be referred to as *Kramers partners*. A orthonormal *Kramers paired basis* can be constructed from a spinor set $\{\psi_i\}$ and the corresponding Kramers partners $\{\overline{\psi}_i\}$. With the introduction of an external vector potential the double degeneracy is lifted. One may use degenerate perturbation theory to obtain the splitting. To zeroth order one obtains the eigenvalues via diagonalization of the 2×2 Hamiltonian matrix in the space of the two Kramers partners as

$$E_{\pm} = \epsilon \pm ec \left| \langle \psi | (\boldsymbol{\alpha} \cdot \mathbf{A}) | \overline{\psi} \rangle \right| .$$

The double degeneracy of the time symmetric Dirac equation suggests that a block diagonalization of the matrix operator is possible. This is indeed true, but at the expense of going from complex to quaternion algebra. First, let us recall the definition of a (real) quaternion number

$$q = \sum_{\Lambda=0}^{3} v_\Lambda e_\Lambda = v_0 + \check{\mathrm{i}} v_1 + \check{\mathrm{j}} v_2 + \check{\mathrm{k}} v_3; \quad v_\Lambda \in \mathcal{R} \tag{6.32}$$

The quaternion units $\check{\mathrm{i}}$, $\check{\mathrm{j}}$ and $\check{\mathrm{k}}$ are equivalent in the sense that they may be interchanged by cyclic permutation $\check{\mathrm{i}} \to \check{\mathrm{j}} \to \check{\mathrm{k}} \to \check{\mathrm{i}}$. It was observed already by Jordan [51] that the algebra of imaginary i times the Pauli spin matrices is that of the quaternion units, that is

$$\check{\mathrm{i}} \leftrightarrow i\sigma_z, \quad \check{\mathrm{j}} \leftrightarrow i\sigma_y, \quad \check{\mathrm{k}} \leftrightarrow i\sigma_x \tag{6.33}$$

The link between time reversal symmetry can then be established by noting that the time-symmetric form of (6.28) can be written in terms of Pauli spin matrices

$$\mathcal{D}_+ = [I_2 \otimes A_R] + [(i\sigma_z) \otimes A_I] + [(i\sigma_y) \otimes B_R] + [(i\sigma_x) \otimes B_I] \tag{6.34}$$

clearly showing the quaternion structure of the matrix operator. The block diagonalization is achieved through the unitary quaternion transformation

$$U^\dagger \mathcal{D}_+ U = \begin{bmatrix} A + B\check{\mathrm{j}} & 0 \\ 0 & -\check{\mathrm{k}}\left(A + B\check{\mathrm{j}}\right)\check{\mathrm{k}} \end{bmatrix}, \quad U = \frac{1}{\sqrt{2}} \begin{bmatrix} I_2 & \check{\mathrm{j}} I_2 \\ \check{\mathrm{j}} I_2 & I_2 \end{bmatrix} \tag{6.35}$$

For the upper block of the quaternion Dirac operator we find the structure

$$\begin{aligned} {}^{Q}\mathcal{D}_+ \;=\; & \begin{bmatrix} mc^2 - e\phi & 0 \\ 0 & -mc^2 - e\phi \end{bmatrix} - \check{\mathrm{i}}c \begin{bmatrix} 0 & d_z \\ d_z & 0 \end{bmatrix} - \\ & -\check{\mathrm{j}}c \begin{bmatrix} 0 & d_y \\ d_y & 0 \end{bmatrix} - \check{\mathrm{k}}c \begin{bmatrix} 0 & d_x \\ d_x & 0 \end{bmatrix} . \end{aligned} \tag{6.36}$$

One observes that the rest mass term and the scalar potential enter the real part of the operator whereas the kinetic energy is represented by the quaternion imaginary part. The quaternion Dirac operator has no preferential axis, in contrast to the conventional form (6.25) where the Pauli spin matrices in their standard form correspond to spin quantization along the z-axis.

Time reversal symmetry provides only a partial compensation for the loss of spin symmetry in the relativistic domain. The coupling of the spin and spatial degrees of freedom by the spin-orbit interaction changes the structure of the equations relative to those of non-relativistic theory. The extra price to be paid due to this coupling can be directly related to the algebra needed to solve the Dirac equation by matrix diagonalization using a finite real basis expansion. In the general case the matrix representation of the symmetric Dirac operator can be block diagonalized through the quaternion unitary transformation (6.35) and one then needs to diagonalize the quaternion subblock $A + B\mathrm{j}$. In the absence of spin-orbit coupling, as in the non-relativistic limit, this subblock becomes real. However, in the relativistic domain symmetry reduction in terms of going from quaternion to complex or real algebra can be achieved by combining time reversal and spatial symmetry [52,53]. One further thing to note is that Kramers partners do not map directly on to spin α and β orbitals. For instance the Kramers partner of a $p_1\alpha$ orbital is $p_{-1}\beta$ and not $p_1\beta$.

1.1.3 Charge conjugation symmetry. The choice $U_C = i\beta\alpha_y$ in (6.22) gives the *charge conjugation operator* $\widehat{\mathcal{C}}$ (usually this term is reserved for the unitary part U_C only). Its application gives

$$\left[-\underbrace{\left\{ \beta mc^2 + c\left(\boldsymbol{\alpha}\cdot\mathbf{p}\right) - i\frac{\partial}{\partial t} \right\}}_{(-)} + \underbrace{e\left\{ c\left(\boldsymbol{\alpha}\cdot\mathbf{A}\right) - \phi \right\}}_{(+)} \right] \widehat{\mathcal{C}}\psi\left(\mathbf{r},t\right) = 0 \quad (6.37)$$

It can be seen that the term containing the 4-potential is symmetric (+) under charge conjugation, whereas the free-particle Dirac equation (6.7) is antisymmetric (−). It follows that if ψ is a solution of the Dirac equation for an electron (thus with charge $-e$) in the 4-potential A_μ, then $\widehat{\mathcal{C}}\psi$ is a solution of the Dirac equation for a particle with charge $+e$ in the *same* potential. In the stationary case the eigenvalues of ψ and $\widehat{\mathcal{C}}\psi$ have the same magnitude, but opposite sign. After an initial false identification with the proton [54], Dirac boldly predicted the existence of the positron [55], confirmed experimentally by Anderson in 1932 [56].

Note, however, that for a given 4-potential the Dirac operator describing an electron is *not* identical to the one describing a positron since the particles couple to the 4-potential through their charge (6.8). Only in the absence of external fields do the two equations become identical.

To see charge conjugation "at work" let us consider a stationary electronic solution ψ of the free-particle Dirac equation (6.7) with eigenvalue ϵ (positive continuum) and it's charge conjugated partner $\widehat{\mathcal{C}}\psi$ with eigenvalue $-\epsilon$ (negative continuum). We now introduce an external 4-potential through minimal coupling (6.8) with the electron charge $-e$, thus adding the term $\hat{V} = -ec\beta\gamma_\mu A_\mu$ to the free-particle Hamiltonian $\hat{h}_{D;0}$. The eigenvalues of the 2×2 Hamiltonian matrix in the space of the two charge conjugated partners is then

$$E_\pm = \Delta \pm \sqrt{\epsilon^2 + \Omega^2}; \quad \begin{cases} \Delta &= \left\langle \psi \middle| \hat{V} \middle| \psi \right\rangle \\ \Omega &= \left| \left\langle \psi \middle| \hat{V} \middle| \widehat{\mathcal{C}}\psi \right\rangle \right| \end{cases} . \tag{6.38}$$

The positive sign gives the electronic solution which can be expanded as

$$E_e = E_+ = \epsilon + \Delta + \frac{1}{2}\eta^1 + O(\eta^2) > \epsilon + \Delta; \quad \eta = \left(\frac{\Omega}{\epsilon}\right)^2 . \tag{6.39}$$

The corresponding positronic solution can be obtained by introducing the 4-potential through minimal coupling with the positronic charge $+e$. Alternatively, it can be obtained through charge conjugation of the solution corresponding to E_- of (6.38). The corresponding energy is

$$E_p = -E_- = \epsilon - \Delta + \frac{1}{2}\eta + O(\eta^2) \tag{6.40}$$

One can easily see that if the electron is attracted by the 4-potential, that is Δ is negative, then the positron is repulsed, due to it's opposite charge. Unless the coupling term Ω dominates Δ the electronic solution descends below $+mc^2$ and the negative energy solution descends further down the negative continuum. However, this does not imply, as is often stated, that for systems with bound electrons all negative energy orbitals can be identified as having energies below $-mc^2$. Potentials are not always purely attractive or repulsive, e.g. in an anion one may observe negative-energy orbitals entering the gap as such solutions far from the nucleus see a negative and thus attractive potential.

1.1.4 Towards the non-relativistic limit. 4-component operators and wave functions are usually taken to imply relativistic theory.

In this section we shall, however, show that also non-relativistic calculations may be carried out at the 4-component level. In fact, as has been discussed extensively by Visscher and Saue [57], a multitude of Hamiltonians, with and without spin-orbit interaction included, may be formulated at the 4-component level of theory. These Hamiltonians are obtained from non-unitary transformations W of the Dirac equation [58]

$$\psi = W\psi' \quad \Rightarrow \quad W^\dagger \left[\hat{h}_{D;A_\mu} - i\frac{\partial}{\partial t}\right] W\psi' = 0, \tag{6.41}$$

possibly followed by the deletion of certain parts of the transformed operators. As starting point for these Hamiltonians we choose the time-independent Dirac equation in the molecular field (6.17)

$$\begin{bmatrix} \hat{V} & c(\boldsymbol{\sigma}\cdot\mathbf{p}) \\ c(\boldsymbol{\sigma}\cdot\mathbf{p}) & \hat{V} - 2mc^2 \end{bmatrix} \begin{bmatrix} \psi^L \\ \psi^S \end{bmatrix} = \begin{bmatrix} I_2 & 0_2 \\ 0_2 & I_2 \end{bmatrix} \begin{bmatrix} \psi^L \\ \psi^S \end{bmatrix} E; \quad \hat{V} = -e\phi \tag{6.42}$$

where the metric is explicitly included since non-unitary transformations will be performed. We have also performed the substitution (6.6) to align relativistic and non-relativistic energy scales.

Consider first the non-relativistic limit, generally obtained as $c \to \infty$. The Dirac operator $\hat{h}_{D;V}$ has terms linear and even quadratic in the speed of light and one can therefore not apply this limit directly. Instead, one first performs the non-unitary transformation

$$\begin{bmatrix} \psi^L \\ \psi^S \end{bmatrix} = \begin{bmatrix} I_2 & 0_2 \\ 0_2 & c^{-1}I_2 \end{bmatrix} \begin{bmatrix} \psi^L \\ \widetilde{\psi}^S \end{bmatrix} \tag{6.43}$$

which gives the transformed equation

$$\begin{bmatrix} \hat{V} & (\boldsymbol{\sigma}\cdot\mathbf{p}) \\ (\boldsymbol{\sigma}\cdot\mathbf{p}) & -2m\left(1 - \dfrac{\hat{V}}{2mc^2}\right) \end{bmatrix} \begin{bmatrix} \psi^L \\ \widetilde{\psi}^S \end{bmatrix} = \begin{bmatrix} I_2 & 0_2 \\ 0_2 & c^{-2}I_2 \end{bmatrix} \begin{bmatrix} \psi^L \\ \widetilde{\psi}^S \end{bmatrix} E \tag{6.44}$$

The speed of light now appears only in inverse powers and the proper non-relativistic limit may be obtained, but with the following restrictions [59]:

1. $|E| \ll c^2$, that is we restrict attention to the positive-energy solutions. This also means that a separate non-relativistic limit exists for the negative-energy solutions.

2. The potential ϕ in $\hat{V}$ must be non-singular. This does not hold for the potential of point charges, but does hold for the extended nuclei commonly used in 4-component relativistic calculations.

With the above restrictions we arrive in the non-relativistic limit at the Levy-Leblond equation [60]

$$\begin{bmatrix} \hat{V} & (\boldsymbol{\sigma}\cdot\mathbf{p}) \\ (\boldsymbol{\sigma}\cdot\mathbf{p}) & -2m \end{bmatrix} \begin{bmatrix} \psi^L \\ \widetilde{\psi}^S \end{bmatrix} = \begin{bmatrix} I_2 & 0_2 \\ 0_2 & 0_2 \end{bmatrix} \begin{bmatrix} \psi^L \\ \widetilde{\psi}^S \end{bmatrix} E \tag{6.45}$$

which forms the starting point of the direct perturbation theory of Kutzelnigg [59]. By elimination of the modified small component $\widetilde{\psi}^S$we obtain the more familiar non-relativistic Schr?dinger equation in the molecular field using the identity $(\boldsymbol{\sigma}\cdot\mathbf{p})(\boldsymbol{\sigma}\cdot\mathbf{p}) = p^2$. However, in some cases the 4-component non-relativistic form (6.45) may be more advantageous than the conventional 1-component form, in particular upon the introduction of external magnetic fields [61].

Another route to the non-relativistic limit, with an interesting stop on the way, is provided by the non-unitary transformation

$$\begin{bmatrix} \psi^L \\ \psi^S \end{bmatrix} = \begin{bmatrix} I_2 & 0_2 \\ 0_2 & \dfrac{1}{2mc}(\boldsymbol{\sigma}\cdot\mathbf{p}) \end{bmatrix} \begin{bmatrix} \psi^L \\ \widetilde{\psi}^S \end{bmatrix} \tag{6.46}$$

which leads to what has been called *the modified Dirac equation* [62]

$$\begin{bmatrix} \hat{V} & \widehat{T} \\ \widehat{T} & \dfrac{1}{4m^2c^2}(\boldsymbol{\sigma}\cdot\mathbf{p})\hat{V}(\boldsymbol{\sigma}\cdot\mathbf{p}) - \widehat{T} \end{bmatrix} \begin{bmatrix} \psi^L \\ \widetilde{\psi}^S \end{bmatrix} = \begin{bmatrix} I_2 & 0_2 \\ 0_2 & \dfrac{1}{2mc^2}\widehat{T} \end{bmatrix} \begin{bmatrix} \psi^L \\ \widetilde{\psi}^S \end{bmatrix} E \tag{6.47}$$

where $\hat{T}$ is the kinetic energy operator. The speed of light again appears only in inverse powers which facilitates taking the non-relativistic limit. Another possibility is to use the identity

$$(\boldsymbol{\sigma}\cdot\mathbf{p})\hat{V}(\boldsymbol{\sigma}\cdot\mathbf{p}) = \mathbf{p}\widehat{V}\cdot\mathbf{p} + i\boldsymbol{\sigma}\cdot\left(\mathbf{p}\widehat{V}\times\mathbf{p}\right) \tag{6.48}$$

By dropping the spin-dependent term on the right hand side one obtains the spin-free form of the modified Dirac equation. It allows scalar relativistic calculations within a 4-component framework, although the uniqueness of the distinction between scalar and spin-orbit relativistic effects has been questioned [63].

1.2 The two-electron part

The extension from one-electron systems to fully interacting many-electron systems is more complicated in the relativistic domain than in the non-relativistic one. From our discussion of Coulomb gauge in section 1.1.1 this can be understood since in the relativistic framework we have

to add the effects of retardation and magnetic interaction to the non-relativistic limit represented by the instantaneous Coulomb interaction. The necessary correction terms can be obtained rigorously by invoking the full machinery of QED where the interaction is described in terms of the exchange of virtual photons. We shall however restrict ourselves to the semiclassical limit, that is continuous electromagnetic fields. To first order the electron-electron interaction is then given by the Coulomb-Breit interaction

$$\hat{g}(1,2) = \hat{g}^{\text{Coulomb}} + \hat{g}^{\text{Breit}} \tag{6.49}$$

The zeroth order term is the Coulomb term

$$\hat{g}^{\text{Coulomb}} = e^2 \frac{I_4 \cdot I_4}{r_{12}}. \tag{6.50}$$

We have inserted 4×4 times identity matrices I_4 to remind the reader that, although at first sight the Coulomb term appears to be identical to the non-relativistic electron-electron interaction, it's physical content is different. Upon reduction to non-relativistic form [37,64–67] through a Foldy-Wouthuysen transformation one finds that the relativistic operator contains for instance spin-own orbit interaction in addition to the instantaneous Coulomb interaction.

The first order term is the Breit interaction [68]

$$\hat{g}^{\text{Breit}} = -\frac{e^2}{2c^2 r_{12}} \left[(c\boldsymbol{\alpha}_1 \cdot c\boldsymbol{\alpha}_2) + \frac{1}{r_{12}^2} (c\boldsymbol{\alpha}_1 \cdot \mathbf{r}_{12}) (c\boldsymbol{\alpha}_2 \cdot \mathbf{r}_{12}) \right]. \tag{6.51}$$

We have written the Breit term in a slightly unusual form using explicitly the relativistic velocity operator $c\boldsymbol{\alpha}$. In this manner one easily recognizes (6.49) as the quantum mechanical analogue of the classical expression (6.16). It is important to note that although the Breit term can be derived as the low-frequency limit of the full electron-electron interaction as described by QED, it can equally well [37] be derived from the quantization of (6.16), which is essentially how it was derived by Breit. In this chapter *we will not go beyond* the semiclassical limit of QED, that is we will not consider quantization of the electromagnetic field since this would open up a whole new level of complexity. The Breit term can be rewritten in the form

$$\hat{g}^{\text{Breit}} = \hat{g}^{\text{Gaunt}} + \hat{g}^{\text{gauge}} \tag{6.52}$$

The first term is the Gaunt term

$$\hat{g}^{\text{Gaunt}} = -e^2 \frac{c\boldsymbol{\alpha}_1 \cdot c\boldsymbol{\alpha}_2}{c^2 r_{12}} \tag{6.53}$$

whereas the second term

$$\hat{g}^{\text{gauge}} = -e^2 \frac{(c\boldsymbol{\alpha}_1 \cdot \boldsymbol{\nabla}_1)(c\boldsymbol{\alpha}_2 \cdot \boldsymbol{\nabla}_2) r_{12}}{2c^2}, \tag{6.54}$$

where $\boldsymbol{\nabla}_1$and $\boldsymbol{\nabla}_2$ act *only* on r_{12} and not on the wave function, disappears in Lorentz (Feynman) gauge. By comparison with (6.11) one sees that the Coulomb and Gaunt terms represent charge-charge and current-current interactions, respectively. One can furthermore show by reduction to the non-relativistic form that the Gaunt term carries all spin-other orbit interaction [69].

The experience accumulated so far indicates that the Breit term has rather minor effects on the spectroscopic constants of molecular systems [21, 70, 71] so that the Coulomb term is usually sufficient. However, it is needed to get spin-orbit splittings correctly, in particular for light systems. From a practical point of view the Gaunt term is then preferred since it involves the same two-electron integrals as the Coulomb term (at least in a scalar basis) and provides the full spin-other orbit interaction.

1.3 Second quantization

Creation and annihilation operators were first introduced by Dirac to describe absorption and emission of photons [72], and the formalism was later extended to fermions by Jordan and Wigner [73, 74]. Although originally conceived to describe processes in which the particle number is not conserved, the second quantization formalism [75, 76] is widely used in molecular electronic-structure theory [31] that considers systems with a fixed particle number. This is so because it allows the derivation and expression of the methodology in an elegant manner, in particular when combined with exponential parametrization. In this section we will consider the second quantized form of the many-electron Hamiltonian at the 4-component relativistic level.

The second-quantized Hamiltonian is obtained from the first-quantized form (6.1) upon the introduction of field operators

$$\Psi(1) = \varphi_p(\mathbf{r}_1)\, a_p = \widetilde{\varphi}_p(\mathbf{r}_1)\, \widetilde{a}_p. \tag{6.55}$$

In the above expression the field operator has been expanded in two different orbital sets $\{\varphi_p\}$ and $\{\widetilde{\varphi}_p\}$ related by a unitary transformation which then defines two different sets of annihilation operators, $\{a_p\}$ and $\{\widetilde{a}_p\}$, related by the inverse transformation. In QED parlance the orbital set obtained as the solution of the free-particle Dirac equation corresponds to the "free" picture, whereas the one obtained with the molecular field (6.17) leads to the Furry [77] or bound-state interaction

picture [78, 79]. The general form of the second-quantized Hamiltonian is

$$\hat{H} = \int \Psi^\dagger(1)\hat{h}(1)\Psi(1)d\tau_1 + \frac{1}{2}\int\int \Psi^\dagger(1)\Psi^\dagger(2)\hat{g}(1,2)\Psi(2)\Psi(1)d\tau_1 d\tau_2 \tag{6.56}$$

where $\hat{g}(1,2)$ is the chosen form of the electron-electron interaction. We will for the moment limit attention to the Coulomb (6.50) and Gaunt term (6.53). At the 4-component level the direct product $\Psi(2)\Psi(1)$ leads to an expansion in terms of vector functions with sixteen components. From this one sees that the two-electron operator $\hat{g}(1,2)$ should be considered a 16×16 matrix operator [37], so that the *dot* products appearing in the Coulomb and Gaunt terms should be replaced by *direct* products. Expanding the field operators in a specific orbital basis the second-quantized Dirac-Coulomb-(Gaunt) Hamiltonian is written as

$$\hat{H} = h_{pq}a_p^\dagger a_q + \frac{1}{4}\mathcal{L}_{pq,rs}a_p^\dagger a_r^\dagger a_s a_q \tag{6.57}$$

in which appear one-electron integrals over the Dirac operator in the molecular field

$$h_{pq} = \int \varphi^\dagger(\mathbf{r}_1)\hat{h}_{D;V}(1)\varphi(\mathbf{r}_1)d\tau_1 \tag{6.58}$$

and where we have introduced antisymmetrized two-electron integrals

$$\mathcal{L}_{pq,rs} = (pq\,|\,rs) - (ps\,|\,rq) = \mathcal{L}_{rs,pq} = -\mathcal{L}_{ps,rq}. \tag{6.59}$$

We write the two-electron integrals as

$$(pq\,|\,rs) = \int\int \frac{\Omega_{pq}(\mathbf{r}_1)\Omega_{rs}(\mathbf{r}_2)}{r_{12}}d\tau_1 d\tau_2 \tag{6.60}$$

where we introduce generalized overlap distributions (including charge)

$$\Omega_{pq}(\mathbf{r}) = \varphi_p^\dagger(\mathbf{r})S_\mu\varphi_q(\mathbf{r}); \quad S_\mu = ie\beta\gamma_\mu = -e\left(-i\boldsymbol{\alpha}, I_4\right). \tag{6.61}$$

The time-like part corresponds to standard overlap distributions and contributes to the Coulomb term, whereas the space part corresponds to current distributions and contributes to the Gaunt term.

2. Variational procedures

There has been considerable discussion as to the variational stability of the Dirac-Coulomb-(Gaunt) Hamiltonian. The discussion originated from an argument put forward by Brown and Ravenhall [5]. They

considered the interaction of two electrons described by this Hamiltonian. Consider for instance the helium atom. In a perturbational approach one can start with the non-interacting system and thus a Slater-determinant consisting of the 1s orbitals obtained as solutions of the hydrogenic atom with $Z = 2$. This Slater determinant is, however, degenerate with an in principle infinite number of Slater determinants containing one orbital from the positive continuum and one from the negative continuum. When the electron-electron interaction is turned on, these determinants will mix in and lead to what has been called a continuum dissolution, meaning that no bound state is obtained. Brown and Ravenhall suggested the use of projection operators to avoid the mixing in of these continuum determinants, a proposal that has been further explored by Sucher and others (see [80] for a review). In this section we will carefully consider variational approaches based on the Dirac-Coulomb-(Gaunt) Hamiltonian using the second quantization formalism introduced in the previous section. This will allow us to employ an exponential parametrization of the wave function in terms of orbital rotations and furthermore make the connection to QED where a true minimization principle is assumed to exist.

2.1 The standard approach

In the second quantization formalism [31] Slater determinants are replaced by occupation-number vectors in Fock space as the fundamental entity. The antisymmetry of the wave function under particle exchange follows from the anticommutation properties of the creation- and annihilation operators

$$[a_p, a_q]_+ = \left[a_p^\dagger, a_q^\dagger\right]_+ = 0; \quad \left[a_p^\dagger, a_q\right]_+ = \delta_{pq} \tag{6.62}$$

Starting with a given set of orthonormal orbitals $\{\varphi_p\}$ the Fock space equivalent of a Slater determinant is generated by acting with the corresponding creation operators on the vacuum state $|0\rangle$

$$|\Phi\rangle = a_1^\dagger a_2^\dagger \ldots a_N^\dagger |0\rangle \tag{6.63}$$

where the vacuum state itself is defined by the relation

$$a_i |0\rangle = 0; \quad \forall a_i. \tag{6.64}$$

The occupation-number vector $|\Phi\rangle$ is an eigenfunction of the *number operator*

$$\hat{N} = a_p^\dagger a_p \tag{6.65}$$

with eigenvalue N corresponding to the number of occupied orbitals. The Fock space formalism goes beyond expansions in Slater determinants by allowing the coupling of vectors with different occupation numbers.

The variational *ansatz* at the Hartree-Fock level of theory is

$$\left|\widetilde{\Phi}\right\rangle = \exp\left[-\widehat{\kappa}\right]|\Phi\rangle \tag{6.66}$$

where $\exp\left[-\widehat{\kappa}\right]$ is an *orbital rotation operator* which is the negative exponential of the single replacement operator

$$\widehat{\kappa} = \kappa_{pq} a_p^\dagger a_q; \quad \kappa_{pq} = -\kappa_{qp}^*. \tag{6.67}$$

It is readily shown that $\widehat{\kappa}$ commutes with the number operator (6.65) which implies that the orbital rotation operator conserves particle number. The antihermiticity of the matrix containing the single replacement amplitudes $\{\kappa_{pq}\}$ guarantees the unitarity of the orbital rotation operator. Using (6.63) we can therefore rewrite the HF wavefunction as

$$\left|\widetilde{\Phi}\right\rangle = \widetilde{a}_1^\dagger \widetilde{a}_2^\dagger \ldots \widetilde{a}_N^\dagger |0\rangle \tag{6.68}$$

in which appear transformed creation operators

$$\widetilde{a}_p^\dagger = \exp\left[-\widehat{\kappa}\right] a_p^\dagger \exp\left[\widehat{\kappa}\right] = a_q^\dagger U_{qp}; \quad U = \exp\left[-\kappa\right]. \tag{6.69}$$

To derive (6.68) we have used the result

$$\exp\left[-\widehat{\kappa}\right]|0\rangle = |0\rangle \tag{6.70}$$

which follows from the fact that annihilation operators appear on the right in the first and higher order terms of the exponential expansion of the orbital rotation operator.

The orbital set corresponding to the transformed creation operators (6.69) is given by

$$\widetilde{\varphi}_p = \varphi_q U_{qp}^* \tag{6.71}$$

and demonstrates that the orbital rotation operator provides a means of parameterizing the wave function in such a manner that orthonormality of the orbitals is assured without the need to introduce Lagrange multipliers. The orbital rotation operator furthermore allows the use of unconstrained optimization techniques by choosing a linearly independent set of elements of the κ matrix as variational parameters. Due to the antihermiticity of the κ matrix this is straightforwardly accomplished by choosing e.g. the upper triangle and the (imaginary) diagonal elements. The $\widehat{\kappa}$ operator can then be written as

$$\widehat{\kappa} = \sum_{p<q} \left[\kappa_{pq} a_p^\dagger a_q - \kappa_{pq}^* a_q^\dagger a_p\right]. \tag{6.72}$$

Table 6.1 Classes of variational parameters in the standard 4-component approach compared to QED.

	Generic	Standard	QED
A	κ_{ia}	$\kappa_{ia}^{++}, \kappa_{ia}^{+-}$	$\kappa_{ia}^{++}, \kappa_{ia}^{-+}$
B	κ_{ij}	κ_{ij}^{++}	$\kappa_{ij}^{++}, \kappa_{ij}^{+-}, \kappa_{ij}^{--}$
C	κ_{ab}	$\kappa_{ab}^{++}, \kappa_{ab}^{+-}, \kappa_{ab}^{--}$	κ_{ab}^{++}

We have discarded the diagonal elements since they only introduce a complex phase in the wave function and do not change the energy. Other redundant parameters should also be eliminated from the set of variational parameters. Within the chosen parametrization this is an easy task, as will be seen shortly. For this purpose it is convenient to introduce classes of orbitals and thereby the elements of the κ matrix. We shall use indices i, j, k and l to identify occupied orbitals. We furthermore employ indices a, b, c and d for virtual orbitals and p, q, r and s as general indices. When needed we shall use superscripts $+$ and $-$ to distinguish positive- and negative-energy orbitals. This of course assumes that the actual potential allows this distinction. We can then identify three classes of variational parameters as given in table 6.1 (the column marked QED should be ignored for the moment). It should be noted that the direct use of the elements of the U matrix (6.69) as variational parameters is less advantageous since they are related in a non-linear manner by the unitary condition $U^\dagger U = I$. It is furthermore difficult to identify redundant parameters in this alternative parametrization.

We now gather the chosen, generally complex variational parameters in the vector

$$\mathbf{K} = \begin{bmatrix} \kappa \\ \kappa^* \end{bmatrix} \tag{6.73}$$

and consider a Taylor expansion of the energy in terms of these. Let $\mathbf{K} = 0$ correspond to the current expansion point, that is the reference determinant (6.63) and the corresponding orbital set. We then have

$$E(\mathbf{K}) = E^{[0]} + \mathbf{K}^\dagger \mathbf{E}^{[1]} + \frac{1}{2}\mathbf{K}^\dagger E^{[2]}\mathbf{K} + O(\kappa^3). \tag{6.74}$$

The various terms of the Taylor expansion can be easily found by comparing with a Baker-Campbell-Hausdorff (BCH) expansion of the energy

expectation value

$$\begin{aligned} E = \left\langle \widetilde{\Phi} \middle| \hat{H} \middle| \widetilde{\Phi} \right\rangle &= \left\langle \Phi \middle| \exp\left[\widehat{\kappa}\right] \hat{H} \exp\left[-\widehat{\kappa}\right] \middle| \Phi \right\rangle \\ &= \left\langle \Phi \middle| \hat{H} \middle| \Phi \right\rangle + \left\langle \Phi \middle| \left[\widehat{\kappa}, \hat{H}\right] \middle| \Phi \right\rangle + \\ &\quad + \frac{1}{2} \left\langle \Phi \middle| \left[\widehat{\kappa}, \left[\widehat{\kappa}, \hat{H}\right]\right] \middle| \Phi \right\rangle + O(\kappa^3) \end{aligned} \tag{6.75}$$

The zeroth order term is the expectation value of the energy with respect to the current Slater determinant

$$E^{[0]} = h_{ii} + \frac{1}{2}\Gamma_{ii}\left[\varphi_j\right]; \quad \Gamma_{pq}\left[\varphi_i\right] = \mathcal{L}_{pqii} \tag{6.76}$$

where we have introduced the mean-field potential $\Gamma\left[\varphi_i\right]$ involving summation over the orbital set $\{\varphi_i\}$. It will turn out to be useful to also consider the explicit form of the energy expression in the algebraic approximation. Consider the expansion of the current orbital set in some set of suitable basis functions (to be discussed in section 3.1) $\varphi_p = \chi_\mu c_{\mu p}$ where Greek indices are used for the AO-basis. The energy (6.76) can then be re-expressed as

$$E = D_{\mu\nu} h_{\nu\mu} + \frac{1}{2} D_{\mu\nu} \mathcal{L}_{\nu\mu\lambda\kappa} D_{\kappa\lambda}; \quad D_{\lambda\kappa} = c_{\lambda i} c^*_{\kappa i} \tag{6.77}$$

in which appears the AO-density matrix D.

The first-order term can be expressed as

$$\begin{aligned} \mathbf{K}^\dagger \mathbf{E}^{[1]} &= \sum_{p<q} \left\{ -\kappa^*_{pq} \left\langle \Phi \middle| \left[a^\dagger_q a_p, \hat{H}\right] \middle| \Phi \right\rangle + \kappa_{pq} \left\langle \Phi \middle| \left[a^\dagger_p a_q, \hat{H}\right] \middle| \Phi \right\rangle \right\} \\ &= \left(F_{ip}\kappa^*_{pi} - \kappa^*_{ip} F_{pi}\right) + \text{c.c.} \end{aligned} \tag{6.78}$$

in which appears the Fock matrix

$$F_{pq} = h_{pq} + \Gamma_{pq}\left[\varphi_i\right] = h_{pq} + \mathcal{L}_{pq\kappa\lambda} D_{\lambda\kappa}. \tag{6.79}$$

From (6.78) one can easily see that derivatives of the energy at the current expansion point ($\mathbf{K} = 0$) with respect to parameter classes B and C (see table 6.1) are identically zero. Since this will hold for *any* expansion point the two parameter classes can be eliminated as redundant. The only non-redundant parameters are rotations between occupied (+) and virtual (±) orbitals, that is parameter class A, and the $\widehat{\kappa}$ can accordingly be written in terms of non-redundant parameters as

$$\widehat{\kappa} = \kappa_{ia} a^\dagger_a a_i - \kappa^*_{ai} a^\dagger_i a_a \tag{6.80}$$

Note that in order to ensure unitarity of the orbital rotation operator the $\widehat{\kappa}$ operator contains de-excitation operators $\left\{a_i^\dagger a_a\right\}$ in addition to excitation operators $\left\{a_a^\dagger a_i\right\}$. This can be contrasted with the exponential operator in a coupled-cluster expansion which is entirely based on excitation operators. In terms of non-redundant parameters the gradient vector can be written as

$$\mathbf{E}^{[1]} = \begin{bmatrix} \mathbf{g} \\ \mathbf{g}^* \end{bmatrix}; \quad g_{ai} = \left.\frac{\partial E}{\partial \kappa_{ai}^*}\right|_{K=0} = \left\langle \Phi \middle| \left[-a_i^\dagger a_a, \hat{H}\right] \middle| \Phi \right\rangle = -F_{ai} \tag{6.81}$$

The current expansion point corresponds to a stationary value of the energy when all the elements of the gradient vector are zero. From the above expression we can see that this corresponds to the occupied-virtual blocks of the Fock matrix being zero. This can be accomplished by diagonalization of the Fock matrix (until convergence of the SCF procedure) and then leads to the canonical Hartree-Fock orbitals with associated orbital energies $\{\epsilon_p\}$. Alternatively one can proceed by second-order methods such as Newton-Raphson. These are generally more expensive since they involve calculation of the Hessian matrix $E^{[2]}$, but are also more robust. The second-order methods lead to a set of orthonormal orbitals not necessarily equal to, but related through a unitary transformation, to the canonical HF orbitals.

To characterize the stationary points we must consider the eigenvalues of the Hessian matrix. It has been defined in such a manner that it is Hermitian and diagonal dominant. It has the structure

$$E^{[2]} = \begin{bmatrix} A & B \\ B^* & A^* \end{bmatrix}; \qquad \begin{aligned} A_{ai,bj} &= \delta_{ij}F_{ab} - \delta_{ab}F_{ij}^* - \mathcal{L}_{abij} \\ B_{ai,bj} &= -\mathcal{L}_{aj,bi} \end{aligned} \tag{6.82}$$

Consider first a non-interacting system, i.e. $\hat{g}(i,j) = 0$. Then all two-electron terms disappear. In canonical orbitals the Hessian furthermore becomes diagonal with diagonal elements

$$A_{ai,ai} = \epsilon_a - \epsilon_i \begin{cases} > 0 & \text{for} \quad \left\{\kappa_{ia}^{++}\right\} \\ < 0 & \text{for} \quad \left\{\kappa_{ia}^{+-}\right\} \end{cases} \quad \text{(no summation !)} \tag{6.83}$$

One sees that the stationary point is a *minimum* with respect to rotations $\left\{\kappa_{ia}^{++}\right\}$ between occupied (+) and positive-energy virtual orbitals, but a *maximum* with respect to rotations $\left\{\kappa_{ia}^{+-}\right\}$ between occupied and (virtual) negative-energy orbitals.

For an interacting system the diagonal elements of the Hessian correspond to energy differences between singly excited determinants $\Phi_{i\to a}$ and the reference determinant

$$A_{ai,ai} = E\left(\Phi_{i\to a}\right) - E\left(\Phi\right) = \epsilon_a - \epsilon_i - \mathcal{L}_{aa,ii} \quad \text{(no summation !)} \quad (6.84)$$

Since the excited determinant is calculated in the orbitals optimized for the reference determinant the diagonal elements of the Hessian constitute a rather poor approximation to excitation energies that goes under the name of the single-transition approximation [81]. A better approximation of the energies needed to reach the manifold of singly excited states with respect to the ground state is obtained at the RPA (random-phase approximation) level (coupled Hartree-Fock) where the single excitation energies from a closed-shell ground state are the eigenvalues of the Hessian matrix. In view of this, it is clearly reasonable to claim that the minimax principle (6.83) applies to interacting systems as well.

The minimax principle for non-interacting systems is not identical to the minimax principle for the Dirac equation proposed by Talman [82] which states that the expectation value of the Dirac operator is a minimum with respect to variations in the large components and a maximum with respect to variations in the small components

$$E = \min_{\psi^L}\left[\max_{\psi^S}\frac{\left\langle\psi\left|\hat{h}_D\right|\psi\right\rangle}{\langle\psi\mid\psi\rangle}\right] \quad (6.85)$$

This minimax principle has been justly criticized by Kutzelnigg [49]. The problem is that the coupling between the large and the small components of the Dirac spinor means that some variations of the large component may lead to energies below the exact energy. We shall discuss this further in section 3.1, but one should note that the minimax principle (6.83) is susceptible to the same problem unless the chosen basis set expansion allows the proper coupling of large and small components. There is a significant difference, though. The Talman minimax principle operationally implies the *separate* variation of the large and small components. However, due to their coupling variations must be done in a *concerted* manner and this is achieved by the minimax defined in (6.83).

2.2 Towards QED

The standard approach to 4-component relativistic molecular calculations is not quantum electrodynamics and does not even constitute its semiclassical limit, that is the level of theory in which the electromagnetic field is not quantized. In this section we shall explore a variational

description of the proper semiclassical limit of QED. This section is very much inspired by two rarely cited papers by Chaix and Iracane [83] on the transition from quantum electrodynamics to mean-field theory, but whereas these authors employ the elements of the U matrix (6.69) as variational parameters, leading to what they call the Bogoliubov-Dirac-Fock formalism, we shall employ the more advantageous parametrization in terms of elements of the κ matrix.

In the previous section we have seen that the standard approach to 4-component relativistic molecular calculations leads to a minimax principle at the Hartree-Fock level. This means that the bound electronic states at this level of theory are excited states and may therefore decay through an infinite succession of transition through various states of the negative-energy continuum, thereby causing a radiative catastrophe [84]. To avoid this difficulty Dirac postulated that the negative-energy orbitals are all occupied so that transitions into the negative-energy continuum, "the Dirac sea", is forbidden by the Pauli exclusion principle. On the other hand, the excitation of an electron from the Dirac sea to a positive-energy orbital, requiring an energy on the order of $2mc^2$, leaves a hole with opposite charge that in time was identified as the positron.

The first step towards proper QED is to introduce a *particle-hole formalism*. The field operators (6.55) are rewritten as

$$\Psi = \varphi_p^+ b_p + \varphi_p^- d_p^\dagger \tag{6.86}$$

in which appears *electron* annihilation operators b_p associated with the positive-energy orbitals φ_p^+ and *positron* creation operators $d_p^\dagger$ describing the creation of positrons whose orbitals are obtained by charge conjugating the associated negative-energy orbitals φ_p^-. This distinction leads to a more involved expression for the second quantized form of the Hamiltonian

$$\begin{aligned}
\hat{H} &= h_{pq}^{++} b_p^\dagger b_q + h_{pq}^{+-} b_p^\dagger d_q^\dagger + h_{pq}^{-+} d_p b_q + h_{pq}^{--} d_p d_q^\dagger \qquad (6.87)\\
&+ \frac{1}{4}\mathcal{L}_{pqrs}^{++++} b_p^\dagger b_r^\dagger b_s b_q + \frac{1}{4}\mathcal{L}_{pqrs}^{+-++} b_p^\dagger b_r^\dagger b_s d_q^\dagger\\
&+ \frac{1}{4}\mathcal{L}_{pqrs}^{+++-} b_p^\dagger b_r^\dagger d_s^\dagger b_q + \frac{1}{4}\mathcal{L}_{pqrs}^{+-+-} b_p^\dagger b_r^\dagger d_s^\dagger d_q^\dagger\\
&+ \frac{1}{4}\mathcal{L}_{pqrs}^{++-+} b_p^\dagger d_r b_s b_q + \frac{1}{4}\mathcal{L}_{pqrs}^{+--+} b_p^\dagger d_r b_s d_q^\dagger\\
&+ \frac{1}{4}\mathcal{L}_{pqrs}^{++--} b_p^\dagger d_r d_s^\dagger b_q + \frac{1}{4}\mathcal{L}_{pqrs}^{+---} b_p^\dagger d_r d_s^\dagger d_q^\dagger\\
&+ \frac{1}{4}\mathcal{L}_{pqrs}^{-+++} d_p b_r^\dagger b_s b_q + \frac{1}{4}\mathcal{L}_{pqrs}^{--++} d_p b_r^\dagger b_s d_q^\dagger\\
&+ \frac{1}{4}\mathcal{L}_{pqrs}^{-++-} d_p b_r^\dagger d_s^\dagger b_q + \frac{1}{4}\mathcal{L}_{pqrs}^{--+-} d_p b_r^\dagger d_s^\dagger d_q^\dagger
\end{aligned}$$

$$
\begin{aligned}
&+ \quad \frac{1}{4}\mathcal{L}_{pqrs}^{-+-+} d_p d_r b_s b_q + \frac{1}{4}\mathcal{L}_{pqrs}^{----+} d_p d_r b_s d_q^\dagger \\
&+ \quad \frac{1}{4}\mathcal{L}_{pqrs}^{-+--} d_p d_r d_s^\dagger b_q + \frac{1}{4}\mathcal{L}_{pqrs}^{----} d_p d_r d_s^\dagger d_q^\dagger
\end{aligned}
$$

By inspection one immediately sees that the QED Hamiltonian couples occupation-number vectors with different particle number. However, we will demonstrate later that charge is conserved.

As in the previous section we consider the description of bound electronic states in terms of a single Slater determinant or, equivalently, in terms of a single occupation-number vector in Fock space

$$
|\Phi\rangle = b_1^\dagger b_2^\dagger \ldots b_n^\dagger |0\rangle . \tag{6.88}
$$

The vacuum state $|0\rangle$ is in this formalism defined by

$$
(b_p |0\rangle = 0, \quad \forall b_p) \quad \text{and} \quad (d_p |0\rangle = 0, \quad \forall d_p) . \tag{6.89}
$$

In analogy with (6.66) we now consider the following variational *ansatz*

$$
\left|\widetilde{\Phi}\right\rangle = \exp\left[-\widehat{\kappa}\right] |\Phi\rangle \tag{6.90}
$$

The $\widehat{\kappa}$ operator appearing in the orbital rotation operator now has the form

$$
\widehat{\kappa} = \underbrace{\kappa_{pq}^{++} b_p^\dagger b_q}_{\widehat{\kappa}^{++}} + \underbrace{\kappa_{pq}^{+-} b_p^\dagger d_q^\dagger}_{\widehat{\kappa}^{+-}} + \underbrace{\kappa_{pq}^{-+} d_p b_q}_{\widehat{\kappa}^{-+}} + \underbrace{\kappa_{pq}^{--} d_p d_q}_{\widehat{\kappa}^{--}} \tag{6.91}
$$

We may next introduce number operators $\hat{N}^e$ and $\hat{N}^p$ for electrons and positrons, respectively

$$
\hat{N}^e = b_p^\dagger b_p; \quad \hat{N}^p = d_p^\dagger d_p. \tag{6.92}
$$

One finds that the $\hat{\kappa}$ operator commutes with neither number operator

$$
\left[\hat{\kappa}, \hat{N}^e\right] = \left[\hat{\kappa}, \hat{N}^p\right] = \hat{\kappa}^{-+} - \hat{\kappa}^{+-}, \tag{6.93}
$$

but with the linear combination

$$
\hat{Q} = e\left(\hat{N}^p - \hat{N}^e\right) \tag{6.94}
$$

which can be identified as the *charge* operator. From this we can conclude that the orbital rotation operator of QED conserves charge but *not* the particle number. The charge operator furthermore commutes with the QED Hamiltonian (6.87), thus demonstrating that the latter conserves charge as well.

Using the unitarity of the orbital rotation operator we may now rewrite the HF ansatz as

$$\left|\widetilde{\Phi}\right\rangle = \widetilde{b}_1^\dagger \widetilde{b}_2^\dagger \ldots \widetilde{b}_n^\dagger \left|\widetilde{0}\right\rangle \tag{6.95}$$

where appear the transformed creation operators

$$\widetilde{b}_p^\dagger = \exp\left[-\widehat{\kappa}\right] b_p^\dagger \exp\left[\widehat{\kappa}\right] = b_q^\dagger U_{qp}; \quad U = \exp\left[-\kappa\right]. \tag{6.96}$$

Note that due to charge conservation we can identify the transformed creation operators with dressed electrons. Equation (6.95) contains not only dressed electrons, but also a *dressed vacuum*

$$\left|\widetilde{0}\right\rangle = \exp\left[-\widehat{\kappa}\right]|0\rangle = \left\{1 - \kappa_{pq}^{--} d_p d_q - \kappa_{pp}^{--} + O(\kappa^2)\right\}|0\rangle \neq |0\rangle. \tag{6.97}$$

This relation may be compared with (6.70) and shows the effect of *vacuum polarization* which is not present in the standard approach described in the previous section.

If we evaluate the expectation value of the Hamiltonian (6.87) with respect to the reference determinant (6.88) we obtain the expression (6.76), but with *all* the negative-energy orbitals included amongst the occupied orbitals, thus leading to an infinite negative energy. In order to avoid working with infinite energies renormalization procedures are introduced in QED. In the present case the infinite negative energy is avoided by writing the Hamiltonian on *reordered* form, that is all creation operators are shifted to the left and all annihilation operators are shifted to the right as if they anticommuted. Using the notation of Chaix and Iracane [83] we write the reordered QED Hamiltonian as

$$\begin{aligned} \hat{H} &= \int N\left[\Psi^\dagger(1)\hat{h}(1)\Psi(1)d\tau_1\right] \\ &+ \frac{1}{2}\int\int N\left[\Psi^\dagger(1)\Psi^\dagger(2)\hat{g}(1,2)\Psi(2)\Psi(1)\right]d\tau_1 d\tau_2 \end{aligned} \tag{6.98}$$

In the orbital set which diagonalizes $\hat{h}$, the one-electron part, can be written as

$$\begin{aligned} \hat{h} &= h_{pq}^{++} b_p^\dagger b_q + h_{pq}^{+-} b_p^\dagger d_q^\dagger + h_{pq}^{-+} d_p b_q - h_{pq}^{--} d_q^\dagger d_p \\ &= \epsilon_p^+ b_p^\dagger b_p + \left(-\epsilon_p^-\right) d_p^\dagger d_p \end{aligned} \tag{6.99}$$

One may observe that on this reordered form electrons and positrons both appear with *positive* energies, but with opposite charges.

To relate the original Hamiltonian (6.87) to the reordered form (6.98) one may employ Wick's theorem [85,86]. For the one-electron part this gives

$$N\left[\Psi^\dagger(1)\Psi(2)\right] = \Psi^\dagger(1)\Psi(2) - \left\langle 0^{(\mathrm{ref})}\left|\Psi^\dagger(1)\Psi(2)\right|0^{(\mathrm{ref})}\right\rangle \tag{6.100}$$

which shows that normal ordering of a one-electron operator corresponds to the subtraction of its vacuum expectation value. We have inserted a superscript (ref) on the vacuum to remind the reader that the definition of the vacuum and thus the reordering depends on the choice of orbital set in which the field operators are expanded. As reference vacuum the *bare* vacuum is employed, corresponding to the orbital sets generated from the solution of the free-particle Dirac equation (6.7). Normal ordering of the two-electron part gives

$$\begin{aligned} N\left[\Psi^\dagger(1)\Psi^\dagger(2)\Psi(3)\Psi(4)\right] &= \Psi^\dagger(1)\Psi^\dagger(2)\Psi(3)\Psi(4) \\ &- N\left[\Psi^\dagger(1)\Psi(4)\right]\Psi^\dagger(2)\Psi(3) \\ &- N\left[\Psi^\dagger(2)\Psi(3)\right]\Psi^\dagger(1)\Psi(4) \\ &+ N\left[\Psi^\dagger(1)\Psi(3)\right]\Psi^\dagger(2)\Psi(4) \\ &+ N\left[\Psi^\dagger(2)\Psi(4)\right]\Psi^\dagger(1)\Psi(3) \\ &- \left\langle 0^{(\mathrm{ref})}\left|\Psi^\dagger(1)\Psi^\dagger(2)\Psi(3)\Psi(4)\right|0^{(\mathrm{ref})}\right\rangle \end{aligned} \tag{6.101}$$

which does *not* correspond to simple subtraction of the vacuum expectation value, even though one readily sees that the bare vacuum expectation value of the reordered Hamiltonian (6.98) is zero.

We have already seen that the particle-hole formalism leads to a rather complicated expression for the Hamiltonian (6.87). With the introduction of reordering more complexity is added and manipulations involving the reordered Hamiltonian become extremely tedious. In order to simplify the ensuing manipulations it is therefore advantageous to go back to the form of the field operators (6.55) introduced in the previous section and instead explicitly define the bare vacuum as filled with all the negative-energy solutions of the free-particle Dirac equation

$$\left|0^{(\mathrm{ref})}\right\rangle = a^\dagger_{[-1]}a^\dagger_{[-2]}\cdots a^\dagger_{[-\infty]}\left|\mathrm{empty}\right\rangle . \tag{6.102}$$

The empty state $|\mathrm{empty}\rangle$ corresponds to the vacuum (6.64) of the standard approach to 4-component relativistic molecular theory. In the above expression as in the following we use *square brackets* (e.g. $h^{--}_{[pq]}$) around indices referring to the negative-energy solutions of the *free-particle* Dirac equation. We can now write the reordered QED Hamiltonian as

$$\hat{H} = \left\{h_{pq} - \Gamma_{pq}\left[\varphi^-_{[i]}\right]\right\} a^\dagger_p a_q + \frac{1}{4}\mathcal{L}_{pqrs}a^\dagger_p a^\dagger_r a_s a_q - h^{--}_{[ii]} + \frac{1}{2}\mathcal{L}^{----}_{[iijj]} \tag{6.103}$$

What we loose by this approach is the physical picture of electron-positron pair creation that was provided by the particle-hole formalism.

Using this reordered Hamiltonian we can now easily find the terms appearing in the Taylor expansion (6.74). The energy at the current expansion point is given by

$$\begin{aligned} E^{[0]}_{QED} &= h^{++}_{ii} + h^{--}_{ii} - h^{--}_{[ii]} + \frac{1}{2}\Gamma^{--}_{[ii]}\left[\varphi^{-}_{[j]}\right] \\ &+ \frac{1}{2}\Gamma^{++}_{ii}\left[\varphi^{+}_{j}\right] + \frac{1}{2}\Gamma^{++}_{ii}\left[\varphi^{-}_{j}\right] + \frac{1}{2}\Gamma^{--}_{ii}\left[\varphi^{+}_{j}\right] + \frac{1}{2}\Gamma^{--}_{ii}\left[\varphi^{-}_{j}\right] \\ &- \frac{1}{2}\Gamma^{++}_{ii}\left[\varphi^{-}_{[j]}\right] - \frac{1}{2}\Gamma^{--}_{ii}\left[\varphi^{-}_{[j]}\right] - \frac{1}{2}\Gamma^{--}_{[ii]}\left[\varphi^{+}_{j}\right] - \frac{1}{2}\Gamma^{--}_{[ii]}\left[\varphi^{-}_{j}\right] \end{aligned} \tag{6.104}$$

This rather formidable expression becomes quite a lot more intelligible when expressed in AO-basis

$$E^{[0]}_{QED} = D^{\mathrm{QED}}_{\mu\nu} h_{\nu\mu} + \frac{1}{2} D^{\mathrm{QED}}_{\mu\nu} \mathcal{L}_{\nu\mu\lambda\kappa} D^{\mathrm{QED}}_{\kappa\lambda} \tag{6.105}$$

in which appears the AO-density matrix of QED

$$D^{\mathrm{QED}}_{\kappa\lambda} = D_{\kappa\lambda} + D^{\mathrm{pol}}_{\kappa\lambda}; \quad D^{\mathrm{pol}}_{\kappa\lambda} = \sum_{i}^{(-)} \left(c_{\kappa i} c^{*}_{\kappa i} - c_{\kappa[i]} c^{*}_{\kappa[i]} \right). \tag{6.106}$$

Comparing with (6.77) one sees that the standard AO-density matrix D has been replaced by the QED counterpart D^{QED} obtained by the addition of the *vacuum polarization density* D^{pol} which reflects how the vacuum density is modified with respect to the reference vacuum upon the introduction of the actual potential.

The gradient vector in semiclassical QED is given by a formula identical to (6.81), except that the Fock matrix of the standard approach is to be replaced by its QED counterpart F^{QED} which is obtained by the substitution $D \to D^{\mathrm{QED}}$ in (6.79). Once again we find that the non-redundant orbital rotations are given by the parameter class A of table 6.1. However, the reader should carefully note that the distribution of the elements of the κ-matrix on the three parameter classes *changes* when going from the standard approach to QED, reflecting that the negative-energy orbitals are now filled and not empty.

The Hessian in semiclassical QED has the same form as in (6.82), but with the substitution $F \to F^{\mathrm{QED}}$. For a non-interacting system the Hessian becomes diagonal like in the standard approach (6.83)

$$A_{ai,ai} = \epsilon_a - \epsilon_i > 0; \quad \forall \kappa_{ia} \tag{6.107}$$

Following the same line of argument as in section 2.1 we may conclude that the Hessian of the interacting systems has all eigenvalues positive as well. We have thereby shown that the electronic ground state of semiclassical QED is characterized by a *minimization principle* at the Hartree-Fock level of theory.

2.3 Discussion

In the previous two subsections we have developed variational theory at the closed-shell Hartree-Fock level according to the standard 4-component approach and QED in the semiclassical limit. In this section we will summarize and discuss our findings. This will allow us to return to and study in more detail the argument of Brown and Ravenhall. It furthermore allows us to consider the extension to the correlated level of theory in the next subsection.

In QED the *negative-energy orbitals are filled,* in accordance with Dirac's proposal. This allows, at sufficiently large energies, to create electron-positron pairs out of the vacuum. Such processes do not conserve particle number, but do conserve charge. The energies of interaction in chemistry are generally too low for real pair creation processes, but the Dirac sea manifests itself through the phenomenon of vacuum polarization. As we have seen, at the closed-shell Hartree-Fock level the QED electronic ground state corresponds to a *true minimum* of the energy and this allows for instance the relativistic extension of the Hohenberg-Kohn theorem of DFT [87]. In contrast, the electronic ground state in the standard approach is characterized by a *minimax principle.* The vacuum is then *empty,* and the negative-energy orbitals are accordingly treated as an *orthogonal complement* to the electronic orbitals. However, and this is a crucial point, retaining the additional degrees of freedom provided by this orthogonal complement (the positronic degrees of freedom) allows the complete relaxation of the electronic ground state.

With the notation and machinery introduced in the two previous subsections we may now revisit the argument of Brown and Ravenhall. We consider a system of two non-interacting electrons and in the standard approach (std) write the ground state as

$$|\Phi_0\rangle = a_i^\dagger a_{\bar{i}}^\dagger |0\rangle_{\text{std}} \tag{6.108}$$

corresponding to the Slater determinant of the degenerate Kramers partners φ_i and $\overline{\varphi}_i$. The ground state energy is $E_0^{(0)} = \epsilon_i + \epsilon_{\bar{i}} = 2\epsilon_i$. We then turn on the two-electron interaction. By standard Rayleigh-Schrödinger perturbation theory the first order amplitudes of the perturbed wave function are

$$a_n = \frac{\langle \Phi_n | \hat{g}(1,2) | \Phi_0 \rangle}{E_0^{(0)} - E_n^{(0)}}. \tag{6.109}$$

One can now straightforwardly construct doubly-excited determinants

$$|\Phi_n\rangle = \left|\Phi_{i\to a^+}^{\bar{i}\to b^-}\right\rangle = a_a^\dagger a_b^\dagger |0\rangle_{\text{std}} \tag{6.110}$$

with one orbital φ_a^+ from the positive continuum and one orbital φ_b^- from the negative continuum such that the energy $E_n^{(0)} = \epsilon_a^+ + \epsilon_b^-$ becomes identical with $E_0^{(0)}$ and perturbation theory breaks down. The solution proposed by Brown and Ravenhall was to embed the Hamiltonian in projection operators Λ_+ onto positive energy orbitals

$$\hat{H} \quad \rightarrow \quad \Lambda_+ \hat{H} \Lambda_+. \tag{6.111}$$

This corresponds to retaining only the purely electronic terms of the QED Hamiltonian (6.87)

$$\hat{H}^{\text{no-pair}} = h_{pq}^{++} b_p^\dagger b_q + \frac{1}{4} \mathcal{L}_{pqrs}^{++++} b_p^\dagger b_r^\dagger b_s b_q. \tag{6.112}$$

Pair creation and annihilation is thereby excluded and this approximation has therefore been referred to as the *no-pair* approximation. However, ***the no-pair Hamiltonian is not unique*** since the distinction between electronic and positronic creation and annihilation operators depends on the orbital set in which the field operators are expanded. One possible choice is the solutions of the free-particle Dirac equation (6.7), giving the "free" picture. Another choice is the solutions of the Dirac equation in the molecular field (6.17) leading to the Furry picture. A third possibility is to continuously update the projection operators through SCF iterations so that they at convergence correspond to the solutions of the combined molecular and mean-field potentials of the Hartree-Fock equations. We shall see that this choice, the "fuzzy" picture, as proposed by Mittleman [88], corresponds to the standard 4-component approach.

Let us, however, first consider the two-electron system discussed by Brown and Ravenhall as described by QED. We write the reference determinant as

$$|\Phi_0\rangle_{\text{QED}} = b_i^\dagger b_{\bar{i}}^\dagger |0\rangle_{\text{QED}} \tag{6.113}$$

where the vacuum is defined by (6.89) and thereby the complete orbital set of the non-interacting system. Using (6.103) we find the QED ground state energy to be

$$E_{\text{QED};0}^{(0)} = 2\epsilon_i^+ + \sum_j^{(-)} \left(\epsilon_j^- - h_{[jj]}^{--} \right). \tag{6.114}$$

Let us next consider the QED analogues of the troublesome doubly excited determinants (6.110). From the reinterpretation of the field operators (6.86) and the definition of the vacuum (6.89) we immediately obtain

$$|\Phi_n\rangle_{\text{QED}} = b_a^\dagger d_b |0\rangle_{\text{QED}} = 0 \quad (!), \tag{6.115}$$

showing that these determinants simply do not occur since all the negative-energy orbitals are already occupied. One may attempt the alternative form

$$|\Phi_n\rangle'_{\text{QED}} = b_a^\dagger d_b^\dagger |0\rangle_{\text{QED}} \tag{6.116}$$

corresponding to the creation of a true electron-positron pair out of the vacuum. However, this determinant corresponds to a different charge (zero and not -2) and does therefore not interact with the two-electron reference determinant since the QED Hamiltonian conserves charge. Such determinants are thus excluded on physical grounds. We can therefore conclude that at the QED level the Brown-Ravenhall disease is easily cured; the reference determinant (6.113) mixes only with purely electronic determinants *for fixed particle number* N. The two-electron part of the QED Hamiltonian (6.87) allows coupling of the reference occupation-number vector to vectors to which are added one or two electron-positron pairs. These can again couple to vectors with more pairs at higher order in perturbation theory. It is perhaps easier to analyze these interacting occupation-number vectors by going from the particle-hole formalism to the original form of the field operators (6.55) and instead fill up all the negative-energy orbitals of the interacting system. The occupation-number vector of the particle-hole formalism containing one and two electron-positron pair(s) then correspond to determinants

$$|\Phi_{k^-\to a^+}\rangle \quad \text{and} \quad \left|\Phi^{i^-\to b^+}_{k^-\to a^+}\right\rangle, \tag{6.117}$$

respectively. The first class of determinants contain the excitation of an electron from the negative-energy orbital k to the virtual positive-energy orbital a. Using the form (6.103) of the reordered QED Hamiltonian with all two-electron terms deleted we find that the unperturbed energy of the determinant $|\Phi_n\rangle = |\Phi_{k^-\to a^+}\rangle$ is

$$E^{(0)}_{\text{QED};n} = 2\epsilon_i^+ + \epsilon_a^+ - \epsilon_k^- + \sum_j^{(-)} \left(\epsilon_j^- - h^{--}_{[jj]}\right) \tag{6.118}$$

Using the full Hamiltonian we can determine the transition moment, that is the numerator of (6.109), and thus obtain the following expression for the first-order amplitude of the perturbed wave function

$$a_n = -\frac{\mathcal{L}^{-+--}_{ka[ii]}}{\epsilon_k^- - \epsilon_a^+} \quad \text{(no summation !)} \tag{6.119}$$

The denominator is clearly of order $O(c^2)$. The numerator $\mathcal{L}^{-+--}_{ka[ii]} = (ka|ii) - (ki|ia)$ contains two-electron integrals in which the integration

over one electron contains the overlap of one positive-energy and one negative-energy orbital. To determine the order of this contribution let us recall from the discussion in section 1.1.1 that for positive-energy solutions the large component is in an averaged sense a factor c larger than the small component, and that for negative-energy solution this role is reversed. We can then conclude that the numerator is on the order of $O(c^{-1})$ and thus the amplitude (6.119) is of order $O(c^{-3})$. By similar arguments we find that the amplitude of doubly-excited determinants $|\Phi_n\rangle = \left|\Phi^{l^- \to b^+}_{k^- \to a^+}\right\rangle$ is

$$a_n = \frac{\mathcal{L}^{-+-+}_{kalb}}{\epsilon^-_k + \epsilon^-_l - \epsilon^+_a - \epsilon^+_b} \tag{6.120}$$

and is of order $O(c^{-4})$. It is important to note that the determinants of (6.117) contain excitations from *occupied* negative-energy orbitals to virtual positive-energy orbitals. They are therefore *absent* in the standard approach since in this approach the vacuum is *empty* and the negative-energy orbitals only serve as an orthogonal complement. The presence of the determinants (6.117) constitute a pure QED effect and our order analysis shows the minuteness of their contribution.

We have seen that the standard approach differs from QED in the semiclassical limit only by the absence of vacuum polarization. This is a rather minute effect, giving rise to the Uehling effect, which is a minor contribution to the Lamb shift [35], and it would therefore be surprising if the elimination of vacuum polarization should lead to a complete breakdown of the theory. In subsection 2.1 we have seen that the electronic ground state in the standard approach can be found by the minimax principle (6.84). However, in practice the solutions are found by vector selection, that is in each iteration of the SCF cycle vectors for the next iteration are not selected according to an *aufbau* principle, rather one selects the lower *electronic orbitals* that are generally easily identified through the energy gap down to the negative-energy orbitals. This procedure corresponds *precisely* to the use of a no-pair Hamiltonian (6.112) with continuously updated projection operators as proposed by Mittleman. Another way of seeing this procedure is to note that the formulas of the standard approach can be recovered from QED by choosing the reference vacuum as the vacuum defined by the self-consistent mean-field potential. The vacuum polarization density D^{pol} (6.106) then goes to zero. Having identified the electronic Hamiltonian of the standard 4-component approach with the no-pair Hamiltonian in the "fuzzy" picture, we can see that the Brown-Ravenhall disease is cured, since the

doubly excited determinants (6.110) leading to continuum dissolution are projected out.

The no-pair Hamiltonian (6.112) depends on the orbital set in which the field operators (6.86) are expanded and thus on the potential generating this orbital. This *non-uniqueness* of the no-pair Hamiltonian is an important point that seems to escape a number of authors. In particular when deriving various approximate 1- or 2-component relativistic Hamiltonians a number of authors embed the Dirac-Coulomb-(Gaunt/Breit) Hamiltonian in projection operators (6.111) *without* specifying the reference orbitals. In an otherwise excellent paper by M. Barysz and A.J.Sadlej [89] one reads: "[...] one should mention that the methods of relativistic quantum chemistry, which are based directly on 4-spinors [...], also neglect the positronic (negative energy) solutions. This is generally known as the *no-pair approximation* [...] and makes the *exact* electronic 2-spinor solutions fully equivalent to four-component electronic solutions. Hence, as long as our knowledge of the pure electronic spectrum of the Dirac equation is sufficient, the 4-spinor formalism becomes obsolete." What the authors miss is the fact that the 4-component methods *update* the projection operators of the no-pair Hamiltonian *until self-consistency* and therefore achieve a complete relaxation of orbitals to the actual potential. The approximate 1- and 2- component methods *freeze* the projection operators before performing an approximate decoupling of the electronic and positronic degrees of freedom. This may lead to excellent approximations that allow relativistic calculations at reduced computational cost, but it is incorrect to state they provide complete equivalence with the 4-component methods.

Just how good these approximations with fixed projection operators are can be easily investigated at the 4-component level in the algebraic approximation. It suffices to generate the orbital set corresponding to the reference potential defining the projection operator and then delete the negative energy vectors from the ensuing calculation in the actual potential. In table 6.2 this procedure is illustrated by 4-component relativistic Hartree-Fock calculations on the radon atom. It can be seen that the use of projection operators defined by the free-particle Dirac equation, the "free" picture, gives rather large deviations, in particular in the core region, compared to the standard approach, the "fuzzy" picture, based on fully relaxed projection operators. On the other hand, the use of projection operators defined by the molecular field (6.17), the Furry picture, compare fairly well with the standard approach. For reference we have also included the results of a 1-component (scalar) second-order Douglas-Kroll calculation in the same basis. Apart from the lack of spin-orbit interaction one can see that the result is rather close to the Furry pic-

ture, which can be considered as infinite-order Douglas-Kroll. An at first sight surprising result is obtained by projecting the standard or "fuzzy" occupied orbitals onto the negative-energy free particle solutions in the same basis. On then finds that the negative-energy free particle solutions contribute only 0.0053 to the total density of 86 electrons! However, albeit minute, one should keep in mind that the negative-energy orbitals contribute very large energies and this explains the large deviations of the "free" picture result from the standard approach.

2.4 The correlated level

Let us now consider the extension to the correlated level. The most general variational parametrization is provided by the MCSCF *ansatz*

$$\left|\Psi^{\mathrm{MCSCF}}\right\rangle = \exp\left[-\widehat{\kappa}\right] \sum_i c_i \left|\Phi_i\right\rangle \tag{6.121}$$

in which the orbital rotation parameters $\{\kappa_{pq}\}$ are supplemented by the coefficients $\{c_i\}$ of the CI expansion in Slater-determinants $\{|\Phi_i\rangle\}$. At the Hartree-Fock level the orbital rotation parameters provide relaxation of orbitals. At the correlated level orbital relaxation, in addition to correlation, is also provided by the CI expansion coefficients. In fact, in the non-relativistic domain the orbital rotation parameters become redundant in the limit of a complete CI-expansion within the given orbital basis, showing that in this domain the exact solution within a given 1-particle basis is provided by full CI.

At the 4-component relativistic level the choice of CI-expansion becomes more difficult since one employs a no-pair Hamiltonian with projection operators that in principle should be allowed to relax completely to the actual potential of the system. At the MCSCF level the relaxation is provided by the orbital rotation parameters that can be employed in conjunction with an expansion in purely electronic determinants, that is containing only positive-energy orbitals. In CI and CC methods the orbital basis is frozen, and the conventional approach is to employ the no-pair Hamiltonian (6.112) defined by Hartree-Fock orbitals. This means that determinantal expansions are restricted to purely electronic determinants generated from this orbital set. Complete relaxation of the projection operators is therefore not possible, although the projection operators defined by the Hartree-Fock orbitals can be expected to constitute a very good approximation. In the limit of full CI the orbital parameters κ_{ia}^{++} describing rotations between occupied and virtual positive energy orbitals become redundant, but the parameters κ_{ia}^{+-} , describing rotations between occupied positive energy orbitals and virtual negative energy orbitals are not accounted for by the CI-expansion. This tells us that at

Table 6.2 The effect of embedding the Dirac-Coulomb Hamiltonian by projection operators onto positive energy orbitals as illustrated by a Hartree-Fock calculation on the radon atom. The calculations were carried out using a point nucleus and an uncontracted 32s32p17d11f family Gaussian large component basis. The small component basis was generated by restricted kinetic balance. For comparison we have included the results of a scalar second-order Douglas-Kroll calculation (DK2) in the same basis.

	Fuzzy	Furry	Free	DK2
E(total)	-23610.98632	-23611.01630	-24153.25409	-23533.64569
$1s_{1/2}$	-3644.74282	-3644.75635	-3859.56081	-3626.81594
$2s_{1/2}$	-669.37883	-669.38209	-694.44791	-667.27997
$2p_{1/2}$	-642.35771	-642.36308	-650.93434	-570.13212
$2p_{3/2}$	-541.08440	-541.08776	-540.98657	idem
$3s_{1/2}$	-166.96715	-166.96783	-172.50957	-166.54445
$3p_{1/2}$	-154.90291	-154.90395	-156.89683	-138.48586
$3p_{3/2}$	-131.72668	-131.72734	-131.61723	idem
$3d_{3/2}$	-112.56321	-112.56374	-112.25150	-109.69442
$3d_{5/2}$	-107.75599	-107.75642	-107.45065	idem
$4s_{1/2}$	-41.34840	-41.34854	-42.76820	-41.25251
$4p_{1/2}$	-36.02132	-36.02153	-36.50780	-31.85484
$4p_{3/2}$	-30.11915	-30.11927	-30.06259	idem
$4d_{3/2}$	-21.54718	-21.54726	-21.44792	-20.89499
$4d_{5/2}$	-20.43800	-20.43805	-20.34020	idem
$4f_{5/2}$	-9.19411	-9.19409	-9.11432	-9.06496
$4f_{7/2}$	-8.92842	-8.92840	-8.85031	idem
$5s_{1/2}$	-8.41670	-8.41671	-8.72474	-8.39894
$5p_{1/2}$	-6.40907	-6.40910	-6.49582	-5.54050
$5p_{3/2}$	-5.17528	-5.17529	-5.14742	idem
$5d_{3/2}$	-2.18932	-2.18932	-2.15957	-2.09081
$5d_{5/2}$	-2.01625	-2.01625	-1.98766	idem
$6s_{1/2}$	-1.07263	-1.07263	-1.12104	-1.06787
$6p_{1/2}$	-0.54033	-0.54033	-0.54932	-0.42777
$6p_{3/2}$	-0.38390	-0.38390	-0.37708	idem

the 4-component relativistic level the exact solution in a given 1-particle basis is not provided by full CI, but by MCSCF.

Bunge *et al.* [90] has advocated 4-component relativistic CI using in addition to purely electronic determinants also mixed determinants, that is Slater determinants containing both positive- and negative-energy orbitals. A subclass of these determinants are precisely the doubly excited determinants that appear in the argument of Brown and Ravenhall analyzed in the previous section. It is our firm conviction that the methods advocated by Bunge *et al.* are plain wrong and our argument against the use of these methods runs as follows: Consider CI at the QED level of theory, or rather in the semiclassical limit that was analyzed in section 2.2. The CI *ansatz* is

$$\left|\Psi^{\mathrm{CI}}\right\rangle = \sum_i c_i \left|\Phi_i\right\rangle \tag{6.122}$$

which is simply the MCSCF *ansatz* (6.121) with the orbital rotation operator deleted. We may assume that we start with the orbital set generated at the Hartree-Fock level. We want to describe a system of N electrons and so our Hartree-Fock reference is simply an occupation-number vector of N electrons as in (6.88). The QED Hamiltonian (6.98) does not conserve particle number and so the CI-expansion (6.122) will contain occupation-number vectors with particle number $N + 2n$, where n is the number of electron-positron pairs generated from the reference determinant. On the other hand, the QED Hamiltonian does conserve charge and so the occupation-number vectors with N particles must all be *purely* electronic since they are the only ones that couple to the reference determinant through the QED Hamiltonian. The occupation-number vectors with more than N particles correspond to determinants (6.117) involving one or more excitations of electrons from occupied negative-energy orbitals to virtual positive-energy orbitals. The inclusion of these determinants will provide complete relaxation of the orbital set. However, as emphasized already in the previous section, these determinants are *absent* in the standard approach since all the negative-energy states are empty. The mixed determinants included by Bunge *et al.* in the CI-expansion simply do not exist at the QED level. They are forbidden by the Pauli exclusion principle since they involve the double occupation of negative-energy orbitals. Their inclusion can precisely lead to the continuum dissolution predicted by Brown and Ravenhall. Bunge *et al.* claims variational control using the Hylleraas-Undheim theorem which implies that the ordered sequence of eigenvalues of a CI-matrix with one determinant added to the expansion are interlaced with those of the original CI-matrix. However, the Hylleraas-Undheim theorem only connects sequences of *eigenvalues* and not *eigenstates*. It is well known in direct-

CI methods that upon enlarging the trial vector space *root flipping* can occur, that is two states may change order, and this is precisely the possibility that precludes variational control in the approach advocated by Bunge *et al.* [90].

3. Implementation and Computational Scaling

Now that the necessary general theory has been introduced in the preceding sections we can direct our attention to the application to molecules. This concerns both the implementation of algorithms and their computational scaling in comparison to the "spinfree" algorithms that are used in non-relativistic quantum chemistry. We start by considering basis set expansion techniques.

3.1 The algebraic approximation

While Hartree-Fock equations for atoms can be solved via numerical integration one needs a basis set expansion to apply the method to general molecular systems. In order to obtain a viable scheme one would like to choose functions that are readily integrated, preferably using the same techniques as employed in non-relativistic quantum chemistry, so that one can benefit from the large body of experience and implementations that are available in this field. Non-relativistic orbitals are, however, usually chosen as real functions of the space coordinates only, whereas the Dirac spinors are complex functions of space and spin coordinates. How can one best exploit the available basis set technology in this domain ?

Basis set expansion is usually done in the LCAO approximation where the molecular orbitals are expressed as linear combinations of atomic orbitals. These atomic orbitals are in turn expressed as fixed linear combinations of simpler functions called primitives. Consider the solution of the time-independent Dirac equation for a molecular field (6.42) in the algebraic approximation. We expand the large and small component in two different sets of primitives

$$\psi_p^X = \chi_\mu^X c_{\mu p}^X; \quad X = L, S. \tag{6.123}$$

We then obtain the eigenvalue equation

$$\begin{bmatrix} V^{LL} & c\Pi^{LS} \\ c\Pi^{SL} & V^{SS} - 2mc^2 S^{SS} \end{bmatrix} \begin{bmatrix} \mathbf{c}_p^L \\ \mathbf{c}_p^S \end{bmatrix} = \begin{bmatrix} S^{LL} & 0 \\ 0 & S^{SS} \end{bmatrix} \begin{bmatrix} \mathbf{c}_p^L \\ \mathbf{c}_p^S \end{bmatrix} \epsilon_p \tag{6.124}$$

in which appear the matrix elements

$$S_{\mu\nu}^{XY} = \langle \chi_\mu^X \mid \chi_\nu^Y \rangle; \quad V_{\mu\nu}^{XY} = \left\langle \chi_\mu^X \middle| \hat{V} \middle| \chi_\nu^Y \right\rangle; \quad \Pi_{\mu\nu}^{XY} = \langle \chi_\mu^X \mid (\boldsymbol{\sigma} \cdot \mathbf{p}) \mid \chi_\nu^Y \rangle \tag{6.125}$$

The first attempts along these lines failed rather miserably, even for one-electron systems. The origin of the problem was the neglect of the coupling of the large and small components in the Dirac equation

$$2mc\psi_p^S(\mathbf{r}) = \widehat{R}_p(\boldsymbol{\sigma}\cdot\mathbf{p})\psi_p^L(\mathbf{r}); \quad \widehat{R}_p = \left[1 + \frac{\epsilon_p - \hat{V}}{2mc^2}\right]^{-1} \tag{6.126}$$

We obtain the finite basis equivalent of this relation by first writing out (6.124) in terms of two matrix equations

$$V^{LL}\mathbf{c}_p^L + c\Pi^{LS}\mathbf{c}_p^S = S^{LL}\mathbf{c}_p^L\epsilon_p \tag{6.127}$$

$$c\Pi^{SL} + \left(V^{SS} - 2mc^2S^{SS}\right)\mathbf{c}_p^S = S^{SS}\mathbf{c}_p^S\epsilon_p \tag{6.128}$$

and solve for the vector $\mathbf{c}_p^S$ of small component expansion coefficients. This gives the relation

$$\mathbf{c}_p^S = \frac{1}{2mc}\left[S^{SS} + \frac{\epsilon_p S^{SS} - V^{SS}}{2mc^2}\right]^{-1}\Pi^{SL}\mathbf{c}_p^L. \tag{6.129}$$

From (6.126) or, alternatively, (6.129) we see that the small component wave function can be regarded as the result of the consecutive action of the operators $(\boldsymbol{\sigma}\cdot\mathbf{p})$ and $\widehat{R}_p$ on the large component wave function. The energy-dependent operator $\widehat{R}_p$ is totally symmetric, but the operator $(\boldsymbol{\sigma}\cdot\mathbf{p})$ couples functions of opposite parity which indicates that separate basis set expansions are needed for the large and small components, as was anticipated by (6.123). We thus see that the coupling of the large and small components generally leads to the use of larger basis sets and thereby increased computational cost at the 4-component relativistic level compared to non-relativistic methods. For instance, at the Hartree-Fock level three classes of integrals over the Coulomb operator (6.50) appear — $(LL\,|\,LL)$, $(SS\,|\,LL)$ and $(SS\,|\,SS)$ — where the first and smaller class (all indices correspond to large component basis functions) constitute the two-electron integrals of a non-relativistic calculation. On the other hand, we shall see that a closer study of the coupling relation provides suggestions as how to reduce computational cost.

Before entering a detailed discussion of the coupling (6.126), let us first consider the choice of primitives in the basis set expansions in relativistic calculations. We know that the exact solutions of the relativistic hydrogenic atom [91] differ from the non-relativistic ones in having a singularity at the nucleus and having a coupling between the spatial and spin coordinates. The singularity is somewhat artificial because it appears in the exact solution for a model in which the nucleus is represented

by a point charge. A more realistic finite nucleus model [92] gives the wave functions an approximately Gaussian shape in this region. The second difference, coupling of the spatial and spin degrees of freedom, leads to more complications. An expansion in 2-spinor functions was suggested by the Oxford group [15] who defined basis functions as

$$\begin{aligned} \chi_\mu^L(\mathbf{r}_A) &= N_\mu^L f_\mu^L(r_A)\,\xi_{\kappa_\mu,m_\mu}(\theta_A,\varphi_A) \\ \chi_\mu^S(\mathbf{r}_A) &= N_\mu^S f_\mu^S(r_A)\,\xi_{-\kappa_\mu,m_\mu}(\theta_A,\varphi_A) \end{aligned} \tag{6.130}$$

The radial functions $f_\mu^L(r_A)$ and $f_\mu^S(r_A)$ depend only on the distance to expansion center A, all the angular and spin dependence is carried by the 2-spinor functions $\xi_{\kappa_\mu,m_\mu}(\theta_A,\varphi_A)$ for which the analytic form is known [6]. The problem with this approach is that, due to the changed angular dependence relative to non-relativistic theory, completely new integral evaluation routines need to be developed. This made the actual implementation for molecular systems appear relatively late [15,16]. Implementations of a more pragmatic approach with scalar expansion functions were available about a decade earlier [13,14,62,93,94] because they employed non-relativistic integral evaluation packages [95]. In such schemes one chooses expansion functions in which only one component of the 4-spinor is non-zero :

$$\psi_p^X = \begin{bmatrix} \boldsymbol{\chi}^X & 0 \\ 0 & \boldsymbol{\chi}^X \end{bmatrix} \begin{bmatrix} \mathbf{c}_p^{X\alpha} \\ \mathbf{c}_p^{X\beta} \end{bmatrix}; \quad X = L,S \tag{6.131}$$

Here $\boldsymbol{\chi}^X$ is a row vector of primitives and $\mathbf{c}_p^{X\alpha}$ and $\mathbf{c}_p^{X\beta}$ are column vectors of the corresponding expansion coefficients. Note that the same set of primitives is used for the α and β components. The scalar functions $\chi_\mu(\mathbf{r}_A)$ are again chosen as functions of the position of the electron relative to expansion centers A. One may still separate the radial and angular parts by choosing the spherical form

$$\chi_\mu(\mathbf{r}_A) = N_\mu^l r_A^{\ell_\mu} f_\mu(r_A)\, Y_{\ell_\mu,m_\mu}(\theta_A,\varphi_A) \tag{6.132}$$

but this gives now only a marginal advantage over the Cartesian form

$$\chi_\mu(\mathbf{r}_A) = N_\mu^{\prime\prime} x_A^{n_\mu^x} y_A^{n_\mu^y} z_A^{n_\mu^z} f_\mu(r_A) \tag{6.133}$$

since neither has the correct angular dependence. The correct angular dependence is in this approach of course still achieved at the Hartree-Fock stage once the actual spinors are found.

In all three models — 2-spinor, spherical or Cartesian — one still needs to choose the specific form of the radial expansion functions $f_\mu(r_A)$.

Again one can take the exact solutions for the hydrogenic atom as a guideline. Slater functions $f_\mu(r_A) = e^{-\zeta_\mu r_A}$ have the correct long range behavior, but do not have the correct shape close to the nuclei. They neither represent the singularity found in the point nucleus model nor the approximate Gaussian shape appropriate for finite nuclear models. There may thus be an advantage for expansion in Gaussian type functions $f_\mu(r_A) = e^{-\zeta_\mu r_A^2}$ for properties that depend on the precise shape near extended nuclei, while properties that depend on the electron density in the outer regions of the molecule are better described using Slater type functions. In practice, however, decisive is the more efficient evaluation of multi-center integrals that makes Gaussian based expansions the method of choice for both kind of properties. In both the scalar and the two-spinor expansion schemes one can then employ integration schemes developed for Gaussian type functions [31].

As said before, the advantage of the scalar function approach is that they require very little adaptation of existing non-relativistic integral evaluation routines. A disadvantage is, however, that the expansion in N^L large and N^S small component primitives is unnecessarily long. To see why this is so we need to consider the relation (6.126) between the large and the small component part of the wavefunction in more detail. For electronic orbitals *and* non-singular potentials ϕ, e.g. finite nuclei, the coupling reduces in the non-relativistic limit to

$$\lim_{c\to\infty} 2mc\, \psi_p^S(\mathbf{r}) = (\boldsymbol{\sigma}\cdot\mathbf{p})\, \psi_p^L(\mathbf{r}) \tag{6.134}$$

and equivalently, in the algebraic approximation, to

$$\lim_{c\to\infty} 2mc\, \mathbf{c}_p^S = \left[S^{SS}\right]^{-1} \Pi^{SL}\mathbf{c}_p^L \tag{6.135}$$

since the operator $\hat{R}_p$ then goes to unity. In practice one obtains this result for point nuclei as well in the algebraic approximation because Gaussian basis functions are not able to describe the singularities at nuclei. When using basis set expansions, one usually ignores the effect of $\hat{R}_p$ since this operator, even in the relativistic regime, is close to unity due to the large value of $2mc^2$. This is called the kinetic balance procedure [3, 96] since it guarantees proper representation of the operator identity $(\boldsymbol{\sigma}\cdot\mathbf{p})(\boldsymbol{\sigma}\cdot\mathbf{p}) = p^2$ in matrix form. We can see this better by inserting the non-relativistic coupling (6.135) into the matrix equation (6.127). We then obtain

$$V^{LL}\mathbf{c}_p^L + \frac{1}{2m}\Pi^{LS}\left[S^{SS}\right]^{-1}\Pi^{SL}\mathbf{c}_p^L = S^{LL}\mathbf{c}_p^L\epsilon_p \tag{6.136}$$

which gives the matrix representation of the non-relativistic Schrödinger equation provided that the relation

$$\langle \chi_\mu^L | p^2 | \chi_\nu^L \rangle = \langle \chi_\mu^L | (\boldsymbol{\sigma} \cdot \mathbf{p}) \, \Omega \, (\boldsymbol{\sigma} \cdot \mathbf{p}) | \chi_\nu^L \rangle \tag{6.137}$$

holds. The term

$$\Omega = \sum_{\kappa\lambda} |\chi^S\rangle_\kappa \left[\left(S^{SS} \right)^{-1} \right]_{\kappa\lambda} \langle \chi_\lambda^S | \tag{6.138}$$

has the form of the resolution of identity in a non-orthogonal basis. As carefully analyzed by Dyall *et al.* [97] it is not necessary to have a complete small component basis in order for relation (6.137) to hold; it suffices that the small component basis *spans* the result of the operator $(\boldsymbol{\sigma} \cdot \mathbf{p})$ acting on the large component basis. This observation explains the weakness of the Talman minimax principle (6.85) alluded to in section 2.1. Assume that we have the exact solution. If the large component function is now varied by adding new primitives *without* conjointly adding small component primitives that span the effect of $(\boldsymbol{\sigma} \cdot \mathbf{p})$ on these new functions, then relation (6.137) will not hold. The kinetic energy will be underestimated, and one may observe that the energy falls below the exact energy, contrary to the Talman minimax principle. The kinetic balance recipe in practice prevents this so-called variational collapse. It does not mean that kinetically balanced basis sets always provide an upper limit of the true energy since the relation (6.135) does not represent the exact coupling (6.129). The effect of the operator $\hat{R}_p$ can be seen in figure 6.1 where we compare the small component radial function of the $1s_{1/2}$ orbital of the radon atom from a Hartree-Fock calculation using a finite nucleus with the function generated by kinetic balance from the corresponding large component radial function. It can be seen that close to the nucleus there is a marked discrepancy between the two functions, illustrating that the kinetic balance prescription gives a rather poor description of the coupling of the large and small components in this region. However, since this breakdown occurs in the close vicinity of nuclei, well within the radial expectation value of the $1s_{1/2}$ orbital, it is reasonable to assume that it occurs in a region of local atomic symmetry, even for molecular systems. This implies that large component s functions then only couple to small component p functions and not to other angular momentum types. With a sufficiently flexible basis the kinetic balance prescription will therefore allow the establishment of the correct coupling. In most cases energy optimizing a sequence of uncontracted kinetically balanced basis sets shows monotonous convergence from above upon extending the basis. For very large basis sets one sometimes sees that the energy in a kinetic balance basis set expansion is slightly lower than the

reference value that is obtained via numeric integration [98]. There is, however, ample numerical evidence that such small deviations do not present a real problem, and the kinetic balance procedure has therefore become the standard approach in developing basis sets for 4-component relativistic calculations.

Since it suffices to span the range of functions $\chi_\mu^{SA}(\mathbf{r}) = (\boldsymbol{\sigma} \cdot \mathbf{p})\,\chi_\mu^{LA}(\mathbf{r})$ in the small component basis, kinetic balance can be realized in different ways. In 2-component basis sets one can directly include one small component expansion function for each large component function . This 1:1 relation between the large and small component basis functions has been denoted *restricted* kinetic balance. In scalar basis sets one usually considers all three components of the $\mathbf{p}$ separately, which is then denoted *unrestricted* kinetic balance. Still, the separate one-component functions can be recombined in the transformation to the orthogonal basis when the Hartree-Fock matrix equation is solved. If this is done, the final result becomes identical to that of the 2-component procedure, with as only difference the calculation of primitive integrals and the construction of the Fock matrix. In these steps the scalar expansion method needs significantly more primitive functions than needed in the comparable two-spinor expansion. As example we take the representation of the 2p spinors. The large component is expressed as a linear combination of $2p_x$, $2p_y$, and $2p_z$ Cartesian Gaussian functions using the same exponents for the whole set of p-functions. The small component is then expanded in the set of functions that are generated by operation with the three components of the gradient operator on the three scalar 2p functions. This gives seven unique functions ($1s$, $3s$ and $3d$) to balance three large component functions. This overrepresentation can be reduced using so-called dual family basis sets [98] in which the exponents of the d-functions are a subset of those of s-functions, and the exponents of f-functions a subset of those of p-functions, etc. This is efficient because small component scalar functions are then used to balance two large component functions at the same time. Still, one always ends up with a longer expansion than used in an qualitatively equivalent two-spinor expansion. The superfluous linear combinations are usually projected away because they may give problems with linear dependencies. The problem is enhanced in heavier elements because the $p_{1/2}$ and $p_{3/2}$ orbitals then have markedly different radial extent [99]. A scalar expansion scheme does not permit distinction between these subshells which means that the tight functions needed in the expansion set for the $p_{1/2}$ will also be included in the set used for the $p_{3/2}$. This illustrates that a two-spinor expansion is to be preferred on theoretical grounds . It is, however, also a matter of strategy whether this reduction in application time really warrants the

additional effort in constructing and maintaining a dedicated integral evaluation implementation for relativistic calculations. An implementation of the scalar expansion scheme that shares most of its inner kernels with a non-relativistic implementation will benefit easily from new advances in non-relativistic integral evaluation techniques, while these need to be rederived and separately implemented in a two-spinor scheme. Another issue is the interface of non-relativistic and relativistic schemes, an approach advocated by Dyall [100–103], where it also may be easier to work with primitive scalar expansion functions throughout.

Let us now direct attention to the $\hat{R}$ operator (6.126) that modifies the function $(\boldsymbol{\sigma} \cdot \mathbf{p})\, \psi^L(\mathbf{r})$ in regions where the potential $\phi(\mathbf{r})$ is large. This is the case in the vicinity of nuclei and has important implications for the kinetic balance procedure for contracted basis sets. The kinetic balance prescription has proven to be a valid method to generate primitive small component basis sets. However, it is clear from figure 6.1 that it fails when applied to the large component part of an eigenspinor. The dramatic consequences can easily be verified for hydrogenic systems [104]. It means that the simple kinetic balance procedure can not be applied to heavily contracted basis functions (that approach the exact large component solution) because the generated small component functions do not provide sufficient flexibility to establish the correct coupling. The proper procedure is to take both the large and the small component coefficients directly from uncontracted atomic reference calculations. This has been referred to as atomic balance [104]. As a side remark we note that the sometimes advocated [105] use of non-relativistic functions to expand the large component, combined with application of the kinetic balance prescription for the small component, also prevents the divergences but at the expense of having wrong expansion functions for both the large and the small component. Again, contraction with the atomic spinor coefficients is easier in two-spinor expansion schemes than in scalar expansion schemes because the former makes it possible to define specific contractions for the spin-orbit split subshells ($j = l - 1/2$ and $j = l + 1/2$). In the latter scheme one needs to give one set of contraction coefficients for a given nl shell which makes it necessary to compromise.

The $\hat{R}$-operator is also of interest when studying the long-range behavior of the small component wave function. In regions of negligible potential it reduces to a constant factor of

$$\hat{R}_p = \left[1 + \frac{\epsilon_p}{2mc^2}\right]^{-1} \tag{6.139}$$

Since the amplitude of the large component wave function in this region is dominated by that from the HOMO with a small value of ε_p and only

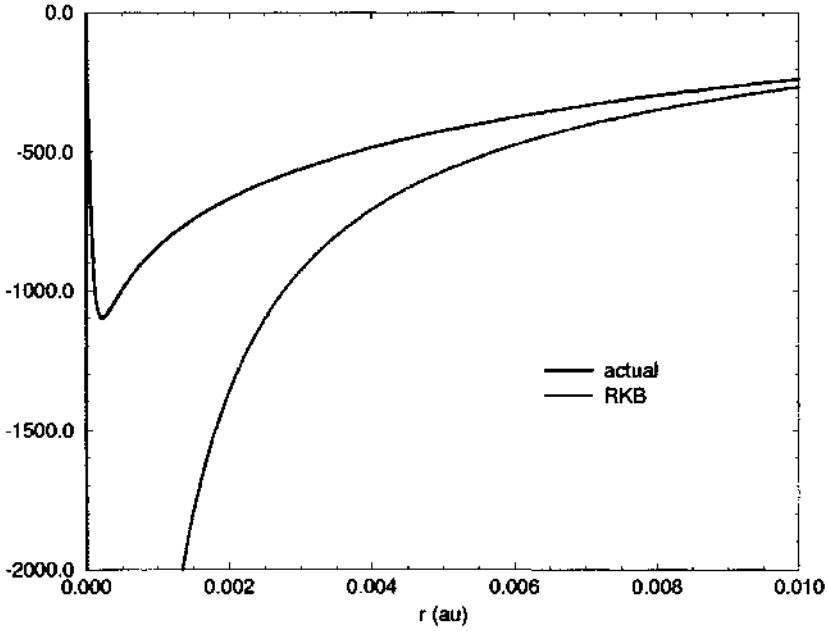

Figure 6.1 The actual small component radial function $[r^{-1}Q(r)\ ]$ of the $1s_{1/2}$ orbital of radon obtained from a numerical GRASP calculation with Gaussian nucleus, as compared with the radial small component function $[r^{-1}P(r)\ ]$ generated from restricted kinetic balance (RKB). For comparison the radial expectation value of the $1s_{1/2}$ orbital is 0.0015 a.u.

a small gradient, the small component wave function will have nearly zero amplitude in this region. The small component density is therefore rather localized and atomic in nature. This observation has made it possible to calculate spectroscopic constants of molecular systems where the complete set of $(SS \mid SS)$ integrals is eliminated and the potential curve is corrected by a simple Coulombic correction [106]. This constitute a perturbational correction, but more elaborate schemes of integral modeling have been developed in order to reduce computational cost. Recently a scheme was presented in which all overlap between small component basis functions located on different expansion centers was neglected in the evaluation of potential energy matrix elements [107]. The promising results obtained in these pilot calculations indicate that in the long run it will probably suffice to restrict evaluation of potential energy inte-

grals in the small component basis to those that share a common center. In this approximation the scaling of integral evaluation then becomes $aN_L^4 + bN_SN_L^2 + cN_S$ where the first term is comparable to that of a non-relativistic all-electron calculation. This means that the preceding discussion on the efficiency of integral evaluation in two-spinor versus scalar expansion schemes looses some of its significance because it will apply mainly to small systems. For larger systems the integral evaluation cost will be dominated by the "non-relativistic" first term and it becomes more important to employ efficient integral-direct or multipole expansion techniques to improve the computational efficiency than to optimize the calculation of integrals over the small component basis.

For small molecules, molecular symmetry may of course also help to increase computational efficiency. In the two-spinors expansion one can resort directly to double group symmetry and apply projection operators or other techniques to create the appropriate symmetric linear combinations of atomic two-spinors. When scalar functions are chosen as expansion basis it is natural to first adapt these using non-relativistic point group symmetry and then combine the resulting functions to obtain double group symmetry adapted functions. In that case one may combine the symmetry adaption of scalar basis functions to single point groups with time reversal symmetry in a quaternion symmetry scheme [52, 53]. The sidestep via non-relativistic symmetry adapted functions also has advantages when approximate, in particular so-called spinfree, algorithms are considered. If one has defined a basis in which the large component scalar functions transform according to the irreps of the appropriate single point group and the small component functions are related by the kinetic balance relation, it becomes possible to identify spin-orbit couplings as arising due to the off-diagonal matrix elements of the Fock operator. Neglecting these contributions becomes then identical to solving the spinfree modified Dirac equation of section 1.1.4 [57, 62] . While this is not very important in the Hartree-Fock stage it offers major saving in the electron correlation procedure. It means that correlation calculations can be carried out using non-relativistic algorithms and implementations. This will be discussed in more detail in the next section.

3.2 Electron correlation methods

The electron correlation methods available for 4-component methods are derived from non-relativistic counterparts. As discussed in section 2.4 a no-pair Hamiltonian (6.111) with fully relaxed projection operators is accessible only at the MCSCF level, where orbital rotations are included.

At the CI or CC level the "best" choice of no-pair Hamiltonian is the one defined by the Hartree-Fock (or MCSCF) orbitals. The generation of the matrix elements appearing in the no-pair Hamiltonian (6.112) is rather costly since it involves summation of integrals over both the large and small component type basis sets. In the scalar expansion scheme this is conveniently expressed in quaternion algebra [108] and gives the following expression in terms of electron repulsion integrals over scalar functions

$$g_{pqrs}^{\Lambda_{12}\Lambda_{34}} = \sum_{X}^{L,S}\sum_{Y}^{L,S}\sum_{\mu,\nu}^{N_X}\sum_{\kappa,\lambda}^{N_Y} B_{\mu\nu,pq}^{XX,\Lambda_{12}} g_{\mu\nu\kappa\lambda}^{XXYY} B_{\kappa\lambda,rs}^{YY,\Lambda_{34}} \quad (\Lambda_{12},\Lambda_{34}=0,1,2,3) \tag{6.140}$$

where the B-matrices are quaternion density matrices

$$B_{\mu\nu,pq}^{XX,\Lambda_{12}} e_{\Lambda_{12}} = \sum_{\Lambda_1=0}^{3}\sum_{\Lambda_1=0}^{3} c_{\mu p}^{X,\Lambda_1} c_{\nu q}^{X,\Lambda_2} e_{\Lambda_1}^{*} e_{\Lambda_2}. \tag{6.141}$$

Each quaternion integral $g_{pqrs}^{\Lambda_{12}\Lambda_{34}}$ can be expressed as a sum of 16 individual real numbers multiplied by a quaternion phase $e_{\Lambda_{12}}$ for electron 1 and a quaternion phase $e_{\Lambda_{34}}$ for electron 2. This is fully equivalent to the more conventional notation in terms of barred and unbarred partners of Kramers pairs. One can see that the effect of spin-orbit coupling translates into making the density matrices complex instead of real, while the use of a 4-component instead of a 2-component formalism leads to the additional summation over the small component basis functions. Together this makes the 4-index formation step, though still scaling as a fifth power with the number of basis functions, much more costly than the same step in non-relativistic calculations. Let M be the number of active Kramers pairs (or spatial orbitals in the non-relativistic case) in a correlated calculation. Pernpointner et al. [109] take the realistic assumption that the primitive small component basis is about twice the size of the primitive large component basis, that is $N_S \approx 2N_L$ and arrive using $M = N_L$ at a non-relativistic/relativistic operation count ratio of 1:130 for the first halftransformation and a ratio of 1:88 for the second halftransformation. The increase in the first steps is largely due to the presence of the small component basis set, while that in the last steps is caused by the coupling of the spin and spatial degrees of freedom. The computational scaling in the first steps can be reduced by using two-spinor expansion functions (so that $N_S = N_L$) and/or by using one-center approximations and it is probable that this will not present a major problem in the near future. The limiting ratio will then be that of a two-spinor algorithm that gives a scaling of 1:10 in the first halftransformation and 1:24 in the second. The later steps remain more demanding due to the fact that

spin-orbit couplings, that are neglected in a purely non-relativistic theory, are taken into account. This gives a shift from real to complex or quaternion algebra and a loss of permutational symmetry. Here one may only improve the scaling in cases that these couplings are so small that approximate algorithms can be used. This is similar to the situation with 2-component methods where spin-orbit coupling are often neglected in the Hartree-Fock procedure and introduced in a CI step. Precisely the same treatment with similar computational gains (and loss of accuracy in some cases) is possible for the 4-component scheme. After the index transformation we end up with a second quantized Hamiltonian that can be used in various correlation treatments. The computations are then identical to those necessary in 2-component calculations.

A number of algorithms and implementations have been developed that tackle the electron correlation problem in the 2- or 4-component no-pair approximation. We will here only consider the algorithms that assume true 4- or 2-spinors and not the methods that neglect the effect on spin-orbit couplings in the Hartree-Fock stage. For more complete descriptions of the algorithms we refer to a recent overview by one of us [110]. In this review we will focus on the computational scaling of these methods.

The computationally most efficient treatment is given by many-body perturbation theory, in particular MP2. Since one only needs to sum transformed integrals divided by the orbital energy differences, this method allows for integral-direct implementations, thus opening up for application to larger systems. The method has as drawback that it is only applicable in cases were a single determinant reference already gives a reasonable description of the system. The computational scaling is identical to that of the index transformation step because the summation of the transformed integrals themselves takes a negligible amount of time.

The CI-type methods are more flexible but computationally less efficient and, more importantly, lack the correct scaling of energy with system size. This restricts their application to relatively small model systems in which they can give results close enough to the full CI limit. As orbital generator usually an average-of-configuration Hartree-Fock procedure is used, but work MCSCF algorithms is underway [20]. The computational scaling depends much on the actual implementation and on the type of CI that is used.

The last class of *ab initio* correlated method are the coupled cluster type approaches. They share with the perturbation theory type methods the features of size-extensivity and reasonable computational efficiency, but also the requirement that the reference wave function should be simple. Application of these type of relativistic methods to atoms has been

pioneered by the groups of Lindgren [111] and Kaldor [112,113] who have shown that almost arbitrary accuracy can be reached once a sufficient number of one-particle functions (up to i-type functions) and excitation level is used. While such accurate treatments are feasible due to the high symmetry and relatively few electrons to be correlated in atomic systems, this is still out of reach for molecular applications. It is possible to formulate the theory entirely in terms of Kramers' pairs instead of individual spinors but the corresponding algorithms have not yet been fully developed for the general case. The unrestricted CCSD(T) algorithm that has been implemented can be routinely applied to diatomics but larger systems and basis sets beyond triple or quadruple zeta level are usually still too demanding. These systems are smaller than feasible with efficient non-relativistic implementations of CC methods, which is mainly due to the limiting steps in the necessary index transformation that make this step often more expensive or cumbersome (due to the necessary diskspace and I/O) than the coupled cluster step itself. This situation will improve due to the increasing performance of computer hardware and the development of more efficient (parallel) algorithms, but unless approximations are made that break the notorious seventh power scaling with system size the coupled cluster algorithms will remain only applicable to relatively small systems.

The latter problem is in fact shared among all the correlation methods and is no different from the situation in non-relativistic quantum chemistry. However, while in non-relativistic quantum chemistry rewriting of the algorithms in the atomic orbital basis combined with approximation of long-range interactions via multipole expansions [114,115] permits the development of algorithms that scale much better with system size [116], this is cumbersome in the relativistic case. In order to make AO-direct algorithms feasible one also needs to take into account the large difference in size between the active spinor set and the complete basis set. It is quite common to correlate only 10 % of the electrons in a system, using only the lowest lying virtual spinors. This makes the AO list of functions much longer than MO-list and it takes larger systems before the gain due to approximate treatment of long-range effects starts to pay off. This leaves the implementers of methods with a difficult choice : In the long run one will see that computations for system sizes for which the effort of using AO-based algorithms pays off are easily feasible and that this then enables much larger computations. In the current situation it is, however, still more efficient to use MO-based algorithms.

The observations regarding the computational scaling of the various steps in a conventional *ab initio* calculation (using scalar basis functions) are summarized in table 6.3. The first steps show a linear dependence

on the number of primitive integrals that need to be calculated and contracted with the density matrix. The factors a, b and c depend on the type of basis functions contained in the integrals. Factor c will in general be larger then a because the small component basis contains higher angular momentum type functions than the large component basis. This is the main reason that relativistic Hartree-Fock calculations for small molecules are so much more expensive than comparable non-relativistic calculations. The difference in algebra (quaternion instead of real) furthermore reduces the permutational symmetry of the density matrix making the Fock matrix building and diagonalization procedure more expensive. This algebra difference also shows up in two-spinor methods where the presence of two-electron spin-orbit integrals increases the computation time by a constant factor relative to non-relativistic calculations. Index transformation of two-electron integrals exhibits the well-known fifth order scaling with the number of basis functions. In the transformation of the first two indices one sees mainly the effects of the small component basis set. In the second halftransformation the effect of spin-orbit couplings start to dominate making the scaling of full Dirac-Coulomb and two-spinor approaches comparable. They become fully equivalent in the last step (taken here as a CCSD calculation since this algorithm has been analyzed in detail previously [117]) where the variational inclusion of spin-orbit coupling leads to a 32-fold increase in operation count. The numbers presented here are theoretical estimates and actual measurements may give a somewhat different picture depending on efficiency of implementation and convergence of iterative procedures. Still, we think that it is useful to have such estimates, — both as a guideline for the efficiency of implementation and for the development of a long term strategy. We can for instance deduce that molecules may as well be treated with relativistic coupled cluster methods based on the spinfree Dirac-Coulomb equation than by other scalar relativistic or non-relativistic counterparts since the rate-determining step is the CCSD step which outscales the preliminary Hartree-Fock or index transformation steps. Including spin-orbit coupling increases the computational time, regardless of whether this is done in a 2- or a 4-spinor algorithm. This trend that is already visible in large basis set calculation on diatomics will become even stronger once more powerful computers that allow larger molecules to be treated become available. On the other hand, if we move to the large systems still inaccessible by current coupled cluster algorithms and use only Hartree-Fock or DFT methods we see that the inclusion of spin-orbit couplings is less crucial. The effort should go into the efficient evaluation or approximation of integrals over the small component basis set. For such larger systems one can then use

the effect of the locality of the small component wave function making integrals prescreening and/or one-center expansion methods take effect.

Table 6.3 Theoretical operation counts of steps in a correlated calculation for different approximation of the Dirac Coulomb no-pair Hamiltonian. 2-Spinor is any method that works with frozen no-pair projection operators but keeps the spin-orbit couplings, Spinfree is any method that varies the projection operators but neglects spin-orbit couplings. N is the number of basis functions (with subscripts referring to Large or Small component where appropriate). M is the number of active orbitals or Kramers' pairs (with the subscripts for the CCSD algorithm referring to the subsets of Occupied or Virtual orbitals). The steps considered are: A)Integral evaluation/Hartree-Fock/DFT, B)Index transformation, step 1, C)Index transformation, step 2, D) CCSD

	Non-Relativistic	Spinfree
A	$\frac{1}{8}aN^4$	$\frac{1}{8}\left(aN_L^4 + 4bN_S^2N_L^2 + 4cN_S^4\right)$
B	$\frac{1}{2}MN^4 + \frac{1}{2}M^2N^3$	$\frac{1}{2}M\left(N_L^4 + 4N_S^2N_L^2 + 4N_S^4\right) +$ $+\frac{1}{2}M^2\left(N_L^3 + 4N_SN_L^2 + 4N_S^3\right)$
C	$\frac{1}{2}M^3N^2 + \frac{1}{2}M^4N$	$\frac{1}{2}M^3\left(N_L^2 + 4N_S^2\right) + \frac{1}{2}M^3\left(N_L + 4N_S\right)$
D	$\frac{1}{4}M_o^4M_v^2 + 4M_o^4M_v^2 + \frac{1}{2}M_o^2M_v^4$	$\frac{1}{4}M_o^4M_v^2 + 4M_o^4M_v^2 + \frac{1}{2}M_o^2M_v^4$
	2-spinor	Dirac-Coulomb
A	$\frac{1}{2}aN^4$	$\frac{1}{2}\left(aN_L^4 + bN_S^2N_L^2 + cN_S^4\right)$
B	$2MN^4 + 8M^2N^3$	$2M\left(N_L^4 + N_S^2N_L^2 + N_S^4\right) +$ $+8M^2\left(N_L^3 + N_SN_L^2 + N_S^3\right)$
C	$4M^3N^2 + 16M^4N$	$4M^3\left(N_L^2 + N_S^2\right) + 16M^4\left(N_L + N_S\right)$
D	$8M_o^4M_v^2 + 128M_o^4M_v^2 + 16M_o^2M_v^4$	$8M_o^4M_v^2 + 128M_o^4M_v^2 + 16M_o^2M_v^4$

4. Conclusion

In this chapter we have discussed 4-component relativistic methods and in particular the challenges that arise when extending the application of these methods from atomic to molecular systems, notably arising from the introduction of the algebraic approximation. We have analyzed in detail the variational stability of the Dirac-Coulomb-(Gaunt/Breit) Hamiltonian by comparing the standard approach to 4-component relativistic molecular calculations with QED in the semiclassical limit. We find that we recover the formulas of the standard approach by deleting vacuum polarization from semiclassical QED. The effect is, however, that the minimization principle of QED is replaced by a minimax principle in the standard approach, due to the fact that in QED all negative-energy orbitals are filled whereas they are empty and treated as an orthogonal complement in the standard approach. The standard approach employs a (and not "the" !) no-pair Hamiltonian which corresponds to

surrounding the relativistic many-electron Hamiltonian by projection operators. Contrary to approximate 1-or 2-component approximations the 4-component methods allows a continuous update of the projection operators and thereby of the no-pair Hamiltonian and thus allows a complete relaxation of the electronic wave function to the actual potential of the system.

We insist on the distinction between Hamiltonians and methods. It is then easier to see that the difference in computational cost of relativistic and non-relativistic calculations is a difference in prefactor rather than order, and so it is not like comparing DFT with CCSD. Through a careful analysis of computational cost we furthermore show that one must distinguish the extra computational cost arising from the introduction of larger basis sets, notably the separate expansion of the large and small components, from the cost arising from the transition from non-relativistic to relativistic symmetry, that is the introduction of spin-orbit coupling. This latter contribution is identical at the 2- and 4-component level of theory. We consider how the computational cost can be reduced by exploiting symmetry, in particular time reversal symmetry, and the atomic nature of the small component density. We also outline the dilemma facing the programmer on whether he should choose a scalar basis expansion which allows him to benefit from the continuous development of (integral) codes in the non-relativistic domain or whether he should choose the more natural expansion in terms of 2-spinors which requires a more dedicated programming effort. The area of 4-component relativistic molecular methods continues to be an area of challenge and promise.

References

[1] Wilson S., (2001) *J. Mol. Struct. (Theochem)* **547**, 279.

[2] Grant I.P., (1961) *Proc. R. Soc. London A* **262**, 555.

[3] Schwarz W.H.E., and Wallmeier H., (1982) *Mol. Phys.* **46**, 1045.

[4] Schwarz W.H.E., and Wechsel-Trakowski E., (1984) *Chem. Phys. Lett.* **85**, 94.

[5] Brown G. E., and Ravenhall D. G., (1951) *Proc. Roy. Soc. London A* **208**, 552.

[6] Grant I. P., and Quiney H. M., (1988) *Adv. At. Mol. Phys.* **23**, 37.

[7] Engel E., (1995) *Int. J. Quant. Chem.* **56**, 217.

[8] Swirles B., (1935) *Proc. Roy. Soc. (London) A* **152**, 625.

[9] Matsuoka O., Suzuki N., Aoyama T., and Malli G., (1980) *J. Chem. Phys.* **73**, 1320.

[10] Aoyama T., Yamakawa H., and Matsuoka O., (1980) *J. Chem. Phys.* **73**, 1329.

[11] McClean A.D., and Lee Y.S., (1982) in *Current Aspects of Quantum Chemistry* R. Carbo (ed.), Elsevier.

[12] Visscher L., Visser O., Aerts P.J.C., Merenga H. and Nieuwpoort W.C., (1994) *Comp. Phys. Comm.* **81**, 120.

[13] Dyall K.G., Taylor P.R., Faegri K. jr. and Partridge H., (1991) *J. Chem. Phys.* **95**, 2583.

[14] Saue T., Faegri K. jr., Helgaker T., and Gropen O., (1997) *Mol. Phys.* **91**, 937.

[15] Quiney H.M., Skaane H., and Grant I.P., (1997) *J. Phys. B* **30**, L829.

[16] Yanai T., Nakajima T., Ishikawa Y., and Hirao K., (2001) *J. Chem. Phys.* **114**, 6526.

[17] Dyall K.G., (1994) *Chem. Phys. Lett.* **224**, 186.

[18] Laerdahl J.K., Saue T., and Faegri K. jr., (1997) *Theor. Chem. Acc.* **97**, 177

[19] Jensen H.J.Aa., Dyall K.G., Saue T., and Faegri K. jr., (1996) *J. Chem. Phys.* **104**, 4083.

[20] Thyssen J., (2001) *Ph. D. thesis*, University of Southern Denmark.

[21] Visscher L., Saue T., Nieuwpoort W.C., Fægri K. jr. and Gropen O., (1993) *J. Chem. Phys.* **99**, 6704.

[22] Visscher L., Lee T.J. and Dyall K.G., (1996) *J. Chem. Phys.* **105**, 8769.

[23] Visscher L., Eliav E., and Kaldor U., (2001) *J. Chem. Phys.* **115**, 759.

[24] Varga S., Engel E., Sepp W.-D., and Fricke B., (1999) *Phys. Rev. A* **59**, 4288.

[25] Liu W.J., Hong G.Y., Dai D.D., Li L.M., and Dolg M., (1997) *Theor. Chem. Acc.* **96**, 75.

[26] Yanai T., Iikura H., Nakajima T., Ishikawa Y., and Hirao K., (2001) *J. Chem. Phys.* **115**, 8267.

[27] Saue T., and Helgaker T., (2002) *J. Comp. Chem.* **23**, 814.

[28] Szabo A., and Ostlund N., (1989) *Modern quantum chemistry: introduction to advanced electronic structure theory*, McGraw-Hill, New York.

[29] McWeeny R., (1992) *Methods of Molecular Quantum Mechanics*, Academic Press, London.

[30] B. O. Roos (ed.) (1992) *Lecture Notes in Quantum Chemistry - European Summer School in Quantum Chemistry.*, Lecture Notes in Chemistry **58** Springer, Berlin; (1994) *Lecture Notes in Quantum Chemistry II - European Summer School in Quantum Chemistry.*, Lecture Notes in Chemistry **64** Springer, Berlin.

[31] Helgaker T., Jørgensen P., and Olsen J., (2000) *Molecular Electronic Structure Theory*, John Wiley & Sons, Ltd, Chichester.

[32] Fischer C.F., (2000) *Mol. Phys.* **98**, 1043.

[33] Dirac P.A.M., (1928) *Proc. Roy. Soc. London A* **117**, 714.

[34] Dirac P.A.M., (1928) *Proc. Roy. Soc. London A* **118** 351.

[35] Sakurai J.J., (1967) *Advanced Quantum Mechanics*, Addison-Wesley, Reading, Massachusetts.

[36] Poole C.P., and Farach H.A., (1982) *Found. Phys.* **12**, 719.

[37] R. E. Moss R.E., (1973) *Advanced Molecular Quantum Mechanics*, Chapmann and Hall, London.

[38] Gell-Mann M., (1956) *Nuovo Cimento Suppl.* **4**, 848.

[39] Schwarzschild K., (1903) *Gött. Nach. Math.-Phys. Kl.*, 126.

[40] Saue T., in *Relativistic Electronic Structure Theory. Part 1. Fundamental Aspects*, P. Schwerdtfeger (ed.), Elsevier, to be published.

[41] Schrödinger E., (1930) *Sitzungsber. Phys. Math. Kl.*, 418.

[42] Jackson J.D., and Okun L.B., (2001) *Rev. Mod. Phys.* **73**, 663.

[43] Bloch F., (1961) in *W. Heisenberg und die Physik unserer Zeit*, F. Bopp (ed.), Vieweg & Sohn, Braunschweig.

[44] Griffith D.J., (1999) *Introduction to Electrodynamics*, Prentice-Hall, Upper Saddle River, New Jersey.

[45] Cohen-Tannoudji C., Dupont-Roc J., and Grynberg G., (1987) *Photons et atomes*, Savoirs Actuels, New York.

[46] Heaviside O., (1889) *Philos. Mag., Ser.5* **27**, 324.

[47] Darwin C.G., (1920) *Phil.Mag.* **39**, 537.

[48] Born M. and Oppenheimer J.R., (1927) *Ann. Phys.* **84**, 457.

[49] Kutzelnigg W., (1997) *Chem. Phys.* **225**, 203.

[50] Wigner E., (1932) *Nachrichten der Akad. der Wissensch. zu Göttingen,II,* 546.

[51] Pauli W., (1927) *Z. Phys.* **43**, 601, see footnote 2 on page 607.

[52] Saue T., and Jensen H.J.Aa., (1999) *J. Chem. Phys.* **111**, 6211.

[53] Saue T. and Jensen H.J.Aa., (2000) in *Mathematical Methods for Ab Initio Quantum Chemistry*, M. Defrancheschi and C. Le Bris (eds.), Lecture Notes in Chemistry, Springer, Berlin.

[54] Dirac P.A.M., (1930) *Proc. Roy. Soc. London A* **126**, 360.

[55] Dirac P.A.M., (1932) *Proc. Roy. Soc. London A* **133**, 60.

[56] Anderson C.D., (1932) *Phys.Rev.* **41**, 405.

[57] Visscher L., and Saue T., (2000) *J. Chem. Phys.* **113**, 3996.

[58] Faegri K. jr., and Saue T., (2001) *J. Chem. Phys.* **115**, 2456.

[59] Kutzelnigg W., (1989) *Z. Phys. D.* **11**, 15.

[60] Lévy-Leblond J.-M., (1967) *Commun. Math. Phys.* **6**, 286.

[61] Hennum A.C., Klopper W. and Helgaker T., (2001) *J. Chem. Phys.* **115**, 7356.

[62] Dyall K.G., (1994) *J. Chem. Phys.* **100**, 2118.

[63] Visscher L., and van Lenthe E., (1999) *J. Chem. Phys.* **306**, 357.

[64] Chraplyvy Z.V., (1953) *Phys.Rev.* **91**, 388; (1953) *ibid.* **92** 1310.

[65] Barker W.A., and Glover F.N., (1955) *Phys.Rev.* **99**, 317.

[66] Itoh T., (1965) *Rev. Mod. Phys.* **37**, 159.

[67] Sjovoll M., Fagerli H., Gropen O., Almlof J., Saue T., Olsen J., and Helgaker T., (1997) *J. Chem. Phys.* **107**, 5496.

[68] Breit G., (1929) *Phys.Rev.* **34**, 553.

[69] Saue T., (1996) *Ph. D. thesis*, University of Oslo.

[70] Visser O., Visscher L., Aerts P.J.C., and Nieuwpoort W.C., (1992) *Theor. Chim. Acta* **81**, 405.

[71] Quiney H.M., Skaane H., and Grant I.P., (1998) *Chem. Phys. Lett.* **290** 473.

[72] Dirac P.A.M., (1927) *Proc. Roy. Soc. London A* **113**, 243.

[73] Jordan P., (1927) *Zeit. Phys.* **44**, 473.

[74] Jordan P., and Wigner E., (1928) *Zeit. Phys.* **47**, 631.

[75] Fock V., (1932) *Zeit. Phys.* **75**, 622.

[76] Jordan P., (1932) *Zeit. Phys.* **75**, 648.

[77] Furry W.H., (1951) *Phys. Rev.* **81**, 115.

[78] Sucher J., (1980) *Phys. Rev.* **22**, 348.

[79] Sucher J., (1984) *Int. J. Quant. Chem.: Quant. Chem. Symp.* **25**, 3.

[80] Kutzelnigg W., (1987) *Phys. Scr.* **36**, 416.

[81] Dunning T.H. and McKoy V., (1967) *J. Chem. Phys.* **47**, 1735.

[82] Talman J.D., (1986) *Phys. Rev. Lett.* **57**, 1091.

[83] Chaix P., and Iracane D., (1989) *J. Phys. B: At. Mol. Opt. Phys.* **22**, 3791; (1989) *ibid.* **22**, 3815.

[84] Greiner W., (1990) *Relativistic Quantum Mechanics*, Springer-Verlag, Berlin.

[85] Wick G.C., (1950) *Phys. Rev.* **80**, 268.

[86] Fulde P., (1995) *Electron Correlation in Molecules and Solids*, Springer, Berlin.

[87] Rajagopal A.K., and Callaway J., (1973) *Phys. Rev. B* **7**, 1912.

[88] Mittleman M.H., (1981) *Phys. Rev. A* **24**, 1167.

[89] Barysz M., and Sadlej A.J., (2001) *J. Mol. Struct.* THEOCHEM **573**, 181.

[90] Bunge C.F., Jauregui R., and Ley-Koo E., (1998) *Int. J. Quant. Chem.* **70**, 805.

[91] Bethe H.A., and Salpeter E.E., (1957) *Quantum mechanics of one- and two-electron atoms*, Springer, Berlin.

[92] Visscher L. and Dyall K.G., (1997) *At. Data Nucl. Data Tables* **67**, 207.

[93] Aerts P.J.C., (1986) *Ph. D. thesis*, University of Groningen.

[94] Matsuoka O., (1992) *J. Chem. Phys.* **97** 2271.

[95] McMurchie L.E., and Davidson E.R., *J. Comp. Phys.* **26**, 218 (1978).

[96] Stanton R.E., and Havriliak S., (1984) *J. Chem. Phys.* **81**, 1910.

[97] Dyall K.G., Grant I.P. and Wilson S., (1984) *J. Phys. B* **17**, 493.

[98] Faegri K. jr., (2001) *Theor. Chem. Acc.* **105**, 252.

[99] Saue T., Faegri K. jr., and Gropen O., (1996) *Chem. Phys. Lett.* **263**, 360.

[100] Dyall K.G., (1997) *J. Chem. Phys.* **106**, 9618.

[101] Dyall K.G., (1998) *J. Chem. Phys.* **109**, 4201.

[102] Dyall K.G., and Enevoldsen T., (1999) *J. Chem. Phys.* **111**, 10000

[103] Dyall K.G., (2001) *J. Chem. Phys.* **115**, 9136.

[104] Visscher L., Aerts P.J.C., Visser O., and Nieuwpoort W.C., (1991) *Int. J. Quant. Chem.: Quant. Chem. Symp.* **25**, 131.

[105] Matsuoka O., (1992) *Chem. Phys. Lett.* **195**, 184.

[106] Visscher L., (1997) *Theor. Chem. Acc.* **98**, 68.

[107] de Jong G. Th., and Visscher L., *Theor. Chem. Acc.* published online at http://dx.doi.org/10.1007/s002140020335.

[108] Visscher L., (2002) *J. Comp. Chem.* **23**, 759.

[109] Pernpointner M., Visscher L., de Jong W.A., and Broer R., (2000) *J. Comp. Chem.* **21**, 1176.

[110] Visscher L., in P. Schwerdtfeger(ed.), *Relativistic Electronic Structure Theory. Part 1. Fundamental Aspects*, Elsevier, to be published.

[111] Lindgren I., and Morrison J., (1986) *Atomic Many-Body Theory*, Springer-Verlag, Berlin.

[112] Kaldor U., (1988) *Phys. Rev. A* **38**, 6013; (1998) *J. Chem. Phys.* **88**, 5248.

[113] Kaldor U., (1991) *Theor. Chim. Acta* **80**, 427.

[114] White C.A., Johnson B., Gill P., and Head-Gordon M., (1994) *Chem. Phys. Lett.* **230**, 8.

[115] Schwegler E., and Challacombe M., (1996) *J. Chem. Phys.* **105**, 2726.

[116] Schutz M., and Werner H.-J., (2001) *J. Chem. Phys.* **114**, 661.

[117] Visscher L., Dyall K.G., and Lee T.J., (1995) *Int. Journal of Quant. Chem. : Quant. Chem. Symp.* **29**, 411.

Chapter 7

RELATIVISTIC ELECTRON CORRELATION THEORY

Yasuyuki Ishikawa
Department of Chemistry and The Chemical Physics Program, University of Puerto Rico, San Juan, PR 00931-3346 USA
ishikawa@rrpac.upr.clu.edu

Marius J. Vilkas
Department of Chemistry and The Chemical Physics Program, University of Puerto Rico, San Juan, PR 00931-3346 USA
marius@hpcf.upr.edu

Abstract Accurate determination of relativistic correlation corrections, nondynamic and dynamic, is crucial to the prediction of term energy separations and transition probabilities of heavy atom systems. Relativistic and correlation effects are strongly intertwined and play an essential role in the electronic structure of many-electron systems and they must be approached with a relativistic many-body theory that simultaneously account for relativity and electron correlation. Relativistic dynamic correlation energies of the ground-state noble gas atoms, Ne through Rn, systems in which quasidegeneracy is absent, are computed by means of a single-configuration Dirac-Fock-Breit self-consistent field and relativistic Møller-Plesset perturbation theory based on the no-pair Dirac-Coulomb-Breit Hamiltonian. Nondynamic and dynamic correlation energies of Zn and Pb are computed by means of a recently developed relativistic multireference many-body perturbation theory. These are among the systems in which quasidegeneracy in both the ground and excited states mandate multireference perturbation theory. The contribution to transition energies of the Coulomb and Breit correlation corrections in Zn and Pb are analyzed in detail.

Keywords: Relativistic many-body perturbation theory, Dirac-Coulomb-Breit correlation corrections.

U. Kaldor and S. Wilson (eds.),
Theoretical Chemistry and Physics of Heavy and Superheavy Elements, 269–324.
© 2003 *Kluwer Academic Publishers.*

Introduction

Since important physical and chemical processes involve heavy atoms, there has been increasing interest in the last decade in the accurate description of the electronic structures of heavy atoms, ions and heavy-atom-containing molecules [1–15]. For accurate calculations of heavy-atom systems, it is necessary to discard the Schroedinger equation in favor of the Dirac equation. Although the study of truly many-electron systems is increasing, accurate *ab initio* Dirac 4-spinor calculations on heavy atoms and on molecules that contain heavy atoms are scarce. There are reasons for this scarcity. Heavy-atom species are many-electron systems with very complicated multiplet state structures that push computational techniques to their limits. And relativistic and correlation effects are so important that extant techniques are unsatisfactory; they must be approached with a relativistic many-body theory that simultaneously accounts for relativity and electron correlation. Because relativistic and correlation effects are intertwined and play an essential role in the electronic structure of many-electron atoms and molecules, relativistic many-body perturbation theory (MBPT) [16–19] and relativistic coupled cluster theory (CC) [20–34], have become the subject of active research interest in the last decade.

Construction of an effective many-body theory, e.g., relativistic MBPT and CC, that accurately accounts for both relativistic and electron correlation effects in many-electron systems is a difficult task. Theoretical methods developed to describe the structure of many-electron systems must yield wave functions which can be refined to account for relativistic, electron-correlation and quantum electrodynamic (QED) effects. At the same time they should be accurate, and whatever defects they may have should be consistent and well characterized. They must be computationally efficient because they will have to eventually describe electronic effects in systems which contain very large numbers of electrons. Finally, an approximation should provide wavefunctions which are compact and easy to interpret chemically. These are properties which have caused the wide application of the relativistic version of the basis set expansion Hartree-Fock self-consistent field (HF SCF) method, the so-called matrix Dirac-Fock self-consistent field (DF SCF) method, and its many-body theoretical refinements.

In the next section, effective relativistic N-electron Hamiltonian, the so-called no-pair Dirac-Coulomb-Breit (DCB) Hamiltonian, is introduced and Dirac-Fock-Breit (DFB) self-consistent field (SCF) theory based on the no-pair DCB Hamiltonian discussed. Relativistic Dirac-Coulomb (DC) and Dirac-Coulomb-Breit (DCB) correlation energies are defined.

Single-configuration DFB SCF and relativistic Møller-Plesset (MP) perturbation theory based on the no-pair DCB Hamiltonian is employed to calculate dynamic correlation energies of the ground-state noble gas atoms, Ne through Rn, systems in which quasidegeneracy is absent. In section 2, relativistic nondynamic and dynamic correlation energies of Zn and Pb have been computed by means of a recently developed relativistic multireference many-body perturbation theory (MR-MBPT). These are among the systems in which quasidegeneracy in both the ground and excited states mandate multireference perturbation theory. Analytic basis sets of G spinors (G for "Gaussian") are employed to expand the upper and lower components of the Dirac 4-spinors in the matrix DFB SCF and relativistic many-body perturbation procedures. The effects of the low-frequency Breit interaction on relativistic many-body effects are analyzed. The contributions to transition energies of the DC and Breit correlation corrections are examined in detail.

1. Relativistic electron correlation theory

1.1 The relativistic no-pair Dirac-Coulomb-Breit Hamiltonian

The relativistic many-body Hamiltonian cannot be expressed in closed potential form. This difficulty has to do with the requirement of relativistic covariance in many-body systems and with separation of electrons from positrons, which are not considered in low-energy, atomic and molecular electronic structure calculations. Unlike the Lagrangian in which dynamical variables are expressed in terms of relativistically invariant space-time intervals between interacting particles, the Hamiltonian approach picks out a particular time frame, making it impossible to construct a manifestly covariant theory. However, relativistic many-body theory for atoms and molecules may be developed by employing an effective many-body Hamiltonian expressed in terms of an effective electron-electron interaction derived with arbitrary accuracy from QED. In c-number theory, an approximate relativistic N-electron Hamiltonian (in atomic units) most commonly used for relativistic many-body calculations is the so-called relativistic "no-pair" DC Hamiltonian [35, 36],

$$H_{DC}^{+} = \sum_{i}^{N} h_D(i) + \mathcal{L}_+ \left(\sum_{i>j}^{N} \frac{1}{r_{ij}} \right) \mathcal{L}_+. \tag{7.1}$$

In the no-pair DC Hamiltonian, one-electron effects are treated relativistically while two-electron effects are nonrelativistic. $\mathcal{L}_+ = L_+(1) L_+(2) \ldots L_+(N)$, where $L_+(i)$ is the projection operator onto the space

$D^{(+)}$ spanned by the positive-energy eigenfunctions of the matrix DF SCF equation [36]. $\mathcal{L}_+$ is the projection operator onto the positive-energy space $\mathcal{D}^{(+)}$ spanned by the N-electron configuration-state functions (CSFs) constructed from the positive-energy eigenfunctions ($\in D^{(+)}$) of the matrix DF SCF. In this form, the no-pair Hamiltonian is restricted to contributions from the positive-energy branch of the DF spectrum. It formally takes into account the field-theoretic condition that the negative-energy states are filled and causes the projected DC Hamiltonian to have normalizable bound-state solutions. This approach is called the no-pair approximation [35] because virtual electron-positron pairs are not permitted in the intermediate states. The eigenfunctions of the matrix DF SCF equation clearly separate into two discrete manifolds, $D^{(+)}$ and $D^{(-)}$, respectively, of positive-energy and negative-energy states. As a result, the positive-energy projection operators can be accommodated easily in many-body calculations. The formal conditions on the projection are automatically satisfied when only the positive-energy spinors ($\in D^{(+)}$) are employed. h_D is the Dirac one-electron Hamiltonian (in a.u.)

$$h_D(i) = c(\alpha_i \cdot \mathbf{p}_i) + (\beta_i - 1)c^2 + V_N(r_i). \tag{7.2}$$

Here α and β are the 4×4 Dirac vector and scalar matrices, respectively. c is the speed of light (c = 137.0359895 a.u.). $V_N(r)$ is the nuclear potential, which for each nucleus takes the form

$$V_N(r) = \{ \begin{array}{c} -\frac{Z}{r}, r > R_n, \\ -\frac{Z}{2R_n}(3 - \frac{r^2}{R_n^2}), r \leq R_n \end{array} . \tag{7.3}$$

The nuclei are modeled as spheres of uniform proton-charge distribution; Z is the nuclear charge. R_n (bohr) is the radius of that nucleus and is related to the atomic mass, A (amu), by $R_n = 2.2677 \cdot 10^{-5} A^{1/3}$. The extended representation of the nuclei eliminates the singularity of the electron-nuclear Coulomb potential of point nuclear charge, an artifact which causes singularities in the wavefunction.

Because the electron-electron interaction is approximated by the classical instantaneous Coulomb interactions, $1/r_{ij} = (1/r_{ij})\delta(t_{ij})$, the no-pair DC Hamiltonian is deficient in that it is both noncovariant and inaccurate for precision calculation of fine structure separations and binding energies of inner-shell electrons. The instantaneous Coulomb interaction, however, is the leading term of the covariant interaction in Coulomb gauge. A higher approximation involves modification of the instantaneous Coulomb interaction. The modification is derived from field theory and leads to a well-defined QED perturbation series with α, the

fine-structure constant, as an order parameter. Adding the frequency-independent Breit interaction,

$$B_{12} = -\frac{1}{2}[\alpha_1 \cdot \alpha_2 + (\alpha_1 \cdot \mathbf{r}_{12})(\alpha_2 \cdot \mathbf{r}_{12})/r_{12}^2]/r_{12}, \tag{7.4}$$

to the instantaneous electron-electron Coulomb interaction in Coulomb gauge introduces the leading effects of the transverse photon exchange in QED and remedies the lack of covariance of the no-pair DC Hamiltonian [35]. The Breit interaction is the $O(\alpha^2)$ correction to the instantaneous Coulomb interaction and describes effects attributable to the so-called "spin-spin" and "spin-other-orbit" interactions. Addition of the Breit term yields the no-pair DCB Hamiltonian [35,36]

$$H_{DCB}^{+} = \sum_{i}^{N} h_D(i) + \mathcal{L}_+ \left(\sum_{i>j}^{N} \frac{1}{r_{ij}} + B_{ij} \right) \mathcal{L}_+, \tag{7.5}$$

which is covariant to first order and increases the accuracy of calculated fine-structure splittings and inner-electron binding energies. Higher-order QED effects, which cannot be expressed in closed potential form, appear first in order α^3. These are 1) QED correction to the mass of an electron, the electron self-energy, and 2) corrections to the charge that cause short-range modifications of the Coulomb's Law, the so-called vacuum polarization. Together, these are referred to as the Lamb shift, which causes a discrepancy between the Dirac theory and experiment.

Inclusion of the Breit interaction in the effective electron-electron interaction results in an effective Hamiltonian which contains all effects through order α^2 [35]. Sucher argues that the no-pair DCB Hamiltonian [35] provides a satisfactory starting point for calculations on many-electron systems in the sense that it treats the electrons relativistically, treats the most important part of electron-electron interaction nonperturbatively, and puts the Coulomb and Breit interactions on the same footing in DFB SCF and MBPT calculations [37–40]. The instantaneous Coulomb and frequency-independent Breit interactions are treated as an integral part of the two-electron interaction in both the DFB SCF and MBPT calculations [37–40] in order to study the electron correlation induced by the Breit interaction.

The effective electron-electron interaction in the many-body Hamiltonian depends on the gauge employed, and many-body corrections evaluated numerically in terms of the frequency-independent forms of the Coulomb- and Feynman-gauge interactions may be different in no-pair theory. There is justification for choosing the Coulomb-gauge Breit operator in Eq. 7.4 in the "no-pair" N-electron Hamiltonian rather than

the simpler Gaunt interaction. In a recent study, Sucher [35] analyzed the apparent gauge dependence of the effective potentials between electrons derived in the Coulomb and Feynman gauges, and indicated that the Feynman-gauge form of the interaction should not be used in no-virtual-pair calculations because the leading-order relativistic effects are incompletely determined. Addition of the frequency-independent Breit interaction to the instantaneous Coulomb interaction provides covariance of the effective many-body Hamiltonian to first order and increases accuracy in fine-structure splittings and inner-shell binding energies [41].

1.2 Single-configuration matrix Dirac-Fock SCF for closed- and open-shell systems

Before we present matrix DFB SCF and many-body perturbation theory algorithms, we here outline the method of expansion in kinetically balanced G spinors and the importance of extended nuclear model for providing appropriate boundary conditions with the unbounded Dirac operator. Consider the wavefunction of a hydrogenic system whose upper and lower components are each expanded in sets of basis functions [42].

The radial Dirac equation is

$$h_D(r)\varphi_{n\kappa} = \varepsilon_{n\kappa}\varphi_{n\kappa} \tag{7.6}$$

where

$$h_D(r) = \begin{pmatrix} V_N & c\Pi_\kappa \\ c\Pi_\kappa^+ & V_N - 2c^2 \end{pmatrix} \tag{7.7}$$

with

$$\Pi_\kappa = -\frac{d}{dr} + \frac{\kappa}{r}, \Pi_\kappa^+ = \frac{d}{dr} + \frac{\kappa}{r} \tag{7.8}$$

Here

$$\varphi_{n\kappa} = \begin{pmatrix} P_{n\kappa}(r) \\ Q_{n\kappa}(r) \end{pmatrix} \tag{7.9}$$

where $P_{n\kappa}(r)$ and $Q_{n\kappa}(r)$ are referred to as the large and small component radial functions, respectively. $V_N(r)$ is the nuclear attraction term.

In basis set expansion calculations, the radial large and small components, $P_{n\kappa}(r)$ and $Q_{n\kappa}(r)$, respectively, are expanded in sets of basis functions, $\{X_{\kappa i}^L\}$ and $\{X_{\kappa i}^S\}$,

$$\begin{aligned} P_{n\kappa}(r) &= \Sigma_i X_{\kappa i}^L C_{n\kappa i}^L \\ Q_{n\kappa}(r) &= \Sigma_i X_{\kappa i}^S C_{n\kappa i}^S \end{aligned} \tag{7.10}$$

where $\{C_{n\kappa i}^L\}$ and $\{C_{n\kappa i}^S\}$ are linear variational parameters.

The Schrödinger equation is a single second-order partial differential equation with a squared momentum operator which is bounded below. The Dirac equation yields two coupled first-order equations with an unbounded momentum operator. One obtains two sets of (spatial) solutions, termed the large and small components of the wavefunction. Each of these is, in turn, associated with two spin functions. The wavefunction is composed of 4-component spinors, the spatial parts of which are coupled. Because of this coupling, if one seeks to expand the large and small components in basis sets, care must be taken in choosing the sets of basis functions that they satisfy proper boundary conditions at the origin and that they do not form an unbalanced representation of the components [42–45].

The bound-state spectra of atoms are bounded below, and the bound electronic levels in the Dirac Hamiltonian are bounded below in much the same way as the corresponding Schrodinger Hamiltonian. Thus, if care is taken with the sets of basis functions, one can proceed exactly the way one does in nonrelativistic basis set expansion calculations. However, the Dirac four-component spinors have a rich internal structure and it has been shown that ignoring the need for some criterion of basis set balance can easily produce variational failure [42–47]. In fact the absence of a criterion by which to judge balance in basis sets was the major barrier to the practical application of the matrix DF SCF method to atoms and molecules. It has also been shown that spurious solutions may be obtained if the basis functions do not properly represent the behavior of the wave function in the high field region near the nucleus [2,42,43]. We here discuss how to choose proper sets of basis functions in applications of the basis set expansion method to the one-electron Dirac equation. We then examine the applications to many-electron atoms which serve as the groundwork for extension to high-Z atoms and to molecules in the next subsection.

From Eqs. 7.6 - 7.9, it is seen that the large and small components of the Dirac spinors are coupled through the off-diagonal Π_κ operation. This coupling, through the unbounded Π_κ operator, produces, by a subtle effect, the "variational failure" mentioned earlier. A criterion by which to judge whether or not basis sets chosen to represent the large and small components of a relativistic wavefunction are kinetically balanced may be developed by first solving the Dirac equation for $Q_{n\kappa}(r)$. One obtains

$$Q_{n\kappa}(r) = [\varepsilon_{n\kappa} - (V_N - 2c^2)]^{-1}(c\Pi_\kappa^+)P_{n\kappa}(r) \tag{7.11}$$

This is the relation between $P_{n\kappa}(r)$ and $Q_{n\kappa}(r)$ which must be obeyed by proper solutions. The required relation is simplified by examining equation 7.11 in the non-relativistic limit. As the non-relativistic limit

($c \to \infty$) is approached, $|V_N - \varepsilon_{n\kappa}| << c^2$, and Eq. 7.11 reduces to [42–47],

$$Q_{n\kappa}(r) = \frac{1}{2c}\Pi_\kappa^+ P_{n\kappa}(r) \tag{7.12}$$

Here it is quite obvious that a basis set chosen for $Q_{n\kappa}(r)$ must contain whatever functions are generated by the action of Π_κ^+ on the functions of the large-component basis. The relation is obeyed if the two-spinors generated by operation of Π_κ^+ onto $\{X_{\kappa i}^L\}$ are contained in the basis set $\{X_{\kappa i}^S\}$. In other words the two-spinors $\{\Pi_\kappa^+ X_{\kappa i}^L\}$ must lie within the linear manifold spanned by $\{X_{\kappa i}^S\}$.

$$\{X_{\kappa i}^S\} \in \{\Pi_\kappa^+ X_{\kappa i}^L\} \tag{7.13}$$

Eq. 7.13 is referred to as the condition of "kinetic balance," which provides a criterion by which to judge whether or not basis sets to be used in relativistic calculations are kinetically balanced at the non-relativistic limit [2, 42, 43]. When c is finite, however, the kinetically balanced basis sets generated by Eq. 7.13 alone do not necessarily reproduce the correct relativistic kinematics near the origin.

It has been a common practice to approximate the electron-nuclear interaction in the atomic or molecular Hamiltonian as a point-charge Coulomb attraction. There are advantages with the point charge model: Simple systems such as hydrogenic ions, both at the nonrelativistic and the relativistic DC level, can be solved exactly. Matrix elements for electron-nuclear interaction in the basis set expansion HF SCF method yield simple analytic expressions, and can be evaluated easily. However, there is a major disadvantage with the point charge model in matrix DF SCF calculations. Kinetic balance [2, 46–48] in the expansion of the large and small components of Dirac 4-spinors has proved successful in preventing the blatant variational failure that has plagued matrix DF SCF calculations [44, 49, 50]. The criterion of basis set balance, Eq. 7.13, however, was derived from the Dirac equation assuming that the electron-nuclear interaction potential V satisfies the condition $|V_N| << c^2$. Consequently, for a finite value of c, a conventional kinetically balanced basis does not necessarily satisfy the boundary condition at the origin where, in point nucleus approximation, $V_N \to -\infty$. As a result, such a basis fails to reproduce the correct relativistic kinematics near the origin because it fails to reproduce the exact solutions there [42–44], although it may recover the correct nonrelativistic limit as c approaches infinity.

Besides this major disadvantage, we note two more serious drawbacks with the use of the point charge approximation in practical DF SCF calculations: The first is that, for a large nuclear charge Z, the atomic

energy is appreciably higher for a more realistic, finite or extended representation of the nucleus than for a point representation. With the extended representation of the nucleus, the total energy of the system is higher by approximately $(0.012\ Z)^{4.75}$ a.u. for low-Z systems than in the point representation [51]. The increase in electronic energy depends even more strongly on Z for high-Z systems and reaches more than 10^3 eV for the element Es (Z= 99). The major contribution to the energy increase comes from $s_{1/2}$-spinors, which become destabilized by about 0.3 % for Z =99 and by 0.6 to 1.3 % for Z = 109, (i.e., Mt) in the extended nucleus representation [52]. As for relativistic corrections, the fractional effects in the outer shells of many electron atoms and molecules are much larger than those of hydrogen-like systems; they are comparable in magnitude to those in the inner K-shell [53]. The second drawback is that the singularity of the Coulomb potential of a point charge results in artificial singularities in the wavefunction, which cause difficulties both in variational and perturbational calculations (see e.g. [54]), especially if one employs basis sets of integer Slater spinors (S spinors) or G spinors. This is indeed the case with kinetically balanced G spinor basis calculations that employ the point nucleus approximation. We briefly review how these drawbacks may be removed by forfeiting the point nucleus approximation in favor of a finite nucleus of uniform proton charge distribution.

With a point representation of the nucleus, the radial upper $(P_{n\kappa}(r))$ and lower $(Q_{n\kappa}(r))$ components of the Dirac spinors behave near the nuclear origin as

$$\begin{aligned} P_{n\kappa}(r) &= r^{\gamma}(a_0^{pn} + a_1^{pn} r + a_2^{pn} r^2 + \ldots) \\ Q_{n\kappa}(r) &= r^{\gamma}(b_0^{pn} + b_1^{pn} r + b_2^{pn} r^2 + \ldots) \end{aligned} \tag{7.14}$$

where $\gamma = \sqrt{\kappa^2 - Z^2/c^2}$.

Here κ is the relativistic quantum number. For an extended representation of the nucleus, the behavior of the Dirac spinors close, but external, to the nuclear boundary is similar to Eq. 7.14 because the electron-nuclear potential is identical, i.e., a point-charge Coulombic attraction potential, for $r > R_n$.

As $r \to R_n$, the wavefunction increases steeply up to the outer boundary of the extended nucleus (see Fig. 1.2), which has a radius (in a.u.) of the order of $R_n = 2.2677 \cdot 10^{-5} \cdot A^{1/3}$ where A is the baryon number. For a point nucleus the relativistic wavefunction diverges towards ∞ as $r \to 0$. When the nucleus is represented as a finite sphere of uniform proton charge, the exact $s_{1/2}$ solutions of the Dirac equation near the origin for finite c have the form [55],

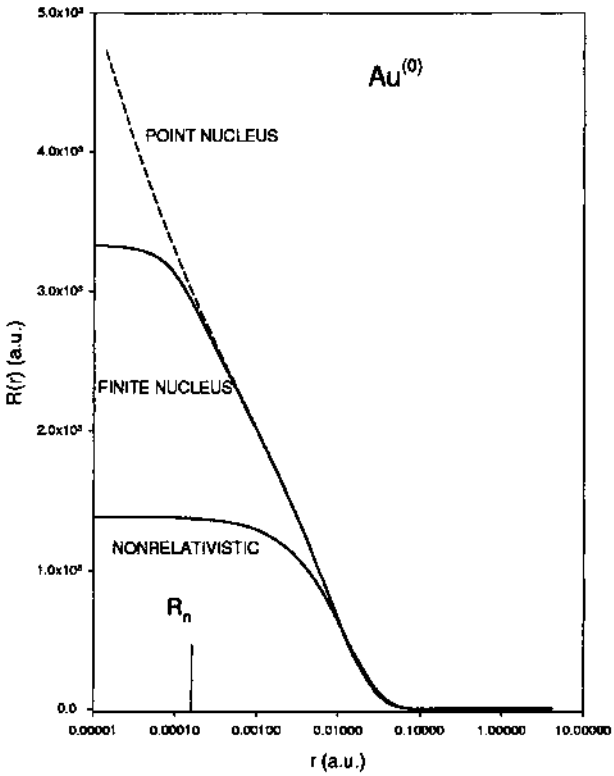

Figure 7.1 $1s_{1/2}$ relativistic wave function, $\frac{1}{r}P_{1s_{1/2}}(r)$, of gold representing the nucleus as a point and a finite sphere of uniform proton charge. Nonrelativistic 1s orbital of gold is also displayed for comparison.

$$\begin{aligned} P_{s1/2}(r)/r &= a_0^{fn} + a_2^{fn} r^2 + a_4^{fn} r^4 + \dots \\ Q_{s1/2}(r)/r &= b_1^{fn} r + b_3^{fn} r^3 + \dots \end{aligned} \tag{7.15}$$

Ishikawa *et al.* [42] showed that G spinors reproduce the relativistic boundary associated with the finite nucleus for finite c, viz.

$$\begin{aligned} P_{s1/2}(r) &= a_0^{fn} r + a_2^{fn} r^3 + a_4^{fn} r^5 + \ldots \approx A r exp(-\gamma r^2) \\ Q_{s1/2}(r) &= b_1^{fn} r^2 + b_3^{fn} r^4 + \ldots \approx B r^2 exp(-\gamma/r^2), \end{aligned} \tag{7.16}$$

where A and B are proportionality constants. Thus, in the finite nuclear model, G spinors of integer power of r are appropriate basis functions for all values of c [42,56] because imposition of the finite nuclear boundary results in a solution which can be accurately represented by kinetically balanced G spinors at the origin. In Refs. [37–40,49–51], we have performed DF G-spinor expansion calculations on one- and many-electron systems with a finite nucleus model. In these studies, we have emphasized alteration of the boundary conditions such that G spinors become the best form for basis functions. Representing the nucleus as a finite body of uniform proton charge accomplishes that feat.

In our matrix DFB SCF calculations, the radial large and small component are expanded in basis sets of G spinors that satisfy the boundary conditions associated with the finite nucleus of uniform proton charge distribution, $\{X_{\kappa i}^L\}$and $\{X_{\kappa i}^S\}$:

$$\begin{aligned} P_{n\kappa}(r) &= \Sigma_i X_{\kappa i}^L C_{n\kappa i}^L \\ Q_{n\kappa}(r) &= \Sigma_i X_{\kappa i}^S C_{n\kappa i}^S \end{aligned} \tag{7.17}$$

where

$$X_{\kappa i}^L = \begin{matrix} N_L r^{|\kappa|} e^{-\zeta r^2} & \kappa < 0 \\ N_L r^{\kappa+1} e^{-\zeta r^2} & \kappa > 0 \end{matrix} \tag{7.18}$$

We have shown that the G spinor basis sets that satisfy the boundary condition associated with the finite nucleus of uniform proton charge distribution automatically satisfy the condition of kinetic balance for all values of c,

$$X_{\kappa i}^S = N_S \Pi_\kappa^+ X_{\kappa i}^L \tag{7.19}$$

Here the $\{C_{n\kappa i}^L\}$ and $\{C_{n\kappa i}^S\}$ are linear variation parameters. N_L and N_S are normalization factors.

In order to be sure that finite basis calculations converge to physical results, one must also devise finite basis sets which can be extended to practical completeness in the Hilbert space of square integrable Dirac spinors. Even-tempered sets of G spinors are suited to this purpose. Very large basis sets of even-tempered G spinors [57, 58] can be used without incurring the near-linear dependence effects encountered with S spinors.

In matrix DFB calculations on closed-shell systems, the SCF equation in the algebraic approximation for symmetry-type κ takes the form

$$\mathbf{F}_\kappa \mathbf{C}_\kappa = \mathbf{S}_\kappa \mathbf{C}_\kappa \mathbf{E}_\kappa. \tag{7.20}$$

Following the notation of Quiney et al. [39, 59], the overlap matrix assumes block-diagonal form,

$$\mathbf{S}_\kappa = \begin{bmatrix} \mathbf{S}_\kappa^{LL} & \mathbf{0} \\ \mathbf{0} & \mathbf{S}_\kappa^{SS} \end{bmatrix}. \tag{7.21}$$

The superscripts LL and SS indicate either the large or the small component basis. The Fock matrix is

$$\mathbf{F}_\kappa = \mathbf{f}_\kappa + \mathbf{g}_\kappa + \mathbf{b}_\kappa. \tag{7.22}$$

where the one-electron part $\mathbf{f}_\kappa$ is

$$\mathbf{f}_\kappa = \begin{bmatrix} \mathbf{V}_\kappa^{LL} & c\Pi_\kappa^{LS} \\ c\Pi_\kappa^{SL} & \mathbf{V}_\kappa^{SS} - 2c^2\mathbf{S}_\kappa^{SS} \end{bmatrix}. \tag{7.23}$$

The two-electron part, $\mathbf{g}_\kappa$, consists of the matrices of two-electron Coulomb and exchange interactions

$$\mathbf{g}_\kappa = \begin{bmatrix} \mathbf{J}_\kappa^{LL} - \mathbf{K}_\kappa^{LL} & -\mathbf{K}_\kappa^{LS} \\ -\mathbf{K}_\kappa^{SL} & \mathbf{J}_\kappa^{SS} - \mathbf{K}_\kappa^{SS} \end{bmatrix}. \tag{7.24}$$

The matrices $\mathbf{J}_\kappa^{TT}$ and $\mathbf{K}_\kappa^{TT'}$, where the subscripts T and $T\prime$ are either L or S, have matrix elements of the form [17, 18, 39, 59]

$$J_{\kappa ij}^{TT} = \sum_{\kappa' kl} (2j' + 1)[D_{\kappa' kl}^{TT} J_{\kappa ij,\kappa' kl}^{0,TT,TT} + D_{\kappa' kl}^{\overline{TT}} J_{\kappa ij,\kappa' kl}^{0,TT,\overline{TT}}] \tag{7.25}$$

$$K_{\kappa ij}^{TT'} = \sum_{\nu} \sum_{\kappa' kl} (2j' + 1) b_\nu(jj') D_{\kappa' kl}^{TT'} K_{\kappa ij,\kappa' kl}^{\nu,TT',TT'} \tag{7.26}$$

Here the superscripts $T\overline{T}$ represent an LS or SL pair. The Coulomb and exchange integrals in Equations (7.25) and (7.26) are given in terms of the G spinors basis functions, $\{X_{\kappa i}^L\}$ and $\{X_{\kappa i}^S\}$ as,

$$J_{\kappa ij,\kappa' kl}^{\nu,TT,T'T'} = \int_0^\infty \int_0^\infty X_{\kappa i}^T(r) X_{\kappa j}^T(r) U_\nu(r,s) X_{\kappa' k}^{T'}(s) X_{\kappa' l}^{T'}(s) ds dr \tag{7.27}$$

$$K_{\kappa ij,\kappa' kl}^{\nu,TT',TT'} = \int_0^\infty \int_0^\infty X_{\kappa i}^T(r) X_{\kappa' k}^T(r) U_\nu(r,s) X_{\kappa j}^{T'}(s) X_{\kappa' l}^{T'}(s) ds dr \tag{7.28}$$

where

$$U_v(r,s) = \begin{matrix} r^v/s^{v+1} & r < s \\ s^v/r^{v+1} & s < r \end{matrix}$$

and

$$D^{TT}_{\kappa ij} = C^T_{\kappa i} C^T_{\kappa j}$$

The frequency-independent Breit interaction in Eq. 7.4 leads to the term $\mathbf{b}_\kappa$ in the matrix SCF equation,

$$\mathbf{b}_\kappa = \begin{bmatrix} \mathbf{B}^{LL}_\kappa & \mathbf{B}^{LS}_\kappa \\ \mathbf{B}^{SL}_\kappa & \mathbf{B}^{SS}_\kappa \end{bmatrix} \tag{7.29}$$

The Breit interaction matrices are given as

$$B^{LL}_{\kappa ij} = \sum_\nu \sum_{\kappa' kl} (2j' + 1) e^{LL}_\nu(\kappa,\kappa) D^{SS}_{\kappa' kl} K^{\nu,LL,SS}_{\kappa ij,\kappa' kl} \tag{7.30}$$

$$B^{SL}_{\kappa ij} = \sum_\nu \sum_{\kappa' kl} (2j' + 1)[f_\nu(\kappa,\kappa') D^{LS}_{\kappa' kl} K^{\nu,SL,LS}_{\kappa ij,\kappa' kl} + g_\nu(\kappa,\kappa') D^{LS}_{\kappa' kl} W^{\nu,SL,LS}_{\kappa ij,\kappa' kl}] \tag{7.31}$$

$$B^{SS}_{\kappa ij} = \sum_\nu \sum_{\kappa kl} (2j' + 1) e^{SS}_\nu(\kappa,\kappa') D^{LL}_{\kappa' kl} K^{\nu,SS,LL}_{\kappa ij,\kappa' kl} \tag{7.32}$$

where

$$W^{\nu,TT,\overline{T}\overline{T}}_{\kappa ij,\kappa' kl} = \int_0^\infty \int_0^r X^T_{\kappa i}(r) X^{\overline{T}}_{\kappa' k}(r) U_\nu(r,s) X^{\overline{T}}_{\kappa j}(s) X^T_{\kappa' l}(s) ds dr -$$

$$\int_0^\infty \int_r^\infty X^T_{\kappa i}(r) X^{\overline{T}}_{\kappa' k}(r) U_\nu(r,s) X^T_{\kappa j}(s) X^{\overline{T}}_{\kappa' l}(s) ds dr$$

The relativistic angular coefficients, $e^{LL}_v(\kappa,\kappa')$, $e^{SS}_v(\kappa,\kappa')$, $f_v(\kappa,\kappa')$ and $g_v(\kappa,\kappa')$ are evaluated by the technique of Grant and Pyper [60].

The frequency-independent Breit interaction, which gives the leading correction to the instantaneous Coulomb interaction in quantum electrodynamics, is a two-body potential of the same general form as the instantaneous Coulomb interaction and this term may be easily incorporated in the SCF procedure of G-spinor expansion DF calculations [41]. Interference between the Coulomb and Breit terms causes large orbital reorganization and one-electron energy shift at large Z, and it can easily be taken into account in the matrix DFB SCF procedure.

Table 7.1 displays the spinor energies of Rn, obtained in matrix DFB SCF calculations. The results of matrix Dirac-Fock-Coulomb (DFC) SCF

Table 7.1 Spinor energies of the Radon atom computed by DFC SCF and DFB SCF methods (a.u.)

ORBITAL	SPINOR ENERGIES DFC SCF	DFB SCF
$1s_{1/2}$	-3641.155	-3627.096
$2s_{1/2}$	-668.8042	-667.1796
$2p_{1/2}$	-642.3244	-639.5933
$2p_{3/2}$	-541.1031	-539.4298
$3s_{1/2}$	-166.8317	-166.5233
$3p_{1/2}$	-154.8936	-154.3637
$3p_{3/2}$	-131.7313	-131.4230
$3d_{3/2}$	-112.5674	-112.3360
$3d_{5/2}$	-107.7595	-107.6086
$4s_{1/2}$	-41.31341	-41.24882
$4p_{1/2}$	-36.01938	-35.90344
$4p_{3/2}$	-30.12091	-30.06253
$4d_{3/2}$	-21.54841	-21.51599
$4d_{5/2}$	-20.43905	-20.42515
$4f_{5/2}$	-9.194284	-9.201396
$4f_{7/2}$	-8.928576	-8.943957
$5s_{1/2}$	-8.409106	-8.398930
$5p_{1/2}$	-6.409060	-6.389847
$5p_{3/2}$	-5.176042	-5.169015
$5d_{3/2}$	-2.189877	-2.189563
$5d_{5/2}$	-2.016767	-2.019221
$6s_{1/2}$	-1.071523	-1.070816
$6p_{1/2}$	-0.5405359	-0.5389305
$6p_{3/2}$	-0.3841743	-0.3840794
Total energy[a]	-23601.9713	-23572.6197

[a] Nonrelativistic (HF) energy: -21866.80 au.

calculations, performed by excluding the Breit interaction in the effective electron-electron interaction, are juxtaposed for comparative purposes. Note that the DFB SCF energy is lower by as much as 1706 a.u. than the nonrelativistic HF SCF energy, -21866.80 a.u., computed with the same basis set, indicating inadequacy in treating heavy systems with nonrelativistic methodologies. The variational Breit interaction energy, $E_B(SCF) = E_{DFB} - E_{DFC}$, is significant, ≈ 30 a.u. The DFB SCF $1s_{1/2}$ orbital energy is higher by 14 hartrees than the DFC SCF. The level shift decreases to ≈ 1.6 hartrees for the $2s_{1/2}$ and ≈ 2.73 hartrees for the $2p_{1/2}$ orbital. These level shifts due to the inclusion of the Breit interaction term in the SCF procedure are much smaller for outer-shell orbitals. In higher Z systems, the major effects of the inclusion of the Breit interaction in the SCF process are the reorganization of the spinors and a large shift in the inner-shell spinor energies. It is usually assumed that Breit energy contributions are small, but even for moderate nuclear charge, the transverse interaction is now known to contribute a substantial part of the correction to mean-field approximations and must be included in any approach that aims to treat relativistic effects to an accuracy of order α^2. A number of studies have demonstrated that large G spinor basis sets can be employed to achieve high accuracy without encountering the numerical near-linear dependency problem reported with S spinor basis sets. Thus G spinor basis set calculations can be regarded as an accurate and versatile approximation in relativistic atomic and molecular structure calculations.

1.3 Relativistic electron correlation: Definition of the Dirac-Coulomb and Dirac-Coulomb-Breit correlation energies

Electron correlation effects are corrections to the independent electron approximation, and their importance depends on the choice of the approximation in which they are calculated. In nonrelativistic many-body calculations, the correlation energy, E_{corr}^{NR} is defined as the difference between the exact eigenvalue of the N-electron Schroedinger Hamiltonian, E_{exact}^{NR} , and the nonrelativistic single-configuration HF energy, E_{HF} [61]:

$$E_{corr}^{NR} = E_{exact}^{NR} - E_{HF} \tag{7.33}$$

This definition of electron correlation energy is inadequate in the framework of relativistic many-body theory. In relativistic quantum theory for atoms and molecules, it is most convenient to replace the HF approximation by the well-defined relativistic independent electron model, the DF SCF method. This choice has the advantage that, as the speed

of light tends to infinity, the DF method smoothly approaches the HF method. Since relativistic N-electron Hamiltonians are approximate and take a variety of forms depending on the degree of approximation with which they are derived from QED, relativistic correlation energy must be defined in terms of the effective Hamiltonian used to construct the relativistic many-body theory.

We employ in our MBPT calculations two different effective N-electron Hamiltonians, the no-pair DCB Hamiltonian and the no-pair DC Hamiltonian. With respect to the two effective many-body Hamiltonians, we can define DCB correlation energy (E_{corr}^{DCB}) as the difference between the exact eigenvalue of the DCB Hamiltonian (E_{exact}^{DCB}) and the DFB SCF energy (E_{DFBSCF}), and DC correlation energy (E_{corr}^{DC}) as the difference between the exact eigenvalue of the DC Hamiltonian (E_{exact}^{DC}) and the DFC SCF energy (E_{DFCSCF}).

$$E_{corr}^{DCB} = E_{exact}^{DCB} - E_{DFBSCF} \tag{7.34}$$

$$E_{corr}^{DC} = E_{exact}^{DC} - E_{DFCSCF} \tag{7.35}$$

The difference between the DCB correlation and the DC correlation, i.e., $E_{BR} = E_{corr}^{DCB} - E_{corr}^{DC}$, is the relativistic many-body shift due to the low-frequency Breit interaction.

1.4 Relativistic Moller-Plesset perturbation theory for systems with closed shells or one valence electron outside a closed core

Accurate treatment of many-electron systems makes it necessary to go beyond the independent-particle level approach to include electron correlation as well as relativistic and quantum electrodynamical effects. In high-Z systems, relativistic and electron correlation effects are strongly intertwined. Therefore, approaches that simultaneously take into account both relativistic and correlation effects are desirable; they can deal with the nonadditive interplay of these effects in atoms and molecules. Relativistic MBPT, which does simultaneously account for both relativistic and correlation effects, has been developed [59, 62–64] using discrete basis sets of "global" functions.

MBPT, introduced into atomic physics by Kelly, provides a powerful and systematic approach to the calculation of atomic and molecular properties. Atomic MBPT calculations using the finite difference method, however, can be laborious because the construction of sufficiently complete sets of functions for correlated calculations is difficult. A relativistic MBPT algorithm based on the algebraic approximation, i.e., expansion

in analytic basis sets, has the distinct advantage over one based on a numerical finite-difference approach. The algebraic approximation provides a compact representation of the Dirac spectrum and results in finite summations in the evaluation of the many-body diagrams. The discrete basis set expansion approach has been shown to be comparable in accuracy with numerical finite-difference calculations. Relativistic MBPT based on the algebraic approximation with G spinor basis sets provides a tractable scheme for calculating relativistic correlation effects in molecules and lends itself to computationally efficient application of relativistic MBPT to atoms and molecules. Many-body perturbation theoretical formalisms based on nonrelativistic many-body Hamiltonian have been successfully applied to atoms and molecules. Perturbative approaches generally confer the advantage of computational efficiency; they permit recovery of the largest fraction of the correlation energy with the least computational effort. Typically 95% to 105% of the correlation energy can be recovered in second order. The results are size consistent, though not variational. Both an advantage and a disadvantage of perturbation approaches is that they must be applied state-by-state. But, because finer effects are determined perturbationally, there is a certain consistency to its use as a tool to compute correlation corrections as well. Although Møller-Plesset perturbation theory was derived for the nonrelativistic closed-shell case, an MP separation may be effected for nonrelativistic and relativistic open-shell and quasi-degenerate systems. In a recent study, we reported a state-specific relativistic MBPT for open-shell systems in which our single Fock operator method is employed to effect a Møller-Plesset type separation of the relativistic many-electron Hamiltonian. The state-specific MBPT involves a full implementation of generalized Møller-Plesset perturbation theory applied to open-shell reference wave functions, and in low order, yields a large fraction of the dynamical correlation. In this subsection, we provide an outline of our recently developed relativistic MP perturbation theory for closed and open-shell systems based on our single DF operator [63, 65].

The N-electron Hamiltonian, H, is partitioned into a model Hamiltonian H_0 and a perturbation V such that $H = H_0 + V$. The zero-order Hamiltonian, H_0, is arbitrary but should be chosen as close to the full Hamiltonian H as possible so that the perturbation series converges rapidly in low order. The zero-order Hamiltonian is usually chosen to be a sum of effective one-electron operators (Møller-Plesset partitioning [66]). In that form, all perturbation corrections describe electron correlation. For closed-shell systems, the best results have been obtained with Møller-Plesset partitioning. In the single Fock operator method of Koc and Ishikawa [65] relativistic MBPT for atomic and molecular

systems with one valence electron outside a closed core retains the essential aspects of Møller-Plesset perturbation theory. The theory provides a hierarchy of well-defined algorithms that allow one to calculate relativistic correlation corrections in non-iterative steps and, in low order, yields a large fraction of the dynamical correlation. The no-pair DCB Hamiltonian H^+_{DCB} is partitioned into an unperturbed Hamiltonian and a perturbation term following Møller and Plesset [66],

$$H^+_{DCB} = H_0 + V, \tag{7.36}$$

where the unperturbed Hamiltonian H_0 is a sum of single DFB SCF Fock operators R_0 for closed [17] or open-shells [62,65],

$$H_0 = \sum_i R_0(i) \qquad V = H^+_{DCB} - \sum_i R_0(i), \tag{7.37}$$

where, for open-shell systems [62],

$$R_0 = \mathcal{P}_c F_c \mathcal{P}_c + \sum_{k(\in O)} \mathcal{P}_k F_k \mathcal{P}_k + \mathcal{P}_v F_c \mathcal{P}_v. \tag{7.38}$$

Here the mean-field operators, F_c and F_k , as well as the projection operators, $\mathcal{P}_c$, $\mathcal{P}_k$, and $\mathcal{P}_v$, are those defined in previous work [62,65]. In this form of partitioning, all perturbation corrections describe relativistic electron correlation including cross contributions between relativistic and correlation effects.

The exact many-electron wave function is expanded in configuration state functions (CSF) $\{\Phi_i(\gamma_i JP); i = 1, 2, \ldots\}$ generated by single, double, triple ... excitations from the reference CSF, $\Phi_0(\gamma_0 JP)$. Individual CSFs are eigenfunctions of the total angular momentum and parity operators and are linear combinations of antisymmetrized products of positive-energy SCF spinors. The SCF spinors are mutually orthogonal so the CSFs $\Phi_i(\gamma_i JP); i = 0, 1, 2, \ldots$ are mutually orthogonal. The unperturbed Hamiltonian is diagonal in this space;

$$H_0 = \sum_i |\Phi_i(\gamma_i JP)\rangle E_i^{(0)} \langle\Phi_i(\gamma_i JP)| \tag{7.39}$$

so that

$$H_0|\Phi_i(\gamma_i JP)\rangle = E_i^{(0)}|\Phi_i(\gamma_i JP)\rangle \qquad (i = 0, 1, 2, ...). \tag{7.40}$$

$E_i^{(0)}$ is a sum of the SCF one-electron energies ε_q;

$$E_i^{(0)} = \sum_q \varepsilon_q N_q n_q[\Phi_i] \tag{7.41}$$

where the occupation number $N_q = 2j_q + 1$ and $n_q[\Phi_i]$ is the occupancy of the qth spinor in $\Phi_i(\gamma_i JP)$.

Application of Rayleigh-Schrödinger perturbation theory provides order-by-order expressions of the perturbation series for the state approximated by $|\Phi_0(\gamma_0 JP)\rangle$ [62],

$$\Psi = \Phi_0(\gamma_0 JP) + \Phi^{(1)}(JP) + ..., \tag{7.42}$$

$$E = E_0^{(0)} + E^{(1)} + E^{(2)} + E^{(3)} + ..., \tag{7.43}$$

where

$$\Phi^{(1)}(JP) = \sum_{i=1} \Phi_i(\gamma_i JP)\{V_{i0}(E_0 - E_i)^{-1}\}, \tag{7.44}$$

$$E_0^{(0)} + E^{(1)} = E_{SCF}, \tag{7.45}$$

$$E^{(2)} = \sum_{i=1} V_{0i} V_{i0}(E_0 - E_i)^{-1}, \tag{7.46}$$

and

$$E^{(3)} = \sum_{i,j=1} V_{0i} W_{ij} V_{j0}(E_0 - E_i)^{-1}(E_0 - E_i)^{-1}. \tag{7.47}$$

Here $V_{ij} =< \Phi_i(\gamma_i JP)|V|\Phi_i(\gamma_i JP) >$ and $W_{ij} =< \Phi_i(\gamma_i JP)\ |W|\ \Phi_i(\gamma_i JP) >$ with $W = V - E^{(1)}$.

In this form, all the perturbation corrections beyond first order describe relativistic electron correlation. Summations over the CSFs in Eqs. 7.44 through 7.47 are restricted to CSFs constructed from the positive-energy branch of the spinors, which effectively incorporates into the computational scheme the "no-pair" projection operator $\mathcal{L}_+$ contained in the DC and DCB Hamiltonians. In generalized Møller-Plesset formalism the CSFs, $\{\Phi_i(\gamma_i JP);\ i \neq 0\}$, generated by single excitations from the reference CSF do not contribute to the second- and third-order energies because the singly-excited CSFs, $\Phi_i(\gamma_i JP)$, generated by the SCF spinors satisfy the generalized Brillouin theorem, $\langle\Phi_i(\gamma_i JP)|\ H_+^{DC}\ |\Phi_0(\gamma_0 JP)\rangle = 0$. Thus $V_{i0} = 0$. CSFs generated by excitations higher than double also do not contribute to the second and third order energies because for them $V_{i0} = 0$ and $H_{i0} = 0$.

1.5 Dirac-Coulomb and Dirac-Coulomb-Breit correlation corrections in noble gas atoms, group-IIB atoms and neonlike ions

Matrix DFB SCF and MBPT calculations on the noble-gas atoms Ne, Ar, Kr, Xe, Rn, and the Group-IIB atoms Zn, Cd and Hg, were performed by using large well-tempered basis sets of G spinors [41]. Calculations were also performed on ions of the neon isoelectronic sequence. For the neonlike ions with Z up to 100, large even-tempered basis sets of G spinors are employed. The order of the partial-wave expansion (L_{max}), the highest angular momentum of the spinors included in the virtual space, was $L_{max} = 6$ throughout the study. The well-tempered basis set exponents were taken from the works of Huzinaga and Klobukowski [67]. Parameters of the even-tempered basis sets were optimized. Table 1.5 displays the SCF energies and the second-order correlation energies for the noble-gas and Group-IIB atoms. The DF SCF and MBPT calculations were also performed by excluding the Breit interaction. These are the matrix DFC SCF and MBPT calculations based on the DC Hamiltonian. The nonrelativistic limit was simulated by setting the speed of light, $c=10^4$. The nuclei are modeled as spheres of uniform proton charge in all the calculations.

The DCB second-order correlation energies, $E^{(2)}_{DCB}$, range from -0.38526 a.u. for Ne (Z=10) to -5.9400 a.u. for Rn (Z=86). Because large G-spinor basis sets were employed to saturate the occupied and virtual spaces in each symmetry, the correlation energies obtained have converged at least to five figures within the i-limit (L_{max}=6). The effect of enlarging the basis sets appears only in the sixth figure or higher. Figure 7.3 shows the variations of the NR, DC, and DCB second-order correlation energies of the neutral atoms as functions of nuclear charge, Z. The correlation energies in the neutral atoms increase almost linearly as Z increases, the least deviation from linearity being the NR correlation energies. The DCB correlation energies show the largest deviation from the linearity.

The difference $E^{(2)}_{DC} - E^{(2)}_{NR}$ is the relativistic DC many-body shift that increases in absolute value as Z increases. This increase arises from the use of relativistic single-particle states but the same two-body interaction, i.e., the classical instantaneous Coulomb interaction. The difference $E^{(2)}_{DCB} - E^{(2)}_{NR}$ in correlation energies is the relativistic DCB many-body shift that arises from the use of relativistic single-particle states and the low-frequency Breit interaction in addition to the classical instantaneous Coulomb interaction in the two-body interactions. In heavy neutral atoms, the increase in the DC correlation energies becomes substantial

Table 7.2 SCF and second-order correlation energies (a.u.)

Z	Atom	Atomic mass	Method	E_{SCF}	E_2
10	Ne	20.18	NR	-128.5470878	-0.3831882
			DC	-128.6919254	-0.3833856
			DCB	-128.6752847	-0.3852591
18	Ar	39.95	NR	-526.8173311	-0.6972791
			DC	-528.6838208	-0.6981223
			DCB	-528.5514977	-0.7060424
30	Zn	65.39	NR	-1777.844400	-1.6506117
			DC	-1794.610963	-1.6611270
			DCB	-1793.849916	-1.6875521
36	Kr	83.80	NR	-2752.047329	-1.8354321
			DC	-2788.861465	-1.8468226
			DCB	-2787.435574	-1.8878912
48	Cd	112.41	NR	-5465.098845	-2.6181147
			DC	-5593.319974	-2.6539737
			DCB	-5589.481095	-2.7362939
54	Xe	131.29	NR	-7232.069451	-2.9211312
			DC	-7446.887980	-2.9587009
			DCB	-7441.118205	-3.0674532
80	Hg	200.59	NR	-18408.53586	-5.0862400
			DC	-19648.84818	-5.2894722
			DCB	-19626.21565	-5.5722140
86	Rn	222	NR	-21866.11626	-5.3920715
			DC	-23601.96583	-5.5874268
			DCB	-23572.61431	-5.9400218

Table 7.3 SCF and second-order correlation energies for neonlike ions (a.u.)

Z	Atom	Atomic mass	Method	E_{SCF}	E_2
20	Ca^{10+}	40.08	NR	-640.3840658	-0.3945152
			DC	-643.2553506	-0.3953778
			DCB	-643.0721885	-0.4051025
30	Zn^{20+}	65.39	NR	-1552.555556	-0.4038468
			DC	-1568.582000	-0.4063782
			DCB	-1567.884988	-0.4300865
40	Zr^{30+}	91.22	NR	-2864.782277	-0.4085616
			DC	-2918.746542	-0.4140520
			DCB	-2916.978729	-0.4578428
50	Sn^{40+}	118.70	NR	-4577.012941	-0.4114717
			DC	-4715.837068	-0.4215601
			DCB	-4712.211476	-0.4918780
60	Nd^{50+}	144.24	NR	-6689.219431	-0.4133766
			DC	-6991.922707	-0.4301778
			DCB	-6985.390129	-0.5340929
70	Yb^{60+}	173.04	NR	-9201.367922	-0.4147801
			DC	-9792.611477	-0.4410812
			DCB	-9781.809926	-0.5868727
80	Hg^{70+}	200.59	NR	-12113.42456	-0.4157677
			DC	-13183.10081	-0.4554500
			DCB	-13166.27570	-0.6532587
90	Th^{80+}	232.04	NR	-15425.33075	-0.4165655
			DC	-17258.51144	-0.4753647
			DCB	-17233.38310	-0.7387175
100	Fm^{90+}	257.00	NR	-19137.06139	-0.4172211
			DC	-22163.34260	-0.5044448
			DCB	-22126.87231	-0.8528151

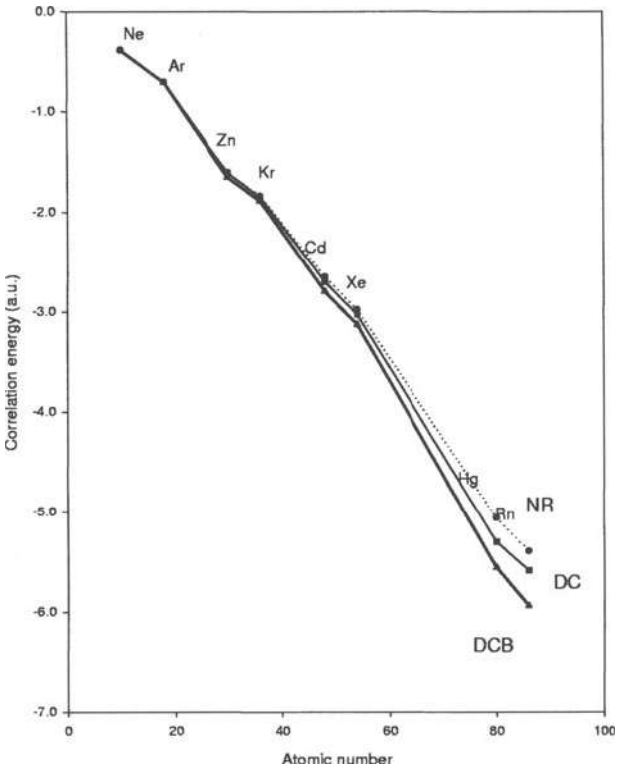

Figure 7.2 Variation of the nonrelativistic, Dirac-Coulomb, and Dirac-Coulomb-Breit second-order energies of the neutral atoms as functions of the atomic number.

due to the large number of bound electrons, e.g. in Rn, the relativistic DCB many-body shift ($E^{(2)}_{DCB} - E^{(2)}_{NR} = 0.548$ a.u.) is 2.8 times larger in magnitude than the relativistic DC many-body shift ($E^{(2)}_{DC} - E^{(2)}_{NR} = 0.195$ a.u.).

The DC second-order correlation energy $E^{(2)}_{DC}$ of Hg is larger by 0.203 a.u. in magnitude than the NR correlation energy. The analysis reveals

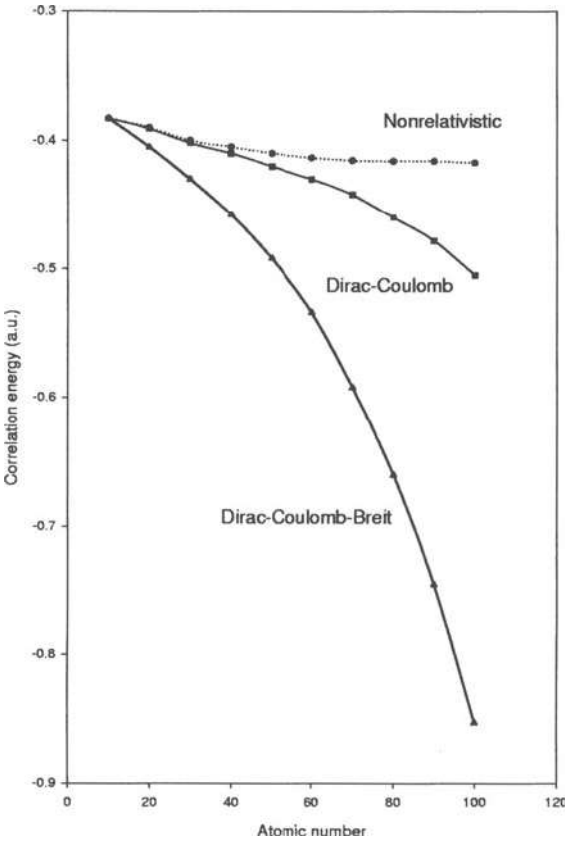

Figure 7.3 Variations in the correlation energies for Ne and neonlike ions as functions of the atomic number.

that the DC many-body shift comes mainly from increases in the DC pair correlation energies of the valence shell electron pairs, e.g., ($5s$,$4f$), ($5p$,$4f$), and ($6s$,$5d$) pairs [41]. The relativistic DCB many-body shift ($E^{(2)}_{DCB} - E^{(2)}_{NR} = 0.486$ a.u.) in Hg is 2.4 times larger than the relativistic DC many-body shift $E^{(2)}_{DC} - E^{(2)}_{NR} = 0.203$ a.u.. Significant increase in magnitude of the pair correlation energies for the inner-shell electron

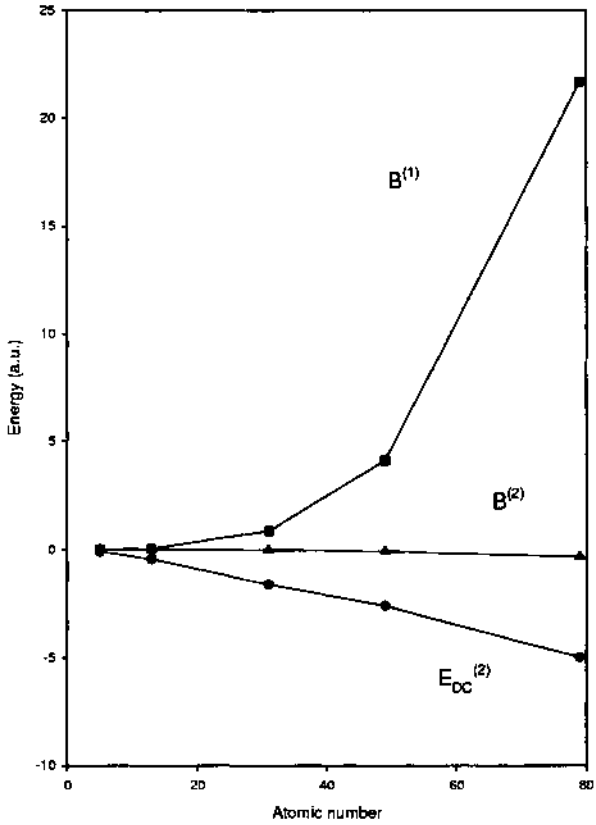

Figure 7.4 Second-order Dirac-Coulomb correlation $E_{DC}^{(2)}$, and first- and second-order Breit corrections, $B^{(1)}$ and $B^{(2)}$, as as functions of the atomic number.

pairs, $(1s,1s)$, $(2p,2p)$ and $(2p,1s)$, as well as the increase in pair correlation energies in the valence-shell electron pairs accounts for the large difference of 0.486 hartrees between the DCB correlation energy and the NR correlation energy.

Table 7.2 displays the results of DFB SCF and MBPT calculations on the ions of the Ne isoelectronic sequence, $Z \leq 100$ [41]. Figure 7.2 shows the variations in the NR, DC and DCB correlation energies for

Ne and Ne-like ions as a function of nuclear charge. The instantaneous Coulomb correlation energy for Ne and ions of the neon isoelectronic sequence computed by using the DC Hamiltonian remains almost constant, with a slight increase in magnitude as nuclear charge, Z, increases. In contrast, the DCB correlation energy, $E^{(2)}_{DCB}$, increases dramatically as Z increases. For the $s_{1/2}$- and $p_{1/2}$-shells, the contribution is most significant because the magnetic interaction, the dominant term in the low-frequency Breit interaction, is a short range interaction which, in the classical limit, behaves as $1/r^3$. Like the highly-ionized He-like ions reported previously [40], the nuclear potential dominates electron-electron interactions in highly-ionized Ne-like ions, and thus the Dirac-Fock independent particle approximation becomes increasingly accurate as Z increases. In these instances, the MBPT series converge very rapidly, and the second-order MBPT energy in general accounts for the total correlation correction to well over 99% accuracy [40].

In their multiconfigurational finite difference DF calculations on the ions of the He isoelectronic sequence Ne^{+8}, Ca^{+18}, Zn^{+28} and Sn^{+48}, Gorceix, Indelicato and Desclaux included the magnetic interaction in the self-consistent field step, and computed the electron correlation energies due to both Coulomb and magnetic interactions [68, 69]. They found that the magnetic correlation energy exceeds in magnitude the Coulomb correlation energy in the region $Z \approx 50$. In a recent study [40], we have computed correlation energies for He and He-like ions employing the DCB Hamiltonian and compared our results with those obtained by Gorceix *et al.* In contrast to the magnetic correlation, the correlation energy due to the low-frequency Breit interaction does not exceed in magnitude the Coulomb correlation energy even at $Z \approx 50$.

Figure 7.2 reveals that the DC correlation energies in Ne-like ions increase noticeably as Z increases. For the neonlike Fm ion (Z=100), the computed relativistic DCB many-body shift, $E^{(2)}_{DCB} - E^{(2)}_{NR}$, amounts to 0.436 a.u. whereas the relativistic DC many-body shift, $E^{(2)}_{DC} - E^{(2)}_{NR}$, is 0.087 a.u. The results of DFC SCF, DFB SCF and MBPT calculations show that the Breit interaction results in a significant modification of relativistic many-body effects in highly-ionized Ne-like ions. The DC Hamiltonian accounts for a fraction of the total relativistic correction to the correlation energy for highly-ionized high-Z species. The bulk of the relativistic correction to the correlation energy comes from one-Coulomb and one-Breit photon diagrams, and these diagrammatic terms are summed to all orders when the spinors are determined self-consistently by the DFB SCF method.

1.6 Dirac-Coulomb and Dirac-Coulomb-Breit correlation in systems with one valence electron outside a closed core: the effects on the ionization energy

Matrix DFC SCF and second-order relativistic MBPT calculations, based on the no-pair Dirac-Coulomb Hamiltonian, on the open-shell ground $^2S_{1/2}$ state of the group-IB atoms (Cu, Ag, Au), the ground $^2P_{1/2}$ state group-IIIA atoms (B, Al, Ga, In), and their singly-ionized closed-shell ions have been done with large well-tempered basis sets of G spinors [63]. All electrons have been included in the relativistic MBPT procedure in order to study the effects of relativity on electron correlation and overall relativity and correlation contributions to the ionization energy in group-IB and -IIIA atoms. The order of the partial-wave expansion (L_{max}), the highest angular momentum of the spinors included in the virtual space, is L_{max}=5. The well-tempered G-spinor basis sets range from 15s13p10d10f10g10h for boron to 24s24p17d13f12g12h for gold. The well-tempered basis set exponents were taken from the work of Huzinaga and Klobukowski [67]. All-electron relativistic MBPT calculations including the frequency-independent Breit interaction in the first and second-orders of perturbation theory were also performed. These relativistic MBPT calculations are based on the no-pair Dirac-Coulomb-Breit Hamiltonian, H^+_{DCB}. The speed of light was taken to be 137.0359895 a.u. The nonrelativistic limit was simulated by setting the speed of light c = 10^4. Nuclei were again modeled as spheres of uniform proton charge in all the calculations.

Table 1.6 displays the DFC SCF energies E_{SCF}, second-order DC correlation energies $E^{(2)}_{DC}$, and first- and second-order Breit interaction energies, $B^{(1)}$ and $B^{(2)}$, for the ground states of the group-IB and -IIIA atoms and their singly-ionized ions. The $B^{(2)}$ are computed as the difference between the second-order correlation correction evaluated with the inclusion of B_{ij} in the effective electron-electron interaction and the second-order DC correlation correction, $E^{(2)}_{DC}$. $B^{(2)}$ in correlation energies is the relativistic many-body shift that arises from incorporation of the frequency-independent Breit interaction into the effective two-body interaction. The second-order energies are necessarily approximate due to the truncation of the partial-wave expansion (L_{max} = 5). $B^{(1)}$ increases by an order of magnitude as the atomic number of group-IB atoms increases from Cu to Ag, and again from Ag to Au. The relativistic many-body shift, $B^{(2)}$, also increases by an order of magnitude from Cu to Au. While the DC correlation energy increases monotonically as the atomic number increases, the first- and second-order Breit interac-

Table 7.4 DF SCF and MBPT energies (a.u.) of the ground states of the group-IB and -IIIA atoms and their singly ionized ions computed with partial-wave expansion $L_{max}=5$.

	E_{SCF}	$E_{DC}^{(2)}$	$B^{(1)}$	$B^{(2)}$	E_{total}
B	-24.536515	-0.103678	0.001506	-0.000336	-24.639023
B^{1+}	-24.245072	-0.086933	0.001481	-0.000336	-24.330860
Al	-242.330338	-0.445635	0.042256	-0.003410	-242.737127
Al^{1+}	-242.128765	-0.430044	0.042217	-0.003408	-242.520000
Ga	-1942.56374	-1.621316	0.852200	-0.026881	-1943.35974
Ga^{1+}	-1942.36137	-1.602937	0.852071	-0.026878	-1943.13911
In	-5880.44102	-2.594151	4.125752	-0.083246	-5878.99267
In^{1+}	-5880.24597	-2.575794	4.125524	-0.083242	-5878.77948
Cu	-1653.45298	-1.62442	0.67793	-0.02375	-1654.42322
Cu^{1+}	-1653.21168	-1.57929	0.67781	-0.02375	-1654.13691
Ag	-5314.63473	-2.51684	3.57295	-0.07983	-5313.65845
Ag^{1+}	-5314.40164	-2.46729	3.57276	-0.07982	-5313.37599
Au	-19035.55977	-4.96537	21.67120	-0.31539	-19019.16933
Au^{1+}	-19035.27726	-4.89618	21.67035	-0.31537	-19018.81846

Table 7.5 DF SCF and MBPT energies (a.u.) of the ground states of the group-IIB atoms, Zn and Cd, and their singly ionized ions.

	E_{SCF}	$E_{DC}^{(2)}$	$B^{(1)}$	$B^{(2)}$	E_{total}
Zn	-1794.61114	-1.62873	0.76145	-0.02502	-1795.50344
	(-1777.84438)	(-1.61799)			(-1779.46237)
Zn^{1+}	-1794.32478	-1.57272	0.76134	-0.02501	-1795.16117
	(-1777.56381)	(-1.56418)			(-1779.12799)
Cd	-5593.32183	-2.57354	3.84216	-0.08161	-5592.13482
	(-5465.09882)	(-2.53824)			(-5467.63706)
Cd^{1+}	-5593.05156	-2.50993	3.84198	-0.08160	-5591.80111
	(-5464.84428)	(-2.48009)			(-5467.32437)

Table 7.6 Contributions from each order of perturbation theory to the ionization energy (in eV) of ground-state Zn and Cd.

$E(A^{1+}) - E(A^0)$	ΔE_{SCF}	$\Delta E_{DC}^{(2)}$	$\Delta B^{(1)}$	$\Delta B^{(2)}$	Total(IE)
Zn					
Relativistic	7.7923	1.5241	-0.0029	0.0002	9.314
Nonrelativistic	7.6347	1.4642	0.0	0.0	9.099
Difference (Rel - NR)	0.1576	0.0599	-0.0029	0.0002	0.215
Cd					
Relativistic	7.3544	1.7309	-0.0049	0.0002	9.081
Nonrelativistic	6.9264	1.5823	0.0	0.0	8.509
Difference (Rel -NR)	0.4280	0.1486	-0.0049	0.0002	0.572

Table 7.7 Ionization energies of neutral atoms (eV).

		Ionization energy			
Atom	This work	Other work			Experiment[a]
B	8.386	8.27[b]	8.26[c]		8.298
Al	5.908	6.08[b]	5.91[c]		5.986
Ga	6.004				5.999
In	5.801	5.48[d]			5.785
Cu	7.791	7.715[e]	7.86[b]	7.46[f]	7.727
Zn	9.314	8.41[b]	9.13[f]		9.39
Ag	7.686	7.42[g]	7.55[h]	7.96[d]	7.574
Cd	9.081	8.72[d]			8.99
Au	9.548	8.39[g]	9.09[i]	8.930[j]	9.226
		9.40[d]	9.41[h]		

[a] - Ref [76], [b] - Ref [79], [c] - Ref [77], [d] - Ref [78], [e] - Ref [73], [f] - Ref [72], [g] - Ref [80], [h] - Ref [74], [i] - Ref [75], [j] - Ref [81].

tion energies increase dramatically and the Breit interaction significantly modifies the relativistic many-body effects. However, for all the atoms except Au, the heaviest system considered in this study, $B^{(1)}$ and $B^{(2)}$ are nearly identical for the neutral atoms and their singly ionized ions, and thus, the valence-shell electron IE is entirely accounted for by the differences in DF SCF energies E_{SCF} and the second-order Coulomb correlation energies $E_{DC}^{(2)}$. This is not the case with the heavy elements in the fifth-row and higher, nor with highly-ionized species. In highly-ionized ions, the second-order correlation correction to the Breit interaction $B^{(2)}$ is comparable in magnitude to the second-order Coulomb correlation correction. The differences in the $B^{(1)}$, $B^{(2)}$, and $E_{DC}^{(2)}$ between ions A^{n+} and $A^{(n+1)+}$ tend to affect the ionization energy (IE) by a comparable amount.

Although group-IIB atoms reveal some quasi-degeneracy in their closed-shell ground state (see next section), single-configuration DF SCF and relativistic MP perturbation theory describe the systems reasonably well [64]. Table 7.4 displays the DF SCF energies, E_{SCF}, second-order Dirac-Coulomb correlation energies, $E_{DC}^{(2)}$, and first- and second-order Breit interaction energies, $B^{(1)}$ and $B^{(2)}$, for ground-state of Zn^0 and Zn^{1+}. The order of the partial-wave expansion is L_{max}=5. The values in parentheses are the nonrelativistic energies computed by setting c = 10^4.

In the second column of Table 7.4, we present the closed-shell DF SCF energies for the ground $^1S_0$ state of Zn^0 as well as the open-shell DF SCF energies for the ground $^2S_{1/2}$ $(3d^{10}4s^1)$ state of Zn^{1+}. The G-spinor basis sets employed are slightly larger than those employed to obtain the results in Table 1.5. The third column of the table gives the second-order Dirac-Coulomb correlation energies $E_{DC}^{(2)}$ in L_{max}=5 partial-wave expansion. The MBPT calculations were also performed with the frequency-independent Breit interaction included. The Breit interaction is introduced into the no-pair DC Hamiltonian, H_{DC}^{+}, by adding the frequency-independent Breit interaction, (Eq. 7.4), to the instantaneous Coulomb interaction $1/r_{ij}$. In the fourth column we present the first-order Breit interaction energies, $B^{(1)}$. In the fifth column the second-order correlation corrections to the Breit interaction, $B^{(2)}$, are given.

The DF energies, -1794.61114 a.u., for the ground $^1S_0$ state Zn^0 atom, computed with a basis of 20s18p13d G spinors agree well with the corresponding numerical DF limit -1794.62 a.u. obtained with the numerical finite difference DF program of Desclaux [70]. The difference between rel-

ativistic DF SCF and its nonrelativistic limit for Zn^0, i.e. the relativistic energy lowering at the SCF level, is 16.76676 a.u.

The difference between the second-order Coulomb correlation correction $E_{DC}^{(2)}$ at c=137.0359895 and its nonrelativistic limit (c=10^4) is the relativistic DC many-body shift that arises from the use of relativistic single-particle states and the instantaneous Coulomb two-body interaction. The relativistic DC many-body shifts are relatively small for Zn^0 and Zn^{1+}, 0.01074 a.u. (0.292 eV) for Zn^0 and 0.00854 a.u. (0.232 eV) for Zn^{1+}. However, the effect on the IE of Zn^0 of the many-body shifts is significant because these values are noticeably different between Zn^0 and Zn^{1+}. For heavier systems, Au and Hg, the relativistic DC many-body shifts are an order of magnitude larger than that in Zn [20, 37].

Table 7.4 also displays the DF SCF energies, E_{SCF}, second-order DC correlation energies, $E_{DC}^{(2)}$, and first- and second-order Breit interaction energies, $B^{(1)}$ and $B^{(2)}$, for the ground $^1S_0$ state of the cadmium atom and its singly-ionized Cd^{1+} ion obtained at L_{max}=5. The relativistic many-body shift, $B^{(2)}$, increases dramatically from Zn to Cd. In going from Zn to Cd, the first- and second-order Breit interaction energies increase four- to five-fold, and the Breit interaction results in a significant modification of relativistic many-body effects. However, $B^{(1)}$ and $B^{(2)}$ are nearly identical for the neutral atoms and their singly ionized ions, and thus the valence-shell electron IE is almost entirely accounted for by the differences in DF energies, E_{SCF}, and the Coulomb correlation energies $E_{DC}^{(2)}$. Such is not the case with the elements of the fifth- and higher-rows, nor with highly-ionized species [37, 62]. In highly ionized ions, $B^{(2)}$ is comparable in magnitude to the second-order Coulomb correlation correction. The differences in $B^{(1)}$, $B^{(2)}$, and $E_{DC}^{(2)}$ between an ion A^{n+} and $A^{(n+1)+}$ tend to affect the IE by similar amounts [37, 62].

Table 7.5 displays the contribution at each order of perturbation theory to the ionization energy of Zn^0 computed at $L_{max} = 5$. These contributions were computed by subtracting the energy of Zn^0 from that of Zn^{1+} in each order of perturbation theory. Relativistic and nonrelativistic results are given respectively in the third and fourth rows. The fifth row gives, for each order, the difference between the relativistic and nonrelativistic contributions given, respectively, in the third and fourth rows. The second column gives the zero-order contribution, ΔE_{SCF}, to the ionization energy, relativistic and nonrelativistic, and their difference. The relativistic zero-order contribution 7.7923 eV, the so-called ΔSCF approximation to the IE, was computed by subtracting the DF SCF energy of Zn^0 from that of Zn^{1+}. The nonrelativistic zero-order contribution, 7.6347 eV, was computed by subtracting the nonrelativistic SCF energy

of Zn^0 from that of Zn^{1+}. Both relativistic and nonrelativistic ΔSCF approaches significantly underestimate the ionization energy. Numerous nonrelativistic and relativistic SCF calculations have demonstrated that single-configuration SCF yields IE which are significantly lower than experimental, indicating that electron correlation effects are important. When the Coulomb correlation correction, $\Delta E^{(2)}_{DC}$ =1.5241 eV, the difference in the second-order DC correlation energies between Zn^{1+} and Zn^0, is taken into account, the computed IE dramatically improves. The effects of Breit interaction corrections on the computed IE, -0.00299 eV and 0.00027 eV respectively for $\Delta B^{(1)}$ and $\Delta B^{(2)}$, on the valence-shell electron IE of Zn^0, are negligible. The Breit interaction is a short-range interaction which primarily affects the inner-shell $s_{1/2}$ and $p_{1/2}$ electrons [37,62]. The IE computed at the nonrelativistic limit, 9.099 eV, underestimates the experimental value by 0.3 eV mainly because of the neglect of relativistic effects.

When one compares experimental IEs of transition metals to those computed by nonrelativistic quantum chemical methods, one must correct for relativistic contributions. Martin and Hay [71] have calculated relativistic contributions to the experimental ionization energies of transition metals at the DF level, assuming that electron correlation does not change the relativistic correction. Raghavachari and Trucks [72] modified the experimental IEs of transition metal atoms Sc through Zn by subtracting the relativistic corrections computed by Martin and Hay [71] from the experimental values. Their corrected "nonrelativistic" IE for Zn^0 is 9.23 eV, in good agreement with their estimate, 9.13 eV, computed by quadratic cofiguration interaction with single and double substitutions and perturbative triples (QCISD(T)). The corrected "nonrelativistic" IE, however, does not take into account the relativistic many-body shift. When this correction is accounted for, the agreement between them improves dramatically. Referring to the third row of Table 7.5, the largest relativistic correction to the nonrelativistic contribution to the ionization energy, 0.1576 eV, comes from the relativistic DF SCF. In an earlier study [71], Martin and Hay estimated this correction to be 0.16 eV, in agreement with our result. The effect of electron correlation on the relativistic corrections, i.e., the relativistic many-body shift, has not hitherto been available for the transition metals. The difference in relativistic many-body shifts between Zn^{1+} and Zn^0 (0.0599 eV) given in the fifth row of Table 7.5, which directly contributes to the IE, is approximately 2/5 of the relativistic SCF contribution (0.1576 eV). The differential effect of relativistic DC correlation on the calculated relativistic corrections to the ionization energy is thus non-negligible. The overall relativistic correction to the IE of the zinc atom is 0.215 eV. When this

correction is subtracted from the experimental IE, one obtains 9.17 eV for the corrected "nonrelativistic" IE for Zn, in excellent agreement with the estimated nonrelativistic IE of 9.13 eV obtained by Raghavachari and Trucks [72]. The residual discrepancy of 0.04 eV is primarily due to the truncation of partial wave to $L_{max} = 3$ in the nonrelativistic QCISD(T) calculations.

Table 7.5 also displays the contribution from each order of perturbation theory to the ionization energy of Cd^0 computed at $L_{max} = 5$. Relativistic and nonrelativistic results are given in the 7th and 8th rows, and the 9th row gives the difference between relativistic and nonrelativistic contributions. The second column gives the zero-order contribution, ΔE_{SCF}, to the ionization energy computed both relativistically and nonrelativistically and their difference. The ΔSCF approximation for IE, 7.3544 eV, was computed by subtracting the DF SCF energy of Cd^0 from that of Cd^{1+}. The nonrelativistic zero-order contribution 6.9264 eV was computed by subtracting the nonrelativistic SCF energy of Cd^0 from that of Cd^{1+}. As in the case of Zn, both relativistic and nonrelativistic ΔSCF approaches underestimate the ionization energy. When the Coulomb correlation correction $\Delta E^{(2)}_{DC}$ =1.7309 eV, the difference in the second-order DC correlation energies between Cd^{1+} and Cd^0, is taken into account, the computed IE improves. The differential effect of relativistic DC correlation on the calculated relativistic corrections to the ionization energy is non-negligible. On the other hand, the effects of Breit interaction corrections on the computed IE, -0.00490 eV and 0.00027 eV, respectively, for $\Delta B^{(1)}$ and $\Delta B^{(2)}$, on the valence-shell electron IE of Cd^0 are still negligible. The IE at the nonrelativistic limit, 8.509 eV, underestimates the experimental value by 0.48 eV because of the neglect of relativistic effects. Referring to the 9th row of Table 7.5, the largest relativistic correction to the nonrelativistic contribution to the ionization energy, 0.4280 eV, comes from the relativistic DF SCF. The difference in relativistic many-body shifts between Cd^{1+} and Cd^0 (0.1486 eV) given in the 9th row of the Table, which directly contributes to the IE, is approximately 1/3 of the relativistic SCF contribution (0.4280 eV). The differential effect of relativistic DC correlation on the calculated relativistic corrections to the ionization energy is thus non-negligible and larger than that in Zn. The over-all relativistic correction to the IE of the cadmium atom is 0.572 eV.

In Table 7.6 the computed IEs for the ground state of the group-IB, -IIB and -IIIA atoms are summarized. These IEs were computed by subtracting the total energies of the neutral atoms given in the last column of Tables 1.6 and 7.4 from those of the singly-ionized ions. In the third column, the IEs computed by means of previous nonrelativistic and rel-

ativistic correlated methods are given for comparison. The experimental IEs are given in the last column [76]. In general our second-order MBPT results tend to slightly overestimate the IEs. For group-IIIA elements, the computed IEs are in good agreement with experiment. The discrepancies between the computed and observed IEs are within 0.1 eV for B through In. Among the group-IIIA elements, the discrepancy between theory and experiment is the largest for boron, the theory overestimating the experimental IE by 0.09 eV. The bulk of the error is due to truncation of the perturbation expansion at second order. For light elements, the effects on the IE of the third-order correlation correction is significant, although it is an order of magnitude smaller than the second order. Recently, Hughes and Kaldor [77] computed the IEs of boron and aluminum by nonrelativistic all-order method, the Fock-space coupled cluster with single and double excitations (CCSD). The all-order method produces an IE for boron (8.26 eV) in closer agreement with experiment (8.298 eV) than does our second-order MBPT estimate. The relativistic correction to the IE of boron is only about 0.001 eV and relativistic DC many-body shift is negligible. Thus, the bulk of the small discrepancy between the IEs obtained by the coupled cluster theory and experiment (0.04 eV) must primarily come from truncation of the partial-wave expansion to L_{max}=3 in their CCSD calculations.

For group-IB elements, the discrepancies between theory and experiment become progressively larger as Z increases. While the computed IE for Cu is only 0.06 eV off the experimental value, the computed IE for Au is 0.34 eV larger than experimental value. The residual discrepancy comes primarily from the truncation of third and higher order correlation corrections in perturbation theory, since previous studies by Eliav, Kaldor and Ishikawa [75] employing an relativistic CC infinite-order method consistently gave better agreement with experiment on heavy atoms. Their relativistic CC calculations on Au, employing up to f-functions (L_{max}=3), gave an IE, 9.09 eV, in excellent agreement with experiment (9.226 eV). Theory underestimates the experimental IE by only 0.14 eV.

Hess and coworkers [80] employed the Douglas-Kroll transformation to decouple the large and small components of the no-pair DC Hamiltonian (Eq. 7.1). Their spin-free no-pair Hamiltonian, derived by separating the spin-free part from the transformed Hamiltonian, is amenable to a variational treatment by matrix formulation. The IEs of silver and gold they computed using the spin-free no-pair Hamiltonian with a partial-wave expansion up to L_{max}=3 are given in the third column of Table 7.6. The computed IE, 7.42 eV, for Ag agrees well with the experimen-

tal IE, 7.57 eV. The computed IE for Au, however, underestimates the experimental IE by 0.8 eV.

The relativistic CC calculations of Eliav, Kaldor and Ishikawa [75] on Au at c=137.037 a.u. and at the nonrelativistic limit (c=10^4 a.u.) give respectively, 9.09 eV and 6.98 eV for the relativistic and nonrelativistic IE of Au indicating that the overall relativistic and correlation contributions to the ionization energy of Au amount to as much as 2 eV. Recent relativistic and nonrelativistic pseudopotential calculations by Schwerdtfeger [81] have also addressed the overall relativistic and correlation contributions to the ionization energy of Au. The multi-electron adjusted pseudopotential QCISD(T) calculations, cited in Table 7.6, reproduce the IEs obtained by the fully relativistic CC method and predict that the overall relativistic and correlation contributions to the ionization energy of Au lie in the range of 1.9 - 2.0 eV.

We have implemented a procedure for performing relativistic MBPT calculations on closed- and open-shell states of atoms that do not exhibit significant near-degeneracy effects. Choosing the zero-order Hamiltonian to be the sum of single Dirac-Fock operators for the closed- and open-shell reference state, we have developed a relativistic MBPT method which fully implements generalized Møller-Plesset perturbation theory for closed- and open-shell systems. The perturbation theory provides a hierarchy of well-defined algorithms that allow one to calculate relativistic correlation corrections in noniterative steps and, in low order, yields a large fraction of the dynamical correlation. In these studies we see that the model used, DF SCF with finite nucleus and all-electron relativistic MBPT corrections, does account for major relativistic and correlation contributions.

2. Nondynamical and dynamical correlation energies

2.1 The matrix multiconfiguration Dirac-Fock SCF method for multiple open-shell systems

Over the years most relativistic atomic and molecular electronic structure calculations have been carried out by relativistic many-body perturbation theory based on single-configuration DF SCF wave functions expanded in analytic basis sets. The multiconfigurational (MC) DF SCF method is most effective in treating nondynamic correlation (i.e. near-degeneracy in the valence shells), but fails to account for the bulk of dynamic correlation. Single-reference many-body perturbation theory has exactly the opposite characteristic; it is effective in accurately describing dynamic correlation but fails to account for nondynamic correlation.

Dynamic correlation is a short-range effect that arises from electron-electron interaction and is the major correction to the Dirac-Fock independent particle model, while nondynamic correlation is a consequence of the existence of nearly degenerate excited states that interact strongly with the reference state. Systems in which only the dynamic correlation is important may be described by a single configuration DF wave function, whereas systems with significant nondynamic correlation cannot be correctly described within single configuration DF wave functions.

Near-degeneracy in the valence spinors gives rise to a manifold of strongly interacting configurations, i.e., strong configuration mixing within a relativistic complex, and makes a MC treatment mandatory. The classic examples in atomic physics are the near-degeneracy effects in ground-state beryllium and open-shell atoms with two or more open valence shells. For reactive and excited-state energy surfaces of molecules, single configuration SCF theory also fails to properly describe the separated fragments because of the near-degeneracy which follows the separation process. As Weiss and Kim [82] showed, relativity alters the magnitude of configuration mixing among the CSFs as Z increases in an isoelectronic sequence. For low-Z ions energy levels are clustered together according to their n quantum number occupancy (i.e., nonrelativistic complex), but as Z increases, they cluster together according to both their n and j quantum number occupancy (i.e., relativistic complex). Strong configuration interaction within a complex due to asymptotic degeneracy is called asymptotic configuration interaction (CI). By including in a zero-order multiconfiguration reference function all the CSFs generated within a complex of given principal quantum number n, relativistic multireference perturbation theory is capable of recovering dynamic correlation energy throughout the isoelectronic sequence. Alteration in the clustering pattern, i.e. asymptotic CI, in increasing Z may be easily accounted for in zero-order by relativistic MC DF SCF. Thus MC DF SCF based on all the CSFs generated within a nonrelativistic complex, is capable of accounting for nondynamic correlation from low to high Z even when the configuration interaction is altered as Z increases. Once the near-degeneracy effects in a complex are accounted for by matrix MC DF SCF, the remaining dynamic correlation may be recovered by a relativistic generalization of nonrelativistic multireference Møller-Plesset (MR-MP) perturbation theory [83, 84].

N-electron eigenfunctions of the no-pair DC Hamiltonian are approximated by a linear combination of M configuration-state functions, $\Phi_I^{(+)}(\gamma_I \mathcal{J} \pi); I = 1, 2, \ldots, M$, constructed from positive-energy eigenfunctions of the matrix DF SCF equation. The M configuration-state

functions form a subspace $\mathcal{P}^{(+)}$ of the positive-energy space $\mathcal{D}^{(+)}$.

$$\psi_K(\gamma_K \mathcal{J}\pi) = \sum_I^M C_{IK}\Phi_I^{(+)}(\gamma_I \mathcal{J}\pi). \tag{7.48}$$

Here the MC DF SCF wave function $\psi_K(\gamma_K \mathcal{J}\pi)$ is an eigenfunction of the angular momentum and parity operators with total angular momentum $\mathcal{J}$ and parity π. γ denotes a set of quantum numbers other than $\mathcal{J}$ and π necessary to specify the state uniquely. The total DC energy of the general MC DF state $|\psi_K(\gamma_K \mathcal{J}\pi)>$ can be expressed as

$$E^{MC}(\gamma_K \mathcal{J}\pi) =< \psi_K(\gamma_K \mathcal{J}\pi)|H_{DC}^{+}|\psi_K(\gamma_K \mathcal{J}\pi) >=$$

$$= \sum_{I,J=1}^{\mathcal{P}(+)} C_{IK}C_{JK} < \Phi_I^{(+)}(\gamma_I \mathcal{J}\pi)|H_{DC}^{+}|\Phi_J^{(+)}(\gamma_J \mathcal{J}\pi) > . \tag{7.49}$$

Here it is assumed that $\psi_K(\gamma_K \mathcal{J}\pi)$ and $\Phi_I^{(+)}(\gamma_I \mathcal{J}\pi)$ are normalized.

Given a trial orthonormal set of one-particle radial spinors $\{\phi_{n_p\kappa_p}^{(0)}(r)\}$ ($\in D^{(+)} \cup D^{(-)}$), the optimum occupied electronic radial spinors $\{\phi_{n_e\kappa_e}^{(+)}(r)\}$ ($\in D^{(+)}$) can be found by a unitary transformation $\mathbf{U} = \mathbf{1}+\mathbf{T}$ via

$$\phi_{n_e\kappa_e}^{(+)}(r) = \frac{1}{r}\begin{pmatrix} P_{n_e\kappa_e}(r) \\ Q_{n_e\kappa_e}(r) \end{pmatrix} = \sum_{p\in D^{(+)}\cup D^{(-)}}^{2N_\kappa} \phi_{n_p\kappa_p}^{(0)}(r)U_{pe} =$$

$$= \sum_p^{2N_\kappa} \phi_{n_p\kappa_p}^{(0)}(r)(T_{pe} + \delta_{pe}). \tag{7.50}$$

Here, the summation extends over both N_κ negative and N_κ positive energy spinors. $P_{n\kappa}(r)$ and $Q_{n\kappa}(r)$ are the large and small radial components and are expanded in N_κ G spinors, $\{\chi_{\kappa i}^L\}$ and $\{\chi_{\kappa i}^L\}$, that satisfy the boundary conditions associated with the finite nucleus [82],

$$\begin{aligned} P_{n\kappa}(r) &= \sum_i^{N_\kappa} \chi_{\kappa i}^L \xi_{n\kappa i}^L \\ Q_{n\kappa}(r) &= \sum_i^{N_\kappa} \chi_{\kappa i}^S \xi_{n\kappa i}^S. \end{aligned} \tag{7.51}$$

Here $\{\xi_{n\kappa i}^L\}$ and $\{\xi_{n\kappa i}^S\}$ are linear variation coefficients. Second-order variation of the MC DF energy (Eq. 7.49) with respect to the parameters

$\{T_{pe}\}$ and configuration mixing coefficients $\{C_{IK}\}$ leads to the Newton-Raphson (NR) equations for second-order MC DF SCF,

$$\begin{pmatrix} g^o_{pe} \\ g^c_\gamma \end{pmatrix} + \sum_{qf\gamma''} \begin{pmatrix} h^{oo}_{pe,qf} & h^{oc}_{pe,\gamma''} \\ h^{co}_{\gamma',qf} & h^{cc}_{\gamma',\gamma''} \end{pmatrix} \begin{pmatrix} T_{qf} \\ B_{\gamma''} \end{pmatrix} = \begin{pmatrix} 0 \\ 0 \end{pmatrix}. \tag{7.52}$$

Here g^o_{pe}, g^c_γ, $h^{oo}_{pe,qf}$, etc. are those defined in previous work [83]. Intermediate coupling is built in through the MC DF SCF process. For the ground electronic state, the Hessian matrix possesses N_κ positive and N_κ negative eigenvalues corresponding to a minimum and a maximum, respectively, in the space of large and small component parameters. Therefore, the energy functional is minimized with respect to spinor rotations between the occupied electronic spinors and the positive energy virtual spinors. The functional is maximized with respect to spinor rotations between the occupied electronic spinors and the negative energy spinors. By maximazing the vacuum charge-current density polarization contribution, the MC DF mean-field potential defines its dressed vacuum [84]. Quiney recently gave a comprehensive account on the participation of the negative-energy states from the point of view of quantum electrodynamics to illustrate how they enter into relativistic mean-field theory [85]. The quadratically convergent NR algorithm for relativistic MC DF SCF calculations has been discussed in detail [83]. To remove the arbitrariness of the MC SCF spinors and density weighting, the canonical SCF spinors are transformed into natural spinors $\{\omega^{(+)}_{n_p\kappa_p}\}$ for subsequent perturbation calculations [86]. The key to successful implementation of the subsequent MR-MP perturbation theory calculations is rapid convergence of our quadratically convergent matrix MC DF SCF method [83] for a general class of MC DF wave functions for open-shell quasidegenerate systems.

2.2 Relativistic multireference many-body perturbation theory for quasidegenerate systems

We have recently developed a relativistic MR-MP theory that combines the strengths of both MC DF SCF and many-body perturbation methods in application to a general class of quasidegenerate systems with multiple open valence shells. The single-reference relativistic many-body perturbation theory discussed earlier is extended to a relativistic MR-MP perturbation theory for systems with a manifold of strongly interacting configurations [83, 84]. The essential feature of the theory is its treatment of the state-specific nondynamic correlation in zero order through quadratically convergent matrix MC DF SCF, and recovery of the re-

maining correlation, which is predominantly dynamic pair correlation, by second-order relativistic MR-MP perturbation theory. We review here the implementation and application of a relativistic MR-MP perturbation theory which takes a general class of MC DF SCF wave functions discussed in previous subsection as reference functions. The multiconfiguration wave functions are computed by a quadratically convergent matrix MC DF SCF method discussed in previous subsection in analytic basis sets of G spinors. A procedure is described by which to perform a relativistic second-order MR-MP perturbation theory calculations for a general class of MC reference functions constructed from Dirac natural spinors.

The no-pair DC Hamiltonian H_{DC}^{+} is partitioned into an unperturbed Hamiltonian and a perturbation term following Møller and Plesset [66],

$$H_{DC}^{+} = H_0 + V, \tag{7.53}$$

where the unperturbed model Hamiltonian H_0 is a sum of "average" DF operators F_{av} ,

$$\begin{aligned} H_0 &= \sum_i^N F_{av}(i) \\ V &= H_{DC}^{+} - \sum_i^N F_{av}(i). \end{aligned} \tag{7.54}$$

Here, the one-body operator F_{av} diagonal in $\{\omega_{n_p\kappa_p}^{(+)}\}$ may be defined by,

$$\begin{aligned} F_{av} &= \sum_{p\in D(+)} |\omega_{n_p\kappa_p}^{(+)}><\omega_{n_p\kappa_p}^{(+)}|f_{av}|\omega_{n_p\kappa_p}^{(+)}><\omega_{n_p\kappa_p}^{(+)}| = \\ &= \sum_{p\in D(+)} |\omega_{n_p\kappa_p}^{(+)}> \varepsilon_p^{+} < \omega_{n_p\kappa_p}^{(+)}|, \end{aligned} \tag{7.55}$$

where

$$\begin{aligned} \varepsilon_p^{+} &=< \omega_{n_p\kappa_p}^{(+)}|f_{av}|\omega_{n_p\kappa_p}^{(+)} > \\ f_{av} &= h_D + \sum_p^{occ} \widetilde{n}_p \left(J_p - K_p\right). \end{aligned} \tag{7.56}$$

The generalized fractional occupation $\widetilde{n}_p$ is related to diagonal matrix elements of the first-order reduced density matrix constructed in natural spinors by,

$$\widetilde{n}_p = D_{pp} = \sum_I^{\mathcal{P}(+)} C_{IK}C_{IK}n_{n_p\kappa_p}[I], \tag{7.57}$$

where $n_{n_p\kappa_p}[I]$ is the occupation number of the κ-symmetry shell in the CSF $\Phi_I(\gamma_I\mathcal{J}\pi)$. J_p and K_p are the usual Coulomb and exchange operators constructed in natural spinors.

The unperturbed Hamiltonian H_0 may be given in second quantized form,

$$H_0 = \sum_{p \in D(+)} \{a_p^+ a_p\} \, \varepsilon_p^+, \tag{7.58}$$

where $\{a_p^+ a_p\}$ is a normal product of creation and annihilation operators, a_p^+ and a_p, respectively. The zero-order Hamiltonian, H_0, is arbitrary but should be chosen as close to the full Hamiltonian H_{DC}^+ as possible so that the perturbation series converges rapidly in low order. The zero-order Hamiltonian is usually chosen to be a sum of effective one-electron operators (Møller-Plesset partitioning [66]). For closed-shell systems, the best results have been obtained with Møller-Plesset partitioning, i.e. with the sum of closed-shell Fock operators as H_0. An effective one-body operator for general MC DF SCF closely related to the closed-shell Fock operator is the "average" DF operator F_{av} , a relativistic generalization of a nonrelativistic average Fock operator [86,87]. The theory provides a hierarchy of well-defined algorithms that allow one to calculate relativistic correlation corrections in non-iterative steps and, in low order, yields a large fraction of the dynamical correlation. In this form of partitioning, perturbation corrections describe relativistic electron correlation, including cross contributions between relativistic and correlation effects.

Many-electron wave functions correct to α^2 may be expanded in a set of CSFs that spans the entire N-electron positive-energy space $\mathcal{D}^{(+)}$, $\{\Phi_I^{(+)}(\gamma_I \mathcal{J} \pi)\}$, constructed in terms of Dirac one-electron spinors. Individual CSFs are eigenfunctions of the total angular momentum and parity operators and are linear combinations of antisymmetrized products of positive-energy spinors ($\in D^{(+)}$). The one-electron spinors are mutually orthogonal so the CSFs $\{\Phi_I^{(+)}(\gamma_I \mathcal{J} \pi)\}$ are mutually orthogonal. The unperturbed Hamiltonian is diagonal in this space;

$$H_0 = \sum_{I}^{\mathcal{D}(+)} |\Phi_I^{(+)}(\gamma_I \mathcal{J} \pi) > E_I^{CSF} < \Phi_I^{(+)}(\gamma_I \mathcal{J} \pi)|, \tag{7.59}$$

so that

$$H_0 |\Phi_I^{(+)}(\gamma_I \mathcal{J} \pi) >= E_I^{CSF} |\Phi_I^{(+)}(\gamma_I \mathcal{J} \pi) > (I = 1, 2, \ldots). \tag{7.60}$$

Since the zero-order Hamiltonian is defined as a sum of one-electron operators F_{av} (Eq. 7.55), E_I^{CSF} is a sum of the products of one-electron energies defined by ε_q^+ and an occupation number $n_{n_q \kappa_q}[I]$ of the κ_q-

symmetry shell in the CSF $\Phi_I^{(+)}(\gamma_I \mathcal{J}\pi)$;

$$E_I^{CSF} = \sum_q^{D(+)} \varepsilon_q^+ n_{n_q \kappa_q}[I]. \tag{7.61}$$

The subset, $\{\Phi_I^{(+)}(\gamma_I \mathcal{J}\pi); I = 1, 2, \ldots, M\}$, with which we expand the MC DF SCF function $\psi_K(\gamma_K \mathcal{J}\pi)$ (Eq. 7.48) also defines an active subspace $\mathcal{P}^{(+)}$ spanned by $\psi_K(\gamma_K \mathcal{J}\pi)$ and its M-1 orthogonal complements, $\{\psi_K(\gamma_K \mathcal{J}\pi); K = 1, 2, \ldots, M\}$. The matrix of H_{DC}^+ in this subspace is diagonal

$$< \psi_K(\gamma_K \mathcal{J}\pi)|H_{DC}^+|\psi_L(\gamma_L \mathcal{J}\pi) >= \delta_{KL}\left(E_K^{(0)} + E_K^{(1)}\right) =$$

$$= \delta_{KL} E^{MC}(\gamma_K \mathcal{J}\pi), \tag{7.62}$$

where

$$E_K^{(0)} =< \psi_K(\gamma_K \mathcal{J}\pi)|H_0|\psi_K(\gamma_K \mathcal{J}\pi) >= \sum_I^M C_{IK} C_{IK} E_I^{CSF} = \sum_p^{occ} \varepsilon_p^+ \tilde{n}_p$$

and

$$E_K^{(1)} =< \psi_K(\gamma_K \mathcal{J}\pi)|V|\psi_K(\gamma_K \mathcal{J}\pi) > .$$

The residual space in the positive-energy subspace is $\mathcal{Q}^{(+)} = \mathcal{D}^{(+)} - \mathcal{P}^{(+)}$, which is spanned by CSFs $\{\Phi_L^{(+)}(\gamma_L \mathcal{J}\pi); L = M+1, M+2, \ldots\}$. Application of Rayleigh-Schrödinger perturbation theory provides order-by-order expressions of the perturbation series for the state approximated by the wavefunction $|\psi_K(\gamma_K \mathcal{J}\pi) >$,

$$E_K(\gamma_K \mathcal{J}\pi) = E^{MC}(\gamma_K \mathcal{J}\pi) + E_K^{(2)} + E_K^{(3)} + \ldots, \tag{7.63}$$

where

$$E_K^{(2)} =< \psi_K(\gamma_K \mathcal{J}\pi)|V\mathcal{R}V|\psi_K(\gamma_K \mathcal{J}\pi) > \tag{7.64}$$

and

$$E_K^{(3)} =< \psi_K(\gamma_K \mathcal{J}\pi)|V\mathcal{R}(H_0 - E_K^{(1)})\mathcal{R}V|\psi_K(\gamma_K \mathcal{J}\pi) > . \tag{7.65}$$

Here, $\mathcal{R}$ is the resolvent operator,

$$\begin{aligned} \mathcal{R} &= Q^{(+)}/(< \Phi_J^{(+)}(\gamma_J \mathcal{J}\pi)|H_0|\Phi_J^{(+)}(\gamma_J \mathcal{J}\pi) > - H_0) \\ Q^{(+)} &= \sum_L^{\mathcal{Q}(+)} |\Phi_L^{(+)}(\gamma_L \mathcal{J}\pi) >< \Phi_L^{(+)}(\gamma_L \mathcal{J}\pi)|. \end{aligned} \tag{7.66}$$

The projection operator $Q^{(+)}$ projects onto the subspace $\mathcal{Q}^{(+)}$ spanned by CSFs $\{\Phi_L^{(+)}(\gamma_L \mathcal{J}\pi); L = M+1, M+2, \ldots\}$. Using the spectral resolution of the resolvent operator acting on $V|\Phi_I^{(+)}(\gamma_I \mathcal{J}\pi) >$, the second-order correction may be expressed as,

$$E_K^{(2)} = \sum_{IJ} C_{IK} C_{JK} < \Phi_I^{(+)}(\gamma_I \mathcal{J}\pi)|V\mathcal{R}V|\Phi_J^{(+)}(\gamma_J \mathcal{J}\pi) >=$$

$$= \sum_{L=M+1}^{\mathcal{Q}(+)} \sum_{I,J=1}^{\mathcal{P}(+)} C_{IK} C_{JK} \frac{< \Phi_I^{(+)}(\gamma_I \mathcal{J}\pi)|V|\Phi_L^{(+)}(\gamma_L \mathcal{J}\pi) >}{E_J^{CSF} - E_L^{CSF}} \cdot$$

$$\cdot < \Phi_L^{(+)}(\gamma_L \mathcal{J}\pi)|V|\Phi_J^{(+)}(\gamma_J \mathcal{J}\pi) > . \tag{7.67}$$

In this form, all perturbation corrections beyond first order describe relativistic electron correlation for the state approximated by the MC DF SCF wavefunction $|\psi_K(\gamma_K \mathcal{J}\pi) >$.

Summations over the CSFs in Eqs. 7.59 through 7.67 are restricted to CSFs ($\in \mathcal{D}^{(+)}$) constructed from the positive-energy branch ($D^{(+)}$) of the spinors, effectively incorporating into the computational scheme the "no-pair" projection operator $\mathcal{L}_+$ contained in the DC and DCB Hamiltonians. Further, the CSFs $\Phi_L^{(+)}(\gamma_L \mathcal{J}\pi)$ ($\in \mathcal{Q}^{(+)}$) generated by excitations higher than double, relative to the reference CSFs $\Phi_I^{(+)}(\gamma_I \mathcal{J}\pi)$ ($\in \mathcal{P}^{(+)}$), do not contribute to the second- and third-order because for them $< \Phi_I^{(+)}(\gamma_I \mathcal{J}\pi)|\ V\ |\Phi_L^{(+)}(\gamma_L \mathcal{J}\pi) >= 0$ and $< \Phi_I^{(+)}(\gamma_I \mathcal{J}\pi)|\ H_{DC}^{+}\ |\Phi_L^{(+)}(\gamma_L \mathcal{J}\pi) >= 0$.

Neglecting interactions with the filled negative-energy sea, i.e. neglecting virtual electron-positron pairs in summing the MBPT diagrams, we have a straightforward extension of nonrelativistic MBPT. Negative energy states ($\in D^{(-)}$), as part of the complete set of states, do play a role in higher-order QED corrections. Studies have appeared which go beyond the "no-pair" approximation where negative-energy states are needed to evaluate the higher-order QED effects [69, 88–90]. Contributions from the negative energy states due to creation of virtual electron-positron pairs are of the order α^3, and estimations of the radiative corrections are necessary in order to achieve spectroscopic accuracy for higher Z. In the relativistic MR-MP calculations on Zn, and Pb described below, the lowest-order radiative corrections were estimated for each state to achieve better accuracy.

2.3 Nondynamic and dynamic correlation energies in Zn

In the previous section, relativistic correlation energies have been computed for the closed-shell ground states of highly correlated Zn and Cd and their singly ionized open-shell ions by means of a relativistic MBPT based on single-configuration DF SCF wave functions as reference functions. The computed ionization energies of the ground-state Zn^0 and Cd^0 agree well with experiment. The theoretical ionization energies differ from experiment by approximately 1%.

In this section, we show that the low-lying ionization energies and term energy splittings of zinc [92] may be computed to unprecedented accuracy using the relativistic MR-MP perturbation theory [84, 93–96] that accurately accounts for relativistic, nondynamic and dynamic correlation energies. The first-row transition metal atoms and their singly-ionized ions exhibit near-degeneracy characteristic of a manifold of strongly interacting configurations arising from different occupations of the $3d$, $4s$ and $4p$ spinors. The ground $3d^{10}4s^2$ $^1S_0$ state of Zn^0 exhibits near-degeneracy within the n=4 complex due to interaction among the ($3d^{10}4s^2$, $3d^{10}4p_{1/2}^2$, and $3d^{10}4p_{3/2}^2$) configurations while the $3d^94s^2$ $^2D_{3/2,5/2}$ states of the singly-ionized Zn^{1+} display interactions within the n=4 complex among the ($3d^94l4l'; l, l' = 0, 1, 2$) configurations. Multireference treatment is necessary to treat these sources of nondynamical correlation. Table 2.3 displays the complete active space (CAS) MC DFB SCF energies E_{DFB}, MR-MP second-order DC ($E_{DC}^{(2)}$) and Breit ($B^{(2)}$) correlation corrections, and the Lamb shift E_{LS} in increasing number of CAS configurations within the n=4 complex. In each entry, the number of CSF, N_{CSF}, arising from increasing active CAS space displayed at the top of the columns, is given. The $^2D_{5/2}$ $-^2$ $D_{3/2}$ fine-structure splittings computed in increasing number of CSFs at the MC DFB and MP-MP level of theories are also given. The last two rows of the table give the Zn^0 ($^1S_0$) $\Rightarrow$ Zn^{1+} ($^2D_{3/2,5/2}$) ionization energies computed at the MR-MP level of theory.

The $^2D_{5/2}$ $-^2$ $D_{3/2}$ fine-structure splitting computed by single-configuration DFB SCF is 2639 cm^{-1}, in good agreement with experiment (2720 cm^{-1}) [91], while the seventeen-configuration CAS DFB SCF yields 2644 cm^{-1}, only a 5 cm^{-1} improvement over single-configuration DFB SCF. Thus the bulk of the FS splitting is due to one-body relativistic effects which are readily reproduced by single-configuration DFB SCF. The residual discrepancy is due to many-body effects and requires relativistic many-body theory. Many-body perturbative improvement based on single-configuration DFB SCF spinors yields a fine structure

Table 7.8 MCDFB energies ($E_{DFB}^{(0+1)}$), second-order Dirac-Coulomb corrections ($E_{DC}^{(2)}$), Lamb shift (E_{LS}), and second-order Breit corrections ($B^{(2)}$) (a.u.), of the the ground $^1S_0$ state of Zn^0 and $^2D_{5/2,3/2}$ states of Zn^{1+} in increasing CSF expansion length. Fine-structure splittings (cm^{-1}), and the ionization energies (eV) for $3d^{10}4s^2$ $^1S_0$ $Zn^0 \Rightarrow 3d^94s^2$ ^2D_J Zn^{1+} appear at the bottom.

		Active CAS orbitals			Experiment
		4s	4s,4p	4s,4p,4d	
Zn^0					
$3d^{10}4s^2$ $^1S_0$	N_{CSF}	1	3	5	
	$E_{DFB}^{(0+1)}$	-1793.849658	-1793.880655	-1793.881219	
	$E_{DC}^{(2)}$	-1.672720	-1.645559	-1.680967	
	E_{LS}	0.506872	0.506858	0.506858	
	$B^{(2)}$	-0.027183	-0.027241	-0.027242	
	E_{total}	-1795.042689	-1795.046597	-1795.082570	
Zn^{1+}					
$3d^94s^2$ $^2D_{5/2}$	N_{CSF}	1	9	17	
	$E_{DFB}^{(0+1)}$	-1793.314358	-1793.348924	-1793.350178	
	$E_{DC}^{(2)}$	-1.557924	-1.525795	-1.579736	
	E_{LS}	0.507130	0.507108	0.507107	
	$B^{(2)}$	-0.027088	-0.027095	-0.027095	
	E_{total}	-1794.392240	-1794.394706	-1794.449902	
$3d^94s^2$ $^2D_{3/2}$	N_{CSF}	1	9	17	
	$E_{DFB}^{(0+1)}$	-1793.302333	-1793.336890	-1793.338133	
	$E_{DC}^{(2)}$	-1.557807	-1.525306	-1.579576	
	E_{LS}	0.507146	0.507124	0.507123	
	$B^{(2)}$	-0.027153	-0.027156	-0.027156	
	E_{total}	-1794.380147	-1794.382228	-1794.437742	
Zn^{1+} $^2D_{5/2}$ - $^2D_{3/2}$ fine structure splitting (cm^{-1})					
FS_{DFB}		2639	2641	2644	2720
FS_{MR-MP}		2665	2748	2679	2720
Ionization energy (eV) $IE_{MR-MP}(Zn^0\ ^1S_0 \Rightarrow Zn^{1+}\ ^2D_{5/2})$					
		17.69002	17.72809	17.20501	17.17083
Ionization energy (eV) $IE_{MR-MP}(Zn^0\ ^1S_0 \Rightarrow Zn^{1+}\ ^2D_{3/2})$					
		18.02042	18.06886	17.53712	17.50807

Table 7.9 $3d^{10}4s^2\ {}^1S_0 \Rightarrow 3d^{10}4s^1\ {}^2S_{1/2}$ ionization energies (cm^{-1}) for zinc.

Method	
Single reference	
$3d^{10}4s^2\ {}^1S_0 \Rightarrow 3d^{10}4s^1\ {}^2S_{1/2}$	
$E_{DFB}^{(0+1)}$	62826
E_{LS}	61
$E_{DC}^{(2)}$	12056
$B^{(2)}$	2
IE[a]	74945
Multireference	
$3d^{10}(4s^2+4p_{1/2}^2+4p_{3/2}^2)\ {}^1S_0 \Rightarrow 3d^{10}4s^1\ {}^2S_{1/2}$	
$E_{DFB}^{(0+1)}$	69629
E_{LS}	64
$E_{DC}^{(2)}$	6095
$B^{(2)}$	14
IE[a]	75802
Experiment	75769.0±0.2

[a] $\mathrm{IE} = E_{DFB}^{(0+1)} + E_{LS} + E_{DC}^{(2)} + B^{(2)}$.

splitting of 2665 cm^{-1}, while MR-MP improves the calculated fine structure splitting to 2679 cm^{-1}, only 40 cm^{-1} shy of the experimental value.

Either single-configuration or MC DFB SCF alone fails to predict accurate $Zn^0(3d^{10}4s^2\ ^1S_0) \Rightarrow Zn^{1+}(3d^94s^2\ ^2D_J)$ ionization energies. The difference between the five-configuration CAS DFB SCF energy of Zn^0, $E_{DFB}^{(0+1)} = -1793.881219$ a.u., and the seventeen-configuration CAS DFB SCF energy of Zn^{1+} , computed in the same $4s$,$4p$,$4d$ active space, $E_{DFB}^{(0+1)} = -1793.350178$ a.u., gives a $Zn^0 3d^{10}4s^2\ ^1S_0 \Rightarrow Zn^{1+}3d^94s^2\ ^2D_{5/2}$ ionization energy of 14.45 eV, underestimating the experimental IE by about 3 eV. The relatively large difference indicates the importance of dynamic correlation. Moderate-size MC SCF alone usually recovers about half the dynamic correlation energy and is suited only to describing nondynamic correlation in the valence shell. Accurate calculation of dynamic correlation in both neutral and ionized zinc is crucial to predicting the ionization energy. Second-order MP perturbation theory based on single-configuration DFB SCF zero-order wavefunctions for Zn^0 and Zn^{1+} significantly improves the calculated IE, yielding the $Zn^0\ ^1S_0 \Rightarrow Zn^{1+}\ ^2D_{5/2}$ IE of 17.690 eV and $Zn^0\ ^1S_0 \Rightarrow Zn^{1+}\ ^2D_{3/2}$ IE of 18.020 eV: The single-reference MP perturbation theory overestimates the IEs by approximately 0.5 eV. The MP correlation corrections, particularly the $E_{DC}^{(2)}$, reduce the percentage error in the computed IE from 15% at the DFB SCF level to 3% at the second-order level.

To achieve higher accuracy, relativistic MR-MP perturbation theory must be employed for both neutral and ionized species to account for both nondynamic and dynamic correlation. CAS DFB SCF, which includes $4s$, $4p$, and $4d$ spinors in the active space, and subsequent MR-MP refinement based on the CAS DFB wavefunctions, improve the calculated IEs dramatically. Because the CSFs arising from $3d^94s^2$ interact noticeably with those involving the 4d spinors in Zn^{1+}, the 4d spinors must be included in the CAS subspace to account for near-degeneracy. MR-MP then yields a computed IE($Zn^0\ ^1S_0 \Rightarrow Zn^{1+}\ ^2D_{5/2}$) of 17.205 eV, and IE($Zn^0\ ^1S_0 \Rightarrow Zn^{1+}\ ^2D_{3/2}$) = 17.537 eV, deviations between theory and experiment being only 0.03 eV in both instances.

Table 7.8 displays the contribution at each order of perturbation theory to the $3d^{10}4s^2\ ^1S_0 \Rightarrow 3d^{10}4s^1\ ^2S_{1/2}$ ionization energy of Zn^0. These contributions were computed by subtracting the energies of Zn^0 from those of corresponding copper-like ion Zn^{1+} in each order of perturbation theory displayed in Table 1.5. The first set of entries in Table 2.3 gives the contribution computed by subtracting single-configuration DFB energies and second-order MP correlation corrections of zinc and zinc-like ions from those of the corresponding copper-like ions. In the

second set of entries, the contributions were computed by subtracting three-configuration MC DFB SCF and multireference MP second-order energies of zinc and zinc-like ions from single-configuration DFB energies and second-order correlation corrections of the corresponding copper-like ions. In the last row of the table, experimental IE is presented along with an estimated error in the extrapolation procedure involved in determining the IE.

Single-reference MP theory yields the IE of Zn^0,74945 cm^{-1}, in good agreement with experiment (75769 cm^{-1}). The residual discrepancy between theory and experiment, 824 cm^{-1}, is primarily due to the near-degeneracy unaccounted for in the single-reference description of ground-state Zn^0. MR-MP theory based on the three-configuration MC DFB SCF wavefunction yields an IE of 75802 cm^{-1}, in excellent agreement with experiment. Accounting for the near-degeneracy in Zn^0 by multireference perturbation theory reduces the residual discrepancy to 33 cm^{-1}.

2.4 Contribution of relativistic correlation energies and Lamb shift to term energy separations in Pb

The computed MC DFB SCF energies E_{MCDFB}, MR-MP second-order DC ($E^{(2)}_{DC}$) and Breit ($B^{(2)}$) correlation corrections, and the Lamb shift E_{LS} for the ^3P_J ($J = 0, 1, 2$) fine-structure states and the excited $^1D_2$ and $^1S_0$ even-parity states of Pb are displayed, respectively, in Tables 2.4 and 7.10. The numbers of CSF in the MC DFB SCF arising from distributing two $6p$ electrons among a minimal ($6p_{1/2}$, $6p_{3/2}$) active space are, respectively, 2, 1, and 2 for the $^3P_0$, $^3P_1$ and $^3P_2$ states.

MCDF SCF calculations were performed to obtain a single set of spinors for all the lowest ^3P_J ($J = 0, 1, 2$) fine-structure states by minimizing the average energy of the $^3P_{0,1,2}$ employing the J-averaged MC energies: $E^{MC}_{J-ave}(\gamma_K\pi) = \sum_J(2J+1)E^{MC}(\gamma_K J\pi)/\sum_{J'}(2J'+1)$ instead of performing state-specific MC DF SCF calculations on each fine-structure state. For neutral atoms with small fine-structure splittings (near degeneracy among $p_{1/2}$ and $p_{3/2}$ spinors), this approach is particularly effective in computing the fine-structure splittings with the subsequent state-by-state MR-MP procedure. The numbers of reference CSFs for state-specific MR-MP calculations were, respectively, 2, 1, and 2 for the J=0, 1, and 2 even-parity states. The MC DF energies of the excited $^1D_2$ and $^1S_0$ even-parity states are those obtained in the $^3P_{J=0,2}$ state MC energy optimization; state-by-state MC DF SCF calculations for the excited states were not done. Thus spinors and configuration mixing co-

Table 7.10 MCDFB, Lamb shift, correlation energies (in a.u.) and fine-structure (FS) separations (in cm−1) for the $6s^26p^2\ ^3P_J$ $(J = 0, 1, 2)$ states of Pb^0.

		Fine-structure separation
$6s^26p^2\ ^3P_0$		
E_{MCDFB}	-20888.990068	
E_{LS}	16.377189	
$E_{DC}^{(2)}$	-5.429900	
$B^{(2)}$	-0.344995	
E_{DCB}^{total}	-20878.387774	
$6s^26p^2\ ^3P_1$		$^3P_1$-$^3P_0$
E_{MCDFB}	-20888.958896	6841
E_{LS}	16.377194	
$E_{DC}^{(2)}$	-5.426621	
$B^{(2)}$	-0.343824	
E_{DCB}^{total}	-20878.352147	7819
Experiment		7819
$6s^26p^2\ ^3P_2$		$^3P_2$-$^3P_0$
E_{MCDFB}	-20888.941608	10636
E_{LS}	16.377194	
$E_{DC}^{(2)}$	-5.430330	
$B^{(2)}$	-0.343527	
E_{DCB}^{total}	-20878.338271	10865
Experiment		10650

efficients employed in MR-MP calculations for the excited states were those obtained in the $^3P_{J=0,2}$ MC DF calculations. All electrons were correlated in the state-specific MR-MP calculations.

In the last column of Tables 2.4 and 7.10, term energy splittings calculated at MC DFB and MR-MP levels of theory are given. The MC DFB SCF yields $^3P_1$ - $^3P_0$ fine-structure splitting of 6841 cm^{-1} and $^3P_2$ - $^3P_0$ splitting of 10636 cm^{-1} while the experimental fine-structure splittings are, respectively, 7819 cm^{-1} and 10650 cm^{-1}. Thus the bulk of the fine-structure splitting is due to one-body relativistic effects which are readily reproduced by MC DFB SCF. The residual discrepancy is due to many-body effects and requires relativistic many-body theory. The MP-MP perturbative improvement based on MC DFB SCF spinors yields a

Table 7.11 MCDFB, Lamb shift, correlation energies (in a.u.) and term energy separations (in cm−1) for $6s^26p^2\ ^1D_2$ and $^1S_0$ states of Pb^0.

		Term energy separation
$6s^26p^2\ ^1D_2$		$^1D_2$-$^3P_0$
E_{MCDFB}	-20888.88972	22024
E_{LS}	16.377198	
$E_{DC}^{(2)}$	-5.446212	
$B^{(2)}$	-0.341254	
E_{DCB}^{total}	-20878.29999	19266
Experiment		21458
$6s^26p^2\ ^1S_0$		$^1S_0$-$^3P_0$
E_{MCDFB}	-20888.84000	32936
E_{LS}	16.377198	
$E_{DC}^{(2)}$	-5.452299	
$B^{(2)}$	-0.341016	
E_{DCB}^{total}	-20878.25612	28895
Experiment		29467

Table 7.12 Effects of correlating increasing number of electronic shells on the $6s^26p^2$ ($^3P_{1,2}$ - $^3P_0$) fine-structure separations (cm^{-1}) of Pb^0.

	$\Delta E_{DCB}^{(2)}$ $6s^26p^2\ ^3P_1$ - $^3P_0$	ΔE_{DCB}^{total}	$\Delta E_{DCB}^{(2)}$ $6s^26p^2\ ^3P_2$ - $^3P_0$	ΔE_{DCB}^{total}
6p	930	7772	370	11007
6s	380	7222	-336	10301
5s	730	7572	-44	10593
4s	947	7789	194	10443
3s	972	7814	223	10860
2s	975	7817	226	10863
1s	977	7819	228	10865
Exp.		7819		10650

Table 7.13 Comparison with experiment of the computed term energy separations (cm^{-1}) of Pb^0.

$6s^26p^2\ 3P_1$	
CC[a]	7531
MCDFB	6841
Biemont[b]	7707
MR-MP DCB2	7819
Experiment	7819
$6s^26p^2\ 3P_2$	
CC[a]	10307
MCDFB	10636
Biemont[b]	10947
MR-MP DCB2	10865
Experiment	10650
$6s^26p^2\ 1D_2$	
CC[a]	20853
MCDFB	22024
Biemont[b]	21283
MR-MP DCB2	19266
Experiment	21458
$6s^26p^2\ 1S_0$	
CC[a]	29259
MCDFB	32936
Biemont[b]	28316
MR-MP DCB2	28895
Experiment	29467

[a] - Ref [97], [b] - Ref [98].

$^3P_1$ - $^3P_0$ fine structure splitting of 7819 cm^{-1}, a fortuitous, four-digit agreement, while the $^3P_2 - ^3P_0$ fine structure splitting computed by MR-MP yields 10865 cm^{-1}, about 200 cm^{-1} off the experimental value. The $^1S_0$ - $^3P_0$ term energy separation computed at the MC DFB SCF level is 32936 cm^{-1}, overestimating experiment (29467 cm^{-1}) by as much as 3500 cm^{-1}. Inclusion of dynamic correlations, $E_{DC}^{(2)}$ and $B^{(2)}$, by MR-MP reduces the term energy separation to 28895 cm^{-1} in reasonable agreement with experiment. Table 7.11 displays the Dirac-Coulomb-Breit ($E_{DC}^{(2)} + B^{(2)}$) correlation contribution from individual correlated shells, the n=1 through 6, to the $^3P_{1,2}$ - $^3P_0$ fine structure separations. Correlating only n=5 and 6 electrons, as is often done in approximate relativistic effective core potential methods, to calculate the $^3P_2$ - $^3P_0$ fine structure separation yields the best, if artifactual, agreement with experiment. Correlating all electrons is seen to yield the calculated fine structure separation in slightly poorer agreement with experiment. Table 7.12 compares the computed MR-MP term energy separations with experiment. Previous theoretical values computed by means of Fock-space relativistic CC [97] and semiempirical scheme by Biemont [98] are also given for comparison.

3. Summary

We have developed the relativistic single- and multireference Møller-Plesset perturbation theory for a general class of open-shell systems with a manifold of configurations which interact strongly due to asymptotic degeneracy. The relativistic many-body perturbation theory for electron correlation is designed to treat a general class of open-shell systems with two or more valence electrons that often exhibit quasidegeneracies. The essential features of the theory are its treatment of the state-specific nondynamic correlation in zero order through open-shell DF and MC DF SCF, and recovery of the remaining correlation, which is predominantly dynamic pair correlation, by second-order perturbation theory. We have reported the successful implementation and application of relativistic single- and multireference Møller-Plesset perturbation theory to the group-IB, -IIB, and -IIIA atoms and their ions. Accurate calculation of term energy separations in such systems requires a method flexible enough to account for the Dirac-Coulomb-Breit static and dynamic correlations, and the Lamb shift that vary considerably from state to state.

References

[1] Pyykkö, P. (1988). *Chem. Rev.*, **88**, 563.

[2] Ishikawa, Y., and Kaldor, U. (1996). In *Computational Chemistry: Reviews of Current Trends*, Vol. 1, J. Leszczynski, Ed., World Scientific, NJ.

[3] Hess, B. A. (1986). *Phys. Rev. A*, **33**, 3742.

[4] Nakajima, T., and Hirao, K. (1999). *Chem. Phys. Lett.*, **302**, 382.

[5] Nakajima, T., Koga, K., and Hirao, K. (2000). *J. Chem. Phys.*, **112**, 10142.

[6] Yanai, T., Nakajima, T., Ishikawa, Y., and Hirao, K. (2001). *J. Chem. Phys.*, **114**, 6526.

[7] Visscher, L., Visser, O., Aerts, H., Merenga, H., and Nieuwpoort, W. C. (1994). *Comput. Phys. Commun.*, **81**, 120.

[8] Saue, T., Faegri, K., Helgaker, T., and Gropen, O. (1997). *Mol. Phys.*, **91**, 937.

[9] Mohanty, A., and Clementi, E. (1991). *Int. J. Quant. Chem.*, **39**, 487.

[10] Dyall, K. G., Taylor, P. R., Faegri, K., and Partridge, H. (1991). *J. Chem. Phys.*, **95**, 2583.

[11] Pisani, L., and Clementi, E. (1994). *J. Comput. Chem.*, **15**, 466.

[12] Chandra, P., and Hess, B. A. (1994). *Theor. Chim. Acta.*, **88**, 183.

[13] Collins, C. L., Dyall, K. G., and Schaefer III, H. F. (1995). *J. Chem. Phys.*, **102**, 2024.

[14] Mohanty, A. K., and Parpia, F. A. (1996). *Phys. Rev. A*, **54**, 2863.

[15] Schwerdtfeger, P., Brown, J. R., and Laerdahl, J. K. (2000). *J. Chem. Phys.*, **113**, 7110.

[16] Johnson, W. R., Idrees, M., and Sapirstein, J. (1987). *Phys. Rev. A*, **35**, 3218.

[17] Ishikawa, Y. (1990). *Phys. Rev. A*, **42**, 1142.

[18] Quiney, H. M., Grant, I. P., and Wilson, S. (1987). *Phys. Scripta*, **36**, 460.

[19] Quiney, H. M., Grant, I. P., and Wilson, S. (1990). *J. Phys. B*, **23**, L271.

[20] Eliav, E., Kaldor, U., and Ishikawa, Y. (1994). *Phys. Rev. A*, **49**, 1724.

[21] Eliav, E., Kaldor, U., and Ishikawa, Y. (1995). *Phys. Rev. A*, **51**, 225.

[22] Eliav, E., Kaldor, U., and Ishikawa, Y. (1995). *Phys. Rev. A*, **52**, 291.

[23] Eliav, E., Kaldor, U., and Ishikawa, Y. (1995). *Phys. Rev. A*, **52**, 2765.

[24] Eliav, E., Kaldor, U., and Ishikawa, Y. (1996). *Phys. Rev. A*, **53**, 3050.

[25] Eliav, E., Kaldor, U., Schwerdtfeger, P., Hess, B. A., and Ishikawa, Y. (1994). *Phys. Rev. Lett.*, **73**, 3203.

[26] Eliav, E., Kaldor, U., and Ishikawa, Y. (1995). *Phys. Rev. Lett.*, **74**, 1079.

[27] Eliav, E., Kaldor, U., Ishikawa, Y., Seth, M., and Pyykkö, P. (1996). *Phys. Rev. A*, **53**, 3926.

[28] Eliav, E., Kaldor, U., Ishikawa, Y., and Pyykkö, P. (1996). *Phys. Rev. Lett.*, **77**, 5350.

[29] Eliav, E., Ishikawa, Y., Pyykkö, P., and Kaldor, U. (1997), *Phys. Rev. A*, **56**, 4532.

[30] Eliav, E., Kaldor, U., and Ishikawa, Y. (1998). *Mol. Phys.*, **94**, 181.

[31] Eliav, E., Shmulyian, S., Kaldor, U., and Ishikawa, Y. (1998). *J. Chem. Phys.*, **109**, 3954.

[32] Blundell, S. A., Johnson, W. R., and Sapirstein, J. (1991). *Phys. Rev. Lett.*, **65** 1411.

[33] Blundell, S. A., Johnson, W. R., and Sapirstein, J. (1992). *Phys. Rev. D*, **45**, 1602.

[34] Avgoustoglou, E., Johnson, W. R., Liu, Z. W., and Sapirstein, J. (1995). *Phys. Rev. A*, **51**, 1196.

[35] Sucher, J. (1980). *Phys. Rev. A*, **22**, 348.

[36] Mittleman, M. H. (1981). *Phys. Rev. A*, **24**, 1167.

[37] Ishikawa, Y. (1990). *Chem. Phys. Lett.*, **166**, 321.

[38] Ishikawa, Y. (1990). *Int. J. Quant. Chem.*, **S24**, 383.

[39] Ishikawa, Y., Quiney, H. M., and Malli, G. L. (1991). *Phys. Rev. A*, **43**, 3270.

[40] Ishikawa, Y., and Quiney, H. M. (1993). *Phys. Rev. A*, **47**, 1732.

[41] Ishikawa, Y., and Koc, K. (1994). *Phys. Rev. A*, **50**, 4733.

[42] Ishikawa, Y., Baretty, R., and Binning, R. C. (1985). *Chem. Phys. Lett.*, **121**, 130.

[43] Ishikawa, Y., Baretty, R., and Binning, R. C. (1985). *Intern. J. Quantum Chem.*, **S19**, 285.

[44] Ishikawa, Y., Binning, R. C. Jr., and Sando, K. M. (1984). *Chem. Phys. Lett.*, **105**, 189.

[45] Ishikawa, Y., Binning, R. C. Jr., and Sando, K. M. (1983). *Chem. Phys. Lett.*, **101**, 111.

[46] Lee, Y. S., and McLean, A. D. (1982). *J. Chem. Phys.*, **76**, 76.

[47] Dyall, K. G., Grant, I. P., and Wilson, S. (1984). *J. Phys. B*, **17**, 1201.

[48] Aerts, P. J. C., and Nieuwpoort, W. (1986). *Chem. Phys. Lett.*, **125**, 83.

[49] Ishikawa, Y., and Sekino, H. (1988). *Intern. J. Quantum Chem.*, **S22**, 457.

[50] Ishikawa, Y., and Sekino, H., (1990). *Chem. Phys. Lett.*, **165**, 243.

[51] Ishikawa, Y., Koc, K., and Schwarz, W. H. E. (1997). *Chem. Phys.*, **225**, 239.

[52] Visscher, L., and Dyall, K. G. (1997). *At. Data Nucl. Data Tables*, **67**, 207.

[53] Molzberger, K., and Schwarz, W. H. E. (1996). *Theor. Chim. Acta*, **94**, 213.

[54] Kutzelnigg, W. (1990). *Z. Phys. D*, **12**, 27.

[55] Bohr, A., and Weisskopf, V. F. (1950). *Phys. Rev.*, **77**, 94.

[56] Ishikawa, Y., and Quiney, H. M. (1987). *Intern. J. Quantum Chem.*, **S21**, 523.

[57] Malli, G. L., Da Silva, A. B. F., and Ishikawa, Y. (1993). *Phys. Rev. A*, **47**, 143.

[58] Malli, G. L., Da Silva, A. B. F., and Ishikawa, Y. (1994). *J. Chem. Phys.*, **101**, 6829.

[59] Quiney, H. M., Grant, I. P., and Wilson, S. (1989). *In Many-body methods in Quantum Chemistry*, edited by U. Kaldor, Lecture notes in Chemistry, Vol. 52 (Springer, Berlin).

[60] Grant, I. P., and Pyper, N. C. (1976). *J. Phys. B*, **9** 761.

[61] Lowdin, P. O. (1959). *Adv. Chem. Phys.*, **2**, 207.

[62] Ishikawa, Y., Koc, K. (1996). *Phys. Rev. A*, **53**, 3966.

[63] Ishikawa, Y., Koc, K. (1997). *Phys. Rev. A*, **56**, 1295.

[64] Ishikawa, Y., Koc, K. (1997). *Int. J. Quant. Chem.*, **65**, 545.

[65] Koc, K., and Ishikawa, Y. (1994). *Phys. Rev. A*, **49**, 794.

[66] Møller, C., and Plesset, M. S. (1934). *Phys. Rev.*, **46**, 618.

[67] Huzinaga, S., and Klobukowski, M. (1985). . *J. Mol. Structure(Theochem)*, **63**, 1812.

[68] Gorciex, O., Indelicato P., and Desclaux, J. P. (1987). *J. Phys. B*, **20**, 639.

[69] Indelicato, P., Gorceix, O., and Desclaux, J. P. (1987). *J. Phys. B*, **20**, 651.

[70] Desclaux, J. P. (1975). *Computer Phys. Comm.* , **9**, 31.

[71] Martin, R. L., and Hay, P. J. (1981). *J. Chem. Phys.*, **75**, 4539.

[72] Raghavachari, K., and Trucks, G. W. (1989). *J. Chem. Phys.*, **91**, 2457.

[73] Johnson, W. R., Blundell, S. A., and Sapirtsein, J. (1988). *Phys. Rev. A*, **37**, 307.

[74] Koc, K., and Migdalek, J. (1990). *J. Phys. B*, bf 23, L5.

[75] Eliav, E., Kaldor, U., and Ishikawa, Y. (1994). *Phys. Rev. A*, **50**, 1121.

[76] Moore, C. E. (1971). *Atomic Energy Levels*, Natl. Bur. Stand. Ref. Data Ser. Natl. Bur. Stand, (US) Circ. No. 35 (U.S. GPO, Washington, D.C.).

[77] Hughes, S. R., and Kaldor, U. (1993). *Phys. Rev. A*, **47**, 4705.

[78] Guo, Y., and Whitehead, M. A. (1988). *Phys. Rev. A*, **38**, 3166.

[79] Vijayakumar, M., and Gopinathan, M. S. (1992). *J. Chem. Phys.*, **97**, 6639

[80] Samzow, R., Hess, B. A., and Jansen, G. (1992). *J. Chem. Phys.*, **96**, 1227.

[81] Schwerdtfeger, P. (1991). *Chem. Phys. Lett.*, **183**, 457.

[82] Weiss, A. W., and Kim, Y.-K. (1995). *Phys. Rev. A*, **51**, 4487.

[83] Vilkas, M. J., Ishikawa, Y., and Koc, K. (1998). *Phys. Rev. E*, **58**, 5096.

[84] Vilkas, M. J., Koc, K., and Ishikawa, Y. (2001). In *Progress in Theoretical Chemistry and Physics*, Kluwer: Dordrecht.

[85] Quiney, H. M. (2001). In *Progress in Theoretical Chemistry and Physics*, Kluwer: Dordrecht.

[86] Hirao, K. (1992). *Chem. Phys. Lett.*, **190**, 374.

[87] Hirao, K. (1993). *Chem. Phys. Lett.*, **201**, 59.

[88] Mohr, P. J. (1992). *Phys. Rev. A*, **46**, 4421.

[89] Blundell, S. A., Mohr, P. J., Johnson, W. R., and Sapirstein, J. (1993). *Phys. Rev. A*, **48**, 2615.

[90] Labzowsky, L., Karasiev, V., Lindgren, I., Persson, H., Salomonson, S. (1993). *Phys. Scripta*, **T46**, 150.

[91] Fuhr, J. R., Martin, W. C., Musgrove, A., Sugar, J., and Wiese, W. L. (1997). *NIST Atomic Spectroscopic Database*, available at http://physics.nist.gov/ PhysRefData/ contents.html.

[92] Vilkas, M. J., Ishikawa, Y., and Hirao, K. (2000). *Chem. Phys. Lett.*, **321**, 243.

[93] Vilkas, M. J., Koc, K., and Ishikawa, Y. (1998). *Chem. Phys. Lett.*, **296**, 68.

[94] Vilkas, M. J., Ishikawa, Y., and Koc, K. (1999). *Phys. Rev. A*, **60**, 2808.

[95] Ishikawa, Y.,Vilkas, M. J., and Koc, K. (2000). *Int. J. Quantum Chem.*, **77**, 433.

[96] Ishikawa, Y., and Vilkas, M. J. (2001). *Phys. Rev. A*, 042506.

[97] Landau, A., Eliav, E., Ishikawa, Y., and Kaldor, U. (2001). *J. Chem. Phys.*, **114**, 2977.

[98] Biemont, E., and Quinet, P. (1996). *Phys. Scripta*, **54**, 36.

Chapter 8

MATRIX APPROXIMATIONS TO THE DIRAC HAMILTONIAN FOR MOLECULAR CALCULATIONS.

Kenneth G. Dyall

Eloret Corporation, 690 W. Fremont Ave. Suite 8, Sunnyvale, CA 94087, U. S. A.

kgdyall@earthlink.net

Abstract This chapter develops several approximate methodologies for the solution of the Dirac equation in a finite basis set. The approximations are made in the matrix formalism rather than in the operator formalism. The operator equation that underlies the developments is the modified Dirac equation, which enables a spin separation similar to that found in the Breit-Pauli or the Douglas-Kroll formalism. The small component is eliminated by a non-unitary transformation that generates a non-unit metric, but one on which the large component is normalized. The transformation depends on the one-particle eigenstates. In the first approximation this dependence is frozen at the atomic level and subsumed into the contraction coefficients of the atomic basis sets. The second approximation classifies atoms as "relativistic" or "nonrelativistic", allowing relativistic effects to be incorporated into an otherwise nonrelativistic calculation. To both of these approximations is added a further approximation for scalar relativistic effects in which the two-electron terms are treated approximately, and only the one-electron integrals need be modified. The errors in the first approximation are negligible for most chemical purposes, and the errors in the last approximation are also mostly negligible. The errors made in treating atoms nonrelativistically has a large Z dependence, but is sufficiently accurate for most chemical purposes for elements up to Ar.

Keywords: Modified Dirac equation, matrix approximations, scalar relativistic effects

U. Kaldor and S. Wilson (eds.),
Theoretical Chemistry and Physics of Heavy and Superheavy Elements, 325–347.
© 2003 *Kluwer Academic Publishers.*

Introduction

The development of approximate methods which can be applied to molecules containing heavy and superheavy atoms has largely followed the line of approximating the Dirac Hamiltonian operator itself, using either the elimination of the small component (ESC) [1,2] or a unitary transformation which block-diagonalizes the Dirac operator to some order in a suitable expansion parameter [3–7]. The approximations each have their cost in the complexity of the resultant operators. In the ESC approaches, either the energy or the potential is contained in the denominator of some expression. The transformation approaches result either in simple but singular operators and divergent series, or in convergent series with non-trivial functions of the square of the momentum operator. None of these forms lend themselves well to the usual methods of quantum chemistry. The ESC-derived operators can be evaluated if the potential is tabulated on a grid, or if further approximations are made [8], and the transformation-derived operators require further approximations which are usually made in some suitable basis set.

Since the majority of relativistic (and nonrelativistic) molecular calculations expand the wave function in a finite basis set, thus reducing the Dirac operator equation to a matrix equation, it makes sense to seek approximations to the matrix form of the Dirac equation rather than to the operator form. Matrices are easy to manipulate, and the approximations can be made on the basis of numerical magnitude as well as on the basis of principle. In fact, most quantum chemistry programs use screening techniques based on the numerical magnitude of matrix elements, especially in direct SCF programs, and such methods have been applied to four-component Dirac-Hartree-Fock (DHF) programs as well [9,10].

In this chapter, we present a series of approximations at the matrix level which start from the matrix Dirac or Dirac-Hartree-Fock equation. Because of this, the integrals over the operators remain simple and can be evaluated readily. The approximations are based on considerations of the physics and chemistry and are motivated by the desire for methods that can be relatively easily incorporated into standard nonrelativistic quantum chemistry codes, and by the desire for methods whose numerical accuracy can be tested against some known standard. One important advantage of retaining simple operators is that the derivatives of the matrix elements with respect to geometric displacements are easy to evaluate, making it possible to perform geometry optimizations and calculate harmonic frequencies using analytic derivative techniques. These

approximations have been developed in a series of papers by the author [12–15].

The easiest implementation of such approximations in standard non-relativistic programs must, because of the symmetry of the operators involved, include only scalar relativistic effects. For this reason, the developments of this chapter are made in terms of the modified Dirac equation in which the separation of scalar and spin-dependent relativistic effects can be done rigorously. The first section of this chapter presents the modified Dirac equation [11] in some detail, not only for the purposes of this chapter but also because the scalar approximation is useful in its own right.

Subsequent sections develop the operator then the matrix versions of the Foldy-Wouthuysen transformation and the elimination of the small component and discuss the properties of the resulting methods, then present approximations to the transformed Hamiltonian matrix. We conclude with a discussion of electric and magnetic properties in the matrix approximations.

1. The Modified Dirac Equation

The foundation of most developments of relativistic approximations is the time-independent Dirac equation, which we write here in what we call its standard form,

$$\hat{H}_{\mathrm{D}}\Psi = \begin{pmatrix} V & c\sigma\cdot\mathbf{p} \\ c\sigma\cdot\mathbf{p} & V-2mc^2 \end{pmatrix}\begin{pmatrix} \Psi^L \\ \Psi^S \end{pmatrix} = \begin{pmatrix} \Psi^L \\ \Psi^S \end{pmatrix} E \tag{8.1}$$

In this standard form, the Dirac equation does not lend itself either to spin separation or to approximations based on the magnitude of the speed of light, c. The second of these issues is readily addressed by scaling the small component of the wave function, Ψ^S by c, so that it is of the same order of magnitude as the large component, Ψ^L. Then the Dirac equation becomes

$$\begin{pmatrix} V & \sigma\cdot\mathbf{p} \\ \sigma\cdot\mathbf{p} & V/c^2-2m \end{pmatrix}\begin{pmatrix} \Psi^L \\ c\Psi^S \end{pmatrix} = \begin{pmatrix} 1 & 0 \\ 0 & 1/c^2 \end{pmatrix}\begin{pmatrix} \Psi^L \\ c\Psi^S \end{pmatrix} E \tag{8.2}$$

It is obvious that one ought to be able to expand this equation in powers of $1/c^2$ with a modified small component, $\Phi^S = c\Psi^S$. This form of the Dirac equation was used for the development of Direct Perturbation Theory [16,17].

However, it is the first issue that must be addressed to develop scalar relativistic approximations, and again this is achieved by modifying the

small component. In addition to changing the magnitude of the modified small component, we also extract the operator $\sigma \cdot \mathbf{p}$ to obtain a function that has very similar properties to the large component, and which we call the pseudo-large component,

$$\Phi^L = \frac{\sigma \cdot \mathbf{p}}{2mc} \Psi^S \tag{8.3}$$

The pseudo-large component has the same symmetry properties as the large component, and in the nonrelativistic limit is identical with the large component.

We can regard the modification to the small component as a transformation of the wave function,

$$\begin{pmatrix} \Psi^L \\ \Psi^S \end{pmatrix} = \begin{pmatrix} 1 & 0 \\ 0 & \sigma \cdot \mathbf{p}/2mc \end{pmatrix} \begin{pmatrix} \Psi^L \\ \Phi^L \end{pmatrix} \tag{8.4}$$

Substituting this expression into the standard Dirac equation and premultiplying by the transformation matrix, we obtain the modified Dirac equation,

$$\begin{pmatrix} V & T \\ T & W/4m^2c^2 - T \end{pmatrix} \begin{pmatrix} \Psi^L \\ \Phi^L \end{pmatrix} = \begin{pmatrix} 1 & 0 \\ 0 & T/2mc^2 \end{pmatrix} \begin{pmatrix} \Psi^L \\ \Phi^L \end{pmatrix} E. \tag{8.5}$$

Here, T is the nonrelativistic kinetic energy operator, $T = p^2/2m$, and the operator W is given by

$$W = \sigma \cdot \mathbf{p} V \sigma \cdot \mathbf{p} = \mathbf{p} V \cdot \mathbf{p} + i\sigma \cdot (\mathbf{p} V) \times \mathbf{p}, \tag{8.6}$$

where the Dirac relation has been used to obtain the final result, and the parentheses indicate that the momentum operator acts only on V.

There are several important features of the modified Dirac equation. The first is that all the operators are simple operators. The most complicated operator is W, which contains two momentum operators. However, it is relatively easy to evaluate the integrals over these operators, because the momentum operators can be applied to the basis functions instead of to the potential, V. This is a simple matter of integration by parts. There are no complicated functions of the momentum or of the potential that require further approximations to evaluate the integrals. The second is that all the spin-dependence appears in W, and W separates cleanly into a spin-free or scalar part, and a spin-dependent part which is none other than the familiar spin-orbit operator from Breit-Pauli theory.

It has been pointed out that there are many possible ways of performing spin separation [18], and these ways do not necessarily give equivalent

results [19], but the current approach satisfies the goal of keeping the operators simple and interfacing as easily as possible with nonrelativistic programs.

We mentioned above that the large and the pseudo-large components become identical in the nonrelativistic limit. This is easily shown by taking c to infinity in equation (8.5), which yields

$$V\Psi^L + T\Phi^L = E\Psi^L \tag{8.7}$$

$$T\Psi^L - T\Phi^L = 0 \tag{8.8}$$

Substitution of the second equation into the first yields the Schrödinger equation for the large component, and the only non-trivial solution of the second equation, given the form of the solution to first equation, is $\Psi^L = \Phi^L$.

As Kutzelnigg has pointed out [17], there are problems with taking the limit $c \to \infty$ when the potential is a Coulomb potential, because the potential W does not vanish at $r = 0$. In this case, the pseudo-large component approaches the large component for $r > 0$. This can be demonstrated with the radial large and small components for the $1s$ state of a hydrogenic atom, $\Psi_r^X = N^X r^{\gamma-1} e^{-Zr}$, with $\gamma^2 = \kappa^2 - Z^2/c^2$ and $X = L, S$. Taking advantage of spherical symmetry, equation 8.3 can be written as

$$\Phi_r^L = N^S \int r^{\gamma-1} e^{-Zr} dr \tag{8.9}$$

If we integrate by parts to obtain a power series expansion, the result is

$$\Phi_r^L = (N^S/\gamma) r^\gamma e^{-Zr} \left(1 + \frac{Zr}{\gamma+1} + \dots\right), \tag{8.10}$$

which, on taking the limit $c \to \infty$ ($\gamma \to 1$) yields the result $\Phi_r^L \approx r\Psi_r^L$ for small r. This behavior can be demonstrated for all solutions of the modified Dirac equation, and is necessary to make the integrals over W non-singular. If instead we integrate by parts to obtain an asymptotic expansion, the result is

$$\Phi_r^L = (N^S/Z) r^{\gamma-1} e^{-Zr} \left(1 + \frac{\gamma-1}{Zr} + \dots\right). \tag{8.11}$$

This series reduces to the correct nonrelativistic limit, but only for $r > 0$. Here, the subscript r has been used to indicate the radial part of the wave function.

For a finite nuclear size, there is no such problem, because the potential remains finite for all r, and both the large and pseudo-large components

behave as r^ℓ at the origin. The potential W, having no negative powers of r in its series expansion, is also finite for all r.

Examining the properties of the large and pseudo-large components near the nucleus, it has been found that the magnitude of the pseudo-large component is much smaller than that of the large component. This finding makes sense in the light of the extra factor of r in the pseudo-large component for a point nucleus. For a finite nucleus, the potential rapidly becomes Coulombic outside the nuclear radius, so the behavior of the pseudo-large component should be similar in this region to that of the point nucleus pseudo-large component. The implication of this finding is that the potential for the pseudo-large component must be more repulsive than that for the large component.

From here on, we will drop the superscript L from the components, and use the notation Ψ for the large component and Φ for the pseudo-large component.

The transformation for the two-electron terms follows straightforwardly from the definitions of the operators, and the result is a set of operators that are similar to the Breit-Pauli operators, and can be classified into spin-free, spin-orbit, spin-other-orbit, and spin-spin categories. In addition to the terms that are of order c^{-2} there are also terms that are of order c^{-4} arising from the relativistic Coulomb interaction. The representation of these operators is not entirely simple because it involves matrices for both electron coordinates.

The transformation of the Coulomb operator generates four operators, which can be expressed as

$$g_{ij}^{00} = g_{ij}\mathbf{I}_2 \tag{8.12}$$

$$g_{ij}^{20} = \sigma_i \cdot \mathbf{p}_i \; g_{ij} \; \sigma_i \cdot \mathbf{p}_i / 4m^2c^2 \tag{8.13}$$

$$g_{ij}^{02} = \sigma_j \cdot \mathbf{p}_j \; g_{ij} \; \sigma_j \cdot \mathbf{p}_j / 4m^2c^2 \tag{8.14}$$

$$g_{ij}^{22} = \sigma_i \cdot \mathbf{p}_i \; \sigma_j \cdot \mathbf{p}_j \; g_{ij} \; \sigma_j \cdot \mathbf{p}_j \; \sigma_i \cdot \mathbf{p}_i / 16m^4c^4 \tag{8.15}$$

where $g_{ij} = 1/r_{ij}$. Applying the Dirac relation to reduce the number of spin matrices, the second and third operators yield a spin-free and a spin-orbit operator in analogy to the one-electron operator, and the fourth yields a more complicated operator that has spin-free, spin-orbit and spin-spin terms. These four operators must be combined with the matrix projectors onto the large component and the pseudo-large component, $\mathbf{P}$ and $\mathbf{R}$,

$$\mathbf{P} = \begin{pmatrix} 1 & 0 \\ 0 & 0 \end{pmatrix}; \qquad \mathbf{R} = \begin{pmatrix} 0 & 0 \\ 0 & 1 \end{pmatrix}. \tag{8.16}$$

These matrices operate on the two component vector that appears in eq. (8.4). The transformed Coulomb operator can finally be written as

$$\begin{aligned} g_{ij}^{\text{mod}} &= \mathbf{P}_i\mathbf{P}_j g_{ij}^{00}\mathbf{P}_j\mathbf{P}_i + \mathbf{P}_i\mathbf{R}_j g_{ij}^{02}\mathbf{R}_j\mathbf{P}_i \\ &\quad + \mathbf{R}_i\mathbf{P}_j g_{ij}^{20}\mathbf{P}_j\mathbf{R}_i + \mathbf{R}_i\mathbf{R}_j g_{ij}^{22}\mathbf{R}_j\mathbf{R}_i. \end{aligned} \tag{8.17}$$

Here the direct product of projection operators and g operators is to be taken. The transformation of the Gaunt or Breit operators can be performed in a similar fashion. The results are reported in the original paper [11].

The spin-free version of the modified Dirac equation has the same spectral properties as the standard Dirac equation, and can be used in the same way. Its advantage is that the spin can be factored out and, after some suitable SCF solutions have been obtained, the machinery of nonrelativistic correlation methods can be used with modified integrals.

The modified electric property operators have the same form as for the potential. For a scalar potential U, the modified operator is

$$\begin{pmatrix} U & 0 \\ 0 & \sigma\cdot\mathbf{p}\, U\, \sigma\cdot\mathbf{p}/4m^2c^2 \end{pmatrix} \tag{8.18}$$

For magnetic properties, the modified form of the vector potential is needed, which is

$$\frac{1}{2m}\begin{pmatrix} 0 & \sigma\cdot\mathbf{A}\,\sigma\cdot\mathbf{p} \\ \sigma\cdot\mathbf{p}\,\sigma\cdot\mathbf{A} & 0 \end{pmatrix}. \tag{8.19}$$

Both operators can be separated into a scalar and a spin-dependent term. The terms for the electric operator follow from the analogous terms in the nuclear attraction. The magnetic term separates as follows:

$$\frac{1}{2m}\begin{pmatrix} 0 & \mathbf{A}\cdot\mathbf{p} \\ \mathbf{p}\cdot\mathbf{A} & 0 \end{pmatrix} + \frac{i}{2m}\begin{pmatrix} 0 & \sigma\cdot\mathbf{A}\times\mathbf{p} \\ \sigma\cdot\mathbf{p}\times\mathbf{A} & 0 \end{pmatrix}. \tag{8.20}$$

The spin-dependent term includes the interaction of the spin with a magnetic field.

2. Elimination of the Small Component and the Foldy-Wouthuysen Transformation

The first stage in most relativistic approximations is the elimination of the small component, either by mathematical manipulation or by a unitary transformation of the Dirac operator. Such transformations we will refer to as Foldy-Wouthuysen transformations, even though the original transformation was developed into an expansion in powers of $1/c$ that yields the Breit-Pauli Hamiltonian. This set of approximations presented here is no exception, but before we present the matrix versions, we give an overview of the operator equivalents. Here, we will use Hartree atomic units $\hbar = e = m1$ and replace the inverse of the speed of light $1/c$ with the fine-structure constant α.

The general form of a Foldy-Wouthuysen transformation of the Dirac Hamiltonian as presented by Kutzelnigg [17] must be adapted for the modified Dirac equation because of the non-unit metric. In addition, the transformation can be factorized into an orthogonal transformation and a normalization, with the following result,

$$\hat{U} = \begin{pmatrix} 1 & -\frac{\alpha^2}{2}\hat{X}^\dagger T \\ \hat{X} & 1 \end{pmatrix} \begin{pmatrix} (1+\frac{\alpha^2}{2}\hat{X}^\dagger T\hat{X})^{-1/2} & 0 \\ 0 & (\frac{\alpha^2}{2}T + \frac{\alpha^4}{4}T\hat{X}\hat{X}^\dagger T)^{-1/2} \end{pmatrix} \tag{8.21}$$

where $\hat{X}$ is an operator to be defined. Each of the operators in the matrices are 2×2 matrix operators. The exact transformation converts the 4×4 modified Dirac Hamiltonian into a form with 2×2 matrix operators on the diagonal and 2×2 zero matrices off-diagonal, which separates the positive energy and the negative energy states. For this case, the operator $\hat{X}$ is the operator that converts the pseudo-large component into the large component.

From the transformed Hamiltonian, $\mathbf{U}^\dagger \hat{H}_D \mathbf{U}$, the transformed equation for the positive energy states is

$$\begin{aligned} &\frac{1}{\sqrt{1+\frac{\alpha^2}{2}\hat{X}^\dagger T\hat{X}}}\Bigg[V + \frac{\alpha^2}{4}\hat{X}^\dagger W\hat{X} \\ &\qquad + T\hat{X} + \hat{X}^\dagger T - \hat{X}^\dagger T\hat{X}\Bigg]\frac{1}{\sqrt{1+\frac{\alpha^2}{2}\hat{X}^\dagger T\hat{X}}}\Phi^{\mathrm{FW}} \\ &= E\frac{1}{\sqrt{1+\frac{\alpha^2}{2}\hat{X}^\dagger T\hat{X}}}\left[1+\frac{\alpha^2}{2}\hat{X}^\dagger T\hat{X}\right]\frac{1}{\sqrt{1+\frac{\alpha^2}{2}\hat{X}^\dagger T\hat{X}}}\Phi^{\mathrm{FW}}. \end{aligned} \tag{8.22}$$

The metric has been included explicitly here; it is of course the 2×2 unit matrix. Apart from the difficulty that the operator $\hat{X}$ is unknown, this equation contains functions of $\hat{X}$ that make it difficult to evaluate. In the case of the Douglas-Kroll transformation these are usually evaluated using matrix methods [5].

The complicated operators arise from the requirement that the transformed wave function be normalized on the unit metric. If we do not require a unit metric, we can perform an orthogonal transformation that is much simpler in form,

$$\hat{U}' = \begin{pmatrix} 1 & -\frac{\alpha^2}{2}\hat{X}^\dagger T \\ \hat{X} & 1 \end{pmatrix} \tag{8.23}$$

and obtain an equation for the large component instead of the transformed wave function,

$$\left[V + \frac{\alpha^2}{4}\hat{X}^\dagger W \hat{X}^2 + T\hat{X} + \hat{X}^\dagger T - \hat{X}^\dagger T \hat{X}\right] \Psi^L = E\left[1 + \frac{\alpha^2}{2}\hat{X}^\dagger T \hat{X}\right] \Psi^L. \tag{8.24}$$

This equation has a non-unit metric, and clearly the large component and the transformed wave function are related by a renormalization,

$$\Phi^{\mathrm{FW}} = \sqrt{1 + \frac{\alpha^2}{2}\hat{X}^\dagger T \hat{X}}\ \Psi^L. \tag{8.25}$$

The equivalent equations in the unmodified Dirac equation were obtained by van Lenthe *et al.* [20].

The traditional elimination of the small component (ESC) also gives an equation for the large component. It proceeds by expressing the small component in terms of the large component using the second line of the (modified) Dirac equation as expressed in two-component form, which we can write in terms of $\hat{X}$,

$$\Phi^L = \hat{X}\Psi^L. \tag{8.26}$$

Substituting into the first line of the modified Dirac equation yields an equation for the large component,

$$\left[V + T\hat{X}\right] \Psi^L = E\Psi^L. \tag{8.27}$$

Using the modified Dirac equation, we can write $\hat{X}$ as

$$\hat{X} = \left[(1 + \frac{\alpha^2}{2}E)T - \frac{\alpha^2}{4}W\right]^{-1} T \tag{8.28}$$

and thus we see that the operator $T\hat{X}$ is Hermitian. In addition we see that $\hat{X} = 1 + \mathcal{O}(\alpha^2)$.

We now have two equations for the large component, one from the "traditional" elimination of the small component, and one from an orthogonal transformation of the Dirac Hamiltonian. The latter equation can also be derived by premultiplying the second line of equation (8.5) by $\hat{X}^\dagger$, eliminating Φ and adding to the first.

The equation from the orthogonal transformation has a non-unit metric. This metric is important because it is the metric on which the large component is normalized. The method that uses this equation is therefore termed the Normalized Elimination of Small Components (NESC). In contrast, the traditional ESC has a unit metric, and the large component must be renormalized. This method is therefore termed the Unnormalized Elimination of Small Components (UESC). More than that, the large components for different energies are not orthogonal on the unit metric, whereas they are orthogonal on the non-unit metric of the NESC equation. This is a very important consideration when multiple one-particle solutions are desired such as in SCF methods. As a result of the differences in metric, the energy obtained from the NESC equation for an approximate $\hat{X}$ differs from the exact result by $\mathcal{O}(c^{-4})$, but the energy obtained from the correpsonding UESC equation differs from the exact result by $\mathcal{O}(c^{-2})$. Further discussion of the properties of the NESC and UESC approximations can be found in the original paper [11].

The unitary transformation has to be applied to the two-electron operators as well as to the one-electron operators, and is now no longer exact. For if the transformation block-digaonalizes the one-electron operator, it will certainly not block-diagonalize the two-electron operator as well. The result is a transformed Hamiltonian that is correct to some order in c^{-1}. The term that connects only positive energy states is

$$\hat{g}_{ij}^{\mathrm{FW,mod}} = \frac{1}{\sqrt{1+\frac{\alpha^2}{2}\hat{X}_i{}^\dagger T_i \hat{X}_i}} \frac{1}{\sqrt{1+\frac{\alpha^2}{2}\hat{X}_j{}^\dagger T_j \hat{X}_j}} \Big[g_{ij} + \hat{X}_i{}^\dagger g_{ij}^{20} \hat{X}_i$$
$$+ \hat{X}_j{}^\dagger g_{ij}^{02} \hat{X}_j + \hat{X}_j{}^\dagger \hat{X}_i{}^\dagger g_{ij}^{22} \hat{X}_i \hat{X}_j \Big] \frac{1}{\sqrt{1+\frac{\alpha^2}{2}\hat{X}_j{}^\dagger T_j \hat{X}_j}} \frac{1}{\sqrt{1+\frac{\alpha^2}{2}\hat{X}_i{}^\dagger T_i \hat{X}_i}}. \tag{8.29}$$

When only the scalar terms are considered, it is a reasonably good approximation to neglect the commutator of the transformation with the Coulomb interaction, and use the bare Coulomb operator $1/r_{ij}$ with the transformed wave function. The neglected term is a renormalized two-electron Darwin term, which is usually very small. This approach

— transforming only the one-electron operator and neglecting the transformation of the two-electron operator in a scalar approximation — was pioneered by Hess [5], who used the Douglas-Kroll transformation [4] to second order in the external potential. This approximation cannot be used with the spin-orbit operators, because they arise from the commutator that is neglected. Instead, the transformed spin-orbit operators must be used.

3. Matrix Elimination of the Small Component

When it comes to the actual calculations, the wave function is expanded in some finite basis set, the matrix elements of the operators over the basis are evaluated, and the equations are solved using matrix techniques. Thus we can perform the same kinds of transformations of the matrix equations as was done for the operator equations, with the finite basis set results for the original equation as the "exact" or reference value against which the approximation can be tested.

Because the large component and the pseudo-large component have the same symmetry, they can be expanded in the same basis set:

$$\Psi = \sum_{k=1}^{n} a_k \chi_k; \qquad \Phi = \sum_{k=1}^{n} b_k \chi_k. \tag{8.30}$$

Inserting these expansions into equation (8.5), the modified Dirac equation in matrix form is obtained,

$$\begin{pmatrix} \mathbf{V} & \mathbf{T} \\ \mathbf{T} & \frac{\alpha^2}{4}\mathbf{W} - \mathbf{T} \end{pmatrix} \begin{pmatrix} \mathbf{a} \\ \mathbf{b} \end{pmatrix} = \begin{pmatrix} \mathbf{S} & 0 \\ 0 & \frac{\alpha^2}{2}\mathbf{T} \end{pmatrix} \begin{pmatrix} \mathbf{a} \\ \mathbf{b} \end{pmatrix} E. \tag{8.31}$$

where $\mathbf{a}$ and $\mathbf{b}$ are the coefficient vectors defined in equation (8.30), $\mathbf{V}$ and $\mathbf{W}$ are the matrices of V and $W = \sigma \cdot \mathbf{p} V \sigma \cdot \mathbf{p}$, $\mathbf{T}$ is the matrix of the kinetic energy operator, $\mathbf{S}$ the overlap matrix, and E the eigenvalue.

The elimination of the small component is now a matrix operation. The matrix equivalent of equation (8.26) is

$$\mathbf{b} = \mathbf{X}\mathbf{a}. \tag{8.32}$$

The matrix $\mathbf{X}$ plays the same role as the operator $\hat{X}$ in the operator equation, and we can use it to construct a unitary transformation matrix $\mathbf{U}$, or an orthogonal transformation matrix. Applying the orthogonal transformation to the matrix modified Dirac equation yields the matrix

NESC equation,

$$\left[\mathbf{V} + \frac{\alpha^2}{4}\mathbf{X}^\dagger\mathbf{W}\mathbf{X} + \mathbf{T}\mathbf{X} + \mathbf{X}^\dagger\mathbf{T} - \mathbf{X}^\dagger\mathbf{T}\mathbf{X}\right]\mathbf{a} = \left[\mathbf{S} + \frac{\alpha^2}{2}\mathbf{X}^\dagger\mathbf{T}\mathbf{X}\right]\mathbf{a}E, \tag{8.33}$$

which is the equation for the large component vector that results from neglecting the off-diagonal block of the transformed modified Dirac matrix. The exact transformation $\mathbf{X}$ can be constructed using the eigenvalue and the second of the equations in analogy to equation (8.28),

$$\mathbf{X} = \left[(1 + \frac{\alpha^2}{2}E)\mathbf{T} - \frac{\alpha^2}{4}\mathbf{W}\right]^{-1}\mathbf{T}. \tag{8.34}$$

From the matrix NESC equation we can construct a modified potential energy matrix, a modified kinetic energy matrix and a modified overlap matrix,

$$\tilde{\mathbf{T}} = \mathbf{T}\mathbf{X} + \mathbf{X}^\dagger\mathbf{T} - \mathbf{X}^\dagger\mathbf{T}\mathbf{X} = \mathbf{T} - (\mathbf{I} - \mathbf{X})^\dagger\ \mathbf{T}\ (\mathbf{I} - \mathbf{X}), \tag{8.35}$$

$$\tilde{\mathbf{V}} = \mathbf{V} + \frac{\alpha^2}{4}\mathbf{X}^\dagger\mathbf{W}\mathbf{X}, \tag{8.36}$$

$$\tilde{\mathbf{S}} = \mathbf{S} + \frac{\alpha^2}{2}\mathbf{X}^\dagger\mathbf{T}\mathbf{X}. \tag{8.37}$$

All of these reduce to the correct nonrelativistic limit. The reduction of the modified kinetic energy matrix follows from the fact that $\mathbf{X} = \mathbf{I} + \mathcal{O}(\alpha^2)$, which can easily be demonstrated from equation (8.34).

Performing the usual ESC leads to the matrix UESC equation,

$$[\mathbf{V} + \mathbf{T}\mathbf{X}]\,\mathbf{a} = \mathbf{S}\mathbf{a}E. \tag{8.38}$$

which yields only a modified kinetic energy matrix,

$$\overline{\mathbf{T}} = \mathbf{T}\mathbf{X} \tag{8.39}$$

This matrix also has the correct nonrelativistic limit, because of the properties of $\mathbf{X}$.

These equations are both valid equations for the large component, but they have different properties, some of which have been discussed in the previous section. One property of note is that if we set $\mathbf{X}$ to $\mathbf{I}$ without setting α to zero, the UESC equation reduces to the nonrelativistic Schrödinger equation, but the NESC equation reduces to a relativistic equation that is correct to order c^{-2}. This equation is the equivalent of the Pauli equation, and cannot be solved variationally.

Just as the operator version of the UESC equation led to difficulties with orthonormality, so does the matrix version. Extending from a single

vector to a set of vectors for all the positive energy states, we write the matrix modified Dirac equation as two equations,

$$\mathbf{VA} + \mathbf{TB} = \mathbf{SAE} \tag{8.40}$$

$$\mathbf{TA} + \frac{\alpha^2}{4}\mathbf{WB} - \mathbf{TB} = \frac{\alpha^2}{2}\mathbf{TBE} \tag{8.41}$$

where $\mathbf{A}$ and $\mathbf{B}$ are the $n \times n$ matrices of coefficients of the large and pseudo-large components, and $\mathbf{E}$ is the diagonal $n \times n$ matrix of the eigenvalues. To eliminate the small component for all vectors simultaneously, we must use the first equation to define $\mathbf{X}$,

$$\mathbf{X} = \mathbf{BA}^{-1} = \mathbf{T}^{-1}\left[\mathbf{SAEA}^{-1} - \mathbf{V}\right] \tag{8.42}$$

Having used this equation to define $\mathbf{X}$, we cannot now use it to eliminate the small component from the same equation. And even if we did arrive at some meaningful equation, the vectors in $\mathbf{A}$ are not orthonormal on the UESC metric, $\mathbf{S}$, but they are orthonormal on the NESC metric, $\tilde{\mathbf{S}}$.

The change in the definition of $\mathbf{X}$ has some practical implcations. When solving for $\mathbf{X}$ using a single vector, it was possible to use the second equation and the eigenvalue E, to obtain a definition of $\mathbf{X}$ that only depended on the single eigenvalue. For the entire set of solutions, the definition depends on all the eigenvalues and all the eigenvectors. In an iterative scheme, the eigenvalues and eigenvectors from the last completed iteration could be taken to define $\mathbf{X}$ for the current iteration.

The modified one-electron matrices for the entire set of solutions have the same form as the modified one-electron matrices for a single solution. The only difference is in the definition of $\mathbf{X}$.

As a method in its own right, NESC has many advantages over UESC. Apart from the fact that its eigenvalues differ from the exact eigenvalues by $\mathcal{O}(\alpha^4)$ rather than by $\mathcal{O}(\alpha^2)$ which is the case for UESC, the ability to use a single equation for all solutions and the lack of a need for orthogonalization is a clear gain, especially when the method is extended from the one-electron Dirac equation to a many-electron Dirac-Hartree-Fock equation. The main drawback is that the metric depends on $\mathbf{X}$ and hence on $\mathbf{E}$, so each iteration requires the solution of a generalized eigenvalue problem. This can be done by performing a symmetric orthonormalization in each iteration. Even with the addition of this extra step, the cost is much less than for UESC.

The extension of NESC to a many-electron method involves the definition of modified two-electron integrals,

$$\begin{aligned}(\tilde{\mu}\tilde{\nu}|\tilde{\kappa}\tilde{\lambda}) &= (\mu\nu|\kappa\lambda) + \frac{\alpha^2}{4} X^*_{\tau\mu}(\hat{\Pi}\tau\hat{\Pi}\rho|\kappa\lambda) X_{\rho\nu} + \frac{\alpha^2}{4} X^*_{\tau\kappa}(\mu\nu|\hat{\Pi}\tau\hat{\Pi}\rho) X_{\rho\lambda} \\ &+ \frac{\alpha^4}{16} X^*_{\tau\mu} X^*_{\zeta\kappa}(\hat{\Pi}\tau\hat{\Pi}\rho|\hat{\Pi}\zeta\hat{\Pi}\eta) X_{\rho\nu} X_{\eta\lambda}. \end{aligned} \tag{8.43}$$

Here the Einstein convention of summation over repeated indices has been used, and $\hat{\Pi} = \sigma \cdot \mathbf{p}$. With these, the Kramers-restricted NESC Fock matrix is

$$\tilde{\mathbf{F}} = \tilde{\mathbf{T}} + \tilde{\mathbf{V}} + 2\tilde{\mathbf{J}} - \tilde{\mathbf{K}} \tag{8.44}$$

where

$$\begin{aligned}\tilde{J}_{\mu\nu} &= (\tilde{\mu}\tilde{\nu}|\tilde{\kappa}\tilde{\lambda}) D_{\kappa\lambda} \\ \tilde{K}_{\mu\nu} &= \left[(\tilde{\mu}\tilde{\lambda}|\tilde{\kappa}\tilde{\nu}) + (\tilde{\mu}\tilde{\bar{\kappa}}|\tilde{\bar{\lambda}}\tilde{\nu})\right] D_{\kappa\lambda} \end{aligned} \tag{8.45}$$

and $D_{\kappa\lambda}$ is the Kramers-restricted density matrix constructed from the large component. Kramers restriction is the equivalent of the nonrelativistic spin restriction; a spinor and its time-reversed partner are termed a Kramers pair, and the latter is distinguished by an overline. The NESC Fock matrix resembles the RHF Fock matrix, and reduces to it in the nonrelativistic limit, provided that the Kramers pairs also reduce to spin-orbitals. This is always possible, since the RHF energy is invariant to rotation among the occupied orbitals. The matrix $\mathbf{X}$ is also different from the one-electron case. The potentials include two-electron terms, and the off-diagonal kinetic energy operators are modified by exchange terms of order α^2. Details can be found in the original paper [12].

In the operator ESC method, it was possible to neglect the commutator of the transformation with the Dirac two-electron Coulomb operator, to obtain a Hamiltonian which uses the bare two-electron Coulomb operator with the transformed one-electron operator. The unitary transformation must be used, and the spin-dependent terms in the one-electron operator must be neglected, for consistency.

The same kind of approximation can be developed for the matrix ESC method. Performing the normalized transformation is equivalent to changing the metric by a transformation. Defining the matrix $\mathbf{Z}$ by

$$\mathbf{Z} = \mathbf{S}^{-1/2}\left[\mathbf{S} + \frac{\alpha^2}{2}\mathbf{X}^\dagger\mathbf{T}\mathbf{X}\right]^{1/2} = \mathbf{S}^{-1/2}\tilde{\mathbf{S}}^{1/2} \tag{8.46}$$

the transformed one-electron equation for the normalized positive energy states $\mathbf{C}$ is

$$(\mathbf{Z}^{-1})^\dagger\left[\tilde{\mathbf{V}} + \tilde{\mathbf{T}}\right]\mathbf{Z}^{-1}\mathbf{C} = \mathbf{S}\mathbf{C}\mathbf{E}. \tag{8.47}$$

The matrix $\mathbf{C}$ is related to the matrix of large component coefficients by

$$\mathbf{C} = \mathbf{ZA}, \tag{8.48}$$

and is normalized on the metric $\mathbf{S}$. The matrix equivalent of neglecting the commutators of the transformation with the two-electron Coulomb operator in this approach is to simply use the untransformed two-electron integrals, $(\mu\nu|\kappa\lambda)$. The advantage of this approach is that the two-electron part of the SCF equations is exactly the same as in nonrelativistic methods. What is different is the transformed renormalized one-electron integrals, for which $\mathbf{X}$ and $\mathbf{Z}$ must be constructed in each iteration. The work in doing this is minimal compared with the work in constructing the two-electron part of the Fock matrix.

4. The Atomic 4-spinor Approximation

The energy- and eigenvalue-dependence of the matrix $\mathbf{X}$ in the matrix NESC equation is not a substantial problem for atomic calculations. For molecular calcuations, especially if the goal is to study large molecules that contain heavy atoms, a further approximation would be desirable, not only for the purpose of reducing the work done but also for the ease of interfacing with existing nonrelativistic methodology.

The most obvious approximation to $\mathbf{X}$ is $\mathbf{X} = \mathbf{I}$. However, this approximation neglects contributions to $\mathbf{X}$ of order α^2, and though these contributions only change the energy to order α^4, they can be significant in the core where relativistic effects are largest. In fact this approximation is the equivalent of the Breit-Pauli approximation, and cannot be used variationally, which is another drawback.

Since most molecular calculations use atomic basis sets, it makes sense to seek an approximation at the atomic level. In doing so, it would be preferable to retain the largest, if not all, of the terms of order α^2 in the approximation to $\mathbf{X}$. To this end, an analysis of $\mathbf{X}$ is necessary, for which equation (8.34) is sufficient. $\mathbf{X}$ is expanded into the unit matrix and a residue,

$$\mathbf{X} = \mathbf{I} + \frac{\alpha^2}{4}\mathbf{T}^{-1}(\mathbf{W} - 2mE\mathbf{T})\left[\mathbf{I} - \frac{\alpha^2}{4}\mathbf{T}^{-1}(\mathbf{W} - 2mE\mathbf{T})\right]^{-1}. \tag{8.49}$$

The size of the off-diagonal matrix elements of $\mathbf{X}$ are determined by the size of the corresponding matrix elements of $\mathbf{W}$ and $\mathbf{T}$. The expression in parentheses is the matrix of $\sigma \cdot \mathbf{p}(V - E)\sigma \cdot \mathbf{p}$, so if E is approximated by the nonrelativistic energy and then replaced with $T + V$, the matrix expression reduces to

$$\mathbf{W} - 2mE\mathbf{T} \simeq 2m\mathbf{T}^2 \tag{8.50}$$

which is essentially a matrix approximation to the lowest order mass-velocity correction to the Hamiltonian. This is a very rough approximation, but sufficient for the present purpose. The size of the off-diagonal matrix elements of **X** therefore approximately scale as the off-diagonal elements of **T**. These are largest for basis functions which describe the core of the same atom, and are smallest for basis functions on different centers, due to the overlap. A reasonable approximation to **X** is therefore to set the elements that connect basis functions on different centers to zero. This approximation does neglect terms of order α^2 but they are small terms. What is more, because the approximation does not expand **X** in powers of α^2, all the higher order terms are present where they matter most: in the atomic core.

What is the nature of this approximation? **X** has been made block-diagonal, with blocks defined by the basis functions on a particular atom. For each diagonal block, **X** is not approximated at all. This means that no approximation is made for the isolated atoms. Because **X** connects the large component with the pseudo-large component, the approximation to **X** means that the ratio of these two components cannot change when the molecule is formed.

Another way to understand this approximation is to consider that a projection has been made onto the positive energy states of the isolated atoms, and the basis set is the set of positive energy atomic 4-spinors of the constituent atoms. To change the ratio of the large and pseudo-large components it is necessary to mix in some of the negative energy states. The effect of this mixing is of order α^4 and because the perturbation to the core on molecule formation is relatively small, the extent of the mixing will also be small.

Calculations on a number of systems [14] in which this approximation is tested in SCF calculations show that the effect on the energy is in the range of tens of microhartrees, and varies slowly with internuclear distance. The effect on the bond lengths and harmonic vibrational frequencies are also negligible for the purposes of chemistry.

In the implementation of this approximation, the matrix **X** becomes part of the atomic basis set specification. It is easily computed from an atomic 4-component calculation using the first equality of equation (8.42). The matrix **A** is non-singular because its vectors are linearly dependent. In an uncontracted basis set, the matrix **X** is all that is needed in addition to the exponents of the basis functions. In a contracted basis set, a set of contraction coefficients derived from **A** is needed in addition to **X**. However, instead of storing **X**, it is preferable to store **B**, because in every place where **X** occurs, it is multiplied by the contraction coefficients derived from **A**, and the product of **X** and **A** is **B**. To illustrate

this point, we can write the one-electron integrals in the contracted basis set as

$$\begin{aligned}\tilde{\mathbf{T}}^{\mathrm{cnt}} = \mathbf{A}^{\dagger}\tilde{\mathbf{T}}\mathbf{A} &= \mathbf{A}^{\dagger}\mathbf{T}\mathbf{X}\mathbf{A} + \mathbf{A}^{\dagger}\mathbf{X}^{\dagger}\mathbf{T}\mathbf{A} - \mathbf{A}^{\dagger}\mathbf{X}^{\dagger}\mathbf{T}\mathbf{X}\mathbf{A} \\ &= \mathbf{A}^{\dagger}\mathbf{T}\mathbf{B} + \mathbf{B}^{\dagger}\mathbf{T}\mathbf{A} - \mathbf{B}^{\dagger}\mathbf{T}\mathbf{B}, \qquad (8.51)\end{aligned}$$

$$\begin{aligned}\tilde{\mathbf{V}}^{\mathrm{cnt}} = \mathbf{A}^{\dagger}\tilde{\mathbf{V}}\mathbf{A} &= \mathbf{A}^{\dagger}\mathbf{V}\mathbf{A} + \frac{\alpha^2}{4}\mathbf{A}^{\dagger}\mathbf{X}^{\dagger}\mathbf{W}\mathbf{X}\mathbf{A} \\ &= \mathbf{A}^{\dagger}\mathbf{V}\mathbf{A} + \frac{\alpha^2}{4}\mathbf{B}^{\dagger}\mathbf{W}\mathbf{B}, \qquad (8.52)\end{aligned}$$

$$\begin{aligned}\tilde{\mathbf{S}}^{\mathrm{cnt}} = \mathbf{A}^{\dagger}\tilde{\mathbf{S}}\mathbf{A} &= \mathbf{A}^{\dagger}\mathbf{S}\mathbf{A} + \frac{\alpha^2}{2}\mathbf{A}^{\dagger}\mathbf{X}^{\dagger}\mathbf{T}\mathbf{X}\mathbf{A} \\ &= \mathbf{A}^{\dagger}\mathbf{S}\mathbf{A} + \frac{\alpha^2}{2}\mathbf{B}^{\dagger}\mathbf{T}\mathbf{B}. \qquad (8.53)\end{aligned}$$

Here, $\mathbf{A}$ and $\mathbf{B}$ are taken to be the matrices of the contraction coefficients. The two-electron integrals in the contracted basis can be expressed similarly, making use of equation (8.43).

Thus, for a contracted calculation, two basis sets are stored, derived from $\mathbf{A}$ and $\mathbf{B}$. This is no different from a contracted calculation for the unapproximated modified Dirac equation: they are precisely the same contraction coefficients. The approximation has the additional requirement that the contractions are not renormalized, because the ratio of $\mathbf{A}$ to $\mathbf{B}$ from the atomic SCF calculation must be preserved, since it defines $\mathbf{X}$.

When it comes to deciding what kind of contraction is to be made of the basis set, there are some constraints imposed by the fact that the relation between $\mathbf{A}$ and $\mathbf{B}$ is fixed. Since the expansion basis is the set of positive energy atomic 4-spinors, the contraction must be a rotation of these functions, or further approximations must be introduced. The most obvious choice is a set of atomic natural spinors (ANSs), the relativistic equivalent of atomic natural orbitals (ANOs), which were introduced by Almlöf and Taylor [21]. Segmented contractions are popular in nonrelativistic calculations, but they are problematic in this context. The reason is that $\mathbf{X}$ is a full matrix, and the segmentation in $\mathbf{A}$ would not produce a corresponding segmentation in $\mathbf{B}$ without further approximation. In particular, the off-diagonal elements of $\mathbf{X}$ are not small in the core region where segmentation is most useful. For a segmented contraction it would then be necessary to store $\mathbf{X}$ and $\mathbf{A}$. Another popular basis set type is the correlation-consistent basis sets developed by Dunning and coworkers [22]. These usually consist of the SCF occupied orbitals supplemented

with primitive Gaussian functions for valence flexibility and correlation. The SCF occupied orbitals present no problems in the present context. For the primitive Gaussians, the same issues arise as for the segmented basis sets. Here, however, the functions are more diffuse than in the case of segmented core basis sets, and the off-diagonal elements of **X** are much smaller. A useful approximation is to neglect the off-diagonal elements of **X** and to use the free-particle ratio for the ratio of the large component to the pseudo-large component. The non-zero coefficients a and b are given by

$$a^2 = (E + c^2)/2E, \qquad b^2 = 2c^4/E(E + c^2), \tag{8.54}$$

where $E = \sqrt{c^4 + c^2p^2}$ and $p^2 = \zeta(2\ell + 3)$. This approximation should be sufficiently accurate for the primitive Gaussians used in these basis sets.

No approximations to the integrals have been made at this stage, so the amount of work needed to evaluate the integrals is no different from the full 4-component method. This also means that in a direct SCF implementation, there is also no change in the amount of work done to construct the Fock matrix. In a conventional implementation, where the integrals are stored, the work done to construct the Fock matrix can be reduced by a factor of 16 if the integral program produces the modified two-electron integrals defined in equation (8.43). In fact, if only the scalar relativistic effects are included, the number of integrals is no different from a nonrelativistic calculation, and the work done to construct the Fock matrix is the same as in a nonrelativistic calculation.

The approximations to the integrals outlined at the end of the previous section could be made within this approximation. In uncontracted basis sets the matrix **Z** would have to be computed and the one-electron integrals transformed using this matrix. In contracted calculations, it would only be necessary to store another set of contraction coefficients, derived from **C** in the same way as the other sets are derived from **A** and **B**. For added primitive functions, the contraction coefficient is simply 1. The two-electron integrals are evaluated with the contraction coefficients from **C**, and the one-electron integrals are evaulated with the contraction coefficients from **A** and **B**. Tests of this approximation [15] show results that are very similar to the Douglas-Kroll-Hess approximation, and in fact the results differ little from results of calculations that include the full scalar two-electron terms.

5. The Nonrelativistic Atom Approximation

The elimination of the small component does not in itself result in a substantial reduction in the work required to solve the Dirac equation,

because it is necessary to evaluate all the two-electron integrals that are used in solving the full 4-component equation. The approximation of neglecting the off-diagonal blocks of $\mathbf{X}$ saves work if a conventional rather than a direct SCF scheme is used in which the integrals are evaluated once and stored as the modified contracted integrals.

The integral evaluation work is in fact a non-negligible component of the calculations because of the gradient operators that appear in the two-electron terms of the modified Dirac Hamiltonian. The work is at least one order of magnitude greater than in an equivalent nonrelativistic calculation and possibly two orders of magnitude greater. Further approximations that reduce the amount of integral work are therefore desirable.

Because relativistic effects scale as Z^4, it should be possible to neglect them for light atoms. This is the basis of the relativistic effective core potentials (RECPs) [23, 24] and relativistic *ab initio* model potentials (AIMPs) [25, 26]: light atoms are treated nonrelativistically and heavy atoms are treated relativistically, by means of a modified potential.

The same classification into light and heavy atoms can be made in the present matrix NESC formalism. Formally, this is done by defining an atom-dependent fine-structure constant α. For light atoms, α is zero, and for heavy atoms, α takes its physical value. To illustrate, we write the one-electron integral matrices with labels for the atomic centers A and B as

$$\tilde{\mathbf{T}}^{AB} = \mathbf{T}^{AB} - (\mathbf{I} - \mathbf{X}^A)^\dagger \mathbf{T}^{AB} (\mathbf{I} - \mathbf{X}^B), \tag{8.55}$$

$$\tilde{\mathbf{V}}^{AB} = \mathbf{V}^{AB} + \frac{\alpha^A \alpha^B}{4} (\mathbf{X}^A)^\dagger \mathbf{W}^{AB} \mathbf{X}^B, \tag{8.56}$$

$$\tilde{\mathbf{S}}^{AB} = \mathbf{S}^{AB} + \frac{\alpha^A \alpha^B}{2} (\mathbf{X}^A)^\dagger \mathbf{T}^{AB} \mathbf{X}^B. \tag{8.57}$$

The modified matrices reduce to the nonrelativistic matrices if either α^A or α^B is zero and $\mathbf{X}^A$ or $\mathbf{X}^B$ is the unit matrix. The relativistic corrections to the one-electron integrals are therefore only needed when all atomic centers involved are heavy atoms. Similarly, the two-electron integrals are modified whenever both atomic centers in a density are heavy atoms. This approximation reduces the amount of integral work enormously when there are only a few heavy atoms in the molecule — for example, in organometallic complexes.

The accuracy of this approximation has also been tested in a number of sample calculations [14]. For atoms of the second period (Li – Ne), the errors in the approximation are of the order of a few hundredths of a picometre in bond lengths, and less than 1 kJ mol^{-1} in dissociation energies; for atoms in the third period, errors are a few tenths of a

picometre and a few kJ mol^{-1}, though polarization effects in P and S by a metal atom can produce errors that are larger. The errors (naturally) grow with Z; however, the fact that they are small for the second and third periods means that most biochemical calculations could be carried out with relativistic effects only on metallic centers.

The integral approximation outlined at the end of section 3. can also be applied with the nonrelativistic atom approximation. In this case all the contraction coefficients from **A**, **B** and **C** for the nonrelativistic atoms are the same and are the nonrelativistic contraction coefficients.

6. Properties in the Matrix Approximations

First order properties (linear response properties) can generally be calcuated from the expectation of the wave function over the property operators. The matrices of the properties in the NESC approach are

$$\tilde{\mathbf{U}} = \mathbf{U} + \frac{\alpha^2}{4}\mathbf{X}^\dagger\mathbf{Y}\mathbf{X} \tag{8.58}$$

$$\tilde{\mathbf{M}} = \mathbf{X}^\dagger\mathbf{M}^\dagger + \mathbf{M}\mathbf{X} \tag{8.59}$$

where **Y** is the matrix of $\sigma \cdot \mathbf{p}\ U\ \sigma \cdot \mathbf{p}$ and **M** is the matrix of $\sigma \cdot \mathbf{A}\sigma \cdot \mathbf{p}$. The electric property matrices $\tilde{\mathbf{U}}$ resemble the potential energy matrices. The magnetic property matrices $\tilde{\mathbf{M}}$ resemble the kinetic energy matrices, in that they have no explicit dependence on α, but the relativistic corrections are in **X**.

The elimination of the small component of itself has no effect on the expectation value, but any approximations to the property operators represent an approximation to the property value. As for the energy matrices, the neglect of terms that come from off-diagonal elements of **X** are likely to be small, no matter what kind of property is being considered.

For second order properties, the elimination of the small component introduces some extra approximations, regardless of whether any approximations to **X** are made. In the full 4-component method from the unmodified Dirac equation, the second order properties come from a sum over terms like

$$\sum_k \frac{\langle\psi_0|\hat{P}|\psi_k\rangle\langle\psi_k|\hat{P}|\psi_0\rangle}{E_0 - E_k} \tag{8.60}$$

where $\hat{P}$ is the 4-component property operator and the ψ are 4-component spinors. The sum extends over both positive and negative energy states. The solution of the ESC equations does not provide any negative energy states, so part of the second order property in any ESC-based method is missing.

The lack of negative energy states in ESC is not critical for electric properties, because the contributions from the negative energy states to the property are of order c^{-4}: if k is a negative energy state, $E_k < -2mc^2$ and the matrix element is of order $1/c$. The property operator for magnetic properties connects large and small components, and for the negative energy states, the "small" component is large in magnitude, and is of order c^0, while the "large" component is of order c^{-1}. The matrix element for the magnetic operator $c\alpha \cdot \mathbf{A}$ has contributions of order c and c^{-1}, so the contribution from the sum over negative energy states is of order c^0, which cannot be neglected in any circumstances.

One solution to this problem is to partition the energy of the negative energy states,

$$E_{k-} = -2mc^2 + \Delta E_{k-} \tag{8.61}$$

and then partition the denominator of the perturbation expression,

$$\begin{aligned} \frac{1}{E_0 - E_{k-}} &= \frac{1}{2mc^2 + E_0 - \Delta E_{k-}} \\ &= \frac{1}{2mc^2} - \frac{E_0 - \Delta E_{k-}}{2mc^2(2mc^2 + E_0 - \Delta E_{k-})}. \end{aligned} \tag{8.62}$$

For small energy differences $|E_0 - \Delta E_{k-}| << 2mc^2$, where the property matrix element is likely to be large, the second term in the partitioning of the inverse is of order c^{-4} and hence the corresponding contribution to the energy is of order c^{-2}. For large energies $|E_{k-}|$, the matrix elements between a bound state and a continuum state behave as some inverse power of the energy, so the contribution to the property is in any case small. From the first term, the contribution to the magnetic property is now

$$\sum_{k-} \frac{\langle \psi_0 | \hat{P} | \psi_{k-} \rangle \langle \psi_{k-} | \hat{P} | \psi_0 \rangle}{2mc^2}, \tag{8.63}$$

from which the denominator may be factored out, and the sum corresponds to a projection onto the negative energy states. Using the resolution of the identity,

$$1 = \sum_{k-} |\psi_{k-}\rangle\langle\psi_{k-}| + \sum_{k+} |\psi_{k+}\rangle\langle\psi_{k+}| \tag{8.64}$$

the contribution to the property can be written as

$$\frac{\langle \psi_0 | \hat{P}^2 | \psi_0 \rangle}{2mc^2} - \sum_{k+} \frac{\langle \psi_0 | \hat{P} | \psi_{k+} \rangle \langle \psi_{k+} | \hat{P} | \psi_0 \rangle}{2mc^2}. \tag{8.65}$$

The operator $\hat{P}^2$ is, for magnetic properties, equal to $c^2\mathbf{A}^2$, and the first matrix element becomes the expectation value of the operator $\mathbf{A}^2/2m$. This term is easily incorporated into the matrix approximation as the equivalent of an electric property operator. The sum is a sum over positive energy states which can be added to the existing sum, yielding

$$\sum_{k+} \langle\psi_0|\hat{P}|\psi_{k+}\rangle\langle\psi_{k+}|\hat{P}|\psi_0\rangle \left(\frac{1}{E_0 - E_{k+}} - \frac{1}{2mc^2}\right). \tag{8.66}$$

The remaining term from the negative energy sum, which was discussed above, is of order c^{-2} and contributes to the relativistic correction to the magnetic property. The denominator is always positive, but the numerator changes sign at $\Delta E_{k-} = E_0$. It is likely therefore that there is a large degree of cancellation in the resultant sum, and this term could be negligible. Without numerical tests, however, there is no guarantee that it is negligible, and for accurate relativistic corrections to magnetic properties, it is probably better to use the full 4-component methods [27]. Nevertheless, using the techniques in this section within the matrix approximations should yield results that are sufficiently accurate for most chemical purposes.

References

[1] E. van Lenthe, E. J. Baerends, and J. G. Snijders, J. Chem. Phys. **99**, 4597 (1993); **101**, 9783 (1994).

[2] J. Wood, I. P. Grant and S. Wilson, J. Phys. B **18**, 3027 (1985).

[3] L. L. Foldy and S. A. Wouthuysen, Phys. Rev. **78**, 29 (1950).

[4] M. Douglas and N. M. Kroll, Ann. Phys. (N.Y.) **82**, 89 (1974).

[5] B. A. Hess, Phys. Rev. A **32**, 756 (1985); **33**, 3742 (1986).

[6] T. Nakajima and K. Hirao, J. Chem. Phys. **113**, 7786 (2000).

[7] M. Barysz, A. J. Sadlej and J. G. Snijders, Int. J. Quantum Chem. **65**, 225 (1997).

[8] S. Faas, J. G. Snijders, J. H. van Lenthe and E. van Lenthe, Chem. Phys. Lett. **246**, 632 (1995).

[9] T. Saue, K. Fægri, Jr., T. Helgaker and O. Gropen, Mol. Phys. **91**, 937 (1997).

[10] L. Visscher, Theor. Chem. Acc. **98**, 68 (1997).

[11] K. G. Dyall, J. Chem. Phys. **100**, 2118 (1994).

[12] K. G. Dyall, J. Chem. Phys. **106**, 9618 (1997).

[13] K. G. Dyall, J. Chem. Phys. **109**, 4201 (1998).

[14] K. G. Dyall and T. Enevoldsen, J. Chem. Phys. **111**, 10000 (1999).

[15] K. G. Dyall, J. Chem. Phys. **115**, 9136 (2001).

[16] A. Rutkowski, J. Phys. B: At. Mol. Phys. **19**, 149, 3431, 3443 (1986); Phys. Scr. **38**, 816 (1988).

[17] W. Kutzelnigg, Z. Phys. D **15**, 27 (1990).

[18] A. J. Sadlej and J. G. Snijders, Chem. Phys. Lett. **229**, 435 (1994).

[19] L. Visscher and E. van Lenthe, Chem. Phys. Lett. **306**, 357 (1999).

[20] E. van Lenthe, E. J. Baerends and J. G. Snijders, J. Chem. Phys. **105**, 2373 (1996).

[21] J. Almlöf and P. R. Taylor, J. Chem. Phys. **86** 4070 (1987); J. Chem. Phys. **92** 551 (1990).

[22] T. H. Dunning, Jr., J. Chem. Phys. **90**, 1007 (1989); R. A. Kendall, T. H. Dunning, Jr., and R. J. Harrison, J. Chem. Phys. **96**, 6769 (1992); D. E. Woon and T. H. Dunning, Jr. J. Chem. Phys. **98**, 1358 (1993); A. K. Wilson, D. E. Woon, K. A. Peterson, and T. H. Dunning, Jr., J. Chem. Phys. **110**, 7667 (1999).

[23] Y. S. Lee, W. C. Ermler and K. S. Pitzer, J. Chem. Phys. **67**, 5861 (1977).

[24] P. J. Hay, W. R. Wadt, L. R. Kahn and F. W. Bobrowicz, J. Chem. Phys. **69**, 984 (1978).

[25] M. Klobukowski, J. Comp. Chem. **4**, 350 (1983).

[26] Z. Barandiarán and L. Seijo, Can. J. Chem. **70**, 409 (1992).

[27] L. Visscher, T. Enevoldsen, T. Saue, H. J. Aa. Jensen and J. Oddershede, J. Comp. Chem **20**, 1262 (1999).

Chapter 9

TWO–COMPONENT METHODS

From the Douglas–Kroll to the exact infinite–order method

M. Barysz

Department of Quantum Chemistry, Institute of Chemistry, Nicolaus Copernicus University, Gagarina 7, PL–87100 Toru, Poland

teomjb@chem.uni.torun.pl

Abstract The Douglas–Kroll and other recently developed two–component methods, based on similar ideas, are reviewed and discussed. A unified derivation of these methods through the solution of certain operator equations is presented. These solutions can be obtained by imposing additional conditions on the accuracy of the resulting two–component Hamiltonians. The traditional Douglas–Kroll Hamiltonian is shown to be the best two–component Hamiltonian which approximates the Dirac operator simultaneously through the fourth order in the fine structure constant and through the second order with respect to the external interaction potentials. Several higher order methods are presented as well.

The main attention is focused on the infinite–order solution of the operator equation for the block–diagonalizing transformation of the Dirac Hamiltonian. This is accomplished by a further modification of this equation and leads to the infinite–order two–component theory 'for electrons only', i.e., the resulting two–component Hamiltonian gives the Dirac spectrum of electronic solution. This 'exact' two–component method is combined with the Hess technique to handle the momentum space integrals and its implementation is shown to give the electronic Dirac levels with arbitrarily high accuracy. The new infinite–order method is also shown to save the supersymmetric features of the 4–component theory by reproducing the accidental degeneracies present in the Dirac spectrum. It is concluded that relativistic quantum chemistry 'for electrons only' can be done in exclusively two–component form. The same method produces another two–component Hamiltonian for the negative energy spectrum. This Hamiltonian can be used to build a finite basis set theory of quantum electrodynamic corrections.

U. Kaldor and S. Wilson (eds.),
Theoretical Chemistry and Physics of Heavy and Superheavy Elements, 349–397.
© 2003 *Kluwer Academic Publishers.*

In addition to reviewing the latest developments in two-component relativistic methods rooted in the Douglas–Kroll approach also the problem of the change of picture for other than energy operators is surveyed. The same problem is shown to occur when the two-component methods are extended to deal with electron–electron interactions. Some recent ideas in this area are reviewed.

Keywords: relativistic Hamiltonians; two-component methods in relativity; Douglas–Kroll approximation; Douglass–Kroll–Hess method; exact two-component Hamiltonian; change of picture; relativistic effects on atomic and molecular properties

Introduction

Physics of the XXth century was dominated by two great theories: the theory of relativity and quantum mechanics [1]. The nonrelativistic quantum mechanics and the Schrödinger equation immediately found their way into chemistry [2] and became the major tool to describe chemical bonds. Years of developments have brought spectacular achievements and made the early applications of quantum mechanics to basic chemical problems into a new area of modern chemistry, the (nonrelativistic) quantum chemistry.

For decades the idea of bringing the theory of relativity into chemistry was considered to be at best unnecessary. Although the basic equation of relativistic quantum mechanics was presented shortly after the nonrelativistic theory was completed, its use in quantum chemistry is relatively recent. Dirac himself was quite sceptical [3] considering it rather unlikely that his equation may be of any use for chemistry. However, at that time chemistry was focused mostly on systems bulit of light elements. With the growing interest in heavy atoms and their compounds the relativistic methods began slowly entering quantum chemistry parallel to the recognition of the importance of relativistic effects in heavy element chemistry.

Chemists do not seem to have had any particular problem to accept the nonrelativistic theory. Most of mathematics in nonrelativistic quantum chemistry and basic physical concepts were simple enough to comprehend and most of the results could be interpreted in terms of almost classical ideas. It was quite different with relativistic theory and this could have been also one of the factors slowing down the development of the relativistic quantum chemistry whose understanding requires the knowledge of physics and mathematics much broader than that sufficient for practising nonrelativistic methods. Moreover, several problems which

arise in the context of the Dirac equation are definitely alien to chemistry and chemists as well as to the majority of quantum chemists.

The first of these problems occurs already at the level of the relativistic free particle equation. The energy spectrum consists of two parts [4] which are referred to as the positive and negative energy continua and are separated by a gap of the magnitude of $2mc^2$, where m is the particle mass and c denotes the velocity of light. This finding obviously contrasts the nonrelativistic picture of a particle moving with always positive kinetic energy. Dirac found ingenious solution of this problem by postulating that all negative energy levels are occupied and not seen directly. However, the occupied negative energy levels are there and the two continua may be coupled via electromagnetic field. This has lead to further developments known under the name of quantum electrodynamics [5,6], whose presence in relativistic quantum chemistry is (so far) very limited [7].

In a similar way the problem of the negative energy continuum arises also in the relativistic theory of the electron moving in the external potential and leads to consequences which are unknown in nonrelativistic methods. One of them is the unboundedness of the Dirac Hamiltonian. Without imposing additional conditions on solutions of the Dirac equation this feature of the Dirac Hamiltonian would make impossible the use of powerful variational methods. Additional problems arise in the case of many electron theories based on the one–electron Dirac Hamiltonian and the Coulomb interaction term (the so–called Dirac–Coulomb approximation for many electron systems). The presence of the negative energy continuum in the Dirac spectrum causes the initially bound system to 'dissolve' into continuous states. This is the so–called Brown–Ravenhall disease [8,9] which cannot be remedied by the addition of simple relativistic correction terms like *e.g.* the Breit two–electron interaction [10,11].

This is only a breif survey of some of the problems which may occur in relativistic quantum chemistry based on the Dirac–Coulomb or Dirac–Breit Hamiltonians [10]. One should also add certain conceptual difficulties related to the 4–spinor form of solutions of the Dirac equation. Most chemists are used to scalar solutions of the Schrödinger equation with spin functions considered as an additional multiplicative factor which can be understood as converting scalars into 2–vectors. Both comprehending and handling 4-spinors represents a higher level of theory which is not a part of the general education in physics and mathematics for chemists.

Additional reasons which justify attempts to reduce the 4–spinor Dirac's theory to much easier 2–vector (2–spinor, 2–component) form follow from the consideration of the magnitude of energies involved in

the majority of chemical phenomena. These are primarily either thermal of spectroscopic energies and hardly go beyond 10 eV as compared with 1 MeV of the energy gap between negative and positive continua of the Dirac spectrum. Thus, the excitations from the filled negative energy levels to positive energy levels, *i.e.*, the creation of the electron–positron pairs, is rather unlikely to be important for most of chemistry. One may conclude that relativistic quantum chemistry without these processes, *i.e.*, without quantum electrodynamics, should be sufficient for solving most of relativistic problems in chemistry. Hence, it would be useful to have a relativistic theory which handles only the electronic (positive energy) solutions and judiciously neglects effects of the negative energy eigenspectrum. One can show that such a theory will involve solutions of the 2–vector form. In addition to certain gains on the conceptual side of such a theory, the experience with 4–spinor calculations [10] shows that significant reduction of the computational effort will be achieved by doing relativistic quantum chemistry in the framework of the two–component approach.

The history of this 'reduction' programme goes back to the period before the Dirac equation. The first step in this direction appears to have been made by Pauli in the form of a quasirelativistic Hamiltonian known as the Pauli Hamiltonian [4,11]. This Hamiltonian can be approximately derived from the Dirac Hamiltonian by noting that in the nonrelativistic limit the 4–component Dirac spinors can be subdivided into what is called the large and small 2–vectors [4]. In the nonrelativistic limit the 'large' (the upper) 2–vector part of the Dirac 4-spinor becomes the electronic (positive energy) solution with spin. On this basis one could expect that there is some representation of the Dirac Hamiltonian which completely separates the positive and negative energy spectra and permits to focus all attention only on the electronic part.

Actually the 2–spinor formalism may not be that much an approximation as far as relativistic quantum chemistry is concerned. The ultimate goal of this formalism is to completely separate the electronic and positronic solutions of the Dirac equation, *i.e.*, to separate the so–called positive and negative parts of the Dirac eigenvalue spectrum. The idea of this separation goes back to Foldy and Wouthuysen [12]. The exact separation of the two spectra would be equivalent to the transformation of the Dirac 4–spinors into either electronic or positronic 2–spinors. Alternatively, this means that the 4×4 Dirac Hamiltonian is to be block–diagonalized, *i.e.*, brought into the form of the direct sum of two 2×2 matrix Hamiltonians, one of them corresponding to the electronic spectrum and the other one referring solely to the positronic eigenvalues. Once this is achieved most problems of the relativistic quantum chem-

istry can be formulated solely in terms of electronic 2–spinors. The positronic solutions can be simply abandoned. Obviously, they will be needed in all cases which may involve the electron–positron pair creation processes, *i.e.,* whenever the given problem needs to be considered in the framework of quantum electrodynamics [5, 6, 13]. However, for the majority of problems encountered in relativistic quantum chemistry the use of the advanced apparatus of the quantum field theory does not seem to be urgently required [14].

In this context one should mention that the methods of relativistic quantum chemistry, which are based directly on 4–spinors [10, 15, 16], also neglect the positronic (negative energy) solutions. The variational stability of the 4–component Dirac–Coulomb or Breit Hamiltonian is achieved by imposing the so–called kinetic balance conditions [10] which define the mutual dependence between the large and small small component vectors. It's fullfillment enables the separation of the electronic and the positronic states. The latter ones are simply abandoned and thus the 4–component method becomes eventually a 'for electrons only' scheme. Once the positronic solutions are removed or neglected, the corresponding 4-spinor approach becomes fully equivalent to the 2–component theory 'for electrons only'. In such a case the solution of the Dirac–Coulomb or Dirac–Breit equations in the full 4–component formalism is only an unnecessary dificulty. The same goal can be achieved starting directly from the two–component approach. This is the main idea underlying recent developments in the area of 2–component methods. These developments can be summarized as a search for an efficient 2–component theory for relativistic quantum chemistry, which would be either very close or fully equivalent to the 4–component positive energy (electronic) solutions.

Achieving the goal of the complete separation of the electronic and positronic spectra by the traditional Foldy–Wouthuysen (FW) transformation [12] faces, however, serious problems [4, 17]. In the case of Coulomb potentials the usual expansion in powers of the fine structure constant $\alpha = 1/c$, where c is the velocity of light ($c \approx 137.026$ a.u. of velocity) results in two–component Hamiltonians which are essentially singular [4, 18, 19]. In general, the two–component Hamiltonians derived by the traditional FW transformation are rather useless. Only the lowest, α^2–order approximation, *i.e.,* the Pauli Hamiltonian [11], is of certain importance [20–22].

The failure of the traditional FW transformation to produce useful two–component electronic Hamiltonians is somewhat puzzling. It is known that the Dirac energy of the electron in the Coulomb field is analytic in α^2 [17]. Thus, the failure of the FW transformation should be

rather ascribed to the way this transformation is carried out; the infinite sum of all diverging energy contributions must give the well known finite result [4]. This means that the block–diagonalizing transformation of the Dirac Hamiltonian should be performed in such a way that the diverging terms undergo implicit infinite summation and result in a non–singular 2×2 electronic Hamiltonian. Such a transformation would be a counterpart of the renormalization techniques used in quantum field theory [6]. It would also resemble the infinite summation methods used in many–body perturbation techniques which lead to what is known as the coupled cluster formalism [23]. In the context of the block–diagonalization of the Dirac Hamiltonian this strategy, though perhaps not phrased explicitly that way, was introduced in 1974 by Douglas and Kroll [24].

The real breakthrough based on what is known as the Douglas–Kroll (DK) transformation should be credited to B. A. Hess [25,26] who found an efficient way of handling the matrix elements of the two–component DK Hamiltonian. Since then the Douglas–Kroll–Hess (DKH) numerical method became the most successful 2–component computational tool of the relativistic quantum chemistry. Analogous technique has been also developed by Almlöf *et al.* [27,28]. However, it does not seem to have been made into a routine computational tool.

This review is not aimed at the completeness of the presentation of different two–component methods in relativistic quantum chemistry and is primarily limited to the DK/DKH and related approximations. Particular attention will be given to new iterative schemes developed in our laboratory [29,30] which can lead to essentially exact (within some finite set of basis functions) solution [31] for the FW transformation and result in the complete non–singular separation of the electronic and positronic spectra of the Dirac Hamiltonian. Nevertheless, one should at least name some other techniques developed over the past decade. Some of them have found almost as broad range of applications as the DKH approach.

Among the other, to some extent competitive methods, the priority should be given to the so–called regular Hamiltonian techniques. The lowest, zeroth–order regular Hamiltonian approximation, which is nowadays referred to as the ZORA approach, has been originally proposed by Chang *et al.* [32] and later independently derived by Snijders and co–workers [33–36]. The major advantage of this approach is that the two–component ZORA Hamiltonian is manifestly non–singular. However, the energy eigenvalues are not invariant upon shifting the external potential by a constant. This disadvantage can be significantly reduced either by simple scaling or by passing to higher–order regular approximations.

Different regular Hamiltonian methods can be understood in terms of the perturbation expansion of the norm of the relativistic solution [37]. Some of the latest developments in the area of regular Hamiltonians have been recently described by Dyall and van Lenthe [38]. The results obtained in the ZORA approximation for molecular spectroscopic parameters are highly encouraging [39–41] and make the regular Hamiltonian methods competitive to the DKH approach.

Other schemes leading to the separation of the electronic and positronic spectra have been recently proposed by Rutkowski *et al.* [42, 43] and by Kutzelnigg [44]. All of them are rooted in the particular form of the perturbation approach introduced by Rutkowski [45–47] and shaped by Kutzelnigg [17, 48, 49] into what is nowadays called the direct perturbation theory (DPT). It is appropriate to mention here that DPT by itself can be considered as a powerful computational tool [50,51].

The present review of the two–component methods of relativistic quantum chemistry, which originate from the DK/DKH scheme, is organized as follows. In Section 1 the basic concepts and equations underlying the Dirac theory will be briefly surveyed and the problem of the block–diagonalization, *i.e.,* the problem of the separation of the positive and negative energy spectra of the Dirac Hamiltonian, will be outlined. Particular attention will be given to the possibility of step–by–step block–diagonalization based on the partition of the complete FW transformation into a product of unitary transformations.

The Foldy–Wouthuysen and Douglas–Kroll approach followed by the Hess ideas will be reviewed in Section 2. The new formulation of the Douglas–Kroll–Hess approach and its possible extensions will be presented as well. Some computational aspects of the two–component schemes considered in this paper, necessary for the development of the exact two–component approach, will be discussed in Section 3. Then, the operator equation introduced in Section 2 will be further modified in Section 4 to permit computationally feasible infinite–order solution of the block–diagonalization problem. The broad range of atomic numerical results, mostly quite recent and not published until now will be presented in Section 5. The spin dependent Hamiltonians are diagonalized and its accuracy in comparison to the Douglass–Krolll–Hess and to the Dirac values will be discussed. The possibility to reproduce the degeneracy of the $ns_{1/2}$ and $np_{1/2}$ or $np_{3/2}$ and $nd_{5/2}$ levels in different methods will be shown and discussed.

On passing to the two–component form of the relativistic Hamiltonian, one encounters another problem known as the change of picture for operators [52]. The fact that the form of essentially all operators is affected by the transition from the four– to two–component formalism will be

briefly discussed in Section 6. The two–electron Hamiltonian in the two–component approximation will be presented in Section 7. Finally, in Section 8, the possibility to define other (approximate) two–component Hamiltonians which may be of certain importance in relativistic quantum chemistry of lighter elements will be shown.

1. Unitary transformations of the Dirac Hamiltonian

Most of this this review will be limited to the theory for a single electron moving in the external potential as represented by the potential energy operator V. Actually, as long as the one–electron part of the many–electron Hamiltonian is considered, this limitation is of hardly any importance. Since the main 'relativistic' contribution to the target two–component Hamiltonians comes from the one–electron terms, *i.e.*, from the electron–nucleus interactions, V can be understood as the usual electron–nucleus attraction operator. Also replacing V by the one–electron Dirac–Hartree–Fock potential [10, 53, 54] would not make too much difference for the general theory. Hence, it is sufficient to consider the ordinary time–independent Dirac equation [4]:

$$\mathrm{H}_0\Psi_0 = \epsilon_0\Psi_0 \tag{9.1}$$

for a single electron moving in the Coulomb field. The Dirac Hamiltonian H_0 can be written as a 4×4 operator matrix:

$$\mathrm{H}_0 = c\boldsymbol{\alpha p} + \beta c^2 + (\mathrm{V} - c^2)\mathrm{I} = \begin{pmatrix} \mathrm{V} & c\boldsymbol{\sigma p} \\ c\boldsymbol{\sigma p} & \mathrm{V} - 2c^2 \end{pmatrix}, \tag{9.2}$$

where the standard symbols are used for Dirac $(\boldsymbol{\alpha}, \beta)$ and Pauli spin $(\boldsymbol{\sigma})$ matrices [4, 18], and I is the 4×4 unit matrix. The energy zero has been shifted by $-c^2$ so that a free electron at rest would have the energy equal to zero. The atomic units will be used throughout this paper and the velocity of light c is equal to about 137.036 a.u. of velocity. Its inverse, α, is the traditional ordering parameter in the perturbation treatment of relativistic effects [4, 17, 45].

The idea of Foldy and Wouthuysen was to completely separate the electronic and positronic solutions of the Dirac equation by the van Vleck–type (unitary) transformation of the Dirac Hamiltonian:

$$\mathrm{H}^{\mathcal{U}} = \mathcal{U}^{\dagger}\mathrm{H}_0\mathcal{U}, \tag{9.3}$$

with

$$\mathrm{H}^{\mathcal{U}} = \begin{pmatrix} \mathrm{h}_+ & 0 \\ 0 & \mathrm{h}_- \end{pmatrix}. \tag{9.4}$$

Such a transformation converts the 4×4 Dirac equation (9.2) into two separate eigenvalue problems. The one which corresponds to what is called the positive (electronic) part of the spectrum:

$$\mathrm{h}_+\psi_+ = \epsilon_+\psi_+, \tag{9.5}$$

where ψ_+ is the upper 2–spinor of the transformed 4–component function:

$$\Psi^{\mathcal{U}} = \mathcal{U}^\dagger\Psi_0 = \begin{pmatrix} \psi_+ \\ 0 \end{pmatrix}, \tag{9.6}$$

should convert into the two-component nonrelativistic Schrödinger equation in the limit of $c \to \infty$ (or $\alpha \to 0$).

The FW transformation $\mathcal{U}$ of Eq. (9.3) can be specified in a number of different forms [17]. The most common is the exponential form [18]. Moreover, it can be also expressed as a product of a series of unitary transformations:

$$\mathcal{U} = \mathcal{U}_0\mathcal{U}_1\mathcal{U}_2\ldots \tag{9.7}$$

This way of decomposing the final block–diagonalizing transformation $\mathcal{U}$ in (9.3) is of particular importance for the development of non–singular two–component relativistic Hamiltonians [29]. The benefits of expressing $\mathcal{U}$ in the product form (9.7) have been also stressed recently by Kutzelnigg [44]. Once the final $\mathcal{U}$ is expressed as the product of the unitary operator matrices $\mathcal{U}_k$ ($k = 0, 1, ...$) the transformation (9.3) can be achieved as a sequence of transformations:

$$\mathrm{H}^{\mathcal{U}}_{k+1} = \mathrm{H}_{k+1} = \mathcal{U}_k^\dagger \mathrm{H}_k \mathcal{U}_k, \qquad k = 0,\ 1,\ 2,\ \ldots, \tag{9.8}$$

initialized by the Dirac Hamiltonian H_0 and some suitable operator $\mathcal{U}_0$.

The problem of finding unitary transformations $\mathcal{U}_k$ ($k = 0, 1, ...$) which at each step perform, in general incomplete, block–diagonalization of the Dirac Hamiltonian can be formulated in terms of operator equations [29,55]. At each step (9.8) the transformation $\mathcal{U}_k$ is assumed to be of the form:

$$U_k = \begin{pmatrix} \Omega_+ & R_-\Omega_- \\ R_+\Omega_+ & \Omega_- \end{pmatrix}, \tag{9.9}$$

where

$$\Omega_+ = (1 + R_+^\dagger R_+)^{-1/2},\ \Omega_- = -(1 + R_-^\dagger R_-)^{-1/2},\ R_- = -R_+^\dagger, \tag{9.10}$$

and R_+ is the root of the following operator equation:

$$R = [(H_{k-1})_{22}]^{-1}\left[-(H_{k-1})_{21} + R(H_{k-1})_{11} + R(H_{k-1})_{12}R\right], \tag{9.11}$$

which corresponds to the assumption that $R = R_+$ is a 'small' operator as compared to the other operators in the r.h.s. of Eq. (9.11). In this equation $(H_{k-1})_{ij}$, $i,j = 1,2$, denotes the (ij)th 2×2 block of the Hamiltonian obatined in the $(k-1)$th step.

To build the exact two-component formalism in a finite number of steps means to find a set of transformations $\mathcal{U}_k$ which fully block-diagonalize H_0, *i.e.*,

$$\mathrm{H}_m = \mathcal{U}_m^\dagger .. \mathcal{U}_1^\dagger \mathcal{U}_0^\dagger \mathrm{H}_0 \mathcal{U}_0 \mathcal{U}_1 ... \mathcal{U}_m. = \begin{pmatrix} \mathrm{h}_+ & 0 \\ 0 & \mathrm{h}_- \end{pmatrix}. \tag{9.12}$$

The one-step determination of the block-diagonalizing unitary transformation $\mathcal{U}$ is possible in the case of a free particle. For $V \equiv 0$, the solution of Eq. (9.11) is known and reads:

$$R = \frac{\alpha \boldsymbol{\sigma p}}{e_p + 1}, \tag{9.13}$$

where

$$e_p = \sqrt{1 + \alpha^2 p^2}. \tag{9.14}$$

and the transformation $\mathcal{U}_0$, referred to as the free-particle Foldy-Wouthuysen (fpFW) transformation, has the following form:

$$\mathcal{U}_0 = \begin{pmatrix} \mathrm{A} & \alpha \mathrm{AB} \\ \alpha \mathrm{AB} & -\mathrm{A} \end{pmatrix}, \qquad \mathcal{U}_0{}^\dagger \mathcal{U}_0 = \mathrm{I}, \tag{9.15}$$

where

$$\mathrm{A} = \sqrt{\frac{e_p + 1}{2e_p}}, \qquad \mathrm{B} = \frac{1}{e_p + 1} \boldsymbol{\sigma p}, \tag{9.16}$$

and

$$e_p = \sqrt{1 + \alpha^2 p^2}. \tag{9.17}$$

When applied to the free-particle Dirac Hamiltonian, this transformation brings it into diagonal form:

$$\mathcal{U}_0{}^\dagger \begin{pmatrix} \mathrm{V} & c\boldsymbol{\sigma p} \\ c\boldsymbol{\sigma p} & \mathrm{V} - 2c^2 \end{pmatrix} \mathcal{U}_0 = \begin{pmatrix} \mathrm{T}_p & 0 \\ 0 & -2c^2 - \mathrm{T}_p \end{pmatrix}, \tag{9.18}$$

where

$$\mathrm{T}_p = c^2 (e_p - 1). \tag{9.19}$$

Thus, the positive and negative energy spectra of a free particle become fully separated. In other words one may say that fpFW of Eq. (9.15) accounts for all 'kinetic' relativistic effects.

In the case of Coulombic potentials the one–step determination of the block–diagonalizing unitary transformation $\mathcal{U}$ leads immediately to unsurmountable mathematical problems [4,17–19] and is evidently futile. In the traditional FW transformation of the Dirac Hamiltonian of Eq. (9.2) [4, 12, 18] the essentially singular operators arise either from high powers of p^2 or from their action on the Coulombic term V.

The problems which occur in the case of a one–step FW transformation of (9.2) hint at the possibilty that one could considerably profit by carring out a preliminary fpFW transformation of the initial Dirac Hamiltonian. Obviously, this transformation will not block–diagonalize H_0. However, it may help to obtain a new transformed Hamiltonian H_1 in which the essentially singular operators would either disappear or would be moved to higher orders with respect to α. This is what one learns by comparing the fully transformed free particle problem (9.18) with its α^2–expanded form. The latter involves essentially singular operators whose infinite sum in (9.18) and (9.19) is nonsingular.

The resulting transformed Hamiltonian $\mathrm{H}_1 = \mathcal{U}_0^\dagger \mathrm{H}_0 \mathcal{U}_0$ is:

$$\mathrm{H}_1 = \begin{pmatrix} \mathrm{T}_p + \mathrm{A}(\mathrm{V} + \alpha^2 \mathrm{BVB})\mathrm{A} & \alpha \mathrm{A}[\mathrm{V},\mathrm{B}]\mathrm{A} \\ \alpha \mathrm{A}[\mathrm{B},\mathrm{V}]\mathrm{A} & -2\alpha^{-2} - \mathrm{T}_p + \mathrm{A}(\mathrm{V} + \alpha^2 \mathrm{BVB})\mathrm{A} \end{pmatrix} \tag{9.20}$$

where $[\mathrm{X},\mathrm{Y}] = \mathrm{XY} - \mathrm{YX}$ denotes the commutator of X and Y. The transformed Hamiltonian can be conveniently written as:

$$\mathrm{H}_1 = \mathrm{H}_{1,d} + \mathrm{H}_{1,od}, \tag{9.21}$$

where $\mathrm{H}_{1,d}$ comprises the diagonal blocks of H_1 and $\mathrm{H}_{1,od}$ is built from its off-diagonal blocks.

The preliminary fpFW transformation of H_0 was the major step in the development of (presumably) non–singular two–component Hamiltonians and is to be credited to Douglas and Kroll [24]. The advantages which follow from this transformation are already visible in Eq. (9.20). First, the 'relativistic' order of the off–diagonal part of H_1 is reduced to the order of α as compared to the order of c in the initial Hamiltonian. Second, the awkward $\boldsymbol{\sigma p}\mathrm{V}\boldsymbol{\sigma p}$ operator which arises from the BVB term and could eventually lead to singular behaviour is accompanied by inverses of $e_p + 1$ (see Eq. (9.16)). Thus, whenever $\boldsymbol{\sigma p}\mathrm{V}\boldsymbol{\sigma p}$ assumes large values (*e.g.* in the vicinity of the nucleus) they will be quenched by the corresponding high values of p^2. Moreover, the norm of the αB operator is in the range between 0 (small momenta) and 1 (large momenta).

This shows that only non–essential (Coulomb) singularities may occur in $\alpha^2 BVB$ and in commutators. Similarly the norm of A is in the range between $1/\sqrt{2}$ (large momenta) and 1 (small momenta). This analysis stresses the advantages of the preliminary transformation applied to H_0 by Douglas and Kroll [24].

Suppose that we would like to have $\mathcal{U}$ of (9.3) determined in two steps only. Then, to build the exact two–component formalism would mean that the next step is to define the complementary transformation $\mathcal{U}_1$ which would fully block–diagonalize H_1, *i.e.*,

$$\mathcal{U}_1^\dagger \mathrm{H}_1 \mathcal{U}_1 = \mathcal{U}_1^\dagger \mathcal{U}_0^\dagger \mathrm{H}_0 \mathcal{U}_0 \mathcal{U}_1 = \begin{pmatrix} \mathrm{h}_+ & 0 \\ 0 & \mathrm{h}_- \end{pmatrix}. \tag{9.22}$$

The elements of $\mathcal{U}_1$ of the form (9.9) will be determined by the appropriate solution of the operator equation (9.11). Approximate solutions of this equation would give approximately block–diagonal Hamiltonians. Different approximations can be distinguished by some ordering parameter [29]. In the case of the Douglas–Kroll method this ordering parameter is chosen to be the strength of the interaction between electron and the external potential V. In the first order with respect to V the corresponding approximate Hamiltonian (DK1) will be given by the (11) block of (9.20). What is referred to as the DK method corresponds to the approximate second unitary transformation $\mathcal{U}_1$ which makes the (11) block of the partly block–diagonalized Hamiltonian accurate through terms of the order of V^2. The resulting approximate two–component approximation to h_+ can be thus referred to as the DK2 Hamiltonian.

2. The two–component Douglas–Kroll Hamiltonian and its extensions

One should mention that there is certain freedom in the choice of the form of the unitary transformation matrix $\mathcal{U}$ and the one given by Eq. (9.9) is not very common [29, 55]. In the present case the unitary character of $\mathcal{U}$ is reflected [55] in properties of the operator R. There are, however, other possibilities to define $\mathcal{U}$ in such a way that it becomes manifestly unitary [17], *e.g.*:

$$\mathcal{U} = e^{\mathcal{S}}, \quad \mathcal{S} = -\mathcal{S}^\dagger, \quad \mathcal{S}_d = 0, \tag{9.23}$$

$$\mathcal{U} = \left(\frac{1+\mathcal{X}}{1-\mathcal{X}}\right)^n, \quad \mathcal{X} = -\mathcal{X}^\dagger, \quad \mathcal{X}_d = 0, \tag{9.24}$$

and

$$\mathcal{U} = (1+\mathcal{Z})^{\frac{1}{2}} + \mathcal{Z}, \quad \mathcal{Z} = -\mathcal{Z}^\dagger, \quad \mathcal{Z}_d = 0. \tag{9.25}$$

where $\mathcal{S}_d$, $\mathcal{X}_d$ and $\mathcal{Z}_d$ are the diagonal elements of the respective matrices $\mathcal{U}$. The exponent n in (9.24) is arbitrary. Moreover, the choice $\mathcal{S}_d = 0$ or $\mathcal{X}_d = 0$ is not neccessary, though very convenient. Due to the even–odd rule the three formulations Eq. (9.23) to Eq. (9.25) are strictly equivalent and the conditions $\mathcal{S}_d = 0$ and $\mathcal{X}_d = 0$ or $\mathcal{Z}_d = 0$ imply each other. The equivalence holds also for different values of n in Eq. (9.24).

The form of $\mathcal{U}$ given by Eq. (9.25) was chosen in the orignal derivation of the Douglas–Kroll Hamiltonian [24]. The choice of the exponential form of the transformation (9.23) combined with the use of the Hausdorff commutator formula was made by Foldy and Wouthuysen [12]. The same exponential form of $\mathcal{U}$ was used in the recent analysis of the DK Hamiltonian [29]. It can be shown [29] that the form of the unitary transformation of the Hamiltonian does not influence the final results as it was proven in the earlier work [29]. However, certain particular choice of $\mathcal{U}$ may be of advantage in the approximate block–diagonalization methods and in comparisons between different two–component approaches.

The very important step of the DK method is the preliminary fpFW transformation of the Dirac Hamiltonian [24]. This can be derived from Eq. (9.11). Although Heully *et al.* [55] considered the transformation (9.9) as leading to the complete block–diagonalization of the Dirac Hamiltonian Eq. (9.2), their technique equally well applies et each step of the partial block–diagonalization. In particular one can use the operator equation (9.11) to define the $\mathcal{U}_1$ transformation in Eq. (9.22) which will approximately or exactly block–diagonalize the Dirac Hamiltonian (9.20) obtained from the preliminary fpFW transformation. This way of deriving the different DKn approximations will be followed here [29, 56, 57] The closed–form solution of Eq. (9.11) is available only in the case of the free–particle Dirac Hamiltonian. However, the form of this equation suggests that one may attempt to solve it iteratively. Once the operator R is determined from Eq. (9.11) applied to the fpFW transformed Dirac Hamiltonian, the 'electronic' 2–component Hamiltonian h_+ assumes the following form:

$$\begin{aligned} h_+ &= \Omega_+^\dagger (H_1)_{11} \Omega_+ + \Omega_+^\dagger R_+^\dagger (H_1)_{21} \Omega_+ + \Omega_+^\dagger (H_1)_{12} R_+ \Omega_+ \\ &+ \Omega_+^\dagger R_+^\dagger (H_1)_{22} R_+ \Omega_+ . \end{aligned} \tag{9.26}$$

For the purpose of the general discussion of different iterative approaches to the solution of Eq. (9.11) it is convenient to give its explicit form. After the substitution of the relevant parts of H_1 and some simple

algebra one obtains:

$$\begin{aligned} 2\mathrm{R} + \alpha^2 \mathrm{T_p R} + \alpha^2 \mathrm{R T}_p &= \\ = \alpha^3 \mathrm{A[B,V]A} + \alpha^2 \mathrm{A[V,R]A} &+ \alpha^4 [\mathrm{ABVBA,R}] + \alpha^3 \mathrm{R[B,AVA]R} \end{aligned} \tag{9.27}$$

Let us note that the *l.h.s.* of this equation can be written in several different, though equivalent forms, *e.g.*,

$$\begin{aligned} 2\mathrm{R} + \alpha^2 \mathrm{T_p R} + \alpha^2 \mathrm{R T}_p &\equiv (1+e_p)\mathrm{R} + \alpha^2 \mathrm{R T}_p \\ &\equiv e_p \mathrm{R} + \mathrm{R} e_p \end{aligned} \tag{9.28}$$

Now, one of the possibilities is to find a convenient and fast converging method for the iterative solution of (9.27) [30]. For this purpose it is useful to introduce the concept of the leading order [29] with respect to the expansion parameter α, *i.e.* the order with respect to α which is explicitly present in Eq. (9.27). One should note that the operators A and B both depend on α. However, their leading order with respect to this parameter is α^0. Thus, they will bring terms which are of the higher order in α than those explicitly shown. The iterative route leads to a series of two–component Hamiltonians of increasing accuracy in α^2. They will be denoted by h_{2k} where $2k$ means that the given approximate two–component Hamiltonian contains all terms through the order of α^{2k}, $k = 1, 2, \ldots$. The derivation and discussion of these Hamiltonians will be given in Section 8. Their main advantage is the explicit analytic form which may be useful in the analysis of certain features of approximate two–component methods [52].

Alternative solution of Eq. (9.27) can be obtained in the form of the matrix representation of the operator R. The basis set representation of solutions of the commutator equations is the common practice in the derivation of the DK Hamiltonian [24, 58]. In the present case a convinient way of solving Eq. (9.27) is by using a basis set which diagonalizes the p^2 operator [1]

$$\langle k \mid p^2 \mid k' \rangle = w_k \delta_{k,k'} \tag{9.29}$$

As a consequence the same basis set diagonalizes the e_p, T_p, A, and B operators. In particular:

$$\langle k \mid e_p \mid k' \rangle = E_k \delta_{k,k'}. \tag{9.30}$$

[1] In the original derivation of the DK Hamiltonian [24] the set $\mid k\rangle$ is meant to be the momentum eigenfunctions $\mid \mathbf{k}\rangle$ and the commutator equations are solved for Fourier kernels of the corresponding operators. In implementations of the DK method the momentum basis set is replaced by a set of functions defined in the coordinate space with the usual boundary conditions in infinity [25–27]. The accuracy of this approximation has been recently extensively tested [59].

In the basis set defined by Eq. (9.29), the matrix representation of the operator Eq. (9.27) leads to

$$\begin{aligned} \mathrm{R}_{k,k'} &= \langle k \mid \mathrm{R} \mid k' \rangle = \alpha^3 \frac{1}{E_k + E_{k'}} \langle k \mid \mathrm{A}[\mathrm{B},\mathrm{V}]\mathrm{A} \mid k' \rangle \\ &+ \frac{1}{E_k + E_{k'}} \langle k \mid \alpha^2 \mathrm{A}[\mathrm{V},\mathrm{R}]\mathrm{A} + \alpha^4 [\mathrm{ABVBA},\mathrm{R}] \\ &+ \alpha^3 \mathrm{R}[\mathrm{B},\mathrm{AVA}]\mathrm{R} \mid k' \rangle. \end{aligned} \tag{9.31}$$

Thus, all terms which will be of the lowest leading order of α^3 are absorbed into the first term in the *r.h.s.* of this equation. This could not have been done while working directly in the operator formalism [29,30,57].

According to Douglas and Kroll their method is based on the assumption that the two–component DK Hamiltonian h^{DK} approximates the exact h_+ through quadratic terms in the external interaction V [24]. This is equivalent to approximating R through terms linear in V. Within this assumption the matrix elements of R become:

$$\mathrm{R}_{k,k'} \approx \mathrm{R}^{DK}_{k,k'} = \mathrm{R}^{DK2}_{k,k'} = -\alpha^3 \frac{\mathrm{D}_{kk'}}{E_k + E_{k'}}, \tag{9.32}$$

where

$$\mathrm{D}_{kk'} = \langle k \mid \mathrm{D} \mid k' \rangle = \langle k \mid \mathrm{A}[\mathrm{V},\mathrm{B}]\mathrm{A} \mid k' \rangle. \tag{9.33}$$

One should note that $\mathrm{R}^{DK2}_{k,k'}$ of Eq. (9.32) is equivalent to the exact $\mathrm{R}_{k,k'}$ through the leading order of α^3 and contains some contributions of all higher–orders in α. Simultaneously $\mathrm{R}^{DK2}_{k,k'}$ contains all terms linear in V. The corresponding DK2 Hamiltonian is obtained from (9.26) under the restriction of its truncation beyond the terms quadratic in V and reads [57]:

$$\begin{aligned} \mathrm{h}^{DK2} &= \mathrm{T}_p + \mathrm{A}\left(\mathrm{V} + \alpha^2 \mathrm{BVB}\right)\mathrm{A} \\ &+ \frac{1}{2}\alpha \left((\mathrm{A}[\mathrm{V},\mathrm{B}]\mathrm{A}\mathrm{R}^{DK2} + \mathrm{R}^{DK2\dagger}\mathrm{A}[\mathrm{B},\mathrm{V}]\mathrm{A} \right). \end{aligned} \tag{9.34}$$

Its matrix elements in the basis set defined by (9.29) are given by:

$$\langle k \mid \mathrm{h}^{DK2} \mid k' \rangle = \langle k \mid \mathrm{T}_p + \mathrm{A}(\mathrm{V} + \alpha^2 \mathrm{BVB})\mathrm{A} \mid k' \rangle$$

$$+\frac{1}{2}\alpha^4 \sum_{k''} \left(\mathrm{D}_{kk''} \frac{1}{E_{k''} + E_{k'}} \mathrm{D}^{\dagger}_{k''k'} + \mathrm{D}_{kk''} \frac{1}{E_{k''} + E_k} \mathrm{D}^{\dagger}_{k''k'} \right). \tag{9.35}$$

This form is fully equivalent [57] to the usual expressions for the DK2 Hamiltonian [26, 58, 60].

Actually, the derivation presented in this review appears to be the simplest and the most transparent one [57]. It simulatneously shows that, through terms of the leading order of α^4, the two–component Hamiltonian h^{DK2} contains all terms that would enter the exact h_+. Hence, according to the present classification, this Hamiltonian belongs to the h_4 class of approximate two–component operators. Moreover, by the way of the ordering of terms in Eq. (9.27) the R^{DK2} approximation to R is exact through the leading order of α^3. This means that this is the *best* approximation one can obtain through this order in α. In consequence, h^{DK2} is *the best* Hamiltonian in the h_4 class.

The only disadvantage of the method leading to the DK (DK2) Hamiltonian of Eq. (9.35) is that the operators have to be defined in terms of their matrix elements in the basis which diagonalizes the p^2 operator. Hence, the study of its analytic features may be to some extent hindered by this particular choice [61]. On the other hand, defining h^{DK2} in terms of its matrix elements is anyway what one needs to do in the implementation of the DK method.

The derivation of what is called the higher–order DK (DKn) schemes [62] is also greatly facilitated by the manifestly iterative form of Eq. (9.31). By substituting the zeroth iterative solution (9.32) back into the *r.h.s.* of Eq. (9.31) one obtains the next iterative approximation to R:

$$\mathrm{R}_{k,k'} \approx \mathrm{R}^{DK2}_{k,k'} + \frac{1}{E_k + E_{k'}} \langle k \mid \alpha^2 \mathrm{A}[\mathrm{V}, \mathrm{R}^{DK2}]\mathrm{A} + \alpha^4 [\mathrm{ABVBA}, \mathrm{R}^{DK2}]$$

$$+ \alpha^3 \mathrm{R}^{DK2}[\mathrm{B}, \mathrm{AVA}]\mathrm{R}^{DK2} \mid k' \rangle. \tag{9.36}$$

This iterative process can be continued to infinity and will lead to exact formal expression of $\mathrm{R}_{k,k'}$. Its substitution into (9.26) will result in the exact h_+ Hamiltonian expressed as an infinite series of matrix elements.

It has been stressed several times that (9.32) is never explicitly evaluated numerically. Since the operator R in (9.32) involves terms which are linear in $\boldsymbol{\sigma p}$, the evaluation of its matrix elements would require

to use of the explicit Fourier transform [24, 63]. This would make the method rather useless for molecular relativistic calculations. The success of the Douglas –Kroll method is mostly due to its implementation by Hess [25, 26, 60]. Although the method of Hess solves the problem of avoiding the Fourier transform in the evaluation of (9.35), it cannot cope with the similar problem arising in the case of Eq. (9.32). Thus, going to higher–order approximations means that the corresponding *formal* solutions for the matrix elements of R need to be determined and a new approximation to h_+ must be derived from Eq. (9.26). A similar problem occurs in extensions of the Douglas–Kroll scheme beyond the third–order in V [62].

Different methods for the efficient determination of R in the operator form have been pursued by Barysz *et. al* [29–31]. In higher orders of approximation with respect to either α^2 or V all of them lead to rather involved two–component hamiltionians. Additionally, for high values of the nuclear charge Z the convergence of the α^2 and V expansions becomes quite poor and one needs to derive the corresponding analytic two–component Hamiltonians of a rather high order [30]. These attempts to obtain a useful analytic two–component Hamiltonian of high accuracy with respect to α^2 will be reviewed in Section 8.

More recently [31,56], a method which avoids the explicit step–by–step generation of the h_{2k} Hamiltonians and gives the infinite–order two–component Hamiltonian h_+, has been found. Both the solution of the operator equation which gives the unitary transformation $\mathcal{U}_1$ and the determination of h_+ are carried out in the algebraic approximation. The proposed algebraic approach is rooted in the method of handling the momentum space integrals suggested by Hess [25, 26] in the context of the DK Hamiltonian. It has been found [31, 56] that the same method can be applied to the determination of the operator R with arbitrarily high numerical accuracy.

3. Momentum space integrals: the Douglas–Kroll–Hess method

If the DK method remained in its original formulation [24] with the need for Fourier transforms of operators defined in coordinate, its use in relativistic quantum chemistry would be rather limited. The success of the DK and related approximations is mostly due to excellent and rather bold idea of Hess [25,26] to replace the explicit Fourier transforms [24, 63] by some basis set which diagonalizes the p^2 operator (9.29). Let $\{\zeta_\alpha(\mathbf{r})\}$ be a finite set of some coordinate–dependent functions in which

the eigenvectors $|\, k\rangle$ of p^2:

$$|\, k\rangle = \sum_{\alpha} c_{\alpha k} \zeta_{\alpha}(\mathbf{r}) \tag{9.37}$$

are determined, i.e.,

$$\langle k \mid p^2 \mid k' \rangle = w_k \delta_{kk'}, \tag{9.38}$$

In the basis set $\{|\, k\rangle\}$ the approximate identity resolution is bulit:

$$1 \approx \sum_{k} |\, k\rangle\langle k\,| \tag{9.39}$$

and inserted between operators defined in the coordinate and momentum spaces. Then, for any function of the p^2 operator, say $f(p^2)$ the following approximation is introduced:

$$\langle k \mid f(p^2) \mid k' \rangle = f(w_k)\delta_{kk'}, \tag{9.40}$$

whereas the matrix elements of V and $\boldsymbol{\sigma p} V \boldsymbol{\sigma p}$ can be evaluated directly in the $\mathbf{r}$–space. This, however, removes only some of integrals which are linear in $\boldsymbol{\sigma p}$. What remains are the operators of the form:

$$\boldsymbol{\sigma p} V f(p^2) V \boldsymbol{\sigma p}. \tag{9.41}$$

They will lead to integrals with linear terms in $\boldsymbol{\sigma p}$ whose accurate enough evaluation would require large basis sets with high angular momentum functions. Hess avoided this problem by using the identity:

$$\frac{\boldsymbol{\sigma p \sigma p}}{p^2} = 1, \tag{9.42}$$

whose insertion into (9.41) gives:

$$\boldsymbol{\sigma p} V \boldsymbol{\sigma p} p^{-2} f(p^2) \boldsymbol{\sigma p} V \boldsymbol{\sigma p}. \tag{9.43}$$

The use of eigenvectors of the p^2 operator determined in the $\mathbf{r}$–dependent basis set and of the identity (9.42) reduces all terms needed for the evaluation of (9.35) to rather elementary integrals in the coordinate representation. However, this method when applied to Eq. (9.27) will not remove the cumbersome terms which are linear in $\boldsymbol{\sigma p}$. This means that to go beyond the Douglas–Kroll approximation one needs first to determine the formal analytic solution for certain higher–order approximation to R and derive the explicit formulae for matrix elements of the

corresponding approximation to h_+. Only then the numerical method of Hess can be appplied.

Although the method based on the analytic iterative solution [30] of Eq. (9.27) is infinitely extendable and in the limit will formally give the *exact* two–component Hamiltonian (9.26), reaching this limit would represent a formidable task and appears to be impractical. However, a simple modification of the operator equation (9.27) will be shown to replace the cumbersome $\boldsymbol{\sigma p}$ by functions of p^2. These in turn can be dealt with by the same technique which Hess applied to the DK Hamiltonian.

4. The infinite–order (exact) two–component method

To obtain a counterpart of the R–operator equation (9.27) which can be directly solved in a purely numerical (algebraic) way its modification was recently proposed [31,56]. For this purpose the Eq. (9.27) is multiplied by the operator $\boldsymbol{\sigma p}$. Then with the use of identity (9.42), this equation can be converted into:

$$e_p\mathrm{Y} + \mathrm{Y}e_p = \alpha^3\mathrm{A}\left(\mathrm{b}p^2\mathrm{V} - \mathcal{V}\mathrm{b}\right)\mathrm{A} + \alpha^2\mathrm{A}\left(\mathcal{V}p^{-2}\mathrm{Y} - \mathrm{YV}\right)\mathrm{A}$$
$$+\alpha^4\left(\mathrm{Ab}p^2\mathrm{VbAY} - \mathrm{YAb}\mathcal{V}\mathrm{bA}\right) + \alpha^3\mathrm{Y}\left(\mathrm{Ab}\mathcal{V}\mathrm{A}p^{-2} - \mathrm{AVAb}\right)\mathrm{Y} \tag{9.44}$$

where

$$\mathcal{V} = \boldsymbol{\sigma p}\mathrm{V}\boldsymbol{\sigma p}, \tag{9.45}$$

$$\mathrm{Y} = \boldsymbol{\sigma p}\mathrm{R}, \tag{9.46}$$

and b is defined by:

$$\mathrm{b} = \frac{1}{e_p + 1} \tag{9.47}$$

The alternative formulation of these equations [31] assumes that Eq. (9.44) is additionally multiplied by the p^{-1} operator. The corresponding formulae are rather lengthy and will not be presented in this review. They can be found in Ref. [31]. However, numerically there is hardly any difference between these two ways of defining the Y operator.

Converting the R–operator equation into Eq. (9.44) means that all its matrix elements can be easily evaluated by using the methods surveyed in Sec. 3. All problematic terms linear in $\boldsymbol{p}$ will be replaced by other operators so that only the p^2–dependent terms will remain. In the basis

set (9.37), the determination of matrix elements of the new operator Y will need only the matrix elements of V and $\mathcal{V}$:

$$\mathrm{Y}_{k,k'} = \alpha^3 \tfrac{1}{E_k+E_{k'}} \mathrm{A}_k \left(\mathrm{b}_k w_k \mathrm{V}_{kk'} - \mathcal{V}_{kk'} \mathrm{b}_{k'}\right) \mathrm{A}_{k'}$$

$$+\tfrac{1}{E_k+E_{k'}} \left[\alpha^2 \mathrm{A}_k \textstyle\sum_{k''} \left(\mathcal{V}_{kk''} w_{k''}^{-1} \mathrm{Y}_{k''k'} - \mathrm{Y}_{kk''} \mathrm{V}_{k''k'}\right) \mathrm{A}_{k'}\right.$$

$$+\alpha^4 \textstyle\sum_{k''} \left(\mathrm{A}_k \mathrm{b}_k w_k \mathrm{V}_{kk''} \mathrm{b}_{k''} \mathrm{A}_{k''} \mathrm{Y}_{k''k'} - \mathrm{Y}_{kk''} \mathrm{A}_{k''} \mathrm{b}_{k''} \mathcal{V}_{k''k'} \mathrm{b}_{k'} \mathrm{A}_{k'}\right)$$

$$\left.+\alpha^3 \textstyle\sum_{k''} \sum_{k'''} \mathrm{Y}_{kk''} \left(\mathrm{A}_{k''} \mathrm{b}_{k''} \mathcal{V}_{k''k'''} \mathrm{A}_{k'''} w_{k'''}^{-1} - \mathrm{A}_{k''} \mathrm{V}_{k''k'''} \mathrm{A}_{k'''} \mathrm{b}_{k'''}\right) \mathrm{Y}_{k'''k'}\right] \tag{9.48}$$

where V_{kl} and $\mathcal{V}_{kl}$ denote the (kl)-th matrix element of V and $\mathcal{V}$, respectively.

Though Eq. (9.48) looks forbidding its programming and iterative solution is simple. By choosing the initial approximation for $\mathrm{Y}_{kk'}$ as equal to the first term of the *r.h.s.* of this equation, one can iterate its solution to any desired accuracy [31]. Hence, under the condition that the Hess method is used to evaluate all necessary matrix elements, one obtains essentially the *exact* matrix representation of the operator Y. Then, by inverting Eq. (9.46):

$$\mathrm{R} = p^{-2} \boldsymbol{\sigma p} \mathrm{Y} \tag{9.49}$$

and substituting this result into Eq. (9.26) one can numerically evaluate the matrix elements of the *exact* two–component Hamiltonian h_+:

$$\begin{aligned} \mathrm{h}_+ &= \Omega_+^\dagger \Big[\{\mathrm{H}_1\}_{11} + \{\mathrm{H}_1\}_{12} p^{-2} \boldsymbol{\sigma p} \mathrm{Y} + \mathrm{Y}^\dagger p^{-2} \boldsymbol{\sigma p} \{\mathrm{H}_1\}_{21} \\ &+ \mathrm{Y}^\dagger p^{-2} \boldsymbol{\sigma p} \{\mathrm{H}_1\}_{22} p^{-2} \boldsymbol{\sigma p} \mathrm{Y}\Big] \Omega_+. \end{aligned} \tag{9.50}$$

with

$$\Omega_+ = \Omega_+^\dagger = \left(1 + \mathrm{Y}^\dagger p^{-2} \mathrm{Y}\right)^{-1/2}. \tag{9.51}$$

The matrix elements of (9.50) are all expressed in terms of the known integrals V_{kl} and $\mathcal{V}_{kl}$, and eigenvalues of Eq. (9.40). The determination of matrix elements of the hermitian operator (9.51) is also achieved by the standard method of taking roots of hermitian matrices.

Obviously, the accuracy or exactness of the solution [31] will depend on the choice of the basis set. The standard Gaussian or Slater (with

integer powers of the radial coordinate r) basis sets are incapable of fully representing the logarithmic singularity of the Dirac solution [61]. For this reason they may not reproduce exactly the Dirac solutions. However, this limitation is common for the majority of methods used in relativistic quantum chemistry and does not represent a serious obstacle [10,26,31].

One can conclude that the complete numerical block–diagonalization of the Dirac Hamiltonian was accomplished in the algebraic form. This was possible owing to the determination of the second unitary transformation (9.9). In this context one should mention that the idea to determine the 'exact' FW transformation in the selected basis set has been also considered by Snijders *et al.* [36]. However, their formulation, at variance with the present one, requires some further approximations.

The new method [31,56] deserves to be referred to as the *exact* block–diagonalization technique. The operator equation (9.11) does not involve any approximation. The same applies to its general matrix form (9.31) and to the equivalent form given by Eq. (9.48). Obviously, the solution is generated numerically. However, as illustrated in Section 5, this can be done with arbitrarily high numerical accuracy so that the two–component solutions become essentially the same as the 'electronic' eigenvalues of the Dirac Hamiltonian.

5. The infinite–order two–component method: Numerical results

Initial investigations [31] of the numerical accuracy and convergence of the infinite–order two–component method of Section 4 of this review have been carried out for the $1s_{1/2}$ level in one–electron ions with different values of the nuclear charge Z. This level is known to be very sensitive to the basis set quality, in particular to the shape of basis functions in the nearest vicinity of the nucleus. For this reason both the Slater-type and Gaussian basis sets were investigated.

The first series of calculations uses the basis set $\{\zeta_\alpha(\mathbf{r})\}$ composed of Slater–type $1s$ functions with the following orbital exponents: $1.0 \times 10^m, 2.0 \times 10^m, 4.0 \times^m, 6.0 \times 10^m, 8.0 \times 10^m, 1.0 \times 10^{m+1}, 2.0 \times 10^{m+1}, \ldots,$ $4.0 \times 10^n, 6.0 \times 10^n, 8.0 \times 10^n, 1.0 \times 10^{n+1}$. The size of this basis set is fully specified by the values of m and n.

The results obtained [31] with basis sets of Slater–type functions for $Z = 40, 60, 80, 100$, and 120 are presented in Table 1.1 and compared with the true Dirac energies and the corresponding values calculated within the Douglas–Kroll method. The tabulated data are given in terms of the parameter ϵ which defines the $1s_{1/2}$ energy $E_{1s_{1/2}}$:

$$E_{1s_{1/2}} = -Z^2\epsilon. \tag{9.52}$$

All calculations have been carried out in quadruple precission. No linear dependencies have been found under the threshold of 10^{-10} for the eigenvalues of the basis set overlap matrix. It has been observed that the ϵ values numerically accurate through eight–nine decimals are obtained with the threshold 10^{-7} for the solution of Eq. (9.27). In all these calculations the basis set which defines the eigenvectors of the p^2 operator is assumed to be the same as the basis set in which the h_+ matrix elements are evaluated. This particular choice of the basis set of Slater–type functions gives essentially the non–relativistic limit for eigenvalues of h_+, although the exact eigensolution for this limit may not be actually among the basis functions.

The data of Table 1.1, which are copied here from the earlier paper [31], show that the lowest eigenvalue of the algebraically generated h_+ Hamiltonian quite smoothly converges to the Dirac limit with the increase of the basis set size. This means that the largest Slater–type basis sets used in this study can efficiently simulate the Dirac wave function behavior in the vicinity of the nucleus. However, this points also to the meaning of the accuracy of the method. This method can give results close to the Dirac values only if the basis functions are capable to reproduce sufficiently well the behavior of the exact $1s_{1/2}$ solution in the nearest vicinity of the nucleus. It is well documented that this is the most difucult task.

Another important point is that the selected basis set must exactly or accurately enough reproduce the non–relativistic limit of the theory. In view of the Slater basis set deficiencies it is rather surprising how well the basis sets employed in our investigation can cope with the simulation of the behavior of the exact solution in the vicinity of the Coulomb singularity. It is also worthwhile to stress the exceptionally good performance of the DK Hamiltonian in its implementation based on method of Hess. In terms of the parameter ϵ the DKH results do not appear to be far away from the exact values. However, one should take into account that in terms of energies of the $1s_{1/2}$ level, the error of the order of, say 10^{-3} a.u. in ϵ, actually means that the calculated energy will be in error by $Z^2 \times 10^{-3}$, *e.g.*, by 10^3 a.u. for $Z = 100$. Thus, the absolute inaccuracy of the DKH method for large values of Z is hidden behind the use of the scaled energy parameter ϵ. The discrepancy between the Douglas–Kroll and Dirac energies increases with the value of the nuclear charge. One should point out that the Douglas–Kroll energies lie always above the corresponding Dirac values. This confirms the usefulness of the Douglas–Kroll methods in approximate two–component variational calculations.

Although the Slater–type basis sets are convenient for testing the performance of the presented infinite–order two–component approach, their use in relativistic quantum chemistry is rather limited. Most calculations in relativistic quantum chemistry are carried out in Gaussian basis sets. Thus, it is worthwhile to investigate how well these basis sets can perform within the present method. For this purpose we have used basis sets of 1*s* Gaussians introduced earlier for similar purposes by Hess [25, 26]. These basis sets are defined by Gaussian orbital exponents: $\{8.0 \times 10^m, 1.0 \times 10^{m+1}, 2.0 \times 10^{m+1}, 4.0 \times 10^{m+1}, 8.0 \times^{m+1}, 1.0 \times 10^{m+2}, \ldots, 8.0 \times 10^{n-1}, 1.0 \times 10^n\}$. The study of the convergence of the lowest h_+ eigenvalue with respect to the range (m, n) is presented in Table 1.2 which also follows from the earlier paper [31].

The convergence of the Gaussian basis set results to the Dirac values looks to be slower than that observed for Slater–type functions. For the heaviest system ($Z = 120$) even the largest Hess–type basis set ($n = -3, m = 10$) used in our calculations does not give the corresponding Dirac limit which has been quite accurately calculated with Slater–type functions. Simple extensions of the Gaussian basis set devised by Hess [25, 26] by increasing the range of n and m have been found to only insignificantly improve the calculated ϵ values. However, by increasing of the Hess–type basis set 'density' via the addition of basis functions with orbital exponents equal to $6.0 \times 10^{m+1}, 6.0 \times 10^{m+2}, \ldots, 6.0 \times 10^{n-1}$ the calculated ϵ values for $Z = 120$ are found to slowly approach the Dirac limit (see Table 1.2). For the largest Gaussian basis set used in this convergence study ($m = -3, n = 15$, see Table 1.2) the ϵ value for $Z = 120$ is only 1×10^{-8} a.u. above the Dirac limit.

The data presented in Table 1.2 simply show that the Gaussian basis sets are not the best choice for relativistic calculations in the case of very high values of the nuclear charge. The importance of very high exponents indicates that the problem arises from the singularity of the Coulomb potential and the representation of the shape of the Dirac solution in the nearest vicinity of the nucleus. It is worthwhile to note that the same problem occurs in four–component calculations and has nothing to do with the use of its two–component equivalent.

It has been found that the accuracy of the finite basis set representation of the momentum space integrals as described in Section 3 can be highly improved by using basis sets of the even–tempered structure [59]. In the case of Gaussian functions the corresponding basis sets are generated by using an equidistant set of exponents on the logarithmic scale. With the lowest exponent assumed to be 10^m and the highest exponent equal to 10^n the decimal logarithmic grid becomes $a = (n - m)/(N - 1)$, where $N \geq 2$ denotes the number of basis functions. Thus, with the

assumed values of n and m the basis set density will be fully specified by the selected number of basis functions.

The efficiency of these (n, m, N) basis sets has been found to be superior [59] to that of basis sets generated by the recipe of Hess [25,26], *i.e.*, with the given size N they give a better approximation to the exact value of ϵ. Thus, all other investigations have been carried out with Gaussian basis sets of the even–tempered structure. Thes basis sets were applied to the study of the performance of the infinite–order method in the case of the higher $ns_{1/2}$ levels of hydrogenic ions and the corresponding results are presented in Table 1.3.

The data of Table 1.3 correspond to just one selected [64] Gaussian basis set which can be identified by the label (−6, 7, 80). On comparing the present data with the exact values of ϵ one needs to take into account that the basis set requirements are different for different $ns_{1/2}$ levels. Thus, a single basis set of 80 Gaussian functions meay not be flexible enough to simultaeneously give converged results for *e.g.* $1s_{1/2}$ and $7s_{1/2}$ levels. Indeed this is observed for higher values of the nuclear charge Z and indicates that one would need to increase the value of m, *i.e.*, augment the (−6, 7, 80) by Gaussian functions with higher exponents. With this reservation the performance of the infinite–order two–component method of Section 4 is in general very good. The iterative solution of Eq. 9.48 together with the two–component Hamiltonian 9.50 give essentially the same results as the 4–component theory.

In addition to the results of present infinite–order method and the exact Dirac values of ϵ also the corresponding values obtained with the same basis set from the DKH approach are presented. The largest differences occur for low–lying levels. This means that the total DKH energies of many–electron systems will be significantly affected by the use of the α^4–order approximate two–component Hamiltonian. However, for higher $ns_{1/2}$ levels the DKH method performs quite well.

The study of $ns_{1/2}$ levels [64] has also indicated that the convergence with respect to the basis set size is much faster for the higher–energy states than for the $1s_{1/2}$ state. In this context one may also refer to earlier studies of the Douglas–Kroll Hamiltonian [26] and to more recent investigations in the area of the regular Hamiltonian approximation [38].

The usual practice of approximate relativistic calculations is to reduce the two–component Hamiltonians to the so–called spin–averaged (scalar) form by simply removing all spin–dependent terms. Also the DKH method was originally formulated in this spin–free approximation. The meaning of this approximation applied simultaneously to all one–electron levels in a many–electron system is not quite clear. If the spin–dependent operators were retained in the DK/DKH method one could

expect it to be incapable of accurately predicting the spin–orbit splittings. Also the exact supersymmetry [65, 66] of the Dirac Hamiltonian will be destroyed because of the approximate form of the second unitary transformation. Since the infinite–order two–component method is based on the complete unitary transformation of the Dirac Hamiltonian, the same transformation is applied to Johnson–Lippmann operator [65, 66]. Hence, the resulting two–component operator (9.50) will be supersymmetric. This feature is considered to be very important for future applications of the infinite–order two–component method as compared to those of the DKH approach without spin–averaging. The numerical examples are shown in Tables 1.4 – 1.7.

The study of the degeneracy of the $ns_{1/2}$ and $np_{1/2}$ levels within the infinite–order scheme is presented in Table 1.4 and accompanied by the corresponding DKH data in Table 1.5. Analogous data for the $np_{3/2}$ and $nd_{3/2}$ levels calculated within the infinite–order and DKH two–component methods are displayed in Tables 1.6 and 1.7, respectively. They all confirm the excellent performance of the infinite–order approach; the corresponding results agree quite well with the exact 4–component data. Some discrepansies observed for $np_{1/2}$ levels for very high values of Z arise from defficiencies of the Gaussian basis set used in these calculations and and can be easily diminished by increasing the range of orbital exponents.

It is interesting to note that for the present choice of Gaussian basis sets for $ns_{1/2}$ and $np_{1/2}$ states the infinite–order method gives generally better results in the case of the s states, whereas the two–component DKH scheme gives consistently better results for p states. Moreover, in all cases when the basis set is saturated well eneough to bring the infinite–order results into full agreement with the exact Dirac values, the two–component DKH method leads to different energies of the given pair of $ns_{1/2}$ and $np_{1/2}$ states. This is what one could have expected on the basis of the lack of supersymmetry of the two–component DK Hamiltonian. The two–component DK Hamiltonian commutes with the transformed Johnson–Lippmann operator only thru terms of the order of α^4 and therefore cannot reproduce certain features of the exact Dirac energy spectrum. The same is also observed in the case of other two–component Hamiltonians [67].

The lack of supersymmetry will also affect the results obatined for spin–orbit splittings. This is confirmed by comparing the data for $np_{1/2}$ and $np_{3/2}$ levels calculated within the two–component DKH method (Tables 1.5 and 1.7) with either the exact results of with the values which follow from the infinite–order two–component calculations.

Only some selected results are presented in this review. A wider illustration of the performance of the infinite–order two–component approach, confirming the convergence of its results to the exact Dirac data for several states of different values of the principal quantum number and angular momenta, will be published separately [64].

6. The change of picture problem

The two–component methods, though much simpler than the approaches based on the 4–spinor representation, bring about some new problems in calculations of expectation values of other than energy operators. The same problems occur also for what is called the higher–order atomic and molecular properties [52,68,69]. Obviously, performing any unitary transformation $\mathcal{U}$ on the Dirac Hamiltonian H_0 (9.2) of a particle moving in some potential V will give transformed solutions (9.6). Suppose now that the relativistic system described by the Hamiltonian (9.2) is affected by some external perturbation. For the sake of simplicity we assume that the perturbation operator, H^1, is fully diagonal and spin–independent, *i.e.*,

$$H^1 = q \times I, \tag{9.53}$$

where q is some one–electron operator which may depend on particle's coordinates and momenta. Thus, the perturbed Dirac Hamiltonian reads:

$$H(\mu) = H_0 + \mu H^1 = \begin{pmatrix} V + \mu q & c\boldsymbol{\sigma p} \\ c\boldsymbol{\sigma p} & V + \mu q - 2c^2 \end{pmatrix}, \tag{9.54}$$

and the parameter μ is used to order the perturbation series. The expectation value of the perturbation operator (9.53) in the state Ψ_0 follows then from the Hellmann-Feynman [70] theorem:

$$\langle \Psi_0 \mid H^1 \mid \Psi_0 \rangle \equiv \epsilon^1 = \left(\frac{\partial}{\partial \mu} \epsilon(\mu) \right)_{\mu=0}, \tag{9.55}$$

where $\epsilon(\mu)$ is the μ–dependent eigenvalue of the perturbed problem:

$$H(\mu)\Psi(\mu) = \epsilon(\mu)\Psi(\mu). \tag{9.56}$$

This is the result obtained prior to any transformations and/or approximations to the Dirac Hamiltonian. The equivalent result for ϵ^1 calculated with transformed 4–component spinors (9.6) will be:

$$\begin{aligned} \epsilon^1 &= \langle \Psi_0^{\mathcal{U}} \mid \mathcal{U}^\dagger H^1 \mathcal{U} \mid \Psi_0^{\mathcal{U}} \rangle \\ &= \langle \mathcal{U}\Psi_0^{\mathcal{U}} \mid H^1 \mid \mathcal{U}\Psi_0^{\mathcal{U}} \rangle, \end{aligned} \tag{9.57}$$

i.e. the unitary transformation of the Hamiltonian will induce what is known as the change of 'picture' [12] which amounts to replacing H^1 by its unitary transform $\mathcal{U}^\dagger H^1 \mathcal{U}$ while using the transformed wave function Ψ_0^U. The second line of this expression says that if H^1 is used in its original non-transformed form, the wave function Ψ_0^U must be back transformed to the original representation. This means that the expectation value defined as:

$$\tilde{\epsilon}^1 = \langle \Psi_0^U \mid H^1 \mid \Psi_0^U \rangle \tag{9.58}$$

has no obvious relation to either (9.55) or (9.57). Although Eq. (9.57) is a trivial consequence of the matrix calculus, in quite a few cases the expectation values obtained from approximate relativistic schemes are calculated according to eq. (9.58). Since the results obtained from eq. (9.58) appear to be quite reasonable [58, 68, 71, 72], the error introduced by simultaneously using two different representations needs to be thoroughly investigated.

Although the picture change arising from unitary transformations of the Dirac equation is well known among physicists [19], its full recognition in relativistic quantum chemistry does not seem to be that common [52, 69]. The first study of this problem within the framework of the DK/DKH approximation is to be most likely credited to Kellö *et al.* [68]. These authors have considered the picture change effect upon the calculation of dipole moments and dipole polarizabilities of the coinage metal atoms and their hydrides. The effect was found to be negligible and led to the incorrect conclusion that the difference $\bar{\mathrm{X}} - \bar{\mathrm{x}}$ is of the order of α^4. Later the picture change problem was carefully considered by the present author [52] who found that the picture change effect is of the order of α^2 and may not be negligible for certain operators. One should also mention the analysis of this problem within the ZORA method [33]. The conclusion of this paper, based partly on the earlier findings of Baerends *et al.* [73], was that the picture change effect should be rather small.

The formal investigation of the picture change problem presented in Ref. [52] links the magnitude of the picture change effect to the form of the operator X. For operators which assume large values in the vicinity of nuclei this effect is expected to be quite large. Indeed, it has been found that for electric field gradients at heavy nuclei the picture change contribution is by no means negligible [74]. Since the calculated electric field gradients are used for the determination of nuclear quadrupole moments from molecular quadrupole coupling constants (see *e.g.*, Ref. [75]), this finding leads to rather important consequences concerning the accuracy of the so-called molecular values of nuclear quadrupole moments [75, 76].

One should mention, however, that the importance of the picture change in calculations of electric field gradients has been to some extent objected by Visscher *et al.* [77]. These authors attempted to evaluate the magnitude of this effect from the calculated 4–component (Dirac) functions. The transition from the 4–component to 2–component spinorbitals requires some renormalization which seems to be a little ambiguous and might have affected their conclusions concerning the true value of the picture change effect. Earlier results for electric field gradients [74] and the latest calculations of nuclear quadrupole moments of halides [76] undoubtedly indicate that the picture change effect must be in this case included.

Another operator which assumes large values in the vicinity of nuclei is related to the Hellmann–Feynman force and the calculation of its matrix elements is required in all gradient methods for the molecular geometry optimization [78–80]. The problem arising in this context was already recognized by Nasluzov and Rösch [81], though these authors did not associate it directly with the change of picture of the Hellmann–Feynman force operator. The same idea essentially underlies the recent papers on gradient methods within the regular Hamiltonian approximation [40, 41]. A comprehensive analysis of the picture change in two–component relativistic calculations has been recently carried out by Kellö *et. al* [82]. The numerical illustration reveals that neglecting the picture change effect on the Hellmann-Feynman force operator may lead to totally wrong predictions concerning molecular geometries [82].

The picture change effect has been also found to be quite large for dipole moment derivatives with respect to nuclear coordinates [83]. The same can be expected in the case of the dipole polarizability derivatives. These findings show that two–component calculations of infrared and Raman intensities for heavy systems need to take into account the picture change of the relevant operators. It should be mentioned that for both derivatives the operator which is responsible for the large picture change effect is the intramolecular electric field at the heavy nucleus [84]. The other operator involved in the definition of the dipole moment and polarizability derivatives, *i.e.*, the dipole moment operator, shows a rather negligible picture change effect [68]. This operator assumes large values far away from the heavy nuclei and the picture change effect on its matrix elements should be small [69].

In the case of major molecular electric properties, *i.e.*, multipole moments and multipole polarizabilities [85] the change of picture effect should be, in general, rather small. This brings some consolation, showing that the two–component calculations of these important properties can be carried out without modification of the corresponding operators.

Recently a general formulation of the picture change problem for second-order properties [85] has been presented [86]. The picture change contribution to these properties is also of the order of α^2. For electric polarizabilities its numerical values are relatively small and become important only for deep core levels [86]. However, the contribution of these levels to total polarizabilities is negligible. In the context of the picture change effect on higher-order atomic and molecular properties one should also refer to the recent paper by Dyall [87] who extensively analysed the picture change problem for different models of the two-component relativistic Hamiltonians with particular attention given to the evaluation of magnetic properties.

One of the puzzling questions arising in the context of the picture change effect is related to the use of relativistic core potentials [88]. Although these pseudpotentials can perform surprisingly well in energy-oriented calculations, the evaluation of expectation values and higher-order molecular properties from the resulting one- or two-component wave functions [89] should be sensitive to the picture change effect. This effect is not considered at all, although the relativistic pseudopotentials are derived by the reduction of all-electron relativistic equations [88, 90, 91]. Moreover, the evaluation of different expectation values and higher-order properties, including energy gradients, is carried out with the usual Schrödinger form of the corresponding operators. It might be that the picture change effects are partly taken care of by the fitted analytic form of relativistic pseudpotentials. Another reason could be that the accuracy of these calculations is too poor to reveal a rather subtle feature of the conversion from the 4-spinor to either 2-spinor or spinless formalisms. Nonetheless, this problem appears to be worth investigating.

The current experience in two-component relativistic calculations of expectation values and higher-order atomic and molecular properties shows that for certain operators the change of picture effect must be taken into account. In principle this would mean that one has to use the transformed operators as defined by Eq. (9.57). Several purely numerical techniques have been developed [68, 74, 82, 92–94] to avoid the explicit use of transformed operators (9.57). All these methods attempt to model the given operator by additional nuclear attraction operators. The latter can be simply included in V whose transformation is available. This approach, though quite successful, means that expectation values and other properties are calculated as the numerical derivatives of energies. Achieving high enough accuracy [93, 94], in particular for higher-order properties could pose some numerical problems. On the other hand, if the method described in Section 2 [25, 26] is used for the calculation of matrix elements of the given Hamiltonian, it can be also employed for

the calculation of (9.57) with the transformation $\mathcal{U}$ specified by the given two–component technique.

It is also appropriate to mention that the picture change problem is by no means restricted to one–electron operators, although the way of phrasing it in the case of the Coulomb repulsion terms is usually somewhat different from the one presented here. For instance, Sucher [54] considered the modification of the Coulomb repulsion operator caused by the no–pair approximation. The expression he derived is simply the interaction operator in the very approximate two–component formalism based on solutions of h_2 operators of Eq. (9.34). This form of the Coulomb interaction operator was also investigated by Samzow *et al.* [95]. They found that for valence orbitals of heavy systems the corresponding modification of two–electron integrals is relatively small.

7. The two–electron Hamiltonian in the two–component approximation

The attention of the present study was focused on the electronic part of the Dirac spectrum and this appears to be sufficient for the majority of relativistic studies in quantum chemistry. However, since both the h_+ and h_- spectra can be generated in the same way one can, if needed, proceed towards quantum electrodynamics formulated in finite basis sets. The first step in this direction will be the appropriate definition of the electron–electron interaction. The theory investigated in this paper is the one electron theory. However, the electron–electron interaction can be included by passing to the field–theoretic formalism. In the lowest order of the coupling between the electronic and electromagnetic fields the interaction term will be given by [6, 54, 96]:

$$V_{int} = \int\int \Psi_D^\dagger(\mathbf{r}_1)\Psi_D^\dagger(\mathbf{r}_2)\frac{1}{r_{12}}\Psi_D(\mathbf{r}_2)\Psi_D(\mathbf{r}_1)d^3\mathbf{r}_1 d^3\mathbf{r}_2, \qquad (9.59)$$

where Ψ_D denotes the Dirac field operator. If the pair creation processes are neglected, *i.e.*, in the so–called *no–pair* approximation [54], the Dirac field operator can be replaced by the 'large–component' spinor 9.6. Thus, within the *no–pair* approximation the interaction term becomes:

$$V_{int} = \int\int \psi_+^\dagger((\mathbf{r}_1)\psi_+^\dagger(\mathbf{r}_2)v(1,2)\psi_+(\mathbf{r}_2)\psi_+(\mathbf{r}_1)d^3\mathbf{r}_1 d^3\mathbf{r}_2, \qquad (9.60)$$

$$
\begin{aligned}
v(1,2) &= \{\mathcal{U}^\dagger(1)\}_{11}\{\mathcal{U}^\dagger(2)\}_{11}\frac{1}{r_{12}}\{\mathcal{U}(2)\}_{11}\{\mathcal{U}(1)\}_{11} \\
&+ \{\mathcal{U}^\dagger(1)\}_{11}\{\mathcal{U}^\dagger(2)\}_{21}\frac{1}{r_{12}}\{\mathcal{U}(2)\}_{21}\{\mathcal{U}(1)\}_{11} \\
&+ \{\mathcal{U}^\dagger(1)\}_{21}\{\mathcal{U}^\dagger(2)\}_{11}\frac{1}{r_{12}}\{\mathcal{U}(2)\}_{11}\{\mathcal{U}(1)\}_{21} \\
&+ \{\mathcal{U}^\dagger(1)\}_{21}\{\mathcal{U}^\dagger(2)\}_{21}\frac{1}{r_{12}}\{\mathcal{U}(2)\}_{21}\{\mathcal{U}(1)\}_{21} \qquad (9.61)
\end{aligned}
$$

and $\mathcal{U}(i)$, $i = 1, 2$, is the $\mathcal{U}$ transformation matrix for the i-th particle. The subscripts denote the appropriate 2×2 blocks of the transformation matrices. In the many-electron two-component theory the operator given by Eq. (9.61) replaces the usual Coulomb interaction operator. Its present form assumes that the transformation $\mathcal{U}$ is exact, and thus gives the infinite-order extension of the electron-electron interaction operators discussed earlier by Sucher [54] and Samzow *et al.* [95].

For a consistent 2-component form of the intermolecular interaction theory based on approximations to the unitary transformation (9.7) one must require that one- and two-electron terms are transformed by using the same form approximate of $\mathcal{U}(i)$. The same applies to the N-electron Hamiltonian:

$$
h(1, 2, ..., N) = \sum_{i=1}^{N} h_+(i) + \sum_{i<j}^{N} v(i,j) \qquad (9.62)
$$

The use of different trasformations for the one- and two-electron terms is inconsistent. Once the relativistic contributions are large, such a scheme may lead to unpredictable results. Actually such an approach has been used by Samzow *et al.* [95] in the context of the spin-averaged relativistic Hartree-Fock calculations for Ag and Au. They have transformed the one-electron terms with the Douglas-Kroll form of $\mathcal{U}(i)$ whereas the two-electron part was transformed with the free-particle Foldy-Wouthuysen matrix $\mathcal{U}_0(i)$. According to their findings [95] the transformation of the two-electron part did not bring too much change in comparison with the use of the non-transformed Coulomb term. This conclusion follows from all-electron Hartree-Fock calculations and does not tell too much about the corresponding effect on interaction energies.

Finally let us point out that the change of picture for different interaction operators which occurs upon transition from the 4-component to 2-component functions is quite relevant from the point of view of

intermolecular interactions. The problem of the form of the operator which corresponds to the interaction between two 'relativistic" subsystems which are described in the framework of the two–component formalism has been recently investigated [97, 98] and the analytic form of the corresponding operator has been derived.

To conclude this section let us add that all equations presented in this paper can be significantly simplified by the spin–averaging. Then, each 2–component function can be represented by one of the two spinorbitals with the same spatial part. This will bring all operators to the usual scalar form. However, the spin–avergaing means that all spin–orbit coupling terms are removed from the transformed operators. Yet, the spin–averaged methods can be quite useful in studies of interactions between heavy closed shell systems.

8. Step by step solutions for the operator R

At the end of this review the analitical attempt to solve the operator equation 9.27 will be discussed [30]. The iterative solution presented in Section 4 gives the most exactly results possible to achieve nowaday. Hovewer, when light elements are studied or when there is no need for such a high accuracy, another, simpler and cheaper approaches may be used.

The attractive feature of the iterative solutions of Eq. 9.27 is that for certain iterative processes, they can be obtained in a simple operator form , i.e. without any reference to some particular basis set. The major advantage is that such solutions can be easily analysed [52] and used for more general purposes [87].

For the purpose of finding efficient low–order iterative approximations to the solution of the nonlinear Eq. 9.27 we can consider it as a particular case of the more general equation:

$$(1+x)R + R(1+y) = \alpha^3 A[B,V]A + G(R,x,y), \tag{9.63}$$

where the only necessary condition imposed on the operators x and y is that Eqs. (9.27) and (9.63) are completely equivalent. Otherwise, they are completely arbitrary and can be manipulated to obtain the best analytic solution for the initial approximation $R^{(0)}$. The particular form of the R–dependent term $G(R,x,y)$ also depends on the choice of x and y.

Upon multiplying Eq. (9.63) by $1/(1+x)$ from the left and by $1/(1+y)$ from the right and using the identities:

$$\frac{1}{1+x} = 1 - \frac{x}{1+x}, \qquad \frac{1}{1+y} = 1 - \frac{y}{1+y} \tag{9.64}$$

Eq. (9.63) can be transformed into:

$$R = \frac{1}{2}\alpha^3 \frac{1}{1+x} A[B,V]A \frac{1}{1+y} + F(R,x,y). \tag{9.65}$$

where

$$F(R,x,y) = \frac{1}{2}\left(\frac{x}{1+x}R + R\frac{y}{1+y} + \frac{1}{1+x}G(R,x,y)\frac{1}{1+y}\right) \tag{9.66}$$

and is at least linear in R. Then, the initial approximation $R^{(0)}$ for R which follows from Eq. (9.65) becomes:

$$R \approx R^{(0)} = \frac{1}{2}\alpha^3 \frac{1}{1+x} A[B,V]A \frac{1}{1+y}. \tag{9.67}$$

The higher–order iterative approximations for R can be generated by the back substitution of (9.67) into (9.65).

The particular choice $x = y = 0$ corresponds to presumably the simplest nontrivial form of $R(0)$ used earlier [52] for the purpose of the formal analysis of different 2–component Hamiltonians. Such a choice gives:

$$R \approx R^{(0)} = \frac{1}{2}\alpha^3 A[B,V]A \tag{9.68}$$

and results in the h_4 BSS Hamiltonian of Ref. [29]:

$$h_4 = T_p + A(V + \alpha^2 BVB)A + \frac{1}{2}\alpha^4 A[V,B]A^2[B,V]A. \tag{9.69}$$

It is also worthwhile to mention that first two terms of the r.h.s. of this equation correspond to choosing $R^{(0)} = 0$ and represent the lowest–order (h_2) relativistic Hamiltonian which has been thoroughly investigated by Sucher [54] and used in numerical calculations in the early papers by Hess *et al.* [25, 26].

The higher–order iterative approximations will give the 2–component BSS Hamiltonians [29] which are exact through the 6th and higher–orders in α. This method, which in the limit of the infinite–order in α would give the exact $\mathcal{U}_1$, produces transformed Hamiltonians with the (1,1) block approximating h_+ through any desired highest leading order in α^2. They are referred to [29] as the 2–component BSS h_{2k} Hamiltonians, $k = 0, 1, 2, ...$, with h_0 being the 2–component non–relativistic Hamiltonian (see Section 2).

Because of some freedom in the choice of x and y one finds that for each value of k there will be a class of h_{2k} Hamiltonians which are equivalent through the order of α^{2k} and differ in higher–order terms. The BSS

h_{2k} Hamiltonians are just members of the given class. It is rather obvious that for the purpose of computational applications efficient iterative approaches, which include several higher–order terms already in low–order h_{2k} Hamiltonians, can be developed. Since each Hamiltonian of the h_{2k} class contains some contribution from all higher–order terms in α^2, one may expect that the success of the given finite $2k$th–order approximation will significantly depend on the included portion of these higher–order terms, *i.e.*, will depend on the choice of the x and y operators in Eq. (9.66).

From the computational point of view it is convenient to choose x and y in the form of functions of the p^2 operator. Then, in the p^2 basis set [26, 27, 59] these operators are diagonal. Although such a choice is by no means necessary, this feature considerably simplifies numerical calculations [25–27,29,59]. Among different forms of x and y investigated numerically in due course of this study particularly successful choice has been found to be given by:

$$x = y = \alpha^2 T_p = e_p - 1. \tag{9.70}$$

This symmetric choice is partly implied by the l.h.s. of Eq. (9.27) and leads to:

$$R \approx R^{(0)} = \frac{1}{2}\alpha^3 \frac{1}{e_p} A[B,V]A\frac{1}{e_p}. \tag{9.71}$$

Since

$$\frac{1}{e_p} = 1 - \frac{1}{2}\alpha^2 p^2 + o(\alpha^4), \tag{9.72}$$

the initial solutions (9.67) and (9.69) are equivalent through terms of the order of α^3. However, the norm of (9.70) will be smaller than that of (9.67). Hence, in comparison with h_4 of Eq. (9.70) the α^4–order contributions resulting from the 2–component Hamiltonian h_4' derived with (9.70):

$$\begin{aligned} h_4' &= T_p + A(V + \alpha^2 BVB)A + \frac{1}{2}\alpha^4 \left(\frac{1}{e_p} A[V,B]A\frac{1}{e_p} A[B,V]A \right. \\ &\quad + A[V,B]A\frac{1}{e_p} A[B,V]A\frac{1}{e_p} \\ &\quad - \left. \frac{1}{e_p} A[V,B]A\frac{1}{e_p^2} A[B,V]A\frac{1}{e_p} \right), \end{aligned} \tag{9.73}$$

For deep core levels the approximation which is exact through only α^4 terms may not be sufficiently accurate. Hence, it might be of some

interest to further iterate Eq. (9.65) with the initial solution as given by Eq. (9.70). The general first iterative solution $R^{(1)}$ becomes, however, quite awkward. If the target Hamiltonian is assumed to be exact through terms of the leading order of α^6, then one can limit the determination of $R^{(1)}$ to terms of the highest leading order of α^5. Then,

$$h_6' = h_4' + v_{6,2} + v_{6,3} \tag{9.74}$$

where $v_{6,2}$ combines all terms of leading order α^6 and quadratic in V,

$$\begin{aligned} v_{6,2} = -\frac{1}{8}\alpha^6 \Bigg(& \frac{1}{e_p}A[V,B]A\frac{1}{e_p^2}A[B,V]A\frac{1}{e_p}T_p + T_p\frac{1}{e_p}A[V,B]A\frac{1}{e_p^2}A[B,V]A\frac{1}{e_p} \\ + & \frac{2}{e_p}A[V,B]A\frac{1}{e_p^2}A[B,V]A\frac{1}{e_p}T_p\frac{1}{e_p} + \frac{1}{e_p}T_p\frac{1}{e_p}A[V,B]A\frac{1}{e_p^2}A[B,V]A\frac{2}{e_p} \\ - & 2A[V,B]A\frac{1}{e_p}A[B,V]A\frac{1}{e_p}T_p\frac{1}{e_p} - 2\frac{1}{e_p}T_p\frac{1}{e_p}A[V,B]A\frac{1}{e_p}A[B,V]A \\ - & 2A[V,B]A\frac{1}{e_p}T_p\frac{1}{e_p}A[B,V]A\frac{1}{e_p} - 2\frac{1}{e_p}A[V,B]A\frac{1}{e_p}T_p\frac{1}{e_p}A[B,V]A \\ + & 4\frac{1}{e_p}A[V,B]A\frac{1}{e_p}T_p\frac{1}{e_p^2}A[B,V]A\frac{1}{e_p}2\frac{1}{e_p}A[V,B]A\frac{1}{e_p}T_p\frac{1}{e_p}A[B,V]A\frac{1}{e_p}\Bigg) \end{aligned} \tag{9.75}$$

and $v_{6,3}$ comprises all terms of the leading order of α^6 and cubic in V:

$$\begin{aligned} & v_{6,3} = \\ & -\frac{1}{8}\alpha^6 \Bigg(\frac{1}{e_p}A[V,B]A\frac{1}{e_p^2}A[B,V]A\frac{1}{e_p}AVA + AVA\frac{1}{e_p}A[V,B]A\frac{1}{e_p^2}A[B,V]A\frac{1}{e_p} \\ & -2A[V,B]A\frac{1}{e_p}AVA\frac{1}{e_p}A[B,V]A\frac{1}{e_p^2} - 2\frac{1}{e_p^2}A[V,B]A\frac{1}{e_p}AVA\frac{1}{e_p}A[B,V]A \\ & +2A[V,B]A\frac{1}{e_p^2}A[B,V]A\frac{1}{e_p}AVA\frac{1}{e_p} + 2\frac{1}{e_p}AVA\frac{1}{e_p}A[V,B]A\frac{1}{e_p^2}A[B,V]A \\ & +2\frac{1}{e_p}A[V,B]A\frac{1}{e_p^2}AVA\frac{1}{e_p}A[B,V]A\frac{1}{e_p^2} + 2\frac{1}{e_p^2}A[V,B]A\frac{1}{e_p}AVA\frac{1}{e_p^2}A[B,V]A\frac{1}{e_p} \\ & -2\frac{1}{e_p}A[V,B]A\frac{1}{e_p^3}A[B,V]A\frac{1}{e_p}AVA\frac{1}{e_p} - 2\frac{1}{e_p}AVA\frac{1}{e_p}A[V,B]A\frac{1}{e_p^3}A[B,V]A\frac{1}{e_p} \\ & -2\frac{1}{e_p}A[V,B]A\frac{1}{e_p}AVA\frac{1}{e_p}A[B,V]A\frac{1}{e_p}\Bigg) \end{aligned} \tag{9.76}$$

It was shown [30] that the contribution of the α^6–order terms is dominated by $v_{6,2}$. However, the corresponding (truncated) Hamiltonian:

$$h'_6(V^2) = h'_4 + v_{6,2} \tag{9.77}$$

does not belong to the h_6 class of the 2–component operators for it does not account for all contributions of the α^6–order. Although the operators $v_{2k,m}$, $m = 2, 3, \ldots, k$ for higher values of k become quite lengthy and may appear prohibitively complicated, the evaluation of matrix elements of h'_{2k} is only marginally more difficult that that for the lower–order Hamiltonians.

As already mentioned the main advantage of the iterative approach based on Eq. (9.27) is that the resulting Hamiltonians are independent of the particular choice of basis functions used to evaluate their matrix elements. However, it appears that the only way to deal with noncommuting pairs of operators, which are of the leading order of α^3 and occur simultaneously in the *l.h.s* of Eq. (9.27), is by the transition to some basis set in a similar way as it was done in Section 2.

Table 9.1 The $1s_{1/2}$ energies for one-electron atoms expressed in terms of the parameter ϵ (Eq. (9.52)) calculated in different basis sets of Slater–type functions. A study of the convergence of the infinite order two–component results to the Dirac limit. All data in atomic units.

Basis set[a]		Nuclear charge Z				
m	n	40	60	80	100	120
−1	−1	0.51089522	0.52515189	0.54607769	0.57398632	0.60818495
−1	0	0.51112843	0.52656709	0.55182277	0.59329160	0.66786180
−1	1	0.51112966	0.52657816	0.55190281	0.59389385	0.67370693
−1	2	0.51112968	0.52657843	0.55190502	0.59391906	0.67430065
−1	3	0.51112968	0.53657842	0.55190498	0.59391937	0.67435298
−1	4	0.51112968	0.52657842	0.55190499	0.59391950	0.67435964
−1	5	0.51112968	0.52657842	0.55190499	0.59391948	0.67435978
−2	6	0.51112968	0.52657842	0.55190500	0.59391951	0.67435996
Exact[b]		0.51112969	0.52657843	0.55190502	0.59391954	0.67435996
DK[c]		0.51100986	0.52608268	0.55051948	0.59061912	0.66625902

[a]See Sectn. 5 for the definition of the set of Slater–type functions in terms of parameters m and n. [b]Exact Dirac energy. All data presented in this Table are calculated with $c = 137.03499$ a.u. [c] The Douglas–Kroll energy calculated with the largest Slater–type basis set ($m = -2, n = 6$).

Table 9.2 The $1s_{1/2}$ energies for one-electron atoms expressed in terms of the parameter ϵ (Eq. (9.52)) calculated in different basis sets of Gaussian functions. A study of the convergence of the infinite order two–component results to the Dirac limit. All data in atomic units.

Basis set [a]		Nuclear charge Z				
m	n	40	60	80	100	120
Hess–type basis set[b]						
−4	1	0.51011017	0.52431982	0.54649066	0.57953320	0.62808133
−4	2	0.51104682	0.52632433	0.55107990	0.59077645	0.65787370
−4	3	0.51112164	0.52654775	0.55177854	0.59325591	0.66872782
−4	4	0.51112881	0.52657458	0.55188551	0.59378108	0.67247654
−4	5	0.51112956	0.52657791	0.55190197	0.59389073	0.67373615
−4	6	0.51112964	0.52657833	0.55190451	0.59391351	0.67415413
−4	7	0.51112965	0.52657839	0.55190490	0.59391823	0.67429210
−3	8	0.51112965	0.52657839	0.55190496	0.59391921	0.67433755
−3	9	0.51112965	0.52657839	0.55190497	0.59391941	0.67435251
−4	9	0.51112965	0.52657839	0.55190497	0.59391942	0.67435251
−3	10	0.51112965	0.52657839	0.55190497	0.59391946	0.67435743
Hess–type basis set with increased density of exponents[b]						
−4	9	0.51112969	0.52657843	0.55190502	0.59391952	0.67435776
−3	11	0.51112969	0.52657843	0.55190502	0.59391952	0.67435924
−3	13	0.51112969	0.52657843	0.55190502	0.59391953	0.67435988
−3	15	0.51112969	0.52657843	0.55190502	0.59391953	0.67435995
Exact[c]		0.51112969	0.52657843	0.55190502	0.59391954	0.67435996
DK[d]		0.51100986	0.52608269	0.55051951	0.59061919	0.66625909

[a]See Sectn. 5 for the definition of the set of Gaussian functions in terms of parameters m and n.
[b]See Sectn. 5 for the detailed description of basis sets.
[c]Exact Dirac energy. All data presented in this Table are calculated with $c = 137.03499$ a.u.
[d] The Douglas–Kroll energy calculated with the Hess–type Gaussian basis set with increased density of exponents and $(m = -3, n = 15)$.

Table 9.3 The $ns_{1/2}$ energies for one-electron atoms expressed in terms of the parameter ϵ (Eq. (9.52)) calculated in different basis sets of Gaussian-type functions. A comparison of the infinite-order results with exact and DKH values.

Method[a]		Nuclear charge Z				
		40	60	80	100	120
Present	$1s_{1/2}$	0.51112969	0.52657843	0.55190496	0.59391841	0.67429626
Exact[b]		0.51112969	0.52657843	0.55190502	0.59391954	0.67435996
DKH[c]		0.51100986	0.52608269	0.55051951	0.59061873	0.66622141
	$2s_{1/2}$	0.12848570	0.13334905	0.14138246	0.15486538	0.18115814
		0.12848570	0.13334905	0.14138247	0.15486562	0.18117521
		0.12847071	0.13328629	0.14120194	0.15440837	0.17986908
	$3s_{1/2}$	0.05678946	0.05849313	0.06126307	0.06579445	0.07424250
		0.05678946	0.05849313	0.06126308	0.06579452	0.07424756
		0.05678506	0.05847489	0.06121137	0.06566604	0.07389056
	$4s_{1/2}$	0.03181193	0.03258128	0.03381637	0.03579616	0.03935974
		0.03181193	0.03258128	0.03381637	0.03579618	0.03936176
		0.03181008	0.03257370	0.03379513	0.03574435	0.03922202
	$5s_{1/2}$	0.02030021	0.02070874	0.02135864	0.02238546	0.02418912
		0.02030021	0.02070874	0.02135864	0.02238548	0.02419011
		0.02029927	0.02070490	0.02134797	0.02235978	0.02412236
	$6s_{1/2}$	0.01406739	0.01430921	0.01469134	0.01528882	0.01632013
		0.01406739	0.01430921	0.01469135	0.01528882	0.01632069
		0.01406685	0.01430700	0.01468526	0.01527430	0.01628302
	$7s_{1/2}$	0.01031862	0.01047325	0.01071639	0.01109355	0.01173618
		0.01031862	0.01047325	0.01071639	0.01109355	0.01173652
		0.01031828	0.01047187	0.01071259	0.01108457	0.01171350

[a]For each energy level the three rows correspond to the results of the infinite order two-component method, exact values, and those calculated within the DKH approach. The present and DKH data are calculated with the even-tempered Gaussian basis set defined by thre parameters parameters $n = -6$, $m = 7$, and $N = 80$. See Section 5.
[b]Exact Dirac energy. All data presented in this Table are calculated with $c = 137.03499$ a.u.
[c] The Douglas-Kroll energy calculated with the same basis set as that used to obtain the infinite-order results.

Table 9.4 A study of the $ns_{1/2} - np_{1/2}$ degeneracy in one-electron atoms and comparison of the present infinite-order results with the corresponding exact energies. All results calculated with even-tempered Gaussian basis sets are expressed in terms of the parameter ϵ (Eq. (9.52)).

Method[a]		Nuclear charge Z				
		40	60	80	100	120
Present[b]	$2s_{1/2}$	0.12848570	0.13334905	0.14138246	0.15486538	0.18115814
	$2p_{1/2}$	0.12848570	0.13334905	0.14138246	0.15486558	0.18115960
Exact[c]		0.12848570	0.13334905	0.14138247	0.15486562	0.18117521
	$3s_{1/2}$	0.05678946	0.05849313	0.06126307	0.06579445	0.07424250
	$3p_{1/2}$	0.05678946	0.05849313	0.06126307	0.06579451	0.07424225
		0.05678946	0.05849313	0.06126308	0.06579452	0.07424756
	$4s_{1/2}$	0.03181193	0.03258128	0.03381637	0.03579616	0.03935974
	$4p_{1/2}$	0.03181193	0.03258128	0.03381637	0.03579614	0.03935955
		0.03181193	0.03258128	0.03381637	0.03579618	0.03936176
	$5s_{1/2}$	0.02030021	0.02070874	0.02135864	0.02238546	0.02418912
	$5p_{1/2}$	0.02030021	0.02070874	0.02135864	0.02238507	0.02418898
		0.02030021	0.02070874	0.02135864	0.02238548	0.02419011
	$6s_{1/2}$	0.01406739	0.01430921	0.01469134	0.01528882	0.01632013
	$6p_{1/2}$	0.01406738	0.01430920	0.01469134	0.01528699	0.01631968
		0.01406739	0.01430921	0.01469135	0.01528882	0.01632069
	$7s_{1/2}$	0.01031862	0.01047325	0.01071639	0.01109355	0.01173618
	$7p_{1/2}$	0.01031854	0.01047318	0.01071639	0.01108601	0.01173390
		0.01031862	0.01047325	0.01071639	0.01109355	0.01173652

[a] For the given principal quantum number the three rows correspond to the present results for separately calculated $ns_{1/2}$ and $np_{1/2}$ levels and to the common exact value.

[b] The infinite-order two-component (present) results are calculated with even-tempered Gaussian basis sets. The set used for s states is defined by parameters $n = -6$, $m = 7$, and $N = 80$. The set use for p is defined by $n = -5$, $m = 5$, and $N = 50$. See Section 5.

[c] Exact Dirac energy. All data presented in this Table are calculated with $c = 137.03499$ a.u.

Table 9.5 A study of the $ns_{1/2} - np_{1/2}$ degeneracy in one–electron atoms as calculated by the two–component DKH method and comparison with the corresponding exact energies. All results calculated with even–tempered Gaussian basis sets are expressed in terms of the parameter ϵ (Eq. (9.52)).

Method[a]		Nuclear charge Z				
		40	60	80	100	120
DKH[b]	$2s_{1/2}$	0.12847071	0.13328629	0.14120194	0.15440837	0.17986908
	$2p_{1/2}$	0.12848450	0.13333598	0.14130478	0.15450849	0.17952380
Exact[c]		0.12848570	0.13334905	0.14138247	0.15486562	0.18117521
	$3s_{1/2}$	0.05678506	0.05847489	0.06121137	0.06566604	0.07389056
	$3p_{1/2}$	0.05678905	0.05848872	0.06123781	0.06568507	0.07379099
		0.05678946	0.05849313	0.06126308	0.06579452	0.07424756
	$4s_{1/2}$	0.03181008	0.03257369	0.03379513	0.03574435	0.03922202
	$4p_{1/2}$	0.03181175	0.03257936	0.03380559	0.03575092	0.03918282
		0.03181193	0.03258128	0.03381637	0.03579618	0.03936176
	$5s_{1/2}$	0.02029927	0.02070490	0.02134797	0.02235978	0.02412236
	$5p_{1/2}$	0.02030012	0.02070751	0.02135313	0.02236243	0.02410330
		0.02030021	0.02070874	0.02135864	0.02238546	0.02419011
	$6s_{1/2}$	0.01406685	0.01430700	0.01468526	0.01527430	0.01628302
	$6p_{1/2}$	0.01406733	0.01430863	0.01468818	0.01527415	0.01627204
		0.01406739	0.01430921	0.01469135	0.01528882	0.01632069
	$7s_{1/2}$	0.01031828	0.01047187	0.01071259	0.01108457	0.01171350
	$7p_{1/2}$	0.01031850	0.01047282	0.01071440	0.01107811	0.01170480
		0.01031862	0.01047325	0.01071639	0.01109355	0.01173652

[a] For the given principal quantum number the three rows correspond to the present two–component DKH results for separately calculated $ns_{1/2}$ and $np_{1/2}$ levels and to the common exact value.

[b] The two–component DKH results are calculated with even–tempered Gaussian basis sets as those used to obtain the infinite–order two–component results of Table 1.4. The set used for s states is defined by parameters $n = -6$, $m = 7$, and $N = 80$. The set use for p is defined by $n = -5$, $m = 5$, and $N = 50$. See Section 5.

[c] Exact Dirac energy. All data presented in this Table are calculated with $c = 137.03499$ a.u.

Table 9.6 A study of the $np_{3/2} - nd_{3/2}$ degeneracy in one-electron atoms and comparison of the present infinite-order results with the corresponding exact energies. All results calculated with even-tempered Gaussian basis sets are expressed in terms of the parameter ϵ (Eq. (9.52)).

Method[a]		Nuclear charge Z				
		40	60	80	100	120
Present[b]	$3p_{3/2}$	0.05595459	0.05646665	0.05720980	0.05821391	0.05952362
	$3d_{3/2}$	0.05595458	0.05646665	0.05720980	0.05821391	0.05952362
Exact[c]		0.05595459	0.05646665	0.05720980	0.05821391	0.05952362
	$4p_{3/2}$	0.03146037	0.03173018	0.03212143	0.03264948	0.03333726
	$4d_{3/2}$	0.03146037	0.03173018	0.03212143	0.03264948	0.03333726
		0.03146037	0.03173018	0.03212143	0.03264948	0.03333726
	$5p_{3/2}$	0.02012057	0.02027502	0.02049860	0.02079967	0.02119061
	$5d_{3/2}$	0.02012057	0.02027502	0.02049860	0.02079967	0.02119061
		0.02012057	0.02027502	0.02049860	0.02079967	0.02119061
	$6p_{3/2}$	0.01396360	0.01405919	0.01419737	0.01438297	0.01462328
	$6d_{3/2}$	0.01396360	0.01405920	0.01419736	0.01438298	0.01462328
		0.01396361	0.01405920	0.01419737	0.01438298	0.01462328
	$7p_{3/2}$	0.01025327	0.01031624	0.01040720	0.01052897	0.01068631
	$7d_{3/2}$	0.01025331	0.01031628	0.01040717	0.01052902	0.01068636
		0.01025335	0.01031632	0.01040720	0.01052905	0.01068637

[a] For the given principal quantum number the three rows correspond to the present results for separately calculated $np_{3/2}$ and $nd_{3/2}$ levels and to the common exact value.

[b] The infinite-order two-component (present) results are calculated with even-tempered Gaussian basis sets. The set used for p and d states is defined by parameters $n = -5$, $m = 5$, and $N = 50$. See Section 5.

[c] Exact Dirac energy. All data presented in this Table are calculated with $c = 137.03499$ a.u.

Table 9.7 A study of the $np_{3/2} - nd_{3/2}$ degeneracy in one–electron atoms as calculated by the two–component DKH method and comparison with the corresponding exact energies. All results calculated with even–tempered Gaussian basis sets are expressed in terms of the parameter ϵ (Eq. (9.52)).

Method[a]		Nuclear charge Z				
		40	60	80	100	120
DKH[b]	$3p_{3/2}$	0.05595457	0.05646651	0.05720927	0.05821247	0.05952047
	$3d_{3/2}$	0.05595458	0.05646665	0.05720975	0.05821391	0.05952285
Exact[c]		0.05595459	0.05646665	0.05720980	0.05821391	0.05952362
	$4p_{3/2}$	0.03146036	0.03173012	0.03212120	0.03268954	0.03333593
	$4d_{3/2}$	0.03146037	0.03173017	0.03212140	0.03264948	0.03333685
		0.03146037	0.03173018	0.03212143	0.03264948	0.03333726
	$5p_{3/2}$	0.02012057	0.02027498	0.02049848	0.02079935	0.02118993
	$5d_{3/2}$	0.02012057	0.02027501	0.02049859	0.02079967	0.02119038
		0.02012057	0.02027502	0.02049860	0.02079967	0.02119061
	$6p_{3/2}$	0.01396360	0.01405918	0.01419730	0.01438279	0.01462289
	$6d_{3/2}$	0.01396360	0.01405920	0.01419735	0.01438298	0.01462314
		0.01396361	0.01405920	0.01419737	0.01438298	0.01462328
	$7p_{3/2}$	0.01025327	0.01031623	0.01040716	0.01052886	0.01068607
	$7d_{3/2}$	0.01025331	0.01031628	0.01040716	0.01052902	0.01068627
		0.01025335	0.01031632	0.01040720	0.01052905	0.01068637

[a] For the given principal quantum number the three rows correspond to the present two–component DKH results for separately calculated $np_{3/2}$ and $nd_{3/2}$ levels and to the common exact value.

[b] The two–component DKH results are calculated with even–tempered Gaussian basis sets as those used to obtain the infinite–order two–component results of Table 1.5. The set used for p and d states is defined by parameters $n = -5$, $m = 5$, and $N = 50$. See Section 5.

[c] Exact Dirac energy. All data presented in this Table are calculated with $c = 137.03499$ a.u.

9. Summary

Some aspects of the formalism underlying the relativistic quantum chemistry and several recent developments in this area have been reviewed. The methods surveyed in this review are primarily restricted to those which follow from the approach devised by Douglas and Kroll and later implemented by Hess. For all these methods the important initial step consists in performing the free particle FW transformation on the Dirac Hamiltonian prior to further attempts to bring it into partly or completely block–diagonal form. This transformation is believed to either completely remove or at least to weaken the notorious singularities arising from the traditional FW approach. It has been shown that this initial step can be combined with the powerful operator method for the generation of the next block–diagonalizing unitary transformation. By uniting the two approaches one obtains a tool for the generation of the two–component relativistic Hamiltonians of arbitrarily high accuracy. These Hamiltonians can be classified according to their completeness with respect to the usual relativistic parameter α^2.

It has been shown that there are several possibilities of choosing Hamiltonians of the given h_{2k} class. It is to be stressed that the operator method used in their derivation is open–ended and can produce the two–component relativistic Hamiltonians of arbitrarily high accuracy in purely operator form, *i.e.,* without choosing any particular basis set. This can be considered as both the advantage of the operator technique and its disadvantage, for it may not be able to deal with certain terms in the most efficient way. The increase of this efficiency can be achieved by the choice of basis functions which diagonalize the p^2 operator. The price to pay is that the corresponding Hamiltonians are specified only in terms of their matrix elements in the selected set of basis functions.

By using the p^2 eigenvectors the present operator formalism is shown to produce the usual DK Hamiltonian. Within the h_4 class the DK(DK2)/DKH Hamiltonian has been shown to represent the best choice. This Hamiltonian follows from imposing simultaneously two conditions. First, the DK2 Hamiltonian must be equivalent to the exact two–component electronic operator h_+ through terms of the order of α^4. Second, it must comprise all terms through the second–order in V. Under these conditions the DK2 Hamiltonian can be easily derived by using the operator formalism described in this review. The same formalism permits a compact derivation of the higher–order DK-type approximations.

Some modification of the basic operator equation has been shown to result in the solution for the unitary transformation which brings the Dirac Hamiltonian into fully block–diagonal form. It has been found that the

complete reduction of the 4–component formalism to the 2–component electronic part can be achieved with negligible computational effort. Thus, the ultimate goal of the FW transformation method has been reached in the form of what is referred to as the exact two–component Hamiltonian. One needs to stress that this is the best one can do within the no–pair approximation, *i.e.* within the neglect of the hole–particle creation processes. This level of theory appears to be quite sufficient for the majority of relativistic problems in chemistry.

The problem which arises in the context of two–component methods of relativistic quantum chemistry is the way in which the expectation values and higher–order properties related to some external perturbation should be calculated. This problem has been specifically addressed in this review. To take into account the so–called picture change effect one needs to use appropriately transformed operators whose form is quite different from the one used in non–relativistic theories. In some cases this can be avoided by the use of models and numerical differentiation methods. Since the picture change problem is real and may significantly affect the calculated properties, the development of non–numerical approaches becomes one of the future goals in computational relativistic quantum chemistry based on the two–component approximation. This problem will also occur in the theory of interactions between heavy atoms and molecules. The corresponding theory based on the two–component representation of the interacting subsystems has to use appropriately modified interaction operator.

In the context of applications of two–component methods of relativistic quantum chemistry one has to mention that actually most of the corresponding calculations are carried out in the spin–free approximation. This permits that standard nonrelativistic codes can be used with a simple modification of the core Hamiltonian. The future seems to be in the development of the true two–component codes which will be able to deal with the spin–orbit interaction effect [99]. Since the methods based on the complete Dirac formalism may not be expected to reach the efficiency needed for their applications to chemical problems, the future is rather on the side of the two–component methods and the acquaintance with this relatively new area should be quite helpful. The area of relativistic quantum chemistry is still far from being fully explored and exploited.

Acknowledgments

The financial support towards this projects has been provided by the Committee of Scientific Research (KBN), Poland, through the research grants No. 3 T09A 116

17. This project is also a part of the activities of the Working Group PAMALOF (0009/98) of the COST Action D9. The authors acknowledge the use of the Sun Enterprise 6000 at the Regional Multiprocessor Systems Laboratory of the Nicolaus Copernicus University, Toruń, Poland.

References

[1] Weart, S.R., and Phillips, M. (1927). *History of Physics*, AIP, New York.

[2] Heitler, W., and London, F. (1927). *Z. Phys.*, 44:455.

[3] Dirac, P.A.M. (1929). *Proc. Roy. Soc. A*, 123:714.

[4] Moss, R.E. (1973). *Advanced Molecular Quantum Mechanics*, London: Chapman and Hall.

[5] Feynman, R.P. (1961). *Quantum Electrodynamics. A Lecture Note*, New York: Benjamin.

[6] Ryder, L. H. (1992). *Quantum Field Theory*, Cambridge: Cambridge University Press.

[7] Quiney, H.M., Skaane, H., and Grant, I.P. (1998). *Chem. Phys. Lett.*, 290:473.

[8] Brown, G.E., and Ravenhall, D.G. (1951). *Proc. Roy. Soc. A*, 208:552.

[9] Sucher, J. (1981). in: *Relativistic Effects in Atoms, Molecules, and Solids, NATO ASI Series B, Physics*, Malli, G.L. (Ed.), New York: Plenum Press, 87:1.

[10] Visscher, L., Visser, O., Aerts, P.J.C., Merenga, H., and Nieuwpoort, W.C. (1994). *Computer Phys. Commun.*, 81:120.

[11] Bethe, H.A., and Salpeter, E.E. (1957). *Quantum Mechanics of One- and Two-Electron Atoms*, Heidelberg: Springer.

[12] Foldy, L.L., and Wouthuysen, S.A. (1950). *Phys. Rev.*, 78:29.

[13] Grant, I.P., and Quiney, H.M. (1988). Fundamentals of relativistic atomic and molecular structure theory. *Adv. At. Mol. Phys.*, 23:37.

[14] Lindgren, L., Persson, H., Salomonsson, S., and Labzovsky, L. (1995). *Phys. Rev. A*, 51:1167.

[15] Dyall, K.G., Grant, I.P., Johnson, C.T., Parpia, F.A., and Plummer, E.P. (1989). *Computer Phys. Commun.*, 55:425.

[16] Dyall, K.G., Taylor, K., Faegri, P.R., Jr., and Partridge, H. (1991). *J. Chem. Phys.*, 95:2583.

[17] Kutzelnigg, W. (1990). *Z. Phys. D*, 15:27.

[18] Greiner, W. (1987). *Theoretische Physik, Bd. 6, Relativistische Quantenmechanik - Wellengleichungen*, Thun: Harri Deutsch.

[19] Thaller, B. (1992). *The Dirac Equation*, Berlin: Springer.

[20] Cowan, R.D., and Griffin, D.C. (1976). *J. Opt. Soc. Am.*, 66:1010.

[21] Ziegler, T., Snijders, J.G., and Baerends, E.–J. (1981). *J. Chem. Phys.*, 74:1271.

[22] Kellö, V., and Sadlej, A.J. (1990). *J. Chem. Phys.*, 93:8122.

[23] Urban, M., Černušák, I., Kellö, V., and Noga, J. (1987). *Methods in Computational Chemistry, Vol. 1*, Wilson S. (Ed.), New York: Plenum, p. 117, and references therein.

[24] Douglas, M., and Kroll, N.M. (1974). *Ann. Phys.*, 82:89.

[25] Hess, B.A. (1985). *Phys. Rev. A*, 32:756.

[26] Hess, B.A. (1986). *Phys. Rev. A*, 33:3742.

[27] Almlöf, J., Faegri K. Jr., and Grelland, H.H. (1985). *Chem. Phys. Lett.*, 114:53.

[28] Almlöf, J., and Gropen, O. (1996). *Reviews in Computational Chemistry Vol 8*, Lipkowitz, K.B., and Boyd, D.B. (Eds.), New York: VCH Publishers.

[29] Barysz, M., Sadlej, A.J., and J. G. Snijders, J.G. (1997). *Int. J. Quantum Chem.*, 65: 225.

[30] Barysz, M. (2001). *J. Chem. Phys.*, 114:9315.

[31] Barysz, M. and Sadlej, A.J. (2001). *J. Chem. Phys.*, 116:2696.

[32] Chang, C., Pélissier, M., and Durand, P. (1986). *Phys. Scr.*, 34:394.

[33] Van Lenthe, E., Baerends, E.–J., and Snijders, J.G. (1993). *J. Chem. Phys.*, 99:4597.

[34] Van Leeuven, R., van Lenthe, E., Baerends, E–J., and Snijders, J.G. (1994). *J. Chem. Phys.*, 101:1272.

[35] Van Lenthe, E., Baerends, E–J., and Snijders, J.G. (1994). *J. Chem. Phys.*, 101:9783.

[36] Van Lenthe, E., van Leeuven, R., Baerends, E–J., and Snijders, J.G. (1996). *Int. J. Quantum Chem.*, 57:281.

[37] Sadlej, A.J., Snijders, J.G., van Lenthe, E. and Baerends, E–J. (1994). *J. Chem. Phys.*, 102:1758.

[38] Dyall, K.G., and van Lenthe, E. (1999). *J. Chem. Phys.*, 111:1366.

[39] Van Wüllen, C. (1998). *J. Chem. Phys.*, 109:392.

[40] Van Lenthe, E., Ehlers, A., and Baerends, E–J. (1999). *J. Chem. Phys.*, 110:8943.

[41] Van Lenthe, J.H., Faas, S. and Snijders, J.G. (2000). *Chem. Phys. Lett.*, 328:107.

[42] Rutkowski, A. and Schwarz, W.H.E. (1996). *J. Chem. Phys.*, 104:8546.

[43] Rutkowski, A., Schwarz, W.H.E., Kozłowski, R., Bęczek, J., and Franke, R. (1999). *J. Chem. Phys.*, 109:2135.

[44] Kutzelnigg, W. (1999). *J. Chem. Phys.*, 110:8283.

[45] Rutkowski, A. (1986). *J. Phys. B*, 19:149.

[46] Rutkowski, A. (1986). *J. Phys. B*, 19:3419.

[47] Rutkowski, A. (1986). *J. Phys. B*, 19:3434.

[48] Kutzelnigg, W. (1989). *Z. Phys. D*, 11:15.

[49] Kutzelnigg, W. (1996). *Phys. Rev. A*, 54:1183.

[50] Kutzelnigg,W., Ottschofski, E., and Franke, R. (1994). *J. Chem. Phys.*, 102:1740.

[51] Ottschofski, E., and Kutzelnigg, W. (1994). *J. Chem. Phys.*, 102:1752.

[52] Barysz, M., Sadlej, A.J. (1997). *Theor. Chim. Acc.*, 97:260.

[53] Grant, I.P. (1987). In: *Methods in Computational Chemistry, Vol. 2*,, S. Wilson (Ed.), New York: Plenum Press, p.1.

[54] Sucher, J. (1980). *Phys. Rev. A*, 22:348.

[55] Heully, J.–L., Lindgren, I., Lindroth, E., Lundquist, S., and Mårtenson–Pendril, A.–M. (1986). *J. Phys. B*,19:2799.

[56] Barysz, M., and Sadlej, A.J. (2001). *J. Mol. Struct. (Theochem)*, 573:181.

[57] Barysz, M. (2002). *Acta Phys. Polon.*, 100:000, in the press.

[58] Jansen, G., and Hess, B.A. (1989). *Phys. Rev. A*, 39:6016.

[59] Woźniak, D., and Sadlej, A.J. (2000). *Acta Phys. Polon. A*, 98:673.

[60] Hess, B.A., and Chandra, P. (1987). *Phys. Scr.*, 36:412.

[61] Kutzelnigg, W. (1997). *Chem. Phys.*, 225:203.

[62] Nakajima, T., and Hirao, K. (2000). *J. Chem. Phys.*, 113:7786.

[63] Hardekopf, G. and Sucher, J. (1984). *Phys. Rev. A*, 30:703.

[64] Barysz, M., to be published.

[65] Johnson, M.H., and Lippmann, B.A. (1950). *Phys. Rev. A*, 78:329.

[66] Dahl, J.P., and Jørgensen, T. (1995). *Int. J. Quantum Chem.*, 53:161.

[67] Snijders, J.G., and Sadlej, A.J. (1996). *Chem. Phys. Lett.*, 252:51.

[68] Kellö, V., Sadlej, A.J., and Hess, B.A. (1996). *J. Chem. Phys.*, 105:1995.

[69] Barysz, M. (2000). *Pol. J. Chem.*, 74:1329, and references therein.

[70] Hellmann, H. (1937). *Einführung in die Quantenchemie*, Vienna: Fraz Deuticke, p. 285; Feynman, R.P. (1939). *Phys Rev*, 56:340.

[71] Marian, C.M. (1991). *J Chem Phys*, 94:5574;

[72] Kaldor, U., and Hess, B.A. (1994). *Chem. Phys. Lett.*, 230:1.

[73] Baerends, E–J., Schwarz, W.H.E., Schwerdtfeger, P., and Snijders, J.G. (1990). *J. Phys. B*, 23:3225.

[74] Kellö, V., and Sadlej, A.J. (1998). *Int. J. Quantum Chem.*, 68:159.

[75] Kellö, V., and Sadlej, A.J. (1990). *Phys. Rev. A*, 60:3575, and references therein.

[76] Bieroń, J., Kellö, V., Pyykkö, P., Sadlej, A.J., and Sundholm, D. to be published.

[77] Visscher, L., Enevoldsen, T., Saue, T., and Oddershede, J. (1998). *J. Chem. Phys.*, 109:9677.

[78] Gerratt, J., and Mills, I.M. (1968). *J. Chem. Phys.*, 49:1719; Thomsen, K., and Swanstrøm, P. (1973). *Mol. Phys.*, 26:735.

[79] Pulay, P. (1997). In: *Modern Theoretical Chemistry, Vol. 4*, Schaefer, H.F. (Ed.), New York: Plenum, p. 153.

[80] Halkier, A., Koch, H., Christiansen, O., Jørgensen, P., and Helgaker, T. (1997). *J. Chem. Phys.*, 107:849.

[81] Nasluzov, V.A., and Rösch, N. (1996). *Chem. Phys.*, 210:413.

[82] Kellö, V., and Sadlej, A.J. (2001). *J. Mol. Struct. (Theochem)*, 547:35.

[83] Kellö, V., and Sadlej, A.J. (2002) *J. Chem. Phys.*, to be published.

[84] Woliński, K., Roos, B.O, and Sadlej, A.J. (1985). *Theor. Chim. Acta*, 68:431.

[85] Buckingham, A.D. (1967). *Adv. Chem. Phys.*, 12:107.

[86] Turski, P., and Sadlej, A.J. (2001). *Chem. Phys. Lett.*, 338:345.

[87] Dyall, K.G. (2000). *Int. J. Quantum Chem.*, 78:412.

[88] Pyykkö, P., and Stoll, H. (2000). In: *Chemical Modelling. Applications and Theory, Vol. 1*, Hinchliffe, A. (Ed.), London: Royal Society of Chemistry, p. 239, and references therein.

[89] Balasubramanian, K. (1998). In: *Encyclopedia of Computational Chemistry*, von Schleyer, P.R. (Ed.), New York: Wiley, p. 2471, and references therein.

[90] Balasubramanian, K., and Pitzer, K.S. (1987). *Adv. Chem. Phys.*, 67:287.

[91] Ermler, W.C., Ross, R.B., and Christiansen, P.A. (1988). *Adv. Quantum Chem.*, 19:139.

[92] Pernpointner, M., Seth, M., and Schwerdtfeger, P. (1998). *J. Chem. Phys.*, 108:6722.

[93] Kellö, V., and Sadlej, A.J. (2000). *J. Chem. Phys.*, 112:522.

[94] Pernpointner, M., Schwerdtfeger, P., and Hess, B.A. (2000). *Int. J. Quantum Chem.*, 76:371.

[95] Samzow, R., Hess, B.A., and Jansen, G. (1992). *J. Chem. Phys.*, 96 (1992) 1227.

[96] Furry, W.H. (1951). *Phys. Rev.*, 81:115.

[97] Pestka, G., and Sadlej, A.J. (2002) *J. Mol. Struct. (Theochem)*, in the press.

[98] Pestka, G., and Sadlej, A.J. *J. Chem. Phys.*, to be published.

[99] Hess, B.A., Marian, C.M., Peyerimhoff, S.D. (1995). In: *Modern Electronic Structure Theory, Part I*, Yarkony, D.R. (Ed.), Singapore: Word Scientific, p. 152.

Chapter 10

RELATIVISTIC PSEUDOPOTENTIALS

Peter Schwerdtfeger
Department of Chemistry, The University of Auckland, Private Bag 92019, Auckland, New Zealand

Abstract: The pseudopotential approximation is reviewed in detail for heavy and superheavy elements. It is shown that pseudopotentials are an effective and accurate way to treat relativistic effects in heavy element containing systems.

Key words: pseudopotential, effective core potential, model potential, relativistic effects

1. Introduction

The treatment of atoms and molecules with a large number of electrons still remains a challenge to quantum chemists since Hartree-Fock (HF) or density functional theory (DFT) based procedures scale generally like N^m, with N being the number of basis functions involved. Even with the exponential increase in CPU power of computers over the last decades, which at the turn of the century reached the tera-flop region in performance (Figure 1), and the introduction of sophisticated algorithms and approximations to HF, post-HF and DFT methods, which can in some cases yield an almost linear scaling in computer time with increasing number of atoms,[1-3] for large and heavy molecules there is still a need for further approximations without significant loss of accuracy for the calculated properties of interest. Such an approximation is the *pseudopotential approximation* (PPA), also called *effective core potential method* (ECP), originally introduced by Hans G. A. Hellmann[4,5] in 1933 as combined approximation method (kombiniertes Näherungsverfahren).[6] The PPA applies the chemist's very basic idea that only valence electrons are important for the understanding of chemical bonding and processes (Figure 2).

U. Kaldor and S. Wilson (eds.),
Theoretical Chemistry and Physics of Heavy and Superheavy Elements, 399–438.
© 2003 *Kluwer Academic Publishers.*

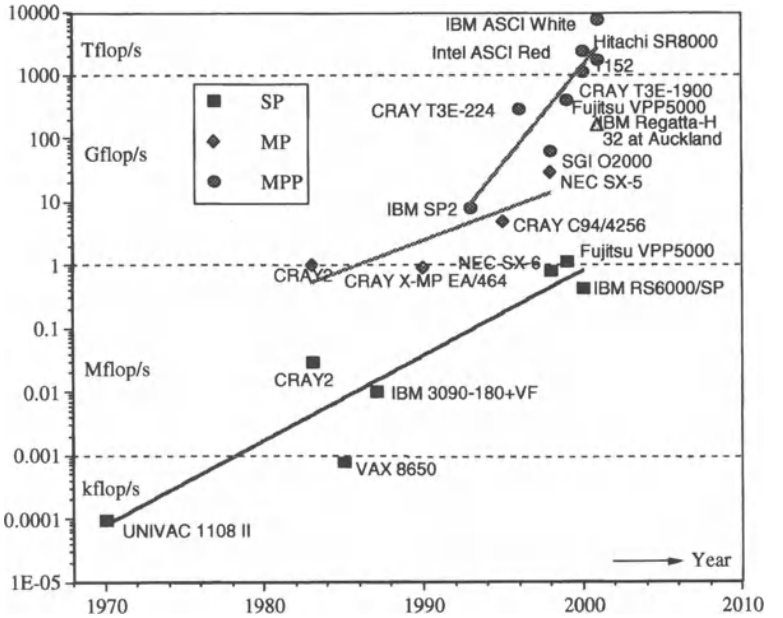

Figure 1. Linpack performance of various computers over the last three decades (in flops/s = floating point operations per second). SP: Single Processor. MP: Multi-processor. MPP: Massive parallel processing. The IBM ASCI White Power 3 (375MHz per processor) at Lawrence Livermore National Laboratory has 8192 processors.

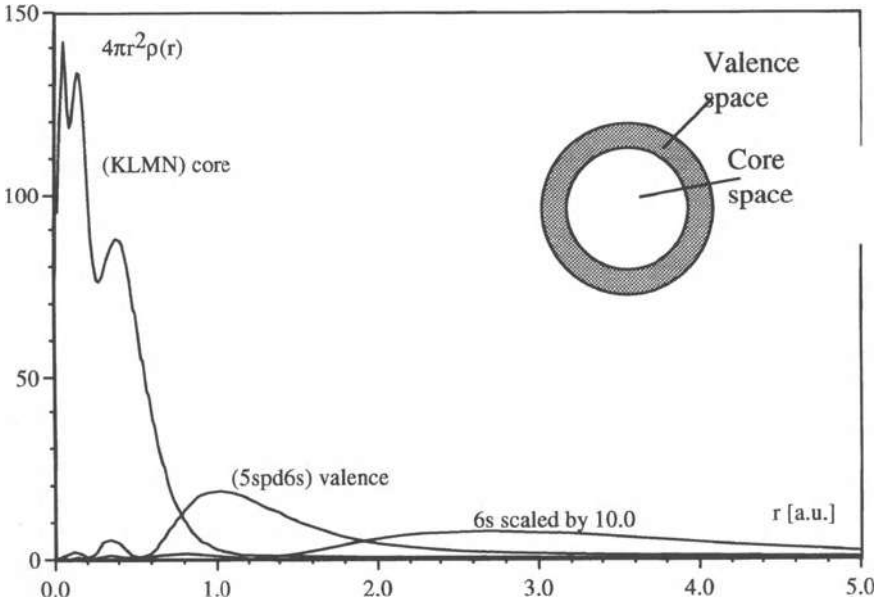

Figure 2. The (KLMN) core - (5spd6s) valence space separation shown for the mercury atom. Core and valence radial densities obtained from all-electron Dirac-Hartree-Fock calculations. The 6s density is increased by a scaling factor of 10.0 for comparison.

The PPA can be introduced in an *ad-hoc* fashion into the molecular electronic Hamiltonian (in au):

$$H_V = -\frac{1}{2}\sum_i^{n_V}\nabla_i^2 + \sum_{i<j}^{n_V}\frac{1}{r_{ij}} + \sum_i^{n_V}\sum_a^{N_C}\left[V_{PP}^a(r_{ai}) - \frac{Q_a}{r_{ai}}\right] + \sum_{a<b}^{N_C}\frac{Q_aQ_b}{r_{ab}} \qquad (1)$$

H_v is the valence electron model Hamiltonian with n_V valence electrons and N_c cores (nuclei), and V_{PP} is the corresponding pseudopotential for the core-valence interaction. The indices a,b run over all cores (nuclei) and i,j over all valences electrons. Q_a is the charge of core a, i.e. $Q_a = Z_a - n_c^a$, n_c^a being the number of core electrons of atom a (for an all-electron treatment of a specific atom we have $Q_a = Z_a$), and the last term in (1) describes the classical (point charge) core-core repulsion. Additional corrections to the last three sums may apply if non-frozen core effects are considered. After almost 70 years of intensive development in pseudopotential theory[7] it is fair to say that the PPA is now the most commonly applied and successful method for the treatment of systems including heavy elements.[8]

For the accurate treatment of heavy elements relativistic effects cannot be neglected anymore.[9] Even though relativistic basis sets for heavy elements become now available,[10-13] and state-of-the-art Dirac-Hartree-Fock (DHF) coupled cluster calculations including Breit interactions for many-electron heavy atomic systems yield properties (ionisation potentials, electron affinities, excitation energies[14,15] or static dipole polarizabilities[16]) of near experimental accuracy, a fully relativistic treatment for larger molecules (currently more than 500 basis functions at the DHF level or 250 basis functions at the relativistic coupled cluster level) is computationally still a formidable task. The main reason is the occurrence of the small component (S) spinor in the Dirac equation which leads to a large number of class (SS|SS) two-electron integrals. Another disadvantage is the required double group treatment for molecules which reduces the symmetry and requires complex wavefunctions. These complications led to the development of techniques for elimination of the small Dirac component and to new Hamiltonians in relativistic quantum theory, e.g. the direct perturbation theory starting from the nonrelativistic limit (the Levy-Leblond equation),[17] the Douglas-Kroll-Hess approximation,[18] the zero (and first) order regular approximation (ZORA, FORA),[19] the Chang-Pelissier-Durand Hamiltonian,[20,21] to name a few. They can either be used at the two-component (spin-orbit coupled) level (which still requires double group symmetry), or at the one-component (scalar relativistic, spin-orbit averaged) level which can easily be implemented in standard nonrelativistic program packages. Nevertheless, an all-electron *ab-initio* treatment using a scalar

relativistic approach say for a medium sized heavy metal cluster (e.g. Pb_{20} with more than 1600 electrons) would not be feasible with the current state-of-the-art computer codes and hardware.

There seems to be two mainstream approaches toward the treatment of large molecules including heavy atoms. One is the relativistic density functional theory (RDFT), that is the relativistic Hamiltonians mentioned above can be easily introduced into a DFT scheme.[22] For example, the Car-Parinello or other DFT methods[23] allow treatment for molecules with large number of atoms such a Ni_{147}.[24] However, current DFT schemes suffer from the fact that they cannot be improved successively to high accuracy for molecular properties even with the development of more accurate functionals within the generalized gradient approximation (GGA).[25] Dispersive (Van der Waals) type of interactions is one well known example where current DFT fails.[26] To illustrate this we consider the solid state of a heavy element system, mercury, which crystallizes in a metallic state of rhombohedral structure (hcp) with lattice parameters $a=b=$ 3.46 Å and $c=$ 6.66 Å, and a relatively small cohesive energy of $\Delta E_{coh}=$ 76 kJ mol^{-1}.[27] Recent DFT calculations gave $a=b=$ 3.55, 3.71, 6.26 Å, $c=$ 8.49, 9.26, 12.2 Å, and $\Delta E_{coh}=$ 42.4, 12.0, 1.7 kJ mol^{-1} at the LDA, PBE and B3LYP level respectively.[28] This is not a very satisfying situation.

The other alternative is to stay with *ab-initio* schemes and reduce significantly the number of electrons in the Hamiltonian. Since for most chemical properties of interest core-electrons are not so important, one might consider to keep the atomic core frozen (*frozen core approximation*) and to apply a *core-valence separation* (Figure 2) to finally arrive at a valence-only description, the PPA. This is however a non-trivial issue since it raises a number of fundamental questions:

- Electrons are indistinguishable and Fermi-Dirac statistics strictly does not allow a separation of the n-particle Hamiltonian into a core only and valence only part. Neither the n-particle wavefunction $\Psi(\vec{r}_i)$ nor the exact one-particle density $\rho(\vec{r})$ can be separated into a core and valence part. If we accept this argument the difficulty still remains how and at what level of approximation (DFT, Hartree-Fock or correlated schemes) one can introduce the PPA.
- Once we introduce the PPA at the *ab-initio* or DFT level, the question of transferability arises, e.g. the applicability of the PPA for different valence states.[29] Therefore, current PPA schemes derive their parameters from specific atomic calculations including important valence reference states. However, electrons and nuclei from other atoms will polarise the core and at small interatomic distances core repulsion effects become important.
- There is some ambiguity in the PPA because all current schemes include adjusted pseudopotential parameters which are obtained by quite different

fit procedures and data sets. There is currently no scheme at hand to decide which approximation is more accurate and only a large number of calculations and careful comparisons to all-electron calculations will decide if the specific pseudopotential for an atom is sufficiently accurate or not. With this respect, the choice of the core plays a crucial role.

- It is well known that relativistic perturbation operators act in the close vicinity of the nucleus (K- and L-shell region). It is therefore not immediately obvious how a relativistic scheme can be implemented into the PPA using nodeless orbitals.
- Core properties (operators which weigh the inner part of the electronic density, e.g. operators ~ r^{-n} or contain derivatives with respect to r) like electric field gradients of magnetic shielding tensors cannot be obtained directly from pseudopotential schemes using nodeless pseudoorbitals. The core has to be reintroduced in a subsequent step.

Despite all these points raised above the PPA has been tested many times in the past leading to very accurate atomic and molecular valence properties even for systems where relativistic effects are extremely large (Group 11 elements or superheavy elements). For valence properties (structure, bond energies, polarizabilities, dipole moments etc.) there is not one example known (in contrast to current DFT) where the PPA fails badly (if a small-core definition is chosen). This is the main reason for the huge success of the PPA in atomic, molecular and solid state chemistry and physics.

The PPA has a number of distinct features and advantages over all-electron methods:

- Removing the core and using nodeless pseudoorbitals reduces the number of basis functions significantly and thus reduces substantially the CPU time for any atomic or molecular calculation. There is also no need for accurately describing the strong oscillations of the valence orbitals in the core region. The additional cost comes from the evaluation of extra one-electron integrals over the pseudopotential operator, which however is relatively small.
- For weakly interacting systems the basis set superposition error is reduced since there is no contribution from the core electrons which contribute mostly to the total energy of the system.
- The accuracy of finite field methods (external electric or magnetic fields) is improved since small perturbations can be evaluated more accurately with a much reduced total electronic energy. That is the numerical noise is reduced considerably.
- Relativistic effects are implicitly considered in the pseudopotential through the adjustment procedure to relativistic atomic calculations. This again eliminates the additional treatment of relativistic perturbation

operators. Two-electron contributions like the Breit interaction can also be considered in this effective potential treatment.

The accuracy of the current PPA to heavy elements is the main subject of this book chapter. The theoretical section is kept at a more general level such that ongoing computational chemists are easily led into this important field of quantum chemistry of the heavy elements. There are a number of excellent and more specialized review articles available on pseudopotential theory and its applications.[30-37] A more concise treatment and discussion of the PPA can be found in a recent overview by Dolg.[38]

2. The pseudopotential approximation

2.1 Selecting the core

The aim is to find a valence-only formalism. This was achieved an early stage of quantum chemistry by Hellmann who realized that the Pauli exclusion principle can be re-expressed into an effective (nonclassical) potential (Abstossungspotential).[6] Later in 1940 Fock, Veselov and Petrashen gave a first expression for the valence Fock operator.[39] While the PPA found quickly its way into solid state physics through the orthogonalized plane wave method (OPW),[40] it was Preuss who implemented the PPA in a local form into atomic and molecular quantum chemistry codes.[41] The first important step in pseudopotential theory came in 1959 by Phillips and Kleinman who demonstrated explicitly that the orthogonality between valence and core orbitals can be replaced by an effective (local) potential.[42] A more general treatment for many valence electron systems was given in 1972 by Kahn, Baybutt and Truhlar.[43]

We start with the nonrelativistic Hartree-Fock equation for an n-electron atom (for more details see ref.7):

$$F\,\varphi_i = \varepsilon_i\,\varphi_i \qquad \text{with} \qquad \langle \varphi_i | \varphi_j \rangle = \delta_{ij} \tag{2}$$

and for convenience we use $\varphi \equiv |\varphi\rangle$. In a neutral atom with n_c core electrons and $n_v = Z\text{-}n_c$ valence electrons we have to select a suitable core. There are a number of ways in achieving *core-valence* separation from an all-electron Hartree-Fock calculation:

– If we define the core and valence densities respectively,

$$\rho_c(\vec{r}) = \sum_{i \in \text{core}} n_i\,|\varphi_i(\vec{r})|^2 \qquad \rho_v(\vec{r}) = \sum_{i \in \text{valence}} n_i\,|\varphi_i(\vec{r})|^2 \tag{3}$$

where n_i are the occupation numbers, we search for a closed-shell core with n_c core electrons where the overlap between both densities is relatively small (see Figure 2). This can be achieved in various ways by comparing the outermost core orbital with the innermost valence orbital (separation of orbital energies, overlap region, r-expectation values, etc.)

- The static dipole polarizability of the core, that is the ion with n_c core electrons, should be small, i.e. $\alpha_D < 1$ a.u. This defines a hard core where polarisation by all other electrons and nuclei is relatively small. The core usually consists of filled p-, d- and f- outermost orbitals. Relativistic effects (indirect and spin-orbit effects) may increase the core polarizability and the choice of the core from a nonrelativistic calculation may not be suitable for the heavier elements.
- The core density $\rho_c(\vec{r})$ should not change significantly by either removing or adding valence electrons important in chemical bonding or in electronic excitations out of the valence space, thus assuring that the *frozen-core approximation* works. For example, for CuH we might get away with a one-valence electron description for copper (α_D = 0.9 a.u. for Cu^+).[44] For CuF_4^- this would not be a good approximation since we have copper in the oxidation state +3 and we expect substantial mixing between the "core" 3d- and the valence 4s-orbitals.
- Valence electrons of other atoms should not penetrate into the core, that is the smallest interatomic distance in a molecule should not should not be smaller than the sum of the core radius plus the atomic radius of a partner atom. This also avoids larger errors coming from overlap between two cores.

Figure 3 shows the dipole polarizabilities of the positively charged Group 1 metals. We see that Li and perhaps Na can be reasonably well described by a one-valence electron pseudopotential, but this approximation becomes critical for the heavier atoms. Let us consider a different atom, indium, which is a three-valence electron system and chemists would not expect that the 4d-electrons play a significant role in chemical bonding. Already the large dipole polarizability of In^{3+} with α_D = 3.2 a.u. tells us that considering only the outermost (5s5p) valence electrons may lead to significant errors in the calculation in molecular properties.[45]

Another drawback is that in a molecule the cores belonging to neighbouring atoms slightly overlap. Since these are closed-shell interactions we obtain a splitting into fully occupied bonding and antibonding orbitals. The outermost antibonding orbitals will be more diffuse compared to the atom and the core polarizability increases. That is both core polarisation and core-valence correlation effects are more important in the molecule than in

the atom, and even if core-polarization effects are taken into account the transferability requirement is not fulfilled. It is now evident that defining the core is the first crucial step in the construction of an accurate pseudopotential and a small core definition has to be preferred over a large one.

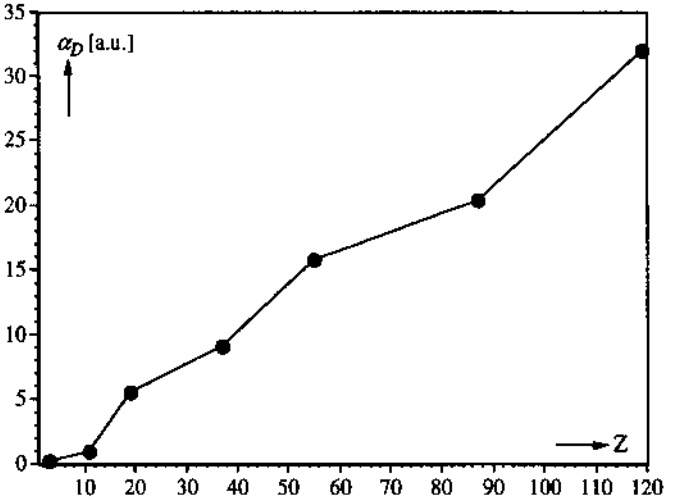

Figure 3. Static core dipole polarisabilities of positively charged alkali atoms from Li^+ to element 119^+ (data taken from ref.46).

2.2 Introducing the pseudopotential approximation at the Hartree-Fock level

We assume that the core with n_c core electrons has been determined. For simplicity we only consider a one-valence electron system and a closed-shell core with $n_c/2$ core orbitals. For a many-valence electron treatment see ref.43.

For a valence electron the atomic Hartree-Fock equation (2) is

$$F\,\varphi_v = \varepsilon_v\,\varphi_v \qquad \text{with} \qquad \langle \varphi_v | \varphi_c \rangle = 0 \tag{4}$$

If we choose a new valence orbital by mixing in core orbitals (the Phillips-Kleinman ansatz)

$$\chi_v = \varphi_v + \sum_c a_{cv}\varphi_c \qquad \text{with} \qquad a_{cv} = \langle \varphi_c | \chi_v \rangle \tag{5}$$

we obtain $$\langle \chi_v | F | \chi_v \rangle = \varepsilon_v + \sum_c a_{cv}^2 \varepsilon_c \tag{6}$$

Since we have complete freedom of choice for the linear combination (5) we can for example select new valence orbital such that the radial part of χ_v becomes nodeless (smooth) in the region (0,∞) which is called the pseudo-orbital transformation. Our aim is to construct a new Fock operator for the valence orbital χ_v such that

$$F' \chi_v = \varepsilon_v \chi_v \tag{7}$$

with ε_v being identical to that in (4). The Hartree-Fock equation for χ_v becomes

$$F \chi_v = \varepsilon_v \varphi_v + \sum_c a_{cv} \varepsilon_c \varphi_c = \varepsilon_v \chi_v + \varepsilon_v (\varphi_v - \chi_v) + \sum_c a_{cv} \varepsilon_c \varphi_c$$

$$= \varepsilon_v \chi_v + \sum_c a_{cv} (\varepsilon_c - \varepsilon_v) \varphi_c = \varepsilon_v \chi_v + \sum_c \langle \chi_v | \varphi_c \rangle (\varepsilon_c - \varepsilon_v) \varphi_c \tag{8}$$

The last term in (8) can be brought to the left hand side and after inserting (5) for the coefficients a_{cv} we obtain

$$[F + P_{core}] \chi_v = F_{PK} \chi_v = \varepsilon_v \chi_v \tag{9}$$

with P_{core} being a specific core projection operator,

$$P_{core} = \sum_c (\varepsilon_v - \varepsilon_c) |\varphi_c\rangle\langle\varphi_c| \tag{10}$$

conveniently written in the Dirac notation which assures that the valence electrons cannot collapse into the core. We can now split the original Fock operator F into

$$F = F_{valence} + F_{core} \tag{11}$$

where $F_{valence}$ is the valence-only Fock operator and all other terms containing core contributions are in F_{core}. We are now able to define the pseudopotential operator for a valence electron at position $\boldsymbol{r}$,

$$V_{PP}(r) = F_{core} + P_{core} = -\frac{n_c}{r} + \sum_c (2J_c - K_c) + P_{core} \tag{12}$$

We obtain some important expectation values for the pseudo-Fock operator $F_{valence} + V_{PP}$,

$$\langle \chi_v | F_{valence} + V_{PP} | \chi_v \rangle / \langle \chi_v | \chi_v \rangle = \langle \varphi_v | F_{valence} + V_{PP} | \varphi_v \rangle \tag{13}$$
$$= \langle \varphi_c | F_{valence} + V_{PP} | \varphi_c \rangle = \varepsilon_v$$

All core energies are shifted up to the valence energy ε_v due to the shift-operator P_{core}. If we use the Fock-operator $F_{valence} + V_{PP}$ instead of F, nothing would be gained. We therefore try to find suitable approximations to V_{PP}.

As mentioned before, the procedure shown here can be easily generalized to a many-electron system (open or closed shell). Equation (12) or its more generalized Phillips-Kleinman form can be seen as the starting point for all pseudopotential approximations using nodeless pseudo-orbitals (effective core potentials, abbreviated as ECP).

2.3 The model core potential approximation

The model core potential schemes (abbreviated as MCP or simply MP) usually start from a slightly different idea than outlined above, i.e. by adding a core level-shift operator to the usual Hamiltonian (the Huzinaga-Cantu equation).[47] This gives valence orbitals which retain their inner nodal structure. We can nevertheless use the pseudopotential operator (12) as a starting point and generalize it in the following way:[48-51]

$$V_{PP}(\vec{r}) = \sum_i A_i r^{n_i} \exp\left(-\alpha_i r^2\right) + \sum_c B_c |\varphi_c\rangle\langle\varphi_c| \tag{14}$$

that is the Coulomb- and exchange and the n_c / r terms are approximated by a local potential which conveniently consists of a linear combination of Gaussian functions. Usually n_i = -1 and 0 is chosen.[52] The core orbitals φ_c are chosen beforehand and the parameters A_i and n_i are obtained from least squares fits to numerical Hartree-Fock core potentials. B_c is chosen such that

$$B_c = -b_c \varepsilon_c \tag{15}$$

with $1 \leq b_c \leq 2$. Note that $B_c > (\varepsilon_v - \varepsilon_c)$ which shifts the core orbitals to relatively high orbital energies such that in a subsequent correlation procedure these core orbitals are only occupied to 10^{-5} or less. This assures that the Pauli principle is approximately fulfilled and correlation contributions are not overestimated substantially. Larger b_c values can lead to numerical problems in the fit procedure.

It is clear that replacing the nonlocal core exchange K_c by a local potential is not such a good approximation and the model potential can be further

improved by replacing K_c by its spectral representation in a finite (non-orthogonal) basis,[53]

$$K_c' = PK_cP \tag{16}$$

with $$P = \sum_{i,j} |\varphi_i\rangle (S^{-1})_{ij} \langle\varphi_j| \tag{17}$$

This extension of the MP method developed by Seijo and co-workers is called the *ab-initio* model potential method (AIMP). In a similar way the total core Coulomb and exchange operator can be used in its spectral representation.[54] Two- and three center integrals are usually approximated in such schemes. Parameters and basis sets for the AIMP approximation can be downloaded from web[55] (see ref.56 for details) and are implemented in program packages like MOLCAS, MOLECULE or COLUMBUS.

2.4 The pseudopotential approximation

The most crude approximation is to replace the complete operator (12) for a specific atom by a local or non-local potential which is bounded from below, for example by a linear combination of Gaussian functions such that integrals over Gaussian type functions (GTO) can easily be evaluated. This removes the core states and produces nodeless pseudo-orbitals which contain admixtures of both the core- and virtual orbitals. The local PPA was the preferred way up to the late seventies[57] in the last century and most widely applied in solid state physics. However, a local approximation is less accurate in describing states of different angular symmetry, and for example cannot alter the sequence in the angular momentum symmetries in a one-valence electron system, i.e. we always obtain $\varepsilon_s \le \varepsilon_p \le \varepsilon_d \le \ldots$ for the lowest eigenstates of each symmetry. For example, in Ca^+ 4s→3d (13650 cm^{-1}) is *below* the 4s→4p (25192 cm^{-1}) transition and a local potential cannot correctly describe such a change in symmetry. One therefore chooses *l*-dependent semi-local pseudopotentials of the form[58-61]

$$\begin{aligned} V_{PP} &\cong V_{PP}^{local}(r) + \sum_{l=0}^{L_{max}} V_{PP}^{l}(r) \sum_{m=-l}^{l} |lm\rangle\langle lm| \\ &= \sum_{n=1}^{N_L} A_n r^{k_n} e^{-\alpha_n r^2} + \sum_{l=0}^{L_{max}} \sum_{n=1}^{N_{SL}} B_{ln} r^{k_{ln}} e^{-\beta_{ln} r^2} \sum_{m=-l}^{l} |lm\rangle\langle lm| \end{aligned} \tag{18}$$

where the sum over the m term is an l-dependent operator projecting onto the Hilbert subspace of angular momentum l, and k is an integer with $k \geq -2$. It is a matter of choice if the local part in (18) is included in the pseudopotential or not. For better accuracy it is necessary to extend the sum in (18) to $L_{max} > max\{l_{core}\}$ and if L_{max} is chosen large enough, the local part in (18) can be neglected. Another common definition used is to treat only all greater L_{max} terms in local form,

$$V_{PP} \cong V_{PP}^{local}(r) + \sum_{l=0}^{L_{max}} \left[V_{PP}^{l}(r) - V_{PP}^{local}(r) \right] \sum_{m=-l}^{l} |lm\rangle\langle lm| \tag{19}$$

The following fit procedures are currently in use which distinguishes the different types of pseudopotentials in use:

a) *Energy consistent pseudopotentials* (EC-PP or EC-ECP). Here the pseudopotential parameters A_n, α_n, B_{ln} *and* β_{ln} in (18) are adjusted to an atomic valence spectrum by a least-squares fit,

$$\sum_i w_i (\Delta E_i^{AE} - \Delta E_i^{PP})^2 = \min. \tag{20}$$

w_i are weight-factors. The reference data ΔE_i^{AE} (ionization potentials, electron affinities and excitation energies of neutral and various charged ions) are obtained beforehand from numerical Hartree-Fock calculations. This technique has been developed and perfected over more than two decades by the Stuttgart group.[62,63] Only up to two or three Gaussians (N_{SL} = 2, 3) per angular symmetry l are required for such a fitting technique.

b) *Shape consistent pseudopotentials* (SC-PP or SC-ECP). Here the parameters A_n, α_n, B_{ln} *and* β_{ln} in (18) or (19) are adjusted such that valence orbitals of specific symmetry are reproduced to high accuracy above a certain cut-off radius R_c. This can be achieved in various ways. Hay and Wadt[64-66] as well as Christiansen and Ermler[67] start by modifying all-electron orbitals such that they are nodeless in the core region below $R < R_c$. Next they use the pseudopotential HF equation applying eq.(19) and adjust the parameters to reproduce these nodeless pseudo-orbitals. This technique has the disadvantage that it requires inversion of the Fock equation to produce l-dependent pseudopotentials which requires a larger number of Gaussian functions in the fit procedure. This can be avoided in a more elegant fit technique developed by the Toulouse group[68,69] and later used by Stevens, Krauss and Basch.[70] Here the 2-norm $\|O\|_2$ of the following operator is minimized,

$$O = \tilde{\varepsilon}_v \left|\tilde{\varphi}_v\right\rangle\left\langle\tilde{\varphi}_v\right| - \varepsilon_v \left|\varphi_v\right\rangle\left\langle\varphi_v\right| \tag{21}$$

The *norm-conserving pseudopotential* (NC-PP or NC-ECP) developed by Bachelet, Schlüter and co-workers[71-75] is a slight modification of the SC-ECP method.

The PPA (18) has been extended further by Titov by dividing the valence space into an outer core part and a valence part. This relatively new procedure is called the generalized pseudopotential approximation (GPPA)[76-78] and is derived from the norm-conserving fitting technique. The analytical form used is,

$$\begin{aligned} V_{GPP} \cong\ & V_{val}^{local}(r) + \sum_{l=0}^{L_{max}+1} \left[V_{val}^{l}(r) - V_{val}^{local}(r)\right] \sum_{m=-l}^{l} \left|lm\right\rangle\left\langle lm\right| \\ & + \sum_{l=0}^{L_{max}} \left[V_{oc}^{l}(r) - V_{val}^{local}(r)\right] \sum_{m=-l}^{l} \left|oc,lm\right\rangle\left\langle oc,lm\right| \\ & + \sum_{l=0}^{L_{max}} \sum_{m=-l}^{l} \left|oc,lm\right\rangle\left\langle oc,lm\right| \left[V_{oc}^{l}(r) - V_{val}^{local}(r)\right] \\ & - \left\langle \varphi_{oc,l}^{*} \left| V_{oc}^{l}(r) - V_{val}^{local}(r) \right| \varphi_{oc,l} \right\rangle \sum_{m=-l}^{l} \left|oc,lm\right\rangle\left\langle oc,lm\right| \end{aligned} \tag{22}$$

The symbol *oc* stands for outer core. Here the sum over the *m* term for the outer core part is an *l*-dependent operator projecting onto the Hilbert subspace of the outer core pseudo-orbitals with angular momentum *l*.

The pseudopotential method using nodeless orbitals is more widely used compared to the AIMP method (although there is no justification for this).[79] The one-electron integrals in both procedures are relatively easy to evaluate (although the non-local part in (18) is more complicated and therefore more CPU intensive, leading to well-known integrals such as the error function, the Dawson integral and the mixed Dawson-error function).[68,80-84] Pseudopotentials are available in almost all standard program packages for molecules like GAUSSIAN, MOLCAS, COLUMBUS, TURBOMOLE, GAMESS, MOLPRO, and in solid state packages like CRYSTAL. Some of these computer codes include analytical first and second derivatives.[85,86]

2.5 Relativistic Pseudopotentials

The notion that only core orbitals are inherently relativistic and relativistic effects indirectly influence valence-orbitals,[87] e.g. by the orthogonality condition (4), has led to the belief that core orbitals are required to correctly describe the complex interplay between direct and indirect relativistic effects in an atom. However, the parametrization to relativistic data (relativistic spectra in the EC-PP scheme or relativistic orbitals in the SC-PP scheme, relativistic parametrization in the MP or AIMP schemes) seems to successfully transfer both direct and indirect relativistic effects into the valence region, i.e. relativistic operators are replaced by pseudo-operators. For example, Seijo and co-workers derive their relativistic AIMP parameters from atomic relativistic Cowan-Griffin calculations.[88-90]

Since the orbitals in MP and AIMP methods retain their inner nodal structure, relativistic perturbation operators (such as Douglas-Kroll or ZORA Hamiltonians) can in principle be implemented in a straight-forward manner into such schemes.[91-93] Thus, the direct relativistic effects are considered explicitly by such relativistic perturbation operators, and indirect relativistic effects are considered in the core potentials. For convenience, we call such a procedure direct relativistic, i.e. DR-AIMP. This scheme has the advantage that all-electron relativistic operators and the AIMPs can be used most conveniently together in one program package. For example, if electronic transitions in heavy transition metal complexes are considered (for example metal-to-ligand charge transfer) the central atom can be treated in an all-electron fashion while the ligands can be treated in a more approximate way using AIMPs. Otherwise, there seems to be no particular advantage of such a scheme and is has to be proven that the accuracy of DR-AIMP methods is far superior compared to a conventional relativistic AIMP scheme.

For pseudopotential schemes using nodeless orbitals relativistic effects have to be taken into the parametrization procedure since relativistic perturbation operators act in the vicinity of the nucleus where pseudo-orbitals have the wrong nodal behaviour. Reference energies or orbitals are taken from scalar relativistic, spin-orbit coupled or even fully relativistic all-electron calculations. It is most convenient to introduce the PPA at the scalar (spin-orbit averaged) relativistic level (common notations are SRPP, ARPP or AREP), or at the two-component level (common notations are SOPP or REP), derived from the 4-component Dirac equation by elimination of the small component. Equations (18) and (19) are used for the SRPPs.

Spin-orbit operators derived from elimination of the small component, for example the Breit-Pauli Hamiltonian, contain operators which weight the inner part of the valence orbital and should not be used in pseudopotential

schemes using nodeless orbitals.[94] Instead, spin-orbit coupled pseudopotentials are of the following analytical form,[95-97]

$$V_{PP} \cong V_{PP}^{local}(r) + \sum_{l=0}^{L_{max}} \sum_{j=|l-1/2|}^{l+1/2} V_{PP}^{l,j}(r) \sum_{m=-j}^{j} |ljm\rangle\langle ljm| \tag{23}$$

$$= \sum_{n=1}^{N_L} A_n r^{k_n} e^{-\alpha_n r^2} + \sum_{l=0}^{L_{max}} \sum_{j=|l-1/2|}^{l+1/2} \sum_{n=1}^{N_{SL}} B_{ljn} r^{k_{ljn}} e^{-\beta_{ljn} r^2} \sum_{m=-j}^{j} |ljm\rangle\langle ljm|$$

If we define $\Delta V_{PP}^{l}(r) = V_{PP}^{l,l+1/2}(r) - V_{PP}^{l,l-1/2}(r)$ (24)

we can rewrite (23) in the following form,[95,98]

$$V_{PP} \cong V_{PP}^{local}(r) + \sum_{l=0}^{L_{max}} (2l+1)^{-1} \left[l \cdot V_{PP}^{l,l-1/2}(r) + (l+1) \cdot V_{PP}^{l,l+1/2} \right] \sum_{m=-l}^{l} |lm\rangle\langle lm|$$

$$+ \vec{s} \cdot \sum_{l=0}^{L_{max}} (l+\tfrac{1}{2})^{-1} \Delta V_{PP}^{l}(r) \sum_{m=-l}^{l} \sum_{m'=-l}^{l} |lm\rangle\langle lm|\vec{l}\,|lm'\rangle\langle lm'| \tag{25}$$

This form is also convenient since the first two terms can be used to produce SRPPs from SOPPs. Again, the parameters in V_{PP} can be fitted to spin-orbit coupled data, e.g. derived from a fully relativistic Dirac-Hartree-Fock treatment. 2-particle spin-orbit terms arising from the Breit interaction can be included in such a fit procedure and are approximated by effective 1-particle operators. The spin-orbit core potential one-electron integrals have been evaluated by Pitzer and Winter.[99]

SOPPs have been implemented by Lee et al. into the fully relativistic program package MOLFDIR utilizing Kramers' symmetry.[100] This treats spin-orbit coupling at the SCF level using double-group symmetry. The other common approach is to perform SRPP calculations (first two operators in (25)) at the SCF level which is computationally more efficient and to treat spin-orbit coupling (third operator in (25)) in the subsequent configuration interaction (CI) treatment.[101] This can be done either directly, that is treating spin-orbit coupling and the CI in the same process, or adding spin-orbit coupling after the CI treatment, which is a relatively good approximation for spin-orbit coupling in lighter elements. These procedures are available in program packages like COLUMBUS or CIPSO.

Finally we mention that pseudopotentials have been used within the fully relativistic (4-component) Dirac-Hartree-Fock scheme simply by replacing the potential in the Dirac equation

$$D = \sum_i \Lambda_i^+ h_D(i) \Lambda_i^+ + \sum_{i<j} \Lambda_i^+ \Lambda_j^+ g(i,j) \Lambda_i^+ \Lambda_j^+ \tag{26}$$

by the corresponding pseudopotential.[102-104] $g(i,j)$ stands for all electron-electron interactions (including Breit) and the Λ_i^+ are projection operators projecting onto the Hilbert subspace of positive energies. The one-particle Dirac operator is

$$h_D(i) = c\vec{\alpha}_i \vec{p}_i + c^2 \beta_i + V(i) \tag{27}$$

The potential $V(i)$ contains the pseudopotential in the usual fashion (see eq.(1)). Such pseudopotentials are called fully relativistic pseudopotentials (FRPP or FRECP).

There seems to be no advantage for introducing 4-component pseudopotentials except that part of the molecule can be treated in a more accurate fully relativistic all-electron way and other parts (e.g. outer ligands) can be treated via pseudopotentials.[105] Otherwise, 2-component SOPPs are sufficient for the accurate treatment of atoms or molecules and it is questionable if the accuracy can be improved substantially by going fully relativistic. First, the small Dirac component has most of its density near the nucleus where pseudo-orbitals are nodeless and the correct kinetic balance condition between the small and large components requires the core-orbitals used in the pseudo-orbital transformation (5). Second, there is no need for including negative energy states in a pseudopotential formalism if the core states are projected out. There is therefore no need to include pseudopotentials in a unitary transformation from 4- to 2-component (large component only) schemes.[106] Instead, pseudopotentials should be introduced either at the 2-component or scalar relativistic level only.

2.6 Valence basis sets

Pseudopotential parameters are usually accompanied by valence basis sets obtained from energy minimization techniques at the HF level of theory. In recent years correlation-consistent basis sets became available for a number of heavy elements in order to reduce significantly the basis set superposition error (BSSE).[107-109] Figure 4 demonstrates this nicely for the weakly interacting system Hg_2.[110] All-electron HF optimised basis sets show large BSSEs as seen by the AE/MVD results using a relatively large (21s17p11d9f)/[13s11p7d4f] set. The basis set by Dolg and Flad is a (9s9p8d4f2g) set and performs much better compared to the all-electron set.[111] This indicates that part of the BSSE comes from the core region. The HF optimised (9s9p6d2f)/[8s7p4d2f] small basis set (SB) shows larger

BSSEs compared to the one by Dolg and Flad. Later, Dolg and Flad reduced the BSSE even further by extending their basis set to (9s8p7d5f5g).[112] However, when the basis set parameters are optimised at the MP2 level and enlarged significantly to a (11s10p9d3f)/[10s8p7d2f] (cc-SB) the BSSE is reduced significantly. Using the cc-SB in its uncontracted form brings another large improvement. Finally, adding more higher momentum functions to a final (11s10p9d4f3g2h) basis set (cc-ULB) increases the BSSE slightly. This clearly demonstrates the usefulness of correlation consistent valence basis sets in relativistic pseudopotential calculations for weakly interacting systems.

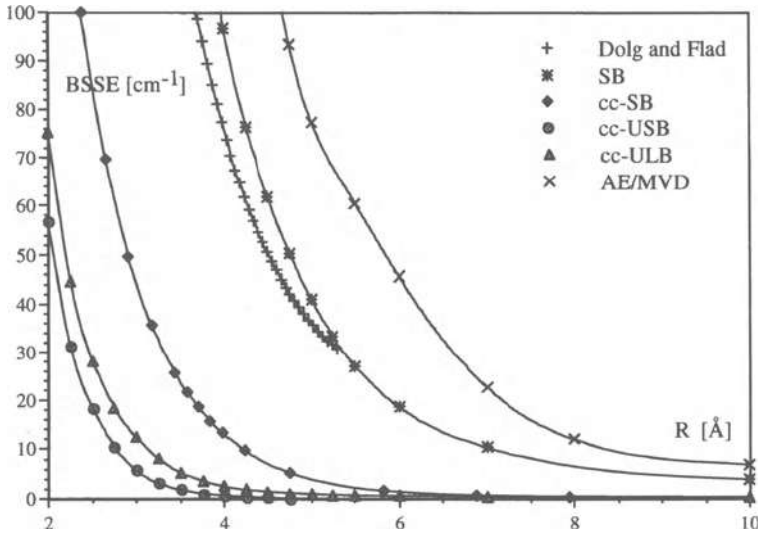

Figure 4. Calculated coupled cluster (CCSD(T)) basis set superposition corrections for the potential energy curve of Hg_2 at various interatomic distances R. AE/MVD: all-electron including the mass-velocity and Darwin term; SB: small valence basis set; LB: large valence basis set; U: uncontracted; cc: correlation consistent.

2.7 Beyond the frozen core approximation

When electrons from another atom penetrate the core of a pseudo-atom (atom described by a pseudopotential) additional repulsion effects between the core and the other nucleus (core) has to be considered since the nucleus in the pseudo-atom is less well screened by the core electrons and the point core charge approximation breaks down. In addition, core-polarization corrections become important as well, which includes static polarization of the core at the HF level and dynamic polarization due to core-valence correlation. There seems to be only a few articles concerned with such

corrections[113-117] and one can avoid the breakdown of the frozen-core approximation by replacing the large core by a smaller core definition. If this is computationally not feasible, one has to modify the core-valence and the core-core interactions in eq.(1),

$$H_V = -\frac{1}{2}\sum_i^{n_V}\nabla_i^2 + \sum_{i<j}^{n_V}\frac{1}{r_{ij}} + \sum_i^{n_V}\sum_a^{N_C}\left[V_{PP}^a(r_{ai}) - \frac{Q_a}{r_{ai}} + V_{CP}^a(r_{ai}, r_{ab})\right] + \sum_{a<b}^{N_C}\left[\frac{Q_a Q_b}{r_{ab}} + V_{CR}^{ab}(r_{ab})\right] \tag{28}$$

$V_{CR}^{ab}(r_{ab})$ is usually obtained from calculations using small-core pseudopotential calculations (for core-core repulsion effects) or directly from the electrostatic potential of the atomic core (for core-nucleus repulsion effects) and adjusted to some analytical function, i.e. a linear combination of exponentials. Figure 5 shows such corrections for Au-Au, Hg-Hg and Tl-Tl interactions with the atoms treated as $6s^n6p^m$ valence electron systems and the 5d-electrons placed into the core. As can be seen the core-repulsion corrections are quite large and cannot be neglected up to distances of 3 Å. Moreover, since relativistic effects narrows the 5d-6s gap (relativistic expansion of the 5d and contraction of the 6s orbitals), core-core and core-polarization effects (V_{CP}^a) are more pronounced at the relativistic level. A simple one-valence electron pseudopotential for Au not corrected for both effects leads to bond distances for AuH and Au_2 which are 0.34 Å and 0.83 Å (!) too short respectively.[118]

Core-polarization also become significant if the core is placed in a strong electric field, i.e. if the pseudo-atom is surrounded by charged ligands. That is AuF_4^- or AuF_6^- can surely not be accurately described by a gold atom with only one-valence electron. This is also in line with chemical intuition, that is the 5d-electrons in gold participate significantly in chemical bonding if gold is in the higher oxidation state +3 or +5 and the frozen 5d-core approximation will break down. Such effects can again be avoided if one chooses a smaller core definition. Alternatively, if core-polarization effects are not too large one can add a core-polarization potential as proposed originally by Meyer and co-workers,[119]

$$V_{CP}^a(r_{ai}, r_{ab}) = -\tfrac{1}{2}\alpha_D^a \vec{f}_a^{\,2} \tag{29}$$

with $$\vec{f}_a = -\frac{\vec{r}_{ai}}{r_{ai}^3}g(r_{ai}) + \sum_{b\neq a}^{N_C} Q_b \frac{\vec{r}_{ab}}{r_{ab}^3} \tag{30}$$

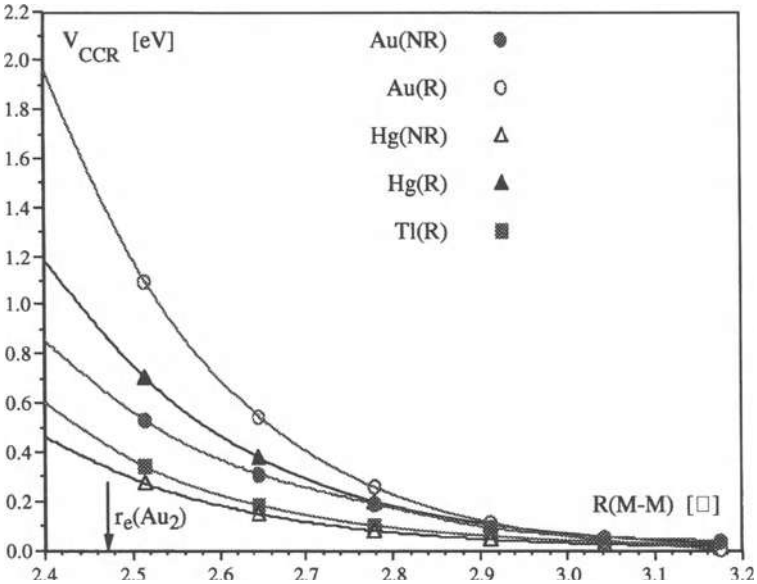

Figure 5. Core-core repulsion (CCR) corrections for Au-Au, Hg-Hg and Tl-Tl interactions using a [Pt]-core definition. NR: nonrelativistic; R: scalar relativistic.

α_D is the dipole polarizability of core a and $\vec{f}_a$ is the field at core a produced by all other surrounding charges (electrons and cores). The r^{-4} dependency of the $\vec{f}_a^2$ term requires the introduction of a cut-off function g to remove the (essential) singularity at the origin,

$$g(r_{ai}) = \left(1 - \exp\left(-\delta_a r_{ai}^2\right)\right)^n \tag{31}$$

Higher order pole corrections can be added as well.[120] The disadvantage is that expression (29) leads to quite complicated integrals[121] and to corrections to two-electron integrals, which makes this method rather ineffective. Nevertheless, for gold in the low oxidation state +1 core-polarization corrections can be quite large as shown in Table 1 for calculations on several 6th row hydrides. The results also show that core polarization effects become less important with increasing number of valence electrons. It is now evident that for Au, Hg and perhaps even for Tl the 5d-core should be part of the valence space. Moreover, the (5s5p) orbitals significantly overlap with the 5d-space and Au and Hg should be treated with the (5s5p5d) included in the valence space. We will discuss this in more detail in the next section.

Table 1. Core-polarization effects for bond distances and dissociation energies of closed shell diatomic hydrides AuH, HgH^+ and TlH calculated by using a [Pt]-core definition for the heavy elements including core-repulsion corrections (CR).

	AuH	HgH^+	TlH
R_e (in Å)			
SRPP+V_{CR}	1.76	1.69	1.88
SRPP+V_{CR}+V_{CP}	1.69	1.65	1.85
Δ_{CP}	0.07	0.04	0.03
D_e (in eV)			
SRPP+V_{CR}	0.70	0.99	1.81
SRPP+V_{CR}+V_{CP}	1.32	1.49	1.88
Δ_{CP}	-0.62	-0.49	-0.07

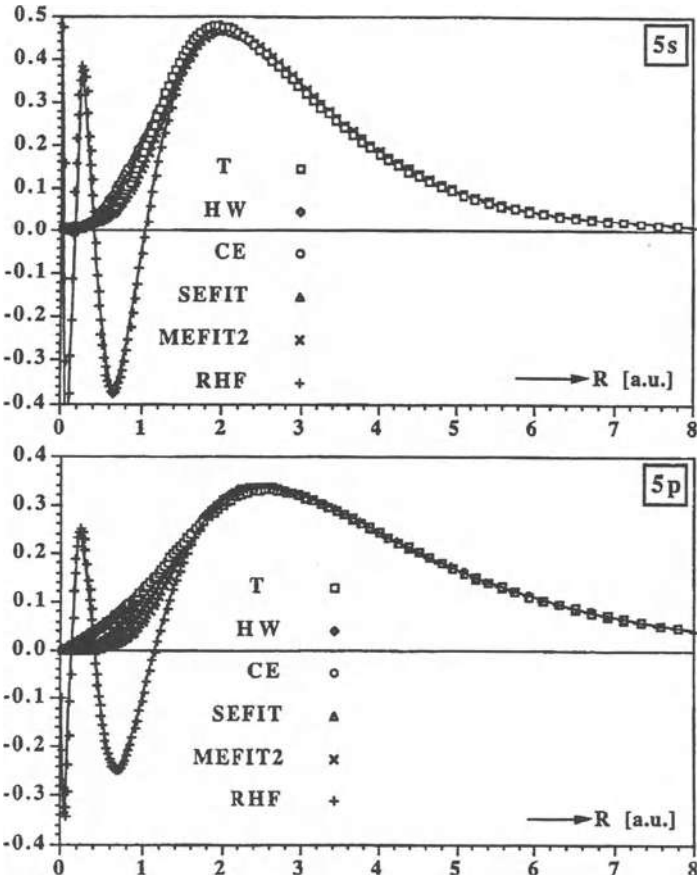

Figure 6. Pseudo-orbitals from various pseudopotentials (PP) in comparison with scalar relativistic all-electron (AE) results (see ref.45 for details). T: Toulouse PP (ref.122); HW: Hay-Wadt PP (refs.65, 66); CE: Christiansen-Ermler PP (ref.123); SEFIT: Single valence electron energy adjusted PP (ref.124); MEFIT2: multi-electron energy adjusted PP from ref.45).

3. The Accuracy of the Pseudopotential approximation

3.1 Test case indium atom

Figure 6 (previous page) shows different pseudoorbitals obtained for a number of 3-valence electron pseudopotentials of indium. Despite the different fit techniques used by different groups, the 5s and 5p pseudoorbitals are almost identical for all pseudopotentials and match closely the all-electron results above a certain core radius, i.e. $R > R_c$. Figure 7 shows the semilocal part of the s- and p-pseudopotentials. Here we see large deviations between the differently adjusted pseudopotentials. The question therefore arises, how these differences will be reflected in the valence energy spectrum of the indium atom. Table 2 shows a few selected states of the valence spectrum. The differences between the pseudopotentials are now obvious. The data also show the advantage of multi-electron energy adjusted pseudopotentials (in this case the MEFIT2 pseudopotential) favoured by the Stuttgart group. Such pseudopotentials are able to describe both the valence orbitals and the valence spectrum correctly. Nevertheless, a 3-valence electron pseudopotential is not sufficiently accurate as has been shown recently for InCl.[45] Core polarization lowers the In-Cl bond distance by 0.04 Å. Even more importantly, around the In-Cl equilibrium distance the Cl 3sp orbitals overlap with indium 4d core orbital leading to an incomplete Pauli repulsion and to bond distances which are too small if such core orbitals are not included.[125] Thus a small-core definition has to be preferred.

Table 2. Total electronic energies for different valence configurations of various pseudopotentials (PP) (see ref.45 for details). All values in atomic units. T: Toulouse PP (ref.122); HW: Hay-Wadt PP (refs.65, 66); CE: Christiansen-Ermler PP (ref.123); SEFIT: Single valence electron energy adjusted PP (ref.124); MEFIT1: multi-electron energy adjusted PP (ref.126); MEFIT2: multi-electron energy adjusted PP from ref.45).

	AE	SEFIT	MEFIT1	MEFIT2	HW	T	CE
$5s^2 5p^1$	-1.79176	-1.79588	-1.79126	-1.79111	-1.78611	-1.81250	-1.80793
$5s^1 5p^2$	-1.60867	-1.61548	-1.60699	-1.60935	-1.60781	-1.62790	-1.62397
$5s^2$	-1.60339	-1.60733	-1.60379	-1.60265	-1.59952	-1.62515	-1.61961
$5s^1 5p^1$	-1.41583	-1.42295	-1.41486	-1.41687	-1.41696	-1.43518	-1.43107
$5p^3$	-1.35986	-1.36636	-1.35407	-1.35931	-1.36075	-1.37327	-1.37074
$5p^2$	-1.16098	-1.16780	-1.15540	-1.16085	-1.16359	-1.17344	-1.17133
$5s^1$	-0.97771	-0.98327	-0.97928	-0.97907	-0.97995	-0.99504	-0.99078
$5p^1$	-0.71963	-0.72489	-0.71578	-0.71987	-0.72288	-0.72872	-0.72710
$6s^1$	-0.43895	-0.44179	-0.43739	-0.43816	-0.44396	-0.44654	-0.44521
$5d^1$	-0.43249	-0.43342	-0.43194	-0.43249	-0.43386	-0.42899	-0.43205

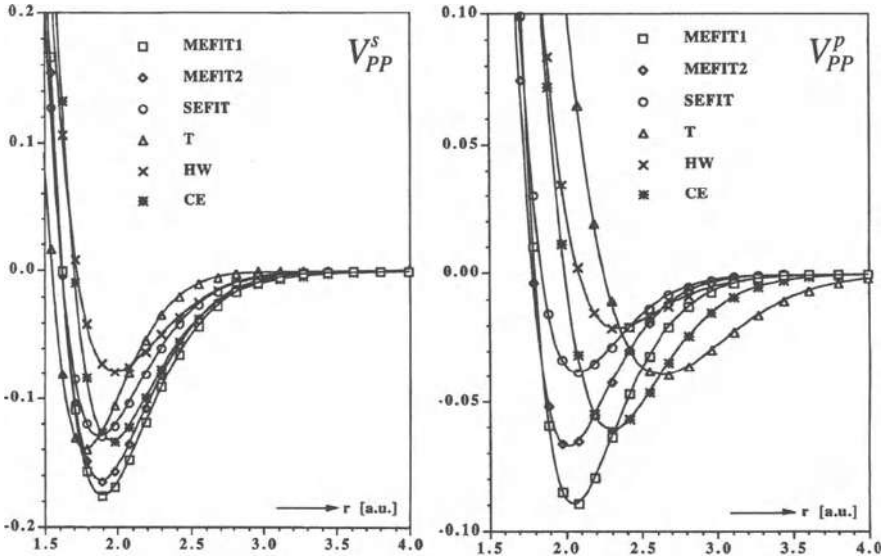

Figure 7. The s- and p- part of various pseudopotentials (PP) (see ref.45 for details). T: Toulouse PP (ref.122); HW: Hay-Wadt PP (refs.65 and 66); CE: Christiansen-Ermler PP (ref.123); SEFIT: Single valence electron energy adjusted PP (ref.124); MEFIT1: multi-electron energy adjusted PP (ref.127); MEFIT2: improved MEFIT1 from ref.125).

3.2 Test case mercury atom

While pseudopotentials can be systematically improved in their accuracy by taking more parameters into the fitting procedure and by using smaller cores, the question remains how well relativistic effects can be reproduced by such an approximation. Table 3 shows recent relativistic coupled cluster calculations by Kaldor and co-workers[128] for the mercury atom which give a good estimate how accurate current all-electron theory is.

The results in Table 3 demonstrate that accuracy of a few 100 cm^{-1} can be achieved by all-electron relativistic coupled cluster techniques for such multielectron systems. Remaining errors are due to the neglect of Breit interactions (which can be up to 250 cm^{-1} for the transitions shown below), other QED effects (of the order of a few 10 cm^{-1}), the finite extension of the nucleus (usually less than 100 cm^{-1}) and basis set and correlation incompleteness. However, the results shown below also demonstrate that correlation out of deeper core regions could become important and for Hg at least a (5spd6s) valence space for the pseudopotential definition has to be preferred.

Table 3. Relativistic Fock-space coupled cluster calculations (RCC) for the mercury atom using the Dirac Hamiltonian without Breit interaction and a point charge nucleus. All data are in cm^{-1}. The numbers behind RCC indicate the number of valence electrons considered in the RCC procedure. For details see refs. 128 and 131. Experimental data from ref.129.

	Exp.	RCC34	RCC20	RCC18	RCC12
$6s^2(^1S_0) \rightarrow$					
$6s^16p^1(^3P_0)$	37645	37471	37260	37545	37208
$6s^16p^1(^3P_1)$	39412	39318	39091	39369	38992
$6s^16p^1(^3P_2)$	44043	44209	43925	44177	43675
$6s^16p^1(^3P_0)$	54069	55419	55095	55328	54769
$6s^16p^1(^1P_1)$	84184	84550	84215	84466	83885
$6s^1(^2S_{1/2}) \rightarrow$					
$6p^1(^2P_{1/2})$	51485	52025	51734	52051	51515
$6p^1(^2P_{3/2})$	60608	61269	60883	61163	60476
$5d^{10}(^1S_0)$	151280	151219	150720	151055	150132

How do pseudopotentials compare with these results? As mentioned before, multi-electron adjustments of small-core pseudopotentials are usually accurate to 10-100 cm^{-1} and in the range of QED effects which can anyway be neglected in molecular calculations even for the most heavy elements.[130] Very recently Titov et al[131] demonstrated that he can reproduce the valence spectrum of the Hg atom at the generalized pseudopotential level extremely well. Table 4 shows a comparison of the GPP[131] with the Stuttgart SOPP adjusted by Dolg[132-134] for the 6p spin-orbit splitting of Hg and Hg^+ excited states. Even so, both results (GPP and EC-PP) are not directly comparable (the GPP results are correlated), the EC-PPA scheme performs well when a larger number of reference states are chosen in the adjustment procedure (as this is the case for Dolg's EC-PP2), and there seems to be no need to divide the valence space into an outer-core and valence space to gain even more accuracy. Moreover, a comparison with the all-electron results show that both PPAs give excellent results for spin-orbit coupled states in atoms.

Figure 8 shows calculated dipole polarizabilities for all Group 12 atoms. It is well recognized that polarizabilities as a second-order response property are more difficult to obtain accurately by *ab-initio* methods. The results clearly demonstrate that relativistic effects become very important for such properties, that pseudopotentials are capable to describe relativistic effects (compare to the all-electron results), and that relativistic pseudopotentials perform extremely well, i.e. we have almost perfect agreement between the EC-ARPP results and experiment.

Table 4. Relativistic Fock-space coupled cluster calculations (RCC) using the Dirac Hamiltonian including Breit interactions (refs. 128, 131). The Dirac-Hartree-Fock (DHF) calculations also include self-energy and vacuum polarization corrections. All data are in cm^{-1}. All PPAs are defined as 20 valence electron systems. GPP are RCC results whereas the EC-PP are relativistic Hartree-Fock results. EC-PP1 from ref.132. EC-PP2 is derived from EC-PP1 by increasing the reference space of energies in the adjustment procedure (ref.134).

	Exp.	RCC	GPP	DHF	EC-PP1	EC-PP2
$6s^16p^1(^3P_0) \rightarrow$						
$6s^16p^1(^3P_1)$	1767	1849	1845	1988	1973	1985
$6s^16p^1(^3P_2)$	6398	6737	6703	6083	6054	6079
$6s^16p^1(^1P_1)$	16424	18000	17924	22994	22980	22985
$6p^1(^2P_{1/2}) \rightarrow$						
$6p^1(^2P_{3/2})$	9123	9239	9169	7765	7751	7765

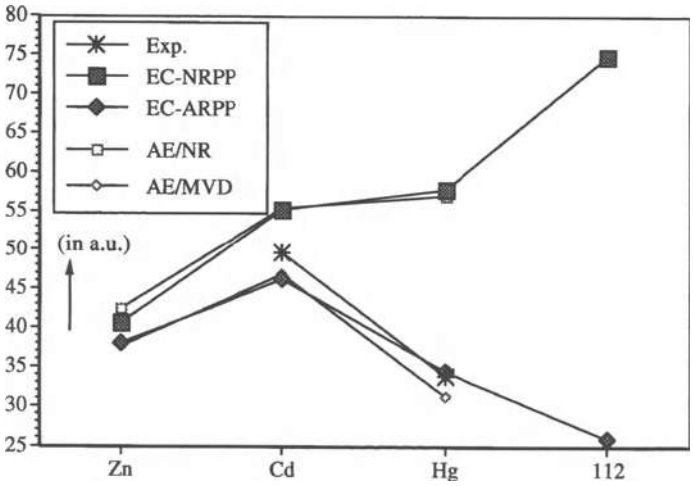

Figure 8. Comparison of energy-adjusted pseudopotential static dipole polarizabilities with all-electron results for the neutral Group 12 metals at the nonrelativistic and scalar relativistic level of theory. Experimental data from refs.135 and 136. All-electron calculations from Sadlej et al using the mass-velocity-Darwin (MVD) term (ref.137).

3.3 Test case Au_2 and AuH

The question if relativistic effects in molecular properties can correctly be reproduced within the PPA, that is if it can be transferred successfully into the valence region, is an important aspect of the relativistic PPA and will therefore be addressed for the gold atom, an atom well known for showing (unusually) large relativistic effects.[138] First we compare relativistic

effects for Au_2 bond distances, dissociation energies and force constants which are summarized in Figures 9 to 11.

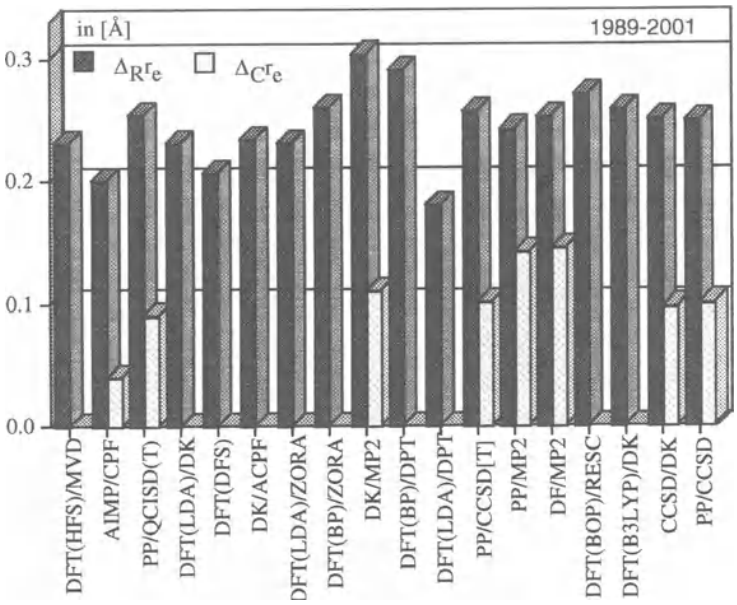

Figure 9. Relativistic bond contractions for Au_2 calculated since 1989 using a variety of different methods. Electron correlation effects at the relativistic level are shown on the right hand side of each bar if available. Relativistic and correlation effects are defined as $\Delta_R r_e = r_e(NR) - r_e(R)$ and $\Delta_C r_e = r_e(HF) - r_e(corr.)$ respectively. DFT denotes density functional theory, otherwise *ab-initio* methods have been applied. From the left to the right: Hartree-Fock-Slater results from Ziegler et al (ref.139); AIMP coupled pair functional results from Stömberg and Wahlgren (ref.140); EC-ARPP results from Schwerdtfeger (ref.141); LDA results from Häberlen and Rösch (ref.142); Dirac-Fock-Slater results from Bastug et al. (ref.143); Douglas-Kroll coupled pair functional results from Hess and Kaldor (ref.144); LDA and GGA ZORA results from van Lenthe et al. (ref.145); Douglas-Kroll MP2 results from Park and Almlöf (ref.146); GGA direct perturbation theory results from van Wüllen (ref.147); PP coupled cluster and MP2, and Dirac-Hartree-Fock results from Wesendrup et al. (ref.148); Relativistic elimination of the small component Becke-88+OP DFT, Douglas-Kroll GGA and coupled cluster, and PP coupled cluster results from Hirao et al (refs.149, 150).

Figure 9 shows that more than a decade ago predictions for relativistic bond contractions varied significantly (between 0.2 and 0.3 Å) but seem now to converge to around 0.25-0.26 Å. This is due to the fact that in the last fifteen years great progress has been made in the development of accurate relativistic methods within both *ab-initio* and density functional schemes. The PPA was often blamed for its poor performance compared to more accurate *ab-initio* methods.[151] In 1990, using a multi-electron adjusted EC-

ARPP for Au within a coupled cluster procedure (QCISD(T); third entry from the left in Figure 9) and a (8s,6p,5d,1f)/[7s,3p,4d,1f] contracted basis set and a full active orbital space in the correlation procedure, the relativistic bond contraction was predicted to be 0.25 Å at the correlated level.[141] At that time the calculation took 1 week on a Fujitsu VP100 supercomputer per point on the potential curve. Electron correlation effects at the relativistic level are important as well leading to a contraction of 0.09 Å. More than 10 years later more sophisticated all-electron and DFT schemes now support this prediction.

The situation is by far more difficult for dissociation energies since relativistic effects very much depend on the level of correlation and basis sets used in the procedure.[141] The latest pseudopotential CCSD(T) calculations using a (10s,8p,7d,4f)/[9s,7p,6d,4f] basis set predict a relativistic increase in the Au_2 dissociation energy of 78 kJ mol^{-1} in agreement with the 1990 calculations. Moreover, the PP MP2 predictions are very close to Dirac-Hartree-Fock MP2 results, Figure 10. Correlation effects increase the dissociation energy by 134 kJ mol^{-1}. In a recent paper by Hess and Kaldor it was shown that correlation from the "core" (5s5p)-orbitals increases the dissociation energy by ca. 5 kJ mol^{-1} which again demonstrates that the (5s5p) electrons should be taken into the valence space for the PPA.[144] g-, h and i-basis functions contributed only by 3 kJ mol^{-1} to the dissociation energy. Spin-orbit effects increase the dissociation energy further by 3 kJ mol^{-1}.[152] Thus it seems safe to predict $\Delta_R D_e \approx 80$ kJ mol^{-1}. We note that the relativistic elimination of the small component scheme (RESC) in its present form as developed by Hirao and co-workers[158] seems to substantially overestimate $\Delta_R D_e$ for Au_2, Figure 10.

Figure 11 shows a similar situation for force constants, that is $\Delta_R k_e$ very much depends on the level of approximation used. However, the PPA performs no worse than any of the other methods applied. Nevertheless, relativistic effects are very large for force constants (which is currently not so well understood),[153] and pseudopotentials seem to predict this quite accurately.

Table 5 shows a comparison of pseudopotential with all-electron Douglas-Kroll results for AuH at the coupled cluster level. The agreement between both methods is obvious. Here, an uncontracted (11s10p7d5f) valence basis set was applied and the basis set superposition error (BSSE) was calculated using the Boys-Bernardi scheme.[107] The BSSE leads to larger errors compared to the PPA itself. B3LYP results at different levels of theory are also shown in Table 5. From these results we conclude that the PPA is very much capable of delivering accurate spectroscopic properties at the relativistic level of theory, as this has also been concluded recently by Hirao et al.[150]

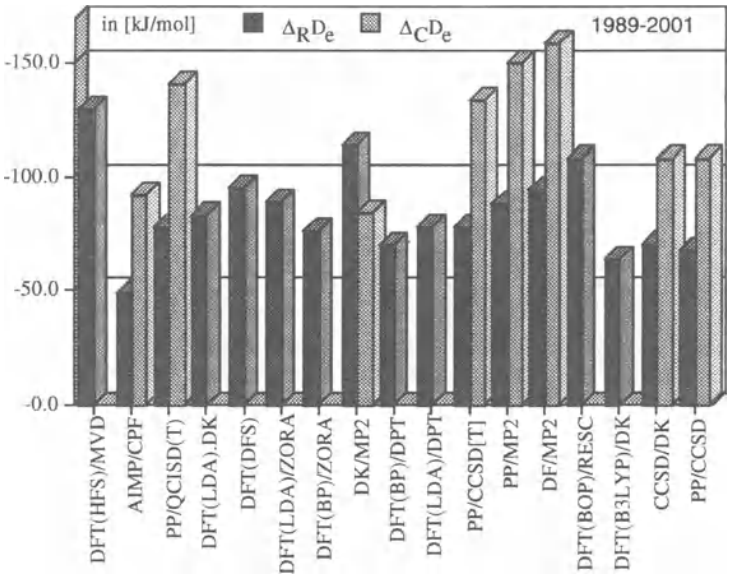

Figure 10. Relativistic increase in dissociation energy for Au_2 calculated since 1989 using a variety of different methods. Electron correlation effects at the relativistic level are shown on the right hand side of each bar if available. Relativistic and correlation effects are defined as $\Delta_R D_e = D_e(NR) - D_e(R)$ and $\Delta_C D_e = D_e(HF) - D_e(corr.)$ respectively. For details see Figure 9.

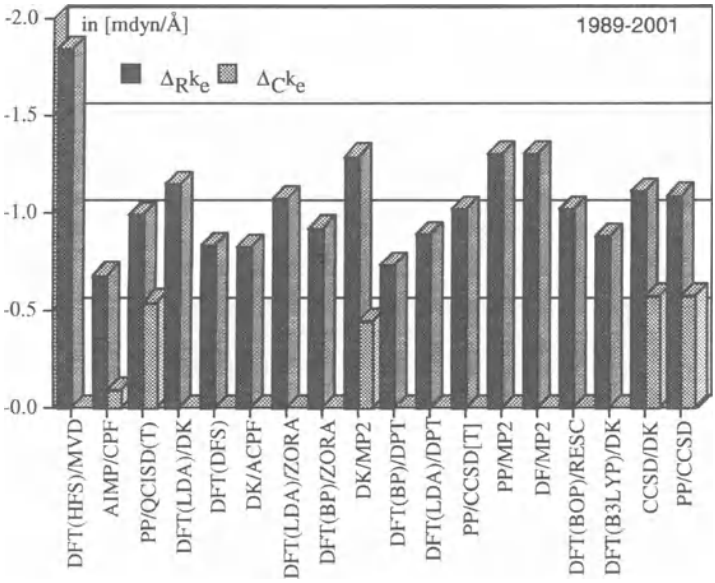

Figure 11. Relativistic increase in force constants for Au_2 calculated since 1989 using a variety of different methods. Electron correlation effects at the relativistic level are shown as well on the right hand side of each bar if available. Relativistic and correlation effects are defined as $\Delta_R r_e = k_e(NR) - k_e(R)$ and $\Delta_C k_e = k_e(HF) - k_e(corr.)$ respectively. For details see Figure 9.

Table 5. Spectroscopic constants for AuH at the CCSD(T) level. Bond distance r_e in Å, dissociation energy D_0 in eV (corrected for zero-point vibrational energy), vibrational frequency ω_e and anharmonicity constant $\omega_e x_e$ in cm^{-1}. +BSSE denotes that the basis set superposition error has been incorporated using the counterpoise method (ref.107). Experimental data are from Huber and Herzberg (ref.154). EC-ARPP results from ref.155. Douglas-Kroll (DK) results from ref.156; shape-consistent spin-orbit coupled PP (ref. 157) results from ref.152. Results from the relativistic elimination of the small component scheme (RESC, ref.158) at the B3LYP level, and normalized elimination of the small component scheme (NESC) by Filatov and Cremer (ref.159) are also shown.

	exp.	EC-ARPP		DK	SC-SOPP	RESC	NESC
			+BSSE		B3LYP	B3LYP	B3LYP
r_e	1.524	1.510	1.527	1.525	1.527	1.525	1.502
D_0	3.22	3.09	2.98	2.92	3.40	3.40	3.54
ω_e	2305	2328	2306	2288	2328	2288	2458
$\omega_e x_e$	43.1	44.9	45.6	42			

3.4 Test case TlH and (113)H

TlH was long seen as an excellent test case for spin-orbit coupled pseudopotentials, since spin-orbit coupling can be quite large in a number of properties, specifically the dissociation energies of thallium compounds. Table 6 shows calculated spectroscopic constants using a variety of different methods for TlH. The most accurate pseudopotential calculations including the AIMP method give bond distances still 0.04 Å above the experimental values, whereas the all-electron calculations (Douglas-Kroll and Dirac-Hartree-Fock) give slightly shorter bond distances (NB: they are not corrected for basis set superposition errors). Anyway, the results by Lee and co-workers demonstrate the importance of spin-orbit coupling in TlH. The relatively large deviations to the experimentally determined bond distance requires further investigations and a smaller core definition (21 valence electrons)[160] and larger basis sets should resolve this discrepancy.

We finally present comparisons between all-electron and pseudopotential results recently calculated for superheavy element 113 (eka-Tl). Experimental results are not available (and probably will not be in distant future). Element 113 shows a very large spin-orbit splitting of the 7p shell, i.e. the $^2P_{1/2}$-$^2P_{3/2}$ splitting is calculated to be 2.8 eV which is of the order of a chemical bond energy.[161] For such atoms scalar relativistic and spin-orbit effects become important in chemical bonding and they present an ideal testing ground for various relativistic approximations. This is indeed the case as the results in Table 7 show. Here spin-obit effects lead to much larger

bond contractions than scalar relativistic effects. The results also show excellent agreement of all-electron and pseudopotential results at the nonrelativistic level of theory. At the relativistic level the agreement is less than satisfactory which is due to a number of facts (basis sets, spin-orbit treatment, definition of scalar relativistic, etc.) which should be further investigated. We note that if spin-orbit effects are very large, different scalar relativistic operators will yield quite different results in atomic or molecular calculations and only a comparison at the spin-orbit coupled level is meaningful.

Table 6. Spectroscopic constants for TlH obtained by recent calculations. Experimental data are from Huber and Herzberg (ref.154). Bond distance r_e in Å, dissociation energy D_e in eV, and vibrational frequency ω_e in cm^{-1}. The number in front of VE indicates either a 3- or 13-valence electron pseudopotential. The last two rows are all-electron results obtained by using the Douglas-Kroll and the Dirac operator.

Method	ref.	r_e	D_e	ω_e
exp.	154	1.870	2.06	1391
3VE-EC-ARPP/QCISD(T)	162	1.912	2.56	1351
13VE-SC-ARPP/CCSD(T)	152	1.931	2.52	1351
13VE-SC-SOPP/CCSD(T)	152	1.910	2.02	1360
13VE-SO-AIMP/CI	163	1.929	2.37	1326
DK+SO/CI	164	1.86	2.13	1386
DHF/CCSD(T)	165	1.885	2.07	1390

Table 7. Spectroscopic constants for (113)H (from ref.165) at the CCSD(T) level of theory. Bond distance r_e in Å, dissociation energy D_e in eV, and force constant k_e in mdyn $Å^{-1}$. The shape-consistent pseudopotential calculations are from Lee and co-workers (ref.166). The parameters of the shape-consistent pseudopotentials originate from Nash (ref.167).

Method	r_e	D_e	k_e
DHF/CCSD(T)	1.789	1.44	1.09
EC-SOPP/CCSD(T)	1.782	1.62	1.37
SC-SOPP/CCSD(T)	1.762	1.37	1.15
DK/CCSD(T)	2.006	2.43	0.87
EC-ARPP/CCSD(T)	1.942	2.60	1.00
SC-ARPP/CCSD(T)	1.970	2.30	0.92
NR/CCSD(T)	2.077	2.52	1.07
NRPP/CCSD(T)	2.072	2.52	1.06

3.5 Do pseudopotentials overestimate electron correlation effects?

Pseudopotential calculations lead sometimes to bond energies very close to the experiment and the question arises if the PPA using nodeless orbitals overestimates electron correlation. Consider electron correlation for a two-electron, two orbital system with double substitution only. We have

$$\Delta E_{cor} = a + \Delta\varepsilon - \left((a+\Delta\varepsilon)^2 + K_{HL}^2\right)^{1/2} \tag{32}$$

with $\Delta\varepsilon = \varepsilon_L - \varepsilon_H$ and $a = 1/2(J_{HH}+J_{LL}) - 2J_{HL} + K_{HL}$. L denotes the LUMO orbital energy and H the corresponding HOMO. J and K are the corresponding Coulomb and exchange matrix elements. If we adjust the pseudopotential parameters such that $\Delta\varepsilon(AE) = \Delta\varepsilon(PP)$ and for the valence orbital $\varphi(AE) = \varphi'(PP)$ for a certain distance $R>R_C$, any difference between all-electron (AE) and pseudopotential calculations of ΔE_{corr} can be traced back to the deviation φ' from the all-electron orbital at distances $R<R_C$. This indeed suggests that nodeless pseudo-orbitals may lead to some errors in the electron correlation, but does not indicate at all that they overestimate such effects. Nevertheless, Figure 6 shows that the differently adjusted pseudopotentials differ substantially in the region $R<R_C$.

We further approximate,

$$\Delta E_{corr} = (a+\Delta\varepsilon)\left[1-\left(1+K_{HL}^2(a+\Delta\varepsilon)^{-2}\right)^{1/2}\right] \cong -\frac{1}{2}K_{HL}^2(a+\Delta\varepsilon)^{-1} \tag{33}$$

If $\Delta\varepsilon(AE) = \Delta\varepsilon(PP)$ and if $\Delta\varepsilon >> a$ (weakly correlated case) then the PPA overestimates electron correlation (within this model) if $K_{HL}^{PP} > K_{HL}^{AE}$. K_{HL} can easily be obtained from numerical Hartree-Fock calculations. In 1977 Teichteil et al.[168] as well as Pittel and Schwarz[169] found that the transformation to pseudoorbitals results in an overestimation of exchange integrals compared to all-electron results. However, the PPA has been improved considerably since, and Dolg recently reinvestigated valence correlation defects of the PPA.[170,171] Figure 12 shows the calculated overestimation of electron correlation effects for the second row elements using [He]-core pseudopotentials from the Stuttgart group together with rather large basis sets to match the all-electron set. The overestimation is at most 6% and much less than previously found. Dolg also found similar results for molecules. Except for fluorine the overall trend is that these deviations increase with increasing number of valence electrons. However,

we see that the curves for the differently charged atoms can cross and it is not immediately evident that ionisation potentials and electron affinities are overestimated as well, although error cancellation reduces these defects in such properties. The same holds for dissociation energies. It is clear that for the heavier elements a small-core definition will reduce this error significantly.

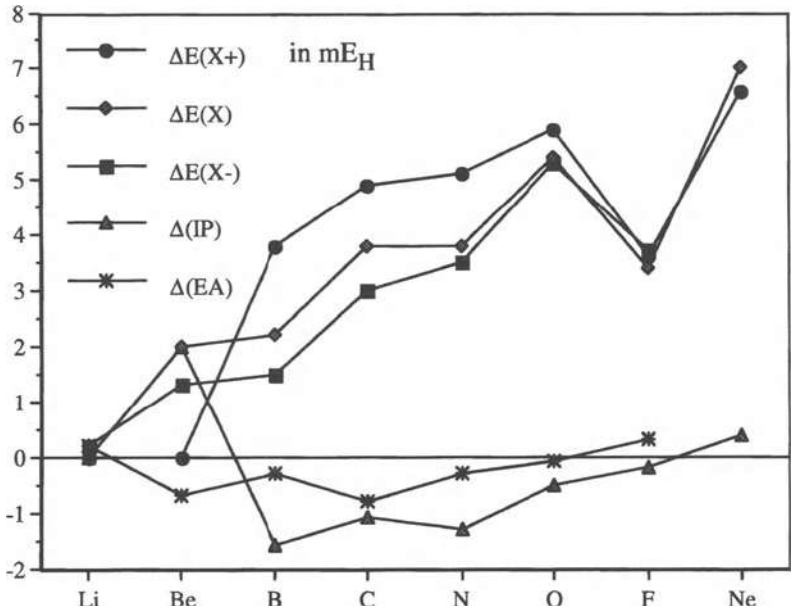

Figure 12. Deviation from all-electron valence energies for the second-row elements using a [He]-core pseudopotential (ref.170).

4. Summary

The PPA is now almost 70 years old and still one of the most successful and accurate methods in use for heavy element containing compounds. It has been implemented into both *ab-initio* and density functional schemes and now applied routinely in quantum chemical calculations. It is clearly the method of choice for larger molecules. If small-core pseudopotentials are used, carefully derived from a multi-electron adjustment procedure, then the PPA is cabable of producing results for valence properties very close to more accurate all-electron *ab-initio* methods. Core-properties like magnetic shielding tensors, electric field gradients, etc. which cannot (and should not) be obtained from pseudopotentials using nodeless orbitals, can be derived in a subsequent step (that is after the geometry optimization within the pseudopotential scheme) from a single-point all-electron calculation, or from

re-introducing the core orbitals with a subsequent orthogonalization procedure (the latter method has not been investigated in detail).[172] The relativistic extension of the PPA through parametrization to relativistic data is an excellent approximation. Previous claims, that the relativistic PPA is inaccurate are unsubstantiated.[173,174]

Acknowledgement

I am grateful to the Marsden fund Wellington (Royal Society of New Zealand) and to the Auckland University Research Committee for financial support. My special thanks are going to Profs. Michael Dolg (Bonn) and Hermann Stoll (Stuttgart) for not only critically reading this chapter but for fruitful collaborations over many years.

References

1 Scuseria, G. E., Ayala, P. Y. (1999). Linear scaling coupled cluster and perturbation theories in the atomic orbital basis. *J. Chem. Phys.* 111: 8330-8343.

2 Burant, J. C., Scuseria, G. E., and Frisch, M. J. (1996). A linear scaling method for Hartree-Fock exchange calculations of large molecules. *J. Chem. Phys.* 105: 8969-8972.

3 Stratmann, R. E., Scuseria, G. E., and Frisch, M. J. (1996). Achieving linear scaling in exchange-correlation density functional quadratures. *Chem. Phys. Lett.* 257: 213-223.

4 Schwarz, W. H. E., Andrae, D., Arnold, S. R., Heidberg J., Hellmann jr., H., Hinze, J., Karachalios, A., Kovner, M. A., Schmidt, P. C., and Zülicke, L. (1999). Hans. G. A. Hellmann (1903-1938). I. Ein Pionier der Quantenchemie. *Ber. Bunsenges* (2) 60-70.

5 Schwarz, W. H. E., Karachalios, A., Arnold, S. R., Zülicke, L., Schmidt, P. C., Kovner, M. A., Hinze, J., Hellmann jr., H., Heidberg J., and Andrae, D. (1999). Hans. G. A. Hellmann (1903-1938). II. Ein deutscher Pionier der Quantenchemie in Moskau. *Ber. Bunsenges* (2) 60-70.

6 Hellmann, H. (1934). A New Approximation Method in the Problem of Many Electrons. *J. Chem. Phys.* 3: 61.

7 Szasz, L. (1985). Pseudopotential Theory of Atoms and Molecules, Wiley, New York.

8 Pseudopotential calculations are less accurate than all-electron calculations, but they simulate the results of the latter often surprisingly well, for substantially smaller expenses. It is therefore not astonishing that in the chemistry of heavy atoms, relativistic pseudopotential theory is practically the method of choice. It is certainly the most successful of all approximate relativistic molecular theories (W. Kutzelnigg, 1987)

9 Pyykkö, P. (1988). Relativistic effects in structural chemistry. *Chem. Rev.* 88: 563-594.

10 Dyall, K. (1998). Relativistic and nonrelativistic finite nucleus optimized double zeta basis sets for the 4p, 5p and 6p elements. *Theor. Chem. Acc.* 99: 366-371.

11 Faegri, K. (1999). Relativistic Gaussian basis sets for the elements K – Uuo. *Theor. Chem. Acc.* 105: 252-258.

12 Tsuchiya, T., Abe, M., Nakajima, T., and Hirao, K. (2001). Accurate relativistic Gaussian basis sets for H through Lr determined by atomic self-consistent field calculations with the third-order Douglas-Kroll approximation. *J. Chem. Phys.* 115: 4463-4472.

13 Tatewaki, H., Mochizuki, Y., Koga, T., and Karwowski, J. (2001). Modification of nonrelativistic Gaussian basis sets for relativistic calculations. *J. Chem. Phys.* 115: 9160-9164.

14 Landau, A., Eliav, E., Ishikawa, E., and Kaldor, U. (2001). Benchmark calculations of electron affinities of the alkali atoms sodium to eka-francium (element 119). *J. Chem. Phys.* 115: 2389-2392.

15 Eliav, E., and Kaldor, U. (1999). High-Accuracy Calculations for Heavy and Super-Heavy Elements. *Adv. Quantum Chem.* 31: 313-336.

[16] Lim, I., Pernpointner, M., Seth, M., Laerdahl, J. K., Schwerdtfeger, P., Neogrady, P., Urban, M. (1999). Accurate Relativistic Coupled Cluster Static Dipole Polarizabilities of the Alkali Metals from Li to Element 119. *Phys. Rev. A* 60: 2822-2828.

[17] Kutzelnigg, W. (1990). Perturbation theory of relativistic corrections. II. Analysis and classification of known and other possible methods. *Z. Phys. D: At., Mol. Clusters* 15: 27-50.

[18] Hess, B. A. (1986). Relativistic electronic-structure calculations employing a two-component no-pair formalism with external field projection operators. *Phys. Rev. A* 33: 3742-3748.

[19] van Lenthe, E., Snijders, J. G., and Baerends, E. J. (1996). The zero-order regular approximation for relativistic effects: The effect of spin-orbit coupling in closed shell molecules. *J. Chem. Phys.* 105: 6505-6516.

[20] Chang, C., Pélissier, M., and Durand, Ph. (1986). Regular two-component Pauli-like effective Hamiltonians in Dirac theory. *Phys. Scr.* 34: 394-404.

[21] Heully, J.-L., Lindgren, I., Lindroth, E., Lundqvist, S., Mårtensson-Pendrill, A.-M. (1986). Diagonalisation of the Dirac Hamiltonian as a basis for a relativistic many-body procedure. *J. Phys. B* 19: 2799-2815.

[22] Knappe, P., and Rösch, N. (1990). A Relativistic Linear Combination of Gaussian-Type Orbitals Density Functional Method Based on a Two-Component Formalism with External Field Projectors. *J. Chem. Phys.* 92: 1153-1161.

[23] Car, R., and Parinello, M. (1985). Unified approach for molecular dynamics and density-functional theory. *Phys. Rev. Lett.* 55: 2471-2474.

[24] Pacchioni, G., Chung, S.-C., Krüger, S., and Rösch, N. (1994). On the Evolution of Cluster to Bulk Properties: a Linear Combination of Gaussian-Type Orbitals Local Density Functional Study of Free and Coordinated Nin Clusters (n = 6 - 147). *Chem. Phys.* 184: 12-137.

[25] Seminario, J. M., and Politzer, P. (1995). *Recent Developments and Applications of Modern Density Functional Theory.* Theoretical and Computational Chemistry, Vol.2 (Elsevier, Amsterdam).

[26] Engel, E., Höck, A., and Dreizler, R. M. (2000). van der Waals bonds in density-functional theory. *Phys. Rev. A* 61: 032502/1-5.

[27] Singh, P. P. (1994). Relativistic effects in mercury: Atoms, clusters, and bulk. *Phys. Rev. B* 49: 4954-4958.

[28] Moyano, G. E., Wesendrup, R., Söhnel, T., Schwerdtfeger, P. (2002). Properties of Small to Medium Sized Mercury Clusters From a Combined *Ab-Initio*, Density-Functional and Simulated Annealing Study. *To be published.*

[29] Goedecker, S., and Maschke, K. (1992). Transferability of pseudopotentials. *Phys. Rev. A* 45: 88-93.

[30] Barthelat, J.C., and Durand, Ph. (1978). Recent Progress of Pseudo-Potential Methods in Quantum Chemistry. *Gazz. Chim. Acta* 108: 225-236.

[31] Krauss, M., and Stevens, W. J. (1984). Effective potentials in molecular quantum chemistry. *Ann. Rev. Phys. Chem.* 35: 357-385.

[32] Christiansen, P. A., Ermler, W. C., and Pitzer, K. S. (1985). Relativistic effects in chemical systems. *Ann. Rev. Phys. Chem.* 36: 407-432.

[33] Ermler, W. C., Ross, R.B., and Christiansen, P. A., (1988). Spin-orbit coupling and other relativistic effects in atoms and molecules. *Adv. Quantum Chem.* 19: 139-182.

[34] Pickett, W. E. (1989). Pseudopotential Methods in Condensed Matter Applications. *Comput. Phys. Rep. 9:* 115-198.

[35] Huzinaga, S. (1995). 1994 Polanyi Award lecture: Concept of active electrons in chemistry. *Can. J. Chem.* 73: 619-628.

[36] Frenking, G., Antes, I., Böhme, M., Dapprich, S., Ehlers, A. W., Jonas, V., Neuhaus, A., Otto, M., Stegmann, R., Veldkamp, A., and Vyboishikov, S. F. (1996). Pseudopotential Calculations

of Transition Metal Compounds. Scope and Limitations. In '*Reviews in Computational Chemistry*', ed. K. B. Lipkowitz and D. B. Boyd, VCH, New York, vol.8; pgs. 63-144.

[37] Pyykkö, P., and Stoll, H. (2000). Relativistic pseudopotential calculations, 1993-June 1999. in *R.S.C. Specialist Periodical Reports, Chemical Modelling, Applications and Theory.* Vol. 1: 239-305.

[38] Dolg, M. (2002). Relativistic Effective Core Potentials. In: Relativistic Electronic Structure Theory. Part 1. Fundamental Aspects. P. Schwerdtfeger (ed.), Elsevier, Amsterdam; in preparation.

[39] Fock, V., Veselov, M., and Petrashen, M. (1940). *J. Expt. Theor. Phys. (USSR)* 10: 723-739.

[40] Herring, C. (1940). A New Method for Calculating Wave Functions in Crystals. *Phys. Rev.* 57: 1169-1177.

[41] Preuss, H. (1955). Untersuchungen zum kombinierten Näherungsverfahren. *Z. Naturforschg.* 10A: 365-373.

[42] Phillips, J. C., and Kleinman, L. (1959). A new method for calculating wavefunctions in crystals and molecules. *Phys. Rev.* 116: 287-294.

[43] Kahn L. R., Baybutt, P., Truhlar, D. G. (1976). Ab initio effective core potentials: Reduction of all-electron molecular structure calculations to calculations involving only valence electrons. *J. Chem. Phys.* 65: 3826-3853.

[44] Schwerdtfeger, P., Bowmaker, G. A. (1994). Relativistic Effects in gold chemistry. V. Group 11 dipole polarizabilities and weak bonding in monocarbonyl compounds. *J. Chem. Phys.* 100: 4487-4497

[45] Schwerdtfeger, P., Fischer, T., Dolg, M., Igel-Mann, G., Nicklass, A., Stoll, H., Haaland, A. (1995). The Accuracy of the Pseudopotential Approximation. I. An Analysis of the Spectroscopic Constants for the Electronic Ground States of InCl and $InCl_3$. *J. Chem. Phys.* 102: 2050-2062.

[46] Lim, I. Laerdahl, J. K., Schwerdtfeger, P. (2002). Fully Relativistic Coupled Cluster Dipole Polarizabilities of the Positively Charged Alkali Ions from Li^+ to Element 119^{+m}, *J. Chem. Phys.* 116: 172-178.

[47] Huzinaga, S., and Cantu, A. A. (1971). Theory of separability of many-electron systems. *J. Chem. Phys.* 55: 5543-5549.

[48] M. Klobukowski, S. Huzinaga, Sakai, Y. (1999). Model Core Potentials: Theory and Applications. in Computational Chemistry, Reviews of Current Trends, J. Leszynski (ed.), World Scientific, Singapore; Vol.3, pgs.49-74.

[49] Sakai, Y., Miyoshi, E., Klobukowski, M., and Huzinaga, S. (1987). Model Potentials for Molecular Calculations. I. The spd-MP Set for Transition Metal Atoms Sc through Hg. *J. Comput. Chem.* 8: 226-255.

[50] Sakai, Y., Miyoshi, E., Klobukowski, M., and Huzinaga, S. (1987). Model Potentials for Molecular Calculations. II. The spd-MP Set for Transition Metal Atoms Sc through Hg. *J. Comput. Chem.* 8: 256-264.

[51] Miyoshi, E., Sakai, Y., Tanaka, K., and Masamura, M. (1998). Relativistic dsp-model core potentials for main group elements in the fourth, fifth and sixth row and their applications. *J. Mol. Struct. (Theochem)* 451: 73-79.

[52] Höjer, G., and Chung, J. (1978). Some aspects of the model potential method. *Int. J. Quantum Chem.* 14: 623-634.

[53] Andzelm, J., Radzio, E., Barandiarán, Z., and Seijo, L. (1985) New developments in the model potential method: ScO molecule. *J. Phys. Chem.* 83: 4565-4572.

[54] Katsuki, S., and Huzinaga, S. (1988). An effective-Hamiltonian method for valence-electron molecular calculations. *Chem. Phys. Lett.* 147: 597-602.

[55] The AIMP parameters and basis sets of Seijo and co-workers can be obtained from: http://www.qui.uam.es/DATA/AIMPLibs.html/.

[56] Casarrubios, M., and Seijo, L. (1999). The *ab-initio* model potential method: Third series transition metal elements. *J. Chem. Phys.* 110: 784-796.

[57] Flad, J., Stoll, H., and Preuss, H. (1979). Calculation of equilibrium geometries and ionization energies of sodium clusters up to Na_8. *J. Chem. Phys.* 71: 3042-3052.

[58] Schwarz, W. H. E. (1968). Hellmann's pseudopotential method. I. Theoretical basis. *Theor. Chim. Acta* 11: 307-324.

[59] Schwarz, W. H. E. (1968). Hellmann's pseudopotential method. III. Calculations on atomic systems with two valence electrons. *Theor. Chim. Acta* 11: 377-384.

[60] Schwarz, W. H. E. (1969). Combined approximation method. II. Correct choice of the effective potential and description of the atomic core-atomic core interaction. *Acta Phys.* 27: 391-403.

[61] Schwarz, W. H. E. (1969). Calculations with the pseudopotential method on alkali-metal molecules. *Theor. Chim. Acta* 15: 235-243.

[62] The Stuttgart group pseudopotentials and valence basis sets of Stoll and co-workers can be obtained from: http://www.theochem.uni-stuttgart.de/pseudopotentials/.

[63] Stoll, H., Metz, B. and Dolg, M. (2002). Relativistic energy-consistent pseudopotentials – recent developments. *J. Comp. Chem.* 23: 767-778.

[64] Hay, P. J., and Wadt, W. R. (1985). *Ab-initio* effective core potentials for molecular calculations. Potentials for the transition metal atoms Sc to Hg. *J. Chem. Phys.* 82: 270-283.

[65] Wadt, W. R., and Hay, P. J. (1985). *Ab-initio* effective core potentials for molecular calculations. Potentials for main group elements Na to Bi. *J. Chem. Phys.* 82: 284-298.

[66] Hay, P. J., and Wadt, W. R. (1985). *Ab-initio* effective core potentials for molecular calculations. Potentials for K to Au including the outermost core orbitals. *J. Chem. Phys.* 82: 299-310.

[67] The pseudopotential parameters and basis sets of Christiansen and co-workers can be obtained from: http://www.clarkson.edu/~pac/reps.html.

[68] Barthelat, J. C., Durand, Ph., and Serafini, A. (1977). Non-empirical pseudopotentials for molecular calculations. I. The PSIBMOL algorithm and test calculations. *Mol. Phys.* 33: 159-180.

[69] Maron, L., and Teichteil, C. (1998). On the accuracy of averaged relativistic shape-consistent pseudopotentials. *Chem. Phys.* 237: 105-122.

[70] Stevens, W. J., Krauss, M., Basch, H., and Jasien, P. G. (1992). Relativistic compact effective potentials and efficient, shared-exponent basis sets for the third-, fourth-, and fifth-row atoms. *Can. J. Chem.* 70: 612-630.

[71] Kleinman, L. (1980). Relativistic norm-conserving pseudopotential. *Phys. Rev. B* 21: 2630-2631.

[72] Hamann, D. R., Schlüter, M., and Chiang, C. (1979). Norm-Conserving Pseudopotentials. *Phys. Rev. Lett.* 43: 1494-1497.

[73] Bachelet, G. B., and Schlüter, M. (1982). Relativistic norm-conserving pseudopotentials. *Phys. Rev. B* 25: 2103-2108.

[74] Focher, P., Lastri, A., Covi, M., and Bachelet, G. B. (1991). Pseudopotentials and physical ions. *Phys. Rev. B* 44: 8486-8495.

[75] Bachelet, G. B., Hamann, D. R., and Schlüter, M. (1982). Pseudopotentials that work: From H to Pu. *Phys. Rev. B* 26: 4199-4228.

[76] Mosyagin, N. S., Titov, A. V., and Tulub, A. V. (1994). Generalized effective-core-potential method: Potentials for the atoms Xe, Pd and Ag. *Phys. Rev. A* 50: 2239-2247.

[77] Titov, A. V., Mitrushenkov, A. O., and Tupitsyn, I. I. (1991). Effective core potential for pseudo-orbitals with nodes. *Chem. Phys. Lett.* 185: 330-334.

[78] Titov, A.V., and Mosyagin, N. S. (1999). Generalized Relativistic Effective Core Potentials: Theoretical Grounds. *Int. J. Quantum Chem.* 71: 359-401.

[79] Klobukowski, M. (1992). Comparison of the effective core potential and model potential methods in studies of electron correlation energy in molecules: Dihalides and halogen hydrides. *Theor. Chim. Acta* 83: 239-248.

[80] Kolar, M. (1981). Pseudopotential matrix elements in the Gaussian basis. *Comput. Phys. Commun.* 23: 275-286.

[81] McMurchie, L. E., and Davidson, E. R. (1981). Calculation of Integrals over ab initio Pseudopotentials. *J. Comput. Phys.* 44: 289-301.

[82] Piccolo, R. (1990). Analytical evaluation of Gaussian pseudopotential matrix elements with any angular momentum. *Phys. Rev. A* 41: 4704-4710.

[83] Pelissier, M., Komiha, N., and Daudey, J. P. (1988). One-Center Expansion for Pseudopotential Matrix Elements. *J. Comput. Chem.* 9: 298-302.

[84] Skylaris, C.-K., Gagliardi, L., and Handy, N. C. (1998). An efficient method for calculating effective core potential integrals which involve projection operators. *Chem Phys. Lett.* 2967: 445-451.

[85] Breidung, J., Thiel, W., and Kormornicki, A. (1988). Analytical second derivatives for effective core potentials. *Chem. Phys. Lett.* 153: 76-81.

[86] Goll, E. (2001). Pseudopotentialintegrale und Energiegradienten. *Diploma Thesis*, Stuttgart.

[87] Datta, S. N., Ewig, C. S., Van Wazer, J. R. (1978). Application of Effective Potentials to Relativistic Hartree-Fock Theory. *Chem Phys. Lett.* 57: 83-89.

[88] Cowan, R. D., and Griffin, D. C. (1976). Approximate relativistic corrections to atomic radial wavefunctions. *J. Opt. Soc. Am.* 66: 1010-1014.

[89] Casarrubios, M., and Seijo, L. (1998). The ab initio model potential method. Relativistic Wood-Boring valence spin-orbit potentials and spin-orbit-corrected basis sets from B(Z=5) to Ba(Z=56). *J. Mol. Stuct.* 426: 59-74.

[90] Barandiarán, Z., and Seijo, L. (1992). The ab initio model potential method. Cowan-Griffin relativistic core potentials and valence basis sets from Li (Z=3) to La (Z=57). *Can. J. Chem.* 70: 409-415.

[91] Wittborn, C., and Wahlgren, U. (1995). New relativistic effective core potentials for heavy elements. *Chem. Phys.* 201: 357-362.

[92] Rakowitz, F., Marian, C. M., Seijo, L., and Wahlgren, U. (1999). Spin-free relativistic no-pair *ab-initio* core model potentials and valence basis sets for the transition metal elements Sc to Hg. II. *J. Chem. Phys.* 111: 10436-10443.

[93] Rakowitz, F., Marian, C. M., and Seijo, L. (1999). Spin-free relativistic no-pair *ab-initio* core model potentials and valence basis sets for the transition metal elements Sc to Hg. Part 1. *J. Chem. Phys.* 110: 3678-3686.

[94] Heinemann, C., Koch, W., and Schwarz, H. (1995). An approximate method for treating spin-orbit effects in platinum. *Chem. Phys. Lett.* 245: 509-518.

[95] Hafner, P., and Schwarz, W. H. E. (1979). Molecular Spinors from the Quasi-Relativistic Pseudopotential Approach. *Chem. Phys. Lett.* 63: 537-541.

[96] Ermler, W. C., Ross, R. R., and Christiansen, P. A. (1988). Spin-Orbit Coupling and Other Relativistic Effects in Atoms and Molecules. *Adv. Quantum Chem.* 19: 139-182.

[97] Ermler, W. C., Lee, Y. S., Christiansen, P. A., and Pitzer, K. S. (1981). Ab intio effective core potentials including relativistic effects. A procedure for the inclusion of spin-orbit coupling in molecular calculations. *Chem. Phys. Lett.* 81: 70-73.

[98] Pitzer, R. M., and Winter, N. W. (1988). Electronic-Structure Methods for Heavy-Atom Molecules. *J. Phys. Chem.* 92: 3061-3063.

[99] Pitzer, R. M., and Winter, N. W. (1991). Spin-Orbit (Core) and Core Potential Integrals. *Int. J. Quantum Chem.* 40: 773-780.

[100] Lee, S. Y., and Lee, Y. S. (1992). Kramers' Restricted Hartree-Fock Method for Polyatomic Molecules Using Ab Initio Relativistic Effective Core Potentials with Spin-Orbit Operators. *J. Comput. Chem.* 5: 595-601.

[101] Yabushita, S., Zhang, Z., and Pitzer, R. M. (1999). *J. Phys. Chem. A* 103: 5791-5800.

[102] Datta, S., Ewig, C. S., and Van Wazer, J. R. (1978). Application of effective potentials to relativistic Hartree-Fock calculations. *Chem. Phys. Lett.* 57: 83-89.

[103] Ishikawa, Y., and Malli, G. L. (1981). Fully relativistic effective core potentials (FRECP). In Relativistic Effects in Atoms, Molecules and Solids, G. L. Malli (ed.), NATO ASI Series B: Physics, Vol. 87, Plenum, New York; pgs. 363-381.

[104] Ishikawa, Y., and Malli, G. L. (1981). Effective core potentials for fully relativistic Dirac-Fock calculations. *J. Chem. Phys.* 75: 5423-5431.

[105] Dolg, M. (1996). Fully relativistic pseudopotentials for alkaline atoms: Dirac-Hartree-Fock and configuration interaction calculations of alkaline monohydrides. *Theor. Chim. Acta* 93: 141-156.

[106] Pyper, N. C. (1980). Relativistic pseudopotential theories and corrections in the Hartree-Fock method. *Mol. Phys.* 39: 1327-1358.

[107] Boys, S. F., and Bernardi, F. (1970). The calculation of small molecular interactions by the differences of separate total energies. Some procedures with reduced errors. *Mol. Phys.* 19: 553-566.

[108] Hermann, H. L., Boche, G., Schwerdtfeger, P. (2001). Metallophilic Interactions between Closed-Shell Copper(I) Molecules – A Theoretical Study. *Chem. Eur. J.* 7: 5333-5342; and references therein.

[109] Martin, J. M., and Sundermann, A. J. (2001). Correlation consistent valence basis sets for use with the Stuttgart-Dresden-Bonn relativistic effective core potentials: The atoms Ga-Kr and In-Xe. *J. Chem. Phys.* 114: 3408-3420.

[110] Schwerdtfeger, P., Wesendrup, R., Moyano, G. E., Sadlej, A. J., Greif, J., Hensel, F. (2001). The Potential Energy Curve and Dipole Polarizability Tensor of Mercury Dimer , *J. Chem. Phys.* 115: 7401-7412

[111] Dolg, M., and Flad, H.-J. (1996). Ground State Properties of Hg_2. 1. A Pseudopotential Configuration Interaction Study. *J. Phys. Chem.* 100: 6147-6151.

[112] Yu, M., and Dolg, M. (1997). Covalent contributions to bonding in group 12 dimers M_2 (M = Zn, Cd, Hg). *Chem. Phys. Lett.* 273: 329-336.

[113] Stoll, H., Fuentealba, P., Dolg, M., Flad, J., Szentpály, L. v., and Preuss, H. (1983). Cu and Ag as one-valence-electron atoms: Pseudopotential results for Cu_2, Ag_2, CuH, AgH, and the corresponding cations. *J. Chem. Phys.* 79: 5532-5542.

[114] Schwerdtfeger, P. (1987). Relativistic effects in molecules: Pseudopotential calculations for TlH^+, TlH and TlH_3. *Phys. Scr.* 36: 453-459.

[115] Bernier, A., Millie, Ph., and Pelissier, M. (1986). Three-electron approach of HgH using relativistic effective core, core polarization and spin-orbit operators: the low-lying states. *Chem. Phys.* 106: 195-203.

[116] Nicklass, A., and Stoll, H. (1995). On the Importance of Core Polarization in Heavy Post-d Elements: a Pseudopotential Calibration Study for X_2H_6 (X = Si, Ge, Sn, Pb), *Mol. Phys.* 86, 317-326.

[117] Jeung, G. H., Spiegelmann, F., Daudey, J. P., and Malrieu, J. P. (1983). Theoretical study of the lowest states of CsH and Cs_2. J. *Phys. B* 16: 2659-2675.

[118] Schwerdtfeger, P. (1986), Pseudopotentials for the Investigation of Relativistic Effects, PhD thesis, University of Stuttgart.

[119] Müller, W., Flesch, J., and Meyer, W. (1984). Treatment of intershell correlation effects in ab initio calculations by use of core polarization potentials. Method and application to alkali and alkaline earth atoms. *J. Chem. Phys.* 80: 3297-3310.

[120] Nicklass, A., Dolg, M., Stoll, H., and Preuss, H. (1995). Ab initio energy-adjusted pseudopotentials for the noble gases Ne through Xe: Calculation of atomic dipole and quadrupole polarizabilities. *J. Chem. Phys.* 102: 8942-8952.

[121] Schwerdtfeger, P., Silberbach, H. (1988). Multicenter integrals over long-range operators using Cartesian Gaussian functions. *Phys. Rev. A* 37: 2834-2842; *ibid.* (1988). 42: 665.

[122] Barthelat, J. C., Pelissier, M., Villemur, P., Devilliers, R., Trinquier, G., and Durand, Ph., (1981). Program PSHONDO (PSATOM), Manuel d'utilisation, Universite de Paul Sabatier, Toulouse, France.

[123] Lajohn, L. A., Christiansen, P. A., Ross, R. B., Atashroo, T., and Ermler, W. C. (1987). Ab initio relativistic effective core potentials with spin-orbit operators. III. Rb through Xe. *J. Chem. Phys.* 87: 2812-2824.

[124] Igel-Mann, G., Stoll, H., and Preuss, H. (1988). Pseudopotentials for main group elements (IIIa through VIIa). *Mol. Phys.* 65: 1321-1328.

[125] Leininger, T., Nicklass, A., Stoll, H., Dolg, M., and Schwerdtfeger, P. (1996). The Accuracy of the Pseudopotential Approximation. II. A Comparison of Various Core Sizes for In Pseudopotentials in Calculations for Spectroscopic Constants of InH, InF, InCl. *J. Chem. Phys.* 105: 1052-1059.

[126] Andrae, D., Häussermann, U., Dolg, M., Stoll, H., and Preuss, H. (1990). Energy-adjusted ab initio pseudopotentials for the second and third row transition elements. *Theor. Chim. Acta* 77: 123-141.

[127] Bergner, A., Dolg, M., Küchle, W., Stoll, H., and Preuss, H. (1993). Ab initio-adjusted pseudopotentials for elements of group 13 through 17. *Mol. Phys.* 80: 1431-1441.

[128] Eliav, E., Kaldor, U., and Ishikawa, Y. (1995). Transition energies of mercury and ekamercury (element 112) by the relativistic coupled-cluster method. *Phys. Rev. A* 52: 2765-27.

[129] Moore, C. E. (1958). *Atomic Energy Levels*, US GPO, Washington.

[130] Dyall, K. G., Bauschlicher Jr., C. W., Schwenke, D. W., and Pyykkö, P. (2001). Is the Lamb shift chemically significant?, *Chem. Phys. Lett.* 348: 497-500.

[131] Mosyagin, N. S., Eliav, E., Titov, A. V., and Kaldor, U. (2000). Comparison of relativistic effective core potential and all-electron Dirac-Coulomb calculations of mercury transition energies by the relativistic coupled-cluster method. *J. Phys. B: At. Mol. Opt. Phys.* 33: 667-676.

[132] Küchle, W., Dolg, M., Stoll, H., and Preuss, H. (1991). Ab initio pseudopotentials for Hg through Rn. I. Parameter sets and atomic calculations. *Mol. Phys.* 74: 1245-1263.

[133] Häussermann, U., Dolg, M., Stoll, H., Preuss, H., Schwerdtfeger, P., and Pitzer, R. M. (1993). Accuracy of energy-adjusted quasirelativistic *ab-initio* pseudopotentials: all-electron and pseudopotential benchmark calculations for Hg, HgH and their cations. *Mol. Phys.* 87: 1211-1224.

[134] Dolg, M., personal communication.

[135] Goebel, D., and Hohm, U. (1995). Dispersion of the refractive index of cadmium vapor and the dipole polarizability of the atomic cadmium $^1S_0$ state. *Phys. Rev. A* 52: 3691-3694.

[136] Goebel, D., and Hohm, U. (1996). Dipole polarizability, Cauchy moments, and related properties of Hg. *J. Phys. Chem.* 100: 7710-7712.

[137] Kellö, V., and Sadlej, A., (1995). Polarized basis sets for high-level-correlated calculations of molecular properties. VIII. Elements of the group IIb: Zn, Cd, Hg. *Theor. Chim. Acta* 91: 353-371.

[138] Siekierski, S., Autschbach, J., Schwerdtfeger, P., Seth, M. and Schwarz, W.H.E. (2002). The dependence of relativistic effects on the electronic configurations in the atoms of the d- and f-block elements. *J. Comput. Chem.*, in press.

[139] Ziegler, T., Tschinke, V., Baerends, E. J., Snijders, J. G., and Ravenek, W. (1989). Calculation of Bond Energies in Compounds of Heavy Elements by a Quasi-Relativistic Approach. *J. Phys. Chem.* 93: 3050-3062.

[140] Strömberg, D., and Wahlgren, U. (1990). First-order relativistic calculations on Au_2 and Hg_2^{2+}. *Chem. Phys. Lett.* 169: 109-115.

[141] Schwerdtfeger, P., (1991). Relativistic and Electron Correlation Contributions in Atomic and Molecular Properties. Benchmark Calculations on Au and Au_2. *Chem Phys. Lett.* 183: 457-463.

[142] Häberlen, O. D., and Rösch, N. (1992). A scalar-relativistic extension of the linear combination of Gaussian-type orbitals local density functional method: application to AuH, AuCl and Au_2. *Chem. Phys. Lett.* 199: 491-496.

[143] Bastug, T., Heinemann, D., Sepp, W.-D., Kolb, D., and Fricke, B. (1993). All-electron Dirac-Fock-Slater SCF calculations of the Au_2 molecule. *Chem. Phys. Lett.* 211: 119-124.

[144] Hess, B. A. and Kaldor, U. (2000). Relativistic all-electron coupled cluster calculations on Au_2 in the framework of the Douglas-Kroll transformation. *J. Chem. Phys.* 112: 1809-1813.

[145] van Lenthe, E., Baerends, E. J., and Snijders, J. G. (1994). Relativistic total energy using regular approximations. *J. Chem. Phys.* 101: 9783-9792.

[146] Park, C., and Almlöf, J. E. (1994). Two-electron relativistic effects in molecules. *Chem. Phys. Lett.* 231: 269-276.

[147] van Wüllen, C. (1995). A relativistic Kohn–Sham density functional procedure by means of direct perturbation theory. *J. Chem. Phys.* 103: 3589-3599.

[148] Wesendrup, R., Laerdahl, J.K., and Schwerdtfeger, P. (1999). Relativistic Effects in Gold Chemistry. VI. Coupled Cluster Calculations for the Isoelectronic Series $AuPt^-$, Au_2 and $AuHg^+$. *J. Chem. Phys.* 110: 9457-9462.

[149] Suzumura, T., Nakajima, T., and Hirao, K. (1999). Ground State Properties of MH, MCl and M_2 (M = Cu, Ag and Au) Calculated by a Scalar Relativistic Density Functional Theory. *Int. J. Quantum Chem.* 75: 757-766.

[150] Han, Y.-K., and Hirao, K. (2000). On the transferability of relativistic pseudopotentials in density-functional calculations: AuH, AuCl and Au_2. *Chem. Phys. Lett.* 324: 453-458.

[151] Collins, C. L., Dyall, K. G., and Schaefer, H. F. (1995). Relativistic and correlation effects in CuH, AgH, and AuH: Comparison of various relativistic methods. *J. Chem. Phys.* 102: 2024-2031.

[152] Lee, H.-S., Han, Y.-K., Kim, M. C., Bae, C., and Lee, Y. S., Spin-orbit effects calculated by two-component coupled-cluster methods: test calculations on AuH, Au_2, TlH and Tl_2. *Chem. Phys. Lett.* 293: 97-102.

[153] Schwerdtfeger, P. Boyd, P. D. W., Burrell, A. K., Taylor, M. J. (1990). Relativistic effects in gold chemistry. III. Gold(I) Complexes. *Inorg. Chem.* 29: 3593-3607.

[154] Huber, K. P., and Herzberg, G. (1979). Molecular Spectra and Molecular Structure, Constants of Diatomic Molecules, Van Nostrand, New York.

[155] Schwerdtfeger, P., Brown, J. R. , Laerdahl, J. K., and Stoll, H. (2000). The accuracy of the pseudopotential approximation. III. A comparison between pseudopotential and all electron methods for Au and AuH. *J. Chem. Phys.* 113: 7110-7118.

[156] Kaldor, U., and Hess, B. A. (1994). Relativistic all-electron coupled-cluster calculations on the gold atom and gold hydride in the framework of the Douglas-Kroll transformation. *Chem. Phys. Lett.* 230: 1-7.

[157] Ross, R. B., Powers, J. M., Atashroo, T., Ermler, W. C. Lajohn, L. A., and Christiansen, P. A. (1990). Ab initio relativistic effective core potentials with spin-orbit operators. IV. Cs through Rn. *J. Chem. Phys.* 93: 6654-6670.

[158] Nakajima, T., and Hirao, K. (1999). A new relativistic theory: a relativistic scheme by eliminating small components (RESC). Chem. Phys. Lett. 302: 383-391.

[159] Filatov, M., and Cremer, D. (2002). A new quasi-relativistic approach for density functional theory based on the normalized elimination of the small component. *Chem. Phys. Lett.* 351: 259-266.

[160] Metz, B., Schweizer, M., Stoll, H., Dolg, M., and Liu, W. (2000). A small-core multiconfiguration Dirac-Hartree-Fock-adjusted pseudopotential for Tl – application to TlX (X= F, Cl, Br, I). *Theor. Chem. Acta* 104: 22-28.

[161] Eliav, E., Kaldor, U., Ishikawa, Y., Seth, M., and Pyykkö, P. (1996). Calculated energy levels of thallium and eka-thallium (element 113). *Phys. Rev. A* 53: 3926-3933.

[162] Schwerdtfeger, P., and Ischtwan, J. (1994). The Convergence of the Møller-Plesset Series in Molecular Properties of Group 13 compounds. Comparison between HF, MP and QCI Calculations of MH and MF (M= B, Al, Ga, In, Tl). *J. Molec. Stuct. (THEOCHEM)* 306: 9-19.

[163] Seijo, L. (1995). Relativistic ab initio model potential calculations including spin-orbit effects through the Wood-Boring Hamiltonian. *J. Chem. Phys.* 102: 8078-8088.

[164] Rakowitz, F.; and Marian, C. M. (1997). An extrapolation for spin-orbit configuration interaction energies to the ground state and excited electronic states of thallium hydride. *Chem. Phys.* 225: 223-238.

[165] Seth, M., Schwerdtfeger, P., and Faegri, K. (1999). The chemistry of superheavy elements. III. Theoretical studies of element 113 compounds. *J. Chem. Phys.* 111: 6422-6433.

[166] Han, Y., Bae, C., and Lee, Y. S. (1999). Two-component calculations for the molecules containing superheavy elements: Spin--orbit effects for (117)H, (113)H, and (113)F. *J. Chem. Phys.* 110: 8969-8975.

[167] Nash, C. S., Bursten, B. E., and Ermler, W. C. (1997). Ab initio relativistic effective potentials with spin-orbit operators. VII. Am through element 118. *J. Chem. Phys.* 106: 5133-5142.

[168] Teichteil, C., Malrieu, J. P., and Barthelat, J. C. (1977). Non-empirical pseudopotentials for molecular calculations. II. Basis set extension and correlation effects on the X_2 molecules (X= f, Cl, Br, I). *Mol. Phys.* 33: 181-197.

[169] Pittel, B., and Schwarz, W. H. E. (1977). Correlation energies from pseudopotential calculations. *Chem. Phys. Lett.* 46: 121-124.

[170] Dolg, M. (1996). Valence correlation energies from pseudopotential calculations. *Chem. Phys. Lett.* 250: 75-79.

[171] Dolg, M. (1996). On the accuracy of valence correlation energies in pseudopotential calculations. *J. Chem. Phys.* 104: 4061-4067.

[172] Hetényi, B., De Angelis, F., Giannozzi, P., and Car, R. (2001). Reconstruction of frozen-core all-electron orbitals from pseudo-orbitals. *J. Chem. Phys.* 115: 5791-5795.

[173] Leininger, T., Riehl, J.-F., Jeung, G.-H., and Pélissier, M. (1993). Comparison of the widely used HF pseudo-potentials: MH^+ (M=Fe, Ru, Os). *Chem. Phys. Lett.* 205: 301-305.

[174] Andrae, D., Dolg, M., Stoll, H., and Ermler, W. C. (1994). Comment on "Comparison of the widely used HF pseudo-potentials: MH^+ (M=Fe, Ru, Os)". *Chem. Phys. Lett.* 220: 341-344.

Chapter 11

RELATIVISTIC DENSITY FUNCTIONAL THEORY

Properties of the Exact Exchange and Construction of Pseudopotentials

E. Engel

Institut fr Theoretische Physik, J.W.Goethe Universitt Frankfurt, D-60054 Frankfurt/Main, Germany

engel@math.uni-frankfurt.de

Abstract An overview of relativistic density functional theory (RDFT) is given, including some illustrative results for atoms and molecules. Starting from quantum electrodynamics, the existence theorem of RDFT and the effective single-particle equations are outlined. In this formalism the ground state four current is the fundamental variable which allows the determination of all ground state observables. The crucial ingredient of the single-particle equations is the relativistic exchange-correlation (xc) potential, which is obtained as the functional derivative of the xc-energy functional with respect to the four current. As standard approximations for the xc-functional, the relativistic local density approximation (RLDA) and the relativistic generalized gradient approximation (RGGA) are reviewed. In particular, it is shown that the RLDA does not provide an adequate description of the relativistic xc-effects in finite systems, while the RGGA performs rather well over the complete periodic table. In contrast to the explicit density functionals RLDA and RGGA, the representation of implicit xc-functionals is not only based on the four current, but also on the effective single-particle spinors of RDFT. The most important implicit functional is the exact exchange. After a summary of the relativistic optimized potential method (ROPM), which is required for the evaluation of the xc-potential corresponding to implicit functionals, the properties of the exact exchange are investigated in detail, addressing in particular the role of the transverse corrections. As RDFT calculations frequently rely on a pseudopotential framework, the fully relativistic construction of normconserving pseudopotentials is presented, including the case of the highly nonlocal exact exchange.

U. Kaldor and S. Wilson (eds.),
Theoretical Chemistry and Physics of Heavy and Superheavy Elements, 439–486.
© 2003 *Kluwer Academic Publishers.*

Finally, some molecular results are given, which illustrate the role of relativity in RDFT.

Keywords: density functional theory, quantum electrodynamics, transverse interaction, exchange-correlation functional, exact exchange, optimized potential method, local density approximation, generalized gradient approximation, normconserving pseudopotentials

1. Introduction

Since the introduction of the generalized gradient approximation (GGA) [1–4] density functional theory (DFT) has gained considerable attention in the quantum chemistry community [5,6]. Most applications of DFT are based on the nonrelativistic formalism (for an overview of DFT see [7]). However, for the physics and chemistry of heavy elements relativity cannot be neglected [8,9], so that corresponding studies have to rely on some variant of relativistic DFT (RDFT).

RDFT has been established by Rajagopal and Callaway [10] who formulated a relativistic generalization of the Hohenberg-Kohn (HK) theorem [11]. Starting from quantum electrodynamics (QED), these authors showed that the ground state $|\Phi\rangle$ of a relativistic many-body system is uniquely determined by the corresponding ground state four current j^μ (up to a gauge transformation — the question of ultraviolet divergencies in ground state observables has been addressed later [12]). This allows to understand all ground state observables as functionals of j^μ, the most important functional being the ground state energy E_{tot}. Minimization of this functional $E_{tot}[j]$ with respect to j^μ then leads to a variational equation in the spirit of the Thomas-Fermi theory [13,14]. While the original work of Rajagopal and Callaway mainly aimed at providing a rigorous foundation for nonrelativistic spin-density functional theory, RDFT has soon been taken seriously as a theory of its own. In fact, attempts to establish relativistic Thomas-Fermi models even date back to the early days of quantum mechanics [15,16]. However, these models were hampered by the occurrence of divergencies which can only be understood within QED. Unfortunately, even if such functionals are derived on the basis of QED, taking into account the inherent need for renormalization of ground state energies and currents, and even if relativistic gradient corrections are included [17], these models are not able to reproduce the quantal nature of electronic states in finite systems. Consequently they are only of very limited use for actual electronic structure calculations.

In order to obtain realistic results one has to utilize effective single-particle equations, which ensures an exact treatment of the quantum mechanical kinetic energy, at least on the noninteracting level. The

single-particle equations of RDFT have simultaneously been put forward by Rajagopal [18] as well as by MacDonald and Vosko [19]. They follow directly from the existence of the functional $E_{tot}[j]$ after a suitable decomposition of this functional. The most important part of $E_{tot}[j]$ is the kinetic energy functional $T_s[j]$. It is most easily defined by application of the relativistic HK-theorem to noninteracting particles. In this case the ground state energy functional consists of only two terms, the kinetic energy of noninteracting particles, T_s, and the coupling between the electrons and the nuclei represented by the external potential V^μ, $\int j_\mu V^\mu$. Although T_s is not explicitly known in terms of the four current, the HK-theorem nevertheless guarantees that T_s is a functional of j^μ, as this is the case for the total ground state energy of the noninteracting system. If one assumes that there exists a noninteracting system with the same ground state four current as the interacting system of actual interest, the energy functional of the latter, $E_{tot}[j]$, can be split into $T_s[j]$, the external potential energy $\int j_\mu V^\mu$, the direct electron-electron repulsion term $E_H[j]$ and a remainder, the so-called exchange-correlation (xc) energy functional $E_{xc}[j]$. The minimization of $E_{tot}[j]$ with respect to j^μ can then be replaced by a minimization with respect to the single-particle spinors of the auxiliary noninteracting system. In this way one ends up with the relativistic Kohn-Sham (RKS) equations, which are Dirac-type equations with a multiplicative effective four potential v_s^μ. Following the decomposition of $E_{tot}[j]$, this potential consists of the external potential, a Hartree component and an xc-potential $v_{xc}^\mu = \delta E_{xc}[j]/\delta j_\mu$.

The only quantity which has to be approximated in the RKS scheme is the xc-functional. Consequently, much work went into the construction of xc-functionals suitable for electronic structure calculations. Three generations of functionals may be distinguished. In the local density approximation (LDA) [20] the homogeneous electron gas (HEG) serves as model system, for which the xc-energy density e_{xc}^{NRHEG} is known as a function of the gas density n_0. For inhomogeneous systems the function $e_{xc}^{NRHEG}(n_0)$ is then utilized with the actual density $n(\boldsymbol{r}) = j^0(\boldsymbol{r})$. In RDFT the same concept can be applied to define the relativistic LDA (RLDA) [18, 19, 21]. Analogous to e_{xc}^{NRHEG}, the xc-energy of the relativistic HEG (RHEG), e_{xc}^{RHEG}, is a function of the gas density only, but not of the spatial components $\boldsymbol{j}$ of the four current, which vanish in the RHEG.

In the second generation of density functionals gradient corrections are added to the LDA. The most suitable form of a gradient corrected functional is the GGA, which combines reasonable accuracy with efficiency. In the GGA the xc-energy is usually represented in terms of two quantities, the density $n(\boldsymbol{r})$ and the first gradient of the density,

$\nabla n(\boldsymbol{r})$, thus taking into account an infinitesimal neighborhood of the point $\boldsymbol{r}$ in question (in some cases also the second gradient of the density is included). A direct extension of the GGA concept to the relativistic domain (RGGA) is also available [22,23]. Finally, in the third generation of xc-functionals the auxiliary RKS spinors are used for the representation of the xc-energy. The most simple and most important functional of this type is the exact exchange of RDFT, which is defined via the Fock expression, written in terms of RKS spinors [24, 25]. In contrast to the RLDA and the RGGA, such implicit density functionals are functionals of the complete j^μ, rather than just the density.

The application of orbital-dependent functionals requires the evaluation of the corresponding multiplicative xc-potential by the relativistic Optimized Potential Method (ROPM) [25–28]. In this approach an integral equation has to be solved simultaneously with the RKS equations, which makes the ROPM much more demanding than standard RLDA or RGGA calculations. Fortunately, an efficient and accurate semi-analytical approximation to the ROPM is available [25, 28], which follows the concept introduced by Krieger, Li and Iafrate (KLI) in the nonrelativistic context [29]. On the basis of the KLI approximation calculations with the exact exchange are possible even for larger molecules. However, routine applications of implicit functionals have to await the derivation of a suitable implicit correlation functional, as the combination of the exact exchange with LDA or GGA correlation often yields unsatisfying results [30].

On the other hand, the exact exchange is an ideal reference standard for judging the quality of approximate density functionals. This is not only the case for the Coulomb exchange, but also for the (retarded) Breit corrections. It turns out that the RLDA does not provide a realistic account of the relativistic xc-effects in atomic systems [27, 31–33], while the RGGA gives rather accurate results over the complete periodic table [22], at least for closed shell systems.

The latter restriction points at the fact that the four current version of RDFT, outlined so far, is not very useful for practical studies of magnetic phenomena. The reason for this is the lack of truly j^μ-dependent xc-functionals (apart from the exact exchange): In the four current version of RDFT the spin degree of freedom is accounted for via the spatial components of j^μ, which do not show up in the RLDA and the standard RGGA form. This deficiency has prompted an alternative form of RDFT, in which the magnetization density $\boldsymbol{m}$ plays the role of $\boldsymbol{j}$. An existence theorem for this variant has been formulated by MacDonald and Vosko [19], the corresponding single-particle equations were given by Ramana and Rajagopal [34] (see also [35]). An $\boldsymbol{m}$-dependent RLDA has been

derived for the exchange part of E_{xc} on the basis of a polarized RHEG [34, 36–38]. However, due to the complicated structure of its single-particle equations this formalism has only rarely been applied in its most general form [39–41]. In most calculations the orientation of the magnetization density is restricted to one direction, $\boldsymbol{m} = (0, 0, m_z)$ (collinear $\boldsymbol{m}$). In this limit the generalized spin-densities

$$n_{\pm}(\boldsymbol{r}) = \frac{1}{2}\left[n(\boldsymbol{r}) \mp \frac{1}{\mu_B} m_z(\boldsymbol{r})\right] \qquad \left(\mu_B = \frac{e}{2mc}\right)$$

may be used as basic variables of RDFT, rather than n and m_z. These direct relativistic extensions of the nonrelativistic spin-densities suggest the application of nonrelativistic spin-density functionals within the collinear RDFT formalism, which constitutes the standard RDFT approach to magnetic (open-shell) systems (see e.g. [42–44]). This scheme is supported by the fact that non-collinearity turned out to be only of limited importance for open-shell atoms [41].

In this contribution an overview of the RDFT formalism for ground states is given, restricting the discussion to the most general, four current form[1]. On the basis of QED the relativistic generalization of the HK theorem and the resulting effective single-particle equations are summarized in Section 2.. For brevity, however, several aspects of the underlying quantum field theory are suppressed. In particular, the issue of virtual electron-positron pair creation and the associated renormalization scheme will not be touched — for a detailed account of the QED renormalization program and its consequences for RDFT the reader is referred to [45]. In this contribution the *no-pair* approximation will be used throughout. On the other hand, the fact that the electron-electron interaction originates from the exchange of photons is not ignored. The resulting transverse corrections to the Coulomb interaction show up both in the basic formalism and in explicit functionals as the RLDA and the RGGA, which are also discussed in Section 2..

The importance of the transverse corrections can be unambiguously analyzed for the exact exchange of RDFT. The ROPM required for the evaluation of the corresponding multiplicative exchange potential and the KLI approximation to the ROPM are outlined in Section 3.. The role of the transverse interaction is then explicitly investigated in Section 4.1, which contains a number of illustrative exchange-only results for atoms. The ROPM values also serve as reference data for an analysis of the exchange components of the RLDA and the RGGA. In the case of the

[1] A review of the $\boldsymbol{m}$-dependent variant of RDFT may be found in [45].

correlation components, on the other hand, one has to resort quantum chemical data [46] in order to assess the quality of the RLDA and RGGA (Section 4.2).

In many DFT applications pseudopotentials (PPs) are utilized. In Section 5.1 a relativistic variant [47] of the most frequently used DFT-based scheme for the construction of PPs [48] is presented. In view of the computational demands of ROPM calculations the use of PPs is particularly attractive for calculations with the exact exchange. A PP construction scheme suitable for fully nonlocal functionals like the exact exchange is summarized in Section 5.2 and illustrated by some exchange-only results for first and second row diatomic molecules.

In Section 6. a few prototype results for molecules and solids are given. First the question of the importance of the relativistic ingredients in the xc-functional is addressed. Next, the impact of transverse corrections on molecular properties is examined for $RfCl_4$. Finally, the relevance of relativity for third row elements is stressed by a study of FeO. The review is concluded by some brief remarks on open questions in Section 7..

No attempt is made to review the wealth of RDFT applications (see e.g. [49–75]) as well as the substantial literature on nonrelativistic xc-functionals. For the discussion of a time-dependent generalization of RDFT [76–79], an RDFT approach to excited states [80] and relativistic, extended Thomas-Fermi models [17, 81–86] the reader is also referred to the original literature.

The notation and units in this work are as follows: The space-time coordinates are denoted as $x = x^\mu = (x^0, \boldsymbol{x}) = (ct, \boldsymbol{r})$, with the metric as in [87]. Greek indices run from 0 to 3, Latin indices from 1 to 3. $\alpha^\mu = \gamma^0\gamma^\mu$, with γ^μ denoting the standard Dirac matrices. The summation convention and $\hbar = 1$ are used throughout.

2. RDFT Formalism

At the most fundamental level the electronic systems of interest are described by QED. Within this framework the electrons interact with each other and all other charged particles (as the nuclei) by the exchange of photons, rather than via some classical interaction potential. However, as soon as the Born-Oppenheimer approximation is applied, the attraction of the electrons by the nuclei may be represented by a stationary external potential $V^\mu(\boldsymbol{x})$ in which the electrons move. The corresponding Hamiltonian can be obtained from the standard Lagrangian of bound

state QED by application of Noether's theorem [88],

$$\hat{H} = \hat{H}_e + \hat{H}_\gamma + \hat{H}_{int} + \hat{H}_{ext} \tag{11.1}$$

$$\hat{H}_e = \int d^3x\ \hat{\psi}^\dagger(x)\Big(-ic\boldsymbol{\alpha}\cdot\boldsymbol{\nabla} + \beta mc^2\Big)\hat{\psi}(x) \tag{11.2}$$

$$\hat{H}_\gamma = -\frac{1}{8\pi}\int d^3x\ \Big\{[\partial^0\hat{A}_\nu(x)][\partial^0\hat{A}^\nu(x)] + \boldsymbol{\nabla}\hat{A}_\nu(x)\cdot\boldsymbol{\nabla}\hat{A}^\nu(x)\Big\} \tag{11.3}$$

$$\hat{H}_{int} = e\int d^3x\ \hat{j}^\mu(x)\ \hat{A}_\mu(x) \tag{11.4}$$

$$\hat{H}_{ext} = e\int d^3x\ \hat{j}^\mu(x)\ V_\mu(\boldsymbol{x})\,. \tag{11.5}$$

Here $\hat{\psi}(x)$ and $\hat{A}_\mu(x)$ denote the fermion and photon field operators and $\hat{j}^\mu$ is the fermionic current operator,

$$\hat{j}^\mu(x) = \hat{\psi}^\dagger(x)\alpha^\nu\hat{\psi}(x)\,. \tag{11.6}$$

For the photon field the covariant quantization scheme has been chosen, in which the two artificial photonic degrees of freedom are eliminated by subsidiary conditions on the states of the Hilbert space [87].

Both the QED Lagrangian $\mathcal{L}$ from which (11.1) is derived and the four current (11.6) are invariant under a gauge transformation of the photon and fermion fields,

$$\hat{A}_\mu(x) \to \hat{A}'_\mu(x) = \hat{A}_\mu(x) + \partial_\mu\Lambda(x) \quad ; \quad \partial_\mu\partial^\mu\Lambda(x) = 0 \tag{11.7}$$

$$\hat{\psi}(x) \to \hat{\psi}'(x) = \exp[-ie\Lambda(x)/c]\ \hat{\psi}(x) \tag{11.8}$$

$$\Longrightarrow\ \mathcal{L}[\hat{\psi}', \hat{A}'] = \mathcal{L}[\hat{\psi}, \hat{A}] \tag{11.9}$$

$$\hat{j}^\mu[\hat{\psi}'] = \hat{j}^\mu[\hat{\psi}]\,. \tag{11.10}$$

This invariance reflects the fact that the covariant quantization does not fix the gauge completely, so that different gauges may be applied in practice. For brevity, Feynman gauge is used in this work. This gauge leads to a particularly simple form of the photon Hamiltonian, i.e. Eq.(11.3), and of the corresponding noninteracting photon propagator,

$$D^0_{\mu\nu}(x-y) = \int \frac{d^4q}{(2\pi)^4}\ e^{-iq\cdot(x-y)}\ D^0_{\mu\nu}(q) \tag{11.11}$$

$$D^0_{\mu\nu}(q) = D^0(q^2)\ g_{\mu\nu} \tag{11.12}$$

$$D^0(q^2) = \frac{-4\pi e^2}{q^2 + i\eta}\,, \tag{11.13}$$

which serves as a retarded interaction in a perturbative treatment of the electron-photon coupling (11.4).

Invariance of $\mathcal{L}$, $\hat{j}^\mu$ and also $\hat{H}$ is found under (static) gauge transformations of the external potential,

$$\begin{aligned} V'_\nu(\boldsymbol{x}) &= V_\nu(\boldsymbol{x}) + \partial_\nu \lambda(\boldsymbol{x}) \quad ; \quad \Delta\lambda(\boldsymbol{x}) = 0 && (11.14)\\ \hat{\psi}'(x) &= \exp[-ie\lambda(\boldsymbol{x})/c]\ \hat{\psi}(x) && (11.15)\\ \Longrightarrow \quad \hat{H}[\hat{\psi}', V'] &= \hat{H}[\hat{\psi}, V] && (11.16)\\ \hat{j}^\mu[\hat{\psi}'] &= \hat{j}^\mu[\hat{\psi}]\,. && (11.17) \end{aligned}$$

As a consequence, the ground state energy and four current of the system,

$$\begin{aligned} E_{tot} &= \langle\Phi|\hat{H}|\Phi\rangle && (11.18)\\ j^\mu(\boldsymbol{x}) &= \langle\Phi|\hat{j}^\mu(x)|\Phi\rangle\,, && (11.19) \end{aligned}$$

are also invariant under the transformation (11.14),(11.15). On the other hand, the ground state $|\Phi\rangle$ itself does depend on the gauge chosen. In the following $|\Phi\rangle$ is always assumed to be nondegenerate, which is generally the case as long as $V_\mu(\boldsymbol{x})$ neither exhibits some spatial symmetry nor vanishes partially.

A generalization of the HK-theorem [11] to relativistic systems was first put forward by Rajagopal and Callaway [10] (see also [18,19]). Utilizing a QED-based Hamiltonian and four current, these authors showed that the ground state energy is a unique functional of the ground state four current. As in the nonrelativistic context this existence proof relies on a *reductio ad absurdum* which makes use of the comparison of energy values obtained with different external potentials. In the framework of QED, however, these energies reflect all features of relativistic quantum field theory, as divergent zero-point energies and ultraviolet-divergencies, but also finite radiative corrections. The same is true for the four current. A rigorous existence proof within QED thus has to be based on renormalized ground state energies and four currents, taking into account the counterterms which keep E_{tot} and j^μ finite. A corresponding argument can be given within a perturbative framework, in which all relevant quantities are expanded in powers of V_μ (for details see [12,45]).

Two statements emerge from the existence proof. On the one hand, there exists a one-to-one correspondence between the class of all those ground states which just differ by gauge transformations and the associated ground state four current. Thus $|\Phi\rangle$ is a unique functional of j^μ as soon as the gauge of $|\Phi\rangle$ is fixed in a unique fashion[2],

$$\left\{|\Phi\rangle \middle| \ |\Phi\rangle \text{ from } V_\mu + \partial_\mu\Lambda\right\} \Longleftrightarrow j^\mu(\boldsymbol{x}) \qquad \Longrightarrow \qquad |\Phi\rangle = |\Phi[j]\rangle\,. \quad (11.20)$$

[2]Recently, in the context of nonrelativistic spin-density functional theory arguments have been given that, under certain conditions, two different magnetic fields can lead to the same

Given the functional $|\Phi[j]\rangle$ one can understand all ground state observables as unique functionals of j^ν, in particular the ground state energy,

$$E_{tot}[j] \;=\; \langle\Phi[j]|\hat{H}|\Phi[j]\rangle\,. \tag{11.21}$$

The second result of the existence proof is a variational principle. Minimization of the energy functional under the subsidiary condition of charge conservation leads to

$$\frac{\delta}{\delta j^\nu(\boldsymbol{r})}\left\{E_{tot}[j] - \mu\int d^3x\; j^0(\boldsymbol{x})\right\} = 0\,. \tag{11.22}$$

Eq.(11.22) opens the possibility to calculate two important quantities of the system without explicit knowledge of the ground state, i.e. the ground state energy and four current.

A direct application of (11.22) with some approximate Thomas-Fermi-type energy functional [15–17], however, misses elementary quantum mechanical features: Due to the continuous density-dependence of these functionals (integer particle numbers are not given any preference), shell structure is not reproduced. One thus resorts to the KS-scheme, which essentially represents a mapping of the interacting many-body problem onto an effective single-particle problem. The starting point for this scheme is the assumption that there exists a noninteracting, relativistic system with the same ground state four current $j^\mu(\boldsymbol{r})$ as the interacting system one is actually interested in. Of course, the external potential $v_s^\mu(\boldsymbol{r})$ of the auxiliary noninteracting system differs from $V^\mu(\boldsymbol{r})$. $v_s^\mu(\boldsymbol{r})$ has to be determined subsequently. The ground state four current j^μ of both systems can then be written in terms of the single-particle spinors ϕ_k of the auxiliary system,

$$j^\mu(\boldsymbol{r}) \;=\; \sum_k \Theta_k\phi_k^\dagger(\boldsymbol{r})\alpha^\mu\phi_k(\boldsymbol{r}) = \Big(n(\boldsymbol{r}), \boldsymbol{j}(\boldsymbol{r})/c\Big) \tag{11.23}$$

$$\Theta_k \;=\; \begin{cases} 0 & \text{for} \quad \epsilon_k \le -mc^2 \\ 1 & \text{for} \quad -mc^2 < \epsilon_k \le \epsilon_F \\ 0 & \text{for} \quad \epsilon_F < \epsilon_k \end{cases}\,, \tag{11.24}$$

where the Fermi level ϵ_F distinguishes occupied from unoccupied auxiliary states. In (11.23) the *no-pair* approximation has already been

ground state [89, 90]. This questions the existence of a unique map between the set of potentials V^μ and the corresponding set of ground states in RDFT (this issue has not been explicitly studied within RDFT up to now). Note, however, that such a unique map is not required for establishing a unique ground state density functional $|\Phi[j]\rangle$ (up to gauge transformations). The existence of $|\Phi[j]\rangle$ only relies on the one-to-one correspondence between $|\Phi\rangle$ and j^μ which can be explicitly proven [45].

utilized, which eliminates the vacuum polarization contributions present in the complete, field theoretical form of j^μ. In the following, the *no-pair* approximation will be consistently used in all relations without further reference. For a detailed discussion of the field theoretical variant of RDFT see [45].

One can then decompose the total ground state energy functional (11.21) as

$$E_{tot} = T_s + E_{ext} + E_H + E_{xc}\,. \tag{11.25}$$

The individual components are defined as follows: T_s represents the kinetic energy of the auxiliary system,

$$T_s \;=\; \sum_k \Theta_k \int d^3r\, \phi_k^\dagger(\boldsymbol{r})\big[-ic\boldsymbol{\alpha}\cdot\boldsymbol{\nabla} + (\beta-1)mc^2\big]\phi_k(\boldsymbol{r})\,, \tag{11.26}$$

E_{ext} is the external potential energy,

$$E_{ext}[j] = e\int d^3r\, j_\mu(\boldsymbol{r})\; V^\mu(\boldsymbol{r})\,, \tag{11.27}$$

and E_H denotes the (direct) Hartree energy,

$$E_H[j] \;=\; \frac{1}{2}\int d^3x \int d^4y\; j^\mu(\boldsymbol{x})\; D^0_{\mu\nu}(x-y)\; j^\nu(\boldsymbol{y})\,. \tag{11.28}$$

E_H has been defined in terms of the complete noninteracting photon propagator (11.11), so that it includes the direct matrix elements of the transverse interaction. E_H may be split into a Coulomb contribution E_H^{C} and a transverse remainder E_H^{T},

$$E_H[j] \;=\; E_H^{\mathrm{C}} + E_H^{\mathrm{T}} \tag{11.29}$$

$$E_H^{\mathrm{C}} \;=\; \frac{e^2}{2}\int d^3r \int d^3r'\, \frac{n(\boldsymbol{r})\; n(\boldsymbol{r}')}{|\boldsymbol{r}-\boldsymbol{r}'|} \tag{11.30}$$

$$E_H^{\mathrm{T}} \;=\; -\frac{e^2}{2c^2}\int d^3r \int d^3r'\, \frac{\boldsymbol{j}(\boldsymbol{r})\cdot\boldsymbol{j}(\boldsymbol{r}')}{|\boldsymbol{r}-\boldsymbol{r}'|}\,. \tag{11.31}$$

Finally, the xc-energy functional E_{xc} is defined by (11.25). It contains all complicated many-body contributions to $E_{tot}[j]$. As the HK argument is also valid for noninteracting systems, for which $E_{tot} = T_s + E_{ext}$, one can state that T_s is a functional of j^μ, $T_s[j]$, in spite of its orbital-dependent form. With this information and E_{ext} and E_H being obvious density functionals also E_{xc} is a functional of j^ν, $E_{xc}[j]$.

The single-particle equations of the auxiliary system are given by

$$\Big\{-ic\boldsymbol{\alpha}\cdot\boldsymbol{\nabla} + (\beta-1)mc^2 + \alpha_\mu v_s^\mu(\boldsymbol{r})\Big\}\phi_k(\boldsymbol{r}) = \epsilon_k\phi_k(\boldsymbol{r})\,. \tag{11.32}$$

The potential v_s^μ can be determined by comparison of the variational equation (11.22) of the interacting system with that for the auxiliary system. One finds that v_s^μ consists of the sum of V^μ, the Hartree potential v_H^μ and the xc-potential v_{xc}^μ,

$$v_s^\mu(\boldsymbol{r}) = eV^\mu(\boldsymbol{r}) + v_H^\mu(\boldsymbol{r}) + v_{xc}^\mu(\boldsymbol{r}) \tag{11.33}$$

$$v_H^\mu(\boldsymbol{r}) = e^2 \int d^3r' \, \frac{j^\mu(\boldsymbol{r}')}{|\boldsymbol{r}-\boldsymbol{r}'|} \tag{11.34}$$

$$v_{xc}^\mu(\boldsymbol{r}) = \frac{\delta E_{xc}[j]}{\delta j_\mu(\boldsymbol{r})} \, . \tag{11.35}$$

The set of equations (11.23)-(11.35) has to be solved selfconsistently as both v_H^μ and v_{xc}^μ depend on j^μ. If the exact $E_{xc}[j]$ is used, the solution provides the exact ground state four current and energy of the interacting system (but not its ground state).

The next task is to construct a suitable approximation for $E_{xc}[j]$. To this aim it is very helpful to decompose E_{xc} into an exchange (x) and a correlation (c) contribution,

$$E_{xc} = E_x + E_c \, . \tag{11.36}$$

The exchange energy is most suitably defined via the standard Fock expression (including the transverse interaction), written in terms of the auxiliary spinors,

$$\begin{aligned} E_x &= -\frac{e^2}{2} \sum_{k,l} \Theta_k \Theta_l \int d^3r \int d^3r' \, \frac{\cos(\omega_{kl}|\boldsymbol{r}-\boldsymbol{r}'|)}{|\boldsymbol{r}-\boldsymbol{r}'|} \\ &\quad \times \phi_k^\dagger(\boldsymbol{r}) \alpha_\mu \phi_l(\boldsymbol{r}) \; \phi_l^\dagger(\boldsymbol{r}') \alpha^\mu \phi_k(\boldsymbol{r}') \end{aligned} \tag{11.37}$$

($\omega_{kl} = |\epsilon_k - \epsilon_l|/c$). In (11.37) E_x has been specified in Feynman gauge. This is the most appropriate choice in the case of the RDFT exchange, as E_x is gauge invariant even in the *no-pair* approximation, in contrast to the transverse Dirac-Fock exchange [25]. The exchange (11.37) provides an exact cancellation of the electronic self-interaction energy contained in E_H, Eq.(11.29). Similar to E_H, the exchange energy can be split into the standard Coulomb component and a transverse remainder,

$$E_x^{\mathrm{C}} = -\frac{e^2}{2} \sum_{k,l} \Theta_k \Theta_l \int d^3r \int d^3r' \, \frac{\phi_k^\dagger(\boldsymbol{r}) \phi_l(\boldsymbol{r}) \; \phi_l^\dagger(\boldsymbol{r}') \phi_k(\boldsymbol{r}')}{|\boldsymbol{r}-\boldsymbol{r}'|} \tag{11.38}$$

$$E_x^{\mathrm{T}} = E_x - E_x^{\mathrm{C}} \, . \tag{11.39}$$

The expressions (11.37)-(11.39) represent implicit functionals of the four current in the same sense as T_s.

Approximate relativistic xc-functionals have been established along the same lines which have been pursued in nonrelativistic DFT. The relativistic local density approximation (RLDA) is defined in complete analogy to the nonrelativistic LDA. In the RLDA one inserts the local density $n(\boldsymbol{r})$ of the actual system into the xc-energy density $e_{xc}^{\mathrm{RHEG}}(n_0)$ of a relativistic homogeneous electron gas (RHEG) with density n_0,

$$E_{xc}^{\mathrm{RLDA}}[n] = \int d^3r\, e_{xc}^{\mathrm{RHEG}}(n(\boldsymbol{r}))\,. \tag{11.40}$$

There is no current-dependence in the RLDA as the spatial components of j^μ vanish for the electron gas. The exchange component of e_{xc}^{RHEG} can be evaluated analytically [18, 19, 91–93]. It can be expressed in terms of the nonrelativistic exchange energy density e_x^{NRHEG} and a relativistic correction factor Φ_x. Separation into its Coulomb and transverse part according to (11.37)-(11.39) yields

$$e_x^{\mathrm{RHEG,C/T}}(n) = e_x^{\mathrm{NRHEG}}(n)\ \Phi_x^{\mathrm{C/T}}(\beta)\,, \tag{11.41}$$

with the correction factors

$$\begin{aligned}
\Phi_x^{\mathrm{C}}(\beta) &= \frac{5}{6} + \frac{1}{3\beta^2} + \frac{2\eta}{3\beta}\mathrm{arsinh}(\beta) - \frac{2\eta^4}{3\beta^4}\ln(\eta) - \frac{1}{2}\left(\frac{\eta}{\beta} - \frac{\mathrm{arsinh}(\beta)}{\beta^2}\right)^2 \\
\Phi_x^{\mathrm{T}}(\beta) &= \frac{1}{6} - \frac{1}{3\beta^2} - \frac{2\eta}{3\beta}\mathrm{arsinh}(\beta) + \frac{2\eta^4}{3\beta^4}\ln(\eta) - \left(\frac{\eta}{\beta} - \frac{\mathrm{arsinh}(\beta)}{\beta^2}\right)^2
\end{aligned}$$

and β being a dimensionless measure of the importance of relativity,

$$\beta = \frac{(3\pi^2 n)^{\frac{1}{3}}}{mc} \qquad ; \qquad \eta = (1+\beta^2)^{\frac{1}{2}}\,. \tag{11.42}$$

For the correlation energy of the RHEG only the ring contributions (or random phase approximation — RPA) have been evaluated, including the full transverse interaction [21]. In contrast to the case of the exchange no closed analytical expression can be given for $e_c^{\mathrm{RHEG,RPA}}$. However, the numerical results for the RPA correction factor can be accurately parameterized as [23]

$$\Phi_c^{\mathrm{RPA}}(\beta) = \frac{1 + a_1\beta^3\ln(\beta) + a_2\beta^4 + a_3(1+\beta^2)^2\beta^4}{1 + b_1\beta^3\ln(\beta) + b_2\beta^4 + b_3[A\ln(\beta) + B]\beta^7}\,, \tag{11.43}$$

which incorporates the analytically known high-density limits of both the relativistic as well as the nonrelativistic RPA. While in the nonrelativistic

case the complete e_c^{NRHEG} approaches the RPA in the high density limit, this is no longer true for the RHEG. In the case of the RHEG the second order exchange term also contributes sizably, as can be concluded from its known high-density limit (for details see [24]). Unfortunately, the complete density-dependence of this expression is not available. In view of this fact E_c^{RLDA} must necessarily be based on the RPA correction factor (11.43). Two forms are possible. On the one hand, one can restrict the relativistic ingredients of E_c^{RLDA} to the known RPA contributions,

$$e_c^{\mathrm{RHEG}}(n) \simeq e_c^{\mathrm{RHEG,RPA}}(n) - e_c^{\mathrm{NRHEG,RPA}}(n) + e_c^{\mathrm{NRHEG}}(n)\,, \qquad (11.44)$$

thus hoping that the relativistic corrections to the second order exchange terms are not relevant in practice [27]. Alternatively, one can use Φ_c^{RPA} with the complete nonrelativistic energy density e_c^{NRHEG},

$$e_c^{\mathrm{RHEG}}(n) \simeq \Phi_c^{\mathrm{RPA}}(n)\, e_c^{\mathrm{NRHEG}}(n)\,, \qquad (11.45)$$

thus hoping that Φ_c^{RPA} is also appropriate for the second order exchange terms [23].

A relativistic extension of the generalized gradient approximation (RGGA) has also been presented in the literature [22, 23]. Focusing first on exchange, the structure of the nonrelativistic GGA functional is

$$E_x^{\mathrm{GGA}} = \int d^3r\; e_x^{\mathrm{NRHEG}}(n)\,\left[1 + g(\xi)\right]\,, \qquad (11.46)$$

with ξ denoting the characteristic dimensionless density gradient,

$$\xi = \left(\frac{\nabla n(\boldsymbol{r})}{2[3\pi^2 n(\boldsymbol{r})]^{1/3} n(\boldsymbol{r})}\right)^2 . \qquad (11.47)$$

The most important ingredient of any GGA is the lowest order gradient term proportional to $(\nabla n)^2$, i.e. the leading term of an expansion of $g(\xi)$ in powers of ξ. The structure of this term is determined by the long-wavelength expansion of the linear response function of the electron gas [11]. The same is true for the relativistic gradient expansion [24]. However, the derivation of the gradient correction turned out to be rather intricate even in the nonrelativistic limit and no result is available in the relativistic case. Consequently, a semi-empirical construction of RGGAs is unavoidable. Neglecting a possible current-dependence, the most appropriate form of the RGGA for E_x is

$$E_x^{\mathrm{RGGA}} = \int d^3r\; e_x^{\mathrm{NRHEG}}(n)\,\left[\Phi_x(\beta) + g(\xi)\Phi_x^{\mathrm{GGA}}(\beta)\right]\,, \qquad (11.48)$$

so that the RGGA consists of the sum of the RLDA and a relativistically corrected gradient term. As one has no first-principles information on Φ_x^{GGA} one makes an ansatz and fits its free coefficients to a suitable data set. In practice a [2/2] Padé approximant provides sufficient flexibility,

$$\Phi_x^{\mathrm{GGA}}(\beta) = \frac{1 + a_1\beta^2 + a_2\beta^4}{1 + b_1\beta^2 + b_2\beta^4}\,. \tag{11.49}$$

Given the success of the Becke GGA [3], the most obvious strategy for the determination of the a_i and b_i is a fit to the exact relativistic exchange energies of atoms [22]. This approach is corroborated by the fact that the resulting $\Phi_x^{\mathrm{GGA}}(\beta)$ depends only weakly on the underlying nonrelativistic $g(\xi)$, as has been verified for the two most frequently used forms of GGAs [3,4].

Even less information is available about gradient corrections in the case of correlation. As explained earlier even the RLDA is not known completely. In view of the limited importance of relativistic contributions to $E_c[n]$ thus a more modest approach to a RGGA seems legitimate, in which only one overall correction factor for the complete GGA is used,

$$E_c^{\mathrm{RGGA}}[n] = \int d^3r\; e_c^{\mathrm{GGA}}(n, (\boldsymbol{\nabla} n)^2, ...)\; \Phi_c^{\mathrm{GGA}}(\beta)\,. \tag{11.50}$$

For the determination of Φ_c^{GGA} the same concept can be applied as in the case of Φ_x^{GGA} [23, 94]. For a given nonrelativistic GGA $e_c^{\mathrm{GGA}}(n, (\boldsymbol{\nabla} n)^2, ...)$ a Padé approximant of the form (11.49) is fitted to a set of relativistic atomic correlation energies. As the exact relativistic E_c of neutral heavy atoms are not available, one resorts to the relativistic MP2 results for the Ne isoelectronic series on the basis of the DCB Hamiltonian [46], which appears to be the most systematic data set for the relativistic E_c in the literature. The inherent limitations of these second order correlation energies are suppressed as much as possible by fitting Φ_c^{GGA} to the ratio between relativistic and nonrelativistic MP2 data.

It seems worthwhile to emphasize that for the functionals (11.40)-(11.50) the single-particle equations (11.25) simplify considerably as the spatial components of v_{xc}^{μ} and thus v_s^{μ} vanish (provided that the spatial components of the external potential also vanish). In fact, lacking a truly current-dependent xc-functional, the RKS equations (11.32) have always been applied with purely density-dependent xc-functionals up to now. On the other hand, in order to deal with magnetic systems a variant of the RKS equations has been introduced [19, 34] which depends on the magnetization density, rather than on $\boldsymbol{j}$. For a review of this form of RDFT the reader is referred to [45].

3. Exact Exchange Functional: Relativistic Optimized Potential Method

As already pointed out, the exact exchange (11.37) represents a functional of j^μ in the same sense as T_s is a functional of the ground state four current. The HK theorem for noninteracting relativistic particles ensures that the auxiliary spinors ϕ_k can be interpreted as unique functionals of j^μ. Given this fact one might ask whether it is possible to evaluate the functional derivative of the expression (11.37) with respect to j^μ? The method which allows the calculation of v_x^μ for such implicit functionals has been established in the nonrelativistic context many years ago [95,96]. A relativistic extension of this optimized potential method (OPM) to E_x^{C} has also been presented [26–28] and recently been generalized to the full RDFT exchange [25]. Using the chain rule for functional differentiation, one can transform the initial derivative (11.35) into derivatives with respect to ϕ_k and ϵ_k,

$$\frac{\delta E_{xc}[\phi_k^{(\dagger)},\epsilon_k]}{\delta j^\mu(\boldsymbol{r})} = \int d^3r' \frac{\delta v_s^\rho(\boldsymbol{r}')}{\delta j^\mu(\boldsymbol{r})} \sum_k \left\{ \int d^3r'' \left[\frac{\delta\phi_k^\dagger(\boldsymbol{r}'')}{\delta v_s^\rho(\boldsymbol{r}')} \frac{\delta E_{xc}}{\delta\phi_k^\dagger(\boldsymbol{r}'')} + c.c. \right] + \frac{\delta\epsilon_k}{\delta v_s^\rho(\boldsymbol{r}')} \frac{\partial E_{xc}}{\partial\epsilon_k} \right\}. \tag{11.51}$$

The required functional derivatives of $\phi_k^{(\dagger)}$ and ϵ_k with respect to v_s^ρ are readily evaluated via first order perturbation theory,

$$\frac{\delta\phi_k^\dagger(\boldsymbol{r})}{\delta v_s^\rho(\boldsymbol{r}')} = -\,\phi_k^\dagger(\boldsymbol{r}')\,\alpha_\rho\,G_k(\boldsymbol{r}',\boldsymbol{r}) \tag{11.52}$$

$$G_k(\boldsymbol{r},\boldsymbol{r}') = \sum_{l\neq k} \frac{\phi_l(\boldsymbol{r})\,\phi_l^\dagger(\boldsymbol{r}')}{\epsilon_l-\epsilon_k} \tag{11.53}$$

$$\frac{\delta\epsilon_k}{\delta v_s^\rho(\boldsymbol{r})} = \phi_k^\dagger(\boldsymbol{r})\,\alpha_\rho\,\phi_k(\boldsymbol{r})\,. \tag{11.54}$$

One can then multiply Eq.(11.51) by the static KS response function,

$$\begin{aligned}\chi_0^{\mu\nu}(\boldsymbol{r},\boldsymbol{r}') &= \frac{\delta j^\mu(\boldsymbol{r})}{\delta v_{s,\nu}(\boldsymbol{r}')} \\ &= -\sum_k \Theta_k\,\phi_k^\dagger(\boldsymbol{r})\,\alpha^\mu G_k(\boldsymbol{r},\boldsymbol{r}')\,\alpha^\nu\phi_k(\boldsymbol{r}') + c.c.\,,\end{aligned} \tag{11.55}$$

to derive an integral equation which allows the determination of v_{xc}^{μ},

$$\begin{aligned}
&\int d^3r'\, \chi_0^{\mu\nu}(\boldsymbol{r},\boldsymbol{r}')\, v_{xc,\nu}(\boldsymbol{r}') \\
= \; & -\sum_k \int d^3r' \left[\phi_k^\dagger(\boldsymbol{r}) \alpha^\mu G_k(\boldsymbol{r},\boldsymbol{r}') \frac{\delta E_{xc}}{\delta \phi_k^\dagger(\boldsymbol{r}')} + c.c. \right] \\
& + \sum_k \phi_k^\dagger(\boldsymbol{r}) \alpha^\mu \phi_k(\boldsymbol{r}) \frac{\partial E_{xc}}{\partial \epsilon_k} . \qquad (11.56)
\end{aligned}$$

In (11.51), (11.53), (11.55) and (11.56) the sums over k are restricted to positive energy states only if the *no-pair* approximation is used. The integral equation (11.56) has to be solved selfconsistently together with the single-particle equations (11.32).

Eq.(11.56) determines the time-like component v_{xc}^0 of the xc-potential only up to an additive constant, as $\chi_0^{\mu 0}$ has to reflect charge conservation, $\int d^3r'\, \chi_0^{\mu 0}(\boldsymbol{r},\boldsymbol{r}') = 0$. This overall normalization may be fixed by the requirement $v_{xc}^0(\boldsymbol{r}) \underset{|\boldsymbol{r}|\to\infty}{\longrightarrow} 0$ in the case of finite systems and by setting the average of v_{xc}^0 in the unit cell to zero in the case of infinite systems.

An important property of the exact exchange is the asymptotic behavior of v_x^0 for finite systems. For the functional (11.37) an analysis of the ROPM integral equation (11.56) yields [25]

$$v_x^0(r) \underset{r\to\infty}{\longrightarrow} -\frac{e^2}{r} . \qquad (11.57)$$

Eq.(11.57) reflects the exact cancellation of the electronic self-interaction contained in v_H^0, Eq.(11.34): An electron which is far away from the other $N-1$ electrons has to experience their net charge, rather than the complete v_H^0 which asymptotically vanishes like Ne^2/r.

The numerical solution of Eq.(11.56) is rather demanding as the evaluation of G_k requires a summation over the complete positive energy spectrum even within the *no-pair* approximation. Consequently an approximate solution of (11.56) which avoids the evaluation of unoccupied states is highly desirable. Such a solution has been suggested by Krieger, Li and Iafrate (KLI) [29] in the nonrelativistic case. The KLI approximation was shown to be both efficient and accurate in the case of the exact exchange [97,98]. The KLI concept is readily extended to the relativistic domain [25,28]. Use of a closure approximation for G_k,

$$G_k(\boldsymbol{r},\boldsymbol{r}') \approx \sum_{l\neq k} \frac{\phi_l(\boldsymbol{r})\phi_l^\dagger(\boldsymbol{r}')}{\Delta\bar{\epsilon}} = \frac{\delta^{(3)}(\boldsymbol{r}-\boldsymbol{r}') - \phi_k(\boldsymbol{r})\phi_k^\dagger(\boldsymbol{r}')}{\Delta\bar{\epsilon}} , \qquad (11.58)$$

in (11.55), (11.56) and neglect of the $\partial E_{xc}/\partial \epsilon_k$-term in (11.56) leads to

$$v^{\mu}_{xc}(\boldsymbol{r}) = \frac{1}{2n(\boldsymbol{r})}\left\{ -g^{\mu}_{\nu} + g^{\mu 0} g_{\nu 0} + \frac{j^{\mu}(\boldsymbol{r}) j_{\nu}(\boldsymbol{r})}{j^{\rho}(\boldsymbol{r}) j_{\rho}(\boldsymbol{r})} \right\}$$
$$\times \left\{ \sum_k \left[\phi^{\dagger}_k(\boldsymbol{r}) \alpha^{\nu} \frac{\delta E_{xc}}{\delta \phi^{\dagger}_k(\boldsymbol{r})} + j^{\nu}_k(\boldsymbol{r})(\Theta_k \overline{v}_k - \overline{e}_k) \right] + c.c. \right\} \quad (11.59)$$

$$\overline{e}_k = \int d^3r\, \phi^{\dagger}_k(\boldsymbol{r}) \frac{\delta E_{xc}}{\delta \phi^{\dagger}_k(\boldsymbol{r})} \quad ; \quad \overline{v}_k = \int d^3r\, j_{k,\lambda}(\boldsymbol{r}) v^{\lambda}_{xc}(\boldsymbol{r}) \quad (11.60)$$

$$j^{\lambda}_k(\boldsymbol{r}) = \phi^{\dagger}_k(\boldsymbol{r}) \alpha^{\lambda} \phi_k(\boldsymbol{r}) . \quad (11.61)$$

One can show that the KLI approximation satisfies the relation (11.57), so that the potential (11.59) is self-interaction free. A careful look at (11.59) reveals that, as a matter of principle, this relation still represents an integral equation for v^{λ}_{xc}. However, the first term on the right-hand side of (11.59) dominates over the contribution from $j^{\nu}_k \Theta_k \overline{v}_k - \overline{e}_k$, so that (11.59) can be easily solved iteratively, either in each cycle of the RKS selfconsistency procedure or in the course of the RKS iteration.

4. RDFT Results for Atoms

4.1 Exchange-only limit: Role of transverse interaction

Until now the ROPM equation (11.56) has only been solved for atoms [25, 27]. Using an ensemble average in the case of open subshells, the set of four coupled equations in (11.56) reduces to one equation for the time-like component of v^{μ}_{xc}. Moreover, as the ensemble average implies a spherical average, only an integral equation with respect to the radial coordinate remains to be solved numerically. This is usually done by recasting the radial integral as a set of linear equations by use of the trapezoidal rule. Utilizing sufficiently dense radial grids, rather high accuracy can be achieved in this way. Results for closed-subshell atoms obtained by complete neglect of correlation (exchange-only limit) are given in Tables 11.1-11.4 and Figs.11.1,11.2.

Table 11.1 lists the ground state energies resulting from three different forms of E_x, the Coulomb limit (11.38), the fully relativistic exchange (11.37) and the weakly relativistic Coulomb-Breit form, in which (11.37) is expanded to first order in ω^2_{kl}. The first question which can be addressed at this point is that of the relation between the x-only ROPM and the standard relativistic Hartree-Fock (RHF) approach. In both schemes the same energy expression is minimized once the treatment of

Table 11.1 Exchange-only ground state energies from ROPM and RHF calculations for closed subshell atoms: Coulomb(C)- and Coulomb-Breit(C+B)-limit in comparison with complete transverse exchange (C+T) [25]. For the RHF approximation the energy difference with respect to the ROPM is given, $\Delta E = E_{tot}(\text{RHF}) - E_{tot}(\text{ROPM})$, providing results from (a) finite differences calculations [99] and (b) a basis set expansion [46] (all energies in mHartree — nuclear model and c as in [46]).

Atom	$-E_{tot}^{C}$ ROPM	ΔE^{C} RHF[a]	ΔE^{C} RHF[b]	$-E_{tot}^{C+B}$ ROPM	ΔE^{C+B} RHF[b]	$-E_{tot}^{C+T}$ ROPM
He	2862	0	0	2862	0	2862
Be	14575	−1		14575		14575
Ne	128690	−2	−2	128674	−2	128674
Mg	199932	−3		199900		199900
Ar	528678	−5	−5	528546	−5	528546
Ca	679704	−6		679513		679513
Zn	1794598	−14		1793838	−12	1793841
Kr	2788849	−13	−12	2787423	−12	2787431
Sr	3178067	−13		3176350		3176360
Pd	5044384	−16		5041074		5041101
Cd	5593299	−20		5589466	−15	5589500
Xe	7446882	−19	−6	7441115	−3	7441179
Ba	8135625	−19		8129091		8129168
Yb	14067621	−48		14053517		14053764
Hg	19648826	−39		19626225	9	19626715
Rn	23601947	−35	−19	23572625	11	23573332
Ra	25028027	−34		24996118		24996912
No	36740625	−57		36685157		36686790

the transverse interaction has been chosen. However, while the RHF procedure provides a free minimization of the x-only energy, the ROPM includes a subsidiary condition, i.e. it restricts the exchange potential to be multiplicative. Consequently the x-only ROPM leads to ground state energies which are higher than their RHF counterparts. However, as Table 11.1 shows the actual differences are very small (note that these differences are absorbed into the RDFT correlation energy). This statement is rigorously verified in the Coulomb limit in which an unambiguous comparison of the finite differences ROPM with finite differences RHF

data [99] is possible. Even for the heaviest atoms the additional energy gain by the nonlocal RHF potential is below 60 mHartree. The energy differences are of the same order of magnitude as those which one finds between finite differences and basis set RHF results [46, 100]. The fact that the Coulomb-Breit RHF energies of the heaviest atoms are above the corresponding ROPM values could thus be interpreted as a basis set deficiency. In addition, the gauge dependence of the CB-RHF data could play a role.

A comparison of the ROPM energies obtained with the three forms of the interaction shows the impact of the transverse exchange. While the size of the Breit contribution is well known from RHF calculations, Table 11.1 also provides results for the retardation corrections to the Breit interaction. For instance, for Radium they amount to 22 eV and even for Xenon one finds 1.8 eV.

The last column of Table 11.1 has been obtained by a fully selfconsistent handling of E_x^{T}. In view of the standard practice in the RHF scheme one might ask whether a first order perturbative treatment of E_x^{T} is sufficient. This question is addressed in Table 11.2 (Note the different nuclear models underlying Tables 11.1 and 11.2). Two perturbative approaches may be distinguished: On the one hand, the complete E_x^{T} can be added *a posteriori*. Alternatively, only the retardation corrections to the Breit interaction (T−B) can be treated perturbatively, while the Coulomb-Breit interaction is included on the selfconsistent level. As Table 11.2 demonstrates the latter procedure gives essentially the same energies as the fully selfconsistent approach. As the T−B-terms are the most time-consuming contributions to E_x^{T}, this scheme suggests itself for practical calculations. On the other hand, a fully perturbative handling of E_x^{T} leads to errors of the order of 1 eV in the case of heavy atoms, so that it depends on the application whether this represents a relevant loss of accuracy, or not.

This result is corroborated by an explicit analysis of the associated exchange potentials. In Fig.11.1 the complete relativistic exchange potential of Mercury including v_x^{T} is compared with the Coulomb-Breit approximation and the pure Coulomb limit as well as the nonrelativistic v_x. It is obvious that the CB-potential follows the exact result closely even for rather small r. On the other hand, the deviations of the Coulomb exchange are as large as the differences between the fully relativistic and the nonrelativistic v_x. For instance, in the region of the L-shell (0.069 Bohr) the transverse exchange contributes 0.9 Hartree and even for the M-shell (0.18 Bohr) one finds 0.1 Hartree. The transverse exchange potential is also visible in the single-particle spectrum, as is illustrated for the case of Mercury in Table 11.3. Even the $5s$-level experiences a 10 mHartree

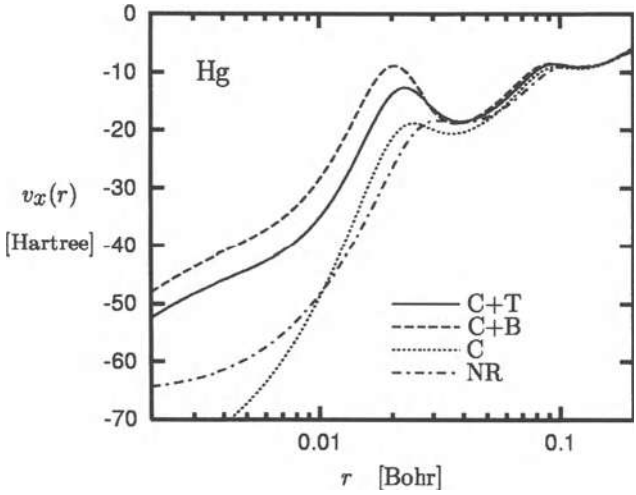

Figure 11.1 ROPM exchange-only potentials for neutral Hg: Selfconsistent Coulomb (C), Coulomb-Breit (C+B) and fully transverse (C+T) results in comparison with nonrelativistic limit (NR). The r-expectation value of the 1s-level is 0.017 Bohr.

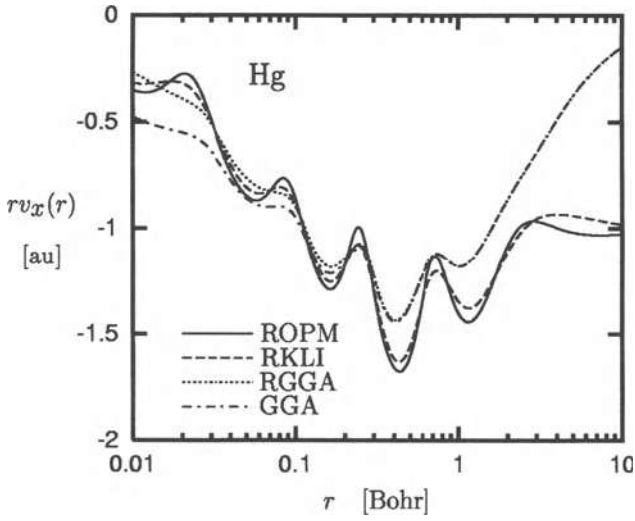

Figure 11.2 Exchange-only potentials for neutral Hg: Exact exchange (ROPM) versus RKLI approximation, relativistic (RGGA) and nonrelativistic B88-GGA.

Table 11.2 Exchange-only ground state energies from ROPM, RKLI, RLDA and PW91-RGGA calculations for closed subshell atoms: In the case of the ROPM the selfconsistent (s) treatment of the complete E_x^{T} (T) is compared with a selfconsistent inclusion of only its Breit (B) limit (together with a first order perturbative (p) evaluation of the beyond Breit contributions (T−B)) as well as a fully perturbative evaluation of E_x^{T} (all energies in mHartree). In all calculations different from Table 11.1 the nuclei were represented by uniformly charged spheres with nuclear radii given by $R_{nuc} = (1.0793A^{1/3} + 0.73587)fm$, A being the atomic mass (weighted by isotopic abundances) taken from Table III.7 of K. Hisaka, et al. (Particle Data Group), Phys. Rev. D 45, Number 11, Part II (1992). The speed of light had been set to $c = 137.0359895$ $a.u.$.

Atom	$-E_{tot}^{\mathrm{C+T}}$	$E_{tot}^{\mathrm{C+T}} - E_{tot}^{\mathrm{C+T}}$[ROPM: s(C+T)]					
	ROPM	ROPM		RKLI	RLDA	RGGA	GGA
s:	C+T	C+B	C	C+T	C+T	C+T	C
p:	—	T−B	T	—	—	—	—
He	2862	0	0	0	138	6	6
Be	14575	0	0	0	351	18	17
Ne	128674	0	0	1	1080	−24	−43
Mg	199900	0	0	1	1408	−1	−37
Ar	528546	0	0	2	2458	41	−111
Ca	679513	0	0	2	2818	26	−195
Zn	1793840	0	1	4	4702	−263	−1146
Kr	2787429	0	2	3	6543	−22	−1683
Sr	3176359	0	2	3	7149	−10	−2014
Pd	5041098	0	5	4	9765	−69	−3953
Cd	5589496	1	6	6	10556	−35	−4537
Xe	7441173	1	10	6	13161	83	−6705
Ba	8129161	1	11	6	14051	58	−7652
Yb	14053750	3	29	11	20888	−894	−17660
Hg	19626705	6	50	10	29161	−257	−27253
Rn	23573354	8	68	9	35207	−9	−35145
Ra	24996946	9	75	9	37395	−22	−38267
No	36687173	16	140	13	56937	−1344	−68097

shift due to the transverse exchange. Only the $5d$ and $6s$ valence levels are unaffected.

Table 11.3 also provides the RHF eigenvalues obtained in the Coulomb limit. Comparison with the corresponding ROPM values reveals substan-

Table 11.3 Exchange-only single particle energies ($-\epsilon_{nlj}$) for neutral Hg from self-consistent ROPM, RHF, RKLI and RGGA calculations, using (i) the complete relativistic exchange-only potential (C+T), (ii) its Coulomb-Breit approximation (C+B), and (iii) its Coulomb (C) limit. The RGGA results have been obtained with the relativistic extension [22] of the B88 GGA [3] (all energies in Hartree).

Level	ROPM			RHF	RKLI	RGGA
	C+T	C+B	C	C	C+T	C+T
$1s1/2$	3036.871	3032.278	3047.431	3074.229	3037.244	3036.453
$2s1/2$	538.444	537.853	540.057	550.251	538.343	538.051
$2p1/2$	516.198	515.546	518.062	526.855	516.083	516.097
$2p3/2$	445.422	445.013	446.683	455.157	445.302	445.276
$3s1/2$	127.956	127.858	128.273	133.113	127.906	127.703
$3p1/2$	117.994	117.885	118.351	122.639	117.966	117.857
$3p3/2$	102.302	102.236	102.537	106.545	102.274	102.152
$3d3/2$	86.069	86.036	86.202	89.437	86.062	85.959
$3d5/2$	82.692	82.665	82.808	86.020	82.687	82.582
$4s1/2$	28.361	28.351	28.428	30.648	28.303	28.037
$4p1/2$	24.090	24.075	24.162	26.124	24.050	23.819
$4p3/2$	20.321	20.315	20.364	22.189	20.269	20.024
$4d3/2$	13.397	13.397	13.412	14.797	13.372	13.151
$4d5/2$	12.689	12.690	12.701	14.053	12.663	12.441
$4f5/2$	3.766	3.770	3.757	4.473	3.764	3.571
$4f7/2$	3.613	3.616	3.603	4.312	3.611	3.417
$5s1/2$	4.394	4.394	4.404	5.103	4.399	4.278
$5p1/2$	3.004	3.002	3.013	3.538	3.004	2.886
$5p3/2$	2.360	2.360	2.364	2.842	2.348	2.219
$5d3/2$	0.507	0.507	0.506	0.650	0.496	0.367
$5d5/2$	0.440	0.441	0.440	0.575	0.430	0.300
$6s1/2$	0.330	0.330	0.330	0.328	0.332	0.222

tial differences, in spite of the similarity of the ROPM and RHF ground state energies. This is not only true for the innermost shells, even the $5d$ energies differ by more than 20%.

In view of the identity of the eigenvalues of the highest occupied KS levels obtained with and without transverse exchange one would expect ionization potentials (IPs) of neutral atoms to be rather insensitive to the inclusion of E_x^{T}. This expectation is confirmed by Table 11.4. A closer

Table 11.4 Exchange-only ionization potentials of neutral atoms calculated from ground state energy differences: For the ROPM the selfconsistent inclusion of the transverse exchange (C+T) is compared with complete neglect of E_x^{T} (C). The RGGA data have been obtained by the relativistic extension of the Becke parameterization [22] (all energies in mHartree).

Atom	ROPM		RKLI	RGGA
	C+T	C	C+T	C+T
Li	196	196	196	179
Na	181	181	181	173
K	147	147	147	143
Rb	139	139	139	137
Cs	127	127	127	127
Fr	132	132	131	132
Be	296	296	295	326
Mg	243	243	243	269
Ca	189	189	189	210
Sr	175	175	175	195
Ba	157	157	157	176
Ra	161	161	161	179
Cu	234	234	232	279
Ag	229	229	228	262
Au	279	280	278	319
Zn	284	284	283	339
Cd	269	269	268	315
Hg	312	313	312	363

look at Table 11.4 also reveals a great similarity of the 6s-eigenvalue of Mercury with the corresponding IP. This feature is not a coincidence but observed for all atoms. In fact, in the nonrelativistic context one can rigorously prove that the eigenvalue of the highest occupied KS level is identical with the IP, if the exact E_{xc} is used [101]. This strict identity is lost in the exchange-only limit considered here. Nevertheless, due to its $-1/r$-dependence, Eq.(11.57), the exact exchange potential dominates v_{xc} in the valence regime, so that even in the x-only limit the highest occupied eigenvalue has to be close to the IP. In other words: The similarity of both quantities is a measure of the degree to which the self-interaction in v_H is canceled by v_x. This cancellation is complete for

the exact exchange, but much less satisfying for the RGGA, as can be extracted from Tables 11.3, 11.4.

On the other hand, the RKLI approximation does provide an accurate treatment of the self-interaction. Both the IPs and the highest occupied eigenvalues are almost identical with their full ROPM counterparts. The $-1/r$-dependence of the RKLI potential, which ensures this behavior, can be explicitly seen in Fig.11.2. The RKLI approximation is also quite accurate in the core region. While it does not completely follow the shell oscillations in the exact v_x, the deviations are much smaller than those of explicit density functionals (compare [102,103]). As a result, the RKLI ground state energies are extremely close to the ROPM data (see Table 11.2). The accuracy of the RKLI approximation thus provides the basis for applications of the exact exchange to more complex systems than atoms.

The exact exchange is an ideal tool to investigate the quality of approximate density functionals. Table 11.2 also contains ground state energies obtained with the RLDA (11.41) and the RGGA (11.48) as well as with the corresponding nonrelativistic GGA (11.46). Two points are immediately obvious. On the one hand, the RLDA underestimates the true ground state energies drastically. In fact, the deviation observed in Table 11.2 is much larger than that found in nonrelativistic DFT. For instance, for Mercury it amounts to 29 Hartree in the relativistic case, but only 13 Hartree in the nonrelativistic limit [30]. This failure mainly originates from the misrepresentation of the transverse exchange [27]. As Table 11.5 shows, atomic E_x^{T} are overestimated by more than 50%, (12 Hartree for Mercury). The RLDA does not account for the relativistic contributions to the exchange functional in a form suitable for finite systems.

On the other hand, the nonrelativistic GGA overestimates ground state energies as much as the RLDA underestimates them. This demonstrates that the relativistic corrections to the exchange functional cannot simply be neglected if one wants to reproduce total energies (or inner shell excitation energies). This leads to the question whether the RGGA provides an accurate account of these corrections? Table 11.2 clearly supports the functional (11.48). The RGGA achieves the same accuracy in the relativistic case as the GGA does in the nonrelativistic limit. The quality of the total RGGA energies is matched by that of the transverse exchange energies (Table 11.5). An improvement is also found for the exchange potential (Fig.11.2) and for the eigenvalues (Table 11.3). The remaining errors reflect the inherent limitations of the semilocal GGA-concept, rather than an inadequate treatment of relativity.

Table 11.5 Transverse exchange energies (E_x^{T}) for closed subshell atoms: Selfconsistent ROPM, RLDA and B88-RGGA results in comparison with perturbative RHF values (Coulomb gauge for E_x^{T} in the case of RHF — all energies in Hartree).

Atom	ROPM	RHF(p)	RLDA	RGGA
He	0.000064	0.000064	0.000147	0.000059
Be	0.00070	0.00070	0.00169	0.00071
Ne	0.0167	0.0166	0.0350	0.0167
Mg	0.0318	0.0318	0.0645	0.0318
Ar	0.132	0.132	0.249	0.132
Ca	0.191	0.191	0.352	0.191
Zn	0.758	0.759	1.318	0.757
Kr	1.417	1.419	2.391	1.415
Sr	1.706	1.710	2.855	1.705
Pd	3.282	3.290	5.331	3.280
Cd	3.797	3.808	6.131	3.796
Xe	5.693	5.711	9.039	5.691
Ba	6.453	6.473	10.197	6.451
Yb	13.842	13.898	21.418	13.837
Hg	22.071	22.168	33.957	22.054
Rn	28.547	28.680	43.979	28.519
Ra	31.006	31.153	47.831	30.971
No	53.313	53.591	84.222	53.101

4.2 Correlation

While a rigorous assessment of the quality of density functionals is possible for the exchange, the situation is more difficult for the correlation functional. For light neutral atoms accurate nonrelativistic correlation energies E_c^{NR} have been extracted by combining variational results for the corresponding two and three electron ions with the experimental IPs for the remaining electrons [104,105] (corrected for relativistic and finite nuclear mass effects). Analogous data for heavy atoms are not available. On the other hand, the overall accuracy of correlation functionals is much lower than that of exchange functionals, so that a more modest reference standard seems to be acceptable. In addition, it is only necessary to judge the quality of the relativistic correction $E_c^{\mathrm{R}} - E_c^{\mathrm{NR}}$ on this basis, rather than the absolute values of the relativistic correlation energy E_c^{R}. As suitable reference standard one can thus use the second order Møller-Plesset

(MP2) results obtained with the Dirac-Coulomb and Dirac-Coulomb-Breit Hamiltonian by Ishikawa and Koc [46], which, to date, appears to be the most systematic set of relativistic atomic correlation energies in the literature. On the present level of accuracy neither the different handling of transverse and vacuum corrections in RDFT and the DCB scheme nor the conceptual difference between the density functional and the conventional correlation energy are relevant. Corresponding numbers

Table 11.6 Correlation energies of neutral noble gas atoms: LDA [106], PW91-GGA [4], MP2 [46] versus exact results [104,105]. Both the nonrelativistic values E_c^{NR} and the difference between the relativistic energies (including transverse corrections) and E_c^{NR} are given. The entry GGA under $E_c^{\mathrm{NR}} - E_c^{\mathrm{R}}$ corresponds to relativistic RKS calculations with the nonrelativistic GGA functional (all energies in mHartree).

Atom	$-E_c^{\mathrm{NR}}$				$E_c^{\mathrm{NR}} - E_c^{\mathrm{R}}$			
	LDA	GGA	MP2	exact	RLDA	GGA	RGGA	RMP2
He	113	46	37	42	0	0	0	0
Ne	746	382	383	390	0	0	2	2
Ar	1431	771	697	722	3	0	8	9
Kr	3284	1914	1835		27	2	47	52
Xe	5199	3149	2921		92	4	141	146
Rn	9027	5706	5392		378	18	502	548

for neutral noble gas atoms are given in Table 11.6, separating the energies obtained with completely nonrelativistic calculations (E_c^{NR}) from the relativistic contributions ($E_c^{\mathrm{R}} - E_c^{\mathrm{NR}}$). One first of all observes the well-known overestimation of nonrelativistic atomic correlation energies by the LDA. The GGA, on the other hand, is fairly accurate. This is not only true for light atoms, but also for heavy elements, if one takes into account that the MP2 values underestimate the exact E_c. If the nonrelativistic GGA is used in relativistic KS calculations, it gives essentially the same values as in fully nonrelativistic calculations, so that the GGA misses the substantial relativistic correction found in the MP2 numbers. Consequently even correlation functionals have to be modified for use in RDFT. However, the RLDA clearly underestimates the correct $E_c^{\mathrm{R}} - E_c^{\mathrm{NR}}$. On the other hand, the RGGA gives a rather accurate account of these corrections. In fact, the quality of the relativistic contribution obtained by the RGGA is much higher than the overall accuracy of the GGA, thus supporting the rather crude approach (11.50).

It seems worth to point out that the neutral atoms listed in Table 11.6 do not belong to the data base to which the relativistic correction factor Φ_c^{GGA} has been fitted.

5. Construction of Relativistic Normconserving Pseudopotentials

5.1 Relativistic Troullier-Martins scheme

The application of PPs is particularly attractive for very heavy elements, even though rather large valence spaces may have to be used. In the framework of DFT usually normconserving PPs are applied. These PPs are nonlocal with respect to the angular coordinates, but local with respect to the radial coordinate r. For each angular momentum l among the valence levels a separate radial PP $v_{\mathrm{ps},l}(r)$ is constructed in such a way that the resulting lowest eigenstate is identical with the corresponding AE valence state for all r larger than some cut-off radius $r_{c,l}$ [107, 108]. In addition, all states with angular momentum higher than some maximum $l_{\max}$ are assumed to experience a common PP v_{loc}. The standard form of normconserving PPs thus is

$$\begin{aligned}\langle \boldsymbol{r}|\hat{v}_{\mathrm{ps}}|\boldsymbol{r}'\rangle &= v_{\mathrm{loc}}(r)\delta^{(3)}(\boldsymbol{r}-\boldsymbol{r}') \\ &\quad + \frac{\delta(r-r')}{r^2}\sum_{l=0}^{l_{\max}}\delta v_l(r)\sum_{m=-l}^{l} Y_{lm}(\Omega)Y^*_{lm}(\Omega') \qquad (11.62)\\ \delta v_l(r) &= v_{\mathrm{ps},l}(r) - v_{\mathrm{loc}}(r)\,. \qquad (11.63)\end{aligned}$$

Typically, one of the $v_{\mathrm{ps},l}$ is used as local potential v_{loc}.

For heavy atoms the construction of PPs has to be based on RDFT. As a matter of principle, relativity comes into play at three stages. First of all, the AE states which determine the form of the PP have to be evaluated by a relativistic KS calculation for the atom of interest. Utilizing an ensemble average in the case of open subshells, the atomic RKS spinors can be written as

$$\begin{aligned}\phi_{nljm}(\boldsymbol{r}) &= \frac{1}{r}\begin{pmatrix} a_{nlj}(r)\,\Omega_{jlm}(\theta,\varphi) \\ i\,b_{nlj}(r)\,\Omega_{j\bar{l}m}(\theta,\varphi)\end{pmatrix} \qquad (11.64)\\ \Omega_{jlm}(\theta,\varphi) &= \sum_{\sigma=\pm 1/2}(l\,m-\sigma,\tfrac{1}{2}\sigma|j\,m)\,Y_{l,m-\sigma}(\theta,\varphi)\,\chi_\sigma\,, \qquad (11.65)\end{aligned}$$

where $(l\,m_l, s\,\sigma|j\,m)$ denotes the Clebsh-Gordan coefficients and χ_σ the two-component Pauli spinors ($\bar{l} = 2j - l$) [109]. The radial spinors a_{nlj} and b_{nlj} are obtained by the solution of the radial form of the RKS

equations (11.32)-(11.35),

$$c\left(\partial_r + \frac{\kappa}{r}\right)a_{nlj}(r) = \left(2mc^2 - v_s(r) + \epsilon_{nlj}\right)b_{nlj}(r) \quad (11.66)$$

$$c\left(\partial_r - \frac{\kappa}{r}\right)b_{nlj}(r) = \left(v_s(r) - \epsilon_{nlj}\right)a_{nlj}(r)\,, \quad (11.67)$$

with

$$v_s(r) = -\frac{Ze^2}{r} + v_H(r) + v_{xc}(r) \quad (11.68)$$

$$v_H(r) = 4\pi e^2\left\{\frac{1}{r}\int_0^r x^2 dx\, n(x) + \int_r^\infty x dx\, n(x)\right\} \quad (11.69)$$

$$n(r) = \sum_{nlj}\Theta_{nlj}\frac{a_{nlj}(r)^2 + b_{nlj}(r)^2}{4\pi r^2}\,, \quad (11.70)$$

and Θ_{nlj} being the occupation of the subshell nlj [$\kappa = -2(j-l)(j+1/2)$].

In addition to the AE calculation, the scheme which generates the radial PPs from the AE information may take into account relativistic corrections. For this second step of the PP construction a number of different strategies have been suggested [48, 107, 108, 110–112], which also differ in their handling of relativity. Among these approaches the inherently nonrelativistic procedure of Troullier and Martins [48] (TM) seems to be most widely used at present. A relativistic variant of the TM scheme has also been introduced recently [47]. In this scheme the large component of the pseudoorbital (PO), $a_{\mathrm{ps},lj}$, is required to be identical with its AE counterpart in the valence region $r > r_{\mathrm{c},l}$. In addition, $a_{\mathrm{ps},lj}$ is required to be nodeless in the core region $r < r_{\mathrm{c},l}$, which is guaranteed by a suitable ansatz,

$$a_{\mathrm{ps},lj}(r) = \begin{cases} a_{nlj}(r) & \text{for } r > r_{\mathrm{c},l} \\ r^{l+1}\exp[p(r)] & \text{for } r \le r_{\mathrm{c},l} \end{cases} \quad (11.71)$$

$$p(r) = \sum_{i=0}^{6} c_{2i} r^{2i}\,. \quad (11.72)$$

The associated small component $b_{\mathrm{ps},lj}$ and the potential $v^{\mathrm{sc}}_{\mathrm{ps},lj}$ for which $a_{\mathrm{ps},lj}$ represents an eigenstate (the so-called screened PP) are obtained from an analysis of the radial equations (11.66),(11.67). In contrast to the nonrelativistic Schrödinger equation, Eqs.(11.66),(11.67) do not allow to express the total potential directly in terms of the radial spinor a_{nlj}. However, one can utilize the fact that for the valence states the relativistic

corrections are comparatively small, so that a first order expansion of $v^{\rm sc}_{{\rm ps},lj}$ in $1/c^2$ is legitimate. This yields [47]

$$v^{\rm sc}_{{\rm ps},lj} = \begin{cases} v_s & \text{for } r > r_{{\rm c},l} \\ v^{\rm sc,nr}_{{\rm ps},lj} + \delta v_{lj} & \text{for } r \le r_{{\rm c},l} \end{cases} \tag{11.73}$$

$$v^{\rm sc,nr}_{{\rm ps},lj} = \epsilon_{nlj} + \frac{l+1}{r}\frac{p'}{m} + \frac{p'' + (p')^2}{2m} \tag{11.74}$$

$$\delta v_{lj} = \frac{(v^{\rm sc,nr}_{{\rm ps},lj} - \epsilon_{nlj})^2}{2mc^2} + \frac{(v^{\rm sc,nr}_{{\rm ps},lj})'}{4m^2c^2}\left(\frac{a'_{{\rm ps},lj}}{a_{{\rm ps},lj}} + \frac{\kappa}{r}\right) \tag{11.75}$$

$$b_{{\rm ps},lj}(r) = \begin{cases} b_{nlj}(r) & \text{for } r > r_{{\rm c},l} \\ \dfrac{c[(l+1+\kappa)/r + p'(r)]a_{{\rm ps},lj}(r)}{2mc^2 - v^{\rm sc}_{{\rm ps},lj}(r) + \epsilon_{nlj}} & \text{for } r \le r_{{\rm c},l} \end{cases} \tag{11.76}$$

where the primes denote derivatives with respect to r. The coefficients c_{2i} are determined by requiring continuity of $a_{{\rm ps},lj}$ and its first four derivatives at the cutoff radius $r_{{\rm c},l}$, a smooth PP at the origin, $(v^{\rm sc,nr}_{{\rm ps},lj})''(0) = 0$, as well as proper normalization,

$$\int_0^{r_{\rm c}} dr\,\left[a_{nlj}(r)^2 + b_{nlj}(r)^2\right] = \int_0^{r_{\rm c}} dr\,\left[a_{{\rm ps},lj}(r)^2 + b_{{\rm ps},lj}(r)^2\right]. \tag{11.77}$$

At this point one has constructed the potential $v^{\rm sc}_{{\rm ps},lj}$ whose lowest eigenstate is the PO. However, $v^{\rm sc}_{{\rm ps},lj}$ cannot be used as external potential in a selfconsistent molecular calculation as in this case the interaction among the valence electrons would be included twice. The valence-valence interaction thus has to be subtracted from $v^{\rm sc}_{{\rm ps},lj}$ in order to obtain the final radial PP. This is easily possible for the Hartree component in $v^{\rm sc}_{{\rm ps},lj}$ as the linearity of v_H, Eq.(11.69), in n allows an exact decomposition into a valence and a core part. The situation is not as simple in the case of the xc-potential which is nonlinear in n. For light atoms often linear unscreening is sufficient in which the nonlinearity of the xc-functional is neglected,

$$v_{{\rm ps},lj}(r) = v^{\rm sc}_{{\rm ps},lj}(r) - v_H([n_{\rm v,ps}];r) - v_{xc}([n_{\rm v,ps}];r) \tag{11.78}$$

$$n_{\rm v,ps}(r) = \sum_{\rm val.orb.} \Theta_{nlj}\frac{a_{{\rm ps},lj}(r)^2 + b_{{\rm ps},lj}(r)^2}{4\pi r^2}. \tag{11.79}$$

On the other hand, for heavier elements the overlap between the valence density $n_{\rm v,ps}$ and the core density is often too large to be completely ignored. In this case one can resort to nonlinear core corrections (nlccs) in

the unscreening procedure [113]. In this scheme essentially the complete $v_{xc}([n];r)$ is subtracted from the screened PP. As a consequence, the atomic core density n_c has to be added to the molecular valence density, when evaluating the molecular v_{xc}. However, in order to avoid the use of basis functions for the core states and/or dense grids for numerical integrations over the core region, n_c is usually smoothened in the inner core regime $r < r_{\rm nlcc} < r_{c,l}$, i.e. for all those r for which the valence density vanishes, e.g.

$$v_{{\rm ps},lj}(r) = v^{\rm sc}_{{\rm ps},lj}(r) - v_H([n_{\rm v,ps}];r) - v_{xc}([n_{\rm c,ps}+n_{\rm v,ps}];r) \quad (11.80)$$

$$n_{\rm c,ps}(r) = \begin{cases} n_0 + \sum_{i=3}^{6} n_i r^i & \text{for} \quad r < r_{\rm nlcc} \\ n_c(r) & \text{for} \quad r \geq r_{\rm nlcc} \end{cases} . \quad (11.81)$$

The n_i are obtained by requiring continuity of $n_{\rm c,ps}$ and its derivatives at the truncation point $r_{\rm nlcc}$.

The relativistic TM procedure yields lj-dependent radial PPs. This points at the fact that a relativistic treatment may also be required in the application of the PP. In this case the lj-dependent radial PPs have to be combined with projection operators which project on states with good l and j, rather than the projection on l only shown in (11.62). However, while the core states directly experience the relativistic effects, the pseudo valence states and potentials are in most cases only indirectly affected via the orthogonality requirement. Thus, as long as the spin-orbit splitting of the valence states does not play an important role in the bonding mechanism one can rely on the l-dependent PP (11.62), using a j-average of the $v_{{\rm ps},lj}$ [107],

$$v_{{\rm ps},l}(r) = \sum_{j=l\pm 1/2} \frac{2j+1}{4l+2} v_{{\rm ps},lj}(r) . \quad (11.82)$$

While in the case of heavy elements a relativistic treatment of the AE problem is the standard in all PP schemes (at least on the scalar relativistic level), relativity is often neglected in the actual construction of $v_{{\rm ps},l}$. However, the PPs resulting from the relativistic TM procedure (11.73) can be different from those generated with the nonrelativistic TM scheme, even if the j-average (11.82) is applied. This is demonstrated in Fig.11.3 for the case of Uranium. For this example a particularly large valence space has been chosen, including the $5s-5f$ electrons. As cut-off radii 0.65, 0.70, 0.82 and 1.00 Bohr have been used for the s-, p-, d- and f-PPs, respectively. In view of the small core nlccs have been neglected.

This PP first of all illustrates the fact that for heavy elements often more than one valence state with a given l has to be included in the valence space. As a consequence one has the choice which of the states

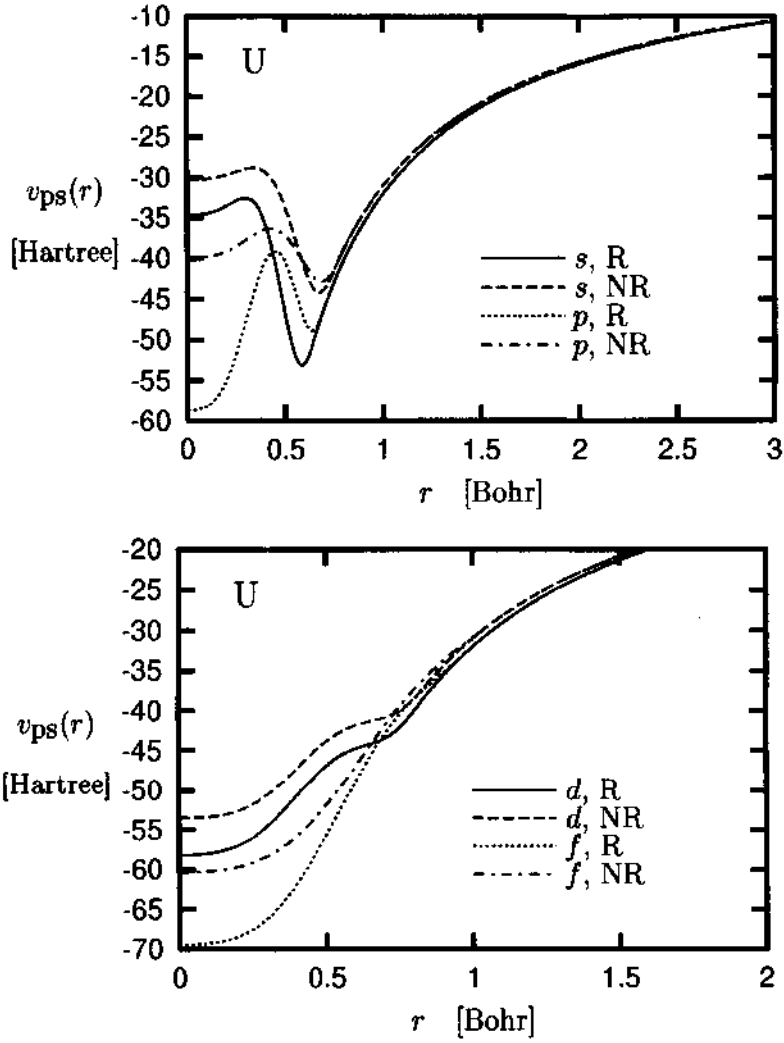

Figure 11.3 TM pseudopotentials for Uranium: Relativistic (R) versus nonrelativistic (NR) PPs obtained with the LDA.

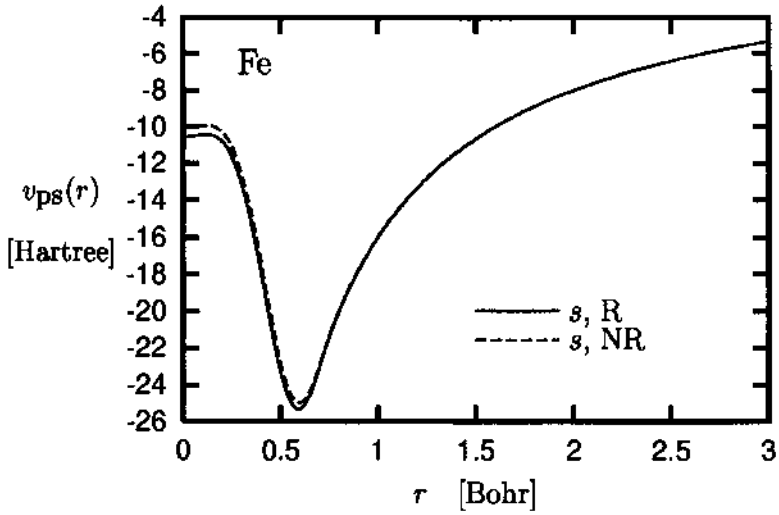

Figure 11.4 TM pseudopotentials for Iron: Relativistic (R) versus nonrelativistic (NR) s-PP obtained with LDA.

is used for the construction of the PP for angular momentum l. The standard choice would be the energetically lowest state, i.e. for the s-PP of Uranium one would utilize the $5s$-level. This necessarily leads to deviations of the $6s$- and $7s$-POs from their AE counterparts in the valence regime, as the $6s$- and $7s$-POs have to be orthogonal to the $5s$-PO. However, the most weakly bound orbital is most important for molecular bonding, so that it seems advantageous to use the energetically highest occupied valence state for the construction of the corresponding PP [47]. In the present case the s-PP has thus been generated from the $7s$-level, requiring the corresponding PO to have two nodes for r >0.65 Bohr. The resulting PP has two energetically lower eigenstates, which, in the valence region, are very close to the AE $5s$- and $6s$-orbitals.

In Fig.11.3 both the PPs resulting from the relativistic TM procedure as well as those obtained from the nonrelativistic TM scheme (with relativistic AE input) are shown. The differences between both approaches are not only sizable for the s-PP (as one might have expected), but also for the f-PP generated from the $5f$-levels. For heavy elements as Uranium obviously a relativistic PP construction is mandatory, even if one applies a j-average. However, relativistic corrections also show up for much lighter elements, as is demonstrated for Iron in Fig.11.4. Of course, the differences between relativistic and nonrelativistic PPs are not huge

for $3d$ elements. Nevertheless, a shift of roughly 100 mHartree in the M-shell regime (0.8 Bohr) is visible in the resulting molecular spectra.

5.2 Exact exchange

The application of PPs is also possible for orbital-dependent xc-functionals as the exact exchange. In fact, the increased computational demands of ROPM calculations (compared to RLDA or RGGA calculations) suggest to resort to PPs even for systems of modest size. The basic scheme for the PP construction outlined in Section 5.1 can equally well be used for orbital-dependent xc-functionals. In this case both the AE xc-potential $v_{xc}[n]$ and the unscreening potential $v_{xc}[n_{\mathrm{v,ps}}]$ have to be calculated by solution of the radial ROPM equation (for its explicit form see [25]). When applied to the exact exchange, however, this straightforward approach leads to spurious long-range components in the final PPs [114,115]. The origin of this feature is the nonlocality of the Fock expression [116]. Due to the integral structure of Eqs.(11.37),(11.38) the form of the orbitals in the core region affects the exchange potential in the valence region via the right-hand side of the ROPM equation (11.56). As a consequence, the core orbitals contribute to the asymptotic behavior of the AE exchange potential and thus to that of v_s and $v^{\mathrm{sc}}_{\mathrm{ps},lj}$ (at least, to a certain extent). On the other hand, the core orbitals are not present in the calculation of $v_{xc}[n_{\mathrm{v,ps}}]$. The asymptotic forms of $v^{\mathrm{sc}}_{\mathrm{ps},lj}$ and $v_{xc}[n_{\mathrm{v,ps}}]$ therefore do not match completely which generates a spurious tail in the unscreened PP (11.78).

These artificial long-range components in the PPs can be eliminated by resorting to a selfconsistent PP construction on the basis of the relativistic TM procedure [116]. In this scheme the strict identity of the POs with the AE orbitals in the valence regime is given up in favor of the correct long-range behavior of the final PP. On the other hand, the identity of the corresponding eigenvalues is kept, so that the POs remain extremely close to the AE orbitals. The scheme starts with a standard TM PP generation, using the AE orbitals, eigenvalues and potential v_s^{AE} as reference quantities. The resulting POs then allow the definition of a new, modified reference potential,

$$\begin{aligned} v_s^{\mathrm{mod}}(r) &= v_s^{\mathrm{AE}}(r) - v_H([n_{\mathrm{v}}^{\mathrm{AE}}], r) - v_{xc}([n_{\mathrm{c}}^{\mathrm{AE}} + n_{\mathrm{v}}^{\mathrm{AE}}], r) \\ &\quad + v_H([n_{\mathrm{v,ps}}], r) + v_{xc}([n_{\mathrm{v,ps}}], r)\,. \end{aligned} \tag{11.83}$$

The construction (11.83) is motivated by the fact that in the asymptotic regime v_s^{AE} is identical to $v_{xc}[n_{\mathrm{c}}^{\mathrm{AE}} + n_{\mathrm{v}}^{\mathrm{AE}}]$, as the nuclear and the Hartree component in v_s^{AE} cancel each other up to contributions which decay exponentially. Thus in v_s^{mod} the asymptotic behavior of the AE potential

is substituted by that of $v_{xc}[n_{\mathrm{v,ps}}]$. In the valence regime the unscreened PP emerging from v_s^{mod} is given by $v_s^{\mathrm{mod}} - v_H[n_{\mathrm{v,ps}}] - v_{xc}[n_{\mathrm{v,ps}}]$. If the eigenstates of v_s^{AE} and v_s^{mod} were identical in the asymptotic regime this unscreened PP would show a clean ionic behavior. However, the eigenstates do not agree completely, so that (11.83) is only the starting point for an iterative scheme.

A complete set of modified reference quantities consistent with v_s^{mod} is obtained by inward integration of the radial RKS equations (11.66), (11.67), using the AE eigenvalues to set up the asymptotic boundary conditions and insisting on the correct normalization in the valence regime,

$$\int_{r_{c,l}}^{\infty} dr \left[a_{\mathrm{ps},lj}^{\mathrm{mod}}(r)^2 + b_{\mathrm{ps},lj}^{\mathrm{mod}}(r)^2\right] = \int_{r_{c,l}}^{\infty} dr \left[a_{nlj}^{\mathrm{AE}}(r)^2 + b_{nlj}^{\mathrm{AE}}(r)^2\right]. \quad (11.84)$$

Due to these conditions $a_{\mathrm{ps},lj}^{\mathrm{mod}}$ and $b_{\mathrm{ps},lj}^{\mathrm{mod}}$ are almost indistinguishable from a_{nlj}^{AE} and b_{nlj}^{AE} for $r > r_{c,l}$. As the TM procedure only uses the reference quantities in the valence regime, the form of v_s^{mod} and the spinors $a_{\mathrm{ps},lj}^{\mathrm{mod}}$, $b_{\mathrm{ps},lj}^{\mathrm{mod}}$ in the core region is irrelevant. One can thus apply the TM scheme to the modified reference quantities which yields new POs and allows the construction of a new reference potential via (11.83). The complete procedure can be iterated until selfconsistency is achieved. The final PP then has the correct long-range behavior.

For light atoms these PPs lead to rather accurate molecular results even without inclusion of nlccs [116]. This is demonstrated in Tables 11.7 and 11.8 in which PP results for the spectroscopic constants of a number of first and second row diatomic molecules are compared with the corresponding AE numbers. One finds average errors of about 0.01 Bohr for bond lengths, 0.05 eV for dissociation energies and 10 cm^{-1} for vibrational frequencies.

PP calculations with the exact exchange also allow an examination of the quality of the LDA and GGA exchange potentials for more complex systems than atoms. An illustration is given in Fig.11.5 which shows the valence exchange potential of bulk Aluminum. While the LDA roughly follows the exact potential, it is obvious from Fig.11.5 that the inclusion of gradient terms does not improve the exchange potential, even if one ignores the spurious peaks in the GGA potential close to the atomic sites. On the other hand, the KLI approximation is rather close to the exact v_x, although it does not quite reach the percentage accuracy observed for atoms.

Corresponding results for heavy elements are not yet available. However, the atomic ROPM results with the exact exchange do allow an investigation of the importance of transverse corrections for the PPs of

Table 11.7 Bond length R_e, dissociation energy D_e (including zero-point energy) and harmonic frequency ω_e of first row diatomic molecules: PP versus AE results obtained with the exact exchange [116].

	mode	R_e [Bohr]	D_e [eV]	ω_e [cm^{-1}]
Li_2	AE	5.266	0.168	338
	PP	5.257	0.171	337
B_2	AE	3.068	0.608	972
	PP	3.063	0.654	972
C_2	AE	2.332	0.281	1933
	PP	2.323	0.379	1939
N_2	AE	2.011	4.972	2736
	PP	2.003	5.142	2749
O_2	AE	2.184	1.441	1981
	PP	2.182	1.466	1971
F_2	AE	2.496	−1.607	1283
	PP	2.498	−1.641	1281
LiH	AE	3.037	1.483	1427
	PP	3.037	1.461	1393
FH	AE	1.694	4.203	4501
	PP	1.694	4.163	4479
CO	AE	2.080	7.530	2444
	PP	2.071	7.692	2456
aver. dev.	PP	0.005	0.067	11

heavy elements. This question is addressed in Fig.11.6 in which two relativistic s-PPs for Uranium are shown, the first obtained in the Coulomb limit, the second with inclusion of the complete transverse interaction. The same valence space as for the LDA has been used (see Section 5.1). The deviations between the two PPs are obvious. While the substantial differences observed for $r < 0.5$ Bohr have only limited impact on molecular results, the transverse exchange still contributes about 420 mHartree

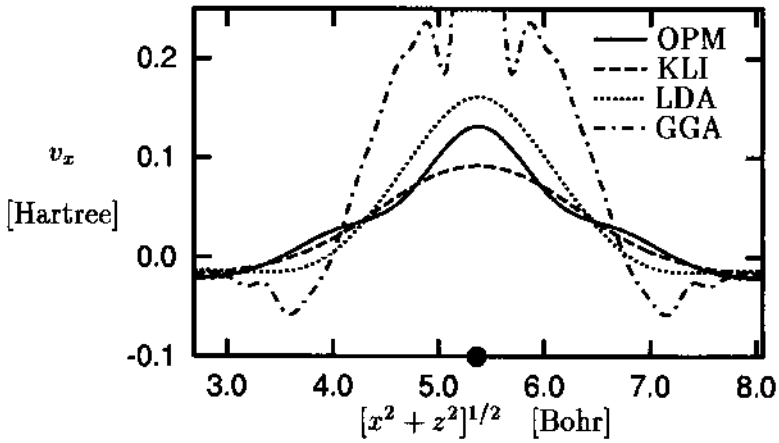

Figure 11.5 Exchange potential of fcc Aluminum in [110] direction: Full OPM versus KLI approximation, LDA and PW91-GGA (• = the position of atom). All results have been obtained by plane-wave pseudopotential calculations (E_{cut} =100Ryd, 44 special k-points). For the OPM calculation 750 states per k-point have been used in G_k.

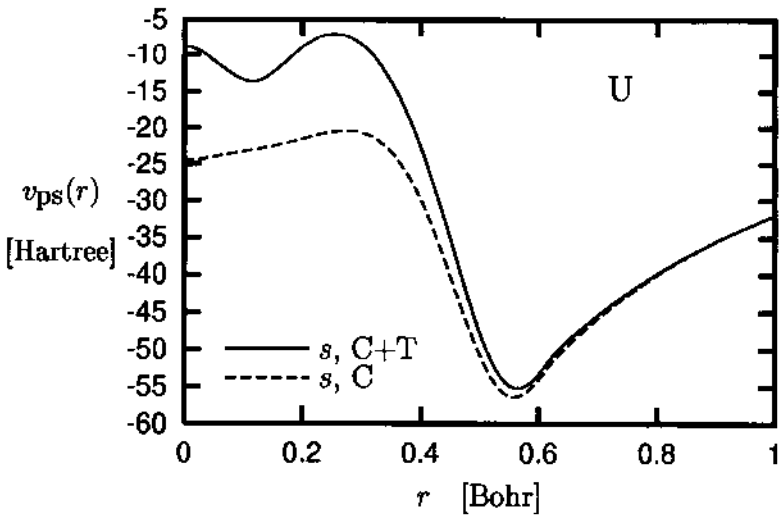

Figure 11.6 TM pseudopotential for $l = 0$ obtained for Uranium with exact exchange: Complete relativistic exchange (C+T) versus Coulomb (C) limit.

Table 11.8 As Table 11.7 for second row dimers.

	mode	R_e [Bohr]	D_e [eV]	ω_e [cm^{-1}]
Na_2	AE	6.050	−0.034	155
	PP	6.011	−0.016	155
Al_2	AE	4.801	0.397	313
	PP	4.826	0.375	311
Si_2	AE	4.184	1.786	575
	PP	4.184	1.790	576
P_2	AE	3.492	1.614	918
	PP	3.493	1.598	913
S_2	AE	3.514	2.154	821
	PP	3.515	2.175	822
Cl_2	AE	3.727	0.715	613
	PP	3.729	0.709	615
aver. dev.	PP	0.011	0.015	2

at r =0.7 Bohr and 25 mHartree at r =1.0 Bohr. Consequently one would expect the transverse exchange to be visible in molecular spectra.

6. Illustrative Results for Molecules

On the basis of RDFT a large variety of molecules have been studied in the literature [49–63]). A review of this vast body of work is beyond the scope of this work. Rather this Section focuses on a few illustrative applications which highlight some of the issues discussed in Sections 2.-5..

The first question which will be addressed is that of the importance of relativistic corrections to the xc-functional for molecular bonding. As emphasized in Section 4., the necessity to include relativistic corrections in the xc-functional is obvious in the case of heavy atoms. On the other hand, relativity mainly affects the innermost electrons, so that one would expect molecular ground state properties to be rather insensitive to relativistic corrections in the xc-functional. This aspect has been investigated both for noble metal compounds [117, 118] and for metallic Gold

and Platinum [23]. Prototype results for Cu_2 and Au_2 are given in Table 11.9. Three calculations are compared which only differ by the handling

Table 11.9 Spectroscopic constants of noble metal dimers: LDA and BP86-GGA [2,3] versus BP86-RGGA (*a*: [47], *b*: [117], *c*: [119]).

		Cu_2			Au_2		
mode	E_{xc}	R_e [Bohr]	D_e [eV]	ω_e [cm^{-1}]	R_e [Bohr]	D_e [eV]	ω_e [cm^{-1}]
PP	LDA^a	4.04	2.83	304	4.61	3.02	198
AE	LDA^{b,c}	4.05	2.86	307	4.64	3.00	196
AE	GGA^b	4.16	2.28	287	4.75	2.30	179
AE	RGGA^b	4.17	2.27	285	4.76	2.27	177
expt.		4.20	2.05	265	4.67	2.30	191

of the xc-effects. In the first calculation the nonrelativistic LDA was applied, the other two rely on a GGA-form, either without or with relativistic corrections. It turns out that even for Au, which usually exhibits the effects of relativity most clearly [8], the impact of the correction factors $\Phi_{x/c}$ on the molecular binding properties is very small. The dissociation energy of Au_2, the quantity which is affected most, changes by 0.03 eV when going from the GGA to the RGGA. Quite generally, the differences are smaller than those resulting from use of two different high-quality basis sets. They are also smaller than those originating from application of different parameterizations of the GGA functional. The same observation is made for solids (Table 11.10). Nevertheless, although the relativistic corrections to the xc-functional turn out to be irrelevant for molecular properties (at least on the present level of accuracy), it seems worthwhile to point out that the application of the RGGA is by no means more difficult or less efficient than that of the corresponding nonrelativistic GGA. There is thus no technical reason for relying on the cancellation of the large errors in the individual ground state energies exhibited in Table 11.2, when calculating energy surfaces.

The second aspect considered here is the quality of the relativistic PPs introduced in Section 5.. Table 11.9 allows a direct comparison of PP and AE results on the basis of the LDA. The excellent agreement is obvious. It seems worthwhile to emphasize that rather large valence spaces have been chosen for the present PP calculation, including the complete M-shell in the case of Copper and the $5s$-$5f$ states for Gold.

Table 11.10 Lattice constant a_0 and cohesive energy E_{coh} of Au and Pt obtained from LAPW calculations with relativistic and nonrelativistic LDA and PW91-GGA [23] in comparison to experiment [120,121].

	Au		Pt	
	a_0 [Bohr]	$-E_{coh}$ [eV]	a_0 [Bohr]	$-E_{coh}$ [eV]
LDA	7.68	4.12	7.36	6.76
RLDA	7.68	4.09	7.37	6.73
GGA	7.87	2.91	7.51	5.34
RGGA	7.88	2.89	7.52	5.30
expt.	7.67	3.78	7.40	5.85

While reasonably accurate spectroscopic constants are already found if just the actual valence states $(n-1)d$ and ns are taken into account, fully converged PP results require the dynamic treatment of the semicore $(n-1)s$ level [47].

As one finds only a very limited effect of the relativistic corrections to the xc-functional in the case of Gold compounds one may ask whether they are more important if superheavy elements are involved. Corresponding results for the ground state of $RfCl_4$ (tetrahedral symmetry) are given in Table 11.11. Both all-electron RLDA and RGGA results

Table 11.11 Spectroscopic constants of $RfCl_4$: PP versus AE [122] results and RHF data [123].

Mode	E_{xc}	R_e [Bohr]	D_e [eV]
AE	RLDA	4.46	21.4
AE	RGGA	4.54	19.5
PP	LDA	4.26	23.34
PP	RLDA	4.27	23.32
AE-RHF: C		4.52	15.56
AE-RHF: C+B			15.53

[122] and LDA pseudopotential data (obtained with the j-averaged PPs discussed in Section 5.) are listed. The valence space chosen for the PPs of Rutherfordium includes the $6s$, $6p$, $6d$ and $7s$ states. In order to account for the large overlap between the $5f$ density and the valence states nlccs are utilized. Two PP calculations are compared: In the first one the nonrelativistic LDA has been applied consistently, i.e. both in the PP construction and in the molecular calculation, in the second case the RLDA has been used. Two points are obvious from Table 11.11. On the one hand, the differences between RLDA and LDA results are again very small, in spite of the huge effect of the relativistic xc-corrections on the atomic data of Rutherfordium (and thus the PP). In fact, the shift of the dissociation energy by 0.02 eV is very close to that observed within the Dirac-Fock approach [123]. On the other hand, the discrepancy between AE and PP RLDA data seems to indicate that the spin-orbit coupling of the valence electrons should not be neglected, as has been done in the present PP calculation.

Table 11.12 Spectroscopic constants of the lowest two states of FeO: PP versus AE results [47] and experimental data [124, 125].

	mode	valence space	E_{xc}	nonrelativistic R_e [Bohr]	nonrelativistic D_e [eV]	nonrelativistic ω_e [cm^{-1}]	relativistic R_e [Bohr]	relativistic D_e [eV]	relativistic ω_e [cm^{-1}]
$^5\Delta$	AE		LDA	3.01	7.06	957			
	PP	$3d4s$+nlcc	LDA	3.05	6.60	956	3.03	6.45	972
	PP	$3s3p3d4s$	LDA	2.99	6.65	962			
	PP	$3s3p3d4s$+nlcc	LDA	2.99	7.00	968	2.97	6.80	984
	PP	$3s3p3d4s$+nlcc	GGA				3.04	5.36	913
	expt.						3.06	4.06	881
$^5\Sigma$	AE		LDA	3.06	6.70	942			
	PP	$3d4s$+nlcc	LDA	3.11	6.46	939	3.09	6.44	956
	PP	$3s3p3d4s$	LDA	3.04	6.45	948			
	PP	$3s3p3d4s$+nlcc	LDA	3.04	6.60	947	3.01	6.59	969

As a further instructive example, results for the ground and the first excited state of FeO are listed in Table 11.12. This molecule is a particularly critical system as three low-lying states are competing for being the ground state and even elaborate Multi-Configuration Hartree-Fock calculations [126] do not reproduce the experimental ground state ($^5\Delta$). Focusing first on the nonrelativistic data, three PP calculations are compared with AE data. In the first PP calculation the standard valence

space has been used for Iron. It contains the $3d$ and $4s$ electrons, while the $3s$ and $3p$ states belong to the core. However, in view of the large overlap between the $3s$, $3p$ and $3d$ densities nlccs are included. The results obtained with this valence space are qualitatively correct, but the binding energies are clearly underestimated. As a consequence the $^5\Delta \longrightarrow ^5\Sigma$ excitation energy is off by more than a factor of 2. All spectroscopic constants are improved if the $3s$ and $3p$ electrons are included in the valence space. Nevertheless, even with this large valence space the energetics of the two states are not accounted for accurately. To obtain accurate dissociation energies one has to augment the large valence space by nlccs representing the L-shell.

This is particularly obvious from the relativistic data. In this case the small valence space predicts the $^5\Sigma$ state to be degenerate with the $^5\Delta$, in contradiction to experiment and the calculation with the large valence space. Comparing the $^5\Delta \longrightarrow ^5\Sigma$ excitation energy from the relativistic PP calculation with its nonrelativistic counterpart one finds a reduction by a factor of 2, which emphasizes the importance of relativity even for $3d$ elements. A comparison of the best LDA PP results with the experimental data finally demonstrates the need for nonlocal corrections. The results are clearly improved by inclusion of gradient terms in the form of the GGA (Table 11.12). The GGA bond length of 3.04 Bohr is already very close to the correct result. The remaining error in the GGA dissociation energy, on the other hand, points at the inherent limitations of the GGA concept. To conclude, this example shows that relativity should not be neglected even for the third row elements and that the nonlinearity of the xc-functional requires the use of nlccs even in calculations with rather small cores.

7. Open Questions

In spite of the three decades which passed since the introduction of the fully relativistic, j-dependent DFT formalism, to date no application of this most rigorous form of RDFT has been published. The reason for this, at first glance surprising, fact is the lack of practical and reliable approximations for the j-dependent xc-energy functional.

In the case of the explicit density functionals RLDA and RGGA only the density n is utilized to represent the xc-energy, but not the spatial components $\boldsymbol{j}$. This problem is unavoidable for the RLDA as the RLDA emerges from the homogeneous electron gas. On the other hand, the most general form of gradient corrections does include $\boldsymbol{j}$-dependent terms [24]. The actual derivation of their detailed structure, however, requires knowledge of the current-current response function of the electron gas.

Unfortunately, not even the long-wavelength limit of the exchange (first order) contribution to this function is available. Thus any systematic derivation of fully j-dependent xc-functionals has to start with a study of the first order current-current response function.

The problem with the $\boldsymbol{j}$-dependence is automatically resolved if one resorts to orbital-dependent xc-functionals as the exact exchange. However, this approach presently suffers from the lack of a suitable implicit correlation functional. First semiempirical [127] and systematic [25, 128] functionals of this type have been suggested. Unfortunately, the semiempirical form does not perform satisfactorily, neither for atoms [30] nor for molecules [129]. The first principles functionals, on the other hand, require the evaluation of the complete single-particle spectrum and corresponding Coulomb matrix elements, so that they drastically increase the computational demands of RDFT calculations. In addition, the most simple functional of this type, which is based on second order perturbation theory, leads to a divergence of the correlation potential in the asymptotic region of finite systems [130]. Thus in the case of implicit functionals the next step must be the derivation of an accurate, universally applicable and efficient correlation functional which can be used with the exact exchange.

Presently, RDFT calculations for systems for which $\boldsymbol{j}$ plays an important role have to rely on the magnetization-dependent variant of RDFT. In practice, this implies the use of nonrelativistic spin-density functionals and thus the neglect of all relativistic corrections to the xc-functional. Any systematic step beyond this hybrid scheme requires an examination of the linear response function of the polarized relativistic electron gas: As the RLDA turned out to be completely inadequate even for closed-shell atoms, one has to go to the RGGA level. As for the j-dependent formalism, the gradient corrections in the $\boldsymbol{m}$-dependent variant are determined by the corresponding response function which remains to be evaluated.

Acknowledgments

The author would like to thank all his colleagues and collaborators, I. Andrejkovics, T. Auth, P. Blaha, H. Bross, N. Chetty, J. A. C. Chevary, R. M. Dreizler, A. Facco Bonetti, G. Fehrenbach, B. Fricke, E. K. U. Gross, L. Gulyás, A. Höck, G. Iseri, S. Keller, T. Kirchner, O. Knospe, T. Kreibich, P. La Rocca, U. Lechner, H.-J. Lüdde, D. H. Madison, C. Mosch, H. Müller, J. P. Perdew, R. N. Schmid, R. Schmidt, U. R. Schmitt, K. Schwarz, W.-D. Sepp, C. Speicher, S. Varga, S. H. Vosko and E. Wüst, for their fruitful contributions to the subject of this review and a vast number of stimulating discussions.

References

[1] J. P. Perdew and Y. Wang. *Phys. Rev. B*, 33:8800, 1986.

[2] J. P. Perdew. *Phys. Rev. B*, 33:8822, 1986.

[3] A. D. Becke. *Phys. Rev. A*, 38:3098, 1988.

[4] J. P. Perdew, J. A. Chevary, S. H. Vosko, K. A. Jackson, M. R. Pederson, D. J. Singh, and C. Fiolhais. *Phys. Rev. B*, 46:6671, 1992.

[5] A. Becke. *J. Chem. Phys.*, 96:2155, 1992.

[6] B. G. Johnson, P. M. Gill, and J. A. Pople. *J. Chem. Phys.*, 98:5612, 1993.

[7] R. M. Dreizler and E. K. U. Gross. *Density Functional Theory*. Springer, Berlin, 1990.

[8] P. Pyykkö. *Chem. Rev.*, 88:563, 1988.

[9] M. Pepper and B. E. Bursten. *Chem. Rev.*, 91:719, 1991.

[10] A. K. Rajagopal and J. Callaway. *Phys. Rev. B*, 7:1912, 1973.

[11] P. Hohenberg and W. Kohn. *Phys. Rev.*, 136 B:864, 1964.

[12] E. Engel, H. Müller, Ch. Speicher, and R M. Dreizler. In E. K. U. Gross and R. M. Dreizler, editors, *Density Functional Theory*, volume 337 of *NATO ASI Series B*, page 65. Plenum, New York, 1995.

[13] L. H. Thomas. *Proc. Cambridge Phil. Soc.*, 23:542, 1927.

[14] E. Fermi. *Z. Phys.*, 48:73, 1928.

[15] M. S. Vallarta and N. Rosen. *Phys. Rev.*, 41:708, 1932.

[16] H. Jensen. *Z. Phys.*, 82:794, 1933.

[17] E. Engel and R. M. Dreizler. *Phys. Rev. A*, 35:3607, 1987.

[18] A. K. Rajagopal. *J. Phys. C*, 11:L943, 1978.

[19] A. H. MacDonald and S. H. Vosko. *J. Phys. C*, 12:2977, 1979.

[20] W. Kohn and L. J. Sham. *Phys. Rev.*, 140 A:1133, 1965.

[21] M. V. Ramana and A. K. Rajagopal. *Phys. Rev. A*, 24:1689, 1981.

[22] E. Engel, S. Keller, and R. M. Dreizler. *Phys. Rev. A*, 53:1367, 1996.

[23] R. N. Schmid, E. Engel, R. M. Dreizler, P. Blaha, and K. Schwarz. *Adv. Quant. Chem.*, 33:209, 1998.

[24] E. Engel and R. M. Dreizler. In R. F. Nalewajski, editor, *Density Functional Theory II*, volume 181 of *Topics in Current Chemistry*, page 1. Springer, Berlin, 1996.

[25] E. Engel, A. Facco Bonetti, S. Keller, I. Andrejkovics, and R. M. Dreizler. *Phys. Rev. A*, 58:964, 1998.

[26] B. A. Shadwick, J. D. Talman, and M. R. Norman. *Comput. Phys. Commun.*, 54:95, 1989.

[27] E. Engel, S. Keller, A. Facco Bonetti, H. Müller, and R. M. Dreizler. *Phys. Rev. A*, 52:2750, 1995.

[28] T. Kreibich, E. K. U. Gross, and E. Engel. *Phys. Rev. A*, 57:138, 1998.

[29] J. B. Krieger, Y. Li, and G. J. Iafrate. *Phys. Lett. A*, 146:256, 1990.

[30] E. Engel and R. M. Dreizler. *J. Comput. Chem.*, 20:31, 1999.

[31] M. P. Das, M. V. Ramana, and A. K. Rajagopal. *Phys. Rev. A*, 22:9, 1980.

[32] M. P. Das. *Phys. Rev. A*, 23:391, 1981.

[33] M. V. Ramana, A. K. Rajagopal, and W. R. Johnson. *Phys. Rev. A*, 25:96, 1982.

[34] M. V. Ramana and A. K. Rajagopal. *J. Phys. C*, 14:4291, 1981.

[35] H. Eschrig, G. Seifert, and P. Ziesche. *Solid State Commun.*, 56:777, 1985.

[36] M. V. Ramana and A. K. Rajagopal. *J. Phys. C*, 12:L845, 1979.

[37] A. H. MacDonald. *J. Phys. C*, 16:3869, 1983.

[38] B. X. Xu, A. K. Rajagopal, and M. V. Ramana. *J. Phys. C*, 17:1339, 1984.

[39] L. Nordström and D. J. Singh. *Phys. Rev. Lett.*, 76:4420, 1996.

[40] L. M. Sandratskii. *Adv. Phys.*, 47:91, 1998.

[41] H. Eschrig and V. D. P. Servedio. *J. Comput. Chem.*, 20:23, 1999.

[42] P. Cortona, S. Doniach, and C. Sommers. *Phys. Rev. A*, 31:2842, 1985.

[43] H. Yamagami, A. Mavromaras, and J. Kübler. *J. Phys.: Condens. Matter*, 9:10881, 1997.

[44] E. Engel, T. Auth, and R. M. Dreizler. *Phys. Rev. B*, 64:235126, 2001.

[45] E. Engel. In P. Schwerdtfeger, editor, *Relativistic Quantum Chemistry, Vol.1*. Elsevier, Amsterdam, 2002.

[46] Y. Ishikawa and K. Koc. *Phys. Rev. A*, 50:4733, 1994.

[47] E. Engel, A. Höck, and S. Varga. *Phys. Rev. B*, 63:125121, 2001.

[48] N. Troullier and J. L. Martins. *Phys. Rev. B*, 43:1993, 1991.

[49] G. te Velde and E. J. Baerends. *J. Comp. Phys.*, 99:84, 1992.

[50] C. Fonseca Guerra et al. Methods and techniques in computational chemistry 95. page 305. STEF, Cagliar, 1995.

[51] E. van Lenthe, J. G. Snijders, and E. J. Baerends. *J. Chem. Phys.*, 105:6505, 1996.

[52] P. H. T. Philipsen, E. van Lenthe, J. G. Snijders, and E. J. Baerends. *Phys. Rev. B*, 56:13556, 1997.

[53] L. Yang, D. Heinemann, and D. Kolb. *Phys. Rev. A*, 48:2700, 1993.

[54] T. Bastug, K. Rashid, W.-D. Sepp, D. Kolb, and B. Fricke. *Phys. Rev. A*, 55:1760, 1997a.

[55] D. Geschke, S. Fritzsche, W.-D. Sepp, B. Fricke, S. Varga, and J. Anton. *Phys. Rev. B*, 62:15439, 2000.

[56] S. Varga, A. Rosén, W.-D. Sepp, and B. Fricke. *Phys. Rev. A*, 63:022510, 2001.

[57] V. Pershina, W.-D. Sepp, B. Fricke, and A. Rosén. *J. Chem. Phys.*, 96:8367, 1992.

[58] V. Pershina, W.-D. Sepp, B. Fricke, D. Kolb, M. Schädel, and G. V. Ionova. *J. Chem. Phys.*, 97:1116, 1992.

[59] C. van Wüllen. *J. Chem. Phys.*, 103:3589, 1995.

[60] W. Liu, G. Hong, D. Dai, L. Li, and M. Dolg. *Theor. Chem. Acc.*, 96:75, 1997.

[61] W. Liu, M. Dolg, and L. Li. *J. Chem. Phys.*, 108:2886, 1998.

[62] W. Liu and M. Dolg. *Phys. Rev. A*, 57:1721, 1998.

[63] W. Liu and C. van Wüllen. *J. Chem. Phys.*, 110:3730, 1999.

[64] A. H. MacDonald, J. M. Daams, S. H. Vosko, and D. D. Koelling. *Phys. Rev. B*, 23:6377, 1981.

[65] A. H. MacDonald, J. M. Daams, S. H. Vosko, and D. D. Koelling. *Phys. Rev. B*, 25:713, 1982.

[66] H. Ebert. *Phys. Rev. B*, 38:9390, 1988.

[67] T. Huhne, C. Zecha, H. Ebert, P. H. Dederichs, and R. Zeller. *Phys. Rev. B*, 58:10236, 1998.

[68] D. Singh and H. Krakauer. *Phys. Rev. B*, 37:3999, 1988.

[69] L. M. Sandratskii and J. Kübler. *Phys. Rev. Lett.*, 75:946, 1995.

[70] M. Körling and J. Häglund. *Phys. Rev. B*, 45:13293, 1992.

[71] H. Reinisch and H. Bross. *Z. Phys. B*, 95:145, 1994.

[72] G. M. Fehrenbach and G. Schmidt. *Phys. Rev. B*, 55:6666, 1997.

[73] P. Dufek, P. Blaha, and K. Schwarz. *Phys. Rev. B*, 50:7279, 1994.

[74] P. Blaha, K. Schwarz, P. Dufek, and R. Augustyn. 1995. WIEN95, Technical University of Vienna (improved and updated Unix version of the original copyrighted WIEN-code, by P. Blaha, K. Schwarz, P. Sorantin, and S. B. Trickey, Comput. Phys. Commun. **59**, 399, (1990)).

[75] P. H. T. Philipsen and E. J. Baerends. *Phys. Rev. B*, 61:1773, 2000.

[76] F. A. Parpia and W. R. Johnson. *J. Phys. B*, 16:L375, 1983.

[77] F. A. Parpia and W. R. Johnson. *Phys. Lett.*, 99 A:172, 1983.

[78] F. A. Parpia and W. R. Johnson. *J. Phys. B*, 17:531, 1984.

[79] A. K. Rajagopal. *Phys. Rev. A*, 50:3759, 1994.

[80] A. Nagy. *Phys. Rev. A*, 49:3074, 1994.

[81] E. K. U. Gross and R. M. Dreizler. *Phys. Lett.*, 81A:447, 1981.

[82] P. Malzacher and R. M. Dreizler. *Z. Phys. D*, 2:37, 1986.

[83] E. Engel and R. M. Dreizler. *Phys. Rev. A*, 38:3909, 1988.

[84] H. Müller, E. Engel, and R. M. Dreizler. *Phys. Rev. A*, 40:5542, 1989.

[85] W. F. Pohlner and R. M. Dreizler. *Phys. Rev. A*, 44:7165, 1991.

[86] H. J. A. C. Stroucken and R. M. Dreizler. *Phys. Rev. A*, 43:3401, 1991.

[87] C. Itzykson and J-B. Zuber. *Quantum Field Theory*. McGraw-Hill, New York, 1980.

[88] A. O. G. Källén. Handbuch der Physik, Band V, Teil 1. Springer, Berlin, 1958.

[89] K. Capelle and G. Vignale. *Phys. Rev. Lett.*, 86:5546, 2001.

[90] H. Eschrig and W.E. Pickett. *Solid State Commun.*, 118:123, 2001.

[91] I. A. Akhiezer and S. V. Peletminskii. *Zh. Eksp. Teor. Fiz.*, 38:1829, 1960. [Sov. Phys. JETP 11, 1316 (1960)].

[92] H. S. Zapolsky. Lns report, Cornell University, 1960.

[93] B. Jancovici. *Nuovo Cim.*, XXV:428, 1962.

[94] E. Engel, S. Keller, and R. M. Dreizler. In J. F. Dobson, G. Vignale, and M. P. Das, editors, *Electronic Density Functional Theory: Recent Progress and New Directions*, page 149. Plenum, New York, 1998.

[95] R. T. Sharp and G. K. Horton. *Phys. Rev.*, 90:317, 1953.

[96] J. D. Talman and W. F. Shadwick. *Phys. Rev. A*, 14:36, 1976.

[97] J. B. Krieger, Y. Li, and G. J. Iafrate. *Phys. Rev. A*, 45:101, 1992.

[98] E. Engel, A. Höck, and R. M. Dreizler. *Phys. Rev. A*, 62:042502, 2000.

[99] K. G. Dyall, I. P. Grant, C. T. Johnson, F. A. Parpia, and E. P. Plummer. *Comput. Phys. Commun.*, 55:425, 1989.

[100] G. L. Malli, A. B. F. da Silva, and Y. Ishikawa. *Can. J. Phys.*, 70:1822, 1992.

[101] C.-O. Almbladh and U. von Barth. *Phys. Rev. B*, 31:3231, 1985.

[102] E. Engel and S. H. Vosko. *Phys. Rev. A*, 47:2800, 1993.

[103] E. Engel and S. H. Vosko. *Phys. Rev. B*, 47:13164, 1993.

[104] E. R. Davidson, S. A. Hagstrom, S. J. Chakravorty, V. Meiser Umar, and C. Froese Fischer. *Phys. Rev. A*, 44:7071, 1991.

[105] S. J. Chakravorty, S. R. Gwaltney, E. R. Davidson, F. A. Parpia, and C. Froese Fischer. *Phys. Rev. A*, 47:3649, 1993.

[106] S. H. Vosko, L. Wilk, and M. Nusair. *Can. J. Phys.*, 58:1200, 1980.

[107] D. R. Hamann, M. Schlüter, and C. Chiang. *Phys. Rev. Lett.*, 43:1494, 1979.

[108] G. B. Bachelet, D. R. Hamann, and M. Schlüter. *Phys. Rev. B*, 26:4199, 1982.

[109] M. E. Rose. *Elementary Theory of Angular Momentum.* Wiley, New York, 1957. The $\Omega_{jlm}, (\theta, \varphi)$ are also often denoted as $\Omega_{jlm}, (\theta, \varphi) = \chi_{-\kappa,m}(\theta, \varphi)$ and $\Omega_{j\bar{l},m}(\theta, \varphi) = \chi_{\kappa,m}(\theta, \varphi)$.

[110] G. P. Kerker. *J. Phys. C*, 13:L189, 1980.

[111] D. Vanderbilt. *Phys. Rev. B*, 32:8412, 1985.

[112] D. R. Hamann. *Phys. Rev. B*, 40:2980, 1989.

[113] S. G. Louie, S. Froyen, and M. L. Cohen. *Phys. Rev. B*, 26:1738, 1982.

[114] D. M. Bylander and L. Kleinman. *Phys. Rev. B*, 52:14566, 1995.

[115] M. Städele, J. A. Majewski, P. Vogl, and A. Görling. *Phys. Rev. Lett.*, 79:2089, 1997.

[116] E. Engel, A. Höck, R. N. Schmid, R. M. Dreizler, and N. Chetty. *Phys. Rev. B*, 64:125111, 2001.

[117] M. Mayer, O. D. Häberlen, and N. Rösch. *Phys. Rev. A*, 54:4775, 1996.

[118] S. Varga, E. Engel, W.-D. Sepp, and B. Fricke. *Phys. Rev. A*, 59, 1999.

[119] W. Liu and C. van Wüllen. *J. Chem. Phys.*, 113:2506, 2000.

[120] L. Brewer. Technical Report Report LBL-3720 Rev., Lawrence Berkeley Laboratory, Univ. of California, Berkeley, 1977.

[121] A. Khein, D. J. Singh, and C. J. Umrigar. *Phys. Rev. B*, 51:4105, 1995.

[122] S. Varga, B. Fricke, M. Hirata, T. Bastug, V. Pershina, and S. Fritzsche. *J. Phys. Chem. A*, 104:6495, 2000.

[123] G. L. Malli and J. Styszynski. *J. Chem. Phys.*, 109:4448, 1998.

[124] E. Murad. *J. Chem. Phys.*, 73:1381, 1980.

[125] A. S. C. Cheung, R. M. Gordon, and A. J. Merer. *J. Mol. Spectrosc.*, 87:289, 1981.

[126] M. Krauss and W. J. Stevens. *J. Chem. Phys.*, 82:5584, 1985.

[127] R. Colle and O. Salvetti. *Theoret. Chim. Acta (Berl.)*, 37:329, 1975.

[128] E. Engel and A. Facco Bonetti. In A. Hernández-Laguna, J. Maruani, R. McWeeny, and S. Wilson, editors, *Quantum Systems in Theoretical Chemistry and Physics, Vol.1: Basic Problems and Model Systems*, page 227. Kluwer, Doordrecht, 2000.

[129] T. Grabo, T. Kreibich, and E. K. U. Gross. *Mol. Engineering*, 7:27, 1997.

[130] A. Facco Bonetti, E. Engel, R. N. Schmid, and R. M. Dreizler. *Phys. Rev. Lett.*, 86:2241, 2001.

Chapter 12

QED EFFECTS IN ATOMS

Leonti Labzowsky and Igor Goidenko
Institute of Physics,
St.Petersburg State University,
198904 Uljanovskaya 1, Petrodvorets,
St.Petersburg, Russia
leonti@landau.phys.spbu.ru

Abstract The QED theory of atoms is reviewed. The interelectron interaction and the radiative corrections to the energy levels (the Lamb Shift) are considered. The applications of QED to the light atoms and to valence electrons in heavy atoms are discussed.

Keywords: Quantum Electrodynamics, QED, atomic structure

Introduction

In this paper we review the recent level of Quantum Electrodynamics (QED) investigations of light and heavy atoms.

The atomic theory was the first field for the application of the modern QED [1–4]. One of the most important achievements of QED was the explanation of the Lamb Shift (LS) between $2s$ and $2p_{1/2}$ states in atomic hydrogen [5–8]. QED is formulated as a perturbation theory (PT) in powers of the coupling constant $\alpha = e^2/\hbar c = 1/137.0359895...$ (e is the electron charge, $\hbar$ is the Planck's constant and c is the speed of light). Due to the smallness of α QED theory for the light atoms is elaborated now up to very high order, demonstrating an excelent agreement with experiment [9].

In QED theory of atoms, apart from the pure QED parameter α the relativistic parameter $\alpha Z \approx v/c$ plays an important role (Z is the charge of the nucleus, v is the characteristic velocity of the atomic electron). For the light atoms an expansion in αZ parameter is commonly used. The

U. Kaldor and S. Wilson (eds.),
Theoretical Chemistry and Physics of Heavy and Superheavy Elements, 487–556.
© 2003 *Kluwer Academic Publishers.*

condition $\alpha Z \ll 1$ does not hold for the inner electron shells in heavy atoms. Moreover it does not hold even for the valence electrons in heavy atoms due to the singularity of QED operators. For the evaluation of the matrix elements of such operators the small distances of the electron from the nucleus become important. At such distances the effective electron charge Z_{eff} for the valence electrons may not be small. Therefore the QED theory without αZ expansion appears to be necessary. Such theory was first introduced in [10] and applied to the K-shell electrons in Hg atom. The further development of this theory can be found in [11].

Another important application of all orders in αZ atomic QED is the theory of the multicharged ions. Nowadays all elements of the Periodic Table up to Uranium (Z=92) can be observed in the laboratory as H-like, He-like etc ions. The recent achievements of the QED theory of the highly charged ions (HCI) are summarized in [11, 12]. In principle, the QED theory of atoms includes the evaluation of the QED corrections to the energy levels and corrections to the hyperfine structure intervals, as well as the QED corrections to the transition probabilities and cross-sections of the different atomic processes: photon and electron scattering, photoionization, electron capture etc. QED corrections can be evaluated also to the different atomic properties in the external fields: bound electron g-factors and polarizabilities. In this review we will concentrate mainly on the corrections to the energy levels which are usually called the "Lamb Shift" (here the "Lamb Shift" should be understood in a more broad sense than the $2s$, $2p_{1/2}$ level shift in a hydrogen) and on the corrections to g-factors.

A question may arise whether there are non-QED corrections comparable in size with QED ones and thus preventing the direct tests of QED in atomic experiments. The most important among these corrections are nuclear ones. The nuclear recoil is usually included in QED theory of atoms [9, 11, 12]. The nuclear size correction even dominates over the QED corrections in HCI [12] and heavy atoms [13,14]. The uncertainty in the determination of the nuclear radius sets the principial limit to the ab initio calculations of the atomic energy levels. For HCI this uncertainty is still smaller than the second-order in α QED corrections [12], but the nuclear polarization corrections are approaching this level [12, 15]. Thus the evaluation of the higher than α^2 QED corrections is unreasonable without the detailization of the nuclear structure theory.

In heavy atoms the nuclear uncertainty is still well below the electron correlation uncertainty, allowing for the evaluation of only the first-order in α QED corrections.

Another possible source of non-QED corrections to the energy levels is the parity - conserving weak interaction between the electron and the

nucleus. The estimates show that these corrections are too small to be considered seriously both in light and heavy atoms and in HCI [9,16]. The parity non - conserving weak interaction can influence atomic transition probabilities. This leads to the observable asymmetry effects in radiation. We should mention that QED effects appear to be observable also in molecules (see the recent publications [17,18]).

Throughout the sections 1, 2, 3 we use the relativistic units $c = \hbar = 1$ ($\alpha = e^2$). In Section 4 where some practical calculations are described the atomic units $m = \hbar = e = 1$ ($\alpha = 1/c^2$) are preferable. Here m denotes the electron mass. We define the scalar product of the two 4-dimensional vectors a and b as :

$$a_\mu b^\mu = a_4 b_4 - \vec{a}\,\vec{b},$$

$$a_\mu = g_{\mu\nu} a^\nu,$$

where the metric tensor $g_{\mu\nu}$ has nonzero components:

$$g_{44} = 1, g_{11} = g_{22} = g_{33} = -1.$$

1. The Furry picture for bound-state QED

1.1 Dirac equation for the electron in an external field

The noncovariant form of the Dirac equation for an electron in an external field is:

$$i\frac{\partial \Psi}{\partial t} = \hat{h}(\vec{r})\Psi(\vec{r}, t), \tag{12.1}$$

where the Dirac Hamiltonian is:

$$\hat{h}(\vec{r}) = \vec{\alpha}\left(\hat{\vec{p}} + e\vec{A}\right) - eV(\vec{r}) + \beta m. \tag{12.2}$$

Here $\hat{\vec{p}} = -i\vec{\nabla}$ is the electron momentum operator, $\vec{\alpha}$, β are the standard Dirac matrices, $\vec{A}$ is the vector potential and V is the scalar potential of the external field. The wave function $\Psi(\vec{r}, t)$ is the four-component spinor. For the stationary state:

$$\Psi_s(\vec{r}, t) = \Psi(\vec{r})e^{-iE_s t}, \tag{12.3}$$

where $\Psi_s(\vec{r})$ is the solution of the stationary Dirac equation:

$$\hat{h}(\vec{r})\Psi_s(\vec{r}) = E_s \Psi_s(\vec{r}). \tag{12.4}$$

Here E_s are the Dirac eigenvalues, index s runs over the complete spectrum of the Dirac Hamiltonian. This spectrum includes the solutions with positive and negative energy values E_s. For the bound-state solutions $\Psi_s(\vec{r})$ the normalization condition is:

$$\int \rho(\vec{r})d\vec{r} = \int \Psi_s^+(\vec{r})\Psi_s(\vec{r})d\vec{r} = 1, \tag{12.5}$$

where $\Psi_s^+(\vec{r})$ is the hermitian - conjugated bispinor. In many cases it is more convenient to use the covariant form of the Dirac equation (1). Introducing the Dirac matrices:

$$\vec{\gamma} = \beta\vec{\alpha}, \gamma_4 = \beta, \tag{12.6}$$

and multiplying both sides of Eq. (1) by γ_4 we arrive at the equation:

$$[i(\not{p} + e\ \not{A}) + m]\,\Psi = 0, \tag{12.7}$$

where $\not{p} = \gamma_\mu p^\mu$ and the 4-vector p is defined as $p_\mu \equiv i\frac{d}{dx_\mu}$, $x_\mu \equiv (\vec{r}, t)$.

The introduction of the Dirac - conjugated wave function $\overline{\Psi}(x) \equiv \Psi^+\gamma_4$ leads to the equation:

$$\overline{\Psi}(x)\,[i(\not{p} - e\ \not{A}) - m] = 0. \tag{12.8}$$

The negative-energy Dirac states within QED are interpreted with the help of the charge conjugation transformation:

$$\Psi^c(x) = \gamma_2\gamma_4\overline{\Psi}^T, \tag{12.9}$$

where the superscript "T" means the transposition of the Dirac bispinor, i.e. transposition of the one-column (Ψ) or the one - row (Ψ) matrix. The charge - conjugated wave function (10) is the solution of the Dirac equation:

$$[i(\not{p} - e\ \not{A}) + m]\,\Psi^c = 0 \tag{12.10}$$

for the positron. Since the charge conjugation (9) includes the complex conjugation, the negative energy Dirac stationary solutions become positive energy solutions for the particle with the opposite sign of charge. However for the summations over intermediate Dirac states it is better to use the negative - energy wave functions. Combined with the positive - energy solutions they give a complete spectrum of the Dirac Hamiltonian (2).

In a central field the solution of Eq. (4) takes the form:

$$\Psi_{EjlM}(\vec{r}) = \begin{pmatrix} g_{Ejl}(r)\Omega_{jlM}(\vec{n}) \\ if_{Ejl}(r)\Omega_{j\bar{l}M}(\vec{n}) \end{pmatrix}, \tag{12.11}$$

where $\Omega_{jlM}(\vec{n})$ is the spherical spinor, $\vec{n} = \vec{r}/r$, $\bar{l} = 2j - l$. The wave function (11) is the eigenfunction of the total electron angular momentum:

$$\hat{\vec{j}} = \hat{\vec{l}} + \hat{\vec{s}}, \tag{12.12}$$

where $\hat{\vec{l}}$ is the orbital angular momentum:

$$\hat{\vec{l}} = \left(\vec{r} \times \hat{\vec{p}}\right) \tag{12.13}$$

and $\hat{\vec{s}}$ is the spin momentum:

$$\hat{\vec{s}} = \frac{1}{2}\hat{\vec{\Sigma}}, \tag{12.14}$$

$$\hat{\vec{\Sigma}} = \begin{pmatrix} \vec{\sigma} & 0 \\ 0 & \vec{\sigma} \end{pmatrix}, \tag{12.15}$$

$\vec{\sigma}$ are the two-component Pauli matrices. This implies the conditions:

$$\hat{\vec{j}}^2 \Psi_{EjlM} = j(j+1)\Psi_{EjlM}, \tag{12.16}$$

$$j_z \Psi_{EjlM} = M\Psi_{EjlM} \tag{12.17}$$

where j, M are the standard angular quantum numbers. The quantum number l defines the parity of the state (the orbital moment $\hat{\vec{l}}$ is not conserved in the Dirac theory):

$$\hat{P}\Psi_{EjlM}(\vec{r}) = (-1)^l \Psi_{EjlM}(\vec{r}), \tag{12.18}$$

where $\hat{P}$ is the inversion operator. In the Dirac theory this operator is defined as:

$$\hat{P}\Psi_{EjlM}(\vec{r}) = \gamma_4 \Psi_{EjlM}(-\vec{r}). \tag{12.19}$$

The equations for the radial functions g, f are:

$$\begin{aligned} &\frac{dg_{Ejl}}{dr} + (1+\kappa_{jl})\frac{1}{r}g_{Ejl} - (E+m+eV)\, f_{Ejl} \quad (a) \\ &\frac{df_{Ejl}}{dr} + (1-\kappa_{jl})\frac{1}{r}f_{Ejl} + (E-m+eV)\, g_{Ejl} \quad (b), \end{aligned} \tag{12.20}$$

where κ_{jl} is the Dirac angular quantum number:

$$\kappa_{jl} = \pm (j + 1/2)\,, \; for \; j = l \mp 1/2. \tag{12.21}$$

It is convenient to introduce the binding energy for the positive- and negative- energy states by definition:

$$E^{(\pm)} = \pm(m + \varepsilon). \tag{12.22}$$

In the nonrelativistic limit:

$$\varepsilon \sim m\,(\alpha Z)^2\,. \tag{12.23}$$

It is also useful to write the Dirac wave function in the two-component form:

$$\Psi_s(\vec{r}) = \begin{pmatrix} \phi_s(\vec{r}) \\ \chi_s(\vec{r}) \end{pmatrix} \tag{12.24}$$

In the nonrelativistic limit:

$$\begin{aligned} \chi_s^{(+)} &\sim \tfrac{\vec{\sigma}\vec{p}}{2m}\phi_s^{(+)} \quad (a) \\ \phi_s^{(-)} &\sim -\tfrac{\vec{\sigma}\vec{p}}{2m}\chi_s^{(-)} \quad (b). \end{aligned} \tag{12.25}$$

It follows from Eq. (23) that the characteristic value of the electron momentum in an atom in the nonrelativistic limit is:

$$p \sim m\,(\alpha Z)\,. \tag{12.26}$$

From Eqs. (25), (26) we deduce that the components $\chi_s^{(+)}$, $\phi_s^{(-)}$ are "small" compared to $\phi_s^{(+)}$, $\chi_s^{(-)}$. Then, after substituting Eqs. (25) in the Dirac equation we see that this equation is split into the two Schrödinger equations for $\phi_s^{(+)}$, $\chi_s^{(-)}$:

$$\begin{aligned} \left(\tfrac{1}{2m}\hat{\vec{p}}^2 - eV - \varepsilon_s\right)\phi_s^{(+)} &= 0 \quad (a) \\ \left(\tfrac{1}{2m}\hat{\vec{p}}^2 + eV - \varepsilon_s\right)\chi_s^{(-)} &= 0 \quad (b). \end{aligned} \tag{12.27}$$

Eqs. (27a) and (27b) describe the non-relativistic electrons and positrons correspondingly. In the case of the positively charged point-like nucleus:

$$V(\vec{r}) = \frac{eZ}{r} \tag{12.28}$$

the binding energy for the electron in the bound states is negative and the binding energy for the positron is always positive. For the negatively charged nucleus (antiproton, Z=-1) the situation is opposite.

1.2 Interaction of the electromagnetic and electron-positron fields

The unique practical way to describe the theory of the interacting fields is by perturbation theory (PT). This is most justified for QED where the coupling parameter is α (see Introduction). The perturbation theory is most conveniently developed within the Hamilton formalism. Therefore we present the total Hamiltonian for the interacting electron-positron and electromagnetic fields as

$$\hat{H} = \hat{H}_0 + \hat{H}_{int}, \tag{12.29}$$

$$\hat{H}_0 = \hat{H}_\gamma + \hat{H}_e, \tag{12.30}$$

where $\hat{H}_\gamma$ is the Hamiltonian for the free electromagnetic field, $\hat{H}_e$ describes the free electron-positron field and the interaction Hamiltonian is denoted by $\hat{H}_{int}$. With the use of the normal products of the operators the expressions for the Hamiltonians $\hat{H}_\gamma$ and $\hat{H}_e$ are:

$$\hat{H}_\gamma = \sum_{k\lambda} w\hat{N}_{k\lambda}, \tag{12.31}$$

$$\hat{H}_e = \sum_{E_s>0} \hat{n}_s^{(+)} E_s - \sum_{E_s<0} \hat{n}_s^{(-)} E_s. \tag{12.32}$$

Here $\hat{N}_{k\lambda}$ is the operator of the number of the photons, $k \equiv (\vec{k}, w)$, $w = |\vec{k}|$ is the photon frequency, $\vec{k}$ is the photon momentum, $\lambda = 1, 2, 3, 4$ denotes the polarization of the photon. The values $\lambda = 1, 2$ coreespond to the transverse polarization, $\lambda = 3$ corresponds to the longitudinal and $\lambda = 4$ to the scalar polarizatoin. The free electromagnetic field have only transverse polarization, so that the longitudinal and scalar polarization should vanish in the expression for any obsevable.

The operators $\hat{n}_s^{(\pm)}$ can be interpreted as the operators of the electron or positron numbers correspondingly. The operators $\hat{N}_{k\lambda}$, $\hat{n}_s^{(\pm)}$ are acting on the state vector $|\Phi\rangle$ that is defined in the Fock space (occupation number space). These operators are defined as the products of the creation and annihilation operators of the corresponding particles. The normal product (N-product) of the creation and annihilation operators is defined in such a way that the positions of the creation operators are always to the left of the positions of the annihilation operators for the same particle. With the use of the N-products the energy of the vacuum state is zero.

By analogy with the classical interaction the interaction Hamiltonian should be:

$$\hat{H}_{int} = -\int \hat{j}_\mu(x)\hat{A}^\mu(x)d\vec{r}. \tag{12.33}$$

Here $\hat{j}_\mu(x)$ is the current density operator of the electron - positron field:

$$\hat{j}_\mu(x) = -ieN\left(\hat{\Psi}^+(x)\hat{\Psi}(x)\right), \tag{12.34}$$

$\hat{\Psi}(x)$, $\hat{\Psi}(x)$ are the electron - positron field operators, $\hat{A}^\mu(x)$ is the electromagnetic field operator, N is the symbol of the N-product.

The Hamiltonian (33), as well as the Hamiltonians (31) and (32) is defined in the Fock space. In the Fock space it is possible to write down the Schrödinger equation for the interacting fields:

$$i\frac{\partial\Psi(t)}{\partial t} = \hat{H}\Psi(t), \tag{12.35}$$

where $\Psi(t) \equiv |\Psi(t)\rangle$ is the state vector in the Schrödinger representation and the operator $\hat{H}$ is defined by Eq. (29). The development of PT is most effective in the interaction representation, where the Schrödinger equation looks like:

$$i\frac{\partial\hat{\Phi}(t)}{\partial t} = \hat{H}_{int}(t)\hat{\Phi}(t). \tag{12.36}$$

Here $\hat{\Phi}$ is the state vector in the interaction representation:

$$\hat{\Phi}(t) = e^{i\hat{H}_0 t}\Psi(t) \tag{12.37}$$

and $\hat{H}_{int}$ is the interaction Hamiltonian in the interaction representation:

$$\hat{H}_{int}(t) = e^{-i\hat{H}_0 t}\hat{H}_{int}e^{i\hat{H}_0 t}. \tag{12.38}$$

The evolution operator $\hat{S}(t, t_0)$ is introduced by the relation :

$$\hat{\Phi}(t) = \hat{S}(t, t_0)\hat{\Phi}(t_0). \tag{12.39}$$

From Eq. (36) follows the equation for $\hat{S}(t, t_0)$:

$$i\frac{\partial\hat{S}(t, t_0)}{\partial t} = \hat{H}_{int}(t)\hat{S}(t, t_0). \tag{12.40}$$

The PT is developed then as the iterative solution of Eq. (40). Combined with the condition:

$$\hat{S}(t_0, t_0) = 1 \tag{12.41}$$

this solution yields:

$$\hat{S}(t, t_0) = 1 + \sum_{l=1}^{\infty} \hat{S}^{(l)}(t, t_0), \tag{12.42}$$

where

$$\hat{S}^{(l)}(t, t_0) = (-1)^l \int_{t_0}^{t} dt_1 ... \int_{t_0}^{t_{l-1}} \hat{H}_{int}(t_1), ..., \hat{H}_{int}(t_l). \tag{12.43}$$

For general purposes it is more convenient to go over the symmetrized form of the expression (43):

$$\hat{S}^{(l)}(t, t_0) = \frac{(-1)^l}{l!} \int_{t_0}^{t} dt_1 ... \int_{t_0}^{t} T\left(\hat{H}_{int}(t_1), ..., \hat{H}_{int}(t_l)\right). \tag{12.44}$$

The symmetrized formula (44) includes the chronological product of the operators (symbol T). This chronological product arrives since the operators $\hat{H}_{int}(t)$ taken at the different time moments do not commute with each other.

The general QED scheme, first formulated for the free electrons, was oriented to the description of arbitrary scattering, decay or capture processes with electrons, positrons and photons. The standard problem considered within this formulation was the following. A set of noninteracting free particles was given at the initial time moment ($t = -\infty$) and another set resulting from the interaction at the intermediate time moments but also containing noninteracting particles was given at the final time moment ($t = \infty$). Then, according to the definition (39):

$$|\Phi(\infty)\rangle = \hat{S}(\infty, -\infty)|\Phi(-\infty)\rangle. \tag{12.45}$$

The evolution operator $\hat{S}(\infty, -\infty)$ is called the S-matrix. Let $|\Phi_a^0\rangle$ be the state vectors for the system of noninteracting electrons (positrons) and photons. These vectors are the eigenfunctions of the Hamiltonian $\hat{H}_0$. We assume that:

$$|\Phi(-\infty)\rangle = |\Phi_a^0\rangle. \tag{12.46}$$

Than it follows from Eq. (45) that:

$$|\Phi(\infty)\rangle = \sum_b \langle\Phi_b^0|\hat{S}(\infty, -\infty)|\Phi_a^0\rangle|\Phi_b^0\rangle, \tag{12.47}$$

where the sum over b extends over the complete set of eigenstates of operator $\hat{H}_0$.

The evaluation of matrix elements of the S-matrix that define the amplitudes of the different processes is the traditional problem of free-electron QED. However the extension of this traditional scheme to bound electrons faces serious difficulties. In particular, these difficulties arise even for the simplest problem of quantum mechanics: evaluation of the energy shift due to the interaction between the particles. The reason is that the interaction in this case is present at all time moments, including $t = \pm\infty$. The discussion of the special approach helping to avoid this difficulty we delay until Section 2.

For the bound electrons (more exactly: for the electrons moving in external fields) it is convenient to develop PT based on the bound electron wave functions. This representation is called Furry representation, or the Furry picture [19]. Within the Furry picture a many-electron atom is considered as a system of electrons moving in the field of a nucleus and interacting with each other via the electromagnetic field.

Formally the interaction constant in QED is e, that enters in Eq. (33). Actually QED corrections are proportional to powers of $e^2 = \alpha$ (in relativistic units).

1.3 Feynman graph techniques for the bound electrons

Inserting $\hat{H}_{int}$ in the form (33) into expression (44) for $\hat{S}(\infty, -\infty)$ we arrive at the so called invariant PT:

$$\hat{S}^{(l)}(\infty, -\infty) = \frac{(-1)^l}{l!} \int d^4x_1 ... d^4x_l T\left(\hat{j}_{\mu_1}(x_1)\hat{A}^{\mu_1}(x_1), ..., \hat{j}_{\mu_l}(x_l)\hat{A}^{\mu_l}(x_l)\right). \tag{12.48}$$

The treatment of the each separate PT term is based on the fundamental Wick's theorem [20]: T - product of the different field operators (of the kind presented by the integrand in Eq. (48)) can be reduced to the sum of N-products with all the possible contractions of the field operators. The contraction of the two field operators $\hat{A}$ and $\hat{B}$ is defined as:

$$\widehat{\hat{A}\hat{B}} \equiv T\left(\hat{A}\hat{B}\right) - N\left(\hat{A}\hat{B}\right). \tag{12.49}$$

Note that in the Furry picture the N-symbol in Eq. (34) should be omitted. Otherwise terms that describe the current induced in the vacuum by the external field will be absent. Unfortunately this leads to the arrival of some additional PT terms that should be omitted for physical

reasons and requires more careful consideration of each PT term from the physical point of view.

It can be shown that the contractions are not the operators in the Fock space but the ordinary functions. They are called also propagators since they describe the propagation of the corresponding particles.

The electron (positron) propagator is defined as:

$$\widehat{\hat{\Psi}_\alpha(x)\hat{\Psi}_\beta(x')} = \mathcal{S}_{\alpha\beta}(x, x'), \tag{12.50}$$

where α, β are spinor indeces. These indices are usually omitted in the evaluations. The photon propagator is:

$$\widehat{\hat{A}_\mu(x)\hat{A}_\nu(x')} = \mathcal{D}_{\mu\nu}(x, x'). \tag{12.51}$$

The field operators that do not enter any contraction act on the right and left state vectors in the S-matrix elements and produce the wave functions for the electrons (positrons) and photons in the initial and final states of the system under consideration.

The graph techniques introduced by Feynman [2] help to write down all the PT terms of given order that contain all the types of contractions. According to Feynman graph techniques each space coordinate x_i in Eq. (48) corresponds to the vertex; each electron that takes part in the particular process corresponds to the solid line connecting different vertices; each photon corresponds to the wavy line that begins or ends at the one of the vertices. Then the outer electron and photon lines (i.e. the lines with one free end) will correspond to the electrons and photons in the initial and final states. To these outer lines the electron and photon wave functions are related. We accept the vertical disposition of the electron lines and will assume that the lower (upper) part of the graph correspond to the initial (final) state of the system. To the electron and photon propagators correspond the internal lines that connect two vertices, i.e. lines without free ends. To distinguish the free electrons from the bound electrons in the Furry picture we will denote the latter by the double solid lines.

In what follows we will consider only the Feynman graphs that describe corrections to energy levels. Then we should retain only the graphs without outer photon lines. The graphs with outer photon lines describe the processes of photon absorption, emission or photon scattering for atomic electrons. The graphs without outer photon lines arrive first in the second-order of PT (they should have two vertices). Thus we have to apply the Wick theorem to the expression:

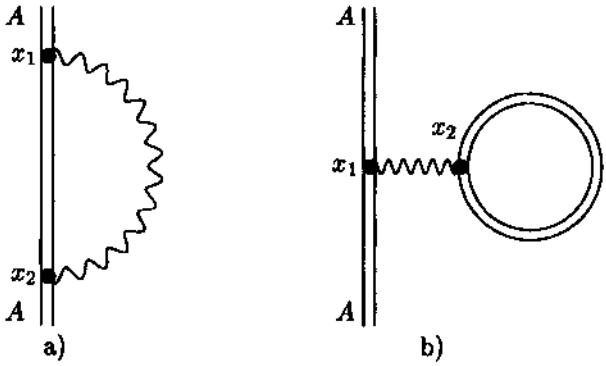

Fig.1
Feynman graphs that describe radiative corrections in one-electron ion with the electron in the state A. The graph a) describes the electron self-energy (SE) and the graph b) describes the vacuum polarization (VP). Notations are given in the text.

$$T\left(\hat{\Psi}^{+}(x_1)\gamma_\mu\hat{\Psi}(x_1)\hat{A}^{\mu}(x_1)\hat{\Psi}^{+}(x_2)\gamma_\nu\hat{\Psi}(x_2)\hat{A}^{\nu}(x_2)\right). \qquad (12.52)$$

We will not list all the possible contractions since most of them should be omitted for physical reasons (see discussion above in this Section). The remaining terms that have physical sense in an one-electron atom arise from the following contractions. First consider the terms with two contractions $\overbrace{\hat{\Psi}(x_1)\hat{\Psi}^{+}}(x_2)$ and $\overbrace{\hat{A}^{\mu}(x_1)\hat{A}^{\nu}}(x_2)$ or with $\overbrace{\hat{\Psi}^{+}(x_1)\hat{\Psi}}(x_2)$ and $\overbrace{\hat{A}^{\mu}(x_1)\hat{A}^{\nu}}(x_2)$. According to the correspondence rules both these terms can be described by the Feynman graph depicted in Fig.1a.

Note that one should not contract the operators $\hat{\Psi}(x_1)\hat{\Psi}(x_2)$ since they contain only the creation operators for the positrons and annihilation operators for the electrons. Hence the product of these operators is always N-ordered. The same concerns the product $\hat{\Psi}^{+}(x_1)\hat{\Psi}^{+}(x_2)$. The next terms that arise in the one-electron atom contain the contractions

$\overbrace{\hat{\Psi}^+(x_1)\hat{\Psi}}(x_1)$ and $\overbrace{\hat{A}^\mu(x_1)\hat{A}^\nu}(x_2)$ or $\overbrace{\hat{\Psi}^+(x_2)\hat{\Psi}}(x_2)$ and $\overbrace{\hat{A}^\mu(x_1)\hat{A}^\nu}(x_2)$ and are described by the graph Fig.1b. The graphs in Fig.1 represent the lowest-order QED corrections to the energy levels of the one-electron atom. These corrections are responsible for most of the Lamb Shift of the atomic levels and are also called radiative corrections. Some terms arising from expression (52) according to Wick's theorem cannot exist in an one-electron atom. The only important term of this kind is the term with unique contraction $\overbrace{\hat{A}^\mu(x_1)\hat{A}^\nu}(x_2)$. In an one-electron atom this term turns out to be zero since one of the two electron annihilation operators from $\hat{\Psi}(x_1)$ or $\hat{\Psi}(x_2)$ will act on the vacuum state. However in the two-electron atom this term is nonzero. Note, that the positron operators from Eq. (52) do not contribute in any case since the real atom consists of electrons. The term with the contraction $\overbrace{\hat{A}^\mu(x_1)\hat{A}^\nu}(x_2)$ describes the lowest-order interelectron interaction. The photon propagator (51) depends on the choice of gauge. The covariant Lorentz-type gauge (in particular applications to the photon propagators in QED it is called the Feynman gauge) is preferable for the description of the radiative corrections. It can be explained by the covariant character of the standard renormalization procedure. However as was already mentioned in Section 1 the Coulomb gauge is more convenient for the description of the interelectron interaction in atoms. Therefore we will distinguish the Coulomb interaction via Coulomb photons and the interaction by the exchange of the transverse photons. The latter contribution is called Breit interaction. Both interactions in the lowest order are depicted in Fig.2.

The explicit expression for the electron propagator is:

$$\mathcal{S}(x_1, x_2) = \frac{1}{2\pi i}\int_{-\infty}^{\infty} dw\ e^{iw(t_1-t_2)} \sum_s \frac{\Psi_s(\vec{r}_1)\overline{\Psi}_s(\vec{r}_2)}{E_s(1-i0)+w}. \tag{12.53}$$

The summation in Eq. (53) is extended over the entire Dirac spectrum and the infinitely small imaginary part in the denominator defines the contour of the integration in the complex w plane (the Feynman contour).

The expression for the photon propagator in the Feynman gauge looks like:

$$\mathcal{D}_{\mu\nu}(x_1 x_2) = \frac{1}{2\pi i}\frac{g_{\mu\nu}}{r_{12}}\int_{-\infty}^{\infty} dw\ e^{i|w|r_{12}-iw(t_1-t_2)}. \tag{12.54}$$

In Coulomb gauge the expression for the Coulomb photon propagator and for the transverse photon propagator are:

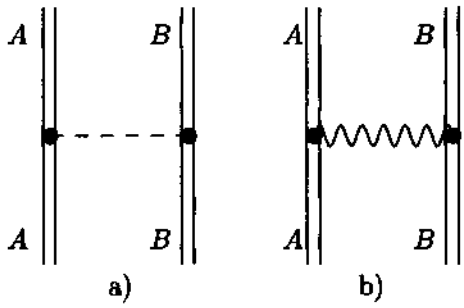

Fig.2

Feynman graphs that describe the lowest-order interelectron interaction in two-electron atom. The graph a) corresponds to the Coulomb interaction (dashed line), the graph b) corresponds to the Breit interaction (wavy line). The letters A, B denote the electron states in the two-electron atom.

$$\mathcal{D}^C_{\mu\nu}(x_1x_2) = \frac{i}{r_{12}}\delta(t_1 - t_2)\delta_{\mu 4}\delta_{\nu 4}, \tag{12.55}$$

$$\mathcal{D}^t_{\mu\nu}(x_1x_2) = \frac{1}{2\pi i}\left\{\frac{g_{\mu\nu}}{r_{12}}\int_{-\infty}^{\infty} dw\; e^{i|w|r_{12} - iw(t_1-t_2)}\right.$$

$$\left. - \nabla_{1\mu}\nabla_{2\mu}\frac{1}{r_{12}}\int_{-\infty}^{\infty} dw\; e^{iw(t_1-t_2)}\frac{e^{i|w|r_{12}} - 1}{w^2}\right\}(1 - \delta_{\mu 4})(1 - \delta_{\nu 4}). \tag{12.56}$$

A detailed description of the Feynman graph techniques and the correspondence rules within the Furry picture for bound-state QED can be found in [11].

1.4 Regularization and renormalization

The radiative corrections depicted in Fig.1 describe the interaction of the electron with the virtual photons (SE) and with vacuum electric current (VP). This interaction results in the shift of the atomic energy levels (Lamb Shift). It appears that not only the energy of the vacuum but also the energy of the interaction between atomic electron and the

vacuum is infinite. Unlike the infinite vacuum energy the infinite interaction energy cannot be simply subtracted and a sophisticated procedure of renormalization is required to obtain the finite values for the radiative corrections to atomic levels. These values are in remarkable agreement with experimental data for the transition energies.

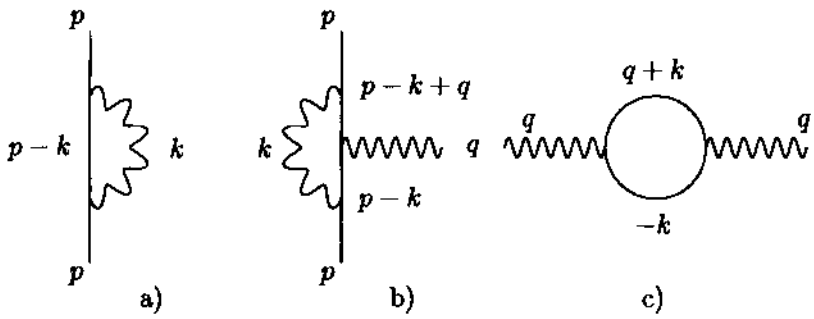

Fig.3
The lowest-order divergent Feynman graphs in the momentum representation. The graph a) corresponds to the electron self-energy graph, the graph b) corresponds to the vertex and the graph c) corresponds to the photon self-energy.

The central idea of the renormalization is that the infinities that arrive in the theory are due to the employment of the wrong values for the electron mass m and charge e. These wrong, or initial, values for m and e are present from the begining in the Dirac equation for the electron in the field of the nucleus and are actually infinite. The interaction with the electromagnetic field, including the interaction with the vacuum, leads to their replacement by the real observable (or renormalized) values m_R and e_R. The values for m_R and e_R are finite and are equal to the experimentally known electron mass and charge. Thus the procedure of the replacement m, e by m_R, e_R absorbs all the divergencies in QED.

The discussion of these divergencies usually starts with free-electron QED. In this case (as well as in bound-electron QED) there are three basic types of the divergent Feynman graphs depicted in Fig.3. In particular Fig.3a represents the lowest-order electron self-energy (SE). In the general case SE is defined as the part of the Feynman graph, connected with the other parts by only two electron lines. The graph Fig.3b shows

the lowest-order vertex. The general definition of the vertex reads: the vertex is the part of the Feynman graph connected with other parts by two electron and one photon lines. Finally, Fig.3c depicts the lowest-order photon self-energy which in the general case is defined as the part of the Feynman graph connected with the other parts only by two photon lines.

The Feynman graphs in Fig.3 are given in the momentum representation; p, q are the outer (real) electron and photon 4-momenta and k is the internal (virtual) photon or electron momentum. It is assumed that the integration is performed over k and these integrals for the graph Fig.3 are divergent when $k \to \infty$. These divergencies are called ultraviolet since for the virtual photons $k \to \infty$ means infinitely large frequencies.

It can be shown that all the possible divergences in QED can be reduced to the combinations of these three basic ones.

The concept of the compact graph plays an important role in the renormalization procedure. The compact electron self-energy graph by definition cannot be divided in two parts connected by only one electron line. The compact photon self-energy graph cannot be divided in two parts connected by only one photon line. The compact vertex is the graph that cannot be divided in two parts connected by only one electron or one photon line. All the graphs in Fig.3 are compact. Other examples of compact graphs are given in Fig.4a, 5a and examples of the noncompact graphs in Fig. 4b, 5b, 6.

Now we can introduce the exact propagators for the electrons $\mathcal{G}^{(e)}(p)$ and photons $\mathcal{G}^{(\gamma)}_{\mu\nu}(k)$ in the momentum space. The propagator $\mathcal{G}^{(e)}(p)$ arises after we insert all the possible electron self-energy graphs into the internal electron line. The propagator $\mathcal{G}^{(\gamma)}_{\mu\nu}(k)$ is defined by all the possible photon self-energy insertions in the internal photon line. In principle, these insertions should be made also in the outer electron and photon lines. This leads to the arrival of so called "exact" (renormalized) wave functions for the real electrons and photons. The exact vertex $\Gamma_\mu(p_1 p_2 k)$ is defined as the sum of all the compact vertices.

The exact propagators satisfy the Dyson equations:

$$\mathcal{G}^{(e)}(p) = \mathcal{S}(p) + \mathcal{S}(p)\Sigma(p)\mathcal{G}^{(e)}(p), \tag{12.57}$$

$$\mathcal{G}^{(\gamma)}_{\mu\nu}(k) = \mathcal{D}_{\mu\nu}(k) + \mathcal{D}_{\mu\lambda}(k)\Pi^{\lambda\pi}(k)\mathcal{G}^{(\gamma)}_{\pi\nu}(k), \tag{12.58}$$

where $\Sigma(p)$ is the sum of the compact electron self-energy graphs and $\Pi^{\lambda\pi}(k)$ is the sum of the compact photon self-energy graphs.

There is no general relation between the vertex $\Gamma_\mu(p_1 p_2 k)$ and the propagators $\mathcal{G}^{(e)}(p)$, $\mathcal{G}^{(\gamma)}_{\mu\nu}(k)$. Still such a relation exists in an impor-

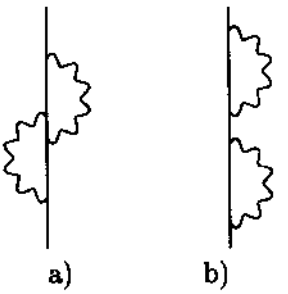

Fig.4
Compact a) and noncompact b) second-order electron self-energy graphs.

tant particular case, when $p_1 = p_2$. This relation is called the "Ward identity". It is convenient to introduce the "short" vertex:

$$\Lambda_\mu(p_1 p_2 k) = \Gamma_\mu(p_1 p_2 k) - \gamma_\mu, \tag{12.59}$$

where γ_μ is the lowest-order (first order in the interaction constant) vertex. Then the Ward identity looks like:

$$\Lambda_\mu(p\ p\ k) = \frac{\partial}{\partial p}\Sigma(p). \tag{12.60}$$

Note that due to the energy conservation $k = p_1 - p_2$, so that $k = 0$ in Eq. (60).

Now we describe the regularization of the divergent graphs in QED. After the regularization the divergences vanish and the main goal of the renormalization theory is to prove that the regularization is equivalent to the renormalization. This means that after subtracting all the divergent parts from the Feynman graphs one can put the observable values m_R and e_R in the remaining finite expressions. With this the renormalization procedure is over.

Regularization of the electron self-energy graph means:

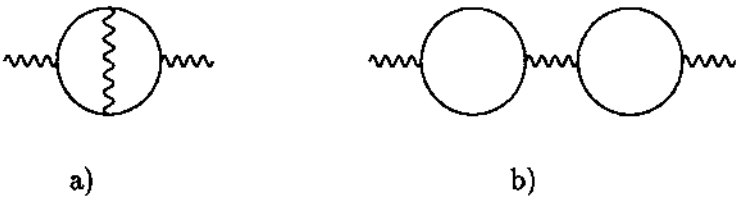

Fig.5
Compact a) and noncompact b) second-order photon self-energy graphs.

$$\Sigma_R(p) = \Sigma(p) - \Sigma(m) - (\not{p} - m)\left(\frac{\partial \Sigma}{\partial p}\right)_{\not{p}=m}, \tag{12.61}$$

where $\Sigma(m) = \Sigma(p)|_{\not{p}=m}$ is the electron self-energy correction on the mass shell, i.e. for the free electron. The relation between the observable and the "initial" mass is:

$$m_R = m + \Sigma(m) \tag{12.62}$$

In Eq. (62) both terms (m and $\Sigma(m)$) are infinite but m_R is finite. The subtraction of the first term in the right-hand side of Eq. (61) corresponds therefore to the "mass renormalization". The subtraction of the second term is related to the "charge renormalization". Eq. (61) shows that the mass renormalization can be achieved by subtraction of the free electron self-energy correction from the bound electron self-energy correction. This circumstance is used directly in some renormalization schemes (see Section 4).

The regularized vertex is:

$$\Lambda_{R\ \mu}(p_1 p_2) = \Lambda_\mu(p_1 p_2) - \Lambda(m, m) \tag{12.63}$$

and the regularized photon self-energy is:

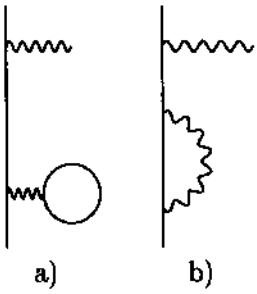

Fig.6
Noncompact vertices in the third order of the interaction constant.

$$\Pi_{R\ \mu\nu}(k) = \Pi_\gamma(k^2)\left(\delta_{\mu\nu} - \frac{k_\mu k_\nu}{k^2}\right), \tag{12.64}$$

$$\Pi_\gamma(k^2) = \Pi(k^2) - \Pi(0) - k^2\left(\frac{d\Pi(k^2)}{d(k^2)}\right)_{k^2=0}. \tag{12.65}$$

For the charge renormalization it is convenient to introduce the renormalization constants Z_1 and Z_3. Then:

$$e_R^2 = Z_3 e^2, \tag{12.66}$$

$$\mathcal{G}_R^{(e)} = \frac{1}{Z_1}\mathcal{G}^{(e)}, \tag{12.67}$$

$$\mathcal{G}_{R\ \mu\nu}^{(\gamma)} = \frac{1}{Z_3}\mathcal{G}_{\mu\nu}^{(\gamma)}, \tag{12.68}$$

$$\Gamma_{R\ \mu} = Z_1\Gamma_\mu, \tag{12.69}$$

$$\Psi_R = Z_1^{1/2}\Psi, \tag{12.70}$$

$$A_{R\,\mu} = Z_3^{1/2} A_\mu. \tag{12.71}$$

It can be proved that the relations (66)–(71) are all consistent with each other and $\mathcal{G}_R^{(e)}$, $\mathcal{G}_{R\,\mu\nu}^{(\gamma)}$ satisfy the Dyson equations with renormalized electron mass $m = m_R$ and renormalized electron and photon self-energies:

$$\Sigma_R = Z_1 \Sigma_\gamma, \tag{12.72}$$

$$\Pi_R = Z_3 \Pi_\gamma. \tag{12.73}$$

The renormalized vertex (69) is connected with the regularized expression (63) by the relation:

$$\Gamma_{R\,\mu} = \gamma_\mu + Z_1 \Lambda_{R\,\mu}. \tag{12.74}$$

The arbitrary matrix element of the $\mathcal{S}$-matrix in n-th order PT can be schematically represented as:

$$\mathcal{S}^{(n)} \sim e^n \int (\Gamma)^n \left(\mathcal{G}^{(e)}\right)^{F_e} \left(\mathcal{G}^{(\gamma)}\right)^{F_\gamma} (\Psi)^{N_e} (A)^{N_\gamma}, \tag{12.75}$$

where F_e, F_γ are the numbers of the internal electron and photon lines in the corresponding Feynman graph and N_e, N_γ are the numbers of the outer electron and photon lines. Inserting in Eq. (75) the renormalized expressions for Γ, $\mathcal{G}^{(e)}$, $\mathcal{G}^{(\gamma)}$, Ψ and A and using Eqs. (66)–(71) we find:

$$\mathcal{S}^{(n)} \sim Z_1^{-n+F_e+\frac{1}{2}N_e} Z_3^{-\frac{1}{2}n+F_\gamma+\frac{1}{2}N_\gamma} e_R^n \times$$

$$\times \int (\Gamma_R)^n \left(\mathcal{G}_R^{(e)}\right)^{F_e} \left(\mathcal{G}_R^{(\gamma)}\right)^{F_\gamma} (\Psi_R)^{N_e} (A_R)^{N_\gamma}. \tag{12.76}$$

The use of the two evident relations:

$$n = F_e + \frac{1}{2} N_e, \tag{12.77}$$

$$n = 2F_\gamma + N_\gamma, \tag{12.78}$$

finally yields:

$$\mathcal{S}^{(n)} \sim e_R^n \int (\Gamma_R)^n \left(\mathcal{G}_R^{(e)}\right)^{F_e} \left(\mathcal{G}_R^{(\gamma)}\right)^{F_\gamma} (\Psi_R)^{N_e} (A_R)^{N_\gamma}. \tag{12.79}$$

The formula (79) presents the final result of the renormalization procedure in QED. It shows that after regularization of the divergent integrals

in $S^{(n)}$ according to prescriptions (62), (63) and (65) we can replace the initial mass and charge values with the observable ones m_R, e_R. After the renormalization is completed for practical calculations we can put $Z_1 = Z_3 = 1$. This shows that the electron and photon wave functions should remain unchanged.

For practical purposes various methods of introducing the regulators are used. The most standard one is the "cut-off" regularization in 4-momentum space. The other options are the Pauli-Willars regularization [21] or the dimensional regularization (see, for example, [22]).

In the following sections we will again use the notation m, e for the observable electron mass and charge.

2. Interelectron interaction in atoms

2.1 Adiabatic S-matrix formalism

Unlike the nonrelativistic theory the Schrödinger equation (35) for quantized interacting fields cannot be used directly for the atomic energy level calculations. The zero-order approximation for the energy of noninteracting electrons in atoms is:

$$E^{(0)} =\rangle\Phi|\hat{H}_e|\Phi\langle= \sum_{s=1}^{N} E_s, \tag{12.80}$$

where E_s are one-electron Dirac energies and the summation is extended over all occupied states. However the shift due to the interelectron interaction via the electromagnetic field is not so easy to introduce. Contrary to the free-electron QED theory, the interaction between the bound electrons is present all the time. One of the most popular ways to avoid this difficulty is the use of the adiabatic S-matrix formalism of Gell-Mann and Low [23]. The main feature of this formalism is the adiabatic switching of the interaction, that is achieved by replacing the interaction Hamiltonian $\hat{H}_{int}(t)$ with the operator:

$$\hat{H}_{int}(t,\gamma) = e^{-\gamma|t|}\hat{H}_{int}(t), \tag{12.81}$$

where $\gamma > 0$ is the adiabatic parameter. Then at times $t = \pm\infty$ the interaction is switched off and at $t = 0$ it is fully switched on. Using the interaction (81) one can perform the calculations in the usual free-electron QED manner and then put $\gamma = 0$, which means the restoration of the interaction for the whole time interval. This allows for the extension of the well-known techniques for calculating the free-electron S-matrix elements to bound electrons in atoms.

Gell-Mann and Low [23] derived a formula which yields the energy shift due to the interaction (81) in terms of the matrix elements of the operator $\hat{S}_\gamma(0,-\infty)$ where $\hat{S}_\gamma$ is the electron operator (39) obtained from Eq. (40) with $\hat{H}_{int}(t)$ replaced by operator (81). Later Sucher [24] derived a symmetrized version of the energy shift formula, containing the matrix elements of the operator $\hat{S}_\gamma(\infty,-\infty)$ and which is more suitable for the renormalization procedure.

The energy shift is determined by:

$$\Delta E_a = \lim_{\gamma\to 0} \frac{i}{2}\gamma e \frac{\frac{\partial}{\partial e}\langle\Phi_a|\hat{S}_\gamma(\infty,-\infty)|\Phi_a\rangle}{\langle\Phi_a|\hat{S}_\gamma(\infty,-\infty)|\Phi_a\rangle}, \tag{12.82}$$

where $\langle\Phi_a|$ is the state vector for the noninteracting electron-positron and electromagnetic fields. Formula (82) enables one to calculate the different kinds of corrections to the energy levels using the Feynman graph techniques in Furry representation for the adiabatic S-matrix elements. All the time integrations should be done explicitly and unlike the free-electron QED each vertex should contain the adiabatic exponent. This program was first realized in [25] where the QED theory of the interelectron interaction in many-electron atoms was developed. For actual calculation it is convenient to expand Eq. (82) in powers of e. The corresponding expansion up to 4th order was given in [25]:

$$\begin{aligned}
\Delta E_a = \lim_{\gamma\to 0} i\gamma \Big\{ & \langle\Phi_a|\hat{S}_\gamma^{(1)}(\infty,-\infty)|\Phi_a\rangle + [\langle\Phi_a|\hat{S}_\gamma^{(2)}(\infty,-\infty)|\Phi_a\rangle \\
& \langle\Phi_a|\hat{S}_\gamma^{(1)}(\infty,-\infty)|\Phi_a\rangle^2] + [3\langle\Phi_a|\hat{S}_\gamma^{(3)}(\infty,-\infty)|\Phi_a\rangle \\
& -3\langle\Phi_a|\hat{S}_\gamma^{(2)}(\infty,-\infty)|\Phi_a\rangle\langle\Phi_a|\hat{S}_\gamma^{(1)}(\infty,-\infty)|\Phi_a\rangle \\
& +\langle\Phi_a|\hat{S}_\gamma^{(1)}(\infty,-\infty)|\Phi_a\rangle^3] + [4\langle\Phi_a|\hat{S}_\gamma^{(4)}(\infty,-\infty)|\Phi_a\rangle \\
& -4\langle\Phi_a|\hat{S}_\gamma^{(3)}(\infty,-\infty)|\Phi_a\rangle\langle\Phi_a|\hat{S}_\gamma^{(1)}(\infty,-\infty)|\Phi_a\rangle \\
& +4\langle\Phi_a|\hat{S}_\gamma^{(2)}(\infty,-\infty)|\Phi_a\rangle\langle\Phi_a|\hat{S}_\gamma^{(1)}(\infty,-\infty)|\Phi_a\rangle^2 \\
& -2\langle\Phi_a|\hat{S}_\gamma^{(2)}(\infty,-\infty)|\Phi_a\rangle^2 - \langle\Phi_a|\hat{S}_\gamma^{(1)}(\infty,-\infty)|\Phi_a\rangle^4]\Big\}.
\end{aligned} \tag{12.83}$$

For the free atom, in the absence of the external fields, the energy corrections contain only S-matrix elements of even order. The reason

is that the perturbation $\hat{H}_{int}$ depends linearly on the operators of the emission or the absorption of photons (see Eq. (33)) and these operators should enter pairwise in the expansion for the energy correction to give the photon vacuum state. Then the equation (83) looks simpler:

$$\Delta E_a = \lim_{\gamma\to 0} i\gamma \Big\{ \langle\Phi_a|\hat{S}_\gamma^{(2)}(\infty,-\infty)|\Phi_a\rangle$$

$$+[4\langle\Phi_a|\hat{S}_\gamma^{(4)}(\infty,-\infty)|\Phi_a\rangle - 2\langle\Phi_a|\hat{S}_\gamma^{(2)}(\infty,-\infty)|\Phi_a\rangle^2]\Big\} \qquad (12.84)$$

It is essential to distinguish the contribution of the "irreducible" and "reducible" graphs (S-matrix elements). In the irreducible graphs the initial or "reference" state is omitted in the summation over intermediate atomic states. The contribution of the "reference" state is described by the "reducible" graphs. The "reducible" S- matrix elements can be expressed as a product of the lower-order S-matrix elements. The calculation of the "reducible" S-matrix elements with the use of Eq. (83) gives rise to the singular terms $1/\gamma$, $1/\gamma^2$ etc. These singularities are cancelled explicitly by the counterterms contained in each set of the square brackets in Eq. (83). The remainder after this cancellation is called the "reference state contribution" (RSC).

For irreducible matrix elements the procedure of the evaluation of the limit $\gamma \to 0$ can be avoided and the adiabatic formula (83) can be replaced by a simpler one [11]:

$$\Delta E_a^{(n),irr} = \langle\Phi_a|U^{(n)}|\Phi_a\rangle, \qquad (12.85)$$

where the "effective potential energy" $U^{(n)}$ is defined as:

$$\langle\Phi_a|\hat{S}^{(n)}|\Phi_a\rangle_{irr} = 2\pi i\delta(E_a^{(0)} - E_b^{(0)})\langle\Phi_a|U^{(n)}|\Phi_a\rangle. \qquad (12.86)$$

A simple proof of Eqs. (85)–(86) is given in [26].

In principle, Eqs. (82)–(84) are valid for the nondegenerate states only. For generalization to the degenerate case we refer to [11]. However, the formulas (82)–(84) remain unchanged in the most important case when the degenerate states differ by symmetry. Reference state corrections for two-electron atoms were first introduced in [27]. They arrive first in the 4th order in e, for the two-photon exchange graphs. For the Coulomb-Coulomb correction the RSC are absent [25]. An explicit expression for the Coulomb-Breit RSC for the ground state of the two-electron atom was derived in [28].

There are other QED approaches to calculations with bound electrons in atoms. One of them is based on the Green function [29] (see also the

related approach in [30]) and the other on the line profile theory [26]. All the methods are equivalent, but the derivations of the corrections differ; it concerns especially the reducible corrections.

2.2 First order interelectron interaction

The first order interelectron interaction in the Coulomb gauge is described by the two second-order in e Feynman graphs Fig.2. These graphs represent the one-photon exchange between the atomic electrons. They are irreducible and for the evaluation of the corresponding energy correction the simplified formulas (85)–(86) can be used. The S-matrix element that corresponds to the Feynman graph Fig.2a looks like:

$$\langle \Phi_b | \hat{S}^{(2)} | \Phi_a \rangle =$$

$$= e^2 \int \left(\overline{\Psi}_{A'}(x_1) \gamma^\mu \Psi_A(x_1) \right) \left(\overline{\Psi}_{B'}(x_2) \gamma^\mu \Psi_B(x_2) \right) \mathcal{D}^C_{\mu\nu}(x_1 x_2) d^4x_1 d^4x_2, \tag{12.87}$$

where one-electron indices A', B' correspond to the atomic state b, and the indices A, B correspond to the state a. The Coulomb photon propagator is defined by Eq. (55). Performing time integration in Eq. (87) and using Eqs. (85) – (86) we obtain the first - order Coulomb energy correction for the atom with the electrons in the state A, B.

Antisymmetrization of the many-electron wave function corresponds to the permutation of the one-electron indices in the upper (or lower) part of the Feynman graph. The "exchange" graphs have the additional factor $(-1)^\zeta$ where ζ is the number of permutations of pairs of indices.

Being applied to the first-order Coulomb graph and its "exchange" counterpart, this yields:

$$\Delta E^C_{AB} = \left(\hat{V}_C \right)_{AB;AB} \tag{12.88}$$

where

$$\hat{V}_C = \frac{e^2}{r_{12}} \tag{12.89}$$

is the Coulomb interaction potential and

$$(\mathcal{F})_{ABCD} = \int \Psi^+_A(\vec{x}_1) \Psi^+_B(\vec{x}_2) \mathcal{F}(\vec{x}_1, \vec{x}_2) \Psi_C(\vec{x}_1) \Psi_D(\vec{x}_2) \tag{12.90}$$

$$(\mathcal{F})_{AB;AB} = (\mathcal{F})_{ABAB} - (\mathcal{F})_{ABBA} \cdot \tag{12.91}$$

The analogous evaluations for the Breit interaction described by the graph Fig.2b, result in:

$$\Delta E^B_{AB} = \frac{e^2}{2}\Big\{ \Big(-\frac{\vec{\alpha}_1\vec{\alpha}_2}{r_{12}} \Big)_{ABAB}$$

$$+ \Big(\frac{1}{r_{12}} + \frac{\vec{\alpha}_1\vec{\alpha}_2 - 1}{r_{12}} \cos((E_A - E_B)r_{12}) \Big)_{ABBA} \Big\}. \qquad (12.92)$$

Eq. (92) includes magnetic interaction and retardation effects. In case of the ground state of the two-electron atom, when $E_A = E_B$, Eq. (92) reduces to:

$$\Delta E^B_{AB} = \frac{e^2}{2} \left(\frac{\vec{\alpha}_1\vec{\alpha}_2}{r_{12}} \right)_{AB;AB}. \qquad (12.93)$$

In Eqs. (92),(93) $\vec{\alpha}_i$ $(i = 1, 2)$ are the Dirac matrices corresponding to the different electrons.

A semirelativistic expression for the Breit interaction with the neglect of retardation can be obtained if we expand $\cos((E_A - E_B)r_{12})$ in Eq. (92) in powers of αZ. In the nonrelativistic limit for the atomic electrons we have $E_A - E_B \sim m(\alpha Z)^2$ in r.u. The characteristic value for r_{12} for the bound electron in atom is $r_{12} \sim a_0/Z \sim (m\alpha Z)^{-1}$, where a_0 is the Bohr radius. Then $(E_A - E_B)r_{12} \sim \alpha Z$ and we can expand the cosine in Eq. (92). Since the $\vec{\alpha}$-matrices also introduce a smallness of order αZ (see Eqs. (24)–(26)) we have to retain only the first term in cosine expansion when it is multiplied by $\vec{\alpha}_1\vec{\alpha}_2$ but to retain the third term when it is multiplied by 1. The second term vanishes due to the orthogonality of the wave functions.

Then the S-matrix element for the first-order Breit interaction can be written in the form:

$$\langle \Phi_b | \hat{S}^{(2)} | \Phi_a \rangle = -2\pi i \delta(E_A - E_B) \langle \Phi_b | \hat{V}_B | \Phi_a \rangle, \qquad (12.94)$$

where $V_B(r_{12})$ is the Breit operator:

$$\hat{V}_B = -\frac{e^2}{2} \left[\frac{\vec{\alpha}_1\vec{\alpha}_2}{r_{12}} + \frac{(\vec{\alpha}_1\vec{r}_{12})(\vec{\alpha}_2\vec{r}_{12})}{r_{12}^3} \right]. \qquad (12.95)$$

It is understood that the matrix elements of this operator should be evaluated with the relativistic 4-component wave function. The approximation (95) is called also the low-frequency approximation, since it arises when energy differences tend to zero: $\Delta E \to 0$. An expression for the Breit operator suitable for the evaluations with the two-component (nonrelativistic) wave functions follows when we expand also the relativistic wave functions using Eqs. (24)–(26):

$$\hat{V}_B = \frac{e^2}{m}\left\{-\pi\delta(\vec{r}_{12}) - \frac{1}{2r_{12}}\left(\hat{\vec{p}}_1\hat{\vec{p}}_2 + \frac{\vec{r}_{12}(\vec{r}_{12}\hat{\vec{p}}_1)\hat{\vec{p}}_2}{r_{12}^2}\right)\right.$$

$$+\frac{1}{4r_{12}^3}\left[-(\vec{\sigma}_1 + 2\vec{\sigma}_2)(\vec{r}_{12}\times\hat{\vec{p}}_1) + (\vec{\sigma}_2 + 2\vec{\sigma}_1)(\vec{r}_{12}\times\hat{\vec{p}}_2)\right]$$

$$\left.+\frac{1}{4}\left[\frac{\vec{\sigma}_1\vec{\sigma}_2}{r_{12}^3} - \frac{3(\vec{\sigma}_1\vec{r}_{12})(\vec{\sigma}_2\vec{r}_{12})}{r_{12}^5} - \frac{8\pi}{3}(\vec{\sigma}_1\vec{\sigma}_2)\delta(\vec{r}_{12})\right]\right\} \qquad (12.96)$$

Here $\hat{\vec{p}}_i$, $\vec{\sigma}_i$ $(i = 1,2)$ are momentum operators and Pauli matrices for different electrons.

All the terms of the operator (96) are the order $Z^{-1}(\alpha Z)^4$ in r.u., i.e. $Z^{-1}(\alpha Z)^2\varepsilon_0$ where ε_0 is the characteristic binding energy. The terms in the first line of Eq. (96) describe the relativistic orbit - orbit interaction, the terms in the second line describe the spin - other orbit interaction (unlike the spin-orbit interaction that is included in the one-electron Dirac equation) and the terms in the third line describe the spin-spin interaction.

It is important to note that both operators (95) and (96) should not be iterated in QED when the negative-energy states may occur as the intermediate states. The full QED theory of the second - order interelectron interaction will be described in the next section.

2.3 Second order interelectron interaction

The full set of the Feynman graphs describing the second-order interelectron interaction (two-photon exchange) in the two-electron atom is depicted in Fig.7 (in the Coulomb gauge). The "exchange" graphs with the interchanged upper electron indices have to be added to the graphs Fig.7. All the "exchange" graphs have the opposite sign compared to the "direct" graphs. Apart from the "box" graphs that do not vanish in the nonrelativistic limit, the "cross" graphs have to be taken into account in the full QED description.

We begin with the most simple Coulomb-Coulomb "box" graph. It is reducible and the evaluation of the corresponding energy shift requires the use of Eq. (84).

The S-matrix element that corresponds to the Feynman graph Fig.7a looks like:

$$\langle\Phi_a|\hat{S}_\gamma^{(4)}|\Phi_a\rangle = e^4\int\left(\overline{\Psi}_A(x_3)\gamma^{\mu_3}\mathcal{S}(x_3x_1)\gamma^{\mu_1}\Psi_A(x_1)\right)$$

$$\times\left(\overline{\Psi}_b(x_4)\gamma^{\mu_4}\mathcal{S}(x_4x_2)\gamma^{\mu_2}\Psi_B(x_2)\right)\mathcal{D}^C_{\mu_1\mu_2}(x_1x_2)\mathcal{D}^C_{\mu_3\mu_4}(x_3x_4)$$

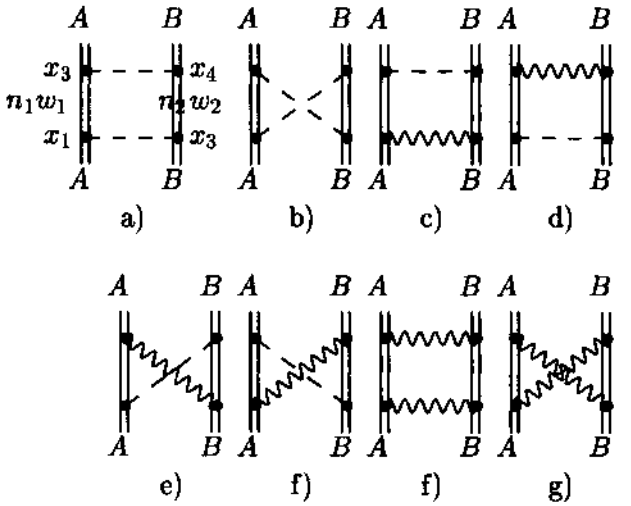

Fig.7
Feynman graphs that describe the second-order interelectron interaction in two-electron atom. Notation is the same as in Fig.2.

$$\times e^{-\alpha(|t|_1+|t|_2+|t|_3+|t|_4)} d^4x_1 d^4x_2 d^4x_3 d^4x_4. \qquad (12.97)$$

The electron propagator $S(x_1x_2)$ is defined by Eq. (53). Inserting these propagators in Eq. (97) we have additional double integration over the frequency variables and the double summation over the Dirac spectrum n_1 n_2.

We perform first the integration over the time variables t_1, ..., t_4 and then the integration over the frequency variables w_1, w_2 in the complex plane using the Feynman contours defined by the denominators in Eq. (53). The terms with $n_1, n_2 = A, B$ in the double sum over n_1 and n_2 should be considered separately since they lead to additional singularity with respect to γ. These terms correspond to the "reference state". Then the integrations result in:

$$\langle \Phi_a | \hat{S}_\gamma^{(4)} | \Phi_a \rangle = e^4$$

$$\times \sum_{n_1 n_2 \ (n_1 n_2 \neq AB)} \left(P_1^{(+)} P_2^{(+)} - P_1^{(-)} P_2^{(-)} \right) \left| \left(\frac{1}{r_{12}} \right)_{n_1 n_2 AB} \right|^2$$

$$\times\left\{\frac{1}{2i\gamma}\frac{1}{E_{n_1}+E_{n_2}-E_A-E_B}+\frac{1}{(E_{n_1}+E_{n_2}-E_A-E_B)^2}\right\}$$

$$-\frac{e^4}{2\gamma^2}\left[\left|\left(\frac{1}{r_{12}}\right)_{ABAB}\right|^2+\left|\left(\frac{1}{r_{12}}\right)_{ABBA}\right|^2\right]. \qquad (12.98)$$

Here $P_1^{\pm}$, $P_2^{\pm}$ are the projectors onto the positive (negative) states in the sums over n_1, n_2. The last term in Eq. (98), proportional to γ^{-2}, corresponds to the reference state contribution. Now we have to use the formula (84) for the energy shift, adding the contributions of the "exchange" graphs. Then the reference state contribution in Eq. (98) will be totally cancelled by the counterterm $\langle\Phi_a|\hat{S}^{(2)}|\Phi_a\rangle^2$ in Eq. (84) and the final result will be:

$$\Delta E_{AB}^{CC,box}=\frac{e^4}{2}\sum_{n_1n_2\ (n_1n_2\neq AB)}\frac{P_1^{(+)}P_2^{(+)}-P_1^{(-)}P_2^{(-)}}{E_{n_1}+E_{n_2}-E_A-E_B}\left|\left(\frac{1}{r_{12}}\right)_{n_1n_2;AB}\right|^2. \qquad (12.99)$$

This formula was first derived in [25]. Note, that the reference state correction is absent for the Coulomb-Coulomb second order interaction. The contribution of the "cross" Coulomb-Coulomb interaction (Fig.7b) is irreducible and can be obtained with the use of the formulas (85) and (86).

The result, also derived first in [25], is:

$$\Delta E_{AB}^{CC,cross}=e^4\sum_{n_1n_2}\left(P_1^{(+)}P_2^{(+)}-P_1^{(-)}P_2^{(-)}\right)\left\{\left|\left(\frac{1}{r_{12}}\right)_{An_1n_2B}\right|^2\right.$$

$$\left.\times\frac{1}{E_A+E_{n_1}-E_{n_2}-E_B}-\left(\frac{1}{r_{12}}\right)^*_{An_1n_2A}\left(\frac{1}{r_{12}}\right)_{Bn_1n_2B}\frac{1}{E_{n_1}-E_{n_2}}\right\}. \qquad (12.100)$$

The expressions for the Coulomb-Breit and Breit-Breit second order interelectron interaction corrections are more complicated. These corrections for the ground and excited states of the two-electron atom were considered in [26, 28, 32–34].

In the case of Coulomb-Breit and Breit-Breit corrections the reducible (reference state) contributions are not zero. The explicit expression for the reducible Coulomb-Breit correction originates from the graphs Fig.7c,d. In the case of the ground state it was first derived in [28]:

$$\Delta E_{AB}^{CB,red} = -\frac{2e^4}{\pi}\left(\frac{1}{r_{12}}\right)_{AB;AB}\left(\frac{(\vec{\alpha}_1\vec{r}_{12})(\vec{\alpha}_2\vec{r}_{12})}{r_{12}^2}\right)_{AB;AB}. \quad (12.101)$$

However it appears that the reference state contribution to the Coulomb - Breit "cross" graph Fig.7e,f exactly cancels the contribution (101) [35]. The graphs Fig 7e,f are irreducible and the reference state contribution to these graphs is not singular. So the origin of the reference state contribution to the "cross" graphs Fig.7e,f is different to the origin of the reference state contribution to the box graphs Fig. 7c,d. In the latter case these contributions are singular and the correction (101) presents the remainder after the cancellation of the singularities in Eq. (84). However it becomes common to define the reference state correction as the sum of the reference state contributions (RSC) to the "box" and "cross" graphs. Then the total RSC for the ground state of the two-electron atom is zero. However, the Coulomb-Breit RSC is not zero for the excited states. The Breit-Breit RSC is not zero also for the ground state [26, 32–34].

2.4 Dirac-Hartree-Fock approximation

An important problem in the application of QED methods to many-electron atoms is the choice of the zero-order approximation. One natural choice is the approximation of noninteracting electrons when the potential V in Eq. (2) is the Coulomb potential of the nucleus (28). This approximation is convenient for highly charged, few-electron ions. For a many-electron neutral atom a better choice is the Dirac-Hartree-Fock (DHF) approximation.

The DHF one-particle functions are the solutions the DHF equation:

$$\left[\hat{h}(\vec{r}) + eV_{DHF}(\vec{r})\right]\Psi_s(\vec{r}) = E_s\Psi_s(\vec{r}). \quad (12.102)$$

The potential V_{DHF} can be defined similarly to the nonrelativistic case:

$$V_{DHF}(\vec{r})f(\vec{r}) = \sum_{s=1}^{N}\int \Psi_s^+(\vec{r}')\frac{e}{|\vec{r}-\vec{r}'|}\Psi_s(\vec{r}')d\vec{r}'f(\vec{r})$$

$$-\sum_{s=1}^{N}\int \Psi_s^+(\vec{r}')\frac{e}{|\vec{r}-\vec{r}'|}f(\vec{r}')d\vec{r}'\Psi_s(\vec{r})d\vec{r}', \quad (12.103)$$

where $f(\vec{r})$ is an arbitrary bispinor wave function. It is understood that the self-consistent field procedure is already done and the one-particle functions Ψ_s present the complete set of the eigenfunctions of Eq. (102).

We can redetermine the perturbation in Eqs. (29), (30):

$$\hat{H} = \hat{H}_0 + \hat{H}_{int} = \hat{H}_0' + \hat{H}_{int}', \tag{12.104}$$

$$\hat{H}_0' = \hat{H}_0 + \hat{H}_{DHF}, \tag{12.105}$$

$$\hat{H}_{int}' = \hat{H}_{int} - \hat{H}_{DHF}, \tag{12.106}$$

where

$$\hat{H}_{DHF} = e \int \hat{\Psi}^+(\vec{r}) V_{DHF}(\vec{r}) \hat{\Psi}(\vec{r}) d\vec{r}. \tag{12.107}$$

Now, apart from the interelectron interaction we have to take into account also the additional interaction with the external field $-eV_{DHF}$. In first order of the perturbation theory (in the interaction constant e) for the two-electron atom we have to consider the additional Feynman graph depicted in Fig.8a, in second order the graph Fig.8b and in third order the graphs Fig.8c,d.

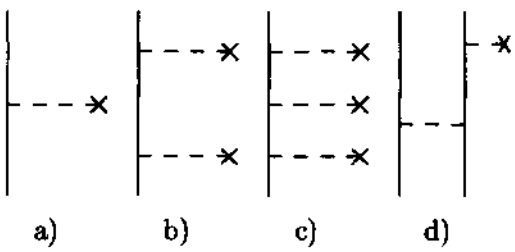

Fig.8

The Feynman graphs that describe the interaction of the atomic electron with DHF self-consistent field in the first a), second b) and third c),d) orders of the perturbation theory. The dashed line with the cross at the end denotes the external field.

However we have to remember that the order of magnitude of the Feynman graph with $2n$ vertices and m external field lines is e^{2n+2m}. The extra powers of e arise from the expression (107) for V_{DHF}. Then the graph 8a we have to combine with the graph 2a and the graph 8b with the graph 7a.

2.5 Dirac-Coulomb-Breit Hamiltonian and beyond

A natural way to generalize the non-relativistic many-body Schrödinger equation is to combine the one-electron Dirac operators and Coulomb and Breit two-electron operators. However such an equation would have serious defects. One of them is the "continuum dissolution" first discussed by Brown and Ravenhall [36]. This means that the Schrödinger-type equation has no stable solutions due to the presence of the negative energy Dirac continuum. An unconstrained variational approach becomes therefore impossible.

A solution of this problem was found in a series of works of different authors [37–39] and was presented in a form which was called Dirac-Coulomb-Breit (DCB) Hamiltonian:

$$\hat{H}_{DCB} = \sum_{i=1}^{N} \hat{h}(\vec{r}) + \sum_{i=1\ (i\neq j)}^{N} \hat{P}_i^{(+)} \hat{P}_j^{(+)} \left[\hat{V}_C(\vec{r}_{ij}) + \hat{V}_B(\vec{r}_{ij})\right] \hat{P}_i^{(+)} \hat{P}_j^{(+)}, \tag{12.108}$$

where $\hat{V}_C$ and $\hat{V}_B$ are the Coulomb and Breit interaction operators. The inclusion of the Breit interaction in Eq. (108) is possible only in the low-frequency approximation (95). Due to the presence of the $\hat{P}^{(+)}$ projectors in Eq. (108) this approximation is called also the "no-pair" approximation.

To understand what remains beyond the DCB Hamiltonian in QED, we have to analyse the relative importance of the different corrections for the different Z values. This analysis was made in [40]. To compare the different corrections it is convenient to use Fig.9. The charge of the nucleus is plotted on the horizontal axis and $\log|\Delta E_i/\Delta E_0|$ is plotted on the vertical axis. Here ΔE_i are the various corrections to the energy and ΔE_0 is the binding energy of the two non-interacting electrons in an ion.

The curve C corresponds to the first order Coulomb interelectron interaction, the curve C^{++} corresponds to the "no pair" approximation for the second-order Coulomb "box" interelectron interaction (Fig.7a). The curve B corresponds to the first order Breit interaction, the curve BC corresponds to the second-order Coulomb-Breit "box" interaction (exchange of the one Coulomb and one transverse photons) Fig.7c,d. The curve denoted by $(*)$ includes the contributions $(*) \equiv CC^{--}$, BB, X, where CC^{--} is the negative-energy contribution to the Coulomb-Coulomb "box" interaction Fig.7a, BB is the Breit-Breit "box" interaction Fig.7g, X denotes all "cross" interactions Fig.7b,e,f,h. The order of magnitude

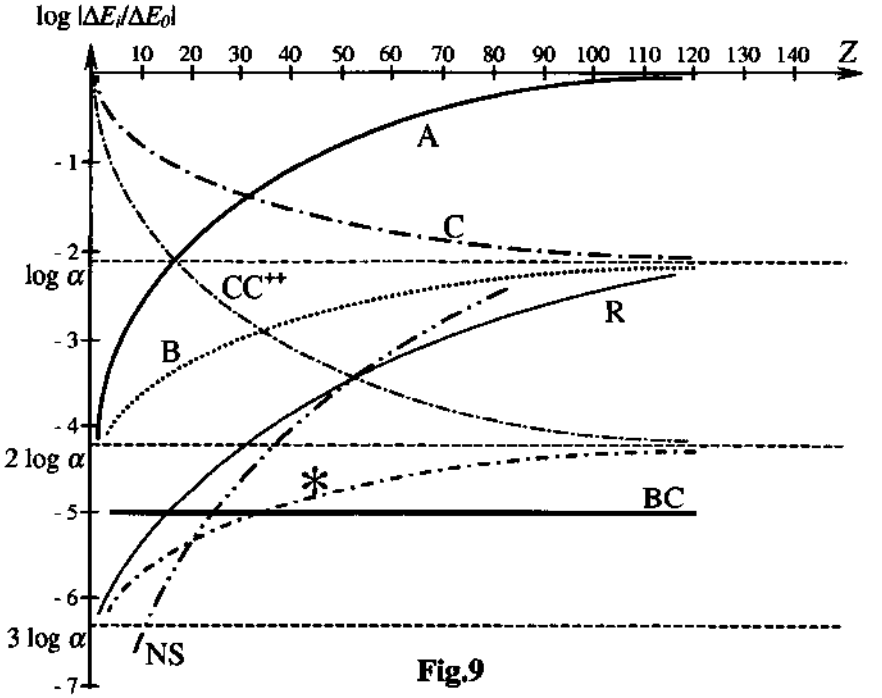

Fig.9

Comparison of the different energy corrections for arbitrary Z values for two-electron ions.

of all (*) corrections is defined by the high-energy intermediate electron state contributions. This means that the corresponding effective interelectron interaction potential does not depend on the external momenta, i.e. it is a constant in momentum space. In a coordinate space such potential is proportional to $\alpha^2\delta(\vec{r})$. The order of magnitude of this potential in r.u. is $m\alpha^2(\alpha Z)^3$ and the order of the ratio $\Delta E_X/\Delta E_0$ is $m\alpha^2(\alpha Z)^3/m(\alpha Z)^2 = \alpha^3 Z$. Thus for $Z = 1$ this ratio is α^3 and for $Z = 137$ it becomes equal to α^2. All the curves in Fig.9 are drawn approximately. The curve R corresponds to the radiative correction, or the Lamb Shift (see Section 3, 4). It is also important to take the nucleus size corrections (NS) into account, which may have the same magnitude as the Lamb Shift.

The curve A corresponds to the one-electron relativistic correction and is given for comparison. For the ground state of the two-electron atom (ion):

$$\Delta E_A = \Delta E_0 - \Delta E_0^{nr} = 2\left[\sqrt{1-(\alpha Z)^2} - 1 + \frac{1}{2}(\alpha Z)^2\right], \qquad (12.109)$$

where ΔE_0^{nr} is the nonrelativistic binding energy. One can see in Fig.8 that the corrections CC^{++} and A become equal when $Z \sim Z_1 \sim 10$. This means that relativistic corrections become larger than electron correlation (defined essentially by CC^{++}) when the charge Z increases and soon dominate over electron correlation. When $Z \sim Z_2 = 30$, the correction ΔE_A becomes equal to ΔE_C, i.e. relativistic corrections become equal to the interelectron interaction. These two important critical values of Z can be obtained also by the simple estimates: $(\alpha Z_1)^2 \sim 1/Z_1^2$ and $(\alpha Z_2)^2 \sim 1/Z_2$.

Fig.8 helps us to understand which of the most important corrections remain beyond the DCB Hamiltonian. Apart from radiative corrections, within second order these corrections include CC^{--}, $BB^{-+,+-,--}$, X and the frequency dependent corrections (retardation) in BB^{++}. According to Fig.8 these nonradiative QED corrections are smaller than the radiative ones for high Z values, but could be comparable for small and intermediate Z.

3. QED theory of light atoms

3.1 Lowest order radiative corrections

In light atoms the parameter αZ is small ($\alpha Z \ll 1$) and one can use an expansion in this parameter. Moreover, the radiative corrections can be evaluated with the nonrelativistic (Schrödinger) wave functions.

The electron self-energy and vacuum polarization corrections can be presented as corrections to the interaction potential between the atomic electron and the nucleus (see graphs Fig.10). These two graphs are the first terms of the expansion of the graphs in Fig.1 in powers of the nuclear potential $V = \frac{Ze}{r}$. Both these graphs are ultraviolet divergent. The use of the renormalized expressions obtained according to the rules given in Sec.1.d leads to the correction [41]:

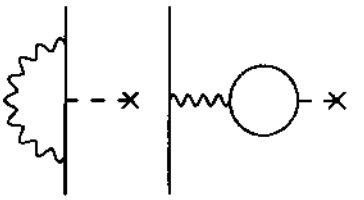

a) b)

Fig.10

Radiative corrections to the interaction with the external field (field of the nucleus in case of the Lamb Shift). Graph a) corresponds to the electron self - energy and graph a) corresponds to the vacuum polarization.

$$e\delta V(\vec{r}) = \frac{e^3}{\pi}\left\{\frac{1}{3m^2}\left(\ln\frac{m}{\lambda} - \frac{3}{8} - \frac{1}{5}\right)\beta + \frac{1}{4m}(\vec{\alpha}\vec{\nabla}V)\right\}. \qquad (12.110)$$

Here λ is the fictitious photon mass that is introduced to avoid the so called "infrared divergency". This divergency occurs in the integral over the virtual photon frequency in Fig.10a. Unlike the ultraviolet divergency it occurs in the small frequency region. To avoid it the photon propagator in the momentum representation, that is $\mathcal{D}_{\mu\nu} = -g_{\mu\nu}/k^2$ (where $k^2 = k_\mu k^\nu$, k_μ is the virtual photon momentum and $g_{\mu\nu}$ is the metric tensor) should be replaced by the expression (in the Feynman gauge):

$$\mathcal{D}_{\mu\nu}(k) = -\frac{g_{\mu\nu}}{k^2 + \lambda^2}. \qquad (12.111)$$

Then the integral becomes finite. However, the infrared divergency occurs only for free electrons, and not for bound ones, since the bound electron graph Fig.1a does not diverge when the virtual photon frequency tends to zero. Therefore the "photon mass" λ should cancel at the end of the calculations.

The term with the coefficient $-1/5$ in Eq. (110) corresponds to the graph Fig.10b (vacuum polarization), the other terms correspond to the graph Fig.10a (electron self-energy).

The radiative correction to the energy arises after averaging the potential (110) with atomic wave functions. Transformation to the nonrelativistic functions (see Eq. (25)) yields:

$$\Delta E_A' = -\frac{e^3}{\pi}\left\{\frac{1}{3m^2}\left(\ln\frac{m}{\lambda}-\frac{1}{5}\right)(\Delta V)_{AA}+\frac{1}{4m^2}\left(\frac{1}{r}\frac{dV}{dr}(\vec{\sigma}\hat{\vec{l}})\right)_{AA}\right\}, \tag{12.112}$$

where $\hat{\vec{l}}$ is the electron angular momentum.

The expression $\Delta E_A'$ presents the "high-energy" contribution to the radiative shift, since in Eq. (110) the electron binding energy was neglected compared to the virtual photon frequency. This means, that we have to add the "low-energy" contribution $\Delta E_A''$ that will cancel the dependence on λ in the total expression.

The low-energy contribution can be written in the frame of nonrelativistic quantum mechanics as [41]:

$$\Delta E_A'' = \sum_{n,\vec{k},\vec{e}} \frac{\left|e\int \vec{j}_{An}(\vec{r})A(\vec{r})d\vec{r}\right|^2}{\varepsilon_A-\varepsilon_n+w}. \tag{12.113}$$

Here $\vec{j}_{An}$ is the nondiagonal electron current:

$$\vec{j}_{An} = \frac{1}{2m}\left[(\hat{\vec{p}}\Psi_A)^*\Psi_n+\Psi_A^*\hat{\vec{p}}\Psi_n\right], \tag{12.114}$$

$\vec{A}$ is the vector potential of the electromagnetic field in the dipole approximation:

$$\vec{A} = \sqrt{\frac{2\pi}{w}}\vec{e}, \tag{12.115}$$

where $\vec{e}$ is the polarization vector. It is assumed that in Eq. (113) the summation over the complete spectrum of the Schrödinger equation for the electron in the field of the nucleus is performed, as well as the integration over the virtual photon momenta and the summation over the

virtual photon polarization. By ε_n we denote the Schrödinger eigenvalues (cf Eq. (22)).

Performing the angular integration over directions of the photon momentum, summation over polarizations, and subtracting from Eq. (113) the corresponding expression for the free electron (mass renormalization) one obtains:

$$\Delta E_A'' = \frac{2}{3\pi}\frac{e^2}{m^2}\int_0^{w_{max}} dw \sum_n \frac{\left|(\hat{\vec{p}})_{An}\right|^2 (\varepsilon_n - \varepsilon_A)}{\varepsilon_n - \varepsilon_A + w}. \tag{12.116}$$

The integral over the photon frequency w diverges when $w \to \infty$, so the integration is limited by w_{max}. Now the integration over w results in [41]:

$$\Delta E_A'' = \frac{1}{3\pi}\frac{e^3}{m^2}\ln\frac{w_{max}}{K_A}(\Delta V)_{AA}, \tag{12.117}$$

where K_A is the Bethe logarithm, defined as:

$$\ln\frac{2K_A}{m(\alpha Z)^2} = \frac{\sum_n \left|(\hat{\vec{p}})_{An}\right|^2 (\varepsilon_n - \varepsilon_A)\ln\frac{2|\varepsilon_n - \varepsilon_A|}{m(\alpha Z)^2}}{\sum_n \left|(\hat{\vec{p}})_{An}\right|^2 (\varepsilon_n - \varepsilon_A)}. \tag{12.118}$$

Since $\varepsilon_n - \varepsilon_A \approx m(\alpha Z)^2$, the quantity $\frac{2K_A}{m(\alpha Z)^2}$ does not depend on Z. It is also rather weakly dependent on the principal quantum number.

The high-energy part $\Delta E_A'$ should be matched with the low-energy part $\Delta E_A''$. This can be easily done if we regularize the high-energy part in a different way, i.e. choosing the frequency value w_{min} as a regulator instead of λ. The relation between λ and w_{min} is [41] :

$$\ln 2w_{min} = \ln\lambda + 5/6. \tag{12.119}$$

Then, putting $w_{min} = w_{max}$ we achieve the matching. The final expression looks like:

$$\Delta E_A = \Delta E_A' + \Delta E_A'' =$$

$$= -\frac{e^3}{\pi m^2}\left\{\frac{1}{3}\left(\ln\frac{m}{2K_A} - \frac{1}{5} + \frac{5}{6}\right)(\Delta V)_{AA} + \frac{1}{4}\left(\frac{1}{r}\frac{dV}{dr}(\vec{\sigma}\hat{\vec{l}})\right)_{AA}\right\}. \tag{12.120}$$

The Poisson equation for the nuclear potential V in the case of the point-like nucleus reads:

$$\Delta V = -4\pi e Z \delta(\vec{r}). \tag{12.121}$$

Then:

$$\Delta E_A = \frac{\alpha^2 Z}{\pi m^2}\left\{\frac{4\pi}{3}\left(\ln\frac{m}{2K_A}+\frac{19}{30}\right)|\Psi_A(0)|^2 - \frac{1}{4}\left(\frac{1}{r^3}(\vec{\sigma}\hat{\vec{l}})\right)_{AA}\right\}. \tag{12.122}$$

For ns-states ($nl = n0$):

$$|\Psi_A(0)|^2 = \frac{(m\alpha)^3}{\pi}\left(\frac{Z}{n}\right)^3.$$

In this case the last term in Eq. (121) becomes zero and

$$\Delta E_{n0} = \frac{4m\alpha^5 Z^4}{3\pi n^3}\left(\ln\frac{1}{(\alpha Z)^2} - \ln\frac{2K_{n0}}{m(\alpha Z)^2} + \frac{19}{30}\right). \tag{12.123}$$

For $l \neq 0$ the final result is :

$$\Delta E_{nlj} = \frac{4m\alpha^5 Z^4}{3\pi n^3}\left\{\ln\frac{1}{(\alpha Z)^2} - \ln\frac{2K_{nl}}{m(\alpha Z)^2}\right.$$
$$\left. + \frac{3[j(j+1)-l(l+1)-3/4]}{16(l+1)(l+1/2)l}\right\}. \tag{12.124}$$

According to Eq. (122) the lowest-order radiative shift is the correction of the order $\alpha(\alpha Z^2)\varepsilon_0$, where ε_0 is the binding energy. Due to the dependence on l this shift leads to the splitting of ns and $np_{1/2}$ (as well as $np_{3/2}$ and $nd_{3/2}$ etc) levels. For $n = 2$ $\Delta E_{2s} = 1034 MHz$, $\Delta E_{2p_{1/2}} = -17 MHz$, so that splitting is $\Delta E_{2s} - \Delta E_{2p_{1/2}} = 1051 MHz$, while the experimental value is $1058 MHz$. The discrepancy is due to the higher-order corrections (see Sec.3.b). This splitting was first measured in the Lamb and Retherford experiment [42].

3.2 Higher orders radiative corrections

The order of magnitude of the correction (120) is $m\alpha(\alpha Z)^4 \ln \alpha Z$ in r.u. for the logarithmic term and $m\alpha(\alpha Z)^4$ for the nonlogarithmic terms. The corrections of the next order $m\alpha(\alpha Z)^5$ and $m\alpha(\alpha Z)^6$ can be obtained by the further expansion of the graphs in Fig.1 in powers of the nuclear potential V. This was done in [43–46] and results in:

$$\Delta E_{njl} = \frac{4\alpha m}{3\pi n^3}\left\{[C_{41}\ln(\alpha Z)^{-2} + C_{40}](\alpha Z)^4 + C_5(\alpha Z)^5 + \right.$$

$$+[C_{62}\ln^2(\alpha Z)^{-2} + C_{61}\ln(\alpha Z)^{-2} + C_{60}](\alpha Z)^6 + ...\}. \qquad (12.125)$$

The coefficient C_{41} and C_{40} are defined by the expressions given in the preceding Sec.3.a and the other coefficients are:

$$C_5 = 3\pi\left[1 + \frac{11}{128} - \frac{1}{2}\ln 2 + \frac{5}{192}\right]\delta_{l0} \qquad (12.126)$$

$$C_{62} = -\frac{3}{4}\delta_{l0}, \qquad (12.127)$$

$$C_{61} = 4\ln 2 - \frac{1}{10} + \left(3\left[\ln\frac{2}{n} + 1 + \frac{1}{2} + ...\frac{1}{n}\right]\right.$$

$$\left. - \frac{601}{240} - \frac{77}{60n^2}\right)\delta_{l0} + \left(1 - \frac{1}{n^2}\right)\left(\frac{1}{10} + \frac{1}{4}\delta_{j,1/2}\right)\delta_{l1}$$

$$+\frac{6 - 2l(l+1)n^{-2}}{(2l+3)l(l+1)(4l^1 - 1)}(1 - \delta_{l0}). \qquad (12.128)$$

The general expression for C_{60} is not known, though the values $C_{60}(n)$ are known up to $n = 4$ [14]. The recent accuracy of the experiment requires also that we take into account the corrections of the order $m\alpha^2(\alpha Z)^4$, $m\alpha^2(\alpha Z)^5$ and partly $m\alpha^2(\alpha Z)^6$. All these corrections can be evaluated in the first order in the nuclear potential V, i.e. with the free - electron formfactors.

The nonperturbative interaction of the free electron with the electromagnetic field (i.e. the most general vertex contribution) can be expressed in the form:

$$\Gamma_\mu(q) = eU(p+q)\left[\gamma_\mu F_1(q^2) + \frac{1}{2m}\sigma_{\mu\nu}\gamma^\nu F_2(q^2)\right]U(p), \qquad (12.129)$$

where $U(p)$ is the free electron bispinor, $\sigma_{\mu\nu} = \frac{1}{2}(\gamma_\mu\gamma_\nu - \gamma_\nu\gamma_\mu)$ and the functions $F_1(q^2)$, $F_2(q^2)$ are called Dirac and Pauli formfactors correspondingly. For the corrections of the order $m\alpha^2(\alpha Z)^4$ the result is (see [9] and the references therein):

$$\Delta E_{nlj}^{(F_1)} = m\left[\frac{3}{4}\zeta(3) - \frac{\pi^2}{2}\ln 2 + \frac{49}{432}\pi^2 + \frac{4819}{5181}\right]\frac{4\alpha^2(\alpha Z)^4}{\pi^2 n^3}\delta_{l0}, \qquad (12.130)$$

where $\zeta(n)$ is the Riemann Zeta function,

$$\Delta E_{nlj}^{(F_2)} = -m\left[\frac{3}{4}\zeta(3) - \frac{\pi^2}{2}\ln 2 + \frac{\pi^2}{12} + \frac{197}{144}\right]$$

$$\times\frac{\alpha^2(\alpha Z)^4}{\pi^2 n^3} \times \begin{cases} 1 & , l = 0 \\ \frac{j(j+1)-l(l+1)-3/4}{l(l+1)(2l+1)} & , l \neq 0 \end{cases} \tag{12.131}$$

Expressions (130), (131) correspond to the two-loop corrections to the graph Fig.10a. The two-loop corrections to the graph Fig.10b give:

$$\Delta E_{nlj}^{(VP)} = -\frac{82}{81}\frac{\alpha^2(\alpha Z)^4}{\pi^2 n^3}\delta_{l0}. \tag{12.132}$$

The expression for $m\alpha^2(\alpha Z)^5$, $m\alpha^2(\alpha Z)^6$ corrections, as well as the recoil corrections and mixed radiative-recoil corrections, can be found in the reviews [6] and [47].

3.3 QED theory of many-electron atoms

An effective Hamiltonian, that contains all QED corrections of the order $m\alpha(\alpha Z)^4$ including radiative and nonradiative ones, was derived by Araki [48] and Sucher [49] for the helium-like atom. Later it was generalized to the N-electron atom [50].

The total relativistic and QED energy shift for many-electron atoms consists of two parts. The first part contains the Bethe logarithm and the other is the average value of some effective potential. Throughout the exact nonrelativistic (Schrödinger) wave functions for the many-electron atom are used. The energy shift is [50]:

$$\Delta E_n = \Delta E_n^{(B)} + (U)_{nn}, \tag{12.133}$$

where $\Delta E_n^{(B)}$ is Bethe's term,

$$\Delta E_n^{(B)} = \frac{2\alpha}{3\pi m^2}\sum_{n'}(\varepsilon_n - \varepsilon_{n'})\left|(\hat{\vec{P}})_{nn'}\right|^2 \ln\left|\frac{\varepsilon_n - \varepsilon_n'}{m\alpha^2}\right|.$$

Here $\hat{\vec{P}} = \sum_{i=1}^{N}\hat{\vec{p}}_i$ and the summation is extended over the complete spectrum of nonrelativistic many-electron Hamiltonian.

The effective potential U reads:

$$U = \sum_{i>k=0}^{N} U_{ik} - \sum_{i=1}^{N}\frac{\hat{\vec{p}}_i^4}{8\mu^3}, \tag{12.134}$$

$$U_{0i} = \frac{\alpha Z\pi}{2m^2}\delta^{(3)}(\vec{r}_i) + \frac{Z\sqrt{\alpha}}{2m}\frac{1}{r_j^3}\left\{(\vec{\mu}_i'[\vec{r}_i\hat{\vec{p}}_i]) - 2\frac{m}{M}\vec{\mu}_i'[\vec{r}_i\hat{\vec{p}}_0])\right\}$$

$$+\frac{\sqrt{\alpha}}{m}\frac{1}{r_j^3}\left(\vec{\mu}_0[\vec{r}_i\hat{\vec{p}}_i]\right)+\frac{\alpha Z}{2mM}\left(\hat{\vec{p}}_i\hat{\vec{p}}_0+\frac{(\hat{\vec{p}}_i\vec{r}_i)(\hat{\vec{p}}_0\vec{r}_i)}{r_i^2}\right)$$

$$+\frac{8\pi}{3}\vec{\mu}_i\vec{\mu}_0\delta^{(3)}(\vec{r}_i)-\left(\mu_i\mu_0-\frac{3(\vec{\mu}_i\vec{r}_i)(\vec{\mu}_0\vec{r}_i)}{r_i^2}\right)\frac{1}{r_i^3}$$

$$+\frac{\alpha^2 Z}{m^2}\left(\frac{38}{45}-\ln(2\alpha^2)\right)\delta^{(3)}(\vec{r}_i), \qquad (12.135)$$

$$U_{ik\ i,k\neq 0}=\frac{\alpha\pi}{m^2}\delta^{(3)}(\vec{r}_{ij})+\frac{\sqrt{\alpha}}{2m}\frac{1}{r_{ik}^3}\left\{(\vec{\mu}_k'[\vec{r}_{ik}\hat{\vec{p}}_k])-(\vec{\mu}_i'[\vec{r}_{ik}\hat{\vec{p}}_i])\right.$$

$$\left.+2(\vec{\mu}_i[\vec{r}_{ik}\hat{\vec{p}}_k])-2(\vec{\mu}_k[\vec{r}_{ik}\hat{\vec{p}}_i])\right\}-\frac{\alpha}{2m}\left(\hat{\vec{p}}_i\hat{\vec{p}}_k+\frac{(\hat{\vec{p}}_i\vec{r}_{ik})(\hat{\vec{p}}_k\vec{r}_{ik})}{r_{ik}^2}\right)$$

$$\times\frac{1}{r_{ik}}-\frac{8\pi}{3}(\vec{\mu}_i\vec{\mu}_k)\delta^{(3)}(\vec{r}_{ij})+\left(\vec{\mu}_i\vec{\mu}_k-\frac{3(\vec{\mu}_i\vec{r}_{ik})(\vec{\mu}_k\vec{r}_{ik})}{r_{ik}^2}\right)\frac{1}{r_{ik}^3}$$

$$+\frac{\alpha^2}{m^2}\left(\frac{14}{3}\ln\alpha+\frac{43}{5}+\frac{5}{3}\vec{\sigma}_i\vec{\sigma}_k\right)\delta^{(3)}(\vec{r}_{ij})$$

$$-\frac{7}{6\pi}\frac{\alpha^2}{m^2}\left\{\frac{1}{r_{ik}^3(a)}+4\pi(\ln(m\alpha a)+C)\delta^{(3)}(\vec{r}_{ij})\right\}. \qquad (12.136)$$

The following notations are used in Eq. (136). The index 0 corresponds to the nucleus, the electrons are numerated by indices i, ... N. The nucleus coordinate is $\vec{r}_0 = 0$; the electrons coordinates are $\vec{r}_j$. The interelectron distances are $\vec{r}_{jk} = \vec{r}_j - \vec{r}_k$; the electron momenta are $\hat{\vec{p}}_i$ $i = 1$ ..., N). The nuclear momentum $\vec{p}_0 = -\vec{P}$ in the center of mass frame of reference. The masses of particles are denoted as M for the nucleus and m for the electrons; $\mu = mM/(m+M)$ is the reduced mass. The magnetic moments of the particles are denoted as $\vec{\mu}_j$. For the electrons $\vec{\mu}_j'$ ($i = 1$ ..., N) are the anomalous magnetic moments:

$$\vec{\mu}_j'=\frac{\sqrt{\alpha}}{2m}\left(1+\frac{\alpha}{\pi}\right)\vec{\sigma}_i.$$

The notation $1/r^3(a) = \theta(r-a)/r^3$ is also used, where $\theta(r-a)$ is the step function, C is the Euler's constant. After averaging the potential U with the wave functions the limit $a \to 0$ should be taken. The singularities with respect to a should cancel.

The expression (136) incorporates the one-electron corrections of order $(\alpha Z)^2\varepsilon_0$ that follow from the Dirac equation for the electron in the field of the nucleus. These corrections are included in the potentials U_{i0}. The Breit operator (96) is also included in the expression for U_{ik}; the corresponding corrections are of order $\alpha^2 Z\varepsilon_0$. The radiative (order $\alpha(\alpha Z)^2\varepsilon_0$) and nonradiative (order $\alpha^2(\alpha Z)\varepsilon_0$) QED corrections are also incorporated in Eq. (136). The radiative corrections, discussed in Sec.3.a are included in the Bethe logarithm term and in the potential U_{i0}. The nonradiative QED corrections discussed in Sec.2.e are included in U_{ik}.

The higher-order QED corrections for He atom can be found in [51–53] and references therein.

4. QED theory of heavy atoms

4.1 Electron self-energy: potential expansion

For electrons in the multicharged ions or even for the valence electrons in heavy atoms the parameter αZ cannot be considered as small. In case of heavy atoms the reason is that the effective QED potentials of the electron interaction with the nucleus are rather short-range and the interaction occurs when the outer electrons penetrate deeply into the core. Therefore the methods described in Section 3 are not valid anymore and all-orders in αZ methods are necessary.

The method that helped to avoid this difficulty was first introduced in [10] and applied to the evaluation of SE for the K-shell electrons in the mercury atom. The general idea of the method is the potential expansion of the SE Feynman graph for the bound electron. This expansion is depicted in Fig.11. The divergency is concentrated in the first two terms of this expansion. These terms are usually called "zero - potential" and "one - potential" terms. The third term, so called "many - potential" term, is finite but the most difficult for numerical evaluations. To avoid the evaluation of ΔE_c the authors of [10] rearranged the three terms of the expansion

$$\Delta E = \Delta E_a + \Delta E_b + \Delta E_c \tag{12.137}$$

after renormalization

$$\Delta E^{(R)} = \Delta E_a^{(R)} + \Delta E_b^{(R)} + \Delta E_c^{(R)} \tag{12.138}$$

in the following way. According to Eq. (61) and Eq. (63) the renormalized expressions for $\Delta E_a^{(R)}$ and $\Delta E_b^{(R)}$ look like:

$$\Delta E_a^{(R)} = \Delta E_a - \Delta E_{a1} - \Delta E_{a2} \tag{12.139}$$

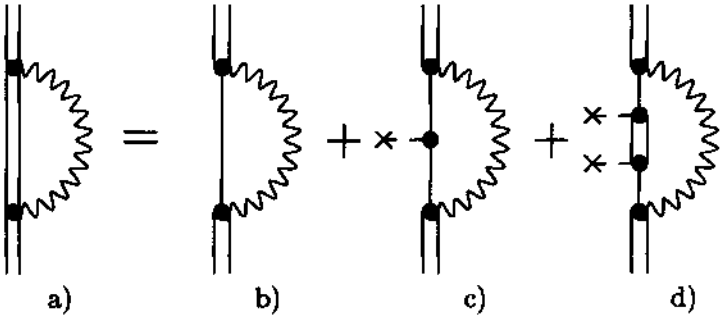

Fig.11
The expansion of the electron self-energy graph in power of the nuclear potential V. The double solid line denotes an electron in the potential field V, and the ordinary solid line denotes the free electron.

$$\Delta E_b^{(R)} = \Delta E_b - \Delta E_{b1} \tag{12.140}$$

Due to the Ward identity $\Delta E_{a2} = \Delta E_{b1}$. The equation results:

$$\Delta E^{(R)} = (\Delta E - \Delta E_a) - \Delta E_a^{(R)} + \Delta E_{a2}. \tag{12.141}$$

The advantage of Eq. (141) is the absence of the cumbersome expression for ΔE_c. Moreover, the ΔE_b contribution is also absent. The main problem is now the evaluation of the difference $(\Delta E - \Delta E_a)$ where the cancellation of the remaining logarithmic ultraviolet divergence should be done numerically. Later the same approach was used in [54] for highly charged ions. The finite nucleus was also taken into account in [54].

The other method of calculating the self - energy correction was developed by Mohr [55] where the Pauli-Willars regularization was used. The advantage of this approach is that the cancellation of the divergences can be done analytically and the evaluation of SE can be performed also for the intermediate and small Z values up to $Z = 5$. The Mohr's method is up to now the most accurate tool for calculating SE for a wide range of Z values. It was generalized for excited electronic states up to principal quantum number values of n=8 in [57–59]. In [61] this method was extended to the small Z region $1 \leq Z \leq 5$ and very accurate results were received.

Still the practical implementation of this method is not so simple and for wider applications to electrons moving in non-Coulomb numerically defined potentials as in heavy atoms the more straightforward approach based on the direct use of the potential expansion can be preferable.

This is mainly due to the development of numerical methods (B-spline approach [62], space discretization [63]) that allow summations to be performed over the complete Dirac spectrum for arbitrary spherically symmetric potentials.

The direct potential expansion of the SE was first analyzed in [64]. Recently it was considered in the Fried-Yennie gauge [65] that allows the extension of calculations to the small Z region. In the Feynman gauge each term of the potential expansion in Eq. (138) for the low Z values contains "spurious" terms of the wrong (too large) order of magnitude in (αZ). These "spurious" terms cancel only in the sum of the zero-potential, one-potential and many-potential contributions. The cancellation of the large "spurious" terms leads to the loss of accuracy in the numerical calculation. In the Fried-Yennie gauge these "spurious" terms are absent. Thus the Fried-Yennie gauge has an advantage for small Z, though it is more complicated than the Feynman gauge. Note that the calculation of the higher-order SE corrections with αZ-expansion [6,47] was performed in the Fried-Yennie gauge.

Numerical calculations of the SE with the use of the direct potential expansion were performed in [66] using the Feynman gauge for Z=70,80,90. A part of the higher-order SE correction was also evaluated for high Z with this method [67].

In the direct potential expansion approach the known expressions for the renormalized contributions $\Delta E_a^{(R)}$ and $\Delta E_b^{(R)}$ are employed. These expressions can be obtained from the corresponding S-matrix elements with the use of the formulas (85), (86) since the graphs in Fig.10 are irreducible. The renormalized expressions are known in the momentum space. For the contribution $\Delta E_a^{(R)}$ we have:

$$\Delta E_a^{(R)} = \int \overline{\Psi}_A(\vec{p})\hat{\Sigma}^{(R)}(\vec{p}, E_A)\Psi_A(\vec{p})d\vec{p}, \tag{12.142}$$

where $\hat{\Sigma}^{(R)}(\vec{p}, E_A)$ is the lowest-order electron self-energy operator off the mass shell (see Sec.1.d), $\Psi_A(\vec{p})$ is the electron wave function in the momentum space. The most general expression for $\hat{\Sigma}^{(R)}(p)$ looks like [68]:

$$\hat{\Sigma}^{(R)}(p) = \frac{\alpha}{4\pi}(\not{p} - m)\left\{\frac{m^2}{p^2}\ln\left|\frac{p^2 - m^2}{m^2}\right|\left(d_0\frac{p^2}{m^2} - 3\right) - \frac{1}{2}\ln\frac{\lambda^2}{m^2}\right.$$

$$\times(6-2d_0)-d_0+\frac{\not p}{m}\left[\frac{m^2}{p^2}\ln\left|\frac{p^2-m^2}{m^2}\right|\left(d_0\frac{p^2}{m^2}-3\right)+d_0\frac{m^2}{p^2}\right]\Bigg\}\ . \tag{12.143}$$

The presence of the photon mass λ in Eq. (143) means the arrival of the infrared divergency after renormalization, d_0 is the parameter defining the gauge. In the Feynman gauge $d_0 = 1$, in the Fried-Yennie gauge $d_0 = 3$. One can see that in the Fried-Yennie gauge the infrared divergency is absent. Inserting Eq. (143) in Eq. (142) we should put $p \equiv (\vec{p}, E_A)$.

The same approach for the contribution $\Delta E_b^{(R)}$ yields:

$$\Delta E_b^{(R)} = \int \overline{\Psi}_A(\vec{p})\Lambda_4(\vec{p}, E_A, \vec{q}, E_A)eV(\vec{p}-\vec{q})\Psi_A(\vec{q})d\vec{p}d\vec{q}, \tag{12.144}$$

An expression for $\Lambda_4(\vec{p}, E_A, \vec{q}, E_A)$ most convinient for numerical evaluations is (in Feynman gauge) [65]:

$$\Lambda_R^0(\vec{p}E_A, \vec{q}E_A) = \tilde{\Lambda}_R^0(\vec{p}E_A, \vec{q}E_A) + \ln\frac{\lambda^2}{m^2}, \tag{12.145}$$

where

$$\Lambda_R^0(\vec{p}E, \vec{q}E) = \gamma_0[4\tilde{C}_{24}-2+2m_e^2C_0-4pp'(C_0+C_{11}+C_{12}+C_{23})-2p^2(C_{11}+C_{21})$$
$$-2p'^{\,2}(C_{12}+C_{22})]+\not p p_0[4(C_{11}+C_{21})]+\not p p_0'[4(C_0+C_{11}+C_{12}+C_{23})]$$
$$+\not p' p_0[4(C_0+C_{11}+C_{21}+C_{23})]+\not p' p_0'[4(C_{12}+C_{22})]-\not p\gamma_0\not p'[2(C_0+C_{11}+C_{12})]$$
$$-p_0[4m_e(C_0+2C_{11})]-p_0'[4m_e(C_0+C_{12})]. \tag{12.146}$$

Here C_0, C_{ij} denote the Feynman parameter integrals:

$$m^2C_0 = \int_0^1 dy\frac{1}{a}\ln\left(\frac{a+b}{b}\right), \tag{12.147}$$

$$m^2C_{11} = -\int_0^1 dy\frac{y}{a}\left[1-\frac{b}{a}\ln\left(\frac{a+b}{b}\right)\right], \tag{12.148}$$

$$m^2C_{12} = -\int_0^1 dy\frac{1-y}{a}\left[1-\frac{b}{a}\ln\left(\frac{a+b}{b}\right)\right], \tag{12.149}$$

$$m^2C_{21} = \int_0^1 dy\frac{y^2}{a}\left[\frac{1}{2}-\frac{b}{a}+\left(\frac{b}{a}\right)^2\ln\left(\frac{a+b}{b}\right)\right], \tag{12.150}$$

$$m^2C_{22} = \int_0^1 dy\frac{(1-y)^2}{a}\left[\frac{1}{2}-\frac{b}{a}+\left(\frac{b}{a}\right)^2\ln\left(\frac{a+b}{b}\right)\right], \tag{12.151}$$

$$m^2 C_{23} = \int_0^1 dy \frac{y(1-y)}{a} \left[\frac{1}{2} - \frac{b}{a} + \left(\frac{b}{a} \right)^2 \ln\left(\frac{a+b}{b} \right) \right], \qquad (12.152)$$

$$C_{24} = \frac{1}{4} \left\{ 1 - \int_0^1 dy \frac{b}{a} \left[1 - \frac{b}{a} \ln\left(\frac{a+b}{b} \right) \right] - \int_0^1 \ln(a+b) \right\}, \quad (12.153)$$

where $b = y\rho - (1-y)\rho'$ and $a + b = 1 - y(1-y)k^2/m^2$, $k^2 = (\vec{p} - \vec{q})^2$, $\rho = (m^2 + p^2 - E_A^2)/m^2$, $\rho' = (m^2 - E_A^2 + q^2)/m^2$ and $p_0 = q_o = E_A$.The infrared divergences in $\Delta E_a^{(R)}$ and $\Delta E_b^{(R)}$ cancel due to the Ward identity and Dirac equation [64,65].

The expression ΔE_c is both ultraviolet and infrared finite, but more difficult for numerical evaluation. It can be treated in the following way. The S-matrix element, corresponding to Fig.11a reads:

$$\langle \Phi_a | S^{(4)} | \Phi_a \rangle = e^4 \int \overline{\Psi}_A(x_1) \gamma^{\mu_1} S^{(0)}(x_1 x_2) \gamma^{\mu_2} e V_{\mu_2}(x_2) \mathcal{S}(x_2 x_3) \times$$

$$\times \gamma^{\mu_3} e V_{\mu_3}(x_3) S^{(0)}(x_3 x_4) \gamma^{\mu_4} \Psi_A(x_4) \mathcal{D}_{\mu_1 \mu_4}(x_1 x_4) d^4 x_1, ..., d^4 x_4, \quad (12.154)$$

where $V_\mu(x) = \delta_{\mu 4} V(\vec{x})$ is the nuclear potential, $S^{(0)}(x_1 x_2)$ is the free electron propagator and $\mathcal{D}_{\mu_1 \mu_4}(x_1 x_4)$ is the photon propagator in the arbitrary gauge. The photon propagator in the arbitrary gauge is (cf Eq. (111)):

$$\mathcal{D}_{\mu_1 \mu_2}(k) = -\frac{1}{k^2} \left(g_{\mu_1 \mu_2} - \frac{k_{\mu_1} k_{\mu_2}}{k^2} \right) - \frac{d_0}{k^2} \frac{k_{\mu_1} k_{\mu_2}}{k^2}. \qquad (12.155)$$

The electron propagators $S^{(0)}$ in the numerical B-spline approach can be treated in the same way as bound propagators with Z=0, so that in total Eq. (154) contains the triple summation over the Dirac spectrum. This summation can be performed numerically with modern computer facilities.

4.2 Electron self-energy: partial wave renormalization

Another simple method that allows for the SE calculations in heavy atoms is the partial wave remormalization (PWR) approach first proposed in [69, 70]. Within this approach the renormalized expression for the lowest-order SE is presented in the form of the partial wave expansion:

$$\Delta E_A^{(R)} = \sum_{l=0}^{\infty} \left[\langle \Psi_A | \hat{\Sigma}_b^{(l)} | \Psi_A \rangle - \langle \Psi_A | \hat{\Sigma}_f^{(l)} | \Psi_A \rangle \right], \tag{12.156}$$

where $\hat{\Sigma}_b^{(l)}$, $\hat{\Sigma}_f^{(l)}$are the terms of the partial wave expansion for the bound and free SE operators respectively. Each term of the partial wave expansion $\langle \Psi_A | \hat{\Sigma}_b^{(l)} | \Psi_A \rangle$ is finite and only the sum over l is divergent. Subtracting the counterterms $\langle \Psi_A | \hat{\Sigma}_f^{(l)} | \Psi_A \rangle$ for each term of the expansion one obtains the convergent expression (156).

The advantage of the PWR approach is its simplicity, the disadvantage is the numerical cancellation of the divergencies which is always less reliable than the analytic one. The disadvantage is partly avoided in another version of PWR based on the multicommutator representation of both the unrenormalized SE expression and its counterterm [71]. In this method the cancellation of divergencies occurs partly analytically and partly numerically.

Within this approach the unrenormalized SE correction to the atomic state A is obtained directly from the S-matrix element for the Feynman graph Fig.1a after the integration over both time and frequency variables. This yields:

$$\Delta E_A = \frac{\alpha}{\pi} \sum_n \left(\frac{1 - \vec{\alpha}_1 \vec{\alpha}_2}{r_{12}} I_{nA}(r_{12}) \right)_{AnnA}. \tag{12.157}$$

The function $I_{nA}(r_{12})$ is defined as (in Feynman gauge):

$$I_{nA}(r_{12}) = \int_{-\infty}^{\infty} \frac{dw e^{i|w|r_{12}}}{E_n(1 - i0) - E_A - w}. \tag{12.158}$$

The evaluation of the integral over w in the complex plane leads to the following expression for the real part of Eq. (157):

$$\begin{aligned} \Delta E_A = & \frac{\alpha}{\pi} \sum_n \frac{\Delta_{nA}}{|\Delta_{nA}|} \left(\frac{1 - \vec{\alpha}_1 \vec{\alpha}_2}{r_{12}} ci(|\Delta_{nA}| r_{12}) \sin(|\Delta_{nA}| r_{12}) \right)_{AnnA} \\ & - \frac{\alpha}{\pi} \sum_n \frac{\Delta_{nA}}{|\Delta_{nA}|} \left(\frac{1 - \vec{\alpha}_1 \vec{\alpha}_2}{r_{12}} si(|\Delta_{nA}| r_{12}) \cos(\Delta_{nA} r_{12}) \right)_{AnnA} \\ & + \frac{\alpha}{4} \sum_n \left(1 + \frac{E_n}{|E_n|} \right) \left(\frac{1 - \vec{\alpha}_1 \vec{\alpha}_2}{r_{12}} \cos(\Delta_{nA} r_{12}) \right)_{AnnA} \end{aligned} \tag{12.159}$$

where $\Delta_{nA} = E_n - E_A$, si and ci are the integral sine and cosine functions. The ultraviolet divergency in Eq. (159) arrives through the summation over the complete Dirac spectrum.

After the subtraction from Eq. (159) of the counterterm corresponding to the free electron, expanding the functions of the argument $\Delta_{nA}r_{12}$ and expressing the powers of this argument through the multiple commutators $[\hat{h}, r_{12}^l]$, we find that most of the divergent terms cancel analytically. The remainder, that still contains some divergent terms to be cancelled numerically reads:

$$\Delta E_A^{(R)} = \frac{\alpha}{\pi} \sum_n \left(\frac{1 - \vec{\alpha}_1 \vec{\alpha}_2}{r_{12}} \tilde{I}_{nA}(r_{12}) \right)_{AnnA} - \tilde{\delta} m_a, \tag{12.160}$$

$$\tilde{I}_{nA}(r_{12}) = \ln|E_n - E_A| \sin(\Delta_{nA} r_{12}) + \frac{\pi}{2} \frac{E_n}{|E_n|} \cos(\Delta_{nA} r_{12}). \tag{12.161}$$

The counterterm $\tilde{\delta} m_a$ is now defined as :

$$\tilde{\delta} m_a = \frac{\alpha}{\pi} \int d\vec{p} \left| \langle \Psi_A(\vec{r}) | \Psi_{\vec{p}}(\vec{r}) \rangle \right|^2 \int d\vec{q} \left(\frac{1 - \vec{\alpha}_1 \vec{\alpha}_2}{r_{12}} \tilde{I}_{nA}(r_{12}) \right)_{\vec{p}\vec{q}\vec{q}\vec{p}}, \tag{12.162}$$

where $\Psi_{\vec{p}}(\vec{r})$ are the spherical wave solutions of the Dirac equation for the free electron, described by the Dirac Hamiltonian (2) with $V = 0$. Integration over p is interpreted as integration over the energies $E_p = \pm\sqrt{p^2 + m^2}$, where p is the absolute value of the electron momentum. The summations over the angular momentum numbers are also understood. Within the B-spline approach the integration over $\vec{p}$, $\vec{q}$ should be replaced by the summations over the Dirac spectrum in the limit $Z \to 0$.

A comparison with accurate SE calculations [56–58,60] shows that for all available principal quantum numbers and $Z \leq 100$ the deviation is less than 2%.

4.3 Vacuum polarization

Apart from the electron self-energy there is another radiative correction of second order in the coupling constant e: the vacuum polarization (VP) correction, described by the Feynman graph Fig.1b. The VP correction may be considered as a correction to the Coulomb interaction of the electron with the nucleus. After integrating over time and frequency variables in the S-matrix element corresponding to the Feynman graph Fig.1b and after using the formulas (85), (86) the VP correction to the energy level A reads:

$$\Delta E_A^{VP} = e \int d\vec{r}_1 \overline{\Psi}_A(\vec{r}_1) \gamma_0 \phi_{VP}(\vec{r}_1) \Psi_A(\vec{r}_1), \tag{12.163}$$

where

$$\phi_{VP}(\vec{r}_1) = e \int \frac{\rho_{VP}(\vec{r}_2) d\vec{r}_2}{|\vec{r}_1 - \vec{r}_2|} \tag{12.164}$$

$$\rho_{VP}(\vec{r}_2) = \frac{1}{2\pi} Sp \left(\int_{-\infty}^{\infty} G_w(\vec{r}_2; \vec{r}_2) dw \gamma_0 \right). \tag{12.165}$$

In Eq. (165) $G_w(\vec{r}_2; \vec{r}_2)$ is the Green function of the Dirac equation (4) and the symbol Sp concerns the spinor indeces.

Expression (165) and, consequently, Eq. (163) are divergent. This divergency follows from the singularity of the Green function

$$\lim_{\vec{r}' \to \vec{r}} G_w(\vec{r}, \vec{r}') = \infty$$

and is actually the same ultraviolet divergency for the photon self-energy in momentum space that was discussed in Sec.1.d. The divergency at high momenta in momentum space corresponds to the divergency at small distances in coordinate space.

For renormalization it is convenient to use again the potential expansion depicted in Fig.12. The first term of this expansion (Fig.12b) gives a zero contribution according to the Furry theorem [72]. This theorem concerns free electron loops with any odd number of vertices (in Fig.12b this number is 1). The divergency is contained only in the second term of the expansion (Fig.12c) and the remainder Fig.12d is finite. In principle, the expansion of the remainder in powers of V also gives one divergent term with three potentials (the term with two potentials is zero due to the Furry theorem). However the divergent integrals in this correction cancel out provided that the gauge invariance is not violated in the calculations. Hence, one should take care with this divergency when the zero-order DHF approximation is used for the evaluation of the remainder term Fig.12d.

The contribution of the graph Fig.12b can be presented in the form:

$$\Delta E_A^U = e \int d\vec{r} \overline{\Psi}_A(\vec{r}) \gamma_0 \phi_U(r) \Psi_A(\vec{r}), \tag{12.166}$$

where $\phi_U(\vec{r})$ is the Uehling potential [73]:

$$\phi_U(r) = \frac{2e^2 Z}{3\pi r} \int_1^{\infty} e^{-2mr\chi} \left(1 + \frac{1}{\chi^2}\right) \frac{\sqrt{\chi^2 - 1}}{\chi^2} d\chi. \tag{12.167}$$

The asymptotic behaviour of the Uehling potential is defined by the expressions:

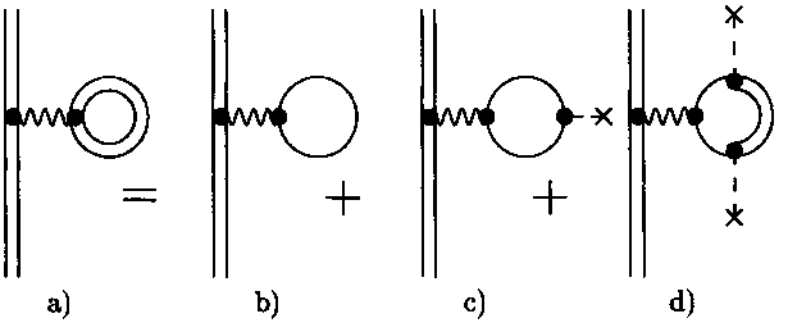

Fig.12
The expansion of the vacuum polarization graph in powers of the nuclear potential V. Notation is the same as in Fig.11.

$$\phi_U(r) = \frac{e^3 Z}{r} \begin{cases} -\frac{1}{3\pi}[5/3 + 2C + 2\ln(mr)] & mr \ll 1 \\ \frac{1}{4\sqrt{\pi}} \frac{e^{-2mr}}{(mr)^{3/2}} & mr \gg 1 \end{cases} \tag{12.168}$$

Remembering that the Bohr radius in relativistic units is $r_0 = 1/m\alpha$, we see that at characteristic atomic distances in the neutral hydrogen atom (Z=1) the deviation from the Coulomb potential is exponentially small:

$$\phi_U(r_0) \approx e^{-1/\alpha}.$$

However, this is not the case for a hydrogenlike ion with a high Z value:

$$\phi_U(r_0) \approx \phi_U(1/m\alpha Z) \approx e^{-1/\alpha Z} \sim 1.$$

The first all orders in αZ evaluation of the remainder term was performed by Wichmann and Kroll [74] for Z=70-90. Later this term (also called the Whichmann-Kroll term) was calculated more accurately for all Z values in [75] (for an extended nucleus) and in [76] (for a point-like nucleus).

The Uehling term usually gives a fairly good approximation for the total VP correction. Even for high Z values deviations from the exact value do not exceed 10%.

4.4 Radiative corrections for the ns valence electrons in heavy atoms

Finally we present results of SE and VP calculations for ns valence electrons in heavy and superheavy atoms with n up to 8 and Z up to 119 [13, 14]. For the calculation of the SE contribution the PWR approach described in Sec.4.b based on the multiple commutator expansion [71] was used. The corrections ΔE^{SE} are given in Table 12.1. Since the B-spline approach requires the employment of the local potential, the local approximation to the DHF potential obtained by the direct parametrization [77] was used. The VP contribution was treated in the Uehling approximation. One can expect that the Uehling term will suffice not only for highly charged ions but in screened systems as well. The Uehling potential was corrected for the extended nucleus [78–80]. The Uehling potential for the point-like nucleus (167) was replaced by the expression:

Table 12.1 SE and VP contributions to the Lamb Shift (eV).

Z	System	State	ΔE^{SE}	ΔE^{VP}
3	Li	$2s$	$3.84\cdot10^{-5}$ [a)]	$-1.38\cdot10^{-6}$
11	Na	$3s$	$2.83\cdot10^{-4}$	$-1.54\cdot10^{-5}$
19	K	$4s$	$4.93\cdot10^{-4}$	$-3.43\cdot10^{-5}$
37	Rb	$5s$	$1.23\cdot10^{-3}$	$-1.31\cdot10^{-4}$
55	Cs	$6s$	$2.15\cdot10^{-3}$	$-2.99\cdot10^{-4}$
87	Fr	$7s$	$6.03\cdot10^{-3}$	$-1.43\cdot10^{-3}$
119		$8s$	$2.74\cdot10^{-2}$	$-1.01\cdot10^{-2}$
29	Cu	$4s$	$2.66\cdot10^{-3}$	$-2.36\cdot10^{-4}$
47	Ag	$5s$	$6.14\cdot10^{-3}$	$-7.34\cdot10^{-4}$
79	Au	$6s$	$2.21\cdot10^{-2}$	$-4.62\cdot10^{-3}$
80	Hg^{+}	$6s$	$3.31\cdot10^{-2}$	$-7.03\cdot10^{-3}$
81	Tl^{++}	$6s$	$4.68\cdot10^{-2}$	$-9.67\cdot10^{-3}$
111		$7s$	$8.66\cdot10^{-2}$	$-3.20\cdot10^{-2}$

[a)] ΔE^{SE} =$3.049\cdot10^{-5}$ [81].

$$V_U(\vec{r}) = -\frac{e^3}{\pi}\int d\vec{r}'\,\rho(r')\int_1^\infty dt\sqrt{t^2-1}\left(\frac{2}{3t^2}+\frac{1}{3t^4}\right)\frac{e^{-2mt|\vec{r}-\vec{r}'|}}{|\vec{r}-\vec{r}'|}, \tag{12.169}$$

where $\rho(r')$ is the nuclear charge density. It is also possible to take the effects of the atomic screening into account and to insert the charge distribution into Eq. (169):

$$\rho(r) = \rho_{nuc}(r) + \rho_c(r), \tag{12.170}$$

where $\rho_{nuc}(r)$ is the nuclear charge density and $\rho_c(r)$ is the core electron density. In this way the electron correlation correction to the vacuum polarization operator will be included. The VP contributions to the Lamb Shift are given in Table 12.1 as well. Electron correlation corrections due to $\rho_c(r)$ in Eq. (169) are always smaller than 1%. For comparison the results of calculations for light atoms are also provided in Table 12.1. The methods of producing SE and VP corrections [14, 71], described in Sec 4.b and 4.c are valid also for the light atoms, though in this case the nonrelativistic QED approach described in Sec.3 is also applicable. Still until now the latter approach has been used only for *Li* atom [81].

The accuracy of the energy level calculations for ns valence electrons in heavy atoms has drastically improved during the last decade.

The all-orders relativistic many-body perturbation theory approach [82, 83], the combination of this approach with the multiconfiguration Dirac - Fock method [84] or the relativistic coupled-cluster approach [85] allow for the evaluation of the energy levels for valence electrons with accuracy of the order of 0.1%. The accuracy of the experimental determination of the ionization potentials in heavy atoms also exceeds the 0.1% level [86]. One can therefore turn to the problem of the evaluation of the lowest-order QED radiative corrections to ns electron levels in heavy atoms as performed in [13, 14].

The importance of QED corrections for heavy atoms is again illustrated in Table 12.2, where the best theoretical values for the ionization potentials are compared to experimental data. The comparison clearly demonstrates that the accuracy achieved recently in heavy atom calculations requires the inclusion of QED corrections.

4.5 Radiative corrections to g-factors of the ns valence electron in heavy atoms

The evaluation of quantum electrodynamical (QED) effects for highly charged ions (HCI) in an external magnetic field, i.e., the QED corrections to the g-factors of bound electrons was the topic of intensive experimental [92–95] and theoretical [96–99] investigations during the last years. In hydrogenlike HCI the QED corrections play a dominant role and their investigation is important for testing bound-state QED in strong fields. In [100] it was pointed out that QED corrections could be also not negligible for ns valence electrons in heavy alkali atoms.

First calculations of the electron self-energy (SE) corrections to the bound-electron g-factors in H-like ions were performed in the framework of the partial wave renormalization (PWR) method (see Section 4.b)

Table 12.2 Comparison of different theoretical values for the first ionization potentials (IP) of selected atoms with experimental data (eV).

Z	System	State	IP theory [82]	IP theory [83]	IP theory [85]	IP exper. [86]	ΔE^{QED}
3	*Li*	$2s$			5.391(5)	5.391716	$3.70 \cdot 10^{-5}$
11	*Na*	$3s$	5.13880(5)		5.127(5)	5.13906	$2.68 \cdot 10^{-4}$
19	*K*	$4s$	4.3347		4.343(4)	4.3407	$4.59 \cdot 10^{-4}$
37	*Rb*	$5s$	4.1719		4.181(4)	4.1771	$1.10 \cdot 10^{-3}$
55	*Cs*	$6s$	3.8760	3.893(4)	3.898(4)	3.8940	$1.85 \cdot 10^{-3}$
			3.8948[a)]				
87	*Fr*	$7s$	4.0586	4.069(4)		4.0778	$4.60 \cdot 10^{-3}$
119		$8s$					$1.73 \cdot 10^{-2}$
29	*Cu*	$4s$	7.715		7.733[f)]	7.727	$2.42 \cdot 10^{-3}$
47	*Ag*	$5s$	7.686[e)]		7.461[f)]	7.574	$5.40 \cdot 10^{-3}$
79	*Au*	$6s$	9.548[e)]		9.123[f)]	9.226	$1.75 \cdot 10^{-2}$
80	Hg^{+}	$6s$			18.75(4)[b)]	18.7563	$2.61 \cdot 10^{-2}$
81	Tl^{++}	$6s$			29.82[c)]	29.8306	$3.71 \cdot 10^{-2}$
111		$7s$			10.60(2)[d)]		$5.47 \cdot 10^{-2}$

[a)] [84], [b)] [87], [c)] [88], [d)] [89], [e)] [90], [f)] [91]

[96]. However, later it was observed that the PWR approach, being applied to the evaluation of the SE correction for the bound electron in the external field, considered as a perturbation, generates the so-called "spurious" terms, arising due to the "noncovariant" character of the PWR approach [101]. The PWR procedure consists of the partial wave expansion of SE contribution and of the corresponding counterterm. Then both expansions are subtracted term by term leading finally to the finite renormalized expression. For the lowest order electron SE (without external field) this procedure was shown to be convergent to the correct limit, but for the SE in the external field, according to [101], finite "spurious" terms arise. An explicit expression has been provided for these "spurious" terms in [101]. In the case of the external central field these "spurious" terms cancel between the different contributions to the perturbation theory (PT) corrections to SE matrix elements: the corrections to the wave functions, the vertex and the reference state correction. This conclusion was later confirmed by numerical evaluation [102] for perturbations to the central Coulomb potential.

In [101] it was also stated that in the case of the external magnetic field the "spurious" terms in perturbation theory do not cancel and that some "spurious" contribution remains after collecting all the contributions.

The situation with the "spurious" terms was clarified in [103] where it was proved that both analytical [101] an numerical [102] occurrence of these terms result from an improper treatment of the unphysical high - energy contribution. Utilizing the nonperturbative method for performing the PWR with the B-spline approximation to the Dirac spectrum in an external magnetic field it was shown that no "spurious" terms are generated in numerical calculations of SE in magnetic field within the level of accuracy of about 0.1%. Still one has to be careful with the high - energy region when performing PWR calculations.

The "spurious" terms problem is fully absent in the potential expansion (see Section 4.a) approach to the evaluation of the electron SE in external field [97–99], which is called "covariant" contrary to PWR procedure that is performed noncovariantly in the coordinate space.

The corrections for the valence ns electrons in alkali metal atoms were first estimated in [100] within the PWR approach by the definition of the effective nuclear charge number Z_{eff} and comparison of the QED corrections in the magnetic field with HCI data. The fully "covariant" evaluation for ns electrons in alkali metal atoms was performed in [104]. In this Section we will follow the Ref. [104].

The magnetic dipole moment $\vec{\mu}$ of a bound electron is connected with its total mechanical moment $\vec{j}$ as:

$$\vec{\mu} = -g_j \frac{e}{2m} \vec{j} = -g_j \frac{\mu_B}{\hbar} \vec{j}, \tag{12.171}$$

where e is the electron charge ($e > 0$), m is the electron mass, μ_B is the Bohr magneton and g_j is the gyromagnetic ratio. For an electron in an ns state, g_j coincide with the bound-electron g-factor.

The energy correction for a bound electron in the state A in an external magnetic field $\vec{B}$ reads:

$$E_A(B) = -\langle A|\vec{\mu}\vec{B}|A\rangle. \tag{12.172}$$

The same quantity can be expressed also using the vector potential $\vec{A}$ for an external field:

$$E_A(B) = \langle A|\vec{\alpha} \cdot e\vec{A}|A\rangle, \tag{12.173}$$

where $\vec{\alpha}$ is the Dirac matrix. We use here the relativistic units $m = c = \hbar = 1$. The expression (173) corresponds to the Feynman graph shown in Fig.13.

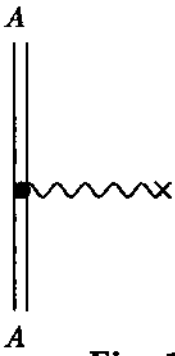

Fig. 13
The Feynman graph describing the interaction of the atomic electron in state A with the external field. The wavy line with the cross at the end denotes the external field.

In the case of a homogeneous magnetic field:

$$\vec{A} = -\frac{1}{2}(\vec{r} \times \vec{B}), \tag{12.174}$$

where $\vec{r}$ is the radius vector for an electron in an atom. Considering a static field aligned in the Z direction and using Eqs.(171)–(173) we obtain the expression for the g-factor of a bound ns electron, first derived by Breit [105]:

$$g^{bound} = \frac{2}{\mu_B B_z}\langle A|\vec{\alpha} \cdot e\vec{A}|A\rangle. \tag{12.175}$$

This value differs from the free - electron value $g^{free} = 2$ which follows from the Dirac equation. The radiative corrections change the value g^{free} [106]:

$$g^{free} = 2.002319304386(20), \tag{12.176}$$

where

$$\delta g^{free}_{QED} = 2319.30 \cdot 10^{-6} \tag{12.177}$$

is the QED correction to the free - electron g-factor. The major part of δg_{Sch}^{free} is incorporated in the Schwinger term:

$$\delta g_{Sch}^{free} = \frac{\alpha}{\pi} = 2322.82 \cdot 10^{-6}. \tag{12.178}$$

The bound-electron corrections to the g-factor are defined as $\delta g = g^{bound} - g^{free}$. In particular, the relativistic correction δg_{rel} is defined as the difference between the value Eq. (175) and $g^{free} = 2$ [105]. The integration over the angles in Eq. (175) yields:

$$\delta g_{rel} = \frac{4}{3} \int_0^\infty dr \; g_{ns}(r) r f_{ns}(r) - 2, \tag{12.179}$$

where $g_{ns}(r)$ and $f_n s(r)$ are the upper and lower radial Dirac wave functions for the ns electron, normalized as:

$$\int_0^\infty dr \; \left(g_{ns}^2(r) + f_{ns}^2(r)\right) = 1. \tag{12.180}$$

The inclusion of the bound-state QED corrections requires the evaluation of the contribution from the Feynman graphs given in Fig.14. The graphs 14a), 14b) correspond to the electron self-energy corrections to the wave function (SE-WF), the graph 14c) represents the vertex correction (VER). The graphs 14d)–14f) describe the vacuum polarization corrections (VP).

It is convenient to divide the contribution of the graphs Fig.14a)–14b) into two parts, namely "irreducible" and "reducible" ones. The "irreducible" part contains no reference state A in the sums over intermediate electron states. The calculation of the "reducible" part should be combined with the calculation of the vertex contribution.

The total bound-state QED correction consists of the following contributions:

$$\delta g_{QED}^{bound} = \delta g_{SE-WF,irr}^{bound} + \delta g_{SE-WF,red}^{bound} + \delta g_{VER}^{bound} + \delta g_{VP}^{bound}. \tag{12.181}$$

The "irreducible" SE-WF contribution to the g-factor of the bound electron reads:

$$\delta g_{SE-WF,irr}^{bound} = \tag{12.182}$$
$$\frac{2}{\mu_B B_z} \sum_{n \neq A} \frac{\left(\hat{\Sigma}^{ren}(E_A)\right)_{An} \left(\vec{\alpha} \cdot e\vec{A}\right)_{nA} + \left(\vec{\alpha} \cdot e\vec{A}\right)_{An} \left(\hat{\Sigma}^{ren}(E_A)\right)_{nA}}{E_A - E_n},$$

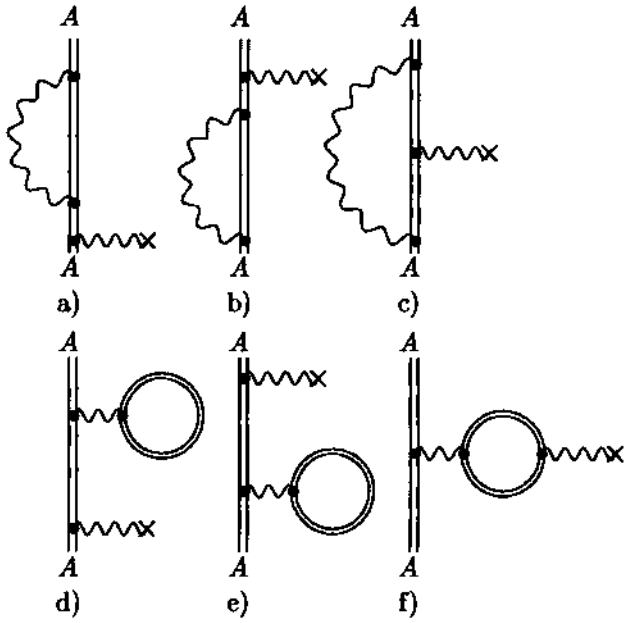

Fig. 14
The Feynman graphs correcponding to the lowest-order QED corrections to the interaction of the bound electron with the external field.

where $\hat{\Sigma}^{ren}(E_A)$ is the renormalized expression for the lowest-order electron self-energy operator. The evaluation of the matrix element of $\hat{\Sigma}^{ren}(E_A)$ and of $\delta g^{bound}_{SE-WF,red}$, δg^{bound}_{VER} we will discuss below.

We discuss next δg^{bound}_{VP}. The contribution of the graphs Fig. 14d)–14e) resembles Eq. (182) but the matrix elements of the electron self-energy operator $\hat{\Sigma}^{ren}$ are replaced by the matrix elements of the vacuum polarization operator $\hat{\Pi}^{ren}$:

$$\delta g^{bound}_{VP} = \frac{2}{\mu_B B_z} \sum_{n \neq A} \frac{\left(\hat{\Pi}^{ren}\right)_{An} \left(\vec{\alpha} \cdot e\vec{A}\right)_{nA} + \left(\vec{\alpha} \cdot e\vec{A}\right)_{An} \left(\hat{\Pi}^{ren}\right)_{nA}}{E_A - E_n}. \tag{12.183}$$

Since the operator $\hat{\Pi}^{ren}$ does not depend on energy, there is no "reducible" VP contribution.

For the evaluation of the correction (183) we employ the Uehling approximation (see Section 4.d). The Uehling contributions to graph Fig. 14f) is exactly zero [96]. Neglecting again the high-order terms we omit thus fully the contribution of Fig. 14f). For alkali metal atoms the numerical results for δg_{VP}^{bound} were elaborated in Refs. [100, 104].

The nondiagonal matrix elements of the electron self-energy operator $(\Sigma^{ren}(E_A))_{An}$ in Eq (182) can be evaluated in the frames of the potential expansion approach in the same way as the diagonal matrix element in Section 4.a.

The numerical calculation of the integrals in Eqs. (142) and (144) was performed with the Simpson method. The wave functions in the momentum space were obtained with the Fourier transformation of the B-spline approximation for the coordinate - space wave function. The integrals in Eqs. (147)–(153) were evaluated by the gaussian method with the number of the integration points 32.

The expression for the MP contribution to the nondiagonal SE matrix element can be written in such a form:

$$\left(\hat{\Sigma}_{OP}^{ren}(E_A)\right)_{An} = -\frac{\alpha}{\pi}\sum_m \int_0^\infty dw \mathcal{R}e\left\{\sum_n \frac{1}{E_a - E_m - iw}\times\right.$$

$$\left.\times \int \phi_m^+(-w,\vec{r_1})\Psi_A(\vec{r_2})\frac{1-\vec{\alpha}_1\vec{\alpha}_2}{r_{12}}exp(-wr_{12})\Psi_n(\vec{r_1})\phi_m(w,\vec{r_2})d\vec{r_1}d\vec{r_2}\right\}. \tag{12.184}$$

Here the sum over m is extended over the total Dirac spectrum for the bound electron, $r_{12} = |\vec{r_1} - \vec{r_2}|$ and $\vec{\alpha}_i$ are the Dirac matrices acting on the different wave functions. The function $\phi_m(w,\vec{r})$ is defined as:

$$\phi_m(w,\vec{r}) = \sum_\nu \frac{(V(\vec{r}))_{\nu m}}{E_a - E_\nu - iw}\Psi_\nu(\vec{r}), \tag{12.185}$$

where the sum over ν is the extended over the total Dirac spectrum for the free electron, $\Psi_\nu(\vec{r})$ and E_ν denote the eigenfunctions and eigenvalues for the free electron Dirac equation.

The triple summation over total Dirac spectrum in Eq.(184) (two summations over the free electron spectrum and one summation over the bound electron spectrum) were performed with the use of B-spline approach [65]. The free-electron spectrum was obtained from the bound-electron spectrum by $Z = 0$. The number of grid points was 150 and the order of splines was equal to 8.

Now we go over to the evaluation of δg_{SE-WF}^{bound} and δg_{VER}^{bound} and begin with the evaluation of $\delta g_{SE-WF,irr}^{bound}$ by the insertion of the expressions

$\left(\hat{\Sigma}^{ren}_{ZP}(E_A)\right)_{An}$, $\left(\hat{\Sigma}^{ren}_{OP}(E_A)\right)_{An}$ and $\left(\hat{\Sigma}^{ren}_{MP}(E_A)\right)_{An}$ in Eq (182). Most easily this calculation is performed by introducing the wave function:

$$\tilde{\Psi}_A(\vec{r}) = \sum_{n\ (E_a \neq E_n)} \frac{\left(e\vec{\alpha}\vec{A}(\vec{r})\right)_{An}}{E_A - E_n} \Psi_n(\vec{r}). \tag{12.186}$$

Then Eq. (182) reduces to:

$$\delta g^{bound}_{SE-WF} = \frac{2}{\mu_B B_z} \left\{ \left(\hat{\Sigma}^{ren}(E_A)\right)_{\tilde{A}A} + \left(\hat{\Sigma}^{ren}(E_A)\right)_{A\tilde{A}} \right\}. \tag{12.187}$$

The evaluation of the matrix elements $\left(\hat{\Sigma}^{ren}_{ZP}(E_A)\right)_{\tilde{A}A}$ and $\left(\hat{\Sigma}^{ren}_{OP}(E_A)\right)_{\tilde{A}A}$ is performed in the momentum space. The direct Fourier transformation of the potential (174) is not convenient for the numerical calculations. More suitable expression was proposed in [98]:

$$\vec{A}(\vec{r}) = \frac{1}{2} \lim_{\zeta \to 0} \left(\vec{r} \times \vec{B}\right) exp\{-(\zeta r/2)^2\}. \tag{12.188}$$

Then in the momentum space one has:

$$\vec{A}(\vec{p}) = \lim_{\zeta \to 0} \frac{i}{\pi^{3/2}\zeta^5} exp\{-(p/\zeta)^2\} \left(\vec{p} \times \vec{B}\right). \tag{12.189}$$

For the practical calculation the values for ζ from 10^{-4} to 10^{-6} should be used since the average value for p in the ion with the nuclear charge Z is $\overline{p} \sim Z$. Practically this means that the order of magnitude of $exp\{-(p/\zeta)^2\}$ is comparable with $(\pi^{3/2}\zeta^5)^{-1}$.

The reducible correction $\delta g^{bound}_{SE-WF,red}$ that corresponds to the irreducible correction Eq (182) looks like:

$$\delta g^{bound}_{SE-WF,red} = \left(\left[\frac{\partial}{\partial E} \hat{\Sigma}^{ren}(E) \right]_{E=E_A} \right)_{AA} \left(e\vec{\alpha}\vec{A}(\vec{r})\right)_{AA}. \tag{12.190}$$

The evaluation of the matrix element of $\left[\frac{\partial}{\partial E}\hat{\Sigma}^{ren}(E)\right]_{E=E_A}$ in Eq (190) is performed again with the use of the potential expansion and the renormalized expressions for $\hat{\Sigma}^{ren}_{ZP}(E)$, $\hat{\Sigma}^{ren}_{OP}(E)$, $\hat{\Sigma}^{ren}_{MP}(E)$. Unlike the case of $\left(\hat{\Sigma}^{ren}(E_A)\right)$, the infrared divergences do not cancel in $\left[\frac{\partial}{\partial E}\hat{\Sigma}^{ren}(E)\right]_{E=E_A}$; the remaining infrared contribution is:

$$\frac{\alpha}{(4\pi)^2} \ln \frac{\lambda^2}{m_e^2} \left(e\vec{\alpha}\vec{A}(\vec{r})\right)_{AA}. \tag{12.191}$$

This contribution will be canceled with the similar term in the vertex correction.

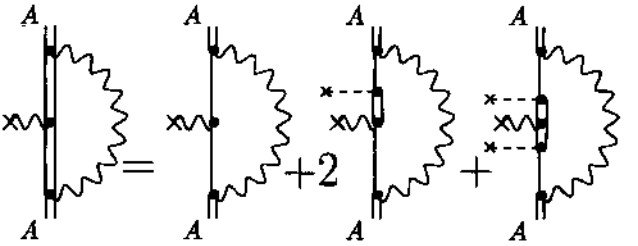

Fig. 15

The potential expansion of the vertex graph. The dashed line with the cross at the end denotes the nuclear Coulomb potential V.

The potential expansion for the vertex correction is depicted in Fig.15. The three terms of this expansion we denote as VER1, VER2 and VER3. Only the VER1 part is divergent. It can be treated exactly in the same way as $\left(\hat{\Sigma}^{ren}_{OP}(E_A)\right)_{AA}$ where the Coulomb potential $V(\vec{p}-\vec{q}) = \alpha Z/\left(\vec{p}-\vec{q}\right)^2$ is replaced by $e\vec{\alpha}\vec{A}(\vec{p})$ and $\vec{A}(\vec{p})$ is the potential of the external magnetic field Eq (189). The infrared divergence will be cancelled by the infrared divergent term Eq (191) in the SE-WF,red contribution [98,99].

The term VER2 is analogous to $\left(\hat{\Sigma}^{ren}_{MP}(E_A)\right)_{AA}$. The only difference is that one of the functions $\phi_m(w,\vec{r})$ in the expression (28) should be replaced by the function, depending on $\left(e\vec{\alpha}\vec{A}(\vec{p})\right)$ instead of the Coulomb potential V. The term VER2 is finite. Now it remains to consider the finite contribution VER3 that will be described below.

The correction δg^{bound}_{VER3}, though finite, is most difficult for the numerical calculations: it contains two bound electron propagators and two free electron propagators. To avoid the computational difficulties the nonperturbative finite basis set method based on the exact solution of the Dirac equation for the atomic electron in the external magnetic field [107] can be applied. Then the correction δg^{bound}_{VER3} results as:

$$\delta g_{VER3}^{bound} = \frac{\left(\hat{\Sigma}_{MP}^{ren}(E_A, B_z)\right)_{AA} - \left(\hat{\Sigma}_{MP}^{ren}(E_A, 0)\right)_{AA}}{\mu_B B_z}. \tag{12.192}$$

It is understood that the magnetic field is included nonperturbatively only in the bound electron propagator in Eq (184) but not in the wave functions $\Psi_A(\vec{r})$. This situation is depicted in Fig. 16.

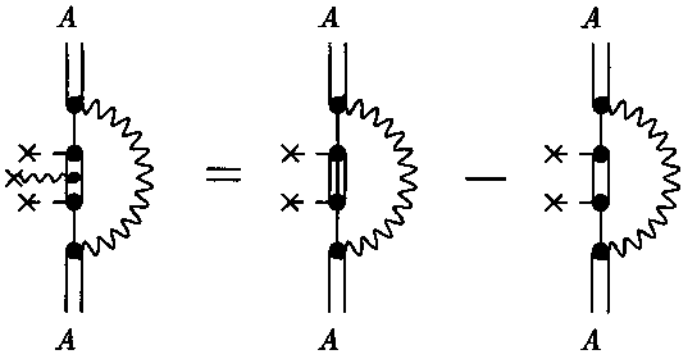

Fig 16.
Graphical representation of the evaluation of δg_{VER3}^{bound}. The triple solid line denotes the atomic electron in an external magnetic field.

The Dirac equation for the atomic electron in an external magnetic field reads:

$$\hat{H}\Psi = E\Psi\,, \tag{12.193}$$

with

$$\hat{H} = \hat{H}_0 + \hat{H}_m \tag{12.194}$$

and

$$\hat{H}_0 = \vec{\alpha}\cdot\vec{p} + \beta m + V(\vec{r}) \tag{12.195}$$

$$\hat{H}_{\rm m} = \frac{1}{2}\vec{\alpha}\cdot\left(\vec{B}\times\vec{r}\right), \tag{12.196}$$

where $\vec{\alpha}$, β denote the Dirac matrices, c is the speed of lihgt, $\vec{B}$ is the magnetic field strength (the magnetic field is supposed to be directed

along the z-axis: $\vec{B} = B\,\vec{e}_z$). For the valence electrons in heavy alkali metal atoms $V(\vec{r})$ includes also the electron core potential. In Eqs. (193)–(196) atomic units are used.

The variational solution of the Dirac equation (193) is obtained according to [107] with the trial functions:

$$\Psi^{\mu}(\vec{r}) = \sum_{s=1}^{2\tilde{N}} \sum_{\kappa}^{\kappa_{\max}} a_s^{\kappa} \Psi_s^{\kappa\mu}(\vec{r})\,. \tag{12.197}$$

The electron wave functions $\Psi^{\mu}(\vec{r})$ in the magnetic field possess cylindrical symmetry and can be expanded with respect to a finite basis set of the functions $\Psi_s^{\kappa\mu}(\vec{r})$ of spherical symmetry. The index κ denotes the Dirac angular quantum number, μ corresponds to the total electron angular momentum projection, a_s^{κ} are the variational coefficients, and $2\tilde{N}$ defines the number of the basis-set functions.

The next step is the use of the B-spline approximation of the functions $\Psi_s^{\kappa\mu}(\vec{r})$ [107].

The variational solution of the Dirac equation (193) with the trial functions (197) reduces to the diagonalization of the Hamiltonian (194) within the finite basis set defined by Eq. (197). As the result one obtains the full set of solutions of the Dirac equation for the atomic electron in an external magnetic field.

Within the B-spline approach the H-like ion is included inside a spherical box of radius $R_{\rm box} \sim \frac{50}{Z}\ a.u.$ with the boundary conditions $rf_n(r)|_{r=0} = rg_n(r)|_{r=0} = rf(r)|_{r=R_{box}} = rg(r)|_{r=R_{box}} = 0$, whehe f_n, g_n are the radial Dirac wave functions. The number of grid points was $N_g = 150$ and the order of splines $k = 8$. This corresponds to $2N = 2(N_g + k - 2) = 312$ energy levels that represent approximately the Dirac spectrum. With this choice the inaccuracy of the spline approximation for the $1s_{1/2}$ state compared to the variational solution [107] becomes less than 10^{-8} [103]. The comparison between the results of the evaluation of Zeeman splitting by the perturbation theory (PT) and by the nonperturbative approach [107] reveals that for field strengths B up to $2 \cdot 10^2$ T the deviation from the PT is about 10^{-8} while for a field strength of about $2 \cdot 10^4$ T the deviation increase up to 10^{-3}. The latter is due to the distortion of the atomic structure by the magnetic field.

In [103] the nonperturbative approach [107] was used for the evaluation of the total correction δg_{QED}^{bound}. For H-like ions with $1 \leq Z \leq 90$ the deviation from the accurate PT results [99] turned out to be smaller than 0.1%.This calculation helped to prove the absence of the "spurious" terms in PWR approach. However this accuracy was not sufficient for obtaining accurate values for δg_{QED}^{bound}. The reason lies in the fact that δg_{QED} correc-

tions are obtained via subtraction of the free-electron QED corrections from the bound-electron QED corrections: $\delta g_{QED} = \delta g_{QED}^{bound} - \delta g_{QED}^{free}$. Since we take into account only the lowest-order QED corrections in δg_{QED}^{bound}, we have to use the Schwinger value for δg_{QED}^{free}. This subtraction leads to severe numerical cancellations that diminish the accuracy of the net result. However, this is not the case when we use the nonperturbative approach only for the part of δg_{QED}^{bound}, namely for the δg_{VER3}^{bound} contribution which is far from dominating in the total result (see the sixth column of Table 12.3). Thus one can claim that 10% accuracy level still holds for the evaluation of δg_{QED}.

Table 12.3 SE corrections to the electron g-factor for the ground state of H-like ions. In the brackets we represent the numerical results from [99]. The units are 1×10^{-6}. The columns are: A: $\delta g_{SE-WF,irr(ZP+OP)}^{bound}$; B: $\delta g_{SE-WF,irr(MP)}^{bound}$; C: $\delta g_{SE-WF,(red+VER1)}^{bound}$; D: $\delta g_{VER2+VER3}^{bound}$; E: δg_{VER3}^{bound}; F: δg_{SE}^{bound}.

Z	A	B	C	D	E	F
1	1.39	0.4012	2320.62	0.43	0.04	2322.84
	(1.39)	(0.1386)	(2320.78)	(0.53)		(2322.84)
10	66.46	12.51	2229.98	17.01	0.06	2325.96
	(66.46)	(12.28)	(2229.83)	(16.97)		(2325.54)
20	193.56	42.40	2076.05	29.14	0.07	2341.15
	(193.56)	(41.61)	(2073.50)	(29.20)		(2337.87)
30	356.80	81.90	1900.17	30.23	0.08	2369.10
	(356.81)	(80.37)	(1899.43)	(29.98)		(2366.59)
40	550.69	128.23	1730.55	13.73	0.08	2423.20
	(550.70)	(125.84)	(1729.58)	(13.27)		(2419.39)
50	774.06	181.98	1570.18	-19.39	0.09	2506.83
	(774.06)	(178.60)	(1569.42)	(-17.25)		(2504.83)
60	1027.85	246.31	1423.05	-62.20	0.10	2635.01
	(1027.87)	(241.80)	(1422.44)	(-58.20)		(2633.91)
70	1315.04	326.47	1289.79	-108.51	0.11	2822.79
	(1315.07)	(320.83)	(1290.52)	(-105.03)		(2821.39)
80	1641.51	430.04	1175.17	-157.67	0.13	3089.05
	(1641.52)	(423.97)	(1174.84)	(-151.87)		(3088.46)

The results of the calculation of the different δg_{SE}^{bound} contributions in comparison with the corresponding results from [98, 99] for H-like ions in the ground state with different Z values are presented in Table 12.3. The mean deviation from [98, 99] in the total δg_{SE}^{bound} value amounts to 0.1%. This deviation originates from our use of the point-like nu-

cleus, while in [98,99] the extended nucleus model was employed. Moreover, in [98,99] the larger number of the partial waves in the evaluation of $\delta g^{bound}_{SE-WF,irr(MP)}$ was employed. However these differences are well within the 10% inaccuracy range, accepted in [104].

The electron g-factor for the number of ns^1 heavy atomic systems and in particular for alkali metal atoms have been accurately measured, showing a clear deviation from the free electron value g^{free} given by Eq (176). Note that $\delta g^{free}_{QED} = g^{free} - 2$ differs from the Schwinger value Eq (178) since it includes higher-order QED terms. A large number of theoretical calculations of $\delta g = g^{bound} - g^{free}$ also exists for alkali metal atoms (see [100]). The reason behind the deviation δg are, however, different in light and in heavy atoms. For light atoms the main contribution is relativistic correction δg_{rel} (see Eq (179)). For a recent status of this correction c.f. [108]. In heavy atoms the core-valence correlation correction δg_{corr} dominants [109–113]. The Breit interaction between the valence and core electrons also leads to an observable contribution δg_{Breit} [109–113].

In most of theoretical studies for the alkali metal atoms it was assumed that the correction δg_{QED} is negligible, i.e. that the QED correction to the g-factor is the same as for the free electron. However, recent calculations for hydrogenlike ions [98], show that the deviation of the bound-state QED correction δg^{bound}_{QED} from the free-electron value δg^{free}_{QED} can be as large as 50% for high Z values.

In [100] it was supposed that the correction δg_{QED} can be observable for heavy alkali metal atoms. This conclusion was confirmed in [104], though the accurate value for δg_{QED} diminished essentially compared to the estimates given in [100].

The evaluation of all the contributions in [104] was performed in one-particle approximation. The approximate Dirac-Hartree-Fock (DHF) wave functions were used. These wave functions were obtained in a local potential field fitted to the DHF potential as was described in [100].

For the summation over the Dirac spectrum the B-spline approach was used with the number of the grid points 150 and the order of spline equal to 8. The number of the partial waves in the MP term varied around 10. Note, that the size of the alkali metal atoms is much larger then the size of HCI. Therefore the radial box was chosen as $R_{box} \sim 100$a.u. Since the magnetic field grows rapidly with the size of the box one has to use relatively small values for the magnetic field ($10T \leq B_z \leq 100T$) for the evaluation of δg^{bound}_{VER3}. This leads to the strong cancellations in Eq (36) but does not affect seriously the accuracy of the total result due to the smallness of δg^{bound}_{VER3} contribution.

The results of the calculations are given in Table 12.4. In the fourth column the values of δg_{VP}^{bound} are shown. In the fifth column we present the sum of the dominant contributions $\delta g_{SE-WF,red}^{bound} + \delta g_{VER1}^{bound}$. The total value of δg_{SE}^{bound} is given in the sixth column and the value for $\delta g_{QED} = \delta g_{QED}^{bound} - \delta g_{Sch}^{free}$ is given in the seventh column of the Table 12.4. The last value should be compared with the experimental data.

Table 12.4 QED corrections to the electron g-factor for the valence ns-electron in alkali metal atoms.

Z	Atom	state	$\delta g_{ns}^{\mathrm{VP}}$	$\delta g_{ns}^{\mathrm{SE,ver[1]+WF,red}}$	$\delta g_{ns}^{\mathrm{SE}}$	δg_{QED}
55	Cs	$6s$	$-3.0\cdot10^{-7}$	$2.29214\cdot10^{-3}$	$2.32333\cdot10^{-3}$	$2.9\cdot10^{-7}$
56	Ba^+	$6s$	$-5.55\cdot10^{-7}$	$2.29174\cdot10^{-3}$	$2.32397\cdot10^{-3}$	$5.9\cdot10^{-7}$
87	Fr	$7s$	$-5.70\cdot10^{-7}$	$2.291591\cdot10^{-3}$	$2.32411\cdot10^{-3}$	$7.2\cdot10^{-7}$

In Table 12.5 the different contributions to δg^{bound} are collected and compared with the experimental data for alkali metal atoms. Here δg_{tot} denotes the sum of the δg_{rel}, δg_{corr}, and δg_{Breit}. The correction δg_{QED} calculated in this work appears to be an order of magnitude smaller than the estimates given for Cs, Ba^+ and Fr in [100]. Still δg_{QED} is not negligible in case of Ba^+ where the most accurate experimental and theoretical data are known. Note, that the theoretical error bars in [113] were introduced mainly to incorporate the possible QED corrections. Then the inclusion of δg_{QED} leads to the better agreement with the experimental value.

References

[1] J. Schwinger, Phys. Rev. **75**, 1912 (1949); Phys. Rev. **75**, 651 (1949).

[2] R. Feynman, Phys. Rev. **76**, 749 (1949); Phys. Rev. **76**, 769 (1949).

[3] S. Tomonaga, Phys. Rev. **74**, 224 (1948).

[4] F. Dyson, Phys. Rev. **75**, 486 (1949); Phys. Rev. **75**, 1736 (1949).

[5] W.E. Lamb and R.C. Retherford, Phys. Rev. **72**, 241 (1947).

[6] H. Bethe, Phys. Rev. **72**, 339 (1947).

[7] N.M. Kroll and W.E. Lamb, Phys. Rev. **75**, 388 (1949).

[8] J.B. French and V.F. Weisskopf, Phys. Rev. **75**, 1240 (1949).

[9] M.I. Eides, H. Grotch and V.A. Shelyuto, Phys. Rep. **342**, 63 (2001).

Table 12.5 Different contributions for alkali metal atoms. The units are 1×10^{-6}.

Z	55	56	87
Atom	Cs	Ba^+	Fr
δg_{rel}	−50. [111] −23. [110] −28.10 [100]	−55.39 [113] −59.71 [100]	−33. [110] −40.01 [100]
δg_{corr}	366. [111] 284. [110]		3370. [110]
δg_{Breit}	1. [111] −7. [110]	−7.08 [113]	−10. [110]
δg_{tot}	317. [111] 254. [110]	171.8±3.0 [113]	3327. [110]
δg_{exp}	223. [114]	172.63±0.03 [95]	2650.±80. [115]
δg_{QED}	0.29	0.59	0.72

[10] G.E. Brown, H.S. Langer and G.W. Schäfer, Proc. Roy. Soc **A 251**, 92 (1959); G.E. Brown and D.F. Mayers, Proc. Roy. Soc **A 251**, 105 (1959).

[11] L.N. Labzowsky, G.L. Klimchitskaya and Yu.Yu. Dmitriev, "Relativistic Effects in Spectra of Atomic Systems" IOP Publishing, Bristol 1993.

[12] P.J. Mohr, G. Plunien and G. Soff, Phys. Rep. **293**, 227 (1998).

[13] P. Pyykkö, M. Tokman and L. Labzowsky, Phys. Rev. **A 57**, R689 (1998).

[14] L. Labzowsky, I. Goidenko, M. Tokman and P. Pyykkö, Phys. Rev. **A 59**, 2701 (1999).

[15] N. Yamanaka, A. Haga, Y. Horikawa and A. Ichimura, Phys. Rev. **A 63**, 062502 (2001).

[16] I. Bednyakov, L. Labzowsky and G. Soff, J. Phys. **B 28**, L719 (1995).

[17] P. Pyykkö, K.G. Dyall, A.G. Csaszar, G. Tarczay, O.L. Polyancky and J. Tennyson, Phys. Rev. **A 63**, 024502 (2001).

[18] K.G. Dyall, C.W. Bauschlicher Jr., D.W. Schwenke and P. Pyykkö, Chem. Phys. Lett. **348**, 497 (2001).

[19] W.H. Furry, Phys. Rev. **81**, 15 (1951).

[20] G.C. Wick, Phys. Rev. **80**, 268 (1950).

[21] W. Pauli and F. Willars, Rev. Mod. Phys. **21**, 434 (1949).

[22] G. Itzykson and J.B. Zuber, "Quantum Field Theory" McGraw Hill, N.Y.1980.

[23] M. Gell-Mann and F. Low, Phys. Rev. **84**, 350 (1951).

[24] J.Sucher, Phys. Rev. **107**, 1448 (1957).

[25] L.N. Labzowsky, Zh. Eksp. Teor. Fiz **59**, 167 (1970) [Engl. Transl. : Sov. Phys. JETP **32**, 94 (1970)].

[26] O.Yu. Andreev, L.N. Labzowsky, G. Plunien and G. Soff, Phys. Rev. **A 64**, 042513 (2001).

[27] M. Brawn and V. Shirokov, Izv. Akad. Nauk USSR ser. fiz. **41**, 2585 (1977); [Engl. Transl. Bull. Acad. Sci. USSR Phys. Ser. **41**, 2585 (1977)]

[28] T.E. Timofeeva and L.N. Labzowsky, Izv. Akad. Nauk USSR ser. fiz. **45**, 2390 (1981); [Engl. Transl. Bull. Acad. Sci. USSR Phys. Ser. **45**, 127 (1981)].

[29] V.M. Shabaev, Phys. Rep. **356**, 119 (2002).

[30] I. Lindgren, Molecular Physics **98**, 1159 (2000).

[31] S. Blundell, P.J. Mohr, W.R. Jonson and J. Sapirstein, Phys. Rev. **A 48**, 2615 (1992).

[32] V. Shabaev and I. Fokeeva, Phys. Rev. **A 49**, 4489 (1994).

[33] I. Lindgren, H. Persson, S. Salomonson and L. Labzowsky, Phys. Rev. **A 51**, 1167 (1995).

[34] P.J. Mohr and J. Sapirstein, Phys. Rev. **A 62**, 052501 (2000).

[35] I. Lindgren, H. Persson, S. Salomonson, V. Karasiev, L. Labzowsky, A. Mitrushenkov and M. Tokman, J. Phys. **B 26**, L503 (1993).

[36] G.E. Brown and D.G. Ravenhall, Proc. Roy. Soc. **A 208**, 552 (1951).

[37] M.H. Mittleman, Phys. Rev. **A 5**, 2395 (1972); Phys. Rev. **A 24**, 1167 (1981).

[38] J. Sucher, Phys. Rev. **A 22**, 348 (1980); "Relativistic, QED and Weak Interaction effects in Atoms" ed. W. Johnson, P. Mohr and J. Sucher (AIP conf. Proc. 189) (New York: American Institute of Physics) p. 29, p. 370 (1989).

[39] I. Lindgren, "Relativistic, QED and Weak Interaction effects in Atoms" ed. W. Johnson, P. Mohr and J. Sucher (AIP conf. Proc. 189) (New York: American Institute of Physics) p. 71 (1989).

[40] G.L. Klimchitskaya and L.N. Labzowsky, Zh. Eksp. Teor. Fiz **60** , 2019 (1971) [Engl. Transl. : Sov. Phys. JETP **33**, 1108 (1971)].

[41] A.I. Akhiezer abd V.B. Berestetskii, "Quantum Electrodynamics" (New York: Wiley Insterscience) 1965.

[42] W.E. Lamb, Jr and R.C. Retherford, Phys. Rev. **72**, 339 (1947).

[43] R. Karplus, A. Klein and J. Schwinger, Phys. Rev. **86**, 288 (1952).

[44] M. Baranger, H. Bethe and R. Feynman, Phys. Rev. **92**, 482 (1953).

[45] H.M. Fried and D.R. Yennie, Phys. Rev. **112**, 1391 (1958).

[46] G.W. Ericksson and D.R. Yennie, Ann. Phys. **35**, 271 (1965).

[47] K. Pachucki, D. Leibfried, M. Weitz, A. Huber, W. König and T.W. Hänsch, J. Phys. **B 29**, 177 (1996).

[48] H. Araki, Prog. Theor. Phys. **17**, 619 (1957).

[49] J. Sucher, Phys. Rev. **109**, 1010 (1958).

[50] M.A. Braun and L.N.Labzowsky, Zh. Eksp. Teor. Fiz **53**, 1176 (1967) [Engl. Transl. : Sov. Phys. JETP **26**, 1017 (1968)].

[51] G.W.F. Drake, Phys. Scripta **T 95**, 22 (2001).

[52] K. Pachucki, Phys. Rev. Lett. **84**, 4561 (2000).

[53] K. Pachucki and J. Sapirstein, J. Phys. **B 33**, 5297 (2000).

[54] A.M. Desiderio and W.R. Johnson, Phys. Rev. **A 3**, 1267 (1971).

[55] P. Mohr, Ann. Phys. NY **88**, 26 (1974). Ann. Phys. NY **88**, 52 (1974).

[56] W.R. Johnson and G. Soff, At. Data Nucl. Data Tables **33**, 405 (1985).

[57] P.J. Mohr and Y.-K. Kim, Phys. Rev. **A 45**, 2727 (1992).

[58] P.J. Mohr, Phys. Rev. **A 46**, 4421 (1992).

[59] P. Indelicato and P.J.Mohr, Hyperfine Interaction **114**, 147 (1998).

[60] E.-O. Le Bigot, P. Indelicato and P.J. Mohr, Phys. Rev. **A 64**, 052508 (2001).

[61] U. Jentschura, G. Soff and P.J. Mohr, Phys. Rev. **A 56**, 1739 (1997).

[62] W.R. Johnson, S.A. Blundell and J. Sapirstein, Phys. Rev. **A 37**, 307 (1988).

[63] S. Salomonson and P. Öster, Phys. Rev. **40**, 5548 (1989).

[64] L.N. Labzowsky, Zh. Eksp. Teor. Fiz **59** , 167 (1970) [Engl. Transl. : Sov. Phys. JETP **32**, 1171 (1970)].

[65] H.J. Snyderman, Ann. Phys. NY **211**, 43 (1991).

[66] S.A. Blundell and H.J. Snyderman, Phys. Rev. **A 44**, R1427 (1991).

[67] A. Mitrushenkov, L. Labzowsky, I. Lindgren, H. Persson and S. Salomonson, Phys. Lett **A 2000**, 51 (1995).

[68] N.N. Bogoljubov and D.V. Shirkov, "Introduction to the Theory of the Quantized Fields" (New York: Wiley) 1959.

[69] H. Persson I. Lindgren and S. Salomonson, Phys. Scr. **T 46**, 125 (1993); I. Lindgren, H. Persson, S. Salomonson and A. Ynnerman, Phys. Rev. **A 47**, R4555 (1993).

[70] H.M. Quiney and I.P. Grant, Phys. Scr. **T 46**, 132 (1993); H.M. Quiney and I.P. Grant, J. Phys. **B 27**, L299 (1994).

[71] L. Labzowsky and I. Goidenko, J. Phys. **B 30**, 177 (1997); L.N. Labzowsky, I.A. Goidenko and A.V. Nefiodov, J. Phys. **B 31**, L477 (1998).

[72] W.H. Furry, Phys. Rev. **51**, 125 (1937).

[73] E.A. Uehling, Phys. Rev. **48**, 55 (1935).

[74] E. Wichmann and N.M. Kroll, Phys. Rev. **101**, 843 (1956).

[75] G. Soff and P.J. Mohr, Phys. Rev. **A 38**, 5066 (1988).

[76] L.N. Manakov, A.A. Nekipelov and A.G. Fainstein, Zh. Eksp. Teor. Fiz **95**, 1167 (1989).

[77] F. Salvat, J.D. Martinez, R. Mayd and J. Parellada, Phys. Rev. **A 36**, 467 (1987).

[78] S. Klarsfeld, Phys. Lett. **B 66**, 86 (1977).

[79] S.A. Blundell, Phys. Rev. **A 46**, 3762 (1992).

[80] H. Persson I. Lindgren, S. Salomonson and P. Sunnergren, Phys. Rev. **A 48**, 2772 (1993).

[81] Z.-C. Yan and G.W.F. Drake, Phys. Rev. Lett. **81**, 774 (1998).

[82] S.A. Blundell, J. Sapirstein and W.R. Johnson, Phys. Rev. **D 45**, 1602 (1992); M.S. Safronova, W.R. Johnson and A. Derevianko, Phys. Rev. **A 60**, 4476 (1999).

[83] V.A. Dzuba, V.V. Flambaum and J.S.M. Ginges, Phys. Rev. **A 63**, 062101 (2001).

[84] M.G. Kozlov, S.G. Porsev and I.I. Tupitsin, Phys. Rev. Lett. **86**, 3620 (2001).

[85] E. Eliav, U. Kaldor and Y. Ishikawa, Phys. Rev. **A 50**, 1121 (1994).

[86] C.E. Moore, "Atomic Energy Levels" Natl. Bur. Stand. (US) GPO, Washington, DC (1948-1971).

[87] E. Eliav, U. Kaldor and Y. Ishikawa, Phys. Rev. **A 52**, 2765 (1995).

[88] E. Eliav, U. Kaldor, Y. Ishikawa, M. Seth and P. Pyykkö, Phys. Rev. **A 53**, 3926 (1996).

[89] E. Eliav, U. Kaldor, B. Hess and Y. Ishikawa, Phys. Rev. Lett. **73**, 3203 (1994).

[90] Y. Ishikawa and K. Koc, Phys. Rev. **a 56**, 1295 (1997).

[91] P. Neogrady, V. Kellö, M. Urban and A. Sadlej, Int. J. Quant. Chem. **63**, 557 (1996).

[92] N. Hermanspahn, W. Quint, S. Stahl, M. Tonges, G. Bollen, H. J. Kluge, R. Ley, R. Mann, and G. Werth, Acta Phys. Pol. **B27**, 351 (1996).

[93] M. Diederich, H. Häffner, N. Hermanspahn, M. Immel, H. J. Kluge, R. Ley, R. Mann, S. Stahl, W. Quint, J. Verdu, and G. Werth, in: *Trapped Charged Particles and Fundamental Physics*, edited by D. H. E. Dubin, and D. Schneider, AIP Conference Proc. N° 457 (AIP, Woodbury, NY, 1999), pp. 43-51.

[94] N. Hermanspahn, T. Beier, H. J. Kluge, W. Quint, S. Stahl, J. Verdu, and G. Werth, Phys. Rev. Lett. **85**, 5308 (2000)

[95] G. Marx, G. Tommaseo, and G. Werth, Eur. Phys. J. **D4**, 279 (1998).

[96] H. Persson, S. Salomonson, P. Sunnergren, and I. Lindgren, Phys. Rev. **A56**, R2499 (1997).

[97] S. A. Blundell, K. T. Cheng, and J. Sapirstein, Phys. Rev. **A55**, 1857 (1997).

[98] T. Beier, I. Lindgren, H. Persson, S. Salomonson, and P. Sunnergren, Phys. Rev. **A62**, 032510 (2000).

[99] T. Beier, Phys. Rep. **339**, 79 (2000)

[100] L. Labzowsky, I. Goidenko, and P. Pyykkö, Phys. Lett. **A258**, 31 (1999).

[101] H. Persson, S. Salomonson and P. Sunnergren, Adv. Quantum Chem. **30**, 379 (1998).

[102] V.A. Yerokhin, Phys. Rev. **A 62**, 012508 (2000).

[103] I. Goidenko, G. Plunien, S. Zschocke, L. Labzowsky, and G. Soff, accepted to Phys. Rev. **A**.

[104] I. Goidenko, L. Labzowsky, G. Soff, and P. Pyykkö, (to be published).

[105] G. Breit, Nature **122**, 649 (1928).

[106] T. Kinoshita, "Quantum Electrodynamics", World Scientific, Singapore, 1990.

[107] Z. Chen and S. Goldman, Phys. Rev. **A44**, 4459 (1991).

[108] P. Marketos, Z. Phys **D 27**, 219 (1993).

[109] V. Flambaum, I. Khriplovich, and O. Sushkov, Zh. Eksp. Teor. Fiz. **75**, 75 (1978) [Engl. Transl. Sov. Phys. JETP **48**, 37 (1978)].

[110] V. Dzuba, V. Flambaum, P. Silvestrov, and O. Sushkov, Phys. Scr **31**, 275 (1985).

[111] G. Anikin, I. Zhogin, Opt. Spectrosc. (USSR) **51**, 303 (1985).

[112] L. Veseth, J. Phys. **B16**, 289 (1983).

[113] E. Lindroth and A. Ynnerman, Phys. Rev. **A47**, 961 (1993).

[114] J. Morton and K. Preston, in: H. Fischer, K. H. Hellwege (Eds.), Magnetic properties of free radicals, Landolt-Börnstein, Group 2, Vol. 9. Springer-Verlag, Berlin, Heidelberg, New York, 1997.

[115] C. Ekström and L. Robertson, VIII ICAP, Abstracts, p. B44, Göteborg, 1982.

Index

2-component 353, 355
2-spinor 353, 354
2-vector 353
4-current 217,218
4-gradient 216
4-momentum 217
4-potential 217
4-spinor 353, 354, 355
4-spinor approximation, atomic 331-334
4-vector 216

A

ab initio model potential method 411
ab initio model potentials 345
accuracy of the pseudopotential approximation 421-431
actinides 164-166
adiabatic S-matrix formalism 510-523
AE/MVD 416
AES 116, 136
AIMP 411, 414
AIMP 345
alchemy 2
ALCHEMY 2, 3
algebraic approximation 34-48, 214, 250-268
algebraic approximation, Dirac equation in 35-39
alkali atoms, electron affinity of 195-198
alkali atoms, ionization potentials of 3, 4, 183-184
anionic states, multiple stable 200
ANO 343
anomalous electron magnetic moment 48
ANS 345
AREP 414
ARPP 414
atomic 4-spinor approximation 341-344
atomic electronic shell, relativistic effects on 61-64
atomic electronic structure methods 171-209
atomic natural orbital 343
atomic natural spinor 343
atomic properties 68-72
atomic units 215
atomic weight 5, 6
atoms, interelectron interaction in 510-521
atoms, QED effects in 493-557
Au_2, accuracy of the pseudopotential approximation 424-428
Auger emission 125, 126
Auger emission spectroscopy 116
AuH, accuracy of the pseudopotential approximation 424-428

B

B3LYP 404
Baker-Campbell-Hausdorff expansion 233
basis set superposition error 416
basis sets, valence 416, 417
BIS 116
Born-Oppenheimer approximation 219, 447
Breit interaction 228-229, 284, 285, 353
Breit operator 174, 333
Breit term, importance of 195
Breit-Pauli operators 332
bremsstrahlung isochromat spectroscopy 116
Brown-Ravenhall diease 214, 244, 353
BSSE 416

C

CAS 313
CCSD 262, 264
CCSD(T) 261
change of picture problem 376-380
Chang-Pelissier-Durand Hamiltonian 403
charge conjugation symmetry 224-225
chemical properties, prediction of 68-86
chemical studies of elements heavier than 108 101-107
chemical studies of the heaviest elements 59-61
chemistry, gas phase 87, 88
chemistry of the heaviest elements 54-114
chemistry, "one-atom-at-a-time" 86-101
chemistry, solution 88, 89
CI 248-249, 259, 260
CIPSO 415
clamped nucleus approximation 219
Clifford algebra 217
COLUMBUS 411, 413, 415
complete active space 313
complex formation, theoretical model for prediction of 80-81
computational scaling 249-263
configuration interaction 248-249, 259
continuum, interaction with a state 155, 156
core and valence electron distributions in heavy elements 115-169
core photoemission 140-146
core, selecting the 406-408
core spectroscopies, complementarity between different 126, 127
core-valence separation 402, 404
correlation corrections in group IIB atoms 290-297
correlation corrections in neon-like ions 290-297
correlation corrections in noble gas atoms 290-297
correlation effects, overestimation of by pseudopotentials 430, 431
correlation, electron 177-182, 271-325, 258-263
correlation energy, Dirac-Coulomb 272, 273, 285, 286, 290-297, 297-305
correlation energy, Dirac-Coulomb-Breit 273, 285, 286, 290-297, 297-305
correlation energy, dynamical 305-320
Coulomb gauge 219, 275, 276
Coulomb-Breit relativistic Hartree-Fock energies 460
coupled cluster approximation 43, 44
coupled cluster method 178-182
coupled cluster method, applications of 182-201
coupled cluster method, Fock space 178-180
coupled cluster method, intermediate Hamiltonian 180-182
coupled cluster theory 216, 248, 259-261, 272, 320, 403
CRYSTAL 413

D

d states 157
DC correlation energy 272, 273, 285, 286, 290-297, 297-305
DCB correlation energy 273, 285, 286, 290-297, 297-305
DCB Hamiltonian 272
density functional theory 216, 404
density functional theory, relativistic 404, 441-490
DFB SCF 272, 273, 275, 276, 281, 284, 290-297, 297-305
DF-SCF 272, 273, 274, 278, 305
DFT 216, 262, 264
DFT, relativistic 441-490
Dirac equation 20, 21, 216, 272, 353, 495-499
Dirac equation in the algebraic approximation 35-38
Dirac equation, modified 329-333
Dirac Hamiltonian 353
Dirac Hamiltonian, matrix approximations to 327-349
Dirac Hamiltonian, unitary transformations of 358-362
Dirac hole theory 11
Dirac matrices 22-27, 217-227
Dirac spectrum 27-29
Dirac-Coulomb correlation energy 272, 273, 285, 286, 290-297, 297-305
Dirac-Coulomb Hamiltonian 173, 174, 175, 353, 355, 467
Dirac-Coulomb-Breit correlation energy 273, 285, 286, 290-297, 297-305
Dirac-Coulomb-Breit Hamiltonian 174, 175, 272, 273-276, 353, 467, 519-521
Dirac-Fock SCF method, multiconfiguration 305-308,308-312,312-317,317-320
Dirac-Fock self-consistent field theory 272, 273
Dirac-Fock-Breit self-consistent field theory 272, 290-297, 297-305
Dirac-Hartree-Fock approximation 518, 519

Dirac-Hartree-Fock approximation, matrix 39-40
Dirac-Hartree-Fock theory 403
direct perturbation theory 329, 357
direct relativistic AIMP 414
discrete x-ray emission 123-125
DK 356, 357, 363-367
DKH 356,357
Douglas-Kroll Hamiltonian 356, 362-367, 413
Douglas-Kroll-Hess approximation 403
Douglas-Kroll-Hess method 356,367-369
DR-AIMP 414
dynamic correlation 187-188
dynamical correlation energy 305-320

E

E103 - gas phase chemistry experiments 89-94
E104 - electronic structures and role of reactivity 73-76
E104 - gas phase chemistry experiments 89-94
E104 - predictions of adsorption enthalpies 77-79
E104 - properties of gas-phase compounds 72-79
E104 - solution chemistry experiments 96-98, 99, 100
E104 - solution chemistry of 81-83
E105 - electronic structures and role of reactivity 73-76
E105 - gas phase chemistry experiments 89-94
E105 - predictions of adsorption enthalpies 77-79
E105 - properties of gas-phase compounds 72-79
E105 - solution chemistry of 83, 84
E106 - electronic structures and role of reactivity 73-76
E106 - gas phase chemistry experiments 89-94
E106 - predictions of adsorption enthalpies 77-79
E106 - properties of gas-phase compounds 72-79
E106 - solution chemistry of 85, 86
E107 - electronic structures and role of reactivity 73-76
E107 - gas phase chemistry experiments 94, 95
E107 - predictions of adsorption enthalpies 77-79
E107 - properties of gas-phase compounds 72-79
E108 - electronic structures and role of reactivity 73-76
E108 - gas phase chemistry experiments 95, 96
E108 - predictions of adsorption enthalpies 77-79
E108 - properties of gas-phase compounds 72-79
E111 184-187
E113 H, accuracy of the pseudopotential approximation 428, 429
E114 190-194
E118 194-195
E121 195
EC-ECP 412
ECP 401-441
EC-PP 412
EELS 116
effective core potential method 401-441
eka actinium (E121) 195
eka-gold (E111) 184-187
eka-lead (E114) 170-174
electromagnetic field, interaction of electron-positron field and 499-502
electron affinities, heavy atom 200
electron affinity 194-195
electron correlation 41-44, 177-182, 271-325
electron distributions in heavy elements 115-169
electron energy loss spectroscopy 166
electron self-energy 47, 528-534
electron spectroscopy 115-169
electron-electron interaction 30-32
electronic configuration 68-69
electron-positron field, interaction of electromagnetic and 499-502
elements 104 through 108: electronic structures and role of reactivity 73-76
elements 104 through 108: predictions of adsorption enthalpies 77-79
elements 104 through 108, properties of gas-phase compounds 72-79
elements heavier than 108, chemical studies of 101-107
elements heavier than 108: experimental investigations and plans 105-107
elements heavier than 108: production of longer-lived isotopes 101, 102
elements heavier than 108: theoretical predictions of chemical properties 102-105

elimination of the small component 328, 334-337, 337-341
energy consistent pseudopotentials 412
erbium 3d emission 153, 154
ESC 328, 347
even-tempered G spinors 282, 290
exchange, exact 473-477
excited states, x-ray 146-158
experimental investigations and plans (for elements heavier than 108) 105-107

F

f states 147
Fermi-Dirac statistics 404
Feynman gauge 275, 276
Feynman graph technique 502-505
fine structure constant 219
finite nuclear models 40, 41, 175, 176, 251, 252, 281
first-order interelectronic interaction 513-515
first-order regular approxiamtion 403
Fock space 178-180, 231
Fock space coupled cluster method 178-180
Foldy-Wouthuysen transformation 334-337, 354-357
FORA 403
four component methods 171-209, 213-269
FRECP 416
frozen core approxiamtion 404
frozen core approximation, beyond 417-420
FRPP 416
full configuration interaction 248-249
Furry picture 229-230
Furry picture for bound-state QED 495-510
Furry picture of quantum electrodynamics 32, 33
FW 354-357

G

G spinors 273, 276, 281,282, 284
GAMESS 413
gas phase chemistry 87,88
Gaunt interaction 228-229
Gaunt operator 333
GAUSSIAN 2, 413
Gaussian basis sets 176, 177
Gaussian type functions 252, 253, 411
generalized gradient approximation 404, 442
generalized gradient approximation, relativistic 444-446, 454, 455, 467, 468, 475, 478, 479, 482, 483
Gesellschaft für Schwerionenforschung mbH 9
GGA 404, 442, 444, 454, 455, 475, 477
GGA, relativistic 444-446, 454, 455, 467, 468, 475-479, 482,483
gold: local maximum of relativistic effects 184-187
Grand Accelerateur National d'Ions Lourds 9
group 13, electron affinites in 199-200
group IIB atoms, correlation corrections in 290-297
G-spinors 176

H

Hamiltonian, Chang-Pelissier-Durand 403
Hamiltonian, Dirac 353
Hamiltonian, Dirac-Coulomb 173, 174, 175, 353, 355, 467
Hamiltonian, Dirac-Coulomb-Breit 174, 175, 272, 467, 353, 355, 519-521
Hamiltonian, Douglas-Kroll 356, 362-367, 413
Hamiltonian, many-electron 215
Hamiltonian, matrix approximations to the Dirac 327-349
Hamiltonian, no pair Dirac-Coulomb 273-276
Hamiltonian, no pair Dirac-Coulomb-Breit 273-276
Hamiltonian, one-electron 216-227
Hamiltonian, relativistic 173, 174
Hamiltonian, two-electron 227-229
Hartree, Douglas 216
Hartree-Fock approach, relativistic 458
Hartree-Fock method, pseudopotential approximation in the 408-410
Hartree-Fock self-consistent field theory 272
Hartree-Fock theory 216, 259, 260
heaviest elements, chemical studies of 59-61
heaviest elements, chemistry of 54-114
heaviest elements, identification of 55-59
heaviest elements, production of 55-59
heaviest elements, timeline for the discovery of 56
heavy atom electron affinities 200
heavy atoms, QED theory of 528-559

heavy atoms, radiative corrections for the NS valence electrons in 536-538
heavy atoms, radiative corrections to G-factors of the NS valence electron in 539-549
heavy elements 2
heavy elements, electron distribution in 115-169
HEG 443
Hessian matrix 235
HF 216, 259, 260
HF-SCF 272, 288
higher orders radiative corrections 524-526
HK theorem 442, 443, 445, 449
Hohenberg-Kohn theorem, relativistic generalization of 442, 443, 445, 449
homogeneous electron gas 443

I

identification of the heaviest elements 55-59
indium atom, accuracy of the pseudopotential approximation 421, 422
Institute of Physical and Chemical Research 10
interaction in atoms, interelectron 510-521
interaction with a state continuum 155, 156
interelectron interaction in atoms 510-521
interelectronic interaction, first-order 513-515
interelectronic interaction, second-order 515-518
intermediate Hamiltonian coupled cluster method 180-182
ionic radii 72
ionization energy 297-305
ionization potentials 69-70
ionization potentials of alkali atoms 183-184
ionization potentials of some alkali atoms 3,4
island of stability 190-194
isotopes, production of longer-lived (of elements heavier than 108) 101, 102
isotopic composition 6

J

Joint Institute for Nuclear Research 9

K

kinetic balance 176, 177, 253-258, 276, 277, 278, 279, 281
kinetic balance, restricted 254
kinetic balance, unrestricted 254
Klein-Gordon hamiltonian 19, 20
KLI (Krieger-Li-Iafrate) 444, 446, 457, 458, 475
Kohn Sham equations 443
Kramers paired basis 223-224
Kramers partners 223-224, 242
Kramer's symmetry 415

L

Lagrangian 447, 448
Lamb shift 317-320
lanthanides 164-166
lanthanum 3d and 4d emissions 150-153
Lawrence Berkeley National Laboratory 9
LCAO approximation 250
LDA 443, 444, 452, 475, 477-479
LDA 404
lead, relativistic correlation energies and Lamb shift to term energy separations in 317-320
Levy-Leblond equation 403
lifetimes 201
liquid drop model 5
local density approximation 443
localized states, transitions between 132-146
long range interactions, approximation of 261
Lorentz frames 216
lowest order radiative corrections 521-524

M

many-body perturbation theory 41-44, 177, 178, 260, 272, 275, 276, 286-289, 290-297, 297-305, 308-312
many-body perturbation theory, multireference 308-312, 312-317, 317-320
many-body systems 29,30
many-electron atoms, QED theory of 526-528
many-electron Hamiltonian 215
matrix approximations to the Dirac Hamiltonian 327-349

matrix Dirac-Fock-Breit calculations 282-285, 290-297
matrix Dirac-Hartree-Fock approximation 39-40
matrix elimination of the small component 337-341
matrix multiconfiguration Dirac-Fock SCF method 305-308, 308-312, 312-317,317-320
maximum (local) of relativistic effects 184-187
Maxwell's equations 218
MBPT 41-44, 177, 178, 272, 275, 276, 286-289, 290-297, 297-305, 308-312
MC DF 128, 177
MC DF SCF 305-308,308-312, 312-317, 317-320
MCP 410, 411
MCSCF 216, 247, 248, 249
mercury atom, accuracy of the pseudopotential approximation 422-424
minimal electromagnetic interaction, principle of 217
Mn K emission spectrum 136-138
model core potential approximation 410,411
model potential method, ab initio 411
modified Dirac equation 329-333
MOLCAS 411, 413
molecular electronic structure methods 215-269
MOLECULE 411
MOLFDIR 415
Moller-Plesset perturbation theory 177, 286-289
Moller-Plesset perturbation theory, multireference 306-308, 308-312, 312-317, 317-320
MOLPRO 413
momentum space integrals 367-369
MP 410, 411, 414
MP2 177, 260
MP2, relativistic 455, 467
MR-MP 308-312, 312-317, 317-320
multiconfiguration Dirac-Fock method 177
multiconfiguration Dirac-Fock SCF method 305-308, 308-312, 312-317, 317-320
multiconfiguration self-consistent field 216, 247, 258, 259
multipole expansions 261
multireference many-body perturbation theory 308-312, 312-317, 317-320
multireference Moller-Plesset perturbation theory 306-308, 308-312, 312-317, 317-320

N

neon-like ions, correlation corrections in 290-297
NESC 345
Newton-Raphson method 235
no pair Dirac-Coulomb Hamiltonian 273-276
no pair Dirac-Coulomb-Breit Hamiltonian 273-276
no virtual pair approximation 41-44
no virtual pair approximation, beyond 44-47
noble gas atoms, correlation corrections in 290-297
Noether's theorem 447
nondynamical correlation energy 305-320
non-relativistic atom approximation 345, 346
non-relativistic limit 225-227
no-pair approximation 243
no-pair Hamiltonian 243
normal emissions, x-ray, and their satellites 133-140
NS valence electron in heavy atoms, radiative corrections to G-factors of the 539-559
NS valence electrons in heavy atoms, radiative corrections for the 536-538
nuclear shell structure 5, 7
nucleus model, finite 40, 41, 175, 176
nucleus model, point 175
nuclides, chart of 59

O

Occupation number vectors 231
"one-atom-at-a-time chemistry 86-101
one-electron Hamiltonian 216-227
OPM 456
optimized potential method, relativistic 444, 446, 455-458, 458-467, 473, 474, 477
orbital rotation operator 232
oxidation states, stabilities of 69-70

P

partial wave renormalization, electron self-energy 532-534
particle-hole formalism 237
Pauli matrices 217, 223

PBE 404
periodic table of the elements 58
perturbation theory, direct 329, 357
perturbation theory, many-body 177, 178, 260, 272, 275, 276, 286-289, 290-297, 297-305, 308-312
perturbation theory, Moller-Plesset 286-289
perturbation theory, Moller-Plesset 177
perturbation theory, multireference many-body 308-312, 312-317, 317-320
perturbation theory, multireference Moller-Plesset 306-308, 308-312, 312-317, 317-320
perturbation theory, Rayleigh-Schrödinger 242
photoemission 122, 123
photoemission, core 140-146
plutonium emission 155
point nucleus 279, 280
point nucleus model 175
Poisson equation 218
polarization, vacuum 534-536
positive-energy solutions 219
positron 237
potential expansion, electron self-energy 528-532
PPA 401-441
Pr^{3+}, importance of dynamic correlation in the f^2 levels of 177-178
production of the heaviest elements 54-60
pseudo-large component 330, 332
pseudopotential approximation 401-441
pseudopotential approximation, accuracy of the 421-431
pseudopotentials 401-441
pseudopotentials 446, 468-473, 473-477
pseudopotentials, energy consistent 412
pseudopotentials, overestimation of correlation effects 430, 431
pseudopotentials, relativistic normconserving 468-473
pseudopotentials, shape consistent 412, 413

Q

QED 174, 177, 236-241, 241-245, 263, 272, 275, 442, 445-447
QED effects in atoms 493-557
QED, Furry picture for bound-state 495-510
QED theory of heavy atoms 528-549
QED theory of many-electron atoms 526-528
quantum chemical calculations, relativistic 65-67
quantum electrodynamics 272, 493-557
quantum electrodynamics, Furry picture of 32, 33
quantum mechanics, history of 10,11,12
quasidegenerate systems 308-312
quaternion algebra 259

R

Racah algebra 216
radiative corrections for the NS valence electrons in heavy atoms 536-538
radiative corrections, higher orders 524-526
radiative corrections, lowest order 521-524
radiative corrections to G-factors of the NS valence electron in heavy atoms 539-549
radii, ionic 72
random phase approximation 453
rare earth x-ray emissions 138, 139
rare gas, electron affinity of 194-195
RASCI 216
Rayleigh-Schrödinger perturbation theory 242
RDFT 441-490
RDFT 404
RECP 345
Redox potentials 70-71
regularization and renormalization 506-510
relativisitic homogeneous electron gas 443, 444
relativistic coupled cluster theory 272
relativistic density functional theory 441-490
relativistic density functional theory 404
relativistic DFT 441-490
relativistic effective core potentials 345
relativistic effects on atomic electronic shells 61-64
relativistic GGA 444, 445, 446, 454, 455, 467, 468, 475, 478, 479, 482, 483
relativistic Hamiltonian 173, 174
relativistic Hartree-Fock approach 458
relativistic Kohn Sham equations 443
relativistic local density approximation 443, 444, 445, 446, 462, 464, 465, 475, 477, 478, 480, 482, 483

relativistic many-body perturbation theory 272, 275, 276, 286-289, 290-297, 297-305, 308-312
relativistic MP2 455, 467
relativistic normconserving pseudopotentials 468-473
relativistic optimized potential method 444, 446, 455-458, 458-467, 473, 474, 477
relativistic pseudopotentials 401-441
relativistic quantum chemical calculations 65-67
relativistic quantum mechanics, basic elements of 15-56
relativistic Troullier-Martins scheme 468-473
renormalization, regularization and 506-510
REP 414
restricted active space configuration interaction 216
restricted kinetic balance 254
RGGA 444, 445, 446, 454, 455, 467, 468, 475, 478, 479, 480, 482, 483
RHEG 443, 444, 445, 453
RHF 458
RKS 443, 444, 455, 458
RLDA 443, 444, 445, 446, 452, 454, 455, 475, 477, 478, 480, 482, 483
ROPM 444, 446, 455-458, 458-467, 483, 484, 487
RPA 453
Rutherford E.R 1
rutherfordium 8,9
Rutherfordium, application of Fock space coupled cluster method 188-190

S

s and p valence electrons, elements with 160-163
satellites, x-ray normal emissions and their 133-140
scaling, computational 249-263
SC-ECP 412, 413
SC-PP 412, 413, 414
second quantization 229-230
second-order interelectronic interaction 515-518
selecting the core 406-408
self-consistent field calculations 177
self-consistent field theory, Dirac-Fock 272, 273
self-consistent field theory, Dirac-Fock Breit 272, 290-297, 297-305
self-consistent field theory, Hartree-Fock 272
self-energy, electron 528-534
self-energy of the electron 47
shape consistent pseudopotentials 412, 413
small component, elimination of 328, 334-337, 337-341
S-matrix formalism, adiabatic 510-513
solids, valence states in 158-160
solution chemistry 88, 89
solution chemistry of elements 104, 105 and 106 79-86
SOPP 414, 415
spectroscopy, Auger emission 116
spectroscopy, bremsstrahlung isochromat 116
spectroscopy, electron 115-169
spectroscopy, electron energy loss 116
spectroscopy, x-ray 114-169
spectroscopy, x-ray emission 116
spectroscopy, x-ray photoemission 116
spectrscopy, x-ray absorption 116
SRPP 414
standard model 12
state continuum, interaction with a 155, 156
superheavy elements 5
surrounding, effects due to the 131, 132
Swirles, Bertha 216

T

theoretical predictions of chemical properties (of elements heavier than 108) 102-105
Thomas-Fermi theory 442, 450
time line for the discovery of the heaviest elements 56
time reversal symmetry 220-224
TlH, accuracy of the pseudopotential approximation 428, 429
transactinide elements 8
transfermium elements, names of 57
transition elements 163, 164
transition probabilities 201
transitions between localized states 132-146
transmutation 1
transuranium elements 7
Troullier-Martins scheme, relativistic 468-473
TURBOMOLE 413
two component approximation, two-electron Hamiltonian in the 380-382

two-component method, (exact) 369-371, 371-376
two-component method, infinite order 369-371, 371-376
two-component methods 351-400
two-electron Hamiltonian 227-229
two-electron Hamiltonian in the two component approximation 380-382

U

unitary transformations of the Dirac Hamiltonian 358-362
unrestricted kinetic balance 254
uranium 3dm 4d and 5d emissions 154, 155
uranium x-ray emissions 139, 140

V

vacuum polarization 47, 534-536
valence basis sets 416, 417
valence electron distributions in heavy elements 115-169
valence states in solids 158-160
variational collapse 176
variational procedures 230-231

W

well-tempered basis set 290

X

XAS 116, 126, 127
XES 116, 117, 126
XPS 116, 117, 126, 127
x-ray absorption spectrscopy 116
x-ray emission, discrete 113-125
x-ray emission spectroscopy 116
x-ray emissions, rare earth 138, 139
x-ray emissions, uranium 139, 140
x-ray excited states 146-158
x-ray excited states, creation of 148,149
x-ray excited states, decay of 149, 150
x-ray normal emissions and their satellites 133-140
x-ray photoemission spectroscopy 116
x-ray spectroscopy 115-169

Z

zero-order regular approximation 403
zinc, nondynamical and dynamical correlation energies in 312-317
Zitterbewegung 218
Zn, nondynamical and dynamical correlation energies in 312-317
ZORA 403, 414
ZORA 356, 357